WL-TR-96-4093

PROCEEDINGS OF THE 1995 USAF STRUCTURAL INTEGRITY PROGRAM CONFERENCE

ASIP

VOLUME I

EDITORS:

Gary K. Waggoner
WL/Materials Directorate
Wright-Patterson AFB OH

John W. Lincoln
ASC/Deputy for Engineering
Wright-Patterson AFB OH

James L. Rudd
WL/Flight Dynamics Directorate
Wright-Patterson AFB OH

USAF Structural Integrity Program Conference
Hilton Palacio del Rio
San Antonio TX

AUGUST 1996

19961025 033

FINAL REPORT FOR 28-30 NOVEMBER 1995

Approved for public release; distribution unlimited

MATERIALS DIRECTORATE
WRIGHT LABORATORY
AIR FORCE MATERIEL COMMAND
WRIGHT-PATTERSON AIR FORCE BASE, OH 45433-7718

DTIC QUALITY INSPECTED 5

NOTICE

When government drawings, specifications, or other data are used for any purpose other than in connection with a definitely related government procurement operation, the United States Government thereby incurs no responsibility or any obligation whatsoever; and the fact that the government may have formulated, furnished, or in any way supplied the said drawings, specifications, or other data, is not to be regarded by implication or otherwise as in any manner licensing the holder or any other person or corporation, or conveying any rights or permission to manufacture use, or sell any patented invention that may in any way be related thereto.

This report has been reviewed by the Office of Public Affairs (ASC/PA) and is releasable to the National Technical Information Service (NTIS). At NTIS, it will be available to the general public, including foreign nationals.

This technical report has been reviewed and is approved for publication.

Gary K. Waggoner

GARY K. WAGGONER
Chief
Systems Support Division

Vincent J. Russo

VINCENT J. RUSSO
Director
Materials Directorate

If your address has changed, if you wish to be removed from our mailing list, or if the addressee is no longer employed by your organization, please notify WL/MLS Bldg 652, 2179 Twelfth St Ste 1, Wright-Patterson AFB, Ohio 45433-7718 to help us maintain a current mailing list.

Copies of this report should not be returned unless return is required by security considerations, contractual obligations, or notice on a specific document.

DISCLAIMER NOTICE

THIS DOCUMENT IS BEST QUALITY AVAILABLE. THE COPY FURNISHED TO DTIC CONTAINED A SIGNIFICANT NUMBER OF PAGES WHICH DO NOT REPRODUCE LEGIBLY.

REPORT DOCUMENTATION PAGE

Form Approved
OMB No. 0704-0188

Public reporting burden for this collection of information is estimated to average 1 hour per response, including the time for reviewing instructions, searching existing data sources, gathering and maintaining the data needed, and completing and reviewing the collection of information. Send comments regarding this burden estimate or any other aspect of this collection of information, including suggestions for reducing this burden, to Washington Headquarters Services, Directorate for Information Operations and Reports, 1215 Jefferson Davis Highway, Suite 1204, Arlington, VA 22202-4302, and to the Office of Management and Budget, Paperwork Reduction Project (0704-0188), Washington, DC 20503.

1. AGENCY USE ONLY *(Leave blank)*	2. REPORT DATE	3. REPORT TYPE AND DATES COVERED
	August 1996	Final, 28-30 November 1995

4. TITLE AND SUBTITLE
Proceedings of the 1995 USAF Structural Integrity Program Conference, Volume I

5. FUNDING NUMBERS
PE 62102F
PR 2418
TA 07
WU 04

6. AUTHOR(S)
1-Thomas D. Cooper, Compiler & Editor; 2-John W. Lincoln, ASC/ENF; and 3-James L. Rudd, WL/FIB, Editors

7. PERFORMING ORGANIZATION NAMES(S) AND ADDRESS(ES)
1-Materials Directorate and 3-Flight Dynamics Directorate, Wright Laboratory;
2-Aeronautical Systems Center, Deputy for Engineering, all three of the
Air Force Materiel Command
Wright-Patterson AFB OH 45433

8. PERFORMING ORGANIZATION REPORT NUMBER
WL-TR-96-4093

9. SPONSORING / MONITORING AGENCY NAME(S) AND ADDRESS(ES)
POC: Gary Waggoner, WL/MLS, 513-255-4651
Materials Directorate
Wright Laboratory
Air Force Materiel Command
Wright-Patterson AFB OH 45433 -7718

10. SPONSORING / MONITORING AGENCY REPORT NUMBER
WL-TR-96-4093

11. SUPPLEMENTARY NOTES
Volume II = WL-TR-96-4094

12a. DISTRIBUTION / AVAILABILITY STATEMENT
Approved for public release; distribution is unlimited.

12b. DISTRIBUTION CODE

13. ABSTRACT *(Maximum 200 words)*

This report contains the proceedings of the 1995 USAF Structural Integrity Program Conference held at the Hilton Palacio del Rio Hotel in San Antonio, Texas, from 28-30 November 1995. The conference, which was sponsored by the Aeronautical Systems Center's Engineering Directorate and the Wright Laboratory's Flight Dynamics and Materials Directorates, was hosted by the San Antonio Air Logistics Center Aircraft Directorate, Aircraft Structural Integrity Branch (SA-ALC/LADD). This conference, as in previous years, was held to permit experts in the field of structural integrity to communicate with each other and to exchange views on how to improve the structural integrity of military weapon systems. Sessions were primarily focused on analysis and testing, engine structural integrity, structural materials and inspections, structural repair, and force management. This year, as in previous years, our friends from outside the U.S. borders provided the audience with outstanding presentations on activities within their countries. It is anticipated this conference will include their contributions in the agenda of future meetings. This year, 16 countries were represented in the audience.

14. SUBJECT TERMS	15. NUMBER OF PAGES
	680
	16. PRICE CODE

17. SECURITY CLASSIFICATION OF REPORT	18. SECURITY CLASSIFICATION OF THIS PAGE	19. SECURITY CLASSIFICATION OF ABSTRACT	20. LIMITATION OF ABSTRACT
UNCLASSIFIED	UNCLASSIFIED	UNCLASSIFIED	SAR

NSN 7540-01-280-5500 COMPUTER GENERATED Standard Form 298 (Rev. 2-89)
Prescribed by ANSI Std. Z39-18
298-102

GENERAL INSTRUCTIONS FOR COMPLETING SF 298

The Report Documentation Page (RDP) is used in announcing and cataloging reports. It is important that this information be consistent with the rest of the report, particularly the cover and title page. Instructions for filling in each block of the form follow. It is important to ***stay within the lines*** to meet ***optical scanning requirements.***

Block 1. Agency Use Only *(Leave Blank).*

Block 2. Report Date. Full publication date including day, month, and year, if available (e.g. 1 Jan 88). Must cite at least the year.

Block 3. Type of Report and Dates Covered. State whether report is interim, final, etc. If applicable, enter inclusive report dates (e.g. 10 Jun 87 - 30 Jun 88).

Block 4. Title and Subtitle. A title is taken from the part of the report that provides the most meaningful and complete information. When a report is prepared in more than one volume, repeat the primary title, add volume number, and include subtitle for the specific volume. On classified documents enter the title classification in parentheses.

Block 5. Funding Numbers. To include contract and grant numbers; may include program element number(s), project number(s), task number(s), and work unit number(s). Use the following labels:

C - Contract	**PR** - Project
G - Grant	**TA** - Task
PE - Program Element	**WU** - Work Unit Accession No.

Block 6. Author(s). Name(s) of person(s) responsible for writing the report, performing the research, or credited with the content of the report. If editor or compiler, this should follow the name(s).

Block 7. Performing Organization Name(s) and Address(es). Self-explanatory.

Block 8. Performing Organization Report Number. Enter the unique alphanumeric report number(s) assigned by the organization performing the report.

Block 9. Sponsoring/Monitoring Agency Name(s) and Address(es). Self-explanatory.

Block 10. Sponsoring/Monitoring Agency Report Number. *(If known)*

Block 11. Supplementary Notes. Enter information not included elsewhere such as: Prepared in cooperation with...; Trans. of...; To be published in.... When a report is revised, include a statement whether the new report supersedes or supplements the older report.

Block 12a. Distribution/Availability Statement. Denotes public availability or limitations. Cite any availability to the public. Enter additional limitations or special markings in all capitals (e.g. NOFORN, REL, ITAR).

DOD - See DoDD 5230.24, "Distribution Statements on Technical Documents."
DOE - See authorities.
NASA - See Handbood NHB 2200.2.
NTIS - Leave blank.

Block 12b. Distribution Code.

DOD - Leave blank.
DOE - Enter DOE distribution categories from the Standard Distribution for Unclassified Scientific and Technical Reports.
NASA - Leave blank.
NTIS - Leave blank.

Block 13. Abstract. Include a brief *(Maximum 200 words)* factual summary of the most significant information contained in the report.

Block 14. Subject Terms. Keywords or phrases identifying major subjects in the report.

Block 15. Number of Pages. Enter the total number of pages.

Block 16. Price Code. Enter appropriate price code *(NTIS only).*

Block 17. - 19. Security Classifications. Self-explanatory. Enter U.S. Security Classification in accordance with U.S. Security Regulations (i.e., UNCLASSIFIED). If form contains classified information, stamp classification on the top and bottom of the page.

Block 20. Limitation of Abstract. This block must be completed to assign a limitation to the abstract. Enter either UL (unlimited) or SAR (same as report). An entry in this block is necessary if the abstract is to be limited. If blank, the abstract is assumed to be unlimited.

H U.S.GPO: 1990-0-273-271

TABLE OF CONTENTS
Volume I

Page

FOREWORD vii

AGENDA ix

INTRODUCTION xv

SESSION I - OVERVIEWS

C-141 Starlifter: An Experience in Aging Aircraft Philosophy 3
J. Cochran

Evaluation of Multiple Site Damage in Lap Joint Specimens 21
A. Grandt Jr., H. Wang and K. Buhler

A New Structural Integrity Policy for the VC10 39
Squadron Leader E. Bittel and C. Hoyle

C17A Durability and Damage Tolerance Test Program 49
K. Liu and C. Babish

CF116 (CF-5) Full Scale Durability and Damage Tolerance Test (FSDADTT) - Final Test/Teardown Results 75
Y. Beauvais

B-1B Aircraft Structural Integrity Program 103
A. Denyer

Understanding Fatigue Failure Analyses Under Random Spectrum Loading Using a C-17 Test Article Failure 129
C. Brooks, K. Lui & R.G. Eastin

Non-Government Standards IPT Findings: The Joint Aeronautical Commanders Group (JACG) Implementation Challenge 149
M. Wilson

SESSION II - STRUCTURAL JOINTS

Local Stresses and Distortions of a Three-Dimensional, Cyclically Loaded, Riveted Lap Joint 165
K. Iyer, P. Bastias, C. Rubin and G. Hahn

Experimental Strain Field Characterization of Boeing 737 Lap Splices with Analytical Correlations 187
D. Jeong, J. Canha, J. Brewer, D. Roach and T. Flournoy

Assessing Structural Integrity of Bonded Joints Using Fracture Mechanics 205
Capt L. Butkus and S. Johnson

Experimental Observation of the Effect of the Contact Parameters on Fretting Fatigue Crack Nucleation 237
G. Harish, M. Szolwinski and T. Farris

Fatigue Crack Growth in Riveted Lap Joints 267
Capt S. Fawaz and Professor J. Schijve

Analytical Methodology to Predict the Onset of Widespread Fatigue Damage in Airframe Structure 279
C. Harris, J. Newman Jr., J. Starnes Jr. & R. Piascik

SESSION III - LOADS

Landing Parameter Surveys of Transport Aircraft 307
R. Micklos

Prediction and Control of Dynamic Loads to Improve Structural Integrity 335
L. Huttsell and L. Shaw

P-3C Fatigue Tracking Methodology Update 359
M. Hoffman, N. Phan and A. Anderjaska

SESSION IV - ROTORCRAFT/DYNAMICS

Lessons Learned from Canadian Forces Helicopter ASIP - Implementation to Retirement 377
T. Padfield and K. Langille

Small Crack Technology for Aging Rotorcraft 409
P. Bates & G. Chamberlain

Helicopter Structural Integrity with I-HUMS 425
G. Cleveland, B. Thompson and B. Sullivan

B-2 Aft Deck Redesign 447
Lt G. Buckner, F. Grimsley and G. Carney

SESSION V - ENGINES

Effect on Machining Processes on the LCF Life of Holes in High Strength Nickel Base Powder Metal Components 471
W. Cowie and S. Kamat

Accelerated Mission Testing: Valuable Tool for Assuring Engine Integrity 491
P. Gatlin

Plan to Control High Cycle Fatigue in Engines 503
Capt N. Huber

F117-PW-100 Tailored ENSIP for Five Peacetime C-17 Missions 523
S. Patel

The Canadian Forces Experience with the Operation of Loads Monitoring Process for Efficient Structural Life Management 551
Capt S. Le Guellec and M. Zgela

SESSION VI - MECSIP

MESCIP Analysis Case Histories - Issues Raised and Beneficial Design Impacts 575
M. Creager and K. Odian

A Damage Tolerance Analysis of a Landing Gear 597
T. Wolff, M. Kaplan and T. Willis

Case Depth and Chemistry Profile Measurements: A Novel NDI Technique 635
S. Pelletier and N. Marchand

Volume II

SESSION VII - ADVANCED MATERIALS AND PROCESSES

Damage Progression in Bolted Composite Structures 663
C. Chamis, P. Gotsis and L. Minnetyan

High-Strength Aluminum Forged Product Durability and Damage Tolerance Capabilities for Weight and Total Life Cycle Cost Saving 681
R. Bucci, R. Bush, A. Hinkle, H. Konish, M. Kulak, R. Wygonik & G. Kuhlman

The Impact of Fastener Hole Quality on Structural Life; A History of Success 703
C. Radcliffe and W.H. Sproat

A Probabilistic Model for Predicting Fatigue Life for Crack Formation at Inclusions Using FASTRAN 727
P. Laz, S. Rohrbaugh and B. Hillberry

The Application of the R-Curve Concept for the Prediction of the Residual Strength of Fiber Metal Laminates 751
T. de Vries & M. Pacchione

Laser Shock Peening - An Analysis in Nearly Closed Form 777
H. Swift

SESSION VIII - NDE/I

Nondestructive Electrochemical Corrosion Measurement: Electrochemical Impedance Pattern Recognition for Detection of Hidden Chemical Corrosion on Aircraft Components 791
J. Bowers, M. Vreeke and A. Sammells

Detecting Weephole Cracks Using Ultrasonic Creeping Waves 821
M. Golis

An Advanced ACPD System for Aircraft Structural Integrity Assessment 827
S. Tiku, N. Marchand and R. Finlayson

SESSION IX - REPAIRS

C-141 Repair Tracking 845
R. Alford and R. Sykes

The ForceTec® Rivetless Nut Plate System and Its Application to Military Aircraft Production and Repair 869
L. Reid and E. Esterbrook

Design Development of a Bonded Fuselage Repair for the C-5A 887
Major R. Fredell, C. Guijt, Lt D. Conley and Lt S. Knighton

An FEAM Based Methodology for Analyzing Composite Patch Repairs of Metallic Structures 903
V. Nagaswamy, D.S. Pipkins and S.N. Atluri

The 1973-1974 F/RF-4C/D Damage Tolerance and Life Assessment Study Revisited 931
R. Bader and R. Howell

SESSION X - CORROSION/FATIGUE

Aircraft Corrosion and Fatigue Damage Assessment 983
R. Wanhill

Fuselage Lap Splice Joint Corrosion 1029
R. Piascik, R. Kelly and S. Williard

The Effect of Corrosion on the Structural Integrity of Fuselage Lap Joints 1063
N. Bellinger and J. Komorowski

Effects of Cyclic Immersion in 3.5% NaCl Solution on Fatigue Crack Propagation Rates in Aluminum 2024-T351 1089
J. Kramer and D. Hoeppner

Corrosion Fatigue Interaction 1113
P. Tong, D. Jeong and G. Neat

SESSION XI - FORCE MANAGEMENT

Automated Readiness Integrated Engineering System (ARIES) 1131
J. Cochran and C. Burke

AMRL Support for RAAF F-111 ASIMP 1139
K. Watters and J. Paul

RNZAF Project KESTREL 1159
Squadron Leader J. ten Have

Application of Object Oriented Technology to an Aircraft Structural Integrity Program - FAA Flight Inspection Learjet Model 60 and Canadair Challenger 601-3R Aircraft 1167
T. Kelley

ATTENDEES LIST 1195

FOREWORD

This report was compiled by the Systems Support Division, Materials Directorate, Wright Laboratory, Wright-Patterson Air Force Base, Ohio. It was initiated under Task 24180704 "Corrosion Control & Failure Analysis" with Gary K. Waggoner as the Project Engineer.

This technical report was submitted by the editors.

The purpose of this 1995 Conference was to bring together technical personnel in DoD and the aerospace industry who are involved in the various technologies required to ensure the structural integrity of aircraft gas turbine engines, airframes and other mechanical systems. It provided a forum to exchange ideas and share new information relating to the critical aspects of durability and damage tolerance technology for aircraft systems. The conference was sponsored by the Air Force Materiel Command (AFMC), Aeronautical Systems Center, Deputy for Engineering and Materials and Flight Dynamics Directorates of the Wright Laboratory, Wright-Patterson Air Force Base, Ohio. It was hosted and co-sponsored by the Aircraft Structural Integrity Branch, Aircraft Directorate of AFMC's San Antonio Air Logistics Center, Kelly Air Force Base, Texas.

FINAL AGENDA

1995 USAF STRUCTURAL INTEGRITY PROGRAM CONFERENCE

28-30 November 1995

Hilton Palacio del Rio

San Antonio, Texas

MONDAY, 27 NOVEMBER 1995

5:00 PM - 7:00 PM	REGISTRATION

TUESDAY, 28 NOVEMBER 1995

7:30 AM - 5:30 PM	REGISTRATION
7:30 AM - 8:10 AM	CONTINENTAL BREAKFAST
8:10 AM - 8:25 AM	Opening Comments *J. Lincoln*, ASC/ENF
	Session I - Overviews Chairman - J. Rudd, WL/CCI
8:25 AM - 8:50 AM	C-141 Starlifter: An Experience in Aging Aircraft Philosophy *J. Cochran*, Lockheed Martin Aeronautical Systems *R. Alford*, WR-ALC/LJLEA
8:50 AM - 9:15 AM	Evaluation of Multiple Site Damage in Lap Joint Specimens *A. Grandt, Jr. and H. Wang*, Purdue University, West Lafayette IN *K. Buhler*, Royal Australian Air Force
9:15 AM - 9:40 AM	Development of a New Structural Integrity Policy for the VC10 *Squadron Leader E. Bittel*, Royal Air Force, HQ Logistics Command, RAF Wyton, United Kingdom *C. Hoyle*, British Aerospace
9:40 AM - 10:05 AM	C-17A Durability and Damage Tolerance Test Program *K. Liu*, McDonnell Douglas Aerospace, Long Beach CA *C. Babish*, Wright-Patterson AFB OH
10:05 AM - 10:35 AM	REFRESHMENT BREAK
10:35 AM - 11:00 AM	CF-5 Full-Scale Durability and Damage Tolerance Test (FSDADTT) - Final Teardown Results *Y. Beauvais,* Bombardier Inc., Marabel, Quebec, Canada
11:00 AM - 11:25 AM	B-1B Aircraft Structural Integrity Program *A. Denyer*, Rockwell International, Seal Beach CA
11:25 AM - 11:50 AM	Understanding Fatigue Failure Analysis Under Random Spectrum Loading Using a C-17 Test Article Failure *C. Brooks*, McDonnell Douglas Aerospace, St Louis MO
11:50 AM - 1:20 PM	LUNCH AND PRESENTATION Non-Government Standards IPT Findings: The Joint Aeronautical Commanders Group (JACG) Implementation Challenge *M. Wilson*, ASC/EN, Wright-Patterson AFB OH

Session II - Structural Joints
Chairman - D. Paul, WL/FIB

1:20 PM - 1:45 PM	Analyses of the Local Stresses and Distortions of a 3-Dimensional, Cyclically Loaded, Riveted Lap Joint *K. Iyer, P. Bastias, C. Rubin and G. Hahn*, Vanderbilt University
1:45 PM - 2:10 PM	Experimental Strain Field Characterization of Boeing 737 Lap Splices with Analytical Correlations *D. Jeong, J. Canha and J. Brewer*, U.S. Department of Transportation, Cambridge MA *D. Roach*, Sandia National Laboratories, Albuquerque NM *T. Flournoy*, Federal Aviation Administration, Atlantic City NJ
2:10 PM - 2:35 PM	Assessing Structural Integrity of Bonded Joints Using Fracture Mechanics *T. Weng and C. Sun*, Purdue University
2:35 PM - 3:00 PM	Experimental Observation of the Effect of the Contact Parameters on Fretting Fatigue Crack Formation *G. Harish, M. Szolwinski and T. Farris*, Purdue University, West Lafayette IN
3:00 PM - 3:30 PM	REFRESHMENT BREAK
3:30 PM - 3:55 PM	Fatigue Crack Growth in Riveted Lap Joints *Capt S. Fawaz*, United States Air Force *Professor J. Schijve*, Delft University of Technology, Delft, The Netherlands
3:55 PM - 4:20 PM	Analytical Methodology to Predict the Onset of Widespread Fatigue Damage in Airframe Structure *C. Harris, J. Newman Jr. and J. Starnes Jr.*, NASA Langley Research Center, Hampton VA

Session III - Loads
Chairman - M. McMahon, NAVAIR

4:20 PM - 4:45 PM	Landing Parameter Surveys of Transport Aircraft *R. Micklos*, Naval Air Warfare Center, Warminster PA
4:45 PM - 5:10 PM	Prediction and Control of Dynamic Loads to Improve Structural Integrity *L. Huttsell and L. Shaw*, WL/FIB, Wright-Patterson AFB OH
5:10 PM - 5:35 PM	P-3C Fatigue Tracking Methodology Update *M. Hoffman*, Naval Air Warfare Center, Warminister PA *N. Phan*, Naval Air Systems Command, Washington DC *A. Anderjaska*, Aerostructures, Inc., Arlington VA
6:00 PM - 7:30 PM	RECEPTION

WEDNESDAY, 29 NOVEMBER 1995

7:30 AM - 5:30 PM REGISTRATION

7:30 AM - 8:00 AM CONTINENTAL BREAKFAST

Session IV - Rotorcraft/Dynamics
Chairman - T. Christian, WR-ALC/MMSR

8:00 AM - 8:25 AM Lessons Learned from Canadian Forces Helicopter ASIP - Implementation to Retirement
T. Padfield, Bristol Aerospace Limited, Winnepeg, Manitoba, Canada
K. Langille, Department of National Defense, Ottawa, Ontario, Canada

8:25 AM - 8:50 AM Small Crack Technology for Aging Rotorcraft
P. Bates, Georgia Tech Research Institute, Atlanta GA

8:50 AM - 9:15 AM Helicopter Structural Integrity with I-HUMS
G. Cleveland, Smiths Industries
B. Thompson, Naval Aviation Engineering Service Unit
B. Sullivan, Chadwick-Helmuth, Inc.

9:15 AM - 9:40 AM B-2 Aft Deck Redesign
Lt G. Buckner and F. Grimsley, ASC/YSDF, Wright-Patterson AFB OH
C. Dever, Northrop-Grumman B-2 Division, Palmdale CA
D. Lies, OC-ALC

9:40 AM - 10:10 AM REFRESHMENT BREAK

Session V - Engines
Chairman - Wing Cmdr C. Pomfret, WL/POTC

10:10 AM - 10:35 AM Effect of Machining Processes on the Fatigue Life of Holes in High Strength Nickel Base Powder Metal Components
W. Cowie and S. Kamat, General Electric

10:35 AM - 11:00 AM Accelerated Mission Testing: A Valuable Tool for Assuring Engine Integrity
P. Gatlin, Pratt & Whitney, West Palm Beach FL

11:00 AM - 11:25 AM Plan to Control HCF in Engines
Capt N. Huber, WL/POTC, Wright-Patterson AFB OH

11:25 AM - 11:50 AM F117-PW-100 Tailored ENSIP for Five Peace Time C-17 Missions
S. Patel, Pratt & Whitney, East Hartford CT

11:50 AM - 1:20 PM LUNCH AND PRESENTATION
The Canadian Forces Experience with the Operation of Loads Monitoring Process for Efficient Structural Life Management
Capt S. Le Guellec, Directorate of Aerospace Support Engineering, National Defense Headquarters, Ottawa, Ontario, Canada
M. Zgela, Martec Limited, Halifax, Nova Scotia, Canada

Session VI - MECSIP
Chairman - R. Berger, ASC/ENFA

1:20 PM - 1:45 PM MECSIP Analysis Case Histories - Issues Raised and Beneficial Design Impacts
M. Creager and K. Odian, Structural Integrity Engineering, Chatsworth CA

1:45 PM - 2:10 PM A Damage Tolerance Analysis of a Landing Gear
T. Wolff, M. Kaplan and T. Willis, Willis & Kaplan Inc., Buffalo Grove IL

2:10 PM - 2:35 PM Case Depth and Chemistry Profile Measurements; A Novel NDI Technique
S. Pelletier and N. Marchand, Montréal Québec, Canada

Session VII - Advanced Materials and Processes
Chairman - R. Meeker, WL/MLS

2:45 PM - 3:00 PM Damage Progression in Bolted Composite Structure
C. Chamis and P. Gotsis, National Aeronautics and Space Administration, Lewis Research Center, Cleveland OH
L. Minnetyan, Clarkson University, Potsdam NY

3:00 PM - 3:30 PM REFRESHMENT BREAK

3:30 PM - 3:55 PM High-Strength Aluminum Forged Product Durability and Damage Tolerance for Weight and Total Life Cycle Cost Saving
R. Bucci, R. Bush, A. Hinkle, H. Konish, M. Kulak and R. Wygonik, Aluminum Company of America, Alcoa Center PA

3:55 PM - 4:20 PM The Impact of Fastener Hole Quality on Structural Life; A History of Success
C. Radcliffe and W.H. Sproat, Measurement Systems Inc., Marietta GA

4:20 PM - 4:45 PM A Probabilistic Model for Predicting Fatigue Life for Crack Nucleation at Inclusions Using FASTRAN
P. Laz, S. Rohrbaugh and B. Hillberry, Purdue University, W Lafayette IN

4:45 PM - 5:10 PM The Application of the R-Curve Concept for the Prediction of the Residual Strength of Fiber Metal Laminates
T. de Vries, Delft University of Technology, The Netherlands

5:10 PM - 5:35 PM Laser Peening - An Analysis in Nearly Closed Form
H. Swift, University of Dayton Research Institute, Dayton OH

THURSDAY, 30 NOVEMBER 1995

7:30 AM - 5:30 PM REGISTRATION

7:30 AM - 8:00 AM CONTINENTAL BREAKFAST

Session VIII - NDE/I
Chairman - R. Paglia, WL/MLS-OL

8:00 AM - 8:25 AM Nondestructive Electrochemical Corrosion Measurement
J. Bowers, M. Vreeke and A. Sammells, Eltron Research Inc., Boulder CO

8:25 AM - 8:50 AM Detecting Weephole Cracks Using Ultrasonic Creeping Waves
M. Golis, Advanced Quality Concepts, Columbus OH

8:50 AM - 9:15 AM Field Level Composite and Composite Repair Evaluation (NDE/I) (Paper Cancelled)
J. Tyson, II, Laser Technology, Inc., Norristown PA

9:15 AM - 9:40 AM An Advanced ACPD System for Aircraft Structural Integrity Assessment
S. Tiku, Départment de Métallurgie et Génie des Matéiaux Ecole Polytechnique, University of Montréal, Montréal, Canada
R. Finlayson, Department of National Defense, Ottawa, Ontario, Canada

9:40 AM - 10:10 AM REFRESHMENT BREAK

Session IX - Repairs
Chairman - J. Mazza, WL/MLSE

10:10 AM - 10:35 AM	C-141 Repair Tracking *R. Alford*, WR-ALC/LJLEA, Robins Air Force Base GA *R. Sykes*, Lockheed Martin Aeronautical Systems, Marietta GA
10:35 AM - 11:00 AM	The ForceTec Rivetless Nut Plate System and Its Application to Military Aircraft Production and Repair *L. Reid and E. Esterbrook,* Fatigue Technology Inc., Seattle WA
11:00 AM - 11:25 AM	Design Development of a Bonded Fuselage Repair for the C/5A *Major R. Fredell and C. Guyt*, United States Air Force Academy, Colorado Springs CO *Lt D. Conley*, WL/FIBE, Wright-Patterson AFB OH *Lt S. Knighton,* San Antonio Air Logistics Center, Kelly AFB
11:25 AM - 11:50 AM	An FEAM Based Methodology for Analyzing Composite Patch Repairs of Metallic Structures *V. Nagaswamy, D.S. Pipkins and S.N. Atluri*, Georgia Tech Computational Modeling Center, Atlanta GA
11:50 AM - 1:20 PM	LUNCH AND PRESENTATION The 1973-1974 F/RF-4C/D Damage Tolerance and Life Assessment Study Revisited *R. Bader*, Consultant, Xenia OH *R. Howell*, OO-ALC/LACM, Hill AFB UT

Session X - Corrosion/Fatigue
Chairman - C. Seher, FAA Tech Center

1:20 PM - 1:45 PM	Aircraft Corrosion and Fatigue Damage Assessment *R. Wanhill*, National Aerospace Laboratory NLR, Amsterdam, The Netherlands
1:45 PM - 2:10 PM	Fuselage Lap Splice Joint Corrosion *R. Piascik*, NASA Langley Research Center, Hampton VA *R. Kelly*, University of Virginia, Charlotteville VA *S. Williard*, Lockheed Engineering and Sciences Co., Hampton VA
2:10 PM - 2:35 PM	The Effect of Corrosion on the Structural Integrity of Fuselage Lap Joints *N. Bellinger and J. Komorowski*, National Research Council Canada, Ottawa, Ontario, Canada
2:45 PM - 3:00 PM	Effects of Cyclic Immersion in 3.5% NaCl Solution of Fatigue Crack Propagation Rates in Aluminum 2024-T351 *J. Kramer and D. Hoeppner*, Department of Mechanical Engineering, University of Utah, Salt Lake City UT
3:00 PM - 3:30 PM	REFRESHMENT BREAK
3:30 PM - 3:55 PM	Corrosion Fatigue Interaction *P. Tong*, The Hong Kong University of Science and Technology *D. Jeong and G. Neat*, U.S. Department of Transportation, Cambridge MA

Session XI - Force Management
Chairman - J. Turner, SA-ALC/LADD

3:55 PM - 4:20 PM	Automated Readiness Integrated Engineering System (ARIES) *J. Cochran and C. Burke*, Lockheed Martin Aeronautical Systems
4:20 PM - 4:45 PM	AMRL Support for RAAF F-111 ASIMP *K. Watters and J. Paul*, Aeronautical and Maritime Research Laboratory, Melbourne, VIC, Australia
4:45 PM - 5:10 PM	RNZAF Project KESTREL *Squadron Leader J. ten Have*, Headquarters NZ Defence Force, Wellington, New Zealand
5:10 PM - 5:35 PM	Application of Object Oriented Technology to an Aircraft Structural Integrity Program - FAA Flight Inspection Learjet Model 60 and Canadair Challenger 601-3R Aircraft *T. Kelley*, E-Systems Greenville Division, Greenville TX

EXHIBITORS

- ADVANCED REPAIR TECHNOLOGY INTERNATIONAL
- BOMBARDIER, CANADAIR DSD
- CANADIAN MARCONI CO.
- ELTRON RESEARCH INC.
- FATIGUE TECHNOLOGY CORP.
- MEASUREMENT SYSTEMS INC.
- METAL IMPROVEMENT CO. INC.
- MOOG ESPRIT
- MTS SYSTEMS CORPORATION
- NONDESTRUCTIVE TESTING INFORMATION ANALYSIS CENTER (NTIAC)
- OGDEN ALC/LACM & MCDONNELL DOUGLAS
- SMITHS INDUSTRIES AEROSPACE
- SOUTHWEST RESEARCH INSTITUTE
- STRUCTURAL LAMINATES COMPANY
- SYSTEMS ELECTRONICS INC. (SEI)
- TEXTRON SPECIALTY MATERIALS
- U. S. AIR FORCE
- WEST COAST INDUSTRIES
- WL/FIBEC FATIGUE, FRACTURE, AND RELIABILITY SECTION

INTRODUCTION

This report contains the proceedings of the 1995 USAF Structural Integrity Program Conference held at the Hilton Palacio del Rio in San Antonio, Texas from 28-30 November 1995. The conference, which was sponsored by the Aeronautical Systems Center's Engineering Directorate and the Wright Laboratory's Flight Dynamics and Materials Directorates, was hosted and co-sponsored by the San Antonio Air Logistics Center Aircraft Directorate, Aircraft Structural Integrity Branch (SA-ALC/LADD).

This conference, as in previous years, was held to permit experts in the field of structural integrity to communicate with each other and to exchange views on how to improve the structural integrity of military weapon systems. Sessions were primarily focused on structural joints, loads, rotorcraft/ dynamics, engines, MECSIP, advanced materials and processes, NDE/I, repairs, corrosion/fatigue and force management. This year, as in previous years, our friends from outside the U.S. borders provided the audience with outstanding presentations on activities within their countries. It is anticipated that this conference will include their contributions in the agenda of future meetings. This year sixteen countries plus NATO were represented in the audience.

The sponsors are indebted to their hosts for their support of the conference. The sponsors are also indebted to the speakers for their contributions. In particular, thanks are due to the three luncheon speakers for their informative presentations, Mr. Mark Wilson, ASC/EN, Aeronautical Systems Center for his update on the Non-Government Standards IPT Findings, Capt S. LeGuellec from National Defense Headquarters, Ottawa Canada on the summary of the Canadian Forces Experiences with the Operation of Loads Monitoring Process for Efficient Structural Life Management and Mr. Bob Bader, Consultant, for an excellent revisit of the 1973-1974 F/RF-4 C/D Damage Tolerance and Life Assessment Study.

As usual, much of the success of the conference is due to the efforts of Jill Jennewine and her staff, including Lori Kilian and Esther Burnett, from Universal Technology Corporation. Their cooperation is greatly appreciated. We are also grateful to Rita Scholes of WL/MLS for her continuing support to the success of this conference.

John W. Lincoln	Gary K. Waggoner	Donald B. Paul	Jimmy Turner
ASC/ENF	WL/MLS	WL/FIB	SA-ALC/LADD

SESSION I

OVERVIEWS

Chairman: *J. Rudd*, WL/CCI

C-141 Starlifter: An Experience In Aging Aircraft Philosophy

Presented To

1995 USAF Aircraft Structural Integrity Program Conference

28-30 November 1995

San Antonio, Texas

Russ Alford
WR-ALC/LJLEA
C-141 ASIP Manager

Joe Cochran
Lockheed Martin
Aeronautical Systems

Today, as an overview, I would like to present an aspect of "aging aircraft" philosophy as related to the C-141 Starlifter, the venerable workhorse of our nation's airlift over the last three decades.

I would like to thank the sponsors of this conference for allowing this presentation to be part of the program. Furthermore, I want to thank my colleague, Mr. Russ Alford for assisting me in putting together this presentation.

Introduction

(Birth of Modern Concept of Aging Aircraft)

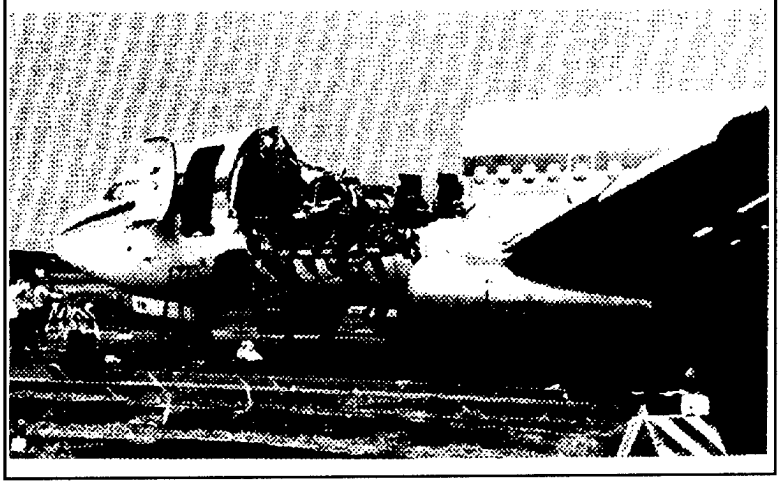

The idea or philosophy of "aging aircraft" is not new. It seems, however, that the Aloha incident pictured here kicked off a frenzy as if the thought of "aging aircraft" never existed. Almost overnight, investigations, special committee formations, new perspectives on aircraft safety, etc.. sprang up with a new sense of urgency. In the eyes of the general public, the phrase "aging aircraft" was born.

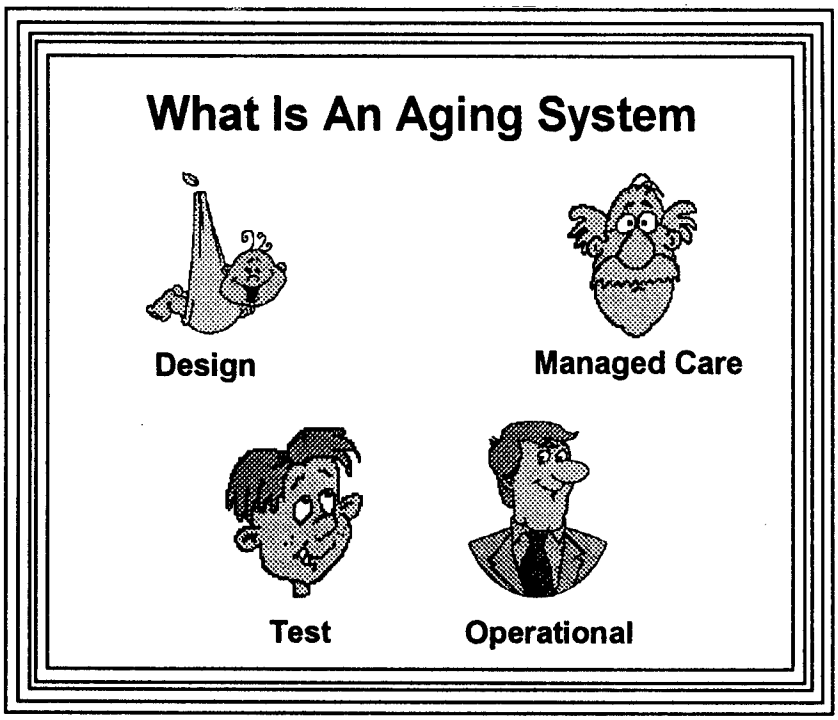

One might ask, "What is an aging system?" The pictorialization presented here might be an over simplification, but the fact of the matter is that everything that is conceived begins to age. Put into terms of an aircraft system, this means that from time of design, through tests and service introduction, through its operational life, and finally into its final years, the "aging" system must be managed with care with respect to its usage and environment through timely (and proper) inspection, repair, and mod programs.

DEFINITION

Any Aircraft System That Is Conceived and Subsequently Funded for Development, Validation and Operational Implementation Is an "Aging" Aircraft System From the Design Board to Day of Retirement.

"Cradle To Grave"

By definition then, we have a "cradle to grave" concept that if implemented would provide the user with a cost effective and efficiently managed weapon system. The ASIP process is probably the best tool we have today to make this concept a reality. However, the ASIP process needs a higher level of authority and/or enforcement that would allow it to make its case in the face of "budget constraints" and other factors inconsistent with the overall mission requirements. Perhaps this could best be served by the establishment of a Total Aircraft System Integrity Program (TASIP) standing committee chaired by a Chief ASIP Engineer and reporting to the AFMC Commander.

INFLUENTIAL FACTORS ON "AGING"

- **Materials (Strength, Durability, Toughness, Etc)**
- **Manufacturing Processes (Cutting, Forming, Drilling, Etc)**
- **Operational Environment**
- **Usage (and Severity of That Usage)**
- **Proper and Timely Maintenance**
- **Force Management Process**

Unless one thinks that the C-141 is the epitome of the aging aircraft, cradle to grave concept, we must be reminded that the aircraft is only a valuable source of information regarding the various factors that are influential on the aging process. It should be noted here that the last two bullets on this chart are the key to giving the aircraft its best "state of readiness" in light of the first four bullets.

AGING AIRCRAFT PHILOSOPHY

- **Understanding the Aircraft**
  - **Design**
  - **Test History**
  - **Mission Profile**
  - **Capability**
- **Understanding Aircraft Health**
  - **Preventative Maintenance**
  - **Scheduled Maintenance by Usage, Environment**
  - **Monitoring Systems (L/ESS, AFSIP, SFDR)**

Any philosophy of aging aircraft should be based on a clear understanding of the aircraft and of its state of health. The things we see here are the ingredients that will enable us to build the foundation of that understanding.

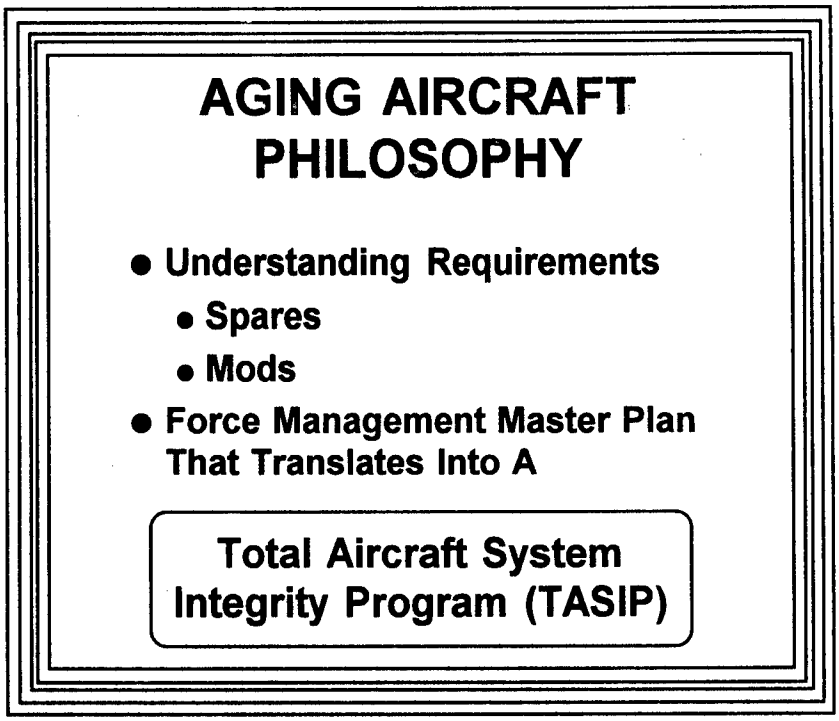

Additionally, to further our understanding of the aging aircraft philosophy, we need to be aware of day to day requirements in terms of resources consistent with mission changes and/or requirements. The best way to do this is through a pro-active force management master plan.

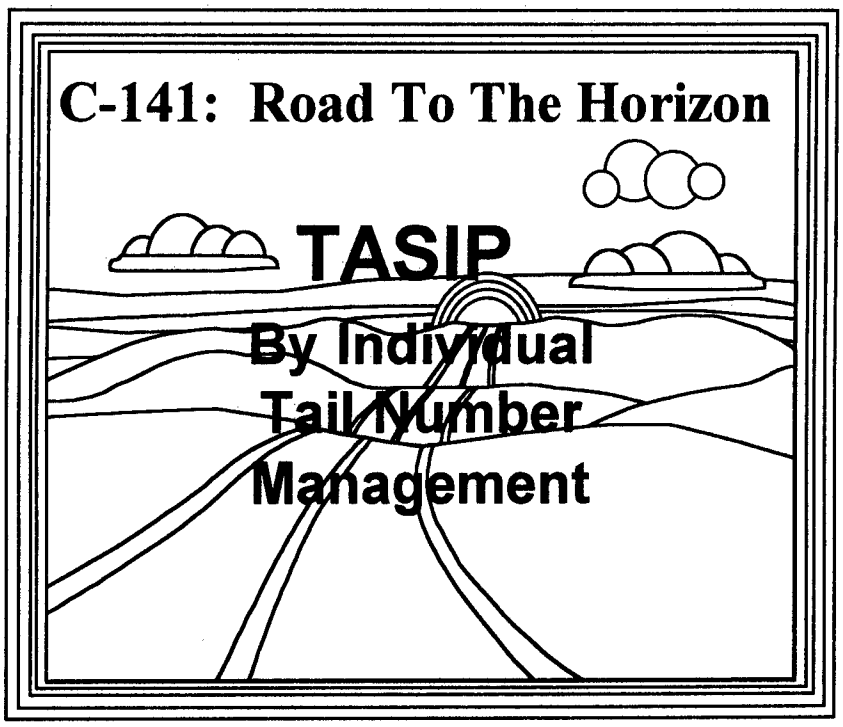

In light of all that has been said to this point, let us look at the C-141 Starlifter as an aging aircraft system, particularly by applying our philosophy to each individual aircraft.

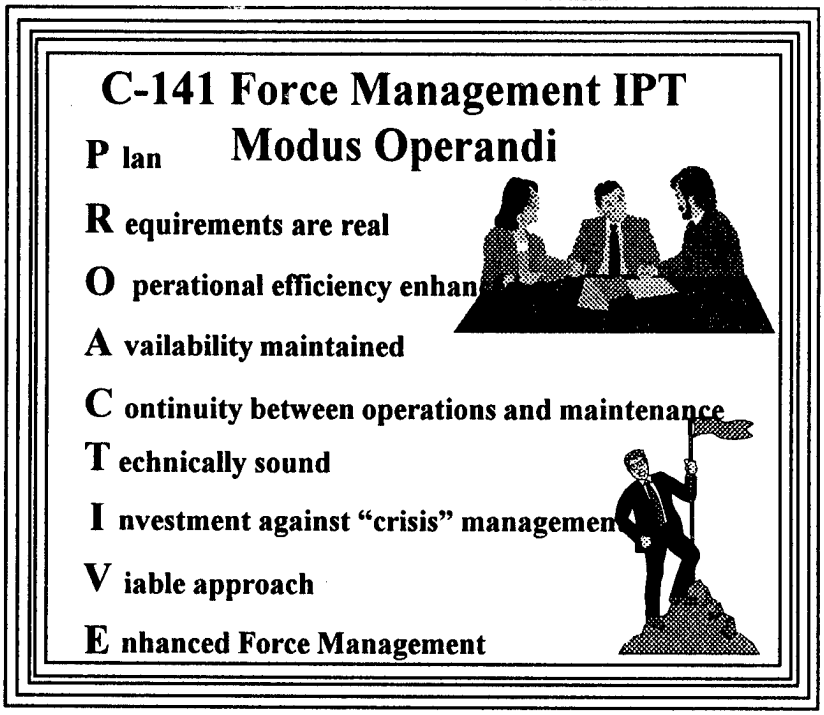

Every since the C-141 went into operation, it has been the philosophy of the ASIP Managers to have a pro-active force management plan. Although we have not been entirely successful, we nevertheless believe that a **p**lan based on real **r**equirements will enhance **o**perational efficiency and maintain aircraft **a**vailability while providing **c**ontinuity between operations and maintenance based on **t**echnically sound decisions. Such a plan is an **i**nvestment against "crisis" management and is a **v**iable approach to an **e**nhanced force management.

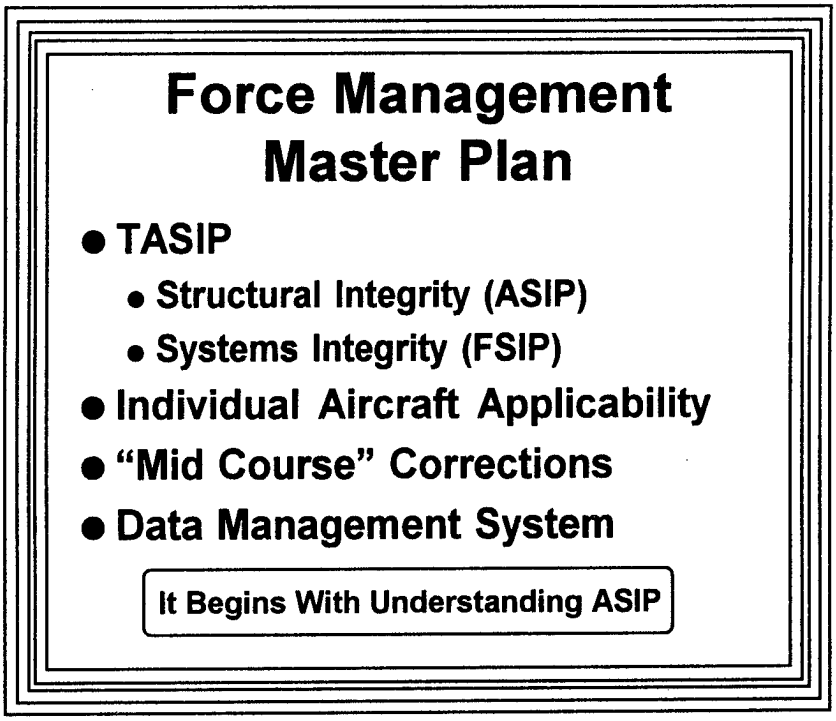

Having a force management master plan and understanding it are two different things. The C-141 has an ASIP(structural integrity) and an FSIP (systems integrity) in place that has individual aircraft applicability. During the years there have been several "mid course" corrections (repairs/mods) that has led us to develop a data management system that we feel is a model for other weapon systems. Any force management plan has to begin with the basics of ASIP.

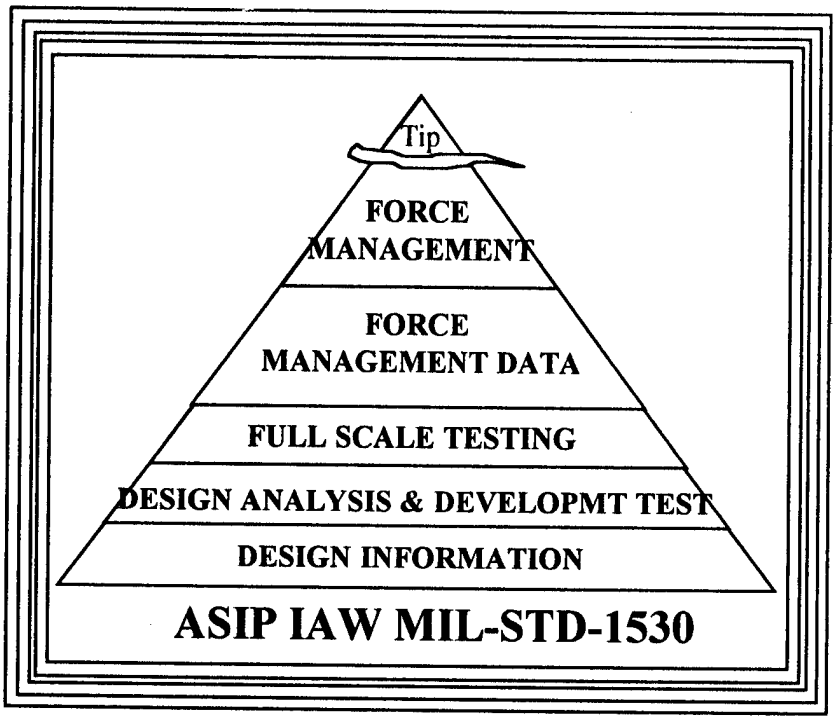

Most of us that are in the force management business recognize the primary tasks as outlined in Mil-Std-1530. However, there are too many of those who operate the aircraft that see ASIP from a "tip of the iceberg" perspective.

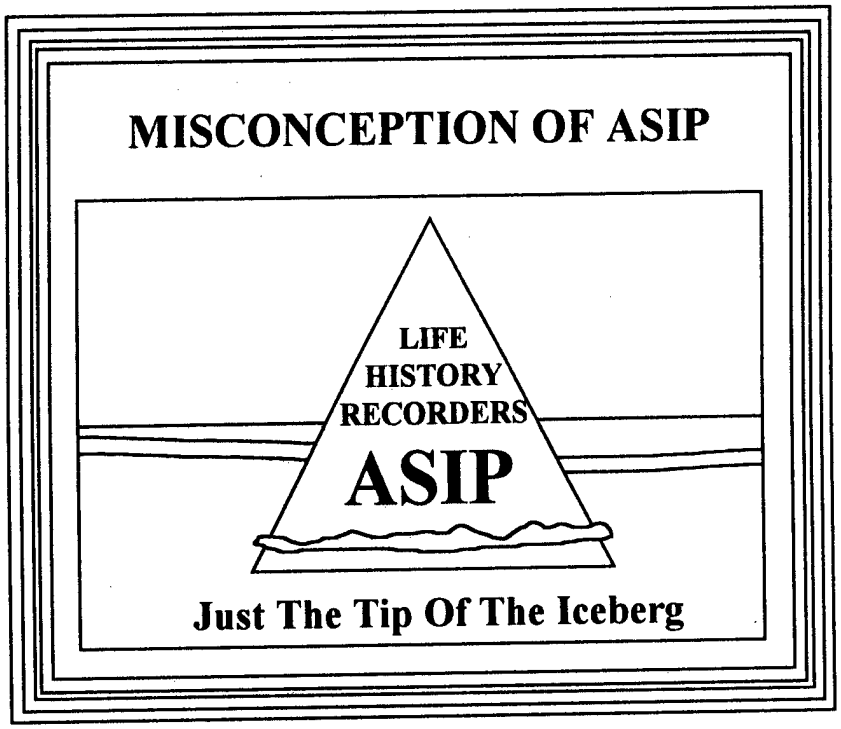

What this means is that the most visible thing pertaining to ASIP is the on-board recorders that gather data on aircraft operational performance and environment.

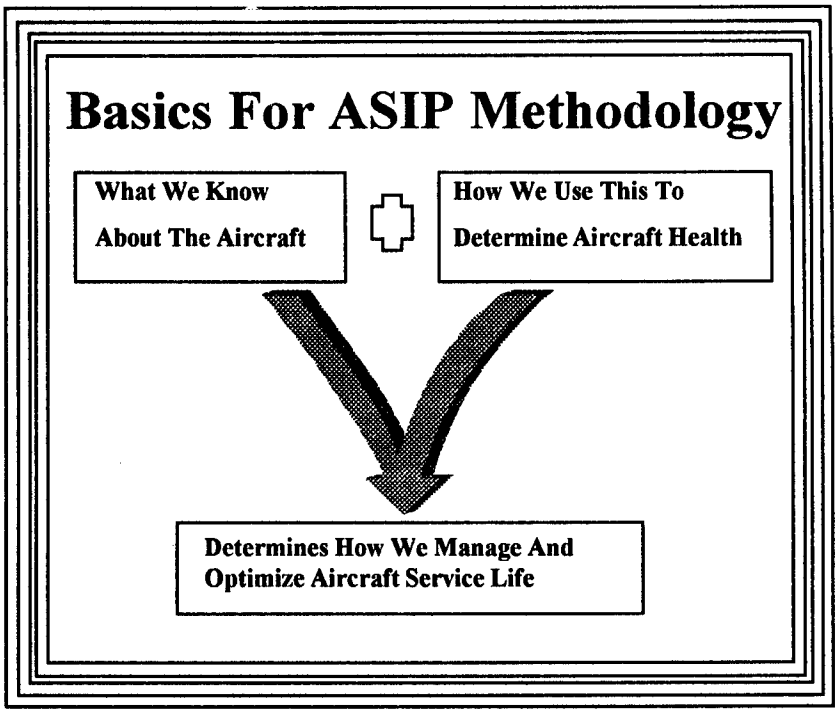

ASIP methodology is basically taking what we know about the aircraft, using that knowledge to determine aircraft state of health at any given time, and from this determine an optimum management for the remaining life of the aircraft.

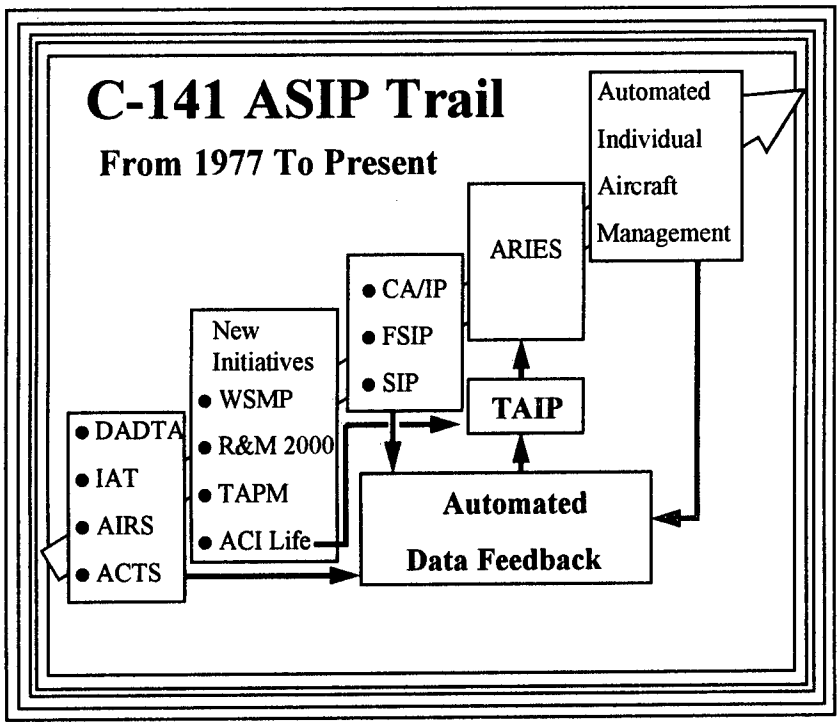

This chart gives a general overview of the C-141 ASIP trail. Not pictured here is the early days of the Individual Aircraft Safe Life Monitoring Program (IASLMP), a fatigue based methodology. Based on a DADTA in 1977, the C-141 instituted a fracture based methodology that led to the development of an individual aircraft tracking program, aircraft corrosion tracking system, and an aircraft information retrieval system. The ensueing years have been addressing pertinent new initiatives, integrity programs enhancement, and development of automated data feedback and management systems.

MID COURSE CORRECTION

- **Service Life Evaluation, i.e., DADTA**
- **Functional Systems Integrity Program (FSIP)**
- **Aircraft Corrosion Tracking System (ACTS)**
- **Center Wing Box (CWB) Repair Program**
- **Air Defensive Systems (ADS), Autopilot Replacement, Fuel Quantity Indicating System (FQIS), Etc**

These are a few of the major mid course corrections that have occurred on the C-141. All of these are a result of sound and responsive actions in keeping with aircraft usage, mission requirements, operational environment, and service life evaluations.

FORCE MANAGEMENT BY TAIL NUMBER

- **Usage Main Driver**
- **Tempered by Environment, Repair and Inspection History**
- **Optimize Downtimes for Proper Maintenance / Inspections**
- **Parts Forecasting**
- **Retirement Forecasting**

Today the C-141 is managed by individual tail number. All the historical knowledge regarding usage, inspections, repairs, and operational environment is brought together through an Automated Readiness Integrated Engineering System (ARIES) (which will be presented later in this conference) to provide the Systems Program Director (SPD) with a useful and dynamic management "tool" for current time status as well as for forecasting needs and/or retirement dates.

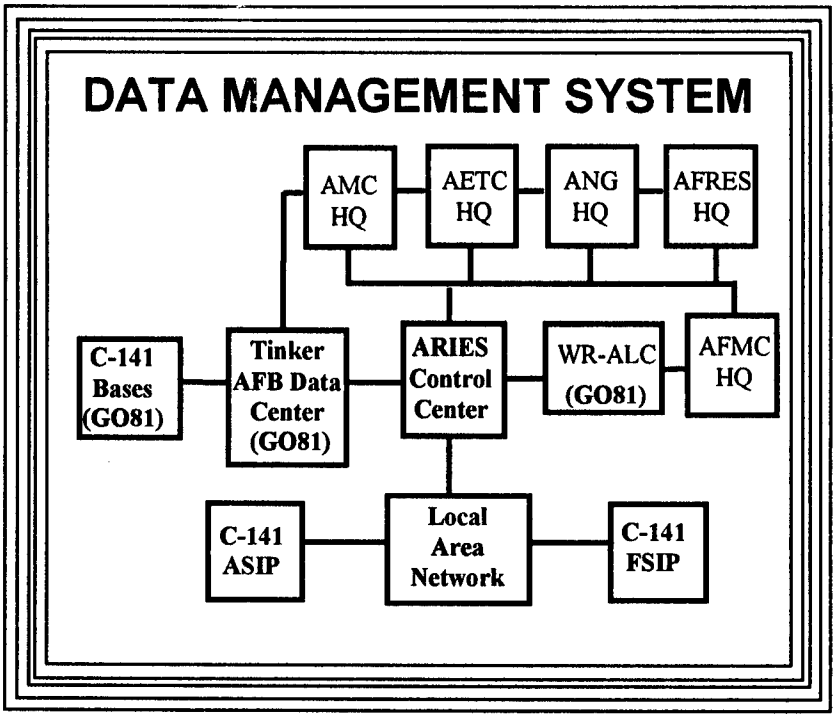

The data management system alluded to throughout this presentation is made more effective by the interlinking of computer terminals between the various commands, the bases, the Tinker AFB Data Center, the appropriate Logistics Center, and the ARIES Control Center. Although this arrangement is not yet fully in place for the C-141, it is making steady progress toward that end. Presently under development/implementation by Lockheed Martin at Marietta, Georgia (where the ARIES Control Center currently resides), the entire data management system will be transferred to WR-ALC, Robins AFB for their daily C-141 management role.

ENFORCING THE CONCEPT

Under The AFMC Commander

- **Form a TASIP Standing Committee To Address USAF Aircraft Current And Future Needs Relative To "Aging" Concerns, i.e., Maintenance Actions, Corrosion, NDI, Mods, Etc.**
- **Committee Briefs The Commander On A Semi-annual Or Annual Basis.**
- **Committee Chaired By A Chief TASIP Engineer.**

As mentioned earlier in this presentation, an aging aircraft philosophy must have some "teeth" if it is to be effective and pro-active. The aforementioned TASIP Standing Committee would formulate and present to the AFMC Commander the various needs, status, concerns, etc. for each weapon system. Reporting should occur annually or semi-annually as deemed appropriate by the committee or the Commander.

Evaluation of Multiple Site Damage in Lap Joint Specimens

by

H. L. Wang,* K. Buhler,** and A. F. Grandt, Jr.***

ABSTRACT

This paper describes research to determine the influence of multiple site damage (MSD) on the fatigue life of lap joint specimens. An MSD life prediction model previously developed for an open hole panel is modified to simulate the fatigue behavior of a structural joint. Simple lap joint specimens which contain MSD in the form of fatigue cracks in one row of rivet holes were cycled to failure under constant amplitude loading. An analytical model for joint load transfer simulates the contact stress in the rivet holes, and is used to predict fatigue life. The load transfer for each rivet is determined as a function of crack propagation. Five specimens were tested with various initial MSD configurations and applied stress levels. Predictions for growth and coalescence of individual cracks are in accordance with the experimental results.

INTRODUCTION

Wide spread fatigue damage is an important concern in aging aircraft. The issue focuses on determining interactions between multiple cracks and establishing appropriate failure criteria [1-2]. Previous research [3,4] has successfully developed a multiple-site damage (MSD) model to predict fatigue crack growth and failure for open hole panels. That model is extended in this paper with an analysis to account for the load transfer by fasteners, and to consider the influence of MSD in lap joints. The benefit of this model is to provide an analytical method for load transfer calculations which can be extended to more complicated structural geometries. Although many analytical and numerical methods have been established to calculate stress intensity factors (SIF) for cracks in open hole panels [3-6], in reality, crack propagation is much more complicated due to joints and stiffeners. The load transfer mechanism through joints, and the relationship between crack lengths and load transfer, has a crucial influence on the fatigue properties of the structure. Although finite element methods [7-10] have been employed to calculate the crack-tip SIF by applying a contact pressure between the rivet and hole, the load transfer mechanism is still not fully understood in those analyses. The goals of this paper are to provide an analytical method to determine load transfer in mechanically fastened joints, to provide a simple method to calculate the crack-tip SIF, and to perform fatigue life predictions.

EXPERIMENTAL PROCEDURE

An experimental program was conducted to study fatigue crack growth and interaction in simple lap joints. The test specimen studied here contained two 4 inch wide by 0.09 inch thick panels joined with 9 fasteners in the simple lap joint configuration shown in Figure 1. As

---

* Graduate Research Assistant, and *** Professor, School of Aeronautics and Astronautics, 1282 Grissom Hall, Purdue University, West Lafayette, IN 47907-1282. ** Flight Lieutenant, Royal Australian Air Force.

indicated, two 2024-T3 aluminum sheets were riveted together with 3 rows of 3/16 inch diameter 2117 aluminum rivets, and the assembled specimen was loaded in remote cyclic tension through pins located in a 7.0 inch wide grip area. The row of rivet holes closest to the grip area in one sheet was precracked prior to assembly to simulate MSD in the specimen. The pre-cracks were formed by first slotting small holes located along the desired crack plane, and then cycling that sheet under remote tension. Once fatigue cracks developed from both sides of the small holes, they were reamed to their final 3/16 inch diameter, removing the pre-slots, and leaving radial fatigue cracks on the order of 0.02 to 0.1 inch. The sheets were then riveted together, and the assembled specimens were cycled to failure under constant amplitude loading. The growth and coalescence of the MSD cracks in the lap joint specimens were monitored with a traveling microscope.

Measurement of the material properties for the 2024-T3 panel is described in Reference 3. The 0.2% yield strength was found to be 54.3 ksi and the ultimate strength was 60.0 ksi. Additionally, the material fatigue crack growth rate da/dN versus cyclic stress intensity factor ΔK relationship was also determined, and is given here by a mathematical representation consisting of a series of line segments which are summarized in Table 1.

ANALYSIS

In order to analyze the results of the fatigue crack growth tests, a preliminary analytical model has been developed for the influence of cracking on load transfer. The model involves two parts: An elastic load transfer solution for an uncracked joint, and determining changes in load transfer due to crack growth from the fastener holes.

Elastic Load Transfer Solution for an Uncracked Structure The numerical model employs the elastic solution for load transferred into fasteners proposed by W. Barrois [11] in 1978. There are two assumptions in this model:

- beam theory is used to determine the deformation of a rivet lying on elastic foundation;
- there is no interference or clearance between the contact surfaces of rivet and the elastic foundation.

The load transfer for two adjacent rivets can be determined by considering displacement compatibility associated with changes in the dimensions ❄ and ✯ shown in Figure 2.

$$_{i} - \delta_{i+1} = \Lambda_{ai} - \Lambda_{bi} \qquad (1)$$

Two different boundary conditions are assumed to account for two extremely different deflections on the contact surface between the rivet head and panels. One is a perfectly clamped rivet head and the other one is a pinned head (Figure 3). These two boundary conditions induce different fastener flexibilities and result in different load transfer ratios among these rivets. The benefit of the Barrois' model over other empirical equations is that it provides an analytical

method for load transfer calculations which can be extended to more complicated structural geometries and different types of rivet heads.

Load Transfer Ratio Associated with Crack Growth The second load transfer issue is to determine the variation in load transfer among the various fasteners as the crack propagates from one of the rivet holes. Having this relation, the SIF can then be calculated and the crack growth rate and fatigue life can be predicted. (The present analysis employs SIF solutions for the load transfer problem given in Reference 13). As the crack grows, the compliance of the cracked structure will decrease, and additional displacement due to crack opening will be induced. The displacement compatibility of in Eq. 1 can be rewritten as

$$_i - \delta_{i+1} = \Lambda_{ai} - \Lambda_{bi} - \delta_{due_to_crack} \qquad (2)$$

Here $\delta_{due_to_crack} = P \times C$, where P is the applied force, and C is the structural compliance derived from Eq. 3. (The derivation of the following equation is given in the Appendix).

$$C = \frac{2\pi}{E_p t}\int_0^a a \times [(\frac{1-R_{lt}}{w})F_0 + \frac{R_{lt}}{D}F_3]^2\, da \qquad (3)$$

In Eq. 3, E_p, t, w and D are the elastic modulus, thickness, unit width and hole diameter for the cracked panel, R_{lt} is the load transfer ratio, and a is the crack length. The terms F_0 and F_3 are geometry factors for the stress intensity factor solutions given in the NASA/FLAGRO 2.0 life prediction program [13]. Two stress intensity factor solutions for a riveted, cracked structure are taken here from the NASA/FLAGRO programs: TC05- Through Crack from Hole in a Plate with a Row of Hole and TC03- Through Crack from an Offset Hole in a Plate.

The crack geometry for these two cases is shown in Figs. 4 and 5. Whenever the relation between the load transfer ratio and crack length is determined, the superposed SIF for the riveted lap joined structure is given by Eq. 4.

$$\begin{aligned} K &= \frac{P}{t}[\frac{1-R_{lt}}{w}F_0 + \frac{R_{lt}}{D}F_3]\sqrt{\pi a} \\ &= Q(a)\frac{P}{wt} \\ &= Q(a)S_{remote} \end{aligned} \qquad (4)$$

Here R_{lt}, the load transfer ratio, is the function of crack length and Q(a) is a new variable defined to include all the terms in SIF solution except remote stress, S_{remote}. The geometric dimensions and Q(a) for the NASA FLAGRO cases TC03 and TC05 are shown in Figures 4 and 5.

Correction Factors The original FLAGRO solutions are restricted to single cracks growing from each rivet hole. Two correction factors were added to consider the double crack case, and to account for interaction between cracks growing towards each other. The following Shah [14] correction factor was used to account for cracks growing from both sides of a rivet hole

$$F_{Shah} = \sqrt{\frac{D+2a}{D+a}} \qquad (5)$$

where D = the hole diameter, and a = the crack length.

Additionally, the solutions were compounded with the following factor [15] to account for crack tip interactions:

$$F_{interaction} = \sqrt{\frac{2L}{\pi(D+2a)} \tan\frac{\pi(D+2a)}{2L}} \qquad (6)$$

where L = the rivet pitch.

Failure Criteria An investigation of several failure criteria for the MSD problem is given in Reference 3. The net section yield and ligament yield criteria [1] (Swift's Model) were utilized in this research. The net section yield criterion states that failure will occur when the failure load P_{Cnet} causes the net section stress to equal or exceed the tensile yield stress (σ_{ys}). This condition may be expressed as follows;

$$\begin{aligned} P_{Cnet} &= \sigma_{ys}\,(W - nD - n_{MSD} \times a_{avg.} - 2 \times a_L) \times t \\ &= \sigma_{ys}\, W_{net}\, t \end{aligned} \qquad (7)$$

Here W is the panel width, n is the total number of rivet holes, D is the average rivet hole diameter, n_{MSD} is the number of MSD cracks, a_{avg}, is the average crack length, a_L is the half-crack length of the central lead crack, and t is the panel thickness.

The Swift ligament yield failure criterion [1] states that the failure occurs when the plastic zones of two approaching crack tips "touch" each other. This failure load, P_{CLY}, is given by Eq. 8.

$$P_{CLY} = \sigma_{ys}\, t W_{net} \times \left[\frac{t}{(a_1 \beta^2_h \beta^2_{i1} + a_2 \beta^2_s \beta^2_{i2})}\right]^{1/2} \qquad (8)$$

In Eq. 8, W_{net} is the net width of the specimen, defined in equation (7), a_1 and a_2 are two approaching radial crack lengths, β_h and β_s are correction factors for radial crack 1 and lead crack 2, β_{i1} and β_{i2} are the stress intensity factor coefficient for two approaching cracks due to

interaction. Since the total specimen width is only 4 inches, and there is no pre-existent lead crack in the test specimens, the predicted failure lives are nearly the same for these two criteria, and therefore, only the net section yield criterion results are presented in the paper. It should be noted, however, that for larger specimens, or for stiffened structures, other failure criteria may be more appropriate.

RESULTS AND DISCUSSION

This section discusses the numerical results, and compares the predictions with results of the lap joint experiments.

Load Transfer versus Crack Length Load transfer ratios based on several empirical solutions [16] for riveted, uncracked structure are compared with Barrios' model in Fig. 6. All load transfer ratios calculated by these empirical formulas are located within these two extreme boundary conditions considered in the Barrios model. The load transfer ratios are approximately 36% for the top and bottom rivet rows in the single-lap joint structure, and 28% for the middle rivet row. The relation between load transfer and crack length is derived from Eqs. (2) and (3), and shown in Fig. 7. For the TC03 case (Fig. 7-a), the load transfer ratio for the top rivet row drops from 36% for an uncracked case to 15% as cracks developed approached the edge of the specimen. For the TC05 case (Fig. 7-b), the load transfer ratio at the top rivet row drops from 37% to 10% when the crack tip approaches the middle line of the rivet pitch. It should be noted that the experimental testing revealed that cracks between the rivets holes did not grow much longer than a maximum of 0.5 inches before the ligaments linked. (This was due to the total ligament length between the rivet holes being only 0.8125 inches.) Hence, only the early part of the inter-rivet solution (TC05) was required in these tests.

The relationship between SIF/ S_{remote} = Q(a) (see Eq. 4) and crack length for the TC03 and TC05 solutions are shown in Figs. 4 and 5. As indicated, a smaller crack has a higher stress intensity value than a longer crack during early stages of crack growth. It seems plausible that a shorter crack, once initiated at the edge of rivet hole, will grow faster than a longer crack, since the pin-loading stress dominates the early growth rate with the highest load transfer ratio. The variable Q for the two types of rivet heads also indicate that the SIFs are almost unaffected for these two types of rivet heads until the crack grows near fracture. The reason is that these two force boundary conditions do not include the clamping force effect of rivet head in the calculation. In real applications, the clamped rivet head not only restricts the deflection of the rivet shank, but also applies a clamping force which generates friction on the panel in the vicinity of the rivet head. The extra clamping force can delay growth of short cracks under the rivet head. An attempt to include these effects in the crack growth prediction by establishing an effective rivet head diameter which defined the local crack delay zone was unsuccessful. Therefore, the "clamped rivet head" utilized here is only a mathematical boundary condition on the panel, and potential clamping pressure is not take into account.

Experimental Life Predictions Since a key objective was to evaluate the ability to predict the growth and coalescence of MSD cracks, predictions were performed for the lap joint tests. The predictions were delayed to start at some point when the cracks were experimentally

observed to grow without the influence of rivet clamping. This prediction was compared with the result obtained by assuming that all cracks propagate when cycling is initiated, and these two different life prediction methods were used to investigate the above rivet clamping effect.

The pre-crack lengths and fatigue loading levels are summarized in Table 2 for the five experiments considered. The pre-cracks were typically on the order of 0.02 to 0.1 inch emanating from both sides of the rivet holes. Among these initial crack lengths, some of the "hidden" cracks would not grow for much of the panel life. Table 2 also shows the initial crack lengths and the delay cycles due to the rivet head clamping effect. For instance, the most delayed cycles of specimens 3, 4 and 6 are 38,000, 45,000 and 40,000 cycles. Compared with the failure life of 39,760, 53,715 and 55,740 cycles, the percentage of delay is 95%, 84% and 68%.

Figure 8 shows plots of crack tip position versus elapsed cycles for specimens 2 and 5. A summary of the life predictions for all 5 specimens is given in Fig. 9 and Table 3. As indicated in Table 3, specimens 3, 4 and 6 exhibit significant clamping effect on crack growth for those cracks under the rivet heads. As a result, the predicted lives are far below the experimental results for these tests. On the contrary, the life predictions agree quite well in comparison with these two methods for specimens 2 and 5. This is due to the fact that the dominate cracks in the latter two specimens begin to propagate early in the fatigue tests (for example, there is almost no cyclic delay of specimen 5). After the first link-up of the dominant cracks, the redistributed load causes the stagnant small cracks to suddenly propagate to specimen failure. The crack tip position is plotted versus elapsed cycle for specimens 2 and 5 in Fig. 8. These plots show that these two life prediction methods are almost identical when there is dominate crack propagation during the tests. These plots also show that the two rivet head assumptions make little difference in life prediction, which is reasonable since the clamping pressure effect was not included in this analysis.

SUMMARY AND CONCLUSIONS

This paper provides an analytical method to predict fatigue crack growth in a simple lap-joint specimen. A load transfer mechanism is established to account for changes in load transfer associated with crack propagation. Although two different rivet heads are utilized in the analysis, more work needed to account for the influence of rivet head clamping effect. This issue is of concern because small "hidden" MSD cracks under the clamping area are hard to detect, and may degrade the aircraft structural integrity.

A fatigue crack growth life prediction program with a load transfer mechanism was obtained by modifying an earlier open-hole MSD program. Two predicted results are presented with respect to rivet head clamping effect. The experimental data indicate that if the pre-existing cracks propagate when the fatigue test starts, the MSD program predicts the results well. Five life predictions are in accordance with the experimental data as the delayed cycles are observed and input the program as the crack growth initiation points.

ACKNOWLEDGMENTS

Portions of this research were sponsored by the Air Force Office of Scientific Research under Grant Number F49620-93-1-0377 with Dr. W. F. Jones as program monitor. FLTLT K. Buhler was also supported by the Royal Australian Air Force during his graduate studies at Purdue University.

REFERENCES

1. T. Swift, "Widespread Fatigue Damage Monitoring Issues and Concern," The 5th International Conference on Structural Airworthiness of New and Aging Aircraft, Hamburg, Germany, June 16-18, 1993.
2. J. Schijve, "Multiple-Site Damage In Aircraft Fuselage Structures," LR-729, Delft University, July, 1993.
3. E. J. Moukawsher, "Fatigue Life and Residual Strength of Panels with Multiple Site Damage," M. S. Thesis, School of Aeronautics and Astronautics, Purdue University, West Lafayette, IN, May 1993.
4. K. Buhler, "A Study of Fatigue Crack Growth of Panels Containing Multiple Site Damage," M. S. Thesis, School of Aeronautics and Astronautics, Purdue University, West Lafayette, IN, December 1993.
5. D. S. Dawicke, J. C. Newman, Jr., "Analysis and Prediction of Multiple-Site Damage (MSD) Fatigue Crack Growth," NASA Technical Paper 3231, 1992.
6. T. Nishimura, Y. Noguchi, and T. Uchimoto, "Damage Tolerance Analysis of Multiple-Site Cracks Emanating from Hole Array," Journal of Testing and Evaluation, JTEVA, Vol. 18, No. 6, Nov. 1990, pp. 401-407.
7. J. L. Beuth, Jr. and J. W. Hutchinson, "Fracture Analysis of Multiple Site Cracking in Fuselage Lap Joints," Division of Applied Sciences, Harvard University, Cambridge, MA 02138, June 1992.
8. R. L. Actis and B. A. Szabo, "Computation of Stress Intensity Factors for Panels with Multiple Site Damage," Center for Computational Mechanics, Washington University, Campus Box 1129, St. Louis, MO 63130, Technical Note WU/CCM-92/3, Dec., 1992.
9. J. H. Park, and S. N. Atluri, "Fatigue Growth of Multiple-Cracks Near a Row of Fastener-Holes in a Fuselage Lap-Joint," Report Number 92-1, Georgia Institute of Technology, Atlanta, Ga. 30332-0356, Dec., 1992.
10. R. Singh, J. H. Park, and S. N. Atluri, "Growth of Multiple Cracks and Their Linkup in a Fuselage Lap Joint," AIAA Journal, Vol. 32, No. 11, Nov. 1994, pp. 2261-2268.
11. W. Barrois, "Stress and Displacements Due to Load Transfer by Fasteners in Structural Assemblies," Engineering Fracture Mechanics, 1978, Vol. 10, pp. 115-176.
12. A. F. Grandt, Jr. and G. M. Sinclair, "Stress Intensity Factors for Surface Cracks in Bending," Stress Analysis and Growth of Cracks, Proceedings of the 1971 National Symposium on Fracture Mechanics, Part I, ASTM STP 513, American Society for Testing and Materials, 1972, pp. 37-58.
13. Appendix C, "Fatigue Crack Growth Computer Program, NASA/FLAGRO Version 2.0," JSC-2267A, Draft, NASA Johnson Space Center, January 1993.

14. R. C. Shah, "Stress Intensity Factors for Through and Part-Through Cracks Originating at Fastener Holes," Mechanics of Crack Growth, ASTM STP 590, American Society for Testing and Materials, Philadelphia, 1976, pp. 429-459.
15. R. J. H. Wanhill, "A Preliminary Study of Fatigue Durability in Terms of Short and Long Crack Growth," NLR TP 92437 L, National Aerospace Laboratory NLR, The Netherlands.
16. H. Huth, "Influence of Fastener Flexibility on the Prediction of Load Transfer and Fatigue Life for Multiple-Row Joints," ASTM STP 927, 1986, pp. 221-250.

Table 1. Coordinates Used to Define the Paris Law Segments for the 2024-T3 Material

ΔK ($ksi\sqrt{in}$)	da/dN (inches/cycle)	ΔK ($ksi\sqrt{in}$)	da/dN (inches/cycle)
3.65	2.40×10^{-7}	14.53	1.38×10^{-5}
6.68	1.07×10^{-6}	19.40	3.83×10^{-5}
7.11	1.58×10^{-6}	23.86	1.45×10^{-4}
8.60	3.02×10^{-6}	24.00	1.00×10^{-2}
11.04	6.94×10^{-6}		

Table 2. Summary of Test Specimen Initial Conditions and Failure Data.

Test Specimen ID								Max Applied Stress (Ksi)	Total Specimen Life (Cycles)
		a1L	a1R	a2L	a2R	a3L	a3R		
Lap #2	Init. Crack Length	**0.04***	0.05	0.06	0.05	0.08	0.05		
	Delay Cycles	17000	5000	10000	5000	5000	5000	13.11	19,840
Lap #3	Init. Crack Length	**0.03***	0.05	**0.02***	**0.02***	0.08	**0.02***		
	Delay Cycles	15000	10000	38000	20000	26000	38000	12.10	39,760
Lap #4	Init. Crack Length	0.06	**0.02***	0.06	**0.02***	0.09	0.05		
	Delay Cycles	20000	45000	20000	45000	25000	25000	10.99	53,715
Lap #5	Init. Crack Length	0.10	0.05	0.06	**0.04***	0.06	**0.02***		
	Delay Cycles	0	0	32000	32000	40000	40000	9.94	55,740
Lap #6	Init. Crack Length	**0.04***	0.09	0.07	0.10	0.09	0.09		
	Delay Cycles	40000	25000	35000	30000	30000	25000	9.94	58,920

*Rivet Shank d= 0.1875 inch; Head D= 0.2840 inch
a < 0.048 : Under Rivet Head
a > 0.048 : Observable Crack

Table 3. Life Prediction

Test Specimen ID	Total Specimen Life (cycles)	Program Prediction			
		with delay		without delay	
		Clamped Head	Pinned Head	Clamped Head	Pinned Head
Lap# 2	19,840	24,525	24,102	19,528	19,104
Lap# 3	39,760	42,703	42,093	25,730	25,182
Lap# 4	53,715	57,437	56,697	32,679	31,947
Lap# 5	55,740	57,909	56,666	52,718	51,423
Lap# 6	58,920	67,815	66,811	40,270	39,209

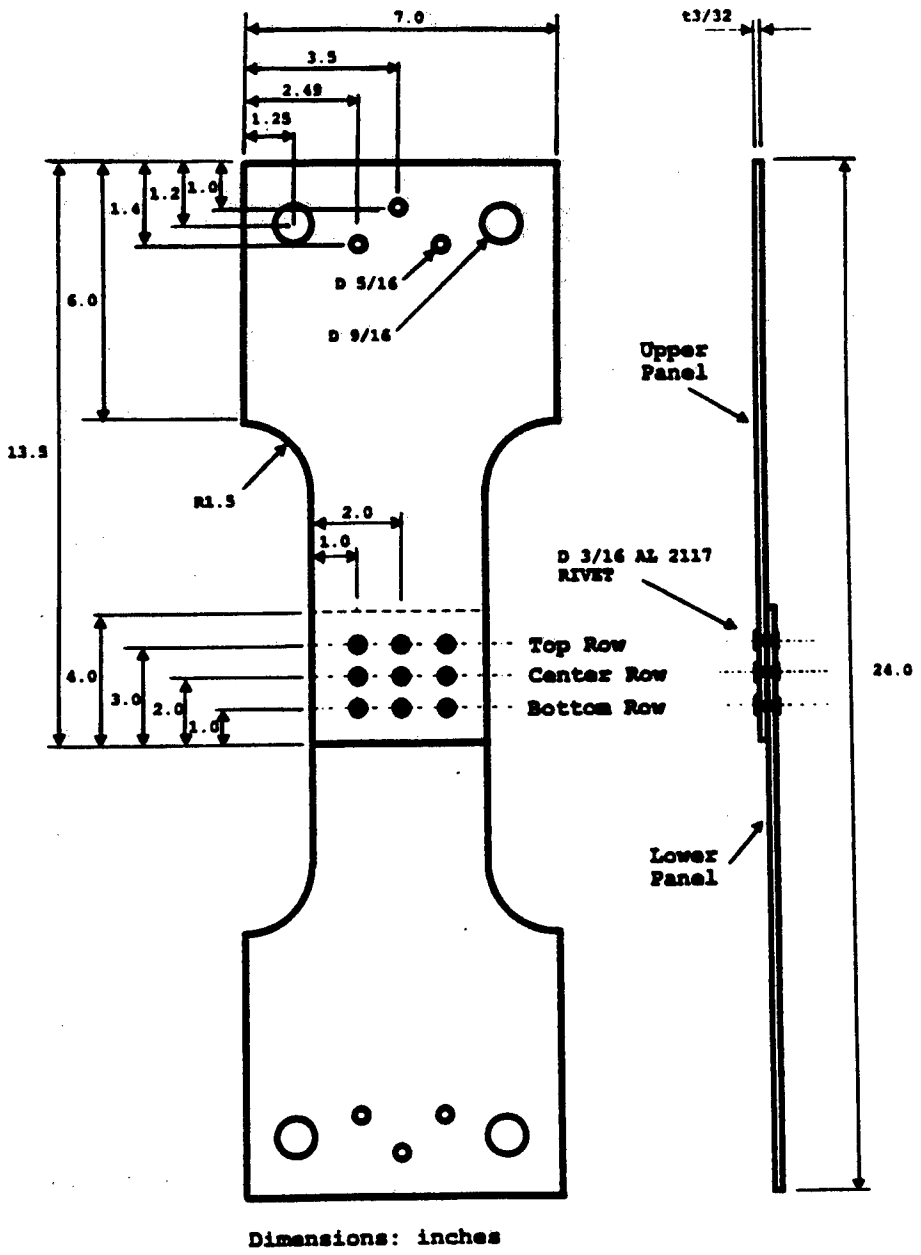

Figure 1. Details of Single Lap Joint Test Specimen.

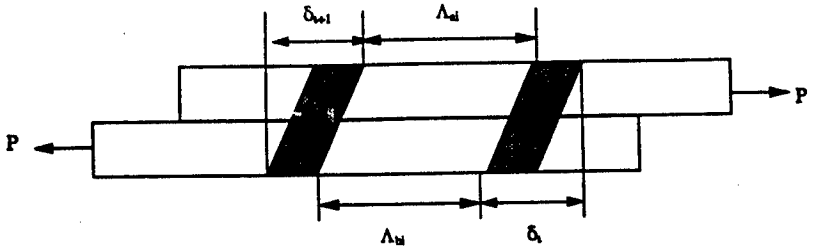

Figure 2. Displacement Compatibility of Two Adjacent rivets.

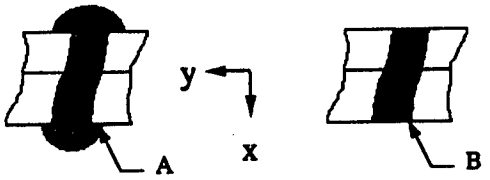

Clamped Rivet Head :

$$\frac{dy}{dx}_{at\ A} = 0$$

Pinned Rivet Head:

$$\frac{dy^2}{d^2x}_{at\ B} = 0$$

Figure 3. Boundary Conditions.

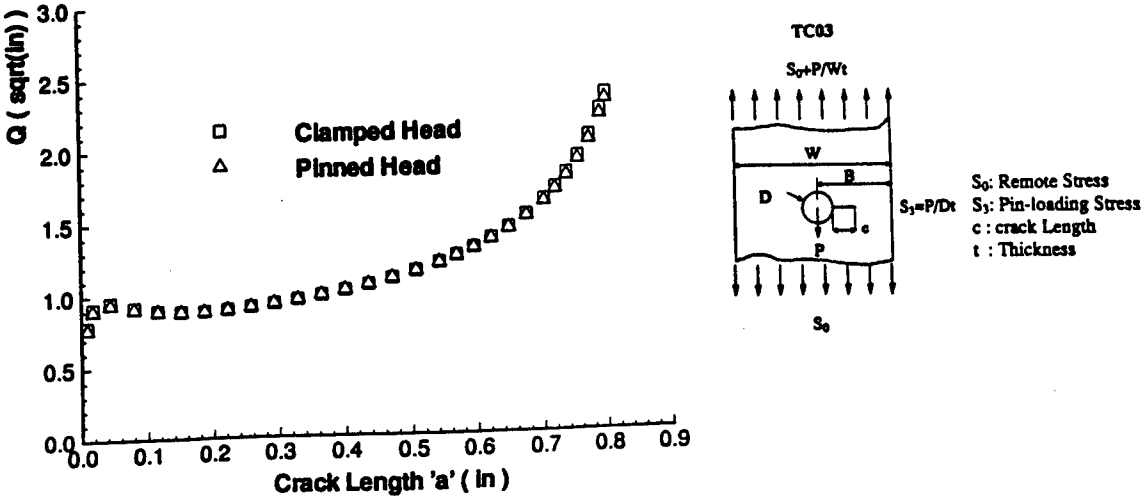

Figure 4. Plot Showing the FLAGRO Solution TC03.

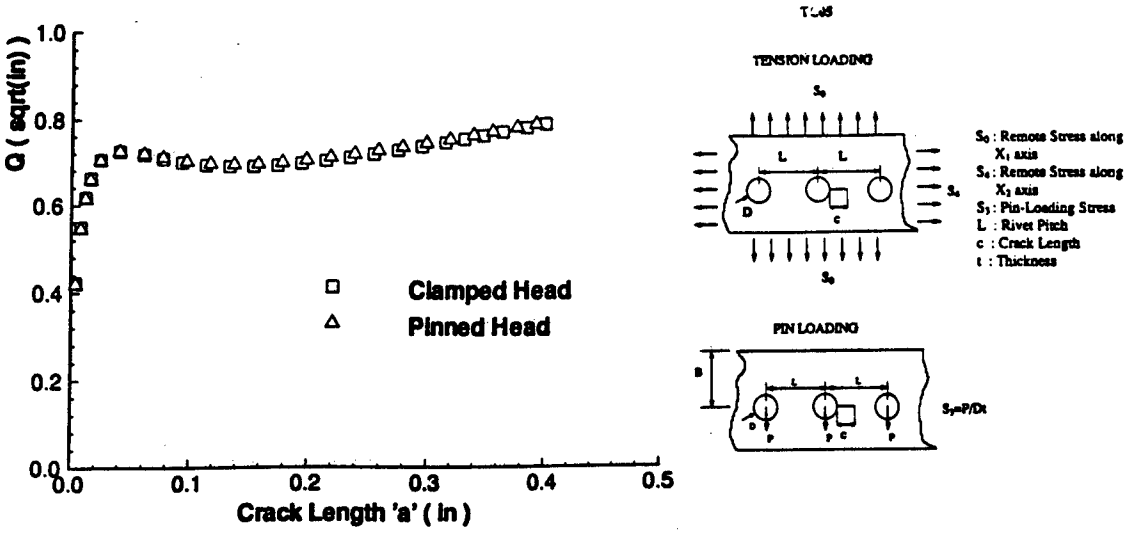

Figure 5. Plot Showing the FLAGRO Solution TC05.

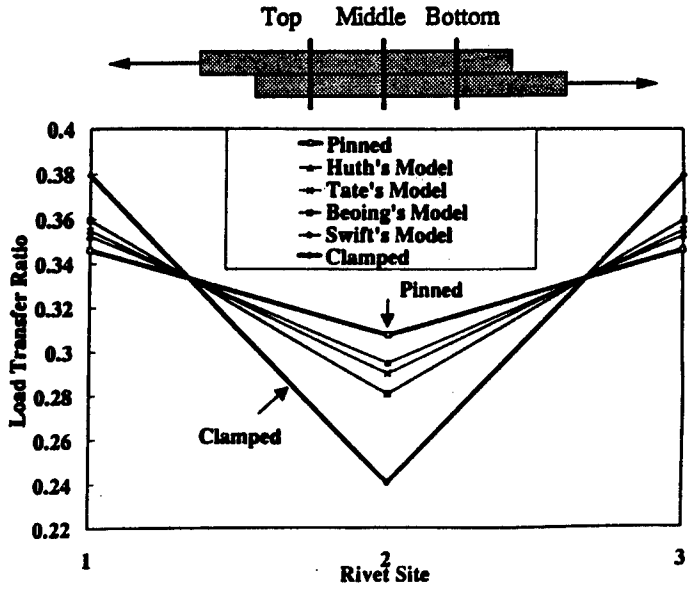

Figure 6. Load Transfer Ratio versus Rivet Position for Single-Lap Joints.

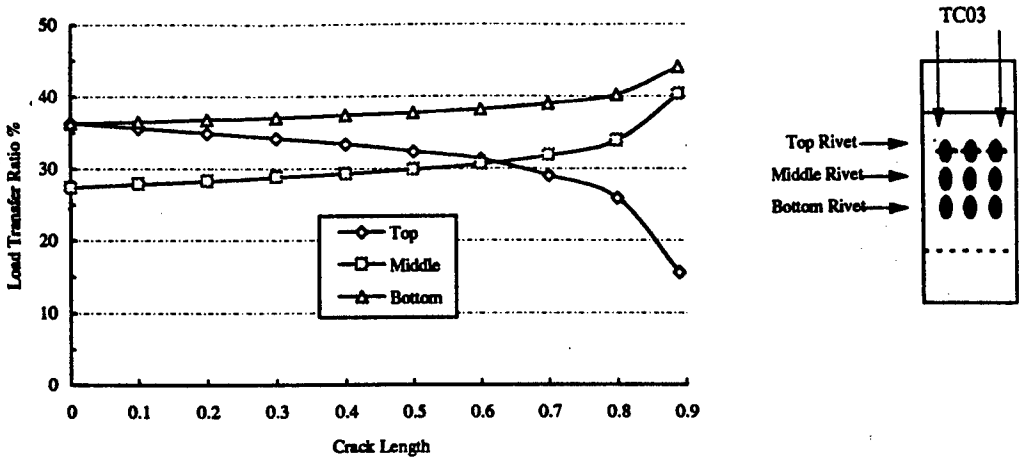

a. TC03 Through Crack from an Offset Hole in a Plate.

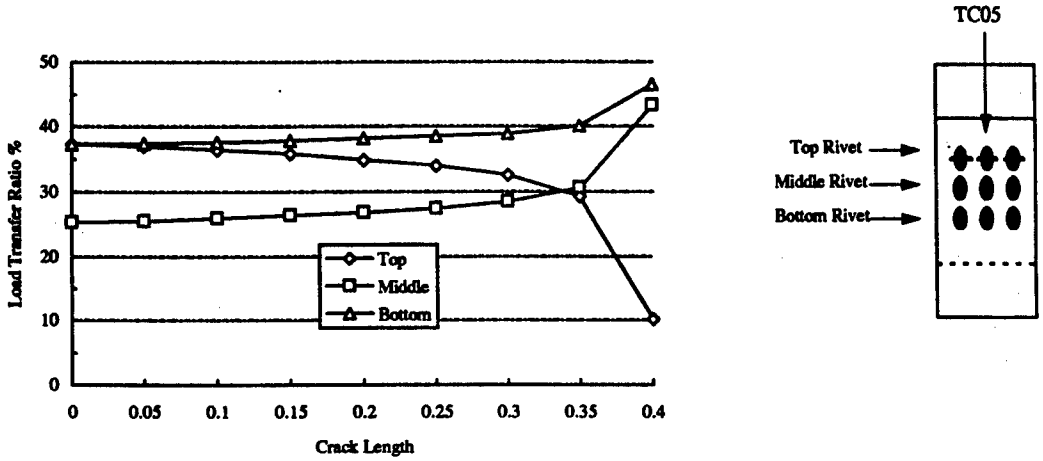

b. TC05 Through from Hole in a Plate with a Row of Hole.

Figure 7. Load Transfer Ratio versus Crack Length.

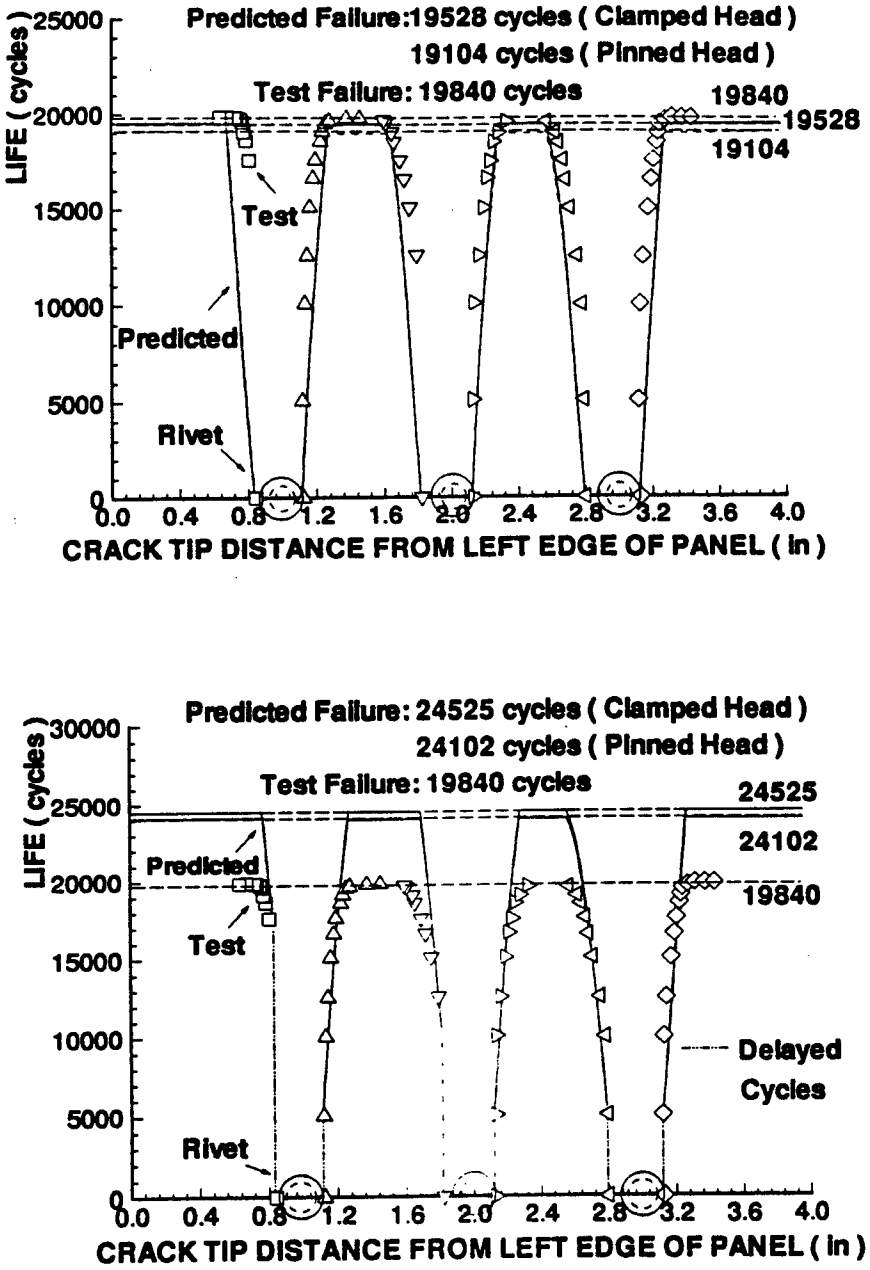

Figure 8-a. Experimental and Predicted Crack Propagation Plot for Lap #2, Tested at a Cyclic Stress Level of 13.1 ksi.
(Upper Plot: Crack Growth without Delay; Lower Plot: with Delay)

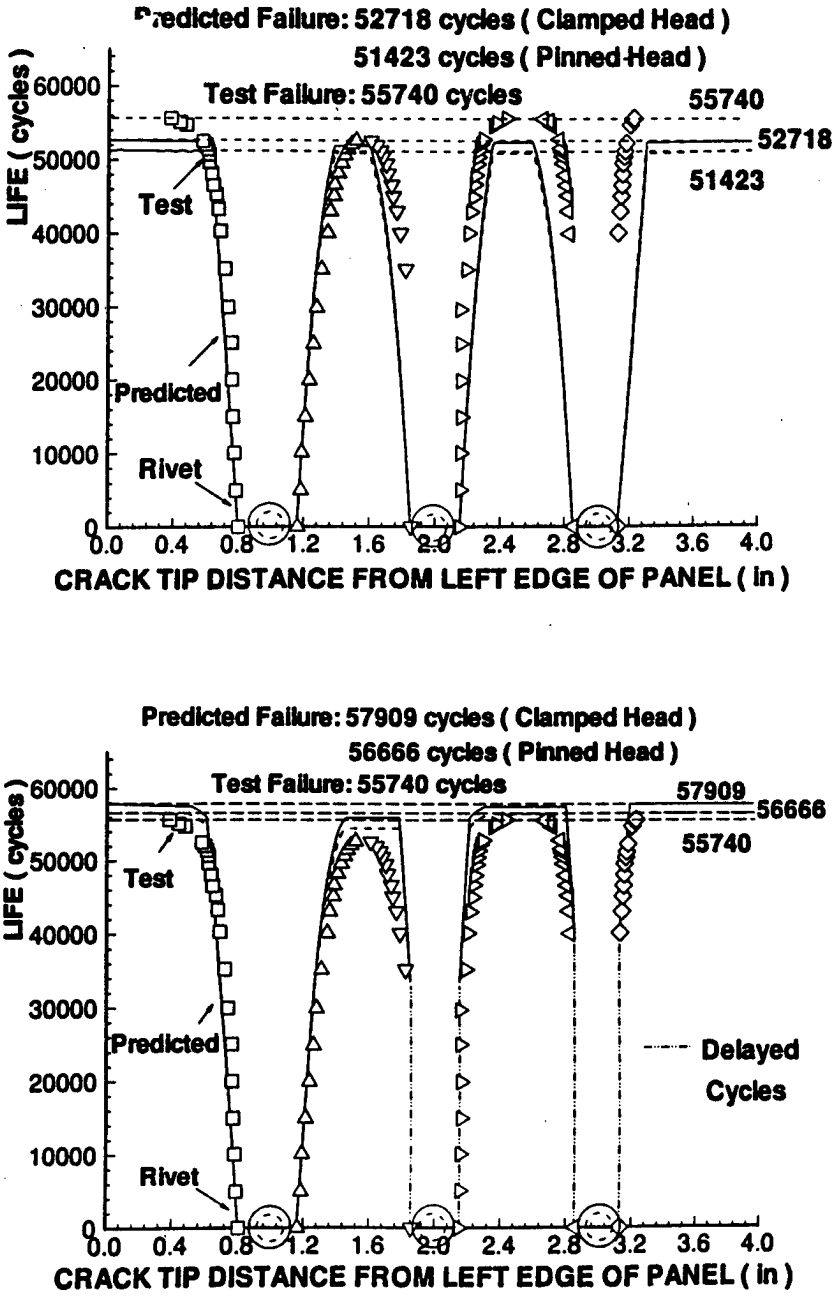

Figure 8-b. Experimental and Predicted Crack Propagation Plot for Lap #5, Tested at a Cyclic Stress Level of 9.9 ksi.
(Upper Plot: Crack Growth without Delay; Lower Plot: with Delay)

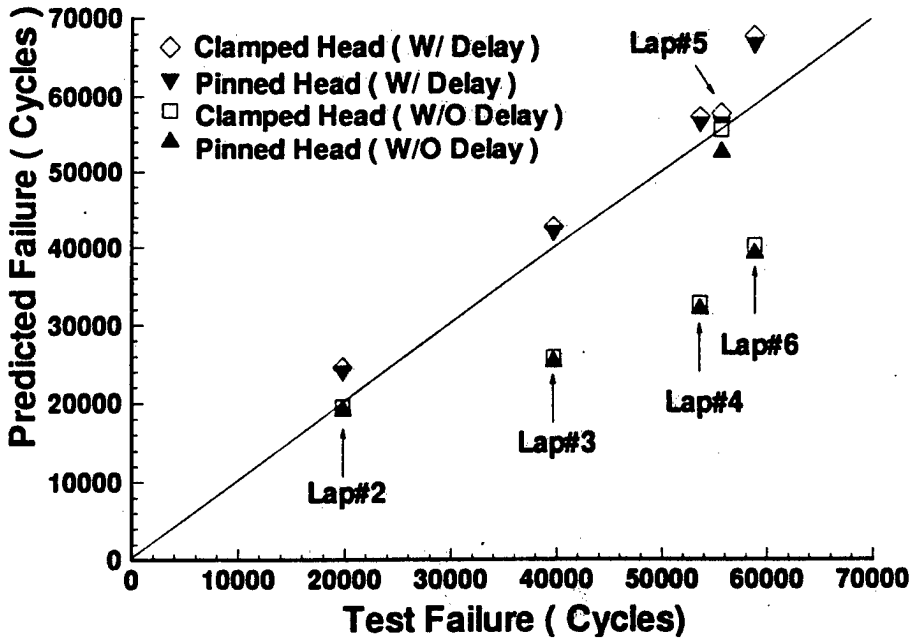

Figure 9. Comparison of Predicted and Measured Lives for All Five Single-Lap Joint Specimens.

APPENDIX

The NASA FLAGRO stress intensity factors solutions TC05 and TC03 involve superposition of two terms, F_0 and F_3, for an open-hole specimen and a loaded-hole specimen (Figure I).

The total SIF of the loaded-hole specimen is

$$K = [S_0 F_0 + S_3 F_3]\sqrt{\pi a} \qquad \text{(a-1)}$$

where

$S_0 = \frac{P}{wt}(1 - R_{lt})$ is the bypassed stress,

$S_3 = \frac{P}{Dt} R_{lt}$ is the bearing stress due to pin loading,

w, t, *and* D = Width, thickness and hole diameter of panel,
R_{lt} = Load transfer ratio for the fastener,
P = Remote force.

Rewriting (a-1),

$$K = \frac{P}{t}[\frac{1 - R_{lt}}{w} F_0 + \frac{R_{lt}}{D} F_3]\sqrt{\pi a} \qquad \text{(a-2)}$$

The Energy release rate for plane stress is induced into the calculation to combine the load transfer effect with the compliance of cracked panel:

$$G = \frac{K^2}{E_p} = \frac{P^2}{2t}\frac{\partial C}{\partial a} \qquad \text{(a-3)}$$

where

C = Compliance of the cracked panel,
a = crack length.

From (a-1) and (a-3), the compliance of the cracked panel can be derived:

$$C = \int_0^a \frac{2t}{P}\frac{K^2}{E_p} da = \frac{2\pi}{E_p t}\int_0^a a \times [(\frac{1 - R_{lt}}{w}) F_0 + \frac{R_{lt}}{D} F_3]^2 da \qquad \text{(a-4)}$$

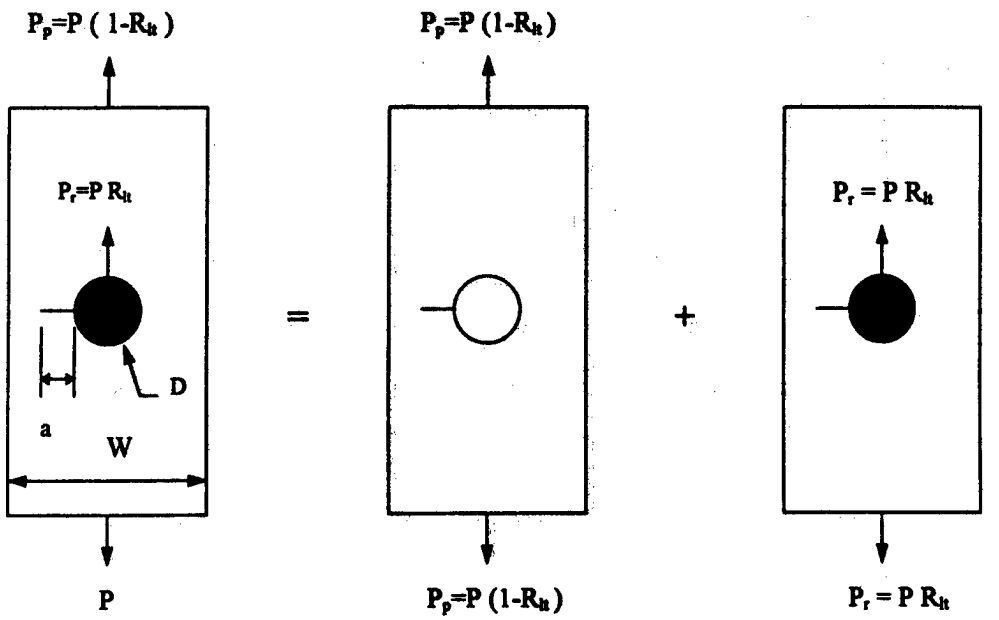

$$K = K_0 + K_3$$

Figure I. Stress Intensity Factor for a Loaded-Hole Specimen

A New Structural Integrity Policy for the VC10

Mr C Hoyle

British Aerospace, Chadderton, Manchester, UK.

Squadron Leader E Bittel,

HQ Logistics Command,

Royal Air Force.

Introduction

The design of the Vickers VC10 commenced at the Weybridge plant in the early 1950s, and was intended to meet a requirement for BOAC, the forerunner of British Airways, for a medium to long range passenger aircraft to fly the flagship BOAC routes. Powered by 4 Rolls Royce Conway engines, and carrying a maximum of 130 passengers, it had a range of 3800 nautical miles.

It was produced in 2 main versions, namely the Standard VC10 and the Super variant which featured an increased wingspan and greater passenger capacity. The design was one of the first British attempts at a fail-safe design, although Vickers carried out a number of fatigue tests aimed at guaranteeing an initial crack-free life. Although it enjoyed a favourable passenger loyalty, its initial acquisition costs and operating economics meant that it did not compete well with its main rival, the Boeing 707, and its overseas sales were limited.

The VC10 C Mk1 entered RAF service in 1966 as a passenger and freight aircraft, and was a hybrid version of the commercial variants in that it comprised a standard VC10 fuselage mounted on a Super VC10 wing. In the early 1980s, the tanker variants started to come into service. The K2 was a conversion of ex-civilian Standard variants, and the K3 and K4 were converted from ex-civilian Super aircraft. The oldest of these aircraft had in excess of 45000 flying hours and 16000 flight cycles at the time of conversion. Eventually, the fleet size reached a total of 27 aircraft in 5 different marks.

In-Service Problems

In 1987, the original design authority at Vickers, closed down, and the DA transferred to British Aerospace at Manchester, previously known as Avro's and best known for a long line of heavy bomber types from the WW2 Lancaster to the Vulcan of the 1960s and 70s. At about the same time, serious cracking (a 15 inch crack in a centre wing spar web), was found in one of the early tanker aircraft, but the location of the cracking was not in line with expectations from the original fatigue clearances. Investigation of this problem by the new DA revealed a number of interesting facts:

a. The fatigue testing had been based on a theoretically derived spectrum for a BOAC standard VC10 operating 3-hour flight plans at an average TOW of 220,000 lb. In contrast, the average TOWs for RAF aircraft were in the range 265,000lb to 285,000lb.

b. The same airframe had been used for both static and fatigue tests. This was not unknown practice in the 1950s, but is not the practice today because we are aware of the crack retardation effects that result from the application of high static loads, and can result in an optimistic estimate of fatigue life. In the case of the VC10 Fatigue Test Specimen, loads equal to or in excess of 50% of the design ultimate had been applied no less than 62 times before fatigue testing commenced.

c. The FTS used a standard VC10 wing, whereas the RAF aircraft had a Super VC10 wing with a 6' greater wingspan than the standard variant. The FTS was thus not representative of the RAF aircraft.

d. There were no Operational Loads Measurement (OLM) results to assess the theoretical loading spectrum which had been applied to the FTS.

Although some of these points could be put down to hindsight, and some to changes in testing philosophy, the simple facts were as follows:

a. The fleet was flying ahead of the safe lives which had been derived for the wing and the fuselage - this was being borne out by the in-service defects.

b. Corrosion would further reduce the calculated or FTS-proven lives.

c. In this situation the only alternative to grounding the fleet was

to underwrite the integrity of the structure by inspecting all areas.

Remedial Proposals

Thus, in order safeguard the integrity of the aircraft for its planned service life of 20 years, BAe Manchester recommended a range of short and long term measures. The long term solution was to change the structural integrity philosophy to wholly damage tolerant, and to produce a complete re-analysis of the airframe using a finite element model. In the short term, inspection intervals were revised to account for the higher RAF operating weights, and the Structural Sampling Programme was refined to include a much greater level of directed inspections. A tailplane refurbishment programme was introduced to counter the growing evidence of stress corrosion in this area. Also, to provide additional assurance for the fuselage, bearing in mind the nature of the Aloha incident, the DA recommended a programme of proof pressure testing.

The concept of proof pressure testing is not new. The method is that the fuselage is subjected to 1.33 times the normal ΔP which is held for a short length of time. Assuming that the pressure shell does not suffer a failure, then a full external NDT inspection of the lap joints is carried out. Any cracking which is found can be rectified, and it may then be assumed that any undetected cracks are, at worst, just sub-critical for that load. It is then possible to calculate an interval over which such cracks will grow at the normal pressurization level and remain sub-critical before a further proof test is required.

In order to provide a degree of assurance that the test aircraft is not about to suffer catastrophic damage, the fuselage is fitted with an array of acoustic emission (AE) sensors to listen for the sound of cracks growing under the proof load. Interestingly, the manufacturers of the AE equipment claim that, by siting the sensors in an accurately defined pattern, it is possible to pinpoint the site of any crack growth by a process of triangulation. Although this is nice to know, the prime purpose of the AE equipment in this application is to prevent an uncontained failure, and not to supplement the NDT inspections.

As for the long term activity, this centres on the project to produce a Fatigue Type Record for the VC10, based on the results of a fatigue and damage tolerance evaluation using the results from a Finite Element Model. This is the largest FEM ever produced in Europe, and work started on it in 1993. The planned end date is October 1996, at which point the evaluation should have provided us with sufficient information to allow the issue of a Fatigue Type Record. This is a formal document, defined in UK Defence

Standards, and comprises these parts:

Part1 — The Historical Record - this summarizes all the fatigue and damage tolerance calculations from the design stage, and includes a synopsis of the major fatigue tests, materials and loading data.

Part 2 — The Reassessment of Fatigue Life - this is a complete re-analysis of the fatigue and damage tolerance calculations, taking account of actual service usage, in-service failures, additional testing, OLM and so on.

Part 3 — The Re-assessment of Inspection Requirements - this section re-assesses the inspection requirements and methods as a result of the work done in Part 2.

Part 4 — Operation Beyond Specified Life - this section provides advice, where it is necessary, on extending the life beyond that which was originally specified. Obviously, this section will not be necessary in the first issue of the FTR.

All this work is necessary to underwrite the structural integrity of the VC10 up to its planned out of service dates, which currently range between 2007 and 2015, depending on the mark of aircraft.

The VC10 Finite Element Model

There are sufficient differences between the 5 VC10 variants to mean that it is necessary to produce, in effect, 5 different versions of the model. The strategy has been to produce the model for the C Mk1, the original RAF version, as the baseline, and then progress to the other variants by modelling the differences. The main elements of the overall programme started in 1992, and will end in October 1996 with the delivery of the final version of the Fatigue Type Record for the K4 tanker variant.

Each version of the model is, at least by European standards, very large indeed, with over 70,000 nodes and nearly 150,000 elements. An early decision was made to run the analysis as a multi-level superelement process, and break the model down into 12 superelements one of which, the port wing, is an image superelement. This was done to reduce the amount of analysis and data storage required for what was essentially a symmetrical section of the structure. This tended to complicate the verification loading cases which were applied to the models.

Verification of the models was by reference to a series of static tests which were carried out on a complete C Mk1 airframe in 1992. The model results were compared, case by case, with strain gauge and deflection data obtained from these static tests. Fig 1 shows the strain gauge positions for the fuselage static tests, and the correlation factors between the model predictions of stresses and the test values. Although the correlation 23 and 28 were not as good as we had hoped, the variation here was mainly due to problems associated with the gauge siting. Fig 2 gives the same information for the verification of the tailplane stresses. The wing verification followed a similar validation process and produced comparable correlation ratios.

Once the verification phase was complete, it was possible to proceed to the actual running of the model, applying the loads for approximately 190 static cases and 120 fatigue cases. Subsequently, work proceeded to the stressing for the baseline model and then the fatigue and damage tolerance evaluation. Currently, about 90% of the work on the static cases has been completed, and the fatigue and damage tolerance calculations are approximately 40% complete. Inspection periodicities are being derived progressively as results become available from the damage tolerance work.

Operational Loads Measurement

It is worthwhile to make mention of our use of direct strain measurement, which we normally call operational loads measurement, or OLM, because this has played a significant part in the development of the VC10 FTR. For the first runs of the model, we were fortunate in having available a quantity of data from an operational loads measurement programme which had been carried out in the mid-1980s to improve our knowledge of the in-service loading which would be experienced by the VC10 in its new air-to-air refuelling role. Specifically, the programme had been devised to provide verification of the wing fatigue life, to re-assess the tailplane life and to obtain qualitative data on fatigue damage in the new operating role.

Fig 3 shows the original strain gauge fit on the aircraft. Part way through the programme, it was found necessary to reconfigure the instrumentation to provide more detailed monitoring of the tailplane, and as a result an additional 6 gauges were installed on the tailplane upper and lower skins. Since the completion of this OLM programme, we have run further 'mini-programmes' to investigate in-service cracking in the area of the wing rear spar and the main undercarriage. The OLM data has also provided us with duty cycles for the rudder, ailerons and elevators. In addition, we will shortly commence a new OLM exercise to measure the loads on the main and nose undercarriages and the associated back-up structures.

Results So Far

Initially, when at the project scoping stage, BAe estimated that the project would probably identify a total of around 200 SSIs and approximately 440 primary damage calculation sites, based on previous experience with civil aircraft. First results from the model indicated however that, in the absence of information from a full-size fatigue test specimen, the numbers could be approaching 500 SSIs and around 1000 damage sites. It has been necessary to expend a great deal of time in reviewing each of the original SSIs to confirm the need to proceed with the analysis, and as much use as possible has been made of read-across by symmetry or between the 5 marks of aircraft. Even so, the analysis task remains significantly greater than the original estimate, at 257 SSIs and 625 primary damage calculation sites; the size of this task is under continuous review as the analysis proceeds. The following areas of difficulty are worthy of particular note:

a. The BAe fatigue software has required significant enhancement to cope with the vast amount of data being generated by the models. Several brand new programs have been written and, naturally, this has generated additional software quality assurance work.

b. The unexpected expansion in the work required has imposed a significant extra workload on the modelling and fatigue specialist departments at BAe Manchester, and it has become necessary to significantly expand the amount of static loads analysis on the wing.

c. The OLM coverage of the aircraft is far from complete, and difficulty has been experienced in deriving load spectra for certain areas of the aircraft, notably the T-tail, the rear fuselage and the engine nacelles.

The Achievements

Of course, these problems have not prevented BAe making encouraging progress with this task and, when reviewing events so far against the short and long term measures which were implemented at the start of this project, the following can be claimed:

a. The tailplane refurbishment programme was completed on time and within budget.

b. The wing inspection programme has revealed various areas requiring attention, in particular the cracking of the centre spar lower boom at ribs 18 and 19 which was not predicted by the original

Weybridge fatigue analysis; appropriate modification action has been taken for this area.

c. The fuselage proof pressure test programme has not revealed any hitherto unknown sources of cracking. Additionally, by using data from a limited monitoring exercise on actual pressurization levels, it has been possible to relax the test interval from 550 cycles to 600 cycles for the C Mk1 and 700 for the tankers. These may be considered small numbers by civil operator standards but, until the Fatigue Type Record is complete, they represent a level of monitoring which is both technically and operationally acceptable.

For the long term measures:

a. BAe have produced the 5 versions of the FEM and have validated the models against static test data.

b. For the baseline aircraft (the C Mk1), 90% of the static stressing is complete, and about 40% of the fatigue and damage tolerance evaluation.

c. 20% of the FDTE results have already been used to amend the aircraft maintenance schedule.

Throughout the project period, there has been no reduction in availability of airframes to the front-line squadrons.

Conclusion

The development of the Fatigue Type Record for the VC10 is the most complicated single project that has ever been undertaken in the UK in support of an ageing aircraft. It is a 4-year project which has required an enormous cooperative effort between BAe and the RAF, and will require much more before it is complete. When it is, the lifing philosophy of this 30 year old fleet will have been completely changed using modern analytical and testing techniques, and this work will have provided the basis for a further 20 years of VC10 operations.

Acknowledgment

The authors are grateful to the Royal Air Force and British Aerospace for permission to publish this paper and for the assistance given by their colleagues. All opinions expressed are those of the authors and do not necessarily reflect RAF or BAe policy.

BRITISH AEROSPACE REGIONAL AIRCRAFT LIMITED
BAE CHADDERTON - MILITARY BUSINESS UNIT

VC10 - FTR

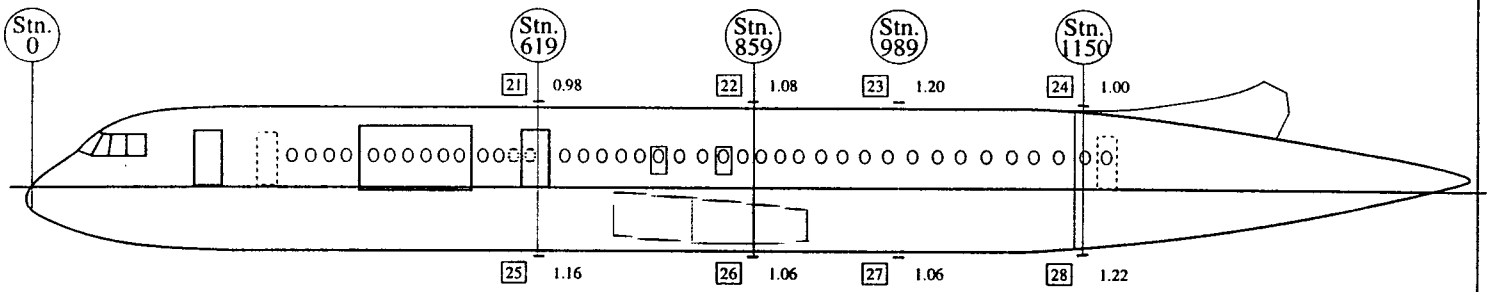

□ - Strain Gauge No

F.E. Model Version :- cn(0)7v(0)4

Strain Gauge No.	Test 3 Stress (lbf/in^2)	Model Stress (lbf/in^2)	Model / Test
21	-3977	-3883	0.98
22	-2386	-2573	1.08
23	-2093	-2509	1.20
24	-2093	-2086	1.00
25	2781	3222	1.16
26	2106	2220	1.06
27	2842	3005	1.06
28	1088	1327	1.22

Figure 1. Correlation of VC10 CMk1 FEM Fuselage Stresses with Test Results

FTR -24

BRITISH AEROSPACE REGIONAL AIRCRAFT LIMITED
BAE CHADDERTON - MILITARY BUSINESS UNIT

VC10 - FTR

Strain Gauge No.	Test 1 Stress lbf/in^2	Model Stress lbf/in^2	Model / Test
41	6652	7000	1.05
42	4605	5115	1.11
43	6210	6827	1.10
44	5566	5081	0.91
45	3868	3862	1.00
46	2888	3985	1.38
47	-7313	-7721	1.06
48	-5356	-5352	1.00
49	-7662	-7049	0.92
50	-6535	-5619	0.86
51	-4410	-4711	1.07
52	-4972	-4742	0.95

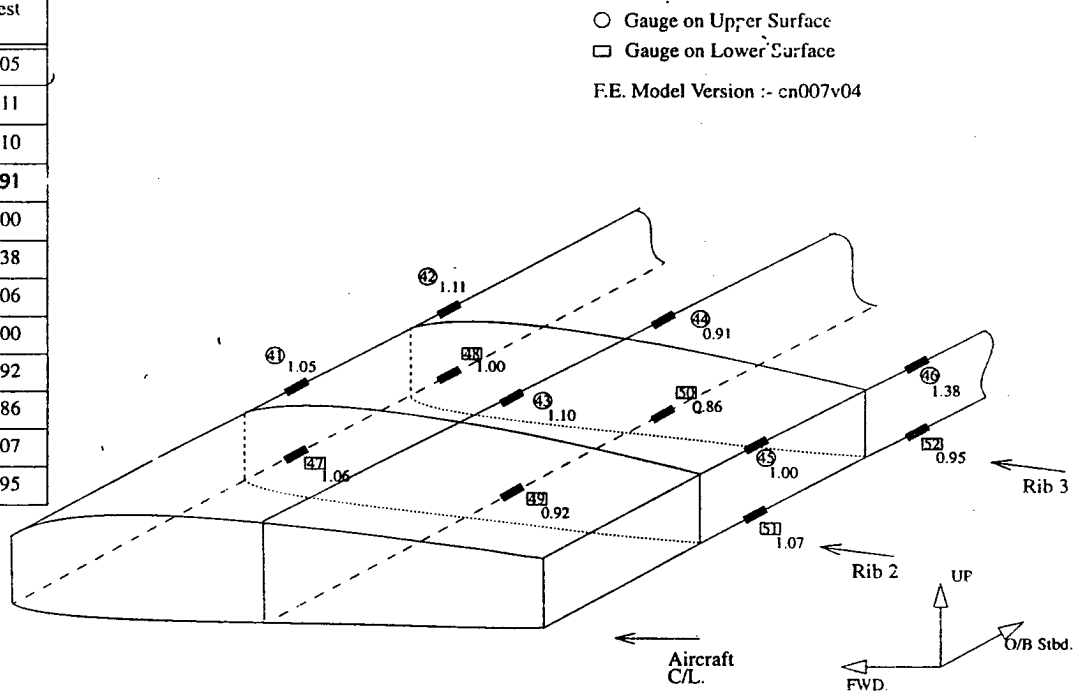

Fig 2

Correlation of VC10 CMk1 F.E.M. Tailplane Stresses with Test REsults (Leading Edges Included)

FTR -28

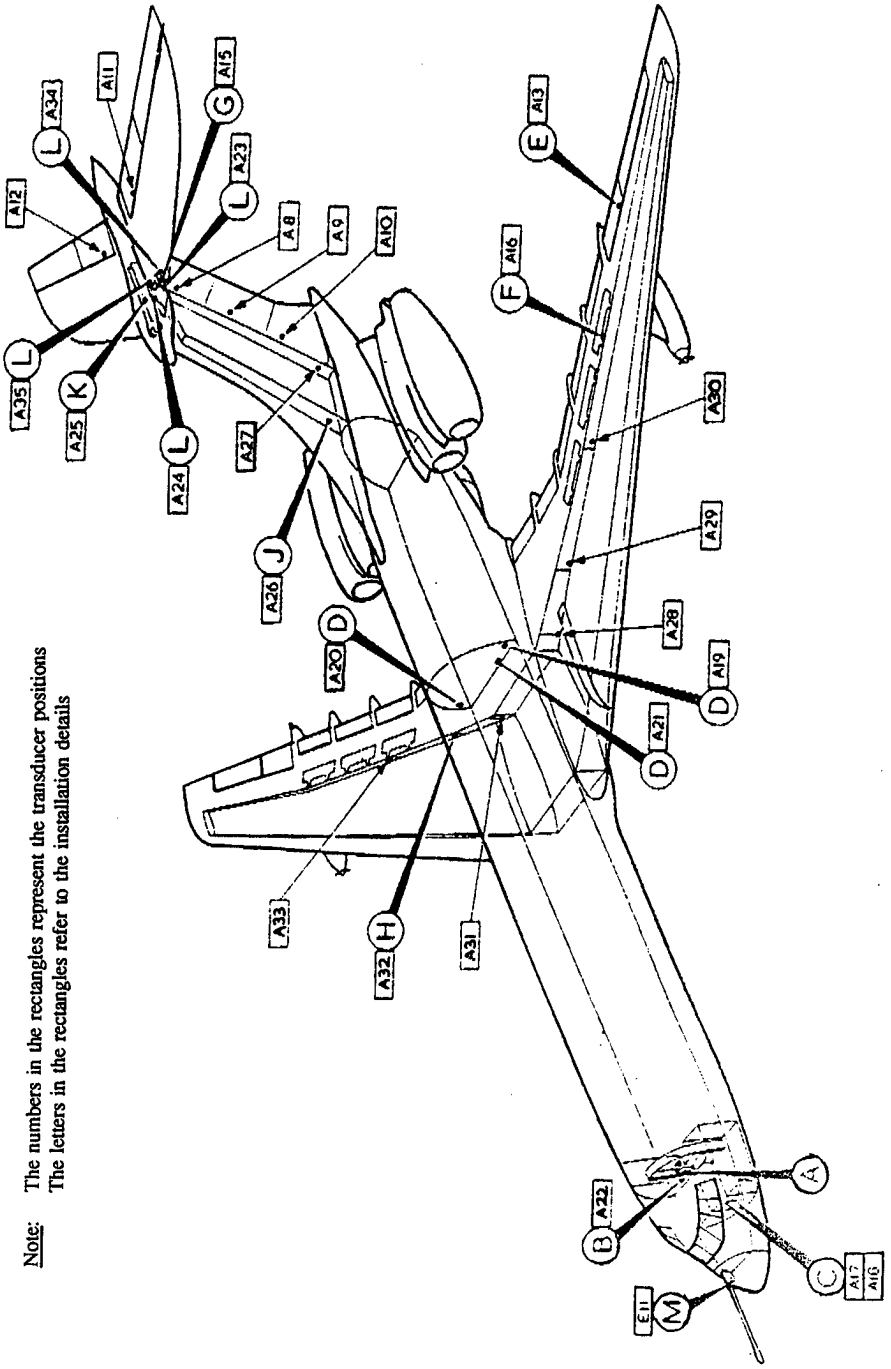

Note: The numbers in the rectangles represent the transducer positions
The letters in the rectangles refer to the installation details

Fig 3 - VC10 OLM - Location of Equipment

C17A DURABILITY AND DAMAGE TOLERANCE TEST PROGRAM

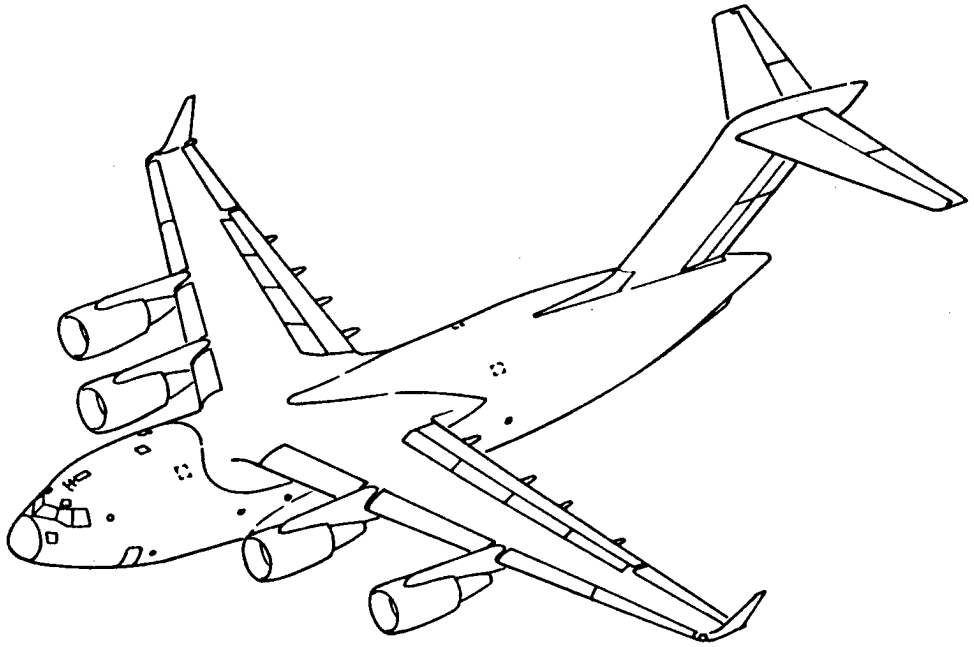

Ko-Wei Liu
McDonnell Douglas Aerospace

Chuck Babish
ASC/YCEF USAF

C17A DURABILITY AND DAMAGE TOLERANCE TEST PROGRAM

DEVELOPMENT AND FULL SCALE DURABILITY TEST PROGRAMS ARE REQUIREMENTS TO BE COMPLIANT WITH USAF AIRCRAFT STRUCTURAL INTEGRITY PROGRAM TASKS (MIL-STD-1530A)

TASKS TO PROVIDE COMPLIANCE WITH BASIC STRUCTURAL DESIGN REQUIREMENTS

TASK II - DESIGN ANALYSES AND DEVELOPMENT TESTS

TASK III - FULL SCALE TESTING

DURABILITY AND DAMAGE TOLERANCE DEVELOPMENT TESTS

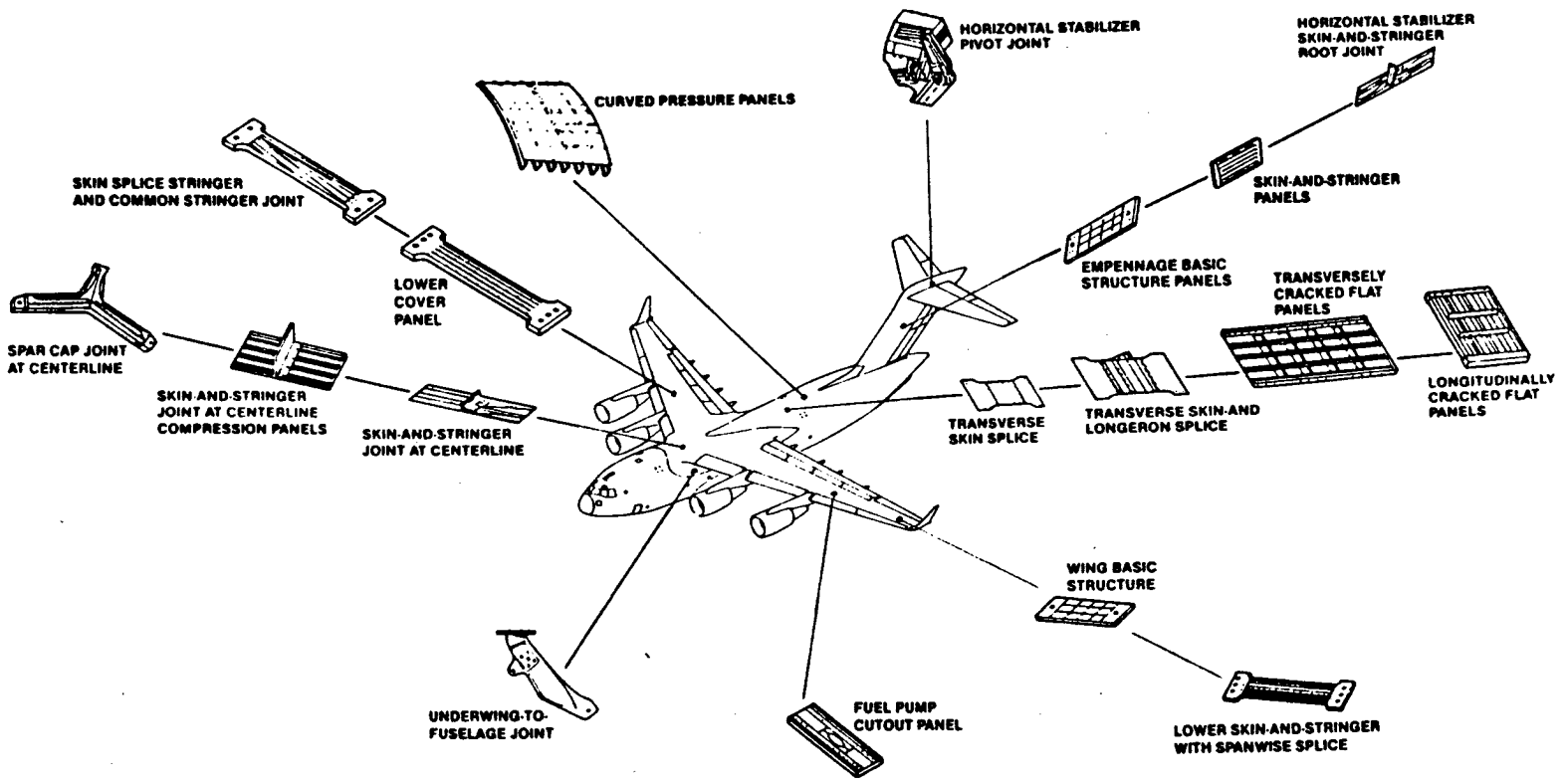

OBJECTIVE

- DEVELOP MATERIAL PROPERTIES DATABASE TO SUPPORT DURABILITY AND DAMAGE TOLERANCE ANALYSIS.
- EVALUATE AND VERIFY OPTIMUM DESIGN APPROACH.
- SUBSTANTIATE ANALYTICAL CRACK GROWTH AND RESIDUAL STRENGTH METHODOLOGY.
- INVESTIGATE THE DURABILITY AND DAMAGE TOLERANCE CHARACTERISTICS OF BUILT-UP STRUCTURE.
- ESTABLISH BASIC STRUCTURE AND JOINTS ALLOWABLES FOR DURABILITY AND DAMAGE TOLERANCE.

DURABILITY AND DAMAGE TOLERANCE MATERIAL TESTS

TYPE OF TESTING	da/dn VS ΔK		FATIGUE S-N	FRACTURE TOUGHNESS		CRACK GROWTH RESISTANCE		STRESS CORROSION	
ENVIRONMENT	LAB AIR AT ROOM TEMP.	DISTILLED WATER AT ROOM TEMP.	LAB AIR AT ROOM TEMP.	LAB AIR AT ROOM TEMP.	-65° F LIQUID NITROGEN	LAB AIR AT ROOM TEMP.	-65° F LIQUID NITROGEN	SUMP TANK WATER AT ROOM TEMP	DISTILLED WATER AT ROOM TEMP.
OBJECTIVE	COLLECT CRACK GROWTH RATE DATA FOR VARIOUS ΔK AND R VALUES		COLLECT FATIGUE LIFE DATA	COLLECT FRACTURE TOUGHNESS K_{IC}		COLLECT R-CURVE DATA		COLLECT CRACK GROWTH RATE DATA AND DETERMINE THRESHOLD STRESS INTENSITY	
TEST OUTPUT	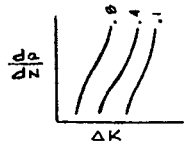			K_{IC}		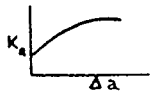		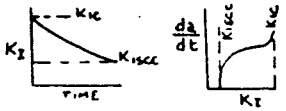	
SPECIMEN TYPE	COMPACT SPECIMEN C(T)	CENTER CRACK TENSION M(T)	SHEET BAR	COMPACT TENSION		COMPACT TENSION C(T)	CENTER CRACK TENSION	DCB	WOL
			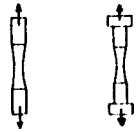			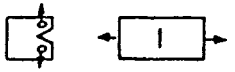		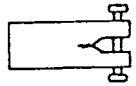	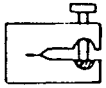
LOADING	CYCLIC CONSTANT AMPLITUDE AT DIFFERENT ΔK AND R		CYCLIC AXIAL FATIGUE TO FAILURE	CYCLIC PRE-CRACK STATIC TO FAILURE		CYCLIC PRE-CRACK DISPLACE-MENT TO FAILURE		BOLT LOADED-CONSTANT DISPLACEMENT TIME TO NO CRACK GROWTH	

- **MATERIAL TESTED:**

  ALUMINUM: 2024, 7050, 7150, 7475, ARALL3, 6013
  TITANIUM: 6Al-4V, 6Al-2Sn-4Zr-2Mo, 10V-2Fe-3Al
  HIGH STRENGTH: 15-5PH, INCO718, PH13-8

- **OVER 2400 SPECIMEN TESTS**

SPECIMEN DESIGN

- MOST SPECIMENS ARE DESIGN TO REPRESENT SPECIFIC LOCATIONS ON THE AIRCRAFT.
- SPECIMENS ARE REPRESENTATIVE OF ACTUAL PRODUCTION STRUCTURE.
- SAME MATERIALS INCLUDING PRODUCT FORM WHEN AVAILABLE.
- SAME DETAIL DESIGN CONCEPTS:
  - STIFFENER SPACING
  - FASTENER TYPES AND SIZING
  - DETAIL PART CONFIGURATION
- REPRESENTATIVE MANUFACTURING PROCESSES USED:
  - SURFACE FINISH AND COATINGS
  - FASTENER AND FAYING SEALANT USED

WING D&D/T DEVELOPMENT TEST PLAN

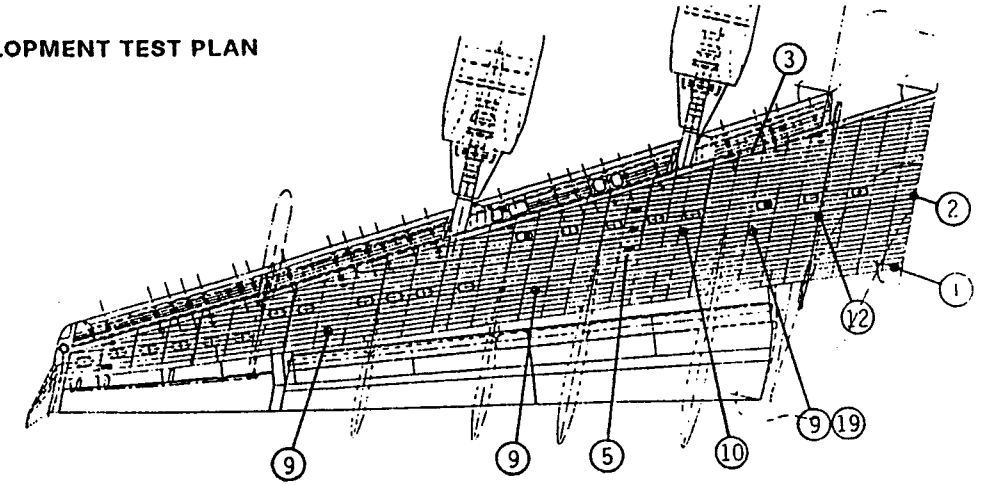

ITEM NO.		1	2A	2B	3	5	9	10	12
ITEM NAME		REAR SPAR CAP	SKIN & STRINGER CENTERLINE JOINT LOWER - STR. RUNOUT CONFIG.	SKIN & STRINGER CENTERLINE JOINT, LOWER	SKIN SPLICE STR. & COMMON / STR. JOINT LOWER	SKIN & STRINGER PANEL WITH FUEL PUMP CUTOUT, LWR	SKIN & STRINGER PANEL LOWER	SKIN & STRINGER PANEL WITH SPANWISE SPLICE LOWER	UNDERWING TO FUSELAGE JOINT
APPROX. SPEC. SIZE		60 X 142	6 X 60	8 X 96	48 X 200	VARIOUS	163 X 52, 200 X 84	70 X 200	8 X 18, 14 X 54
NO. OF SPEC.		2	7	12	2	4	8	3	2
NO. OF CONFIG.		1	7	1	1	4	5	1	2
LOADING		CONST. AMP. FBF SPEC.	CONST. AMP.	CONST. AMP. FBF SPEC.	CONST. AMP. FBF SPEC.	CONST. AMP. FBF SPEC.	CONST. AMP. FBF SPEC.	CONST. AMP. FBF SPEC.	CONST. AMP. FBF SPEC.
TYPE OF TEST	DURA	2	7	12	2	4	2	1	1
	DAM. TOL	-	-	-	-	-	6	2	1

ITEM NO.		19	26	27	28	30	31	32
ITEM NAME		SKIN PANEL BASIC STRUCTURE	SPECTRUM SENSITIVITY FOR RANGE STRESS TRUNCATION	EFFECT OF NEAT FIT PIN ON CRACK GROWTH	DURABILITY OF WET INSTALLED GEMCOR SLUG RIVETS	EFFECT OF FASTENER TYPE ON DURABILITY	CONTROL POINT SIMULATION FOR DAMAGE TOLERANCE	LOWER STRINGER DRAIN GROOVE
APPROX. SPEC. SIZE		14 X 96	4 X 18	4 X 18	3 X 17	2 X 40	4 X 18	2 X 30
NO. OF SPEC.		27	63	24	24	28	65	6
NO. OF CONFIG.		3	7	6	1	7	VARIOUS	3
LOADING		CONST. AMP. FBF SPEC.	FBF SPEC.	CONST. AMP.	CONST. AMP	CONST. AMP.	FBF SPEC.	CONST. AMP.
TYPE OF TEST	DURA	27	-	-	24	28	-	6
	DAM. TOL	-	63	24	-	-	65	-

DEVELOPMENT TEST SPECIMEN

THE TEST SPECIMENS RANGED IN COMPLEXITY FROM SIMPLE COUPONS TO SMALL ELEMENTS TO LARGE COMPONENTS THAT REPRESENT THE ACTUAL STRUCTURE.

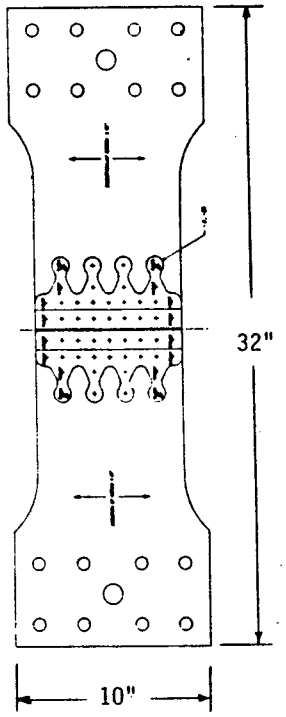

ELEMENT

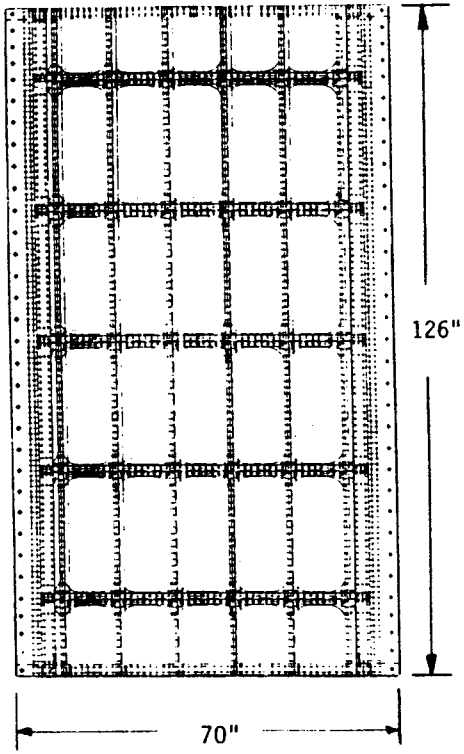

LARGE COMPONENT

WING D&D/T DEVELOPMENT TEST PLAN

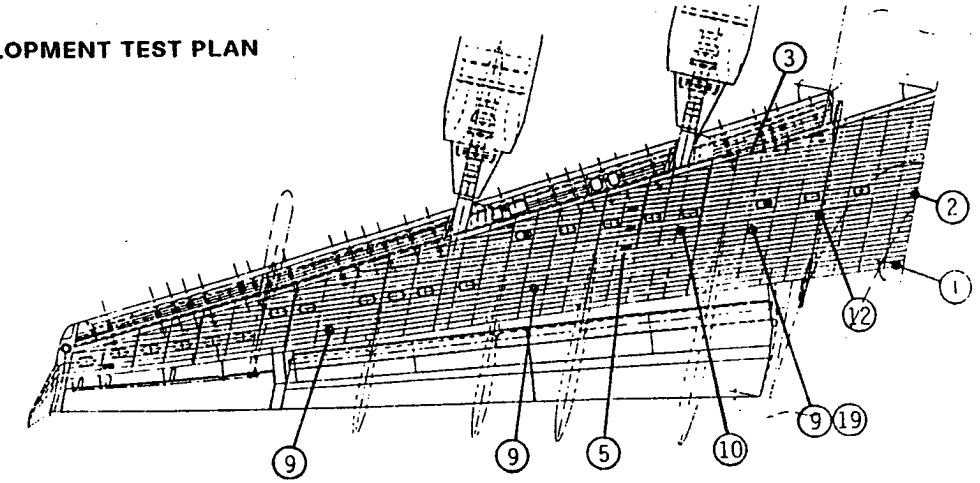

ITEM NO.		1	2A	2B	3	5	9	10	12
ITEM NAME		REAR SPAR CAP	SKIN & STRINGER CENTERLINE JOINT LOWER - STR. RUNOUT CONFIG.	SKIN & STRINGER CENTERLINE JOINT, LOWER	SKIN SPLICE STR. & COMMON / STR. JOINT LOWER	SKIN & STRINGER PANEL WITH FUEL PUMP CUTOUT, LWR	SKIN & STRINGER PANEL LOWER	SKIN & STRINGER PANEL WITH SPANWISE SPLICE LOWER	UNDERWING TO FUSELAGE JOINT
APPROX. SPEC. SIZE		60 X 142	6 X 60	8 X 96	48 X 200	VARIOUS	163 X 52, 200 X 84	70 X 200	8 X 18, 14 X 54
NO. OF SPEC.		2	7	12	2	4	8	3	2
NO. OF CONFIG.		1	7	1	1	4	5	1	2
LOADING		CONST. AMP. FBF SPEC.	CONST. AMP.	CONST. AMP. FBF SPEC.	CONST. AMP. FBF SPEC.	CONST. AMP. FBF SPEC.	CONST. AMP. FBF SPEC.	CONST. AMP. FBF SPEC.	CONST. AMP. FBF SPEC.
TYPE OF TEST	DURA	2	7	12	2	4	2	1	1
	DAM. TOL	-	-	-	-	-	6	2	1

ITEM NO.		19	26	27	28	30	31	32
ITEM NAME		SKIN PANEL BASIC STRUCTURE	SPECTRUM SENSITIVITY FOR RANGE STRESS TRUNCATION	EFFECT OF NEAT FIT PIN ON CRACK GROWTH	DURABILITY OF WET INSTALLED GEMCOR SLUG RIVETS	EFFECT OF FASTENER TYPE ON DURABILITY	CONTROL POINT SIMULATION FOR DAMAGE TOLERANCE	LOWER STRINGER DRAIN GROOVE
APPROX. SPEC. SIZE		14 X 96	4 X 18	4 X 18	3 X 17	2 X 40	4 X 18	2 X 30
NO. OF SPEC.		27	63	24	24	28	65	6
NO. OF CONFIG.		3	7	6	1	7	VARIOUS	3
LOADING		CONST. AMP. FBF SPEC.	FBF SPEC.	CONST. AMP.	CONST. AMP	CONST. AMP.	FBF SPEC.	CONST. AMP.
TYPE OF TEST	DURA	27	-	-	24	28	-	6
	DAM. TOL	-	63	24	-	-	65	-

LARGE COMPONENT TEST SPECIMEN

LARGE COMPONENT TEST SPECIMENS WERE USED TO OBTAIN DURABILITY, CRACK GROWTH AND RESIDUAL STRENGTH DATA FOR ACTUAL PRODUCTION STRUCTURAL PANEL CONFIGURATIONS. THE PANELS WERE SUBJECTED TO 4 LIFETIMES OF DURABILITY TESTING, AFTER WHICH MULTIPLE FLAWS WERE INDUCED TO TO OBTAIN CRACK GROWTH AND RESIDUAL STRENGTH DATA.

WING ITEM 9: LOWER SKIN AND STRINGER PANEL

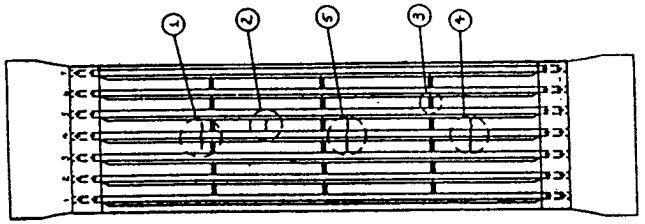

FLAW LOCATION	DAMAGE			FLIGHTS	RESULTS
	CONFIGURATION	INITIAL	FINAL		
1	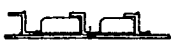	COMMON THRU CRACK AT STR. & SKIN FAST. HOLE a = 0.165"	a = 0.540"	17190	INSIGNIFICANT CRACK GROWTH
2	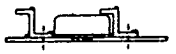	SKIN CRACK MID-BAY 2a = 1.04"	2a = 6.03"	4810	DA/DN DATA COLLECTION
3	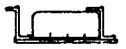	SKIN CRACK AT SHEAR CLIP HOLE a = 0.410"	2a = 5.14"	7222	DA/DN DATA COLLECTION
4		SEVERED STR. & SINGLE CRACK AT SKIN FAST. HOLE a = 0.575"	2a = 0.182"	in. = 4952 fl. = 9553	DA/DN DATA COLLECTION
5		SEVERED STR. & DIAMETRICAL CRACK AT SKIN FAST. HOLE 2 a = 1.385"	2a = 6.020"	in. = 17190 fl = 18478	DA/DN DATA COLLECTION RES. STRENGTH = 39.2 ksi PANEL FAILURE

FUSELAGE D&D/T DEVELOPMENT TEST PLAN

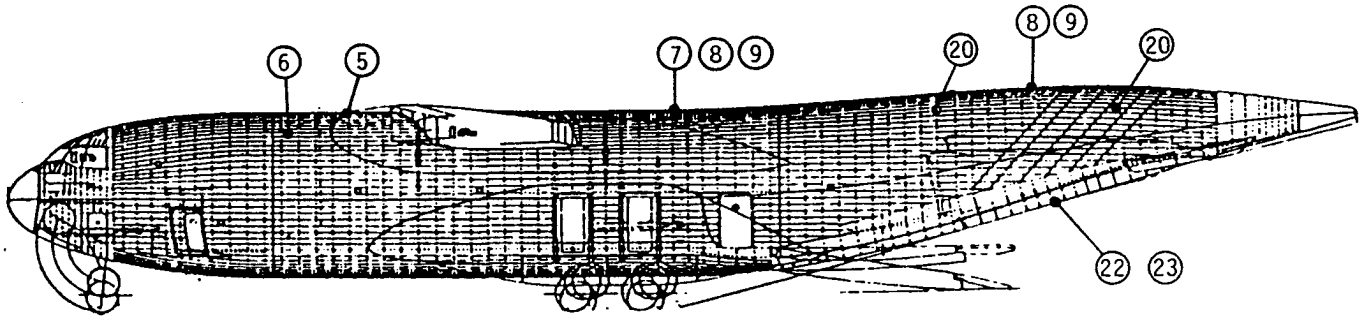

ITEM NO.		5	6	7A	7B	8	9	15	6
ITEM NAME		CURVED PRESSURE PANEL	LONGITUDINAL SKIN SPLICE	TRANSVERSE SKIN SPLICE	TRANSVERSE SKIN AND LONG. SPLICE	TRANSVERSELY CRACKED FLAT PANEL	LONGITUDINALLY CRACKED FLAT PANEL	SHELL FASTENER COMPARISON	CHEMMILLED SKIN COUPONS
APPROX. SPEC. SIZE		108 X 160	10 X 32	10 X 28	16 X 86	63 X 120	70 X 120	VARIOUS	4 X 20
NO. OF SPEC.		1	34	47	13	2	2	162	43
NO. OF CONFIG.		1	10	14	7	2	2	2 BASIC	4
LOADING		COMBINED TEN, COMP, & PRESS	CONST. AMP.	TENSION CONST. AMP.	CONST. AMP FBF SPEC.	CONST. AMP.	CONST. AMP.	CONST. AMP.	CONST. AMP.
TYPE OF TEST	DURA	-	34	47	13	-	-	162	43
	DAM. TOL	1	-	-	-	2	2	-	-

ITEM NO.		20	22	23
ITEM NAME		SHEAR PANEL CHEMMILLED SKIN	TRANSVERSE SKIN SPLICE, ARALL CARGO DOOR	LONGITUDINAL SKIN SPLICE ARALL CARGO DOOR
APPROX. SPEC. SIZE		52 X 60	10 X 32	10 X 32
NO. OF SPEC.		2	5	7
NO. OF CONFIG.		3	-	-
LOADING		CYCLIC SHEAR	FBF SPECTRUM	CONST. AMP
TYPE OF TEST	DURA	2	5	7
	DAM. TOL	-	-	-

EMPENNAGE D&D/T DEVELOPMENT TEST PLAN

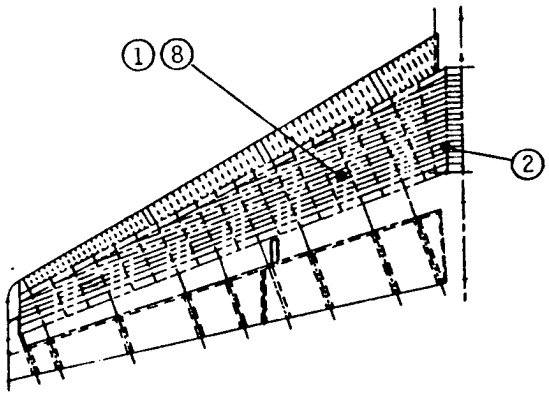

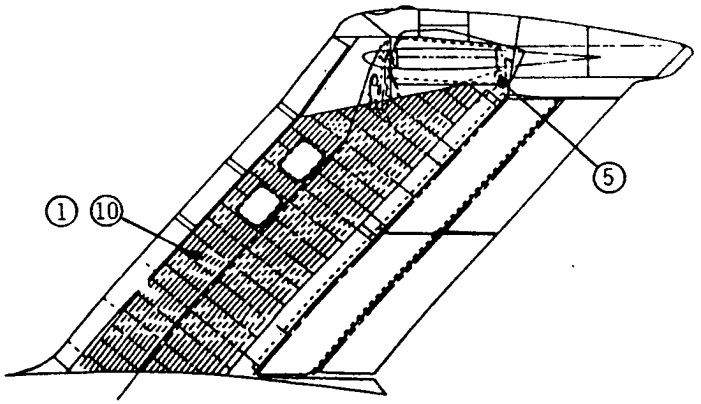

ITEM NO.		1	2	5	8	10
ITEM NAME		HORIZONTAL AND VERTICAL TAIL SKIN PANEL, BASIC STRUCTURE	HORIZONTAL STABILIZER SKIN AND STRINGER ROOT JOINT	HORIZONTAL STABILIZER PIVOT JOINT	HORIZONTAL STABILIZER SKIN AND STRINGER PANEL	VERTICAL STABILIZER SKIN AND STRINGER PANEL
APPROX. SPEC. SIZE		10 X 80	8 X 100		32 X 95	32 X 95
NO. OF SPEC.		18	4	1	2	2
NO. OF CONFIG.		2	2	1	2	2
LOADING		CONST. AMP. FBF SPEC.	CONST. AMP. FBF SPEC.	FBF SPEC.	CONST. AMP. FBF SPEC.	CONST. AMP. FBF SPEC.
TYPE OF TEST	DURA	18	4	1	-	-
	DAM. TOL	-	-	1	2	2

C-17A AIRFRAME DURABILITY TEST

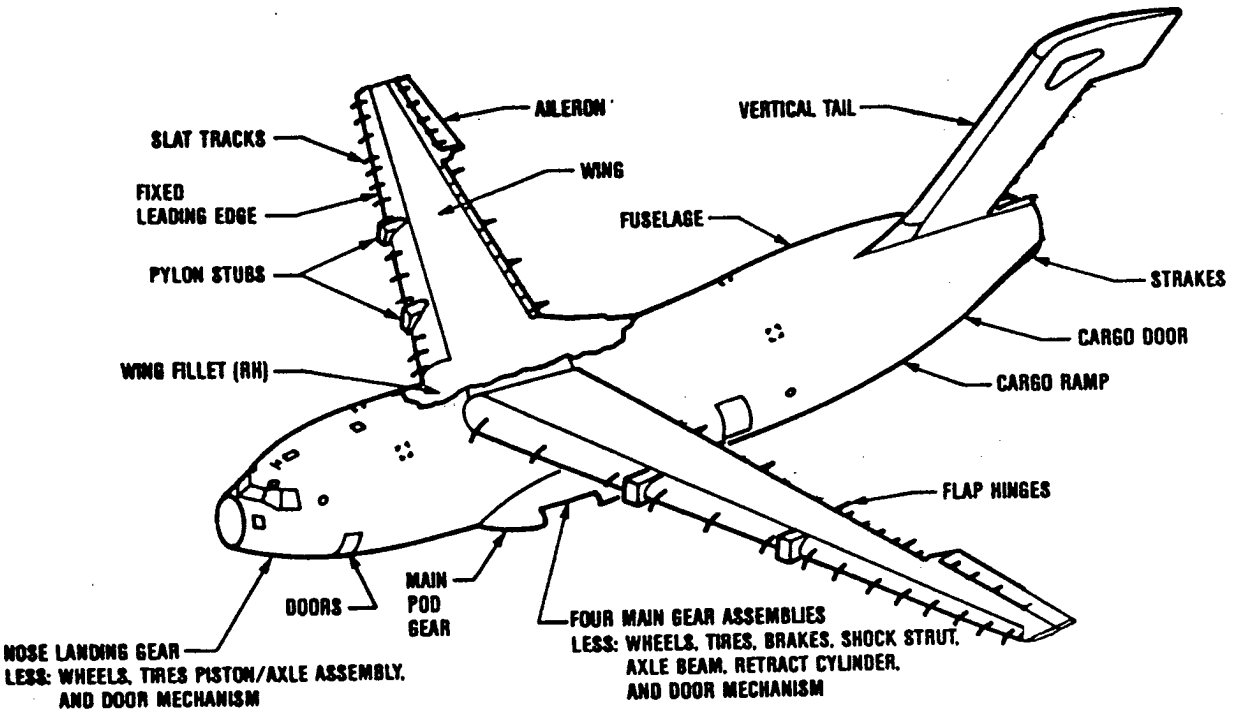

FULL SCALE AIRFRAME DURABILITY TEST

- THE TEST ARTICLE 'D1' IS VIRTUALLY COMPLETE AIRFRAME CONSISTED OF THE FUSELAGE, WING, WING PYLON STUB, LEFT HAND OUTBOARD PYLON AND VERTICAL STABILIZER.
- THE MAJOR OFF-AIRPLANE TEST FULL SCALE DURABILITY COMPONENT TESTS INCLUDES THE HOROZONTAL STABILIZER, INBOARD FLAP, NOSE AND MAIN LANDING GEARS.
- THE 'D1' TEST ARTICLE WAS THE FIFTH AIRFRAME TO BE ASSEMBLED IN THE MANUFACTURING SEQUENCE.
- THE TEST WAS CONDUCTED IN LONG BEACH, CALIFORNIA IN A FIXTURE LOCATED OUTDOOR. THE TEST ARTICLE WAS FINISHED WITH EXTERIOR EPOXY PRIMER.
- THE TEST STARTED IN NOVEMBER OF 1992. FULL RATE CYCLING (AVG. 7 CYCLES PER MINUTE) DID NOT START UNTIL EARLY MARCH 1993.
- COMPLETION OF TWO LIFETIMES FULL SCALE ENGINEERING DEVELOPMENT TESTING WAS ACCOMPLISHED IN MID JULY 1995.

TEST SPECTRUM

- TEST SPECTRUM REPRESENTED ONE TENTH OF A LIFETIME CONSISTED OF 856 FLIGHTS (3000 HOURS) AND 367,019 END CONDITIONS
- MANEUVER LOADS WERE GLOBALLY TRUNCATED USING C.G. INCREMENTAL LOAD FACTOR THRESHOLD OF 0.30 G.
- GUST LOADS WERE TRUNCATED AT AN EQUAL PROBABILITY OF OCCURRENCE LEVEL.
- AUGMENTED CYCLES WERE ADDED TO THE PYLON AND THE VERTICAL STABILIZER GUST SEGMENT IN THE BASELINE TEST SPECTRUM.
- ORDERING OF THE FLIGHTS ARE RANDOM EXCEPT FOR GROUPING OF THE THE MORE DAMAGING FLIGHTS IN THE MIDDLE AND THE END OF THE SEQUENCE TO FACILITATE MARKING.
- THE CABIN PRESSURE SCHEDULE WAS FOLLOW TO DEFINE CABIN PRESSURE THROUGH OUT EACH FLIGHT.
- CARGO RAMP AND DOOR OPENING AND CLOSING CYCLES WERE INCLUDE AND CORRESPOND TO AIR DROP EVENT.

ARTICLE LOADING APPLICATION

- WING AND VERTICAL STABILIZER COVERS ARE LOADED WITH GLUE-ON TENSION PADS.
- AILERON AND LANDING GEAR LOADS APPLIED USING PRODUCTION COMPONENTS.
- FUSELAGE LOADS APPLIED PREDOMINATELY THROUGH THE FLOOR.
- CABIN PRESSURE APPLIED THROUGH CUTOUTS IN THE FUSELAGE.
- FLAP, PYLON, SLAT AND HORIZONTAL STABILIZER LOADS APPLIED USING DUMMY FIXTURES ATTACHED TO PRODUCTION SUPPORT STRUCTURE.
- SPOILER AND RUDDER LOADS ARE LUMPED INTO WING COVER AND VERTICAL STABILIZER COVERS.

TEST SETUP

- 251 HYDRAULIC ACTUATORS TO APPLY LOAD
  - 64 WING BOX
  - 38 AILERONS, FLAPS AND SLATS
  - 25 ENGINE / PYLONS
  - 16 VERTICAL TAIL
  - 14 HORIZONTAL TAIL
  - 61 FUSELAGE
  - 33 LANDING GEAR
- APPROXIMATELY 700 CHANNELS AND 32 DEFLECTION TRANSDUCERS WERE INSTALLED IN THE BEGINNING OF THE TEST.
- ALL LOAD CELLS, STRAIN GAGES AND DEFLECTION TRANSDUCERS ARE RECORDED FOR STRAIN SURVEY CONDITIONS.
- ALL LOAD CELL AND STRAIN GAGES ARE RECORDED AT EVERY END POINT.
- TEST COMPUTER HAS A CIRCULAR BUFFER RECORDING ALL LOAD CELLS, STRAIN GAGES. THE CIRCULAR BUFFER STORES APPROXIMATELY 15 MINUTES OF DATA SCANNING AT A RATE OF 10 READINGS PER SECOND.

INSPECTION REQUIREMENT

THE AIRCRAFT WAS DIVIDED INTO 313 ZONES OF INSPECTION AREA.

- INSPECTION PROGRAM ARE DIVIDED INTO TWO CATEGORIES :
  - MANDATORY 'HARD' INSPECTION OF THE ENTIRE AIRFRAME AT 0.1, 1.0, 1.5 AND 2.0 LIFETIMES.
  - OPPORTUNISTIC INSPECTION OF AREAS PRIORITIZED BASED ON CRITICALITY WHENEVER THE TEST IS STOP WITH MAXIMUM INTERVALS OF 0.1, 0.3 AND 0.5 LIFETIMES.
- INSPECTION METHODS INCLUDE: VISUAL, CLOSED VISUAL, EDDY CURRENT, ULTRASONIC AND DYE PENETRANT.
- LIMITED TEAR DOWN INSPECTION WAS PERFORMED AT THE END OF 1.5 LIFETIMES INSPECTION (CONTRACT WARRANTY PERIOD). APPROXIMATELY 350 FASTENERS WERE REMOVED FOR BOLT HOLE EDDY CURRENT INSPECTION.

FULL SCALE DURABILITY TEST HISTORY

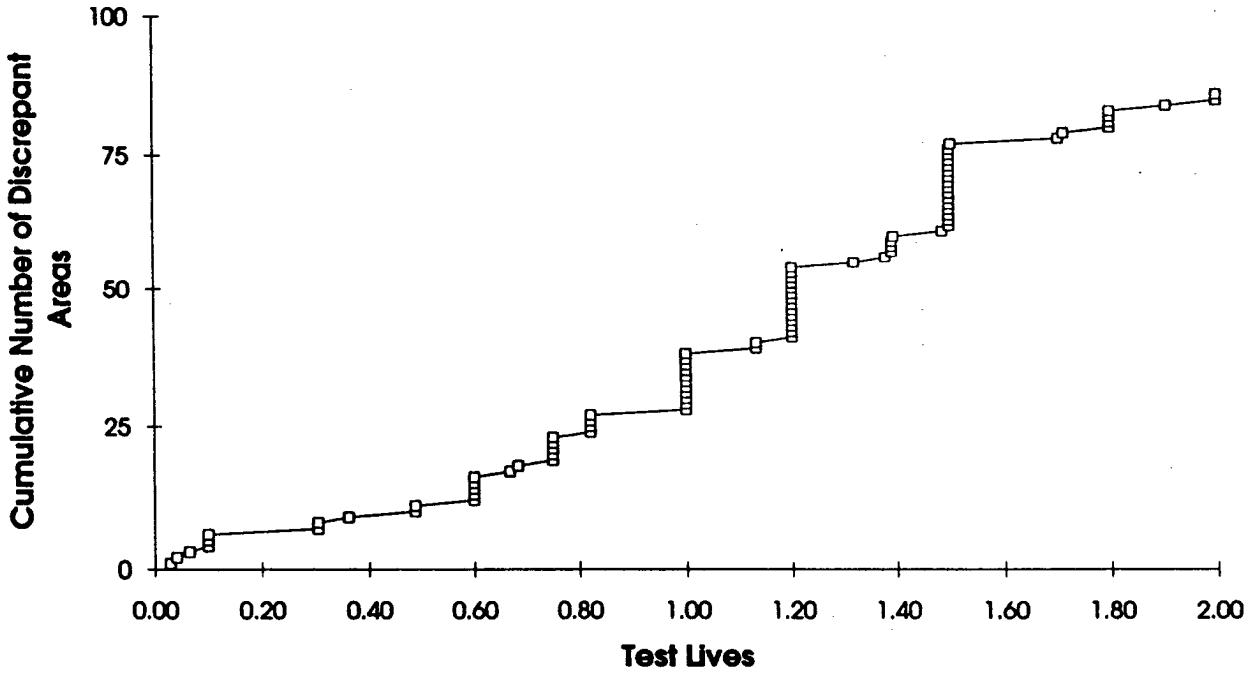

- NUMBER OF DISCREPANCIES : 91
  - NO DESIGN IMPACT : 42
  - MINOR DESIGN IMPACT : 44
  - SIGNIFICANT DESIGN IMPACT : 5

WING AFT TRAPEZOIDAL PANEL TO FUSELAGE SUPPORT STUB

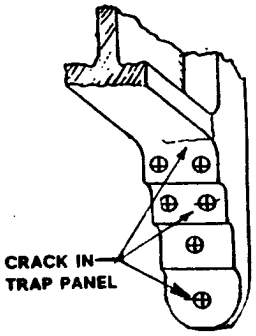

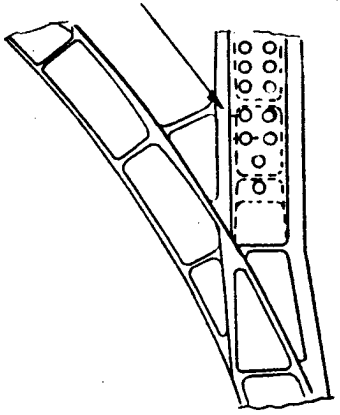

VIEW LOOKING AFT

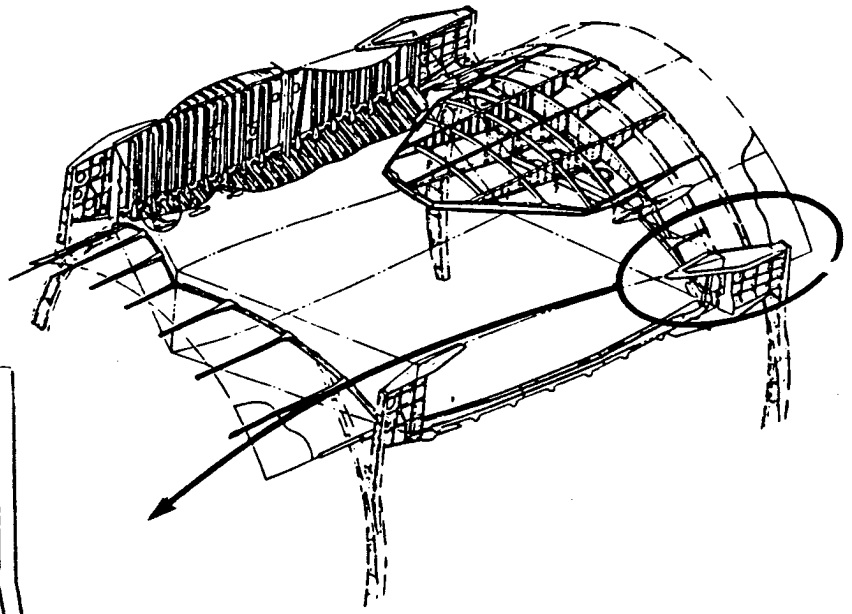

PYLON STUB UPPER CAPS AT 240 JOINT

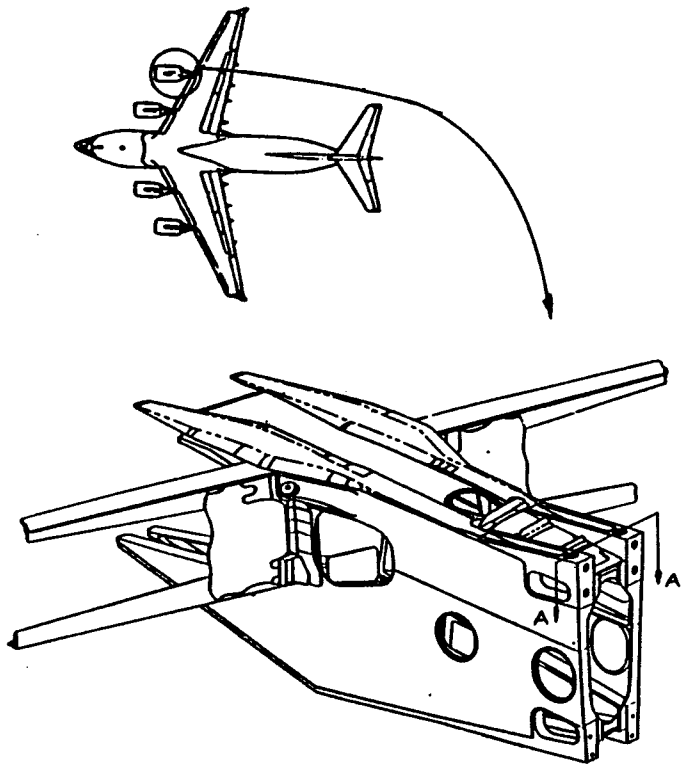

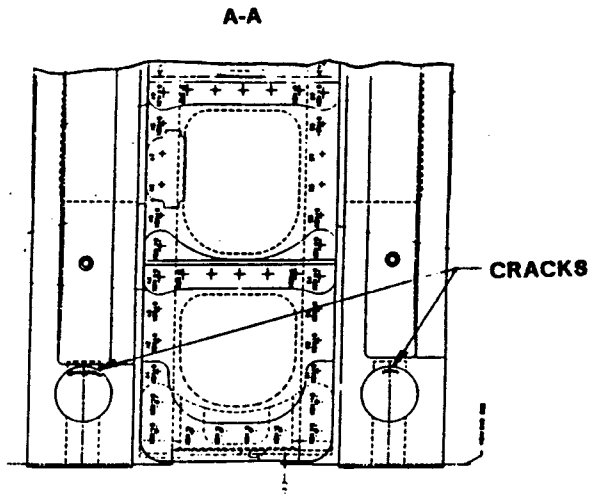

HORIZONTAL STABILIZER FULL SCALE DURABILITY TEST

- TEST ARTICLE WAS A COMPLETE HORIZONTAL STABILIZER CONSISTING OF BOTH LEFT AND RIGHT HAND H.S. BOX WITH THE TIP FAIRING AND TRAILING EDGES REMOVED.
- TEST WAS CONDUCTED AT VOUGHT AIRCRAFT IN TEXAS. TEST STARTED IN APRIL 1992 AND COMPLETED 2 LIFETIMES OF TESTING IN OCTOBER 1993.
- TEST SPECTRUM CONSISTED OF 50,180 END CONDITIONS REPRESENTING ONE TENTH OF A DESIGN SERVICE LIFE.
- 24 ACTUATORS WERE CONNECTED TO TENSION/COMPRESSION WHIFFLETREES ON THE H.S. AND 12 ACTUATORS WERE CONNECTED TO TENSION WHIFFLETREES ON THE ELEVATORS.
- TEARDOWN INSPECTION WAS PERFORMED AFTER THE COMPLETION OF 2 LIFETIMES OF CYCLIC TESTING.
- TOTAL OF 1034 FASTENERS WERE REMOVED FOR INSPECTION. TWO CRACKS AND SOME EVIDENCE OF WEAR WERE FOUND DURING THE INSPECTION.

FLAP FULL SCALE DURABILITY TEST

- TEST ARTICLE WAS A COMPLETE INBOARD FLAP CONSISTING OF FLAP BOX STRUCTURE, AFT FLAP HINGES AND THE ATTACHMENT OF THE VANE SUPPORTS TO THE BOX.
- FLIGHT-BY-FLIGHT TEST SPECTRUM CONSISTED OF 29,450 END CONDITIONS REPRESENTING ONE TENTH OF A DESIGN SERVICE LIFE.
- TEN WHIFFLETREE ASSEMBLIES APPLIED LOAD TO THE FLAP BOX THROUGH THE LOAD PADS, WHILE FIVE WHIFFLETREE ASSEMBLIES SIMULTANEOUSLY APPLIED LOADS THROUGH THE DUMMY VANE.
- TEST WAS CONDUCTED AT MDA TEST FACILITY IN CALIFORNIA. TEST STARTED IN MAY 1994 AND COMPLETED 2 LIFETIMES OF TESTING IN AUGUST 1994.
- NO DISCREPANCIES WERE DISCOVERED THROUGHOUT THE TWO LIFETIMES OF TESTING AND NO DISCREPANCIES WERE FOUND DURING POST TEST INSPECTION.

LANDING GEAR FULL SCALE DURABILITY TESTS

NOSE LANDING GEAR

- THE FULL SCALE DURABILITY TEST IS BEING PERFORMED AT MENASCO IN TORONTO, CANADA.
- TEST STARTED IN DECEMBER 1994 AND COMPLETED 1.5 LIFETIMES OF TESTING IN JULY 1995. THE GEAR WAS DISASSEMBLED AND COMPREHENSIVE TEAR DOWN INSPECTION WAS PERFORMED AT THE COMPLETION OF 1.5 LIFETIMES.
- THE GEAR WAS REASSEMBLED AND TESTING RESUMED IN NOVEMBER OF THIS YEAR. THE PLAN IS TO TEST THE GEAR TO FOUR LIFETIMES.

MAIN LANDING GEARS

- THE AFT MAIN GEAR FULL SCALE DURABILITY TEST IS BEING PERFORMED AT BFG/LGD IN CLEVELAND, OHIO.
- TEST STARTED IN APRIL 1995. THE GEAR HAS CURRENTLY COMPLETED 0.63 LIFETIMES OF TESTING.
- THE PLAN IS TO TEST THE GEAR TO 1.5 LIFETIMES, PERFORM COMPLETE TEAR DOWN INSPECTION, THEN RESUME TESTING TO FOUR LIFETIMES.
- THE CURRENT PLAN IS TO TEST THE FORWARD MAIN LANDING GEAR TO 1.5 LIFETIMES WHILE THE AFT GEAR TEAR DOWN INSPECTION IS BEING PERFORMED. THE FORWARD GEAR WILL THEN UNDERGO A COMPLETE TEAR DOWN INSPECTION WITH TESTING RESUMED AFTER COMPLETION OF THE AFT GEAR TEST TO FOUR LIFETIMES.

ASIP EXTENSION PROGRAM

- THE AIRCRAFT STRUCTURAL INTEGRITY PROGRAM (ASIP) EXTENSION PROGRAM HAS BEEN AUTHORIZED TO CONTINUE THE FULL SCALE AIRFRAME DURABILITY TEST TO THREE LIFETIMES.

- THE THIRD LIFETIME OF DURABILITY TESTING STARTED IN OCTOBER 1995. THE DURABILITY ARTICLE HAS CURRENTLY COMPLETED APPROXIMATELY 2.1 LIFETIMES OF TESTING.

- AN ADDITIONAL 12,000 FULL CABIN PRESSURE CYCLES WILL BE APPLIED TO THE FUSELAGE STRUCTURE AT THE END OF THE THIRD LIFETIME OF TESTING.

- A COMPREHENSIVE TEAR DOWN INSPECTION OF THE AIRFRAME IS PLANNED AT THE END OF THE TEST PROGRAM.

SUMMARY / CONCLUSION

- AN EXTENSIVE DURABILITY AND DAMAGE TOLERANCE DEVELOPMENT TEST PROGRAM CONSISTING OF OVER 2400 SPECIMENS OF VARIOUS COMPLEXITY WAS PERFORMED.

- THE COMPREHENSIVE DEVELOPMENT TEST PROGRAM WAS USED TO ESTABLISH THE DESIGN DETAILS PRIOR TO FINAL DESIGN.

- THE SUCCESS OF THE FULL SCALE AIRFRAME DURABILITY TEST CAN BE LARGELY ATTRIBUTED TO THE COMPREHENSIVE DEVELOPMENT TEST PROGRAM.

CF116 (CF-5) Full Scale Durability and Damage Tolerance Test (FSDADTT) Final Test/Teardown Results

*Mr. Yves Beauvais
Bombardier Inc., Defence Systems Division
10000 Cargo A-4 Street, Mirabel (Quebec)
Canada, J7N-1H3

INTRODUCTION

The F-5 A/B aircraft was originally designed by Northrop Corporation as a 4000 hours safe life airframe to the specifications of the United States Air Force Military Specifications Series MIL-S-5700 "Structural Criteria, Piloted Airplanes", 14 December 1954.

During its service life, the F-5 A/B has experienced numerous cracks in major airframe components, such as the wing spars and ribs, vertical stabilizer and numerous formers. Most of the structural defects were not identified by the Service Life Extension Program (SLEP), which involved an extensive engineering study to extend the airframe safe life from 4000 hours to 6000 hours. Moreover, the usage spectrum used for the SLEP studies was proven to be less severe than the one measured by the Canadian Forces.

As a result of the above, the Canadian Forces (CF) required that a Full Scale Durability and Damage Tolerance Test (FSDADTT) be conducted on a representative CF-5 airframe. The CF also required that all airworthy repairs developed during the FSDADTT be tested and lifed accordingly.

This paper will present a description of the CF-5 Full Scale Durability and Damage Tolerance Test (FSDADTT), performed at Bombardier Inc./Canadair.

First, the rationale for undertaking the Full Scale Test is discussed. The structural modifications incorporated into the airframe over the years are presented, and the impact of different operational usage by the CF on spectrum severity is also covered. The test article selection and preparation will also be discussed, as well as the spectrum development.

Test results will then be presented for the wing, the fuselage, and the empennage. As of end 1993, the test phase was completed and 24000 equivalent flight hours (EFH) have been simulated on the test article, that is six times the original design life of the CF-5 aircraft, and four times the SLEP-calculated life of 6000 flight hours. During this period, test data and results were recorded which have already impacted on fleet management efforts. At the end of the testing, a complete Teardown inspection was carried out on the structure and was completed at the end of 1994. The results of this inspection will also be presented.

Finally, the paper will cover various repair schemes that have been implemented and tested on the FSDADTT, including a boron-epoxy patch installed at a critical location on the wing top skin.

TEST BACKGROUND

The CF-5 was designed in the 1960's using the safe life approach. This approach provided a mean life prediction based on: unflawed lab specimen data, Miner's cumulative damage analysis, a constant scatter factor of 4 and no crack growth analyses requirement. Based on this approach, the design life of the CF-5 was estimated at 4000 flight hours.

In July 1977, a Service Life Extension Program (SLEP) was initiated. This program was based on a new approach: the damage tolerance philosophy. It involved crack growth analyses being carried out using mild, average and severe spectra. A NASTRAN finite element model of the F-5A/B was also used.

Based on these tools, close to 30 critical locations were identified and inspection intervals were determined for each location. Fleet maintenance actions were based on the results of this program.

Thus it was possible to extend the service life of the CF-5 from 4000 to 6000 flight hours, providing that a set of structural inspections be performed regularly.

The Canadian Forces (CF) now rely on the Aircraft Structural Integrity Program (ASIP) concept for most of its aircraft, including the CF-5. This ASIP philosophy is the cornerstone of fatigue life management for the CF and it requires that full scale testing be carried out to validate and substantiate the analyses performed at the design and at various stages of the aircraft service life. Various tests have been performed on the F-5 family aircraft. In the case of the T-38 and F-5 A/B, only components test were performed. The F-5 E is the only member of the family for which a Full Scale Test was performed. However, all these tests do not apply to the CF-5 for various reasons.

First, the CF-5 structure is different from those tested. Although originally the CF-5 was almost identical to the F-5A/B aircraft, several structural components have been redesigned and/or replaced throughout the CF-5 life. The modifications embodied on the CF-5 include:

- Lower wing skin replacement during mid-life R&O
- Several wing spars and ribs replaced during mid-life R&O
- The fuselage dorsal longeron was redesigned and replaced
- The aft fuselage formers were redesigned and replaced

All these modifications have been evaluated analytically, but no test has been done to substantiate these analyses. The F-5E Full Scale Test is not representative either because this later version of the F-5 is significantly different from a structural viewpoint in that many critical locations identified on the F-5A and the CF-5 were completely redesigned for the F-5E model.

Second, the service spectrum of the CF-5 is quite different from that used in the original life estimate, the SLEP life estimate, as well as the various tests carried out on the F-5 family. Figure 1 shows a cumulative exceedance curve for the design, SLEP, F-5E spectra as well as the in-service spectrum of the CF-5 and the FSDADTT test spectrum. It can be seen that the CF-5 spectrum is quite different, and generally more severe, than the other spectra.

In view of the requirement to extend the operational life of the aircraft, continued structural integrity of the CF-5 required that a Full Test be performed.

The Full Scale Test is performed for the following reasons:

- Extend life from 4000 hours to 6000 hours,
- Investigate possible further extension,
- Provide recommendations for inspection schedules to extend the airframe life to 6000 hours and beyond,
- Optimize the aircraft technical support by:
  - substantiating theoretical analyses (D&DTA and FEM)
  - identifying potential problem areas
  - validating inspection techniques
  - establishing spare parts requirements
  - evaluating modifications and repairs schemes (wing component redesign, fuselage dorsal longeron, aft fuselage formers, wing 15% spar repair angle).

Major milestones of the project include the selection and preparation of a test article, the design and construction of a test rig, the development of the test spectrum, testing and regular inspection of the test article for a total of 24000 equivalent flight hours and teardown inspection of the test article after the test.

Test Article Selection

The test article was selected to provide a specimen as representative as possible of the fleet average. It was selected based on the number of flight hours accumulated, the severity of the spectrum flown as well as the structural configuration of the aircraft.

All these factors had to be as close to the fleet average as possible. Structural modifications/repairs were embodied on the test article to bring it to the same structural configuration as that of the CF-5 fleet after the ongoing mid-life R&O.

Test Rig Design

The test rig is designed as a semifree-floating body configuration in a balanced state. The reaction linkages are located at the forward and aft fuselage. A total of 45 actuators are used to apply and distribute the required loads to the test article. Counterbalancing of the test article, using a deadweight system, simulate an approximately weightless condition. The loading and reaction linkages are designed to be easily removed for inspection purposes.

Test Spectrum Development

The Test Spectrum was developed by Canadair to represent as closely as possible the future usage of the aircraft by the Canadian Forces (CF). It represents the average spectrum for the CF-5 fleet in the advanced lead-in trainer role for the CF-18. The spectrum is presented in a 1000 equivalent flight hours (EFH) block in a mission-by-mission format. For each mission, a manoeuvre sequence was determined based on various sources of data. These sources included the wing Flight Load Survey data, the accelerometer data, pilot interviews, and the training syllabus. The flight parameters were analyzed to identify the manoeuvres flown, and they were used to develop a g-spectrum to compare with the accelerometer data collected on the CF-5 fleet. The Nz spectrum and the Vertical Stabilizer spectrum for the FSDADTT are presented in Figures 1 and 2 respectively.

Once the manoeuvre spectrum was completed, the aerodynamic and inertia loads distribution were calculated for each manoeuvre. An optimization program was then used to determine the combination of actuator loads that would reproduce the load distribution for each case.

The test spectrum also incorporates marker blocks to facilitate the evaluation of results and provide crack growth rate data. This feature has already proven useful in the case of the lower wing skin critical radius.

Test Status

The test was completed by the end of 1993 after three 8000 EFH lifetimes were completed. The Teardown inspection planned at the end of the test was completed at the end of 1994.

TEST RESULTS

The test results are presented for the wing, the fuselage and finally, the vertical stabilizer. In general, test failures have been located mainly on the wing, with only a few failures detected on the fuselage. Modification/Repair schemes incorporated to the test article are also discussed.

Wing

The CF-5 wing is the component where most cracks were found during the FSDADTT program. Damage was found starting at 8000 EFH up until 12900 EFH at which time the decision was made to replace the wing and continue testing with more emphasis put on the fuselage and empennage. However, a replacement wing was selected to ensure that the wing loads are redistributed adequately to the fuselage frames. Note that all test lives mentioned are unfactored life, unless specified otherwise.

Lower Wing Skin.

The bulk of the fatigue cracks found on the wing were on the lower wing skin. Those fatigue cracks were mainly at fastener holes. The first four cracked holes were detected at 8000 EFH. Then at 9755 EFH, another 42 fastener hole cracks were detected as well as some drain holes (see Figure 3). Again most of these holes were on the 44% spar line between Wing Station (WS) 25 to 65. Some cracks were also found on the 39% spar line and over the root rib area.

In addition to that, cracks were detected at 9755 EFH in the lower wing skin critical radius, at 11877 EFH and 12890 EFH at the WS 64.8 radius and on the edge of the lower skin at the MLG cut-out.

These damage are summarized in Table 1 and are shown in Figure 3. Analytical life estimates are also presented, when available, in Table 1.

The repair consisted in opening the hole to remove the cracks and the crack tip plastic zone. The holes were then cold worked and a fastener was put back in (except for the drain holes which were left open).

Moreover, at 9755 EFH, it was decided to take the time to cold work every holes in the area limited by WS 70 left to right and the 27% and 44% spar lines (Figure 4). This was done to ensure that testing could proceed without cracks on the lower wing skin slowing the test too much. However, at 11880 EFH, more cracks were found in fastener holes in the 15% spar area (Figure 3).

In the case of the lower wing skin critical radius, a repair was designed for this area. It consists in a titanium patch installed over the critical radius area (Figure 4). The cracked material, including the crack tip plastic zone is removed prior to installing the patch. This repair has been tested successfully from 9755 to 12890 EFH. A composite patch (Boron-Epoxy) was also designed for this location. However, it has not been tested on the Test Article.

At WS 64.8, the area was repaired by blending away the cracked material (including the plastic zone), and then shot-peening the radius.

The largest damage found on the lower skin was located at the 15% spar line at WS 40, after 11880 EFH. There, a crack propagated from the forward edge of the skin (at 15% spar line) to the 21% spar line, over 6 inches away (Figure 3). This damage was particular because it initiated at the radius of a chem-milled pocket. It became unstable before getting through the thickness, hence before being detectable. This area was repaired by removing the cracked material and by installing a steel patch (Figure 4). This repair was tested successfully to 12890 EFH.

After these repair were implemented, testing resumed until 12890 EFH. At that time further cracking was found in the critical radius, the WS 64.8 radius and the edge of the lower skin at the Main Landing Gear cut-out. It was then decided to remove the test wing and continue the testing of the fuselage and empennage with alternate wings. The test wing then went through a teardown inspection. This inspection revealed a lot of cracks in the lower wing skin, as shown in Figure 5.

Wing Spars and Ribs.

The damage found on the wing internal structure is shown in Figures 6 and 7, and summarized in Table 2. Most of this damage was found at the teardown inspection of the wing, after 12890 EFH.

It can be seen that a significant portion of the structure is damaged. The 39% spar, for example, is almost severed at WS 50. It must be noted that this spar, as well as the 21%, 27% and 33% spars, were not replaced as part of the wing R&O program. Therefore, for these components, it was necessary to demonstrate a full 6000 hour life, since they are not replaced at mid-life.

Based on the extent of cracking on the wing, and especially the lower wing skin, it was recommended that the service life of the lower wing skin for the CF-5 fleet be reduced to 2700 flight hours. This corresponds to the time when cracking was first observed (8000 EFH) divided by a scatter factor of three.

However, after reviewing the extent of damage in the internal structure, it was concluded that a complete wing replacement at mid-life was preferable. Such new wing will have a 7475 alloy lower skin, which will greatly improve the crack growth lives in the skin. Also, all fastener holes between WS 64.8 left to right will be cold worked.

Fuselage and Empennage

There has been only a few minor test failures on the fuselage during the test. These test failures are summarized in Table 3, as well as the result of analyses carried out to verify the analytical models of these areas.

The only area of the fuselage that required significant repair during the test is the upper cockpit longeron area (figure 8). Cracking in the area was found at 16000 EFH, at a fastener hole on the longeron. At that time, the hole was oversized to remove the crack and plastic zone and an interference-fit bushing was installed. However, at 18000 EFH, the crack had reappeared and propagated to the edge of the longeron. The area was heavily strain gauged to gather load/stress distribution data in the area and a repair was designed and installed to resume testing. In consisted in a strap bolted over the damaged area, as shown in Figure 8. The cracked area was blended prior to the strap installation.

This repair was successfully tested from 18000 to 24000 EFH. While not being applicable directly for fleet aircraft, this repair provided a lot of data for the development of an airworthy repair.

The test program also provided the opportunity to evaluate two major areas of the fuselage that were modified prior to beginning of the Full Scale Test.

The original aluminium dorsal longeron (Figure 11) was replaced by a new steel longeron designed by Canadair. In 24000 EFH of test, no damage was found on this new longeron nor on the surrounding structure. This redesigned longeron was installed on the entire fleet.

The five fuselage formers underneath the vertical stabilizer (Figure 13) were also replaced on the test article prior to the start of the test. Originally, these formers were made of sheet metal and were cracking early in the aircraft life. The Vertical Stabilizer skin critical radius, located close to this area, was also cracking. Canadair designed new formers section to replace the problem areas. These new formers section are machined with integral bathtub fitting to transfer the vertical stabilizer skin load directly via the attachment angle.

This results in a different load path being available for the stabilizer bending load and reduces the stress (by up to 40%) at the main load path for this load, namely the vertical stabilizer main spar. The stabilizer skin over this area is a very critical location on the CF-5. However, with the new formers, no cracking was found on the Vertical Stabilizer skin in the critical area. The only cracks observed are located at stringer runnouts, as shown in Figure 14. There was also evidence of fretting along the main spar area.

Upper Wing Skin Composite Patch.

When the decision to replace the wing was made, it was decided to take the opportunity to instrument a Boron-Epoxy doubler installed over an area that has experienced cracking in the fleet. This area is the upper wing skin "golden triangle", shown in Figure 4. This boron-epoxy doubler is a fatigue enhancement feature, not a structural component. The doubler was analyzed at Canadair, using NASTRAN, to evaluate the load reduction it would produce on the upper skin. The patch was installed on the test article wing along with many strain gauges. The gauges results matched the NASTRAN results in showing a 40% stress reduction in the critical area. However, the patch failed during testing after approximately 3000 EFH. A large disbound was observed at 16000 EFH as well as matrix cracking. However, evidence of cracking was observed at 15000 EFH. Thus, the useful life of the doubler is estimated at 2000 EFH, based on this test result.

Acoustic Emission

The CF-5 FSDADTT provided an ideal opportunity to evaluate the capability of acoustic emission monitoring with regards to crack detection. A monitoring system was installed on the test article. The monitored region was the wing lower surface.

The acoustic emission system proved to be a valuable tool for the early detection of cracks in that most damages on the lower wing skin were first localized by acoustic emission and then confirmed by other NDT techniques. Had conventional NDT been used without acoustic emission, cracks could have progressed undetected and resulted in early wing failure, possibly causing extensive damage to the rest of the structure. This technique was used on the FSDADTT to highlight the areas where inspections should be carried out in order to save inspection time, and provide advance warning in critical areas.

CONCLUSION

The CF-5 FSDADTT has been a fruitful program. The cracking observed during the test resulted in many changes in the operation and fatigue management efforts for the CF-5. It has also allowed to test major redesigns and repairs, as well as to demonstrate the capability of acoustic emission for early crack detection.

The main conclusions reached at the end of the test program differ for the wing and the rest of the aircraft. In the case of the wing, the conclusion is that this structure is extremely critical and it was decided to limit its life to 3000 hours, which is less than the original design life. Moreover, new wings are being procured at mid-life rather than going through the wing R&O process.

For the fuselage and empennage, the test showed that these structures are damage tolerant and that the SLEP life of 6000 hours is a realistic target, with possible extension. The major critical area of the fuselage is the cockpit longeron, which will require a modification to reach the target life. The test also highlighted the fact that the fuselage modifications (dorsal longeron and aft formers) are quite efficient.

ACKNOWLEDGEMENT

The test is made under contractual arrangements between Bombardier Inc. (Canadair) and the Canadian Department of Supplies and Services. The technical authority is the Canadian Department of National Defence (DAS Eng). The author wishes to acknowledge the support of Maj. J. Miller and Capt. S. LeGuellec, of DAS Eng.

Failure Description	Crack Size	Test time	Analytical Results	Figure
Fastener holes on lower wing skin	0.010" to 0.040"	8000 EFH 9755 EFH Teardown (12890 EFH)	Fatigue = 6730 hr DTA = 200 hr Acrit = 0.060"	3 3 5
Critical Radius at WS 25	0.080"	9755 EFH Teardown (12890 EFH)	Fatigue = 16160 hr DTA = 1050 hr Acrit = 0.095"	3 5
Radius at WS 64.8	0.450"	11877 EFH Teardown (12890 EFH)	Fatigue = 11600 hr DTA = 3700 hr Acrit = 0.487"	3 5
Edge of skin in MLG cut–out	0.040"	Teardown (12890 EFH)		5
Crack form 15% to 21% at WS 33	6.25"	11877 EFH	Fatigue = 10200 hr DTA = 4570 hr Acrit = 0.450"	3

Table 1 – Fatigue Damage found on Lower Wing Skin

Failure Description	Crack Size	Test time	Analytical Results	Figure
15% spar at WS 48 (see note 1)	>1.00"	6000 EFH	Fatigue = 1483 hr DTA = 3420 hr Acrit = 0.090"	6
MLG Uplock Rib	0.250"	12130 EFH		6
Root Rib at 44% spar attachment (upper)	0.200"	9755 EFH	Fatigue = 5176 hr DTA = infinite	6
Crack in 39% spar at WS 49	>2.00'	Teardown (12890 EFH)	Fatigue = 18800 hr DTA = 1030 hr Acrit = 0.330"	6
Cracks in internal Structure in various locations (lower surface)	0.010" to 0.060"	Teardown (12890 EFH)		6
Cracks in internal Structure in various locations (upper surface)	0.010" to 0.060"	Teardown (12890 EFH)		7

Table 2 – Fatigue Damage found on Wing Internal Structure

Failure Description	Crack Size	Test time	Analytical Results	Figure
Upper Cockpit Longeron	0.040"	16700 EFH	Fatigue = 22800 hr DTA = 650 hr Acrit = 0.110"	8
Fuselage Skin Cracks	0.050" to >3.00"	Teardown (12890 EFH)		9
Intake Duct Skin at FS 355 to 370	>3.00"	Teardown (12890 EFH)		10
MLG Door Support Beam – Angle	>1.00"	9755 EFH		9
Cracks in Centre Fuselage internal Structure (various)	0.010" to >5.00"	Teardown (12890 EFH)		11
Cracks in FS 325 Bulkhead	>1.00"	8000 EFH	problem related to corrosion (not a valid test result)	12
Engine Mount Bolts	Bolt Failed	2750 EFH		13
Engine Forward Mount Link	Link Failed	6400 EFH		13
Cracks in Aft Fuselage internal Structure (various)	0.50" to >1.00"	Teardown (12890 EFH)		13
Crack in V/Stab Skin and Internal Structure (various)	>1.00"	Teardown (12890 EFH)		14

Table 3 – Fatigue Damage found on Fuselage and Empennage

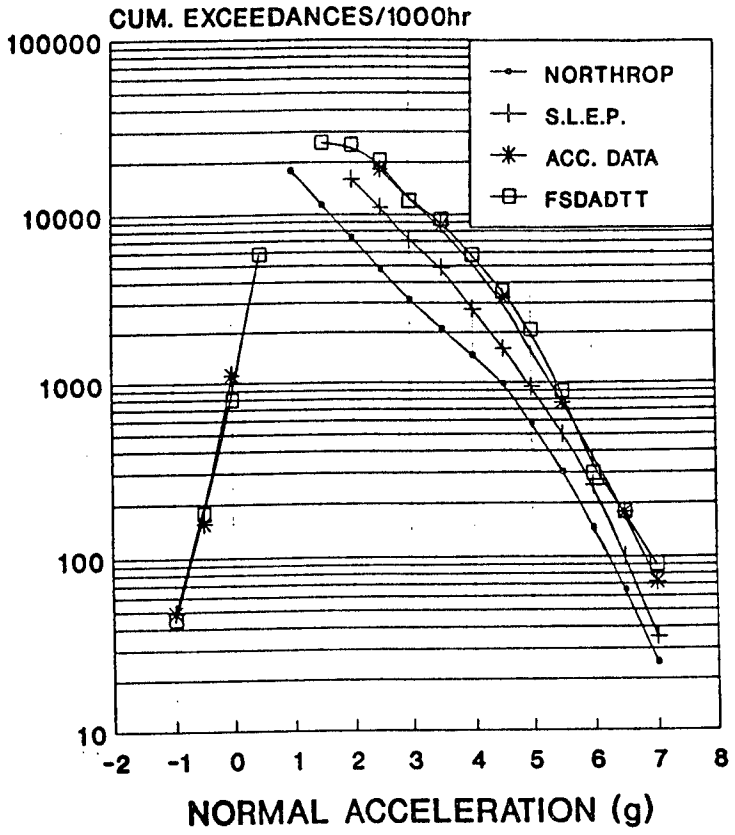

Figure 1 - CF-5 Nz Spectra Comparison

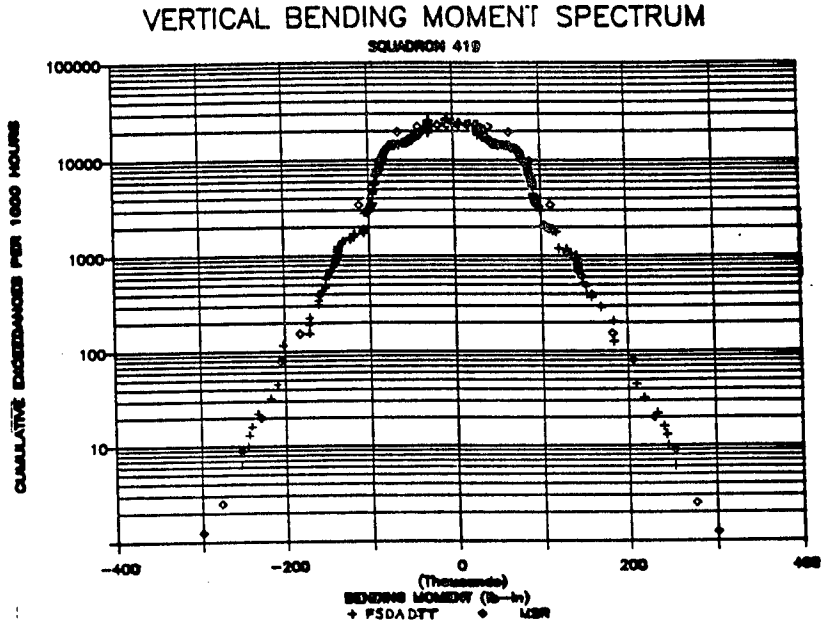

Figure 2 - CF-5 FSDADTT V/Stab Bending Moment Spectrum

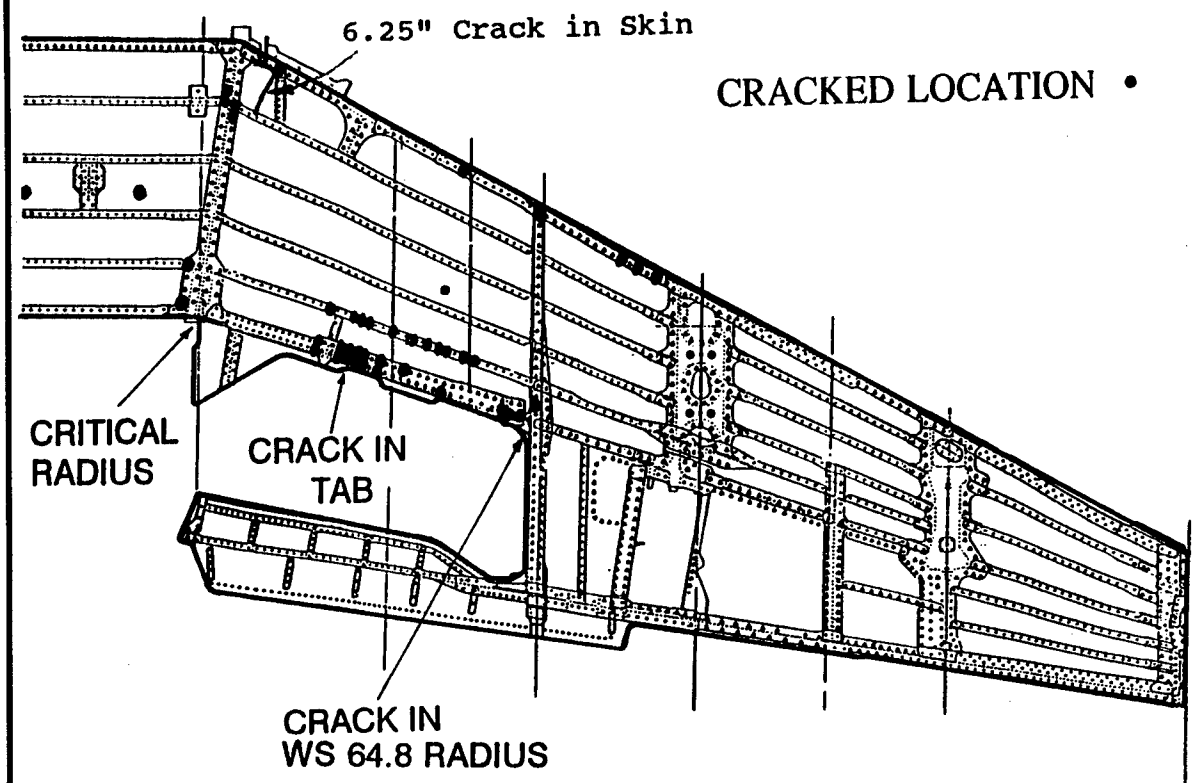

Figure 3 - Cracks on Lower Wing Skin

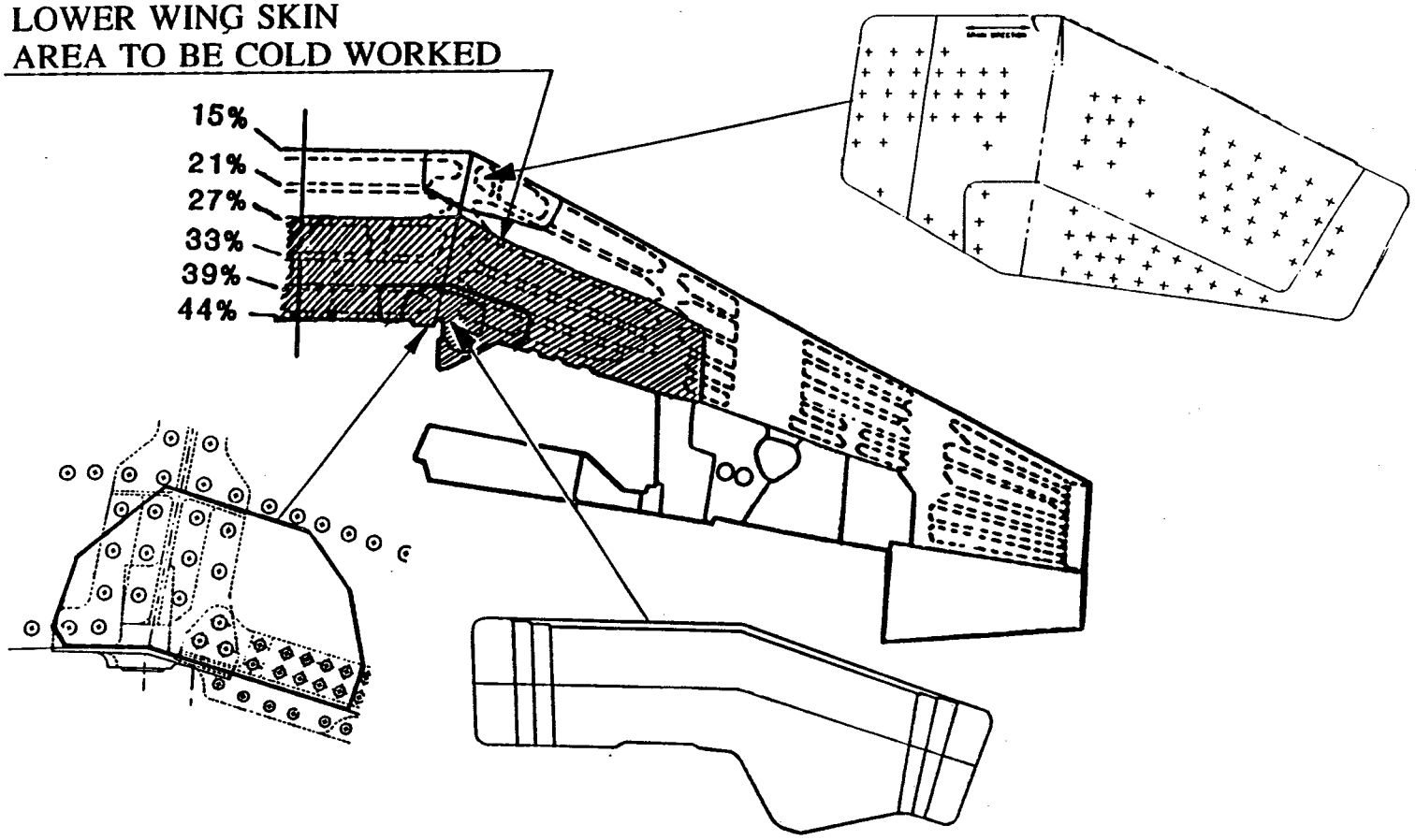

Figure 4 - Repairs Installed on Wing During FSDADTT

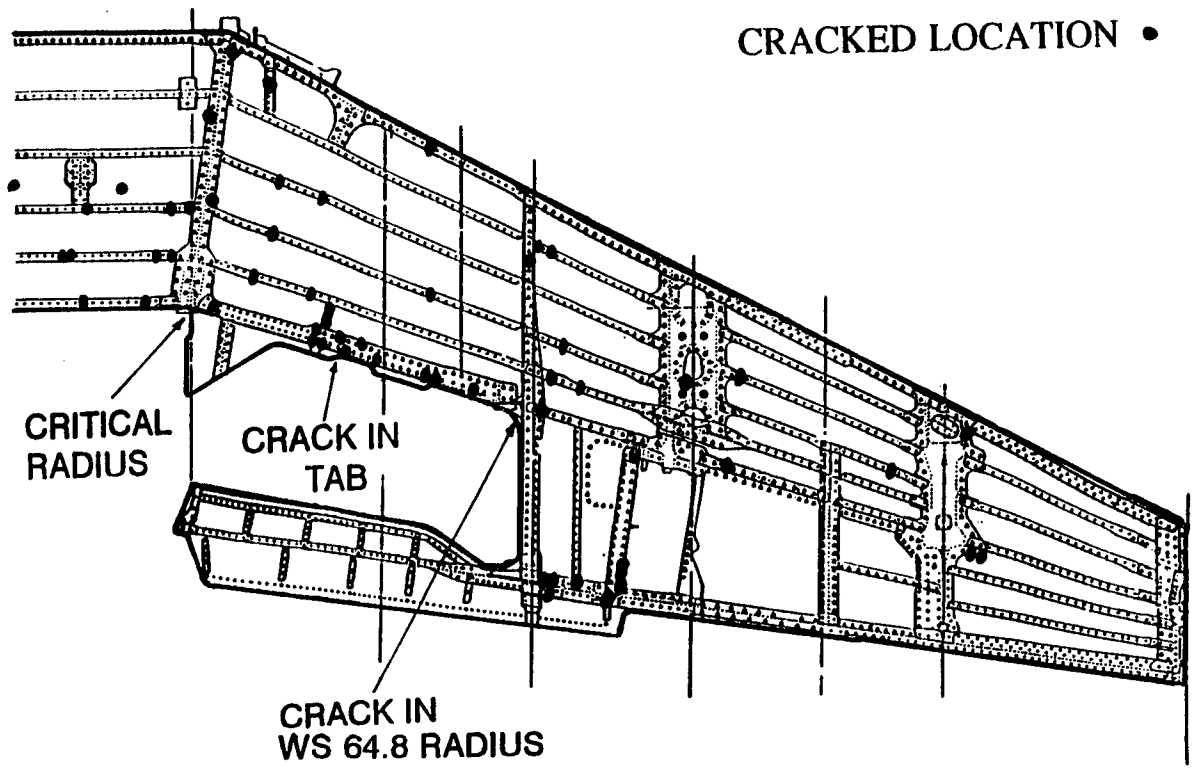

Figure 5 - Cracks on Lower Wing Skin at Teardown

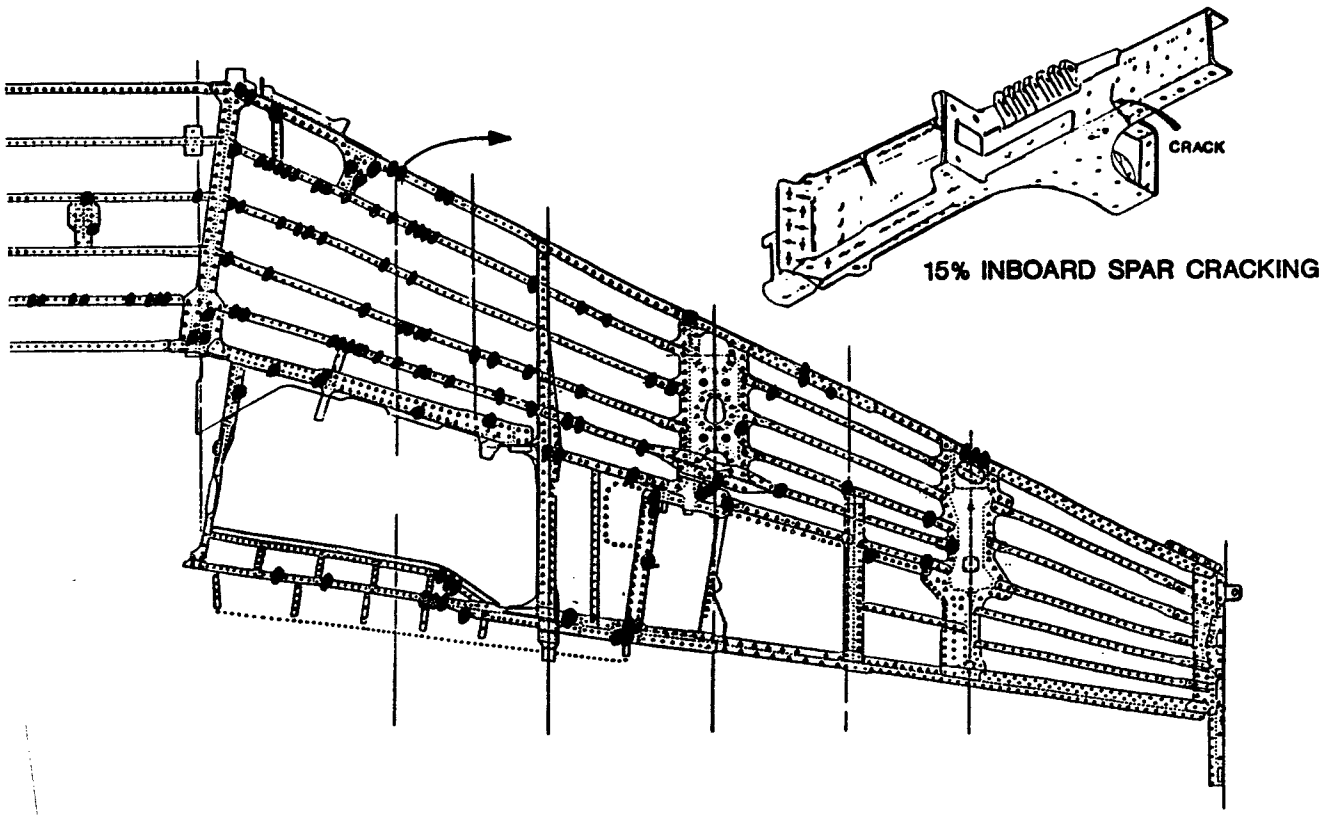

Figure 6 - Cracks on Wing Internal Structure (Lower)

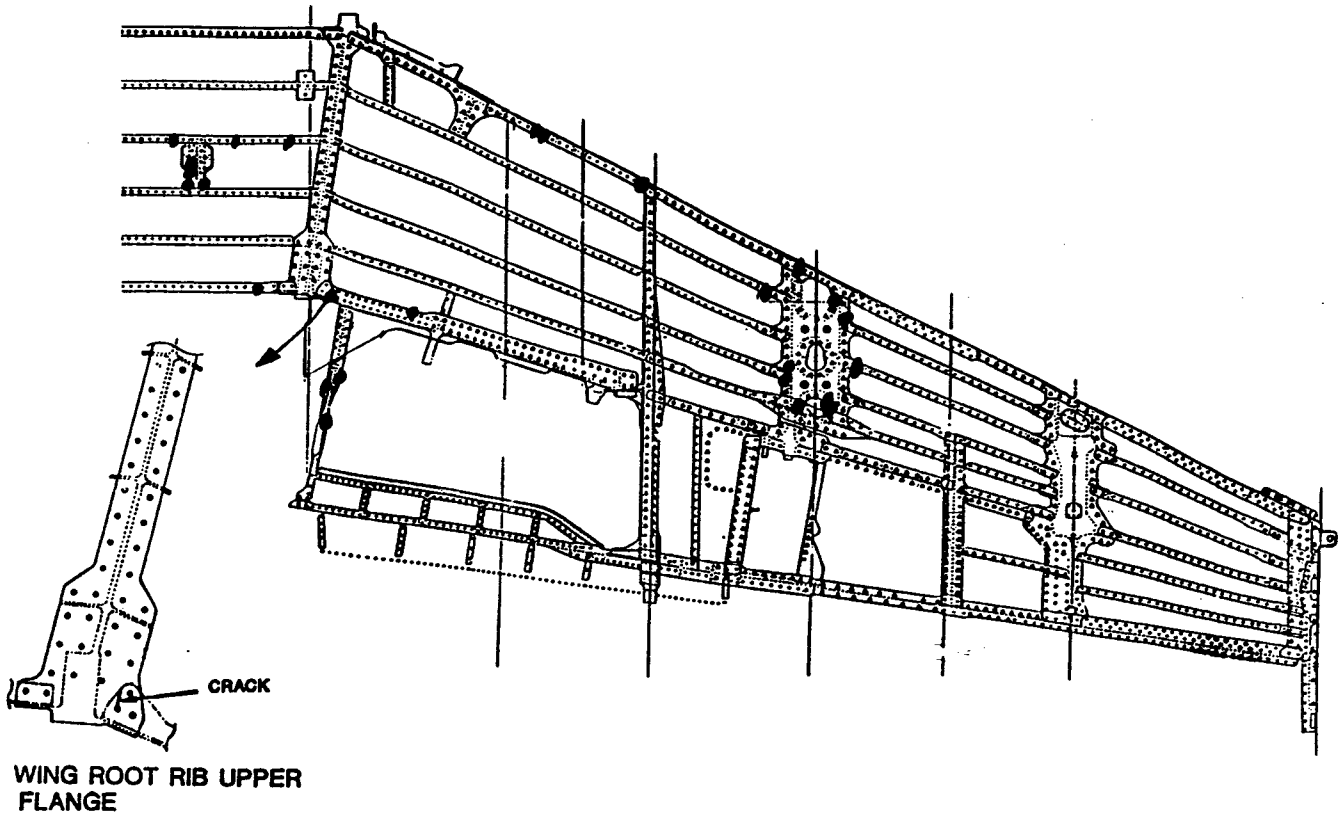

Figure 7 - Cracks on Wing Internal Structure (Upper)

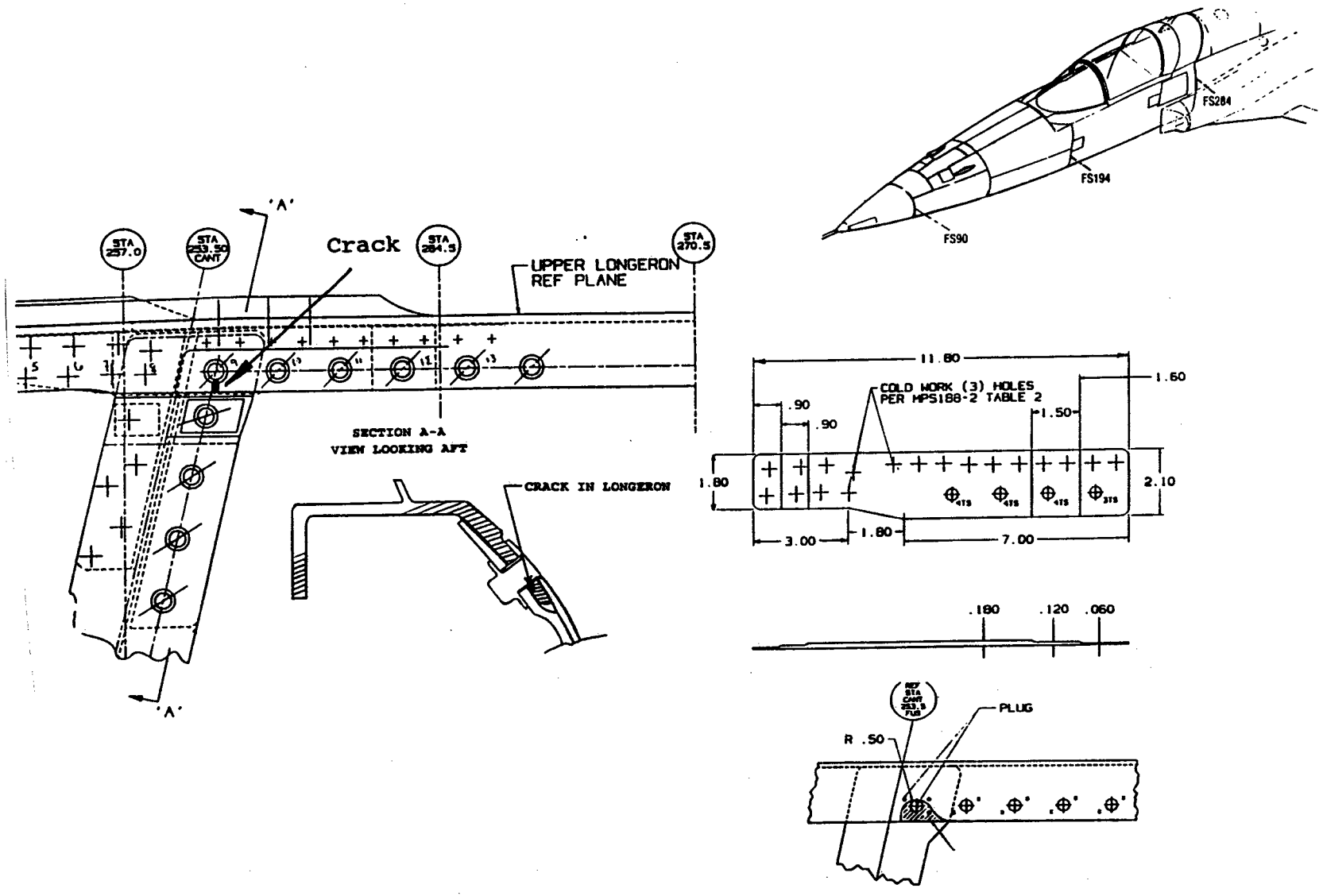

Figure 8 - Crack in Upper Cockpit Longeron

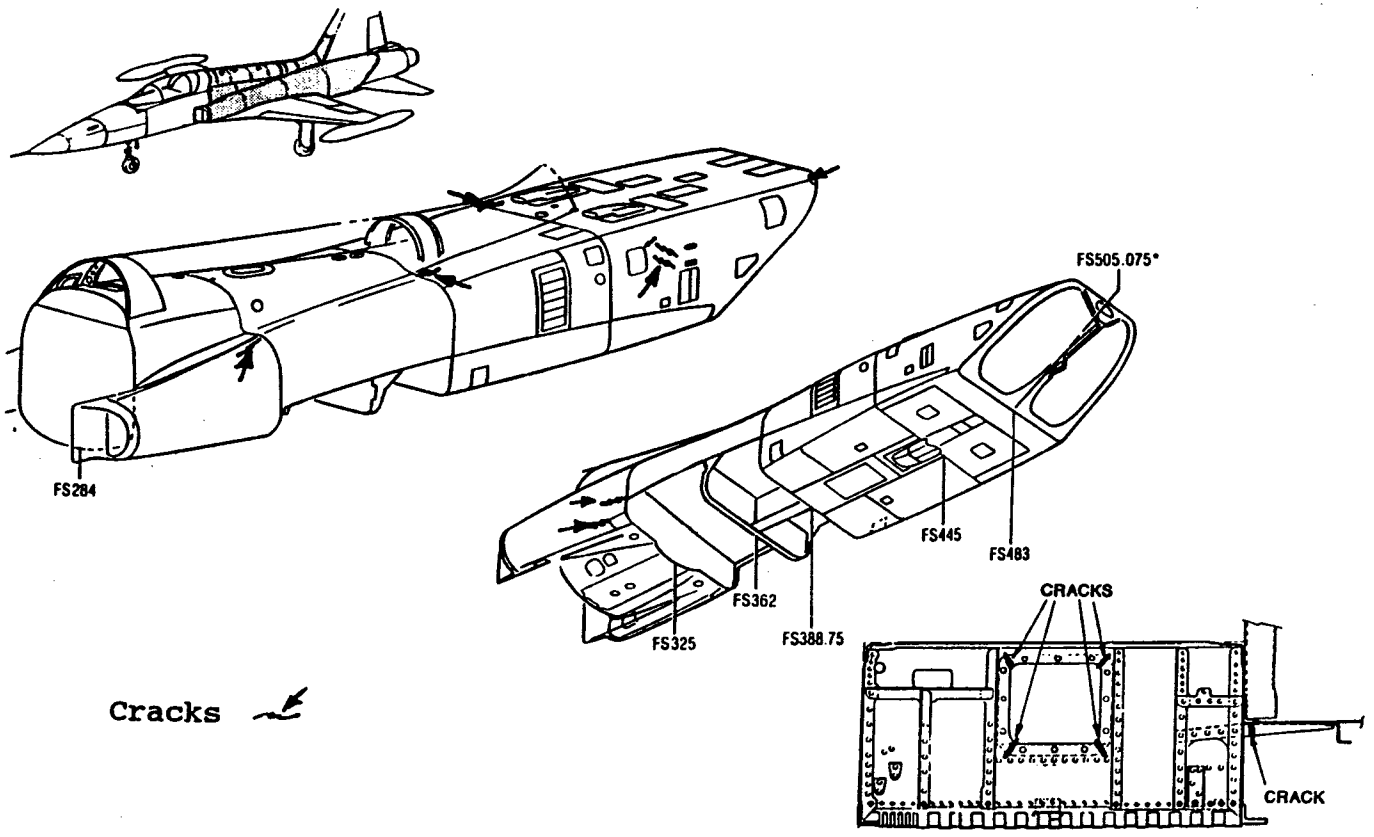

Figure 9 - Cracks on Fuselage Skins

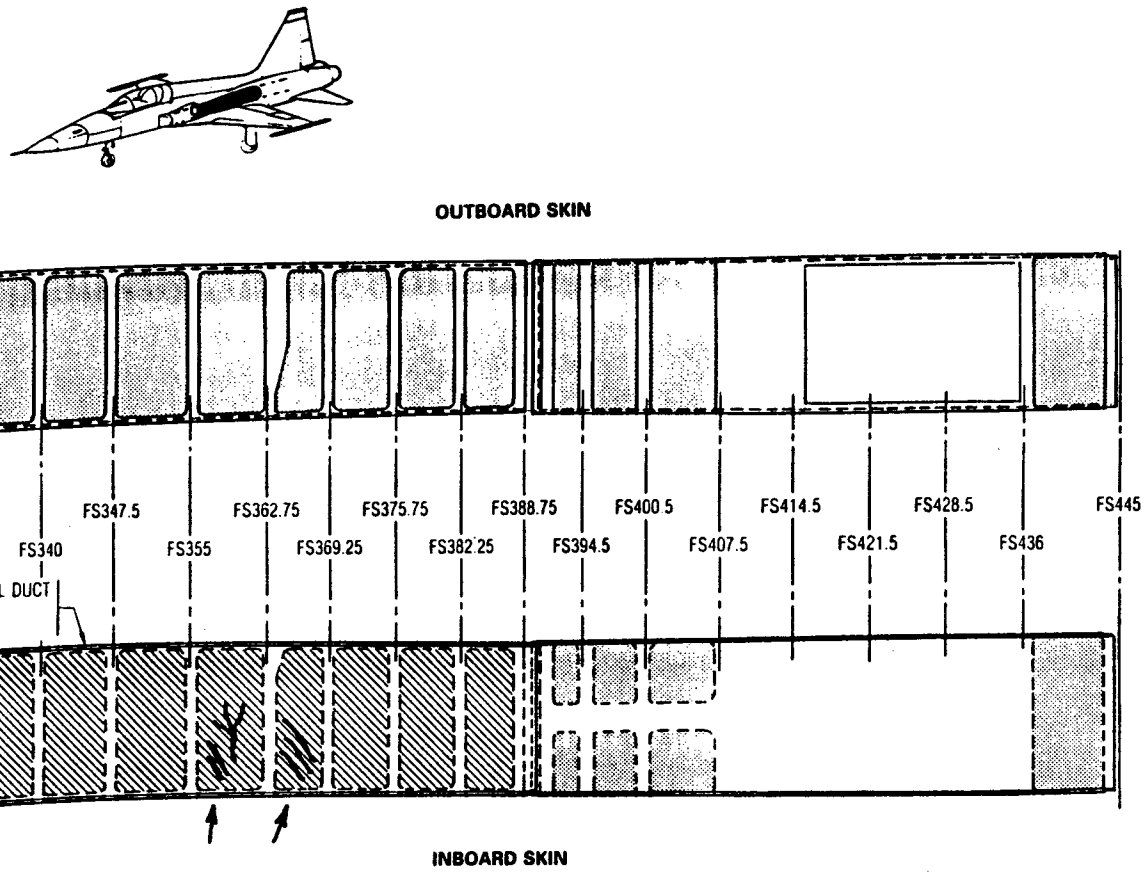

Figure 10 - Cracks in Intake Duct Skins

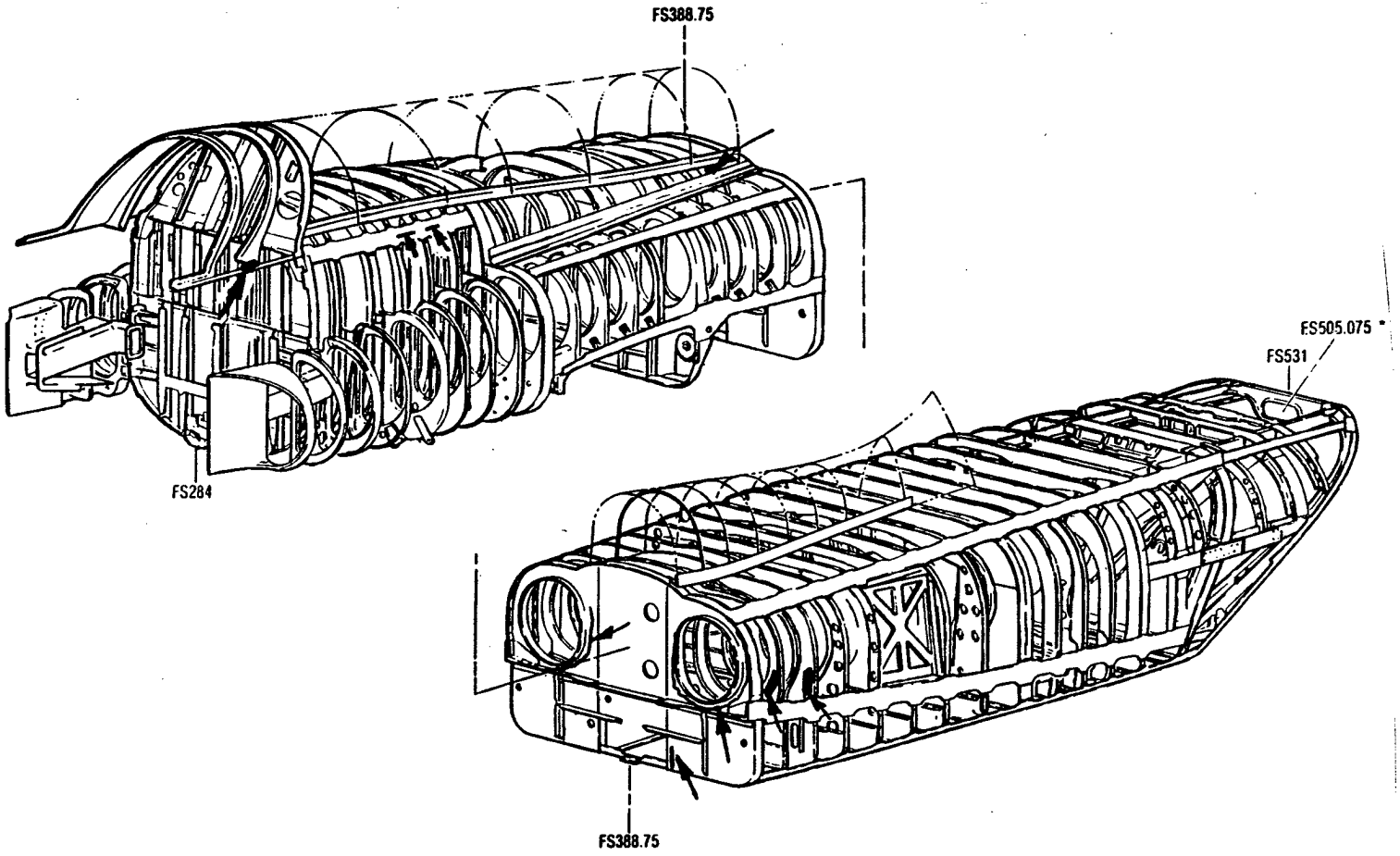

Figure 11 - Cracks in Centre Fuselage Structure

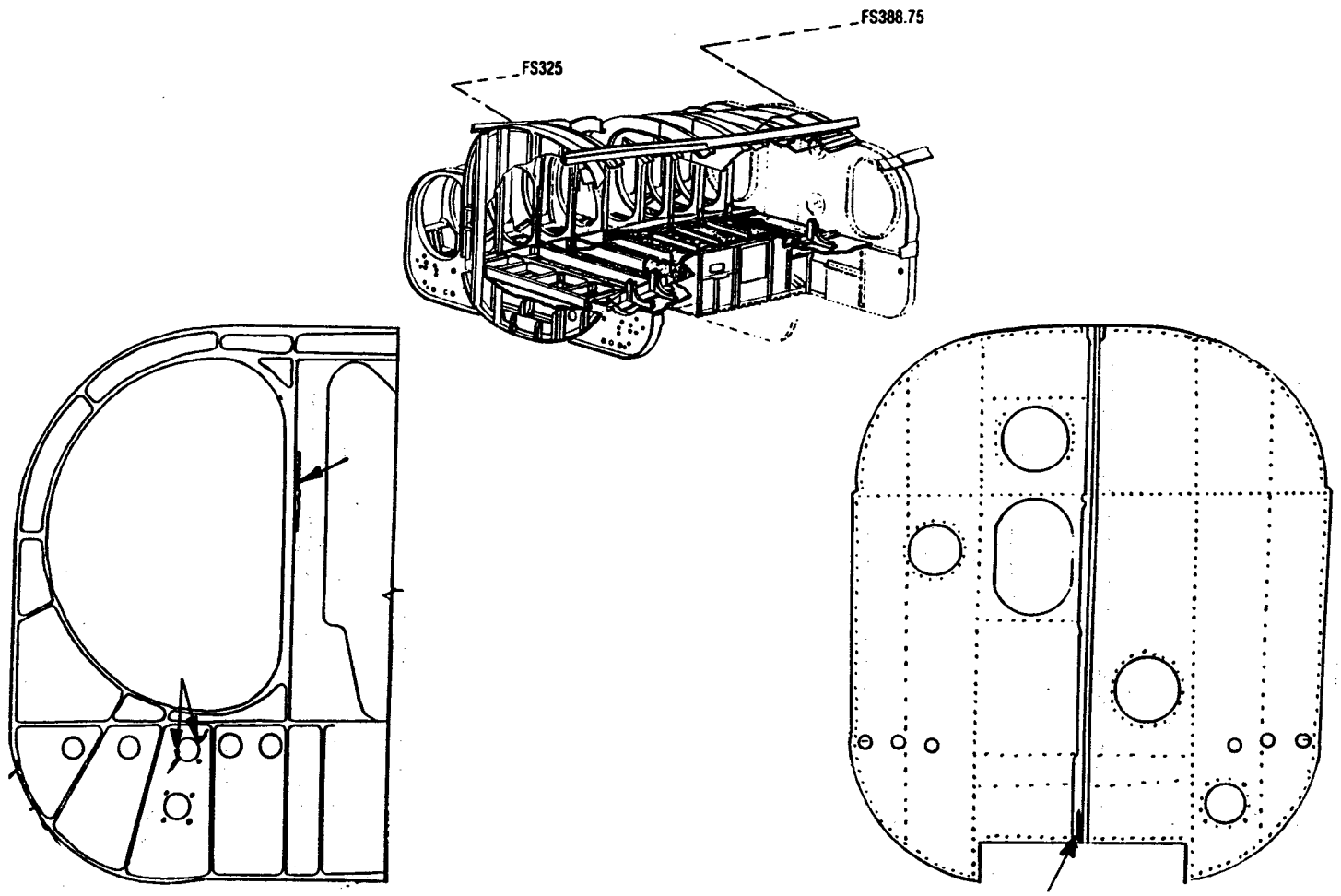

Figure 12 - Cracks on FS 325 Bulkhead

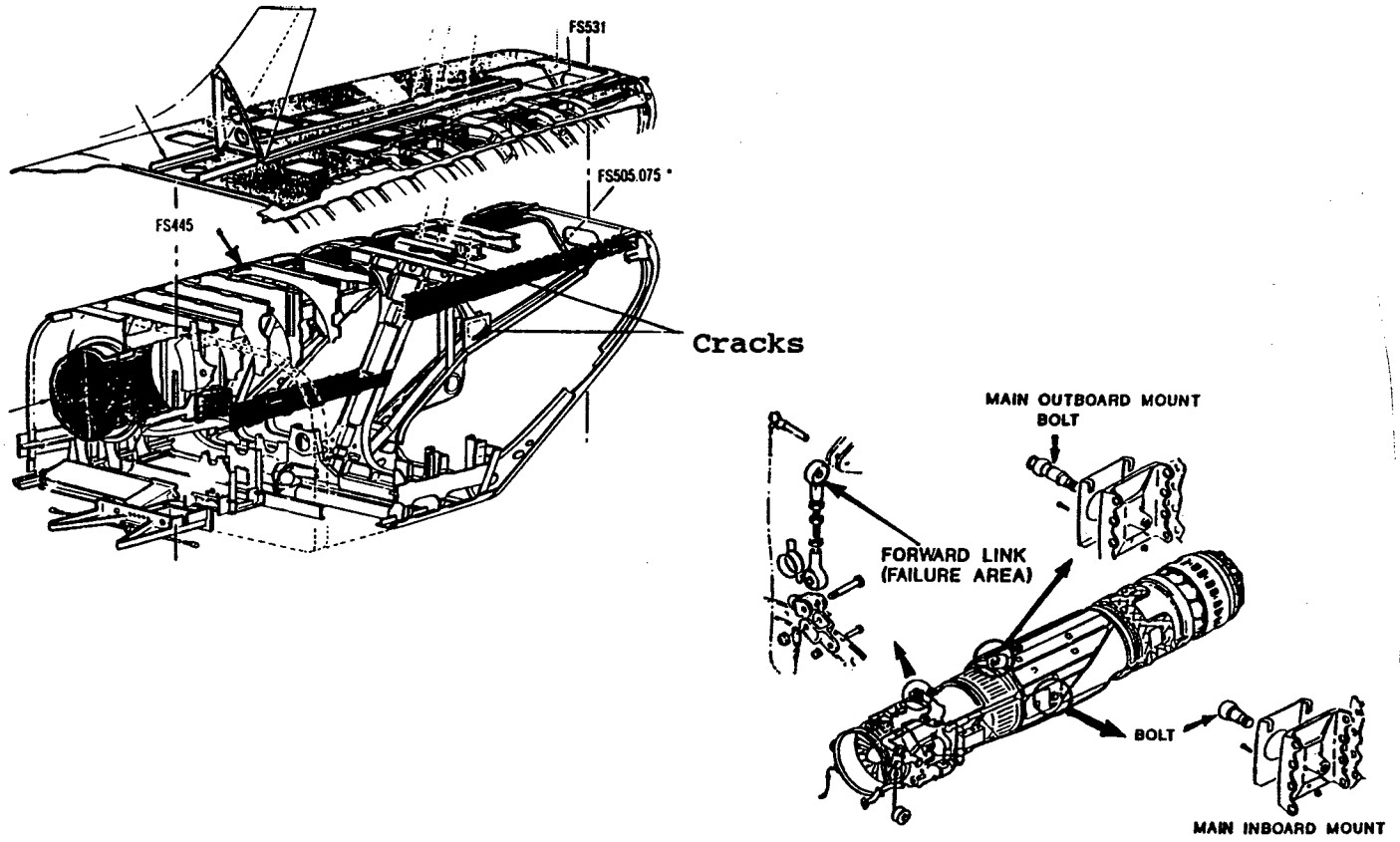

Figure 13 - Cracks in Aft Fuselage Structure

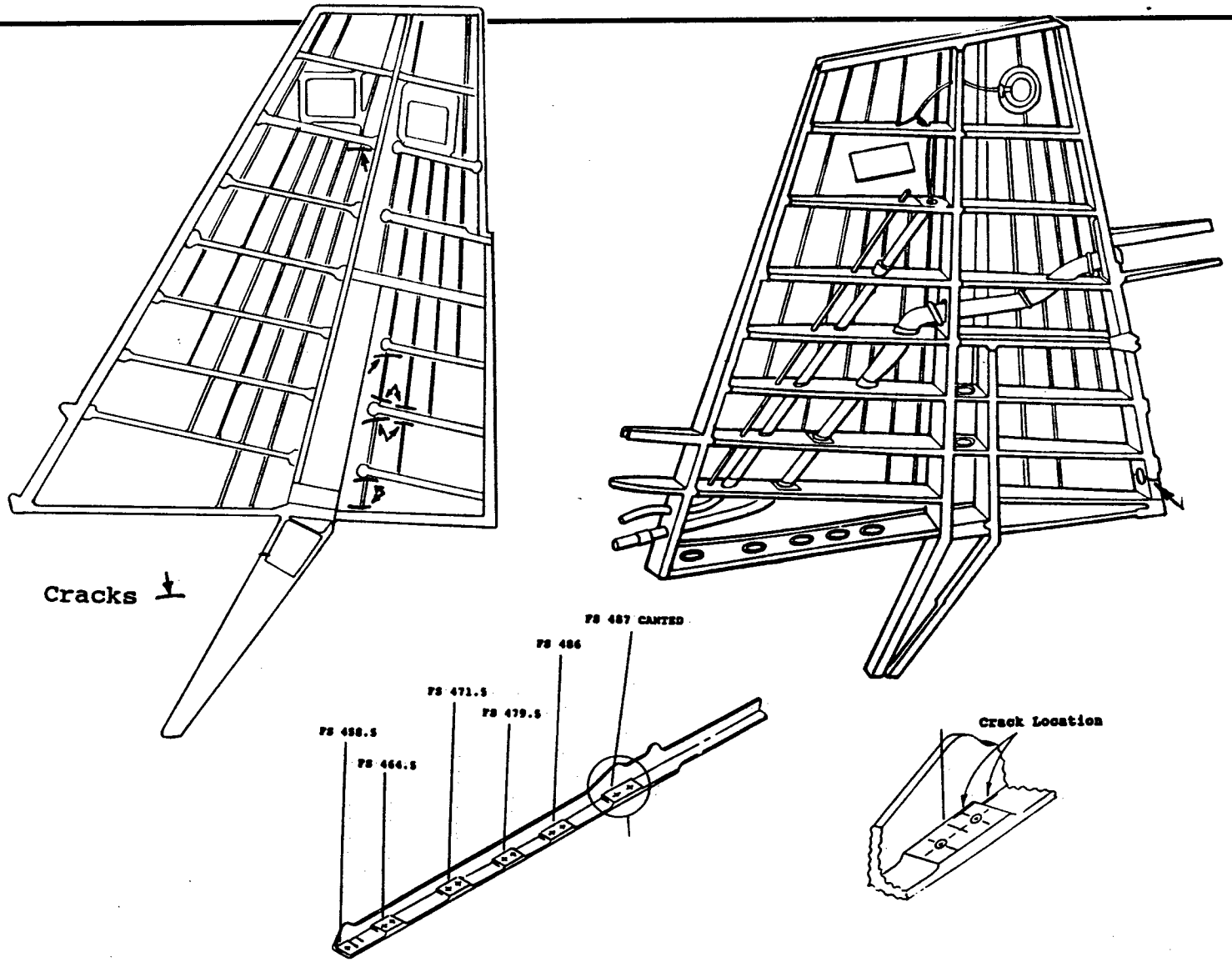

Figure 14 - Cracks on V/Stab Skins and Internal Structure

B-1B Aircraft Structural Integrity Program

A. G. Denyer
Principal Engineering Specialist
Rockwell International

ABSTRACT

The paper presents a review of the impact of the USAF Aircraft Structural Integrity Program (ASIP) on the design, production and eight years of service operations of the USAF B-1B Bomber. The B-1 was the first USAF aircraft procured with fracture mechanics methodology being an integral part of the design requirements, influencing the selection of materials, determination of critical structural components and structural life assessment procedures for both the economic life and the damage tolerance capability of the aircraft. The paper will cover the methodology development, design analysis, structural testing, service life monitoring and the operational experience of the B-1B Aircraft. The paper shows how fracture mechanics was integrated into the design and manufacturing process and how, combined with the service life monitoring aspects of ASIP, it has proven a useful tool for fleet maintenance.

INTRODUCTION

During the 1960's the USAF experienced unexpected early structural failures in service aircraft and in full scale fatigue tests. Particularly disturbing were brittle fractures from small cracks in materials such as D6AC steel and 7178-T6 Aluminum. As a result, the USAF instituted an Aircraft Structural Integrity Program (ASIP), administered under AFR 80-13 (Reference 1) and defined in MIL STD 1530A (Reference 2), to provide a cohesive approach to ensuring structural integrity considerations are not only part of the design and manufacture but are maintained throughout the service life of the aircraft. TABLE 1 shows the major durability and damage tolerance tasks in the ASIP program. For brevity and clarity such tasks as static strength analysis, flutter and dynamics analysis, static tests and flight test have been omitted. The first three phases cover design, development, testing and manufacture while phases four and five cover the maintenance of the structural integrity during the service life time. Phase four is the preparation of the analysis tools that provide the operator with maintenance and inspection requirements for the aircraft while phase five, a USAF responsibility supported by contractor recommendations, is the fleet management, maintenance and reporting procedures that feed back to the analysis programs.

During the same calendar period advances were made in the development of analytic tools to compute the fracture toughness of a component in the presence of a crack and to estimate the rate at which a crack would propagate from an initial crack size to a length at which static failure would occur. In 1970 when the specifications and design requirements for the B-1A Bomber were released they included the ASIP requirements of Reference 2 and the Damage Tolerance Requirements of MIL-A-83444 (Reference 3) which in turn implemented fracture mechanics technology as an integral part of the design approach. The damage tolerance approach as defined in Reference 3 requires single load path structure to be qualified as slow

TABLE 1 - Aircraft Structural Integrity Tasks Involving Durability and Damage Tolerance

PHASE 1	PHASE 2	PHASE 3	PHASE 4	PHASE 5
Design Information	Design Analysis & Development Tests	Full Scale Testing	Force Management Data Package	Force Management
Design Service Life	Loads Analysis	Durability & Damage Tolerance Tests	Final Durability & Damage Tolerance Analysis	Loads/Environment Spectra Survey
Structural Design Criteria	Design Service Loads Spectra	Evaluation of Tests	Force Structrual Maintenance Plan	Individual Aircraft Tracking Program
Durability & Damage Tolerance Control Plans	Stress Analysis		Loads/Environment Spectra Survey	Individual Aircraft Maintenance Times
	Durability & Damage Tolerance Analysis		Individual Aircraft Tracking Program	Structural Maintenance Records
	Design Development Tests			

crack growth while multi-load path structure with crack arrest features may be qualified as slow crack growth or as fail-safe structure.

Rockwell elected to qualify all B-1 safety of flight structure as slow crack growth assuming the presence of flaws in the most unfavorable position and computing the damage tolerance life using the principles of linear elastic fracture mechanics. Implementation of the ASIP program included designing and testing the structure to both durability and damage tolerance requirements and establishing a damage tolerance control plan to ensure the quality of design and manufacturing. Maintenance of structural integrity throughout the service life is accomplished with the aid of the Force Management Data Package (See TABLE 1), a series of programs designed to monitor the force and provide an assessment of the structural capability under service operations.

B-1B BACKGROUND

The B-1B Bomber is a variable geometry (swing wing) aircraft capable of high subsonic speed while terrain following at low altitude (below 500 feet). The aircraft design mission includes low altitude penetration of enemy airspace and weapon delivery combined with long range cruise and in-flight refueling.

The B-1B is a performance enhanced derivative of the B-1A pre-production aircraft which was designed and built in the 1970 through 1976 time period. The design development and design verification tests, proof load and strain survey tests, ground vibration and flight tests accomplished on the B-1A applied to the B-1B for which engineering commenced in 1982 with first flight occurring in 1984. The B-1B design incorporated changes as a result of the B-1A design development, design verification and flight tests. The first aircraft entered service with the USAF in 1985 and the 100th production aircraft was completed in 1988.

METHODOLOGY DEVELOPMENT

In order to meet the analysis requirements of the B-1 contract, Rockwell undertook extensive methodology development programs in the fields of load spectrum generation and in crack growth rate and fracture toughness analysis procedures.

Spectrum Generation Methodology

The spectrum generation studies resulted in the Rockwell Automated Stress Spectrum computer Program (RASSP) shown schematically in FIGURE 1. The major consideration when writing the program was to create an integrated system that would generate local stress spectra at any location within the primary airframe with minimal user input. The spectra would be in flight-by-flight sequence, maintaining the statistics of the mission mix, contain sufficient missions to be representative of the lifetime usage and define the maneuver, gust and ground handling environment. The variable geometry aircraft causes significant changes in mean stress levels as the wings are moved, making the sequence of mission segments within a flight an important consideration. The input data to the program consists of the flight profiles in terms of flight parameters such as weight, Mach number, altitude and aircraft geometry, and the mission mix representing the service life of the aircraft. Both the flight profiles and the aircraft loading environment discussed below are kept on databases for access by the program. The maneuver, gust and ground handling frequency of occurrence statistics are maintained in the form of cumulative occurrences of load factors (Nz) at the aircraft center of gravity. Load factor data were developed to cover the mission segments defined in the mission profiles. MIL-A-8866B (Reference 4) provided the maneuver load factors for all mission segments except terrain following for which the flight simulator was used to generate a load factor trace for selected routes. The gust load factor occurrences were computed using a continuous turbulence approach (power spectral density) according to MIL-A-008861A (Reference 5). The spectrum generation procedure compiles load factor spectra on a flight segment by segment sequence for each mission in the mix. The load factor spectra for multiple missions representing the same flight profile maintain the same segment sequence but the load cycles within each segment differ in magnitude and sequence thus allowing the inclusion of infrequent high loads within the appropriate statistics. Gust and maneuver load cycles are randomly sequenced within a segment. Terrain following at altitudes below 500 feet results in an environment of high maneuver activity in severe gust conditions. The spectrum generation program thus superimposes the gust cycles on the terrain following maneuver spectrum.

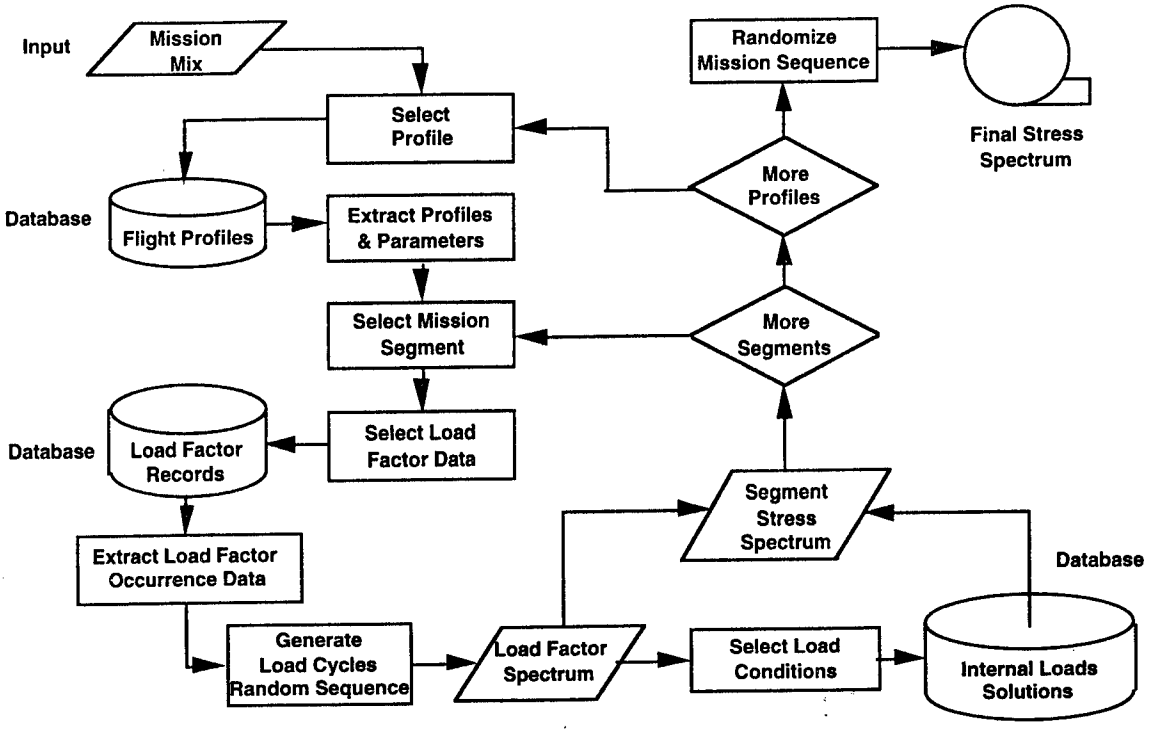

Figure 1 - Spectrum Generation Flow Chart

The load factor spectrum is converted to a stress spectrum at any location in the airframe by linking the spectrum program to a database holding the internal loads for over 100 load conditions covering the envelope of the operational usage in terms of aircraft gross weight, Mach number, altitude and aircraft geometry. These conditions include ground handling operations, symmetric maneuver, roll maneuver, vertical and lateral gust situations. A 77,000 element, 107,000 degrees of freedom, half airframe NASTRAN model (Reference 6) was used to compute the internal loads necessary to support the fatigue analysis.

Crack Growth Methodology Development

The analytical structural damage is accumulated as increasing crack lengths due to the structural loading caused by the aircraft usage. The structural loading takes the form of a sequential stress file developed as defined above. The B-1 analysis methodology is based on the principles of linear elastic fracture mechanics (LEFM) where the stress state at the crack tip is characterized by a single parameter, the stress intensity factor K. Furthermore the sub-critical flaw growth is defined as a function of the cyclic range of the stress intensity factor. The crack growth is computed per cycle (da/dN) using a crack growth rate equation fitted to material property sub critical flaw growth rate data and an integration procedure to obtain the complete crack growth curve. A modified Walker equation (Reference 7) with two slopes covering the range of delta K was selected as the best representation of the test data accounting for the stress ratio effects.

CRACK GROWTH RATE EQUATION

$$\frac{da}{dN} = C\left[(1-R)^{m-1} * \Delta K\right]^n \qquad If\,..\,R \geq 0$$

$$\frac{da}{dN} = C\left[(1-R)^{q} * K_{max}\right]^n \qquad If\,..\,R < 0$$

where

R is *Ratio of applied stress* $\frac{\sigma_{min}}{\sigma_{max}}$

$\Delta K = K_{max} - K_{min}$

K_{max} *Stress Intensity Factor due to applied stress* σ_{max}

K_{min} *Stress Intensity Factor due to applied stress* σ_{min}

C ,n , m and q *Material dependent constants derived from compact tension and center through crack test specimens*

Other parameters used in the modified Walker equation for crack growth predictions are the delta K threshold (a range of K below which no growth occurs) and the values of the stress ratio (R) above and below which the stress ratio changes have no impact. The stress intensity factors are a function of the gross area stress remote from the crack, the local part geometry, the geometry and shape of the flaw. Literature searches and analytical development resulted in a library of stress intensity solutions for both part through and through the thickness cracks originating from holes, edges of plates, surfaces of plates and embedded flaws.

The service loadings of aircraft are of a variable amplitude, and numerous studies have noted the load interaction effects of variable amplitude on the crack growth life. Tensile overloads introduce significant retardation of the crack growth rate while compression loads in a tension / compression spectrum tends to accelerate the crack growth. The load interaction model developed for the B-1 analysis is a modified Willenborg model (Reference 7) which assumes that the overload retardation effect is caused by local variations in the local stress field as the crack grows through the compressive residual stress zone produced by the overload. The effective stress is then defined as the (remote field stress - the local residual stress), and this effective stress is used to calculate the effective stress intensity factor. The Willenborg model predicts that the maximum retardation will occur immediately after the overload and the growth rate will return to its constant amplitude counterpart when the current interaction zone reaches the end of the overload interaction zone. The Willenborg model is modified to reflect an increased growth rate (acceleration) in situations where the spectrum contains compressive loads or underloads (small tension cycles) in low - high sequence loadings.

Test Program in Support of Fracture Mechanics Requirements

The B-1 contract required that "a system of procedures and specifications sufficient to preclude utilization of material with inadequate toughness in critical areas" be developed and implemented. At the inception of the B-1 program, only limited test data was available pertaining to the materials of interest. A comprehensive test program was conducted to determine the fracture mechanics material properties for aluminum, titanium and steel alloys as well as the effects of the welding and diffusion bonding processes. Testing was initiated in December 1970 and continued for four years during which time 1804 tests were made to define material properties (K_{1c}, K_c, K_{1scc} and da/dN) and to verify crack growth spectrum loading models. Tests were conducted on 14 alloys (aluminum 2024, 2124, 2219, 7049, 7050, 7075, and 7175 in selected tempers; titanium alloy Ti-6Al-4V; steel alloys 9Ni-4Co-.20C, 9Ni-4Co-.30C and 300 M; corrosion resistant steel PH13-8Mo; nickel base alloy Inconel 718 and a fastener material MP35N). Approximately 30% of the of the program effort was directed towards evaluations of thirty-one lots of Ti-6Al-4V alloy while another 30% of the effort investigated seven or more lots each of 2024, 2124, 9Ni-4Co-.20 and PH13-8Mo. The specimens used in the testing were of four types: compact tension (CT) for K_{1c} , K_c and da/dN tests, center cracked tension (CCT) for K_c and da/dN tests, and part through crack (PCT) specimens for K_{1c} and da/dN tests and finally double cantilever beam specimens for K_{1scc} tests. The CCT specimen configuration was used for sheet and welds in sheets because the CT sheet specimens buckle under these test conditions. The results of this test program combined with literature data, formed the database for the durability and damage tolerance analysis performed in support of the B-1B design and subsequent analyses.

DESIGN INFORMATION

Design Criteria and Requirements

For the purposes of brevity, this paper will consider only those aspects of the design criteria that affect the integrity of the primary structure from the standpoint of durability and damage tolerance.

The design goal of the B-1B aircraft is 30 years or 9,681 flight hours comprising the mission mix shown in TABLE 2. This differed from the B-1A where the design life was 20 years and 13,500 flight hours. The contract required both analytical and test verification of the structural economic life of one lifetime (9681 flight hours) assuming the initial condition is nominally unflawed structure, as built under normal production and inspection techniques, and also a damage tolerance verification of two lifetimes (19362 flight hours) assuming the initial condition is an undetected flaw equal to the production line inspection capability. The design profiles, a sample of which is shown in FIGURE 2, were provided in the specification for the purposes of fatigue analysis and testing. An indication of the expected load severity may be inferred by the design criteria of 3.0g limit load with the wings aft of 65 degrees and 2.0g limit load when the wings are forward of 65 degrees. Forward wing sweep geometry is used for take offs, landings and subsonic cruise while the aft wing sweep position is used for low level penetration and occasional high speed dash. Atmospheric gusts cause loads comparable in magnitude to the maneuver loads and are especially significant during terrain following operations.

TABLE 2 - B-1B Design Mission Mix

Mission Code	Occurrences. per year	Mission Definition	Mission Flt Hours
1	53	Low altitude training with automatic terrain following	4.21
2	12	Low altitude training with manual terrain following	4.21
3	4	Low altitude training with automatic terrain following (Heavy weight)	4.2
4	7	High altitude training (without air refueling)	2.71
5	3	High altitude training (with air refueling)	3.01
6	2	Dispersal mission	2
8	6	Ground alert	0
		Average	3.98

Figure 2 - Typical Mission Profile

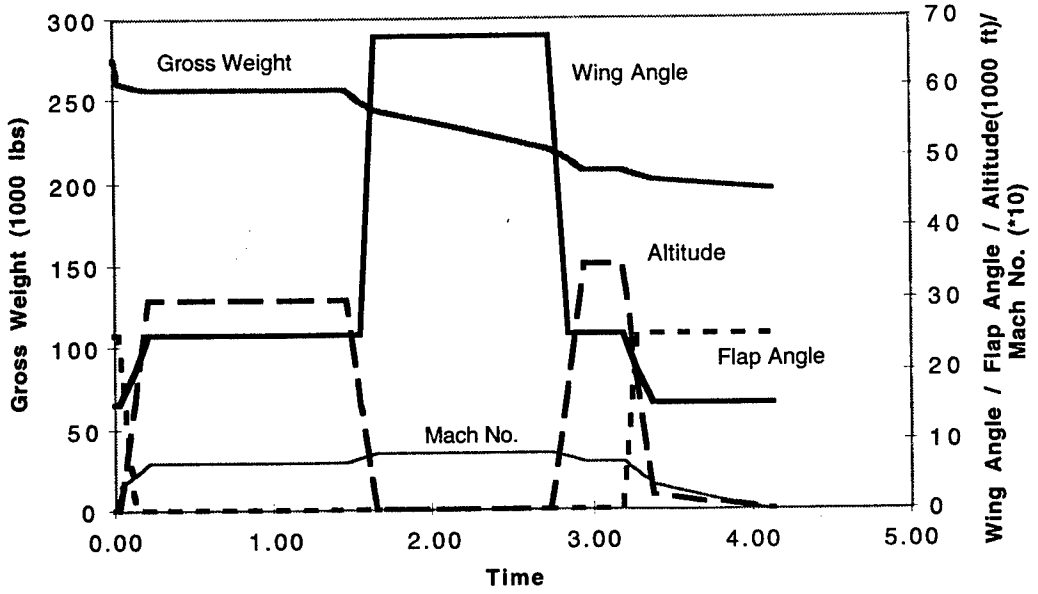

Material Selection

The material selection for the primary structure, shown in FIGURE 3, was significantly influenced by fatigue and fracture mechanics considerations. Forty-three percent of the structural weight is aluminum and within this is the lower cover of the outer wing panel manufactured from 2219-T851 billets selected for the high fracture toughness, slow crack growth capability and quality control in billet manufacture. Other aluminum alloys selected were the well-characterized 2024-T3 for many fuselage and stabilizer skins and 7075 T-73 for forgings and extrusions. The wing carry through structure including the wing pivot lug plates is titanium 6Al-4V. Another major load carrying member is the stabilizer support fitting which carries the horizontal and vertical stabilizers and is built up from four 9Ni-4Co-0.20C steel forgings welded together. The 9Ni-4Co-0.20C steel was also chosen for its toughness and weldability.

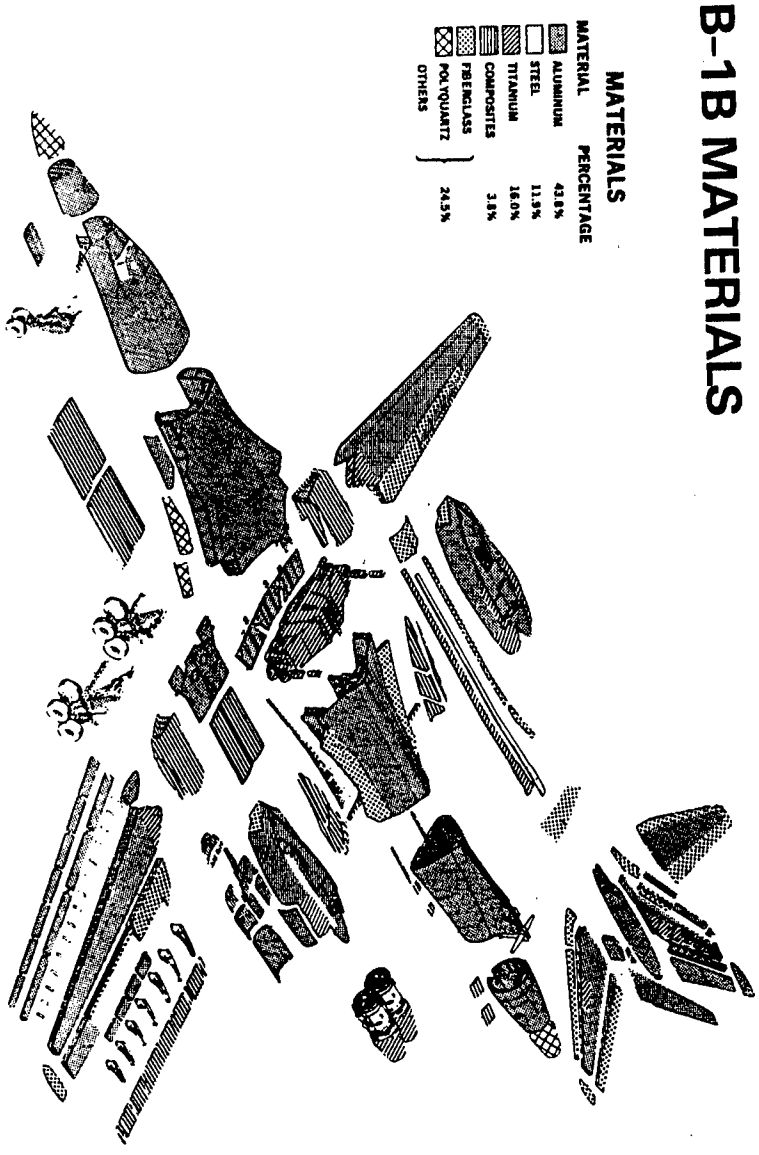

Figure 3 - B-1B Materials

Durability and Damage Tolerance (DADT) Control Plan

Having selected materials which have inherently good durability and damage tolerance the next phase was to ensure a design and manufacturing quality that would meet the life requirements of the contract. A DADT control plan established the following major objectives:

1 Categorize structural members, thus recognizing truly critical components
2 Fracture mechanics analysis supported by tests to verify adequate durability and damage tolerance life
3 Identify fracture critical zones and parts on design drawings for the purposes of ensuring appropriate manufacturing and inspection processes.
4 Preclude utilization of material with inadequate fracture toughness in critical structural areas.
5 Establish traceability records, from the billet to the final assembly, for all fracture toughness controlled parts
6 Develop and implement Non-Destructive Inspection (NDI) techniques to preclude rogue flaws that may cause premature cracking

The structure is categorized as shown in FIGURE 4. Potential DADT critical parts, (i.e. primary structural parts predominantly loaded in tension), were reviewed for both damage tolerance (safety) and durability (economic) impacts. The most critical parts are those whose failure would cause loss of the aircraft and are designated Category 1. All single load path components are designated Category 1. A second damage tolerance group (Category 2) comprises those parts assembled on critical safety of flight components or which are designed by damage tolerance requirements. Designed by damage tolerance requirements in this context means that the part dimensions were increased over that necessary for static strength or that the part was subjected to special processes or assembly techniques to enhance the service reliability. Economic or durability considerations led to two further categories depending on whether the part was economically repairable or was designed by fatigue requirements. Here again, designed by fatigue requirements means that the part dimensions were increased over that necessary for static strength or that the part was subjected to special processes or assembly techniques to enhance the resistance to fatigue cracking. Selected parts were added, by exception, to the various categories when experience with similar parts on other aircraft indicated that benefit would be gained by adding damage tolerance and or durability controls in design and manufacture. As a result of this procedure 53 parts were designated Category 1 damage tolerance critical and 13 parts designated Category 2. 107 structural locations, including those designated fracture critical were defined as durability critical and subjected to durability analysis.

All critical zones of the Category 1 and 2 structure were designated as such on the production drawings with references to the required manufacturing and inspection processes. Further, all Category 1 and 2 structure was made of fracture controlled material requiring fracture toughness (K_{1c}) tests from every raw material billet and in addition a tracking procedure to provide traceability from the billet, through the machining procedures to the final assembly.

Concurrent with the development of analytic methodology, NDI development and implementation ensured manufacturing reliability and high standards consistent with the design assumptions. The holes for the Taper-Lok fasteners in the critical areas of the wing and wing carry through structure, for example, were inspected by both air gage and blue pin methods.

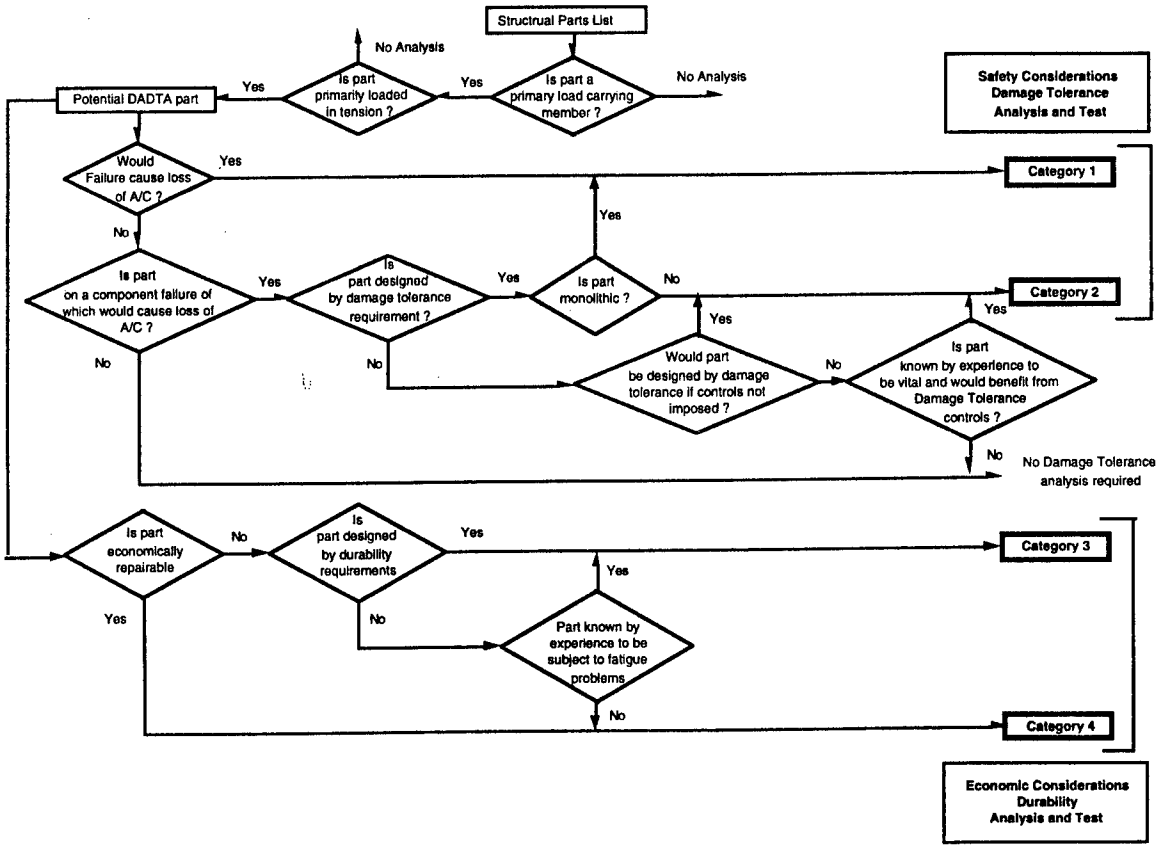

Figure 4 - Structural Parts Classification Logic

DESIGN ANALYSIS AND DEVELOPMENT TEST PHASE

Design Analysis

Both the durability and damage tolerance design analyses used the fracture mechanics approach, the only difference being the selection of initial and final flaw sizes and the criteria of requiring one lifetime of durability and two lifetimes of damage tolerance to preclude any major inspections during the service life.

This approach was selected although many components such as the wing pivot lug plates and the wing carry through lower wing skin were multi-load path. The basis for the design analysis was the anticipated usage shown in TABLE 2 repeated 30 times to represent the lifetime usage. The spectrum was compiled using the RASSP program, described above, which permitted the extraction of a local stress spectrum at any location in the airframe by requesting the appropriate elements from the airframe NASTRAN finite element model. The stress at each critical location is the defined as a function of the loads and stresses in one or more elements of the internal loads model. Typical initial flaw size for durability is 0.01 inches defined as the equivalent initial flaw size (EIFS) such that the crack growth analysis

commencing at this size represents the life of a nominally unflawed part. The final allowable crack size for durability is the minimum of: the crack length that would cause functional impairment (such as fuel leaks); a crack that would be uneconomic to repair; or a crack of a size that would exhibit rapid unstable crack growth if the part be subjected to design limit load. As defined in MIL A-83444, 0.05 inches is the damage tolerance starting crack size for areas of local high stress concentrations, such as bolt holes, while 0.125 inches depth is used for other locations. Based on test demonstration, an exception of 0.01 inch damage tolerance initial flaw was taken for holes, with installed Taper Lok fasteners, that were inspected by both air gage and blue pin procedures. The final flaw size for damage tolerance analysis is that which would exhibit rapid unstable crack growth if the part be subjected to design limit load. The analyses performed on all critical structural locations as defined in the durability and damage tolerance control plan showed durability lives in excess of 9681 flight hours and damage tolerance lives of more than 19362 flight hours.

Design Development Tests

The B-1A Design Development Test (DDT) program accomplished on the B-1A aircraft structure covered a wide range of items throughout the airframe, testing both static strength and fatigue capability of design concepts. The test program is shown in FIGURE 5 . The spectra applied to the fatigue test specimens included constant amplitude and flight by flight sequenced variable amplitude loadings. Since much of the B-1A and B-1B structure is considered common, these tests were applicable to the B-1B design. Additional tests, conducted to cover those areas of concern resulting from design changes, increased loads, new materials and new design features incorporated in the B-1B, are summarized in FIGURE 6.

FULL SCALE TEST PROGRAM

Design Verification Tests

The design verification test program for the B-1A included flight, static strength, ground vibration, flutter, acoustics and fatigue tests. Only the fatigue tests undertaken to verify the durability and damage tolerance capability of the finalized B-1A design will be discussed here. Two major airframe sections shown in FIGURE 7 and defined in detail below were subjected to both durability and damage tolerance tests. Separate fatigue tests were completed on a nacelle beam specimen, a leading edge slat specimen and the main and nose landing gears. All specimens were subjected to flight by flight spectra loading, that was identical to the design analysis spectra with the exception of the elimination of high frequency/low load amplitude cycles. On the basis of crack growth analysis, the eliminated cycles contributed less than 5% of the accumulated structural damage. The B-1A spectrum used in these tests differed from the B-1B spectrum in that the B-1B training missions do not include a supersonic leg, have reduced flight hours per life (9681 compared to 13500 for the B-1A) and an increased number of missions per life (2430 compared to 1280 for the B-1A).

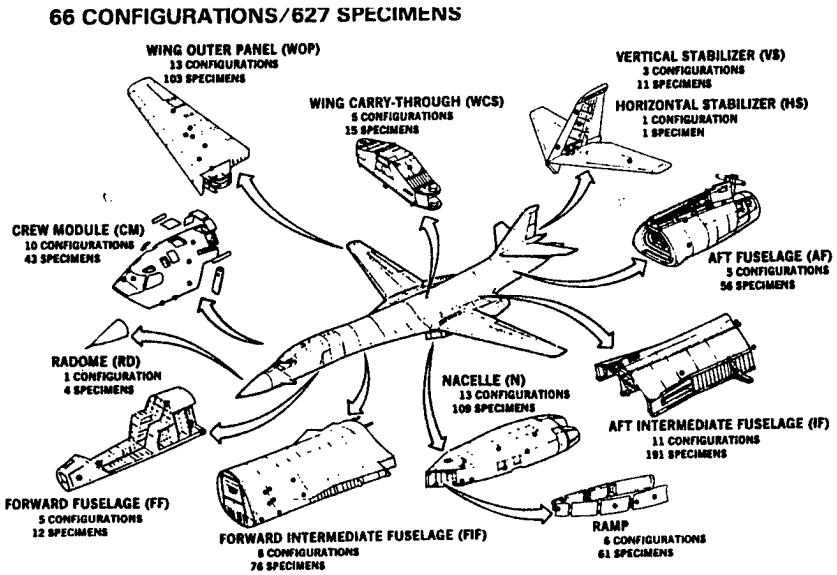

Figure 5 - B-1A Design Development Tests

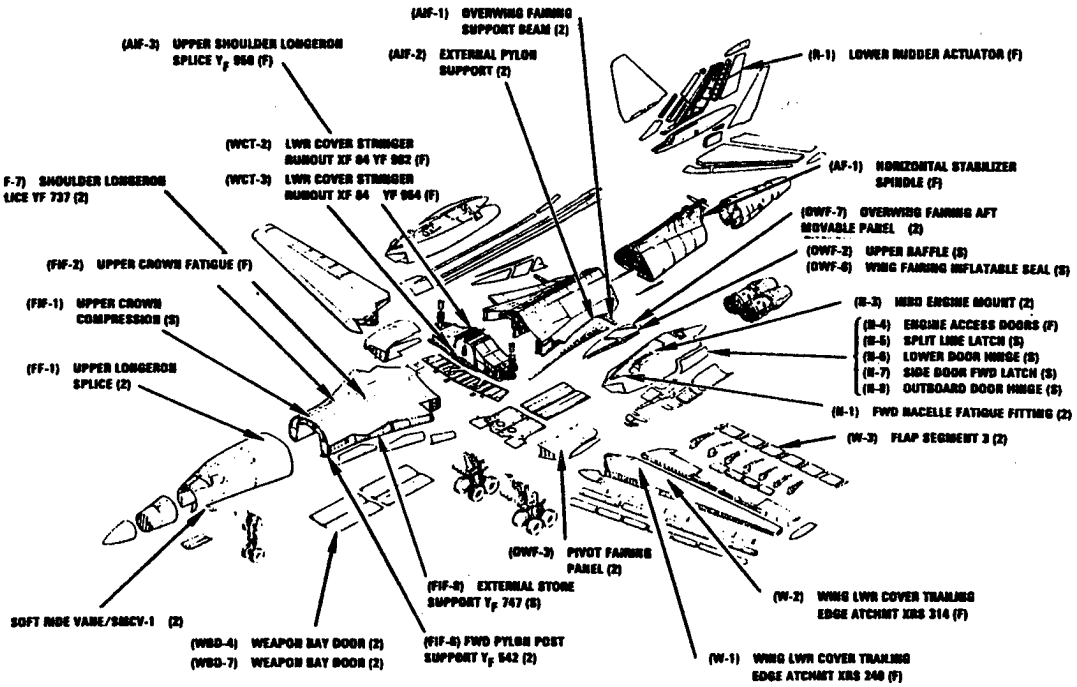

Figure 6 - B-1B Design Development Tests

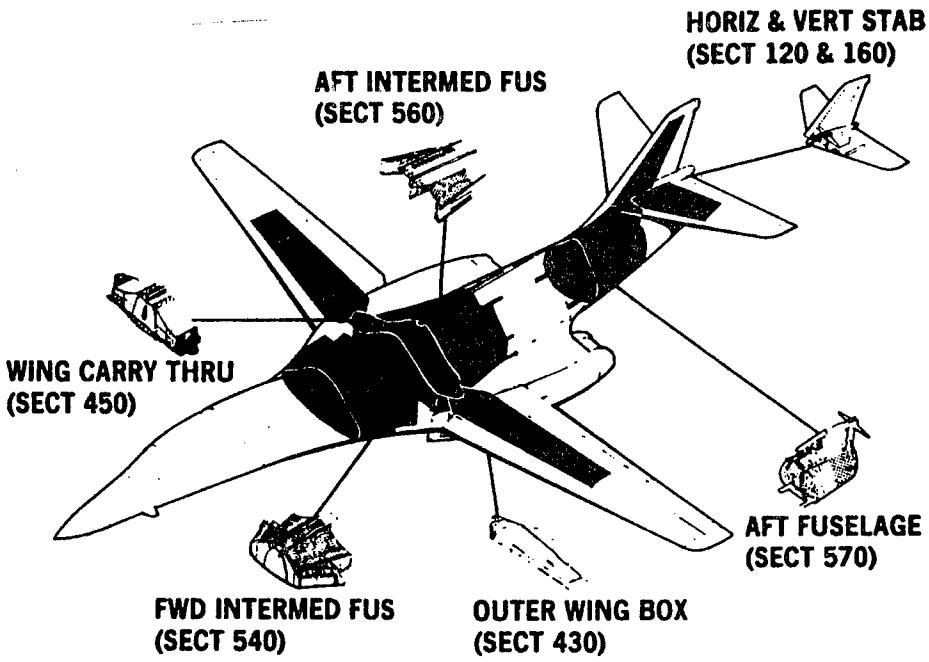

Figure 7 - Design Verification Tests

The nacelle beam test showed no indication of cracks at the completion of the four lifetime test. The slat specimen had cracked ribs and skin after 3.15 lives, was repaired, and the test completed. The landing gears, tested by the manufacturers (Menasco - Nose Gear and Cleveland Pneumatic - Main Gear), completed 4 lifetimes of durability testing without significant damage.

Wing / Wing Carry Through / Center Fuselage Specimen

The structure consisted of the wing carry through box, the wing pivots and large sections of each outboard wing panel and the forward and aft intermediate fuselage. The outer wing panels included simulated flap and slat tracks and the main landing gear fittings were installed on the carry through box. Dummy truss structure was attached to forward and aft fuselage to facilitate the application of fuselage bending loads. The specimen was extensively strain gaged with recordings taken during the first occurrence of the maximum spectrum load and at each life thereafter. The specimen was installed in the loading fixture that was designed to maintain a constant loading on the structure while the wing angle was changed. The loads were applied by hydraulic jacks attached to formers and pads on the structural surfaces and by means of controlled jacks at the specimen boundary members. The applied loads, including the boundary loads, were computed using the NASTRAN finite element model to ensure that the test loads matched the analytic conditions. The spectrum included both flight loads, with the wing sweeps at the appropriate times, and ground loads which were applied at the landing

gear attachment fittings. The wing/wing carry through/center fuselage specimen was subjected to two lifetimes of durability testing. Minor cracking occurred during the test, repairs undertaken and design changes accomplished during B-1B design. Structural changes included refinement in the design of the wing stringer runouts to reduce the stress concentration and an area increase in the forward intermediate dorsal longeron. Selected holes in the dorsal longeron to skin attachment and the dorsal longeron splice were cold worked in the B-1B production. At the completion of the durability test, saw cuts were inserted at selected locations and the specimen subjected to a further one lifetime of loads while monitoring the natural and induced cracks. The specimen was finally subjected to a residual strength test where the design limit load of 2g was applied with the wings in the forward swept position. The specimen demonstrated capability of withstanding design limit load after 1 lifetime of damage tolerance testing. After the test completion the structure was torn down and numerous small cracks were found. Each crack was analyzed to determine if structural design changes were needed on production aircraft.

Aft Fuselage / Empennage Specimen

The aft fuselage / empennage consisted of the aft fuselage, stabilizer support fitting a left hand horizontal stabilizer, dummy right hand stabilizer and the vertical stabilizer.
The specimen was loaded with pads providing the distributed loading over the structural surfaces where applicable, straps on the aft fuselage and as point loads at local attachments. As with the wing carry through specimen the loads were developed with the aid of the NASTRAN finite element model to match the analytic loads. The spectrum included symmetric and roll maneuvers as well as vertical and lateral gust loads. The specimen was extensively strain gaged and the loads recorded during the first application of the maximum spectrum load and at each life thereafter. After 0.7 lifetimes of durability testing, cracks were discovered in the 9Ni-4Co-.20C Steel stabilizer support fitting side plates below the spindle arm. The cracks originated from a weld relief hole in the main weld joining two major forgings. The fractured material was removed for metallurgical examination and the component repaired by welding. After 2.3 lifetimes of durability testing elox manufactured flaws were introduced in critical areas including the armpits of the stabilizer support fitting. The introduced flaws and the naturally formed cracks from the weld area were monitored for an additional 0.7 lifetimes of testing. The specimen was then subjected to 1530 cycles of design limit load (right rolls) to demonstrate residual strength before failure of the component.
The stabilizer support fitting was extensively redesigned for the B-1B. The forgings were changed so that the weld joint was in an area of low stress and the armpit regions of the fitting had significantly increased radius and increased thickness and thus reduced stress levels. Figure 8 reflects the design changes. This redesign was tested to three lifetimes of the B-1B spectrum.

Full Scale, Complete Air-vehicle Fatigue Test

A planned complete air-vehicle fatigue test of the B-1B configuration loaded to the B-1B design spectrum was deleted from the program in the interests of cost and schedule. The B-1B spectrum was determined by analysis to be less severe than the B-1A design and test spectra.

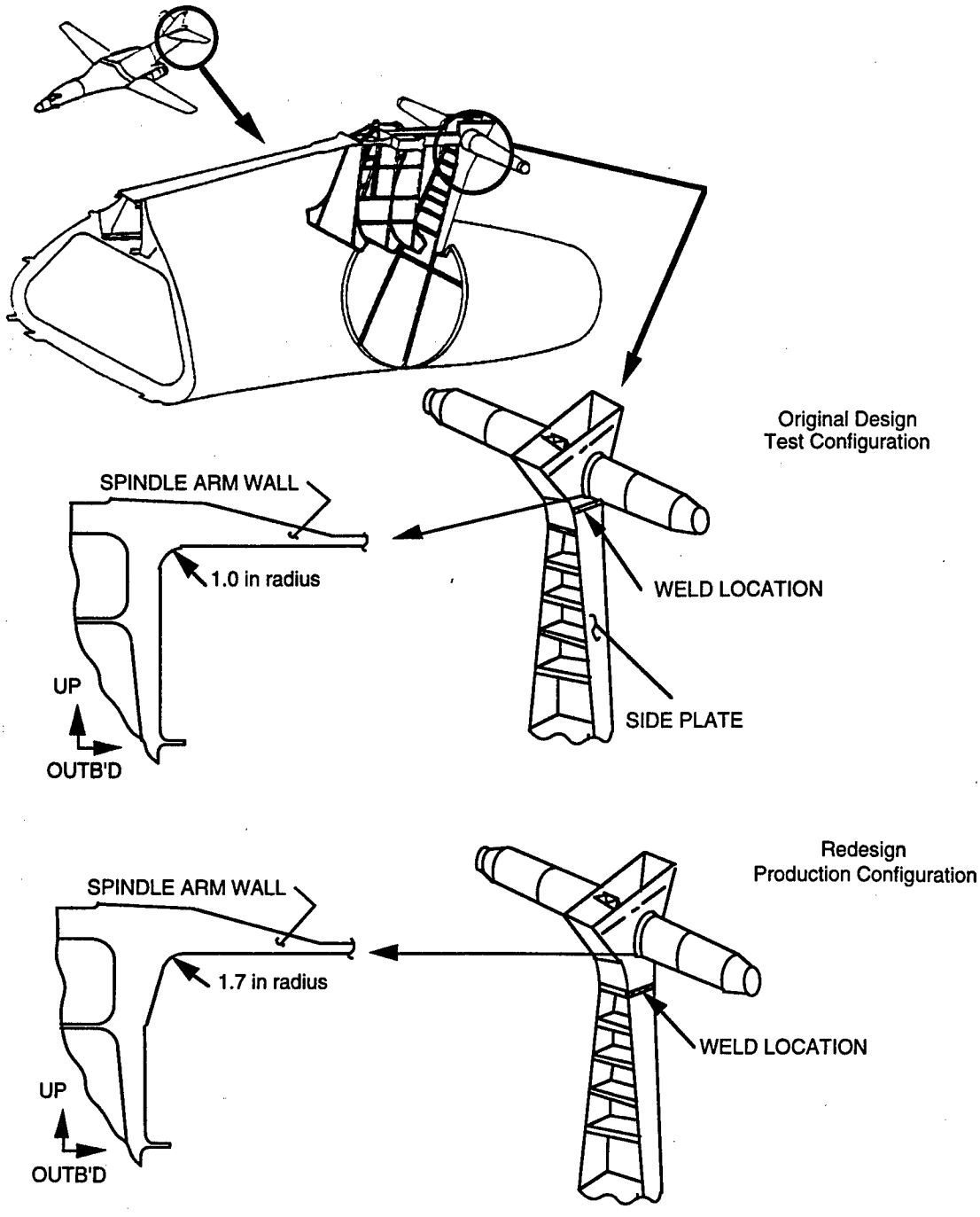

Figure 8 - Stabilizer Support Fitting Design Change

FORCE STRUCTURAL MAINTENANCE PACKAGE

As shown in FIGURE 1, the force structural maintenance package provides the tools necessary to ensure that the structural integrity is maintained throughout the service life. These programs and reports, which collectively provide the service life capability of the fleet and the maintenance requirements, utilize the operational history monitored with an onboard recorder. The Individual Aircraft Tracking Program analyses the flight records of each aircraft to determine the rate at which the useful economic life is being consumed and to define the necessary structural inspections and maintenance. The Loads/Environmental Spectra Survey (L/ESS) Program accumulates the flight load data received from the field into a database that keeps the usage statistics necessary to reconstruct the average B-1B mission profiles, the mission mix, load factor records and strain gage records. The load spectrum generated from the L/ESS database is then used to update the durability and damage tolerance assessment thus reflecting the actual usage. The Force Structural Maintenance Plan (FSMP) provides the inspection and maintenance requirements.

Loads Monitoring Provisions

All of the 100 aircraft fleet are equipped with a microprocessor based solid state data collection and storage device, known as the Structural Data Collector (SDC), linked to 49 sensors. The SDC receives analog inputs from 6 strain gages and from control surface position indicators. The majority of the of the signals received by the SDC are provided via the Central Integrated Test System (CITS) serial digital link. CITS monitors various aircraft systems, including the Central Air Data Computer, Fuel CG Management System, Stability and Control Augmentation System and Engine Monitoring System. TABLE 3 defines the list of parameters monitored and processed by the SDC. The CITS Control and Display Panel allows the manual entry of the necessary mission documentary data shown at the foot of TABLE 3.

Each parameter is monitored at appropriate sample rates shown in TABLE 3 and validated to protect the SDC memory from erroneous information. Validation tests include a maximum and minimum allowable value test, a maximum allowable rate of change test and an excessive activity test. After validation each parameter is processed through data compression algorithms. These algorithms significantly increase the number of flight hours of data that can be stored in the SDC memory by systematically eliminating insignificant or redundant information.

Individual Aircraft Tracking (IAT) Program

The IAT Program monitors each aircraft throughout the lifetime and computes damage assessments at twenty-two selected locations in the airframe and at three locations in each main landing gear structure. The stress history for some tracked locations is compiled directly from strain gage records while for others a predetermined equation relates the stress to the aircraft load factors and the mission parameters such as gross weight, altitude, Mach number and aircraft geometry (wing angle and flap angle). The accumulated structural damage is estimated with the same crack growth approach used for the design analysis and applied to both the durability and damage tolerance regions of the crack growth curve. A realistic assessment of the accumulated damage on any aircraft requires that all missions be included. Inevitably the SDC does not provide records for all flights due to the SDC being inoperative,

TABLE 3 - Mission Parameters Monitored and Processed

Parameter	Unit	Signal Type	Data Compression Method	Sample Rate /sec	Compression Constants	
					Threshold	Delta
Strain Gages						
Stabilizer Support Fitting Left Hand Side	ksi	Analog	PV	40	None	6.19
Stabilizer Support Fitting Right Hand Side	ksi	Analog	PV	40	None	6.19
Stabilizer Support Fitting Side Plate	ksi	Analog	PV	40	None	8.25
Wing Sweep Actuator	k lb	Analog	PV	40	None	42.70
Wing Lower Skin	ksi	Analog	PV	40	None	4.00
Forward Fuselage Dorsal Longeron	ksi	Analog	PV	40	None	8.29
Vertical Acceleration (Nz) (Air)	g	Analog	PV + A	40	0.77/1.2	0.14
Vertical Acceleration (Nz) (Ground)	g	Analog	PV + A	40	0.84/1.13	0.14
Lateral Acceleration (Ny) (Air)	g	Analog	PV + A	20	+/- 0.101	0.10
Lateral Acceleration (Ny) (Ground)	g	Analog	PV + A	20	+/- 0.047	0.05
Longitudinal Acceleration (Nx) (Air)	g	Analog	PV + A	20	+/- 0.094	0.09
Longitudinal Acceleration (Nx) (Ground)	g	Analog	PV + A	20	+/- 0.062	0.06
Pitch Rate	deg/sec	Digital	PV + A	8	+/- 2.10	2.10
Yaw Rate (Air)	deg/sec	Digital	PV + A	8	+/- 4.88	4.88
Yaw Rate (Ground)	deg/sec	Digital	PV + A	8	+/- 2.10	2.10
Roll Rate	deg/sec	Digital	PV + A	8	+/- 1.05	1.05
Pitch Acceleration	deg/sec^2	Digital	PV + A	8	+/- 25.2	5.60
Roll Acceleration	deg/sec^2	Digital	PV + A	8	+/- 46.8	15.62
Yaw Acceleration	deg/sec^2	Digital	PV + A	8	+/- 16.8	5.60
Wing Sweep Angle	degrees	Analog	TH + C	1	None	2.05
Flap Position	degrees	Digital	TH	1	None	4.03
Left Horizontal Stabilizer Position	degrees	Analog	THK A	20	None	None
Right Horizontal Stabilizer Position	degrees	Analog	THK A	20	None	None
Left Inboard Spoiler Position	degrees	Analog	THK A	20	None	None
Right Inboard Spoiler Position	degrees	Analog	THK A	20	None	None
Upper Rudder Position	degrees	Analog	THK A	20	None	None
Gross Weight	lbs	Analog	TH + C + D	1	None	4600.00
Center of Gravity	% MAC	Digital	THK C	1	None	None
Fuel Weight	lbs	Digital	THK D	1	None	None
Mach Number		Digital	TH	1	None	0.02
Airspeed	kts	Digital	TH	1	None	7.66
Altitude (Pressure)	ft	Digital	TH+E	1	None	237.00
Altitude (Radar)	ft	Digital	THK E	1	None	None
Wheel Speed (Main Gear)	kts	Digital	TH	1	None	None
Engine No. 2 Fan Speed	%	Digital	EPV	1	None	None
Engine No. 2 Core Speed	%	Digital	EPV	1	None	None
Engine No. 2 Power Lever Angle	degrees	Digital	EPV	1	None	4.80
Weight on Wheels (on/off)		Digital	disc	1	None	None
Main Gear Down		Digital	disc	1	None	None
Refuel Nozzle Latch (connect/unconnect)		Digital	disc	1	None	None
Structural Mode Control System (on/off)		Digital	disc	1	None	None
Terrain Following Status		Digital	disc	1	None	None
On/Off		Digital	disc	1	None	None
Manual/Auto		Digital	disc	1	None	None
Ride (soft/medium/hard)		Digital	disc	1	None	None
Engine Number 1 Stop		Digital	disc	1	None	None
Engine Number 2 Stop		Digital	disc	1	None	None
Engine Number 3 Stop		Digital	disc	1	None	None
Engine Number 4 Stop		Digital	disc	1	None	None

Disc - Discrete Signal
PV - Peak-Valley Compression Algorithm
EPV - Engine Compression
TH - Time History Compression
TH+C - Time History with group C time hack (typical)
PV+A - Peak Valley with group A time hack (typical)
THK A - Time Hack Parameter Group A (Typical)

DOCUMENTORY ITEMS
Aircraft Serial Number
Mission Date
Take Off Gross Weight
Stores Weight
Mission Type Code
Base Code

not installed in the aircraft, a saturated SDC memory or recorded data being declared invalid. The IAT program receives records of B-1B missions from a USAF maintained database known as the Core Automated Maintenance System (CAMS) which provides, for each flight of each aircraft, the flight length, number of landings, type of mission and the base of operation. From this data and the predefined damage rates kept in the program, for all types of B-1B missions, the IAT program assesses the damage for any flight without SDC records.
The remaining life for each part is determined by commencing the crack growth analysis at the crack size defined by the service history to date and projecting crack growth for the future usage. The projected usage for any aircraft is defined as the average usage for the applicable squadron as compiled from the most recent two years records. The IAT analysis and reporting is updated every six months.

Loads Environment / Spectra Survey

The Loads/Environmental Spectra Survey Program accumulates and validates the SDC recorded field data into a series of databases. The approach is to block the mission data into discrete periods or mission segments characteristic of a particular type of flying or ground taxi operation and to categorize the information into three relational databases. The time history records of the aircraft weight, wing sweep, altitude and Mach number together with documentary data are used to classify each flight profile using a pattern recognition procedure. Once the mission profile has been classified into one of 34 current types, the mission data is broken down into discrete mission segments for which the average values of major flight and geometric parameters are recorded. The other databases contain load factor and the strain gage data which are separated by mission type and flight segment such as terrain following within a given weight, Mach number, altitude and wing angle band. Load factor data is further divided as being due to a gust or pilot induced maneuver. From this database the operational airframe loading spectrum is compiled, compared with design spectrum and serves as the basis for an updated durability and damage tolerance assessment.

Updated Durability and Damage Tolerance Assessment based on Operational Records

In 1993, after collecting 10,000 flight hours of operational data with the L/ESS program, Rockwell re-analyzed the entire airframe to provide an updated assessment of the durability and damage tolerance capability of the B-1B. Continual monitoring of the L/ESS program showed that the operational usage had stabilized after initial fluctuations as the aircraft first entered service. The mix and type of operational mission profiles are shown in TABLE 4 and selected parameters are compared with the design usage in FIGURES 9 through 11. As shown, a significant difference is that the gross weight is 50,000 lb. heavier throughout the mission. This increase is due to increased fuel reserves. The other major difference between the design and the service conditions is the higher than anticipated load factors due to pilot induced maneuvers. FIGURES 10 and 11 show, in exceedance curve format, data for both wings forward and wings aft situations. The increased load factors during the wings forward segments occur during pattern flying where 1.85g is recorded once per hour on the average as compared to the anticipated average once per hour load factor of 1.5g. For the wings aft configuration the design assumed a maximum load factor of 2.4g, the system automatic fly up maneuver in the event of the terrain following radar loosing contact with the ground. Higher load factors have been recorded during manual terrain following.

TABLE 4 - B-1B Service Mission Mix

Mission Code	Occurrences. per 100 flts	Mission Definition	Mission Flt Hours
		Training Missions	
1a	21	2 low altitude/high speed segments & terrain following ON	5.77
1b	21	1 low altitude/high speed segment &terrain following ON	3.91
2a	8	1 low altitude/high speed segment & terrain following OFF with air refuel	5
2b	7	1 low altitude high speed segment & terrain following OFF without refuel	5
3a	10	High Altitude with air refuel	3.65
3b	10	High Altitude without refuel	3.65
1H	2	Heavy weight mission 1	6.14
2H	2	Heavy weight mission 2	6.89
		Other	
4	6	Ferry flight	4.02
5	1	Functional check flight	2.25
11	12	Pilot proficiency flight	0.99
		Average for 100 flights	4.16

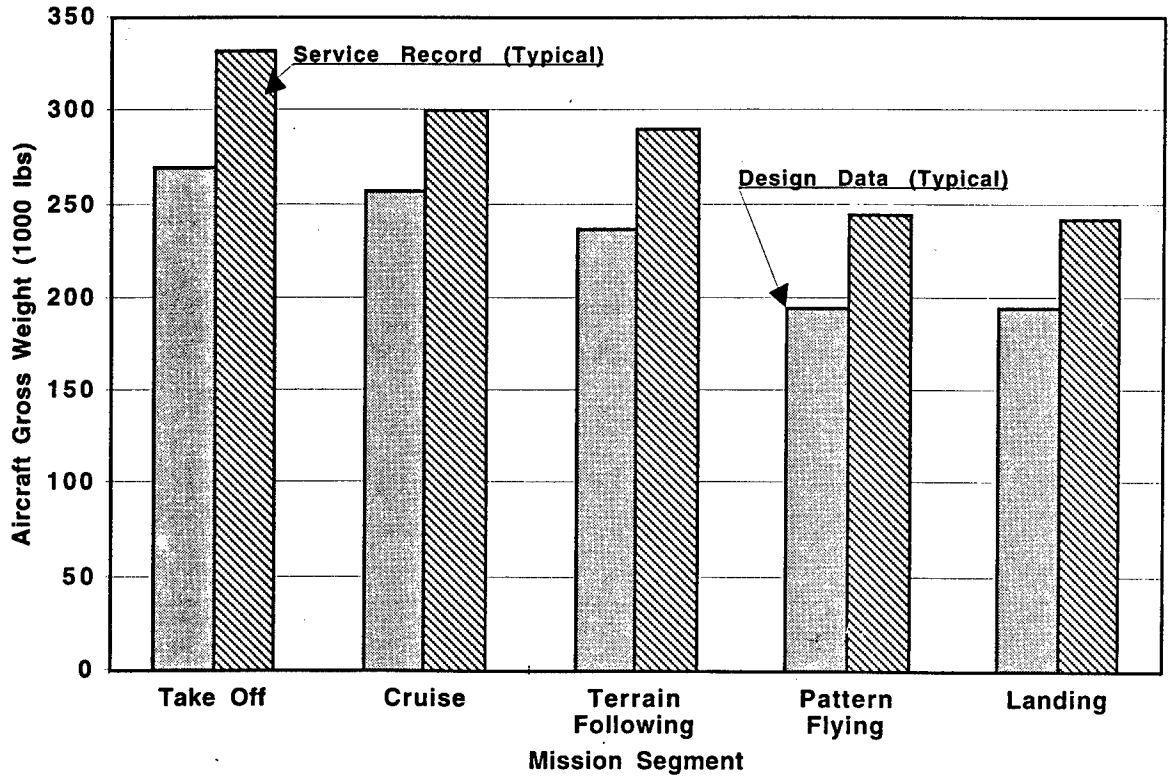

Figure 9 - Design Vs. Service Gross Weights

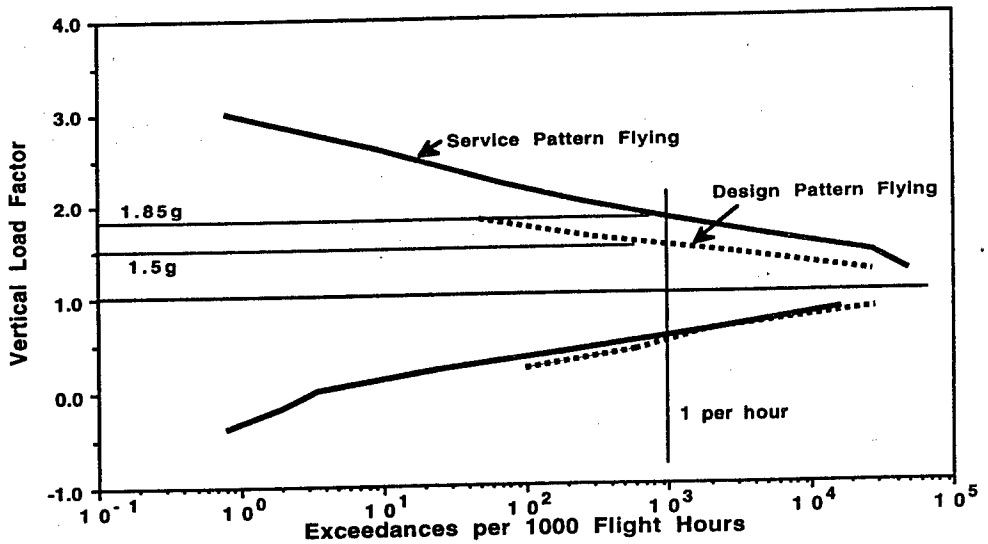

Figure 10. Maneuver Load Factor Spectra (Pattern Flying) - Design Vs. Service

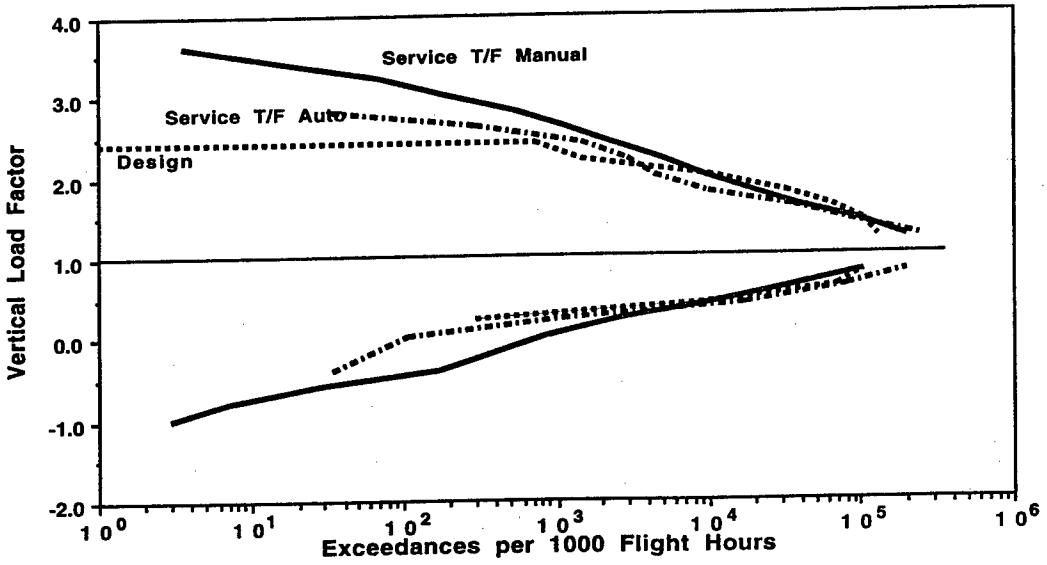

Figure 11- Maneuver Load Factor Spectra (Terrain Following) Design vs. Service

Local stress spectra were compiled and crack growth analysis performed for all locations determined during the design phase to be critical, using the L/ESS mission profiles and load factor data and the NASTRAN finite element model as outlined in Figure 12. Comparison of the design and service stress spectra are shown in FIGURES 13 and 14 for two significant areas, namely a wing location and a wing carry through structure location. These plots show the increase in stress due to both the increase in gross weight and load factors. The lower skin in the wing carry through box, in FIGURE 13 for example, shows a 36% increase in the once per flight stress. The DADT assessment reflected, as expected, a significant reduction in

the economic life and increased inspection requirements if the more severe current usage is continued.

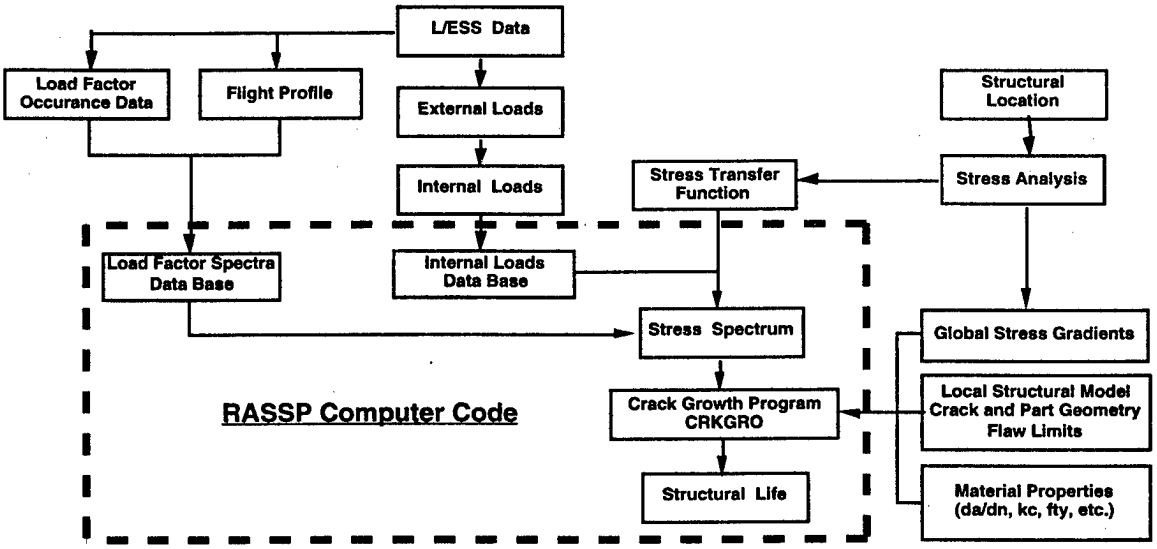

Figure 12 - Durability and Damage Tolerance Assessment Process

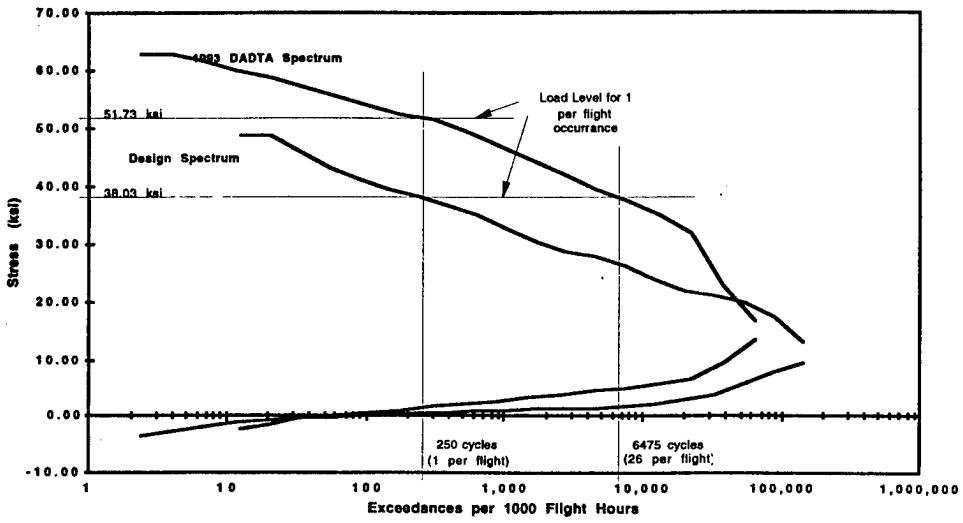

Figure 13 - Typical Stress Exceedance Curves for Wing Carry Through Lower Cover

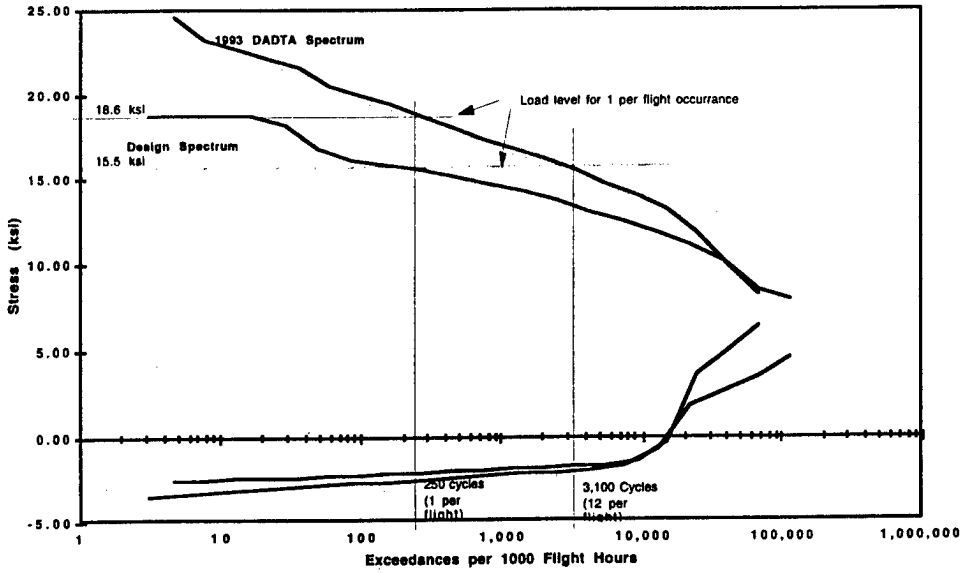

Figure 14 - Typical Stress Exceedance Curves for Wing Outer Panel Lower Cover

FORCE STRUCTURAL MAINTENANCE RECOMMENDATIONS

The inspection and maintenance requirements to ensure structural integrity are issued in the Force Structural Maintenance Plan. The first issue of the plan reflected the inspections and economic life defined as a result of the design analysis and the design verification test program. The inspections in subsequent annual issues incorporated the results of the IAT program and the updated DADT assessment. Inspection intervals are defined as one half of the analytically computed damage tolerance life (time for the inspectable flaw to propagate to critical crack length). The economic life, or the time at which a structural life extension program should be implemented, has also been revised as a result of the updated DADT assessment.

Due to the severity of the service environment the analysis has indicates that a significant reduction may be expected in economic life of the wing carry through structure and that inspections will be necessary on both the wing carry through and wing outer panel to meet the damage tolerance criteria. The critical area is the attachment of the rear spar to the lower wing planks. The analysis is, however, conservative as it does not account for inherent high fatigue capability of the Taper-Lok fasteners. Cracks did not initiate in this area during the DVT test; however, analysis indicates that the test spectrum, while being more severe than the B-1B design spectrum, was significantly less severe than the current spectrum. A test program utilizing test coupons is currently underway to assess the capability of the Taper Lok joint and to compare the current spectrum with that applied to the DVT test specimen.

In addition to the development task referred to above, the following recommendations have been made to the Using Commands to reduce the rate at which the available B-1B life is being consumed:

1) Reduce the fuel reserves from the current 50,000 lb. to 25,000 lb.
2) Reduce the maneuver load factors, particularly during the pattern flying segments and during touch and go landing practice.

The response to these recommendations is being monitored by means of a software program utilizing the Structural Data Collector records and monthly reports issued to the Using Commands. Some reduction in usage severity has been achieved in the 6 months of operating this program.

As the aircraft makes the transition from a nuclear deterrent to a conventional weapons platform the L/ESS and IAT programs must continue to be operated and monitored to detect operational changes which affect the structural life with the possibility that additional durability and damage tolerance assessments may be necessary.

STRUCTURAL EXPERIENCE

As of December 1994 the lead B-1B has exceeded 3000 flight hours and the fleet average is currently at 2200 hours. In the last three years three structural areas, the forward fuselage shoulder longeron, the main landing gear actuator support fitting and the nose landing gear shock strut, have required repairs or modifications as a result of fatigue cracks. In all cases fracture mechanics analysis and the availability of service loads environment from the ASIP Force Management Program have provided the tools for a detailed investigation as to the cause and enabled a timely resolution with minimal impact on service operations. The service load spectrum for the shoulder longeron was generated from the L/ESS program records of the forward fuselage strain gage records utilizing a transfer function based on the flight test records where concurrent strain gage records were recorded for the ASIP forward fuselage and the shoulder longeron. In the case of the landing gear structure cracks, analysis using the recorded L/ESS data demonstrated that the primary damaging operations were the retraction / extension cycles of the gear. Fracture mechanics was then used to confirm that the generated loading would predict the known cracking and also to ensure that the repairs and/or replacement parts will meet the life goals. High local stresses at the crack initiation points were confirmed using RASNA Corporation's "Mechanica" which uses the Polynomial Element (Pcode) approach. This program, not available at the time of the design, also provided the stress intensity factors at the crack tip as the crack length changes. Details of the fatigue cracks and the resolution is shown in the following paragraphs.

Shoulder Longeron

Cracks were found in the shoulder longerons during one of the Analytical Condition Inspections (ACI) performed during 1991 (Reference 8). The cracks were determined to have been caused by a local stress concentration that was introduced during the production redesign after completion of the full scale design verification fatigue test. The shoulder longerons are located at 25 degrees off the top dorsal longeron: the cracks occurring at the juncture of the forward intermediate fuselage and the wing carry through structure (FIGURE 15). The shoulder longerons are two of twelve longerons at that point, but together they carry 30% of the total fuselage bending load. Actual aircraft usage has been more severe than

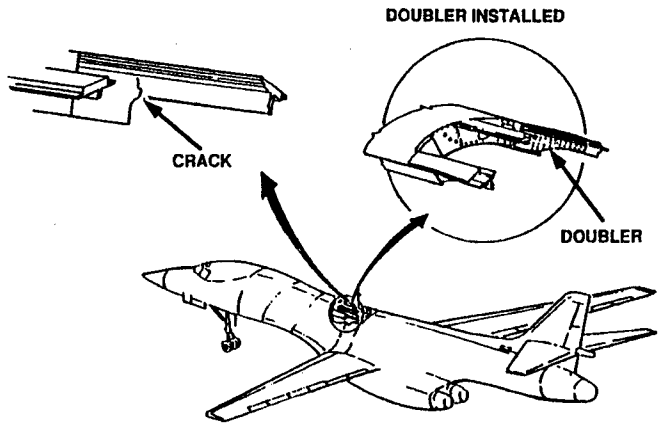

Figure 15 - Longeron Crack Location

design in terms of both gross weight and load factors, and this contributed to the early crack initiation

The shoulder longeron is made of 7075-T73 aluminum alloy forging, is over 17 feet long and attaches to fuselage frames every eight to twelve inches. The longeron cross sectional area is more than five square inches. The longeron was repaired with doublers, both metallic and advanced composite (boron) which were designed to reduce the local stress in the longeron below the crack growth threshold while maintaining low stresses in the doubler. The operating stress levels were confirmed by flight test and a series of coupons and component tests verified the repair.

Nose Landing Gear Shock Strut

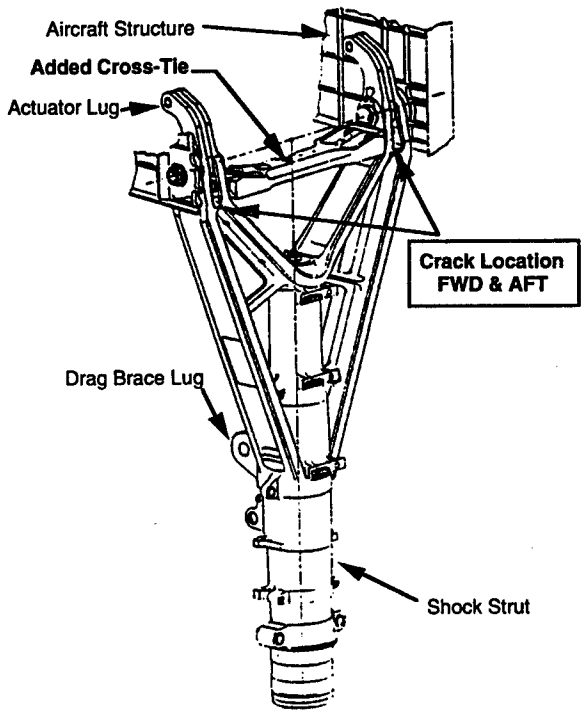

Figure 16 - Nose Landing Gear Shock Strut

Cracks, as shown in Figure 16, have been found in the nose landing gear shock strut in fillet radii, an area of high stress concentration, at the base of the lugs which attach the landing gear to the fuselage. Analyses determined, that stresses due to taxi, ground handling and landing conditions were insignificant at this location compared to those caused by the gear extension / retraction cycles. The entire nose landing gear fatigue test was conducted with the gear in the down and locked position and the loads caused by the extension / retraction cycles were not included in the spectrum. The critical area was thus not tested to a loading environment as severe as experienced in service. The shock struts have been repaired, as shown in Figure 16, by adding a cross tie between the top lugs to reduce the stress level at the location of the crack.

Main Landing Gear Actuator Support Fitting

During periodic depot maintenance, cracks were found in the 6V-4Al titanium forgings which support the main landing gear actuator. The fittings are attached to the rear spar of the wing carry through structure. The cracks occurred in an area of high local stresses where complex machining was necessary to accommodate the fitting in restricted space. The primary loading occurs during the extension and retraction cycles of the main landing gear. The fitting was was not fatigued tested as part of the main landing gear design verification test. The fitting was installed on the wing carry through DVT, however, the main landing gear actuator loads were not included in the wing carry through DVT spectrum. The titanium fittings have been replaced with steel fittings with minor machining changes. The limited available space prevents any significant increase in cross sectional area.

SUMMARY

The Aircraft Structural Integrity Program integrated the design, testing and manufacturing processes to produce a durable and damage tolerant structure. Further the force management tasks are providing early warning of a reduction in the fatigue and damage tolerance capability due to severe usage. The early warning allows changes in operational procedures or alternatively preparing for a life extension program if further analysis and testing deems such a program necessary. It is imperative that service loads monitoring be continued as the role of the B-1B changes, and that interaction between engineering and the Using Commands continue so as to ensure the maximum structural life within the service mission requirements.

Full scale fatigue testing is the best way of locating structural "hot spots" particularly in areas difficult to analyze. The only significant structural problems to date have been in areas that were not tested due to economic constraints or were not subjected to a test loading environment as severe as that demonstrated in service. In retrospect, continuing the full scale design verification tests, beyond the third lifetime and preferably until wide spread cracking occurred, would have provided a measure of the economic life of the structure under the design spectrum that could be extrapolated to the more severe usage experienced in service. Historical evidence has shown that most military aircraft are subjected to more severe usage than predicted in the design specification leading to the conclusion that a more "conservative" spectrum, within the flight envelope, should be considered for the final full scale testing. This alternative would find the fatigue sensitive areas with a shorter and consequently less costly test at the risk of driving structural changes that may be unnecessary if the aircraft was flown to the design missions.

The introduction of fracture mechanics considerations into the design process resulted in the selection of materials that to date have eliminated structural failures from short cracks. For those structural areas where cracks have occurred, the choice of fracture tough materials has ensured that the cracks were found before catastrophic failure. Furthermore, the high fracture toughness of the shoulder longeron (7075 - T73) allowed a repair doubler to be designed such

that the stress in the longeron was below the crack growth threshold. The extensive service loads monitoring, achieved by equipping all aircraft with the structural data collector, and the continued analysis of the recorded data has led to timely response to structural problems both in understanding and in providing a solution.

There were early costs associated with the fracture mechanics requirements applied to the B-1 as the crack growth methodology was in its infancy and the database of material properties was meager. Much of the developed methodology and experience has been used in more recent aircraft designs and the continual improvements of the analysis tools for both crack growth estimates and local stress computations will produce more durable and damage tolerant products in the future.

REFERENCES

1 AFR 80-13 Air Force Regulation -Air Force Structural Integrity Program Department of the Air Force, July 1976

2 MIL STD 1530A Aircraft Structural Integrity Program , Airplane Requirements Department of the Air Force, September 1972

3 MIL-A-83444 Airplane Damage Tolerance Requirements, July 1974

4 MIL-A-8866B Airplane Strength and Rigidity Requirements, Repeated Loads and Fatigue, Department of the Air Force, March 1971

5 MIL-A-8861A Airplane Strength and Rigidity Flight Loads, Department of the Air Force, March 1971

6 TFD-82-431 B-1B NASTRAN Finite Element Model for Fatigue Loads, Rockwell International, December 1982.

7 NA-78-491 Improved Methods for Predicting Spectrum Loading Effects. Rockwell International, September 1979

8 WL-TR-94-4079 B-1B Shoulder Longeron Repair, L.G. Hansen, Rockwell International, Procedings of the 1993 USAF Structural Integrity Program Conference

UNDERSTANDING FATIGUE FAILURE ANALYSES UNDER RANDOM SPECTRUM LOADING USING A C-17 TEST ARTICLE FAILURE

C.L. Brooks
McDonnell Douglas Aerospace
P.O. Box 516 MC 0012741
St. Louis, MO, USA 63166

K. Liu and R.G. Eastin
McDonnell Douglas Aerospace
1510 Hughes Way MC 159-59
Long Beach, CA, USA 90801

ABSTRACT

The determination of the cause of an unanticipated fatigue failure of a structure relies on the ability to perform an accurate failure analysis and assessment. The details of a systematic process for conducting a failure assessment when the failure occurs under random spectrum loading are presented using a crack location on the C-17 full scale test article as a demonstration of the process. Successful use of this process requires efforts from multiple engineering disciplines, and a comprehensive iteration and interaction of stress analysis and life prediction tools.

INTRODUCTION

The C-17 Full Scale Fatigue Test developed a crack in the Wing to Fuselage attachment Trapezoid Panel. The finite element analysis did not show stresses of a magnitude that would produce failure in the time that it occurred. The applied spectrum loading produced a fracture face that could not be readily evaluated to determine the failure scenario. As a result, a process evolved for assessing fatigue failures under random spectrum loading to understand the failure mode and driving mechanisms, and thus provide tools to assist in the re-design to meet fatigue and damage tolerance requirements.

The failure analysis process involved the following steps:

- full characterization of the applied spectrum
- select representative material and analytical models
- global and local finite element stress/strain analyses
- crack nucleation and crack growth analyses
- fractographic examination and fracture face mapping
- correlation, calibrations, and predictions

Subsequent correlation of the analysis results to the fracture face provides confidence in the understanding of the problem and the solution.

Objectives

The primary objective of the failure analysis was to explain the load and stress mechanisms that produced the test article failure. Re-design options could then be evaluated to ensure that life and damage tolerance requirements were met. The tools, techniques, and procedures developed for the failure analysis had to be readily adaptable to support the re-design effort.

The secondary objective of the task was to establish an approach and process for conducting future failure analyses resulting from spectrum loading. The nature of the trap panel failure provided the opportunity for developing techniques to analyze and evaluate a failure when conventional analysis techniques are insufficient and the fracture face difficult to read.

Problem Statement

The trapezoidal panel is a primary load transfer structure between the wing and the fuselage. The design usage spectrum is quite different from other large transport aircraft due to the significant amount of time in low altitude flight. Most of the fatigue damage is due to gust cycles from low altitude heavy gross weight missions. The full scale test article jack-load spectrum represents 1/10 lifetime usage. The spectrum consists of 35 different mission profiles and over 170,000 unique cycles. The two mission types thought to be most damaging were grouped together at the middle and the end of the spectrum in an attempt to mark the fracture surface without introducing arbitrary marker cycles.

The crack developed in the fillet radius at the aft lower end of the panel. The fracture surface revealed evidence of fatigue marker bands. However, due to the multiple crack sites and the crack geometry growth patterns, the crack nucleation and propagation time could not readily be determined from the fracture surface. The initial stress analysis and life assessment did not correlate with the test failure and fracture pattern.

DESCRIPTION OF THE ANALYSIS PROCESS

The poor correlation of the initial analysis with the fatigue life and growth patterns stimulated a study of the stress states and mechanisms that would be required to cause the failure. The process used to conduct this investigation is discussed below along with its application to the C-17 Trap Panel failure.

TASK A: Data Collection

Process. The first step is to collect and review available information that describes the cracked structure. This information includes: details of the structural configuration; the manufacturing process; assembly details; pertinent test procedures, history and data; field history; and material data. The second step is to initiate a metallurgical failure analysis.

This would include visual and macroscopic and microscopic examination, chemical analysis, microstructure examination, and verification of material properties. This information prepares the analyst to develop failure scenarios, understand any mitigating circumstances, and identify key elements of the events that produced the fatigue crack.

Trap Panel Data. The crack location and geometry are shown in Figure 1. The crack originated from multiple origins which linked up early in the life. The final crack size was 0.58 in. (14.7 mm) deep by 0.74 in. (18.8 mm) on the surface. No flaws or defects were noted at the origins. The adjacent surfaces showed a matte finish indicating the local region had been shot peened. A photo of the crack face is shown in Figure 2. Chemical, hardness, and conductivity measurements indicated compliance with the requirements for the 7050-T74 forged material. A black residue on the surface was identified as molydisulfide. The microstructure was uniformly fine without any residual grain flow. No other cracks were observed or detected

TASK B: Spectrum Characterization:

Process. Characterization of the local stress spectrum is the next undertaking. The stress transfer functions used to develop the spectrum should also be verified as part of this task. To facilitate use of the spectrum, the peaks and valleys should be normalized to a reference load; the peak load of the spectrum is often convenient. A sequential plot of each peak and valley, a "spectrum roadmap", should be produced to establish the relationship between events in the spectrum. Peak, valley, stress range and stress ratio exceedance and occurrence plots are also helpful in understanding the contents of a spectrum.

Next the spectrum should be divided into segments based upon the occurrence of similar loadings in proximity to each other. The idea is to group events together that may form distinctive marks on a fracture face. It is often thought that the distinct lines on a fracture face are from the peaks loads. Although this is sometimes the case, a series of low level constant amplitude cycles will appear as a single line unless observed at high magnification. Compression cycles can also produce a change in coloration or appear as markers. High stress ratio clusters can also produce a distinctive mark. The content of each segment should be characterized just as for the full spectrum. The resulting plots should be compared to ascertain the unique features of each segment. Using the characterization the analyst is able is discern the types, magnitudes, ranges, stress ratio, and quantities of cycles that are important for subsequent evaluations.

If the spectrum can be described as completely random without distinctive groups, patterns, or distinctive peaks, there are few failure analysis techniques that can be used to develop an explanation of the failure. Intermediate points on the fracture face, other than the final failure point, are required. The solution in this situation will rely solely on analytical techniques.

Trap Panel Spectrum. The C-17 Full Scale Fatigue Test Spectrum is a fully randomized flight by flight spectrum representing 1/10 lifetime design usage. Each flight occurs only once in the spectrum. The spectrum was assembled so as to provide marker bands to assist with failure assessments. One of the heavy weight, low altitude high speed cruise logistic missions was grouped around the middle of the spectrum, 1500 spectrum hours. The other logistic mission was grouped at the end, of the 3000 hours. A roadmap of the normalized test spectrum for the trap panel is shown in Figure 3. The figure shows the four segments selected for individual characterization. Segments A and C are different from Segments B and D in terms of peak levels and high stress ratio clusters. Although Segment A appears similar to Segment C, and Segment B similar to D, they are each subtly different. Figure 4 is an example of the other characterization plots using Segments A and B plotted together.

TASK C: Material Characterization

Process. Analytical strain-life and crack growth rate curves for design are often constructed to represent general behavior. Proper mechanical properties and material behavior for the cracked component must be used in the investigation. To accomplish this, the information gathered in Task A detailing the material type, product form, grain orientation relative to crack orientation, and the physical properties are used to select the material models for the stress and life prediction analyses. The models should focus on representing typical behavior, but the impact of upper and lower bound behaviors are important for establishing the relative sensitivity of the failure predictions to material properties.

Trap Panel Material Characterization. The trap panel was machined from a 7050-T74 forging with a typical thickness of 5 inches. The crack originated on the surface in the fillet radius. Referring to Figure 1, the longitudinal grain direction is in the "up" direction and the short transverse direction is in the inboard direction. Material properties and models were evaluated for cracking in the L-S orientation for growth along the surface, and L-T & T-L for growth into the depth. Two strain-life curves were used to evaluate the time to initiation of an 0.01 inch (0.25 mm) crack under R=-1 cycles. A 7050-T74 forging curve from tests in the L direction and a 7050-T74 plate curve from tests in the S direction were used for initiation analysis. Although the S direction curve does not represent the orientation in the actual part, it was used to represent the potential lower bound behavior of crack initiation following chemical processing, e.g., etching, chemical milling, anodizing. Thus the two curves provided a means to assess the sensitivity of the crack initiation time.

Analytical crack growth rate curves plotted against basic laboratory data for 7050-T74 forgings considered three stress ratios, R=0, R=0.4 and R=0.8, representing the approximate upper, intermediate, and lower bounds of the stress ratios identified in the spectrum. The initial correlation showed differences at low stress intensities for R=0.8; the crack growth curve was modified to give a better correlation for this assessment. The critical toughness values were also changed to represent appropriate behavior for part-through surface cracks, K_e instead of K_{IC}, as described in the NASA FLAGRO (1) documentation.

TASK D: Stress Analysis

Process. The most important parameter in a failure analysis is the accuracy of the internal loads and local stress state. In general, the finite element model (FEM) created for designing the structure based upon static strength analysis is not adequate for life assessment. The FEM mesh is too coarse and the joints are not modeled in sufficient detail to represent the local stiffness or to obtain the correct load transfer and distribution in the joint. In most cases, individual fasteners have to be modeled to determine the correct load transfer and load distribution. The individual fastener loads will affect the stress intensity. The failure assessment process does not rely on the stress analysis and finite element models for defining the local stress states or even the stress mechanisms required to induce cracking. Subsequent iteration of the life prediction results with the fracture face correlation often provide insight as to the actual stress states and mechanisms causing the failure. This insight can be used to determine the inadequacies of the FEM and how to improve it for the failure analysis, the re-design, or salvages and repairs.

Trap Panel Stress Analysis. The trap panel and the stub frame are connected through common nodes in the same plane without offsets in the original FEM. The FEM did not provide an accurate load transfer between the two parts and overall bending stiffness of the joint. The fillet area where the crack developed was modeled with plate elements representing the horizontal flange and the vertical leg of the trap panel. The high stress in the fillet area was not described by the coarse mesh FEM results (See Figure 5).

The life predictions indicated a significantly higher stress level and a steeper stress gradient were needed. A more detailed global finite element model was created to better approximate the load path, deflection and fastener load transfer between the wing trap panel and fuselage stub frame. The proper offset between the centroid of the trap panel and the stub frame was incorporated to represent the correct bending stiffness of the joint. Individual fasteners were modeled to determine reasonable load transfer and a compression-only element included to simulate the bear-up between the trap panel and the stub frame. The revised FEM showed the aft lower end of the trap panel had significant vertical, aft load and two axes of bending due to relative deflection between the wing and fuselage. The vertical leg of the trap below the fillet transferred 35% of the total vertical shear load in the joint through the bottom 6 bolts.

The failure area is very thick and of complex geometry. The vertical flange, horizontal flange and the web immediately above the fillet have significant affect on the local stress state in the fillet radius. A 3-dimensional solid p-version FEM was used to define the notch stress and the stress distribution in the fillet by applying boundary conditions obtained from the global finite element model (See Figure 5). The 3-D solid model indicated a high stress concentration under the upper web and an associated steep gradient. The stresses obtained from the 3-D solid model correlated well with the strip strain gages installed in the fillet radius and across the width of the fillet.

TASK E: Fatigue Analysis

Process.: Both crack initiation and crack growth analysis are used to approximate the total life of the structure. The stress state should be specified in all crack extension directions. Over or under predictions in the initial life estimate indicate either errors in stress analyses, material models, missed fatigue mechanisms, corrosion interaction, etc. The reasons for any discrepancies is uncovered by systematic iteration through all the tasks outlined here refining the problem description on each pass until the proper solution is demonstrated by the correlation with the fracture surface and the known life of the part.

Crack initiation predictions are performed over a range of $K_t\sigma$ to bound the stress levels necessary to cause failure. The relative fatigue damage contribution for each spectrum segment, as well as the full spectrum, should be noted as a function of stress level. Crack growth predictions are also made over a range of stress levels beginning at the lower bound for crack initiation. The initial inputs for this analyses are based upon the Task A data and initial fracture model. The relative crack extensions for each spectrum segment and the full spectrum should be determined as a function of crack size at each stress level. Comparison of the crack extension caused by each segment provide the relative spacing of marker bands to assist in the pattern recognition. The analyses at different stress levels indicates the sensitivity of the relative spacing to stress intensity.

Trap Panel Fatigue Analysis. The crack initiation analyses for the full spectrum and each of the segments are shown in Figure 6a. The $K_t\sigma$ estimate from the original FEM gave an excess of one lifetime to initiate a crack when the failure occurred at 0.82 lifetimes. Thus the fillet radius had to have a $K_t\sigma$ of at least 55 ksi (380 MPa). The curve also shows that for the early stages of nucleation and small crack growth the Segments A and C are approximately an order of magnitude more damaging than Segments B and D. The bands for segments B and D would be imperceptible at small crack sizes. Since crack initiation techniques only account for the local stress at the surface, this analysis does not change except for the $K_t\sigma$ level used.

For the crack growth analyses, the effects of varying stress distributions, stress levels, aspect ratios, and other parameters were analyzed to observe the analytical effect on the relative spacing that would be expected for each of the segments. An example of one of the plots is shown on Figure 6b. The computations provide insights to the interpretation of the marker band spacing. The sequence of Segment A, B, C, and D would produce a 3.2 :1.0 :3.3 : 1.6 pattern for a uniform stress intensity for an crack size of about 0.105 inch (2.67 mm)

TASK F: Fractographic Observations

Process. The fractographic examination is best conducted using the expertise of laboratory personnel in conjunction with the analyst. Both have complimentary experiences that provide technology transfer and different perspectives to result in a better correlation and understanding. The examination begins with an optical study of the fracture face, origins, paths, colorations, markings, shear lips, over-stress regions, and surface details. A hand sketch of the fracture surface showing the location of all significant details is useful for the subsequent effort. Key dimensions and other important details should also be noted. The sketch and notes are used during the assessment to establish the quantitative correlations of features, bands, and benchmarks.

Trap Panel Fractographic Observations. The fracture face hand sketch of the crack surface observed details is shown on Figure 7. A series of incremental sketches are used to describe the cracking scenario as follows.

Sketch a. Multiple origins developed in the fillet radius perpendicular to the horizontal flange load path. The origins were concentrated beneath the web transition with a slight bias toward the outboard side. No machining or surface discontinuities were evident. A matte finish from shot peening was evident. Most of the origins were semi-elliptical in nature with some appearing spherical and slightly subsurface. The multiple origins indicate a high stress at the origin (low cycle fatigue). The individual origins grew semi-ellipitically for a short distance.

Sketch b. The multiple cracks began to link-up into a dominant crack. During this phase, minimal crack growth is observed into the depth relative to the apparent surface length increase. A high aspect ratio crack is formed. Then the depth extension increases with a reduced extension rate along the surface as the crack shape returns to its preferred aspect ratio.

Sketch c. The dominant crack is well into stable crack growth with the depth and surface growth varying to maintain a constant aspect ratio. Tucking of the surface crack front is noted indicating an influence of the compressive residual stresses from shot peening. The spectrum patterns are discernible and intermittent marker bands are observed. Secondary crack sites to the right of the primary crack are overcome by the primary crack. A slight curvature of the fracture plane is noted for the crack path.

Sketch d. This phase of crack growth shows the onset of region III crack growth to rapid fracture. Crack extensions for single load cycles are observed. A final crack size is readily identified prior to the over-stress zone. The large zone of over-stress is followed by indications of fatigue at the back surface showing arrestment and relief of the crack driving mechanism prior to final fracture (not shown in sketch).

Task G: Correlation of Analysis and Fracture Surface

Process. The information, tools, and analyses generated by the prior tasks are combined to develop an explanation of the failure scenario for correlation with the fracture surface. The analyst develops this explanation based upon the stress analyses, life prediction analyses, normalized and segmented spectrum, and the qualitative crack growth scenario. Correlation of the predictions with the features of the fracture surface confirm the analysis. Lack of correlation starts another iteration through Tasks A to G in an effort to resolve the discrepancies. Often the results indicate a need to refine the FEM to study local effects while maintaining the global internal loads and freebodies. Life predictions are also refined during this phase in response to iterations of the stress analyses. Each iteration should attempt to obtain consistency between the stress analyses, life predictions, and fracture face observations. The resulting set of refined tools ensure that subsequent repairs, redesigns, and future efforts are accurate in providing adequate structure integrity of aircraft structure.

Trap Panel Correlation. The initial life prediction analyses indicated the $K_t\sigma$ at the fillet radius was potentially 40% higher than the FEM was showing, approximately 70 ksi (480 MPa). Uniform stress crack growth solutions provided an approximation of the state of stress at the point of rapid crack growth. A simple 2-D model of the local area was constructed to evaluate the loading scenarios that would produce the high stress at the location of the crack origins and a tensile principal stress distribution perpendicular to the crack path of the primary crack. These studies used individual load components and then combinations of components to assess their affects on the stress states. The results indicated that the web shears induced by the trap panel deflections were the major contributors to the needed stress states. This insight provided direction for the FEM refinements. The original coarse model was refined to establish better internal loads within the trap panel. The internal loads were then used as boundary conditions for the local 3-D model. The surface and depth stress distributions were extracted from the 3-D model along the primary crack paths. The model stress distributions were adjusted to correlate with the strain gage results from the test article. These adjustments gave the stress profile that would have placed the origins of the crack slightly outboard of the web intersection, along the fillet radius, and biased toward the horizontal flange. The maximum principal stress direction would cause the crack to turn and sever the stub flange as it grew, as it did in the test article.

These stresses improved the correlation between the analysis and the fracture face, but did not resolve all the discrepancies. Another iteration of crack growth analyses was made using the local cracking mechanisms identified during the fractographic examination of Task F. Aspect ratio adjustments were incorporated to represent the multiple crack link-up. The surface crack driving stresses and stress intensity solutions were taken at a 12 degree angle below the surface from the point of origin, since the tucking observed at the surface as a result of the shot peening residual stresses indicated the primary crack was being driven by the response slightly subsurface. Figure 8a shows the surface stress distribution with the relative 12 degree stress state. The differences in the stress decay from inboard to outboard growth was also included. The correlation of the point of rapid crack growth required the use of the effective part through surface crack toughness, K_e, as noted in Task C.

An important distinction in this failure analyses was the role that the stress mechanisms (i.e., thru stress, bending stress, and deflections) and their corresponding stress intensity factors had on the correlation. Figure 8b shows the depth stress profile with the mechanisms partitioned out. The rapid decay of deflection induced stress intensity factors as a result of the "relieving effect" of crack opening was needed. Appropriate stress intensities were computed and combined for each mechanism.

The correlation of the marker band spacing on the fracture face with the above analytical crack growth predictions uses the tools described by Task E. An example of one such plot is shown in Figure 9a. The crack extension for each spectrum segment as a function of crack size enables the analyst to associate each marker band with a particular spectrum segment. For marker bands starting at 0.4 inch, Segment B and D would result in 0.03 inch and 0.05 inch of growth, respectively. Segments A and C approximately 0.090 inch each. Comparing this band spacing to the fracture face indicates B or D is being observed. The continued incrementing of subsequent bands and spacing establishes the scenario and order of actual marker band spacings. Figure 9b presents the resulting correlation of each segment to the observed spacing in the respective time order and sequence. Assembling all of the above described procedures and results gives the total scenario for the failure as shown in Figure 10. The life prediction iterations with stress analysis accounting for all attributes of the structure and stress state provides confidence that all mechanisms responsible for the failure were included.

CONCLUSIONS

A structured process was established for analyzing failures which occur under random spectrum loading. The tools and techniques for developing failure scenarios are highlighted using as an example the failure analysis of the C-17 Trap Panel. Several iterations through this process are sometimes necessary in order to capture all the unique features of a failure. This process has proven to be highly successful in resolving very difficult failures. Successful failure assessments are critical in determining that repairs and/or re-designs meet durability, damage tolerance, and structural integrity requirements.

ACKNOWLEDGMENT

The authors would like to acknowledge Jeff Sermersheim and Eric Tuegel for their help in developing the process and in preparing this paper.

REFERENCE

1. "Derivation of Crack Growth Properties of Materials for NASA/FLAGRO 2.0", JSC-26254, June 1994, NASA Johnson Space Center, Houston, Texas.

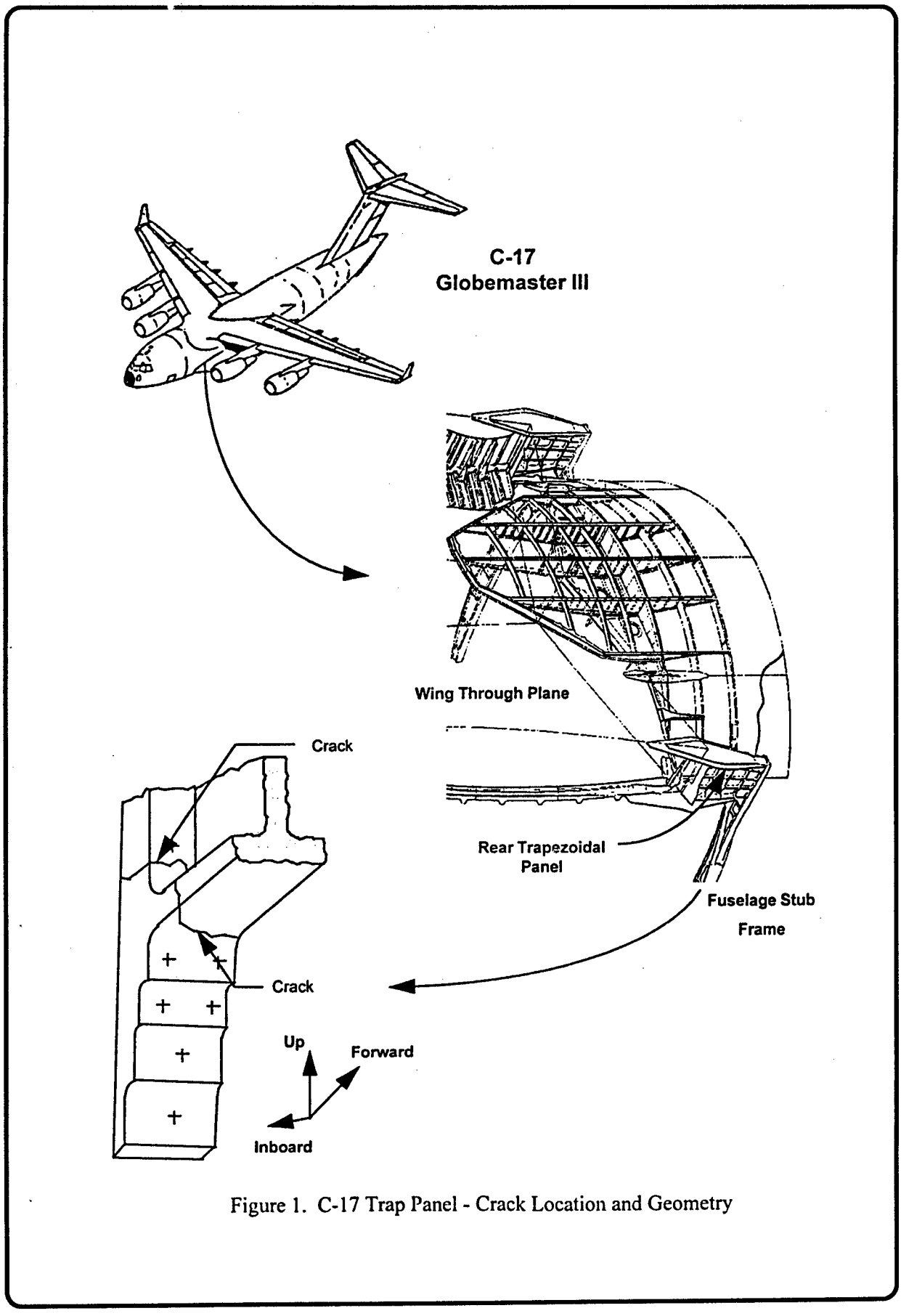

Figure 1. C-17 Trap Panel - Crack Location and Geometry

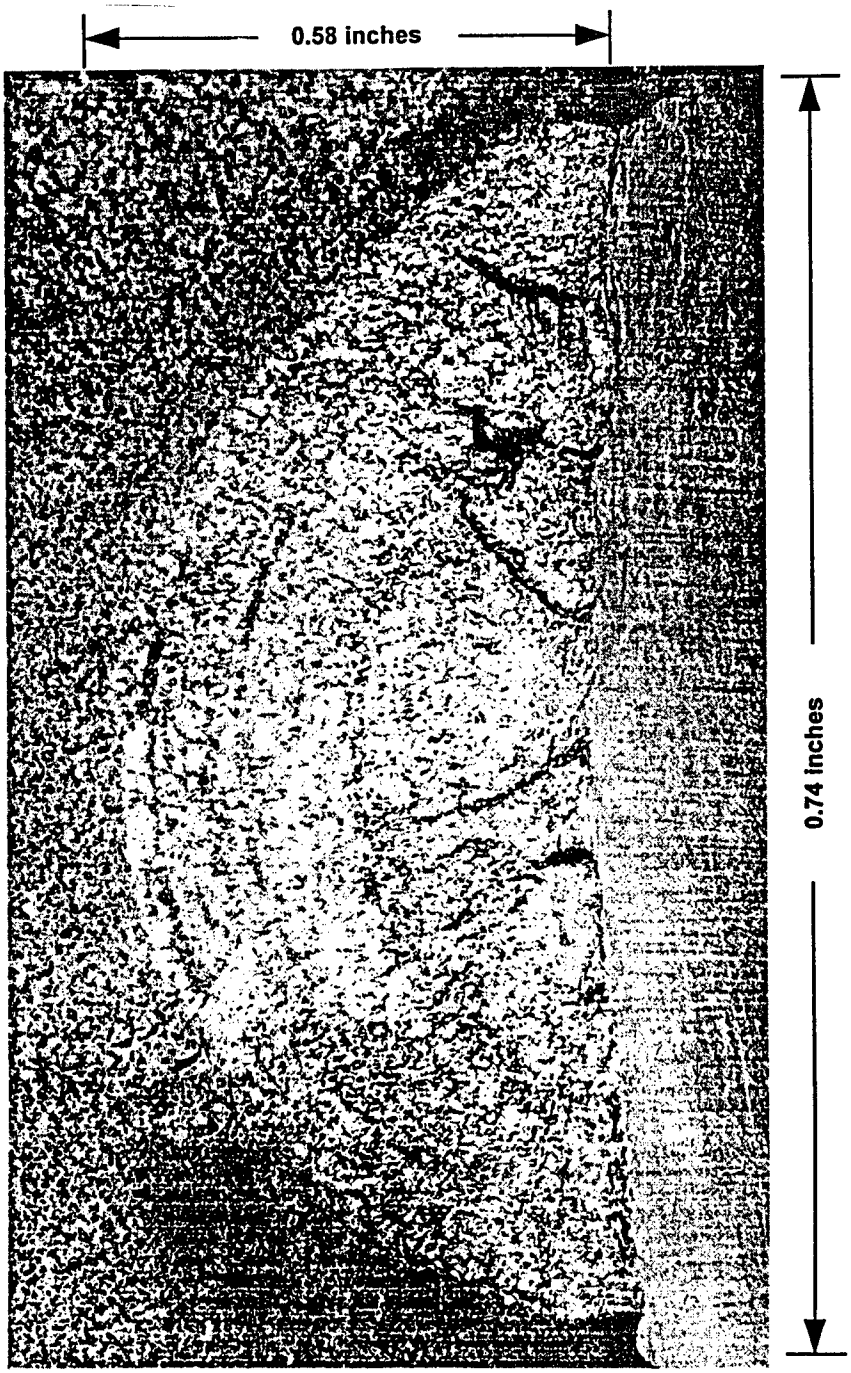

Figure 2. Photograph of the Fracture Face

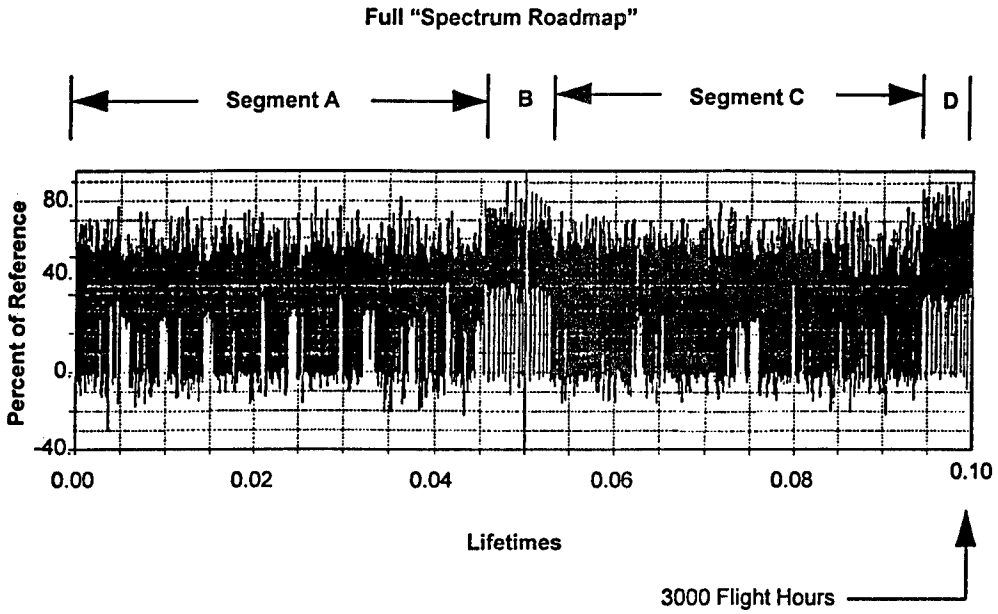

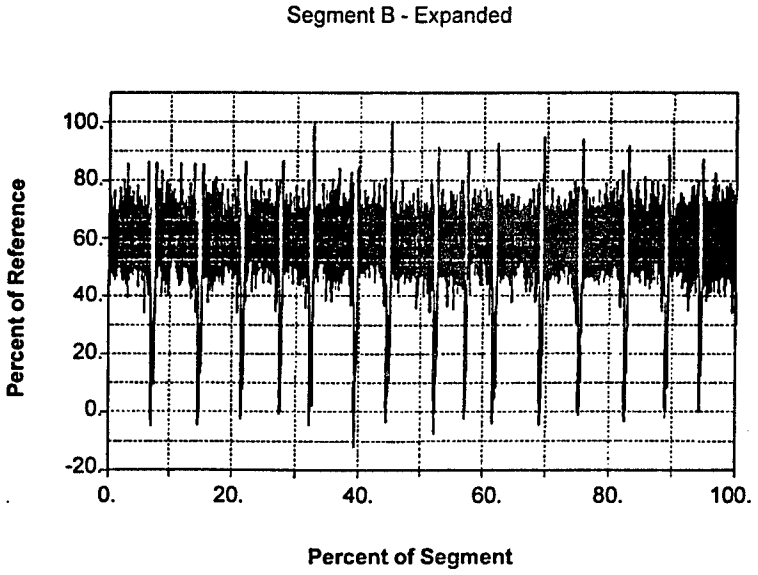

Figure 3. Segmentation of Normalized Test Spectrum

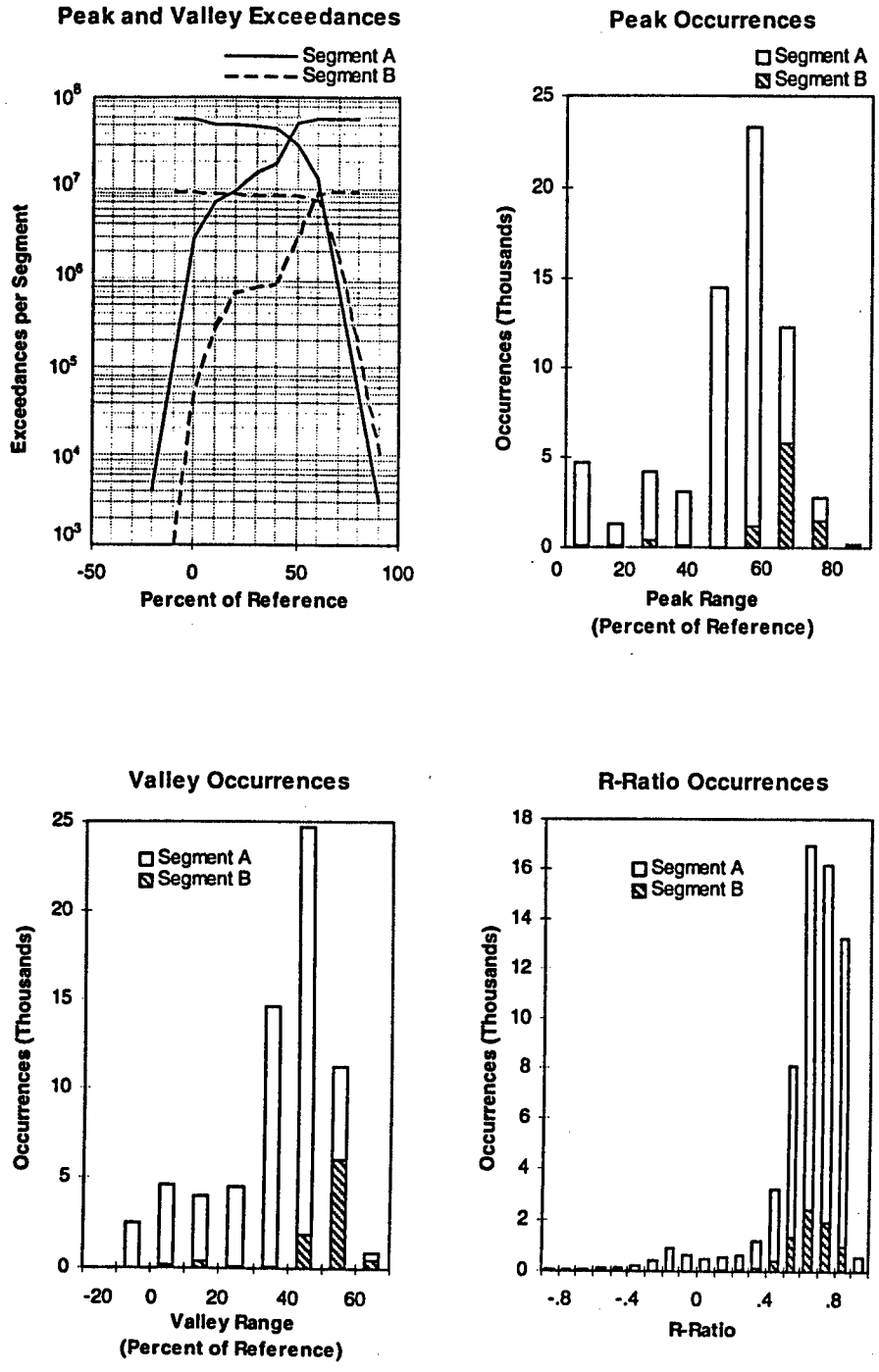

Figure 4. Characterization of Spectrum Segments

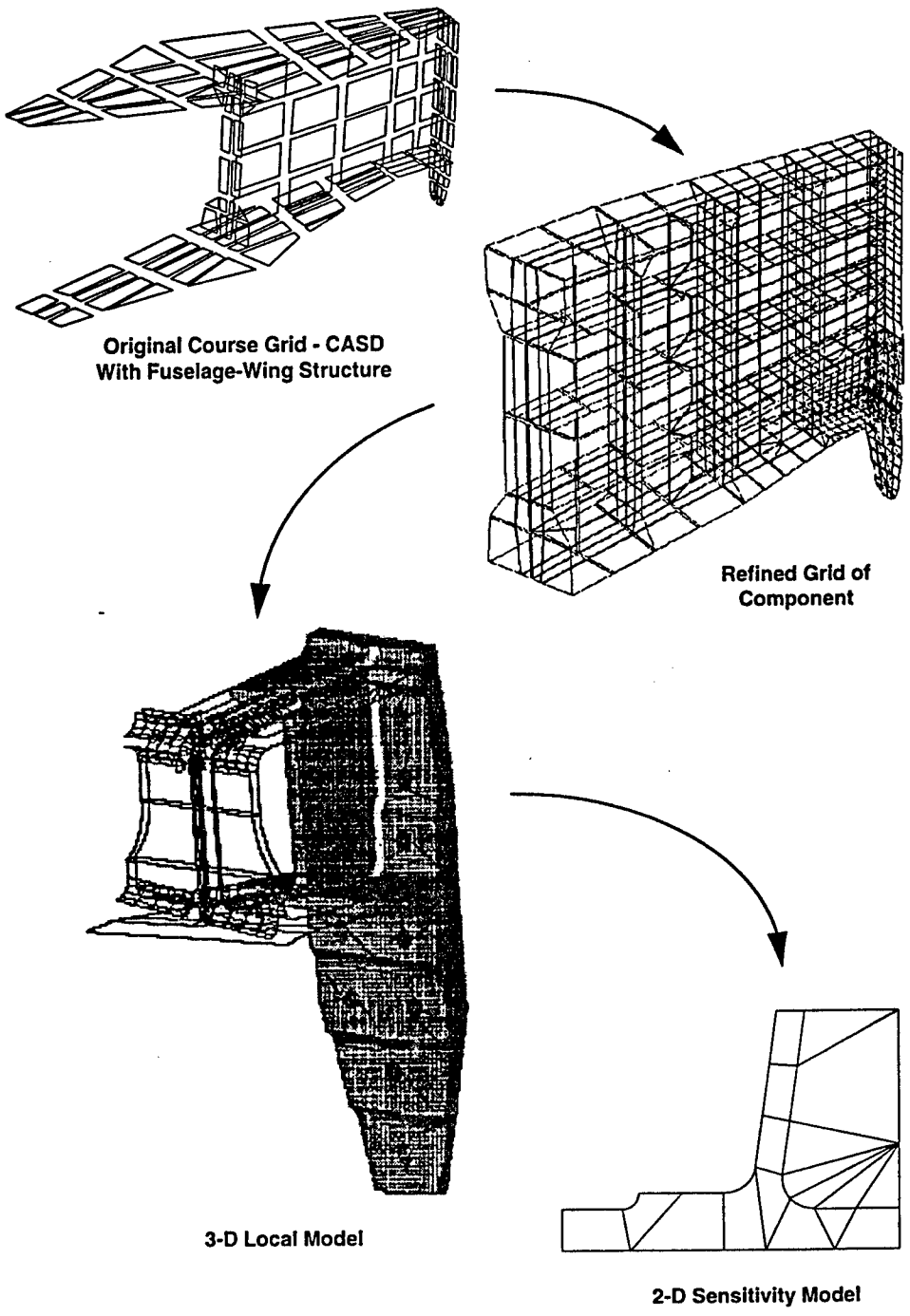

Figure 5. Finite Element Modelling Progression

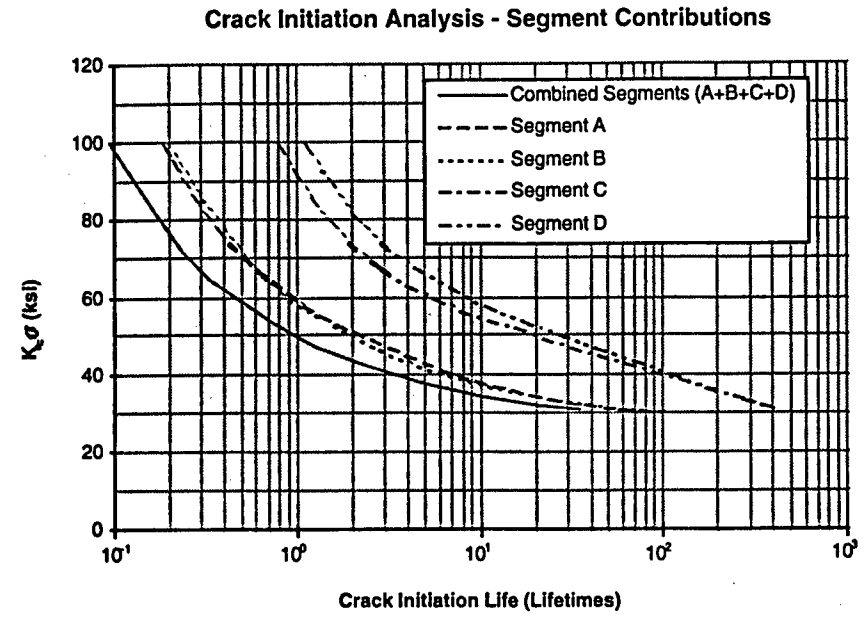

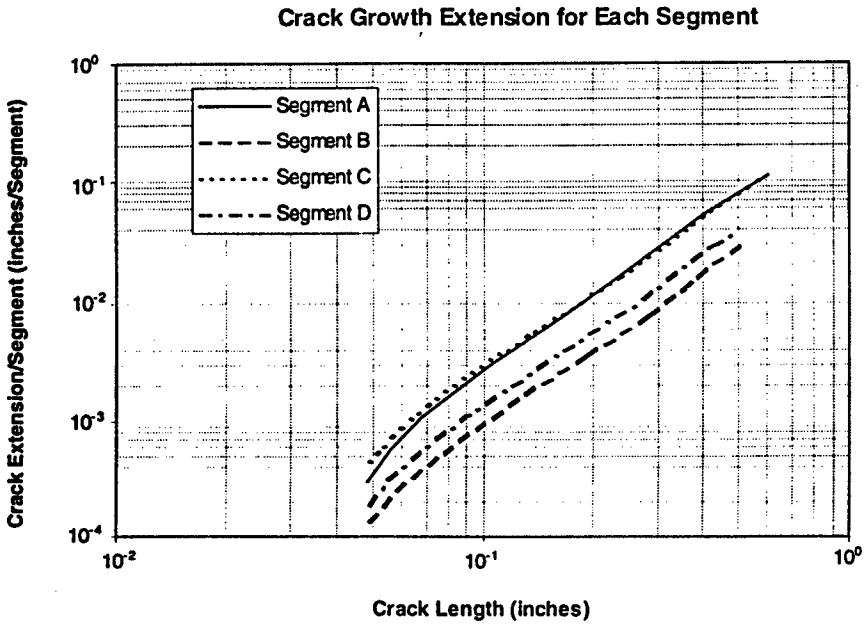

Figure 6. Crack Initiation and Crack Growth Analysis Tools

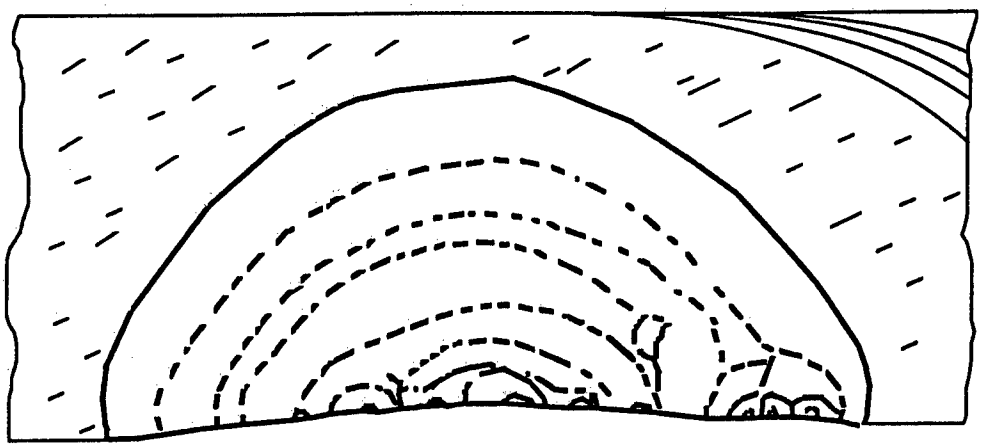

Crack Surface Observed Details

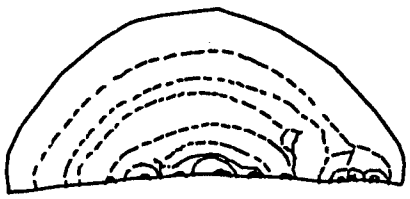

Sketch A

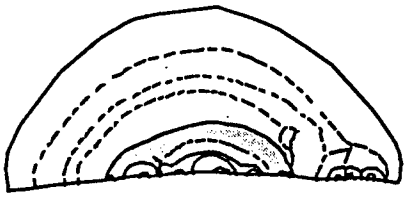

Sketch B

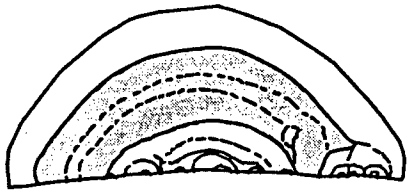

Sketch C

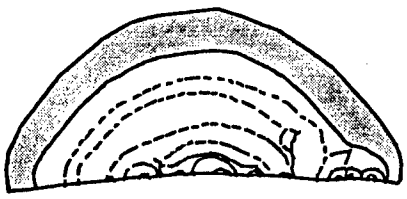

Sketch D

Figure 7. Fractographic Observations and Hand Sketches of Cracking Scenario

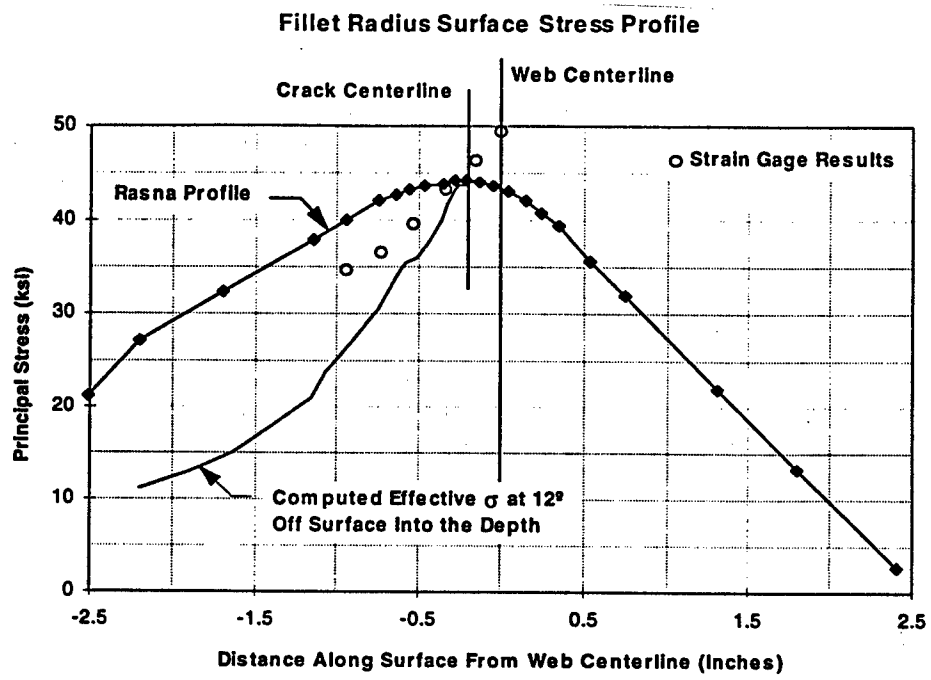

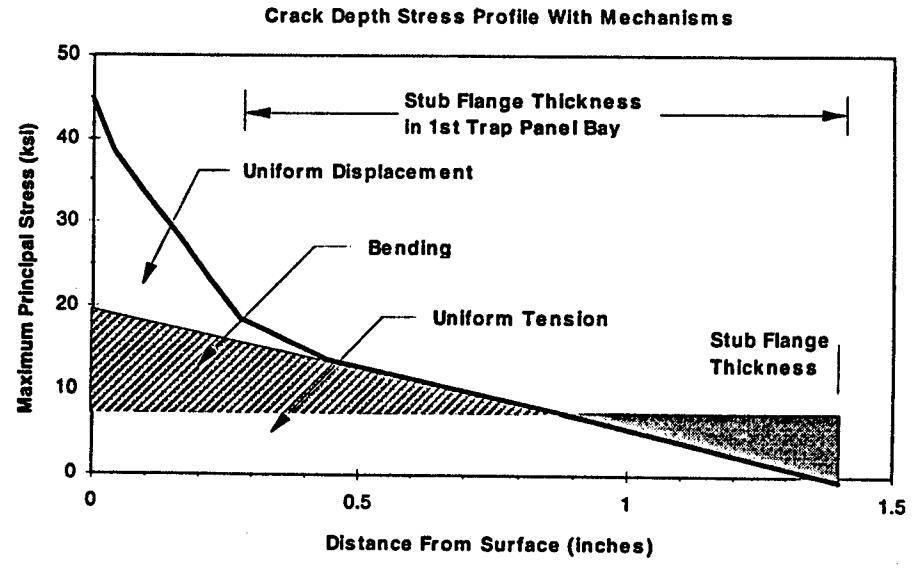

Figure 8. Stress States, Profiles, and Mechanisms

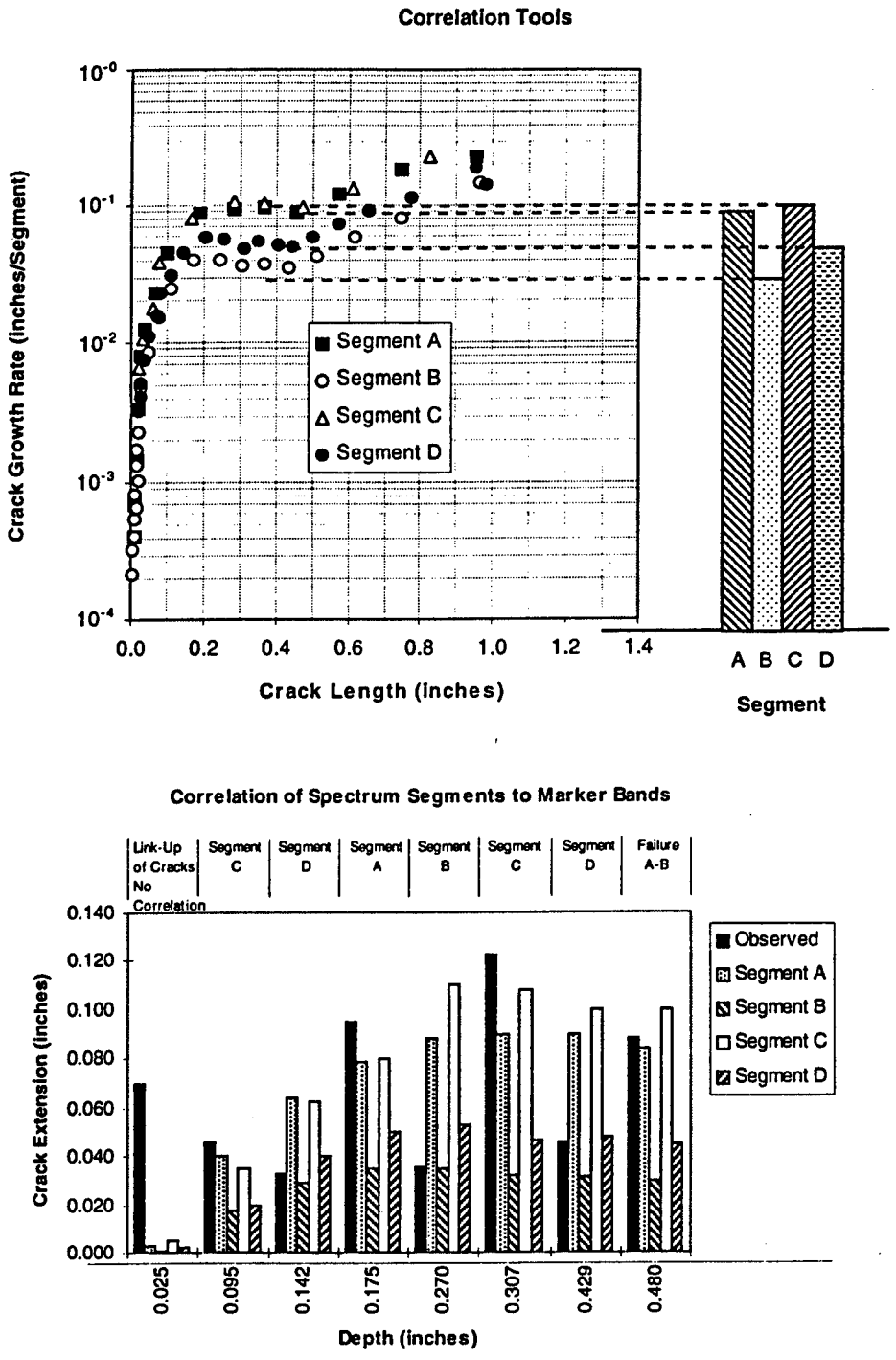

Figure 9. Correlating Analytical to Fracture Face Marker Bands and Spacing

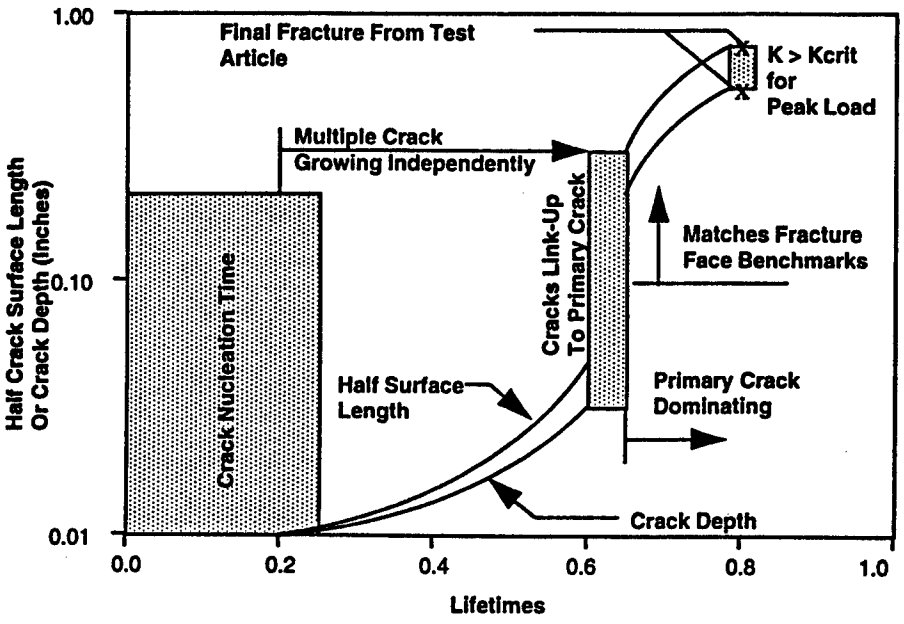

Figure 10. Trap Panel Total Fatigue Failure Scenario

ACQUISITION REFORM

Mark Wilson

ASIP Conference

28 November 1995

Background - The Big Picture

- Dod Budget Cuts
  - Maintain readiness
  - Keep S&T budget line funded
  - Force modernization has suffered
- Strategy to Increase Force Modernization Funding
  - Slow down rate of decrease
  - Base Realignment & Closure (BRAC)
  - Acquisition Reform

Non Government Standards (NGS) IPT

- Initiated at ASC to Develop Methodology to Comply with and Implement Sec. Perry's Reforms
  - Reduction of MIL Specs and Standards
  - Performance Based Specifications
- Endorsed by Joint Aeronautical Commander's Group (JACG)
  - Recommendations to be implemented by JACG
    - If JACG agree with them

IPT Membership

- **Mix of Business Sectors**
  - Aeronautical
  - Aerospace
  - Command, Control, Communication, and Computer (C^4 I)
- **Tri-Service Membership @ SES Level**
  - JACG Lead
- **Industry Membership @ VP, Director and Senior Manager Level**
  - Prime Contractors
  - Major Subcontractors
  - Vendors
- **Cross Functional Representatives**
  - Tech Mangement
  - Program Mangement
  - Business Management
  - Commodity/Reprocurement Mgt
- **Advisers**
  - AIA/CODSIA
  - Government
  - Industry

NGS-IPT GOAL: Derive a Best Practice Approach to Defense System Acquisition

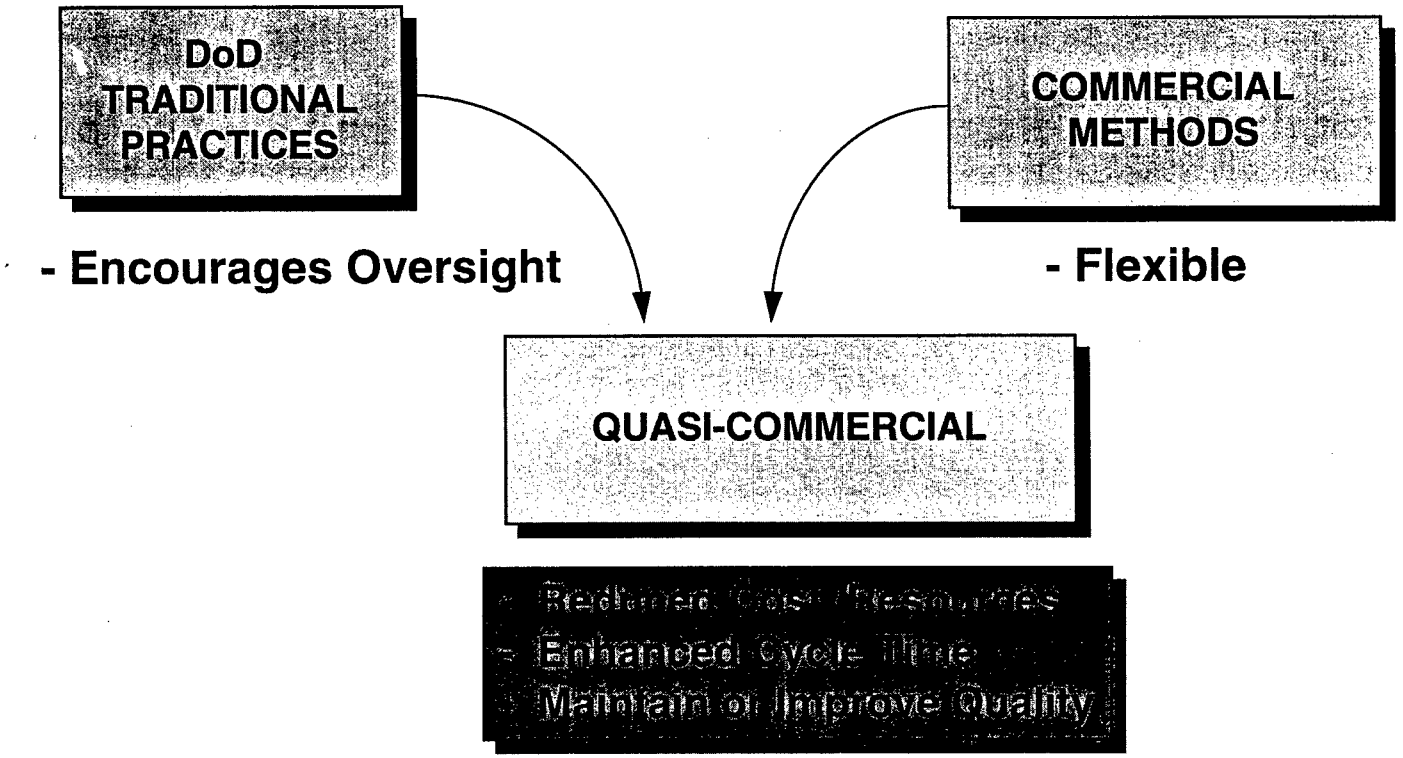

NEW BUSINESS ENVIRONMENT

- **Interface Standards: OK/Necessary**
- **Product Specs/Commercial Item Data**
  - **Description: Common Sense Application**
- **No Fabrication Process MIL STD's**
- **No Tech/Mgt MIL STDs**
- **Contractors Own Their Processes and Compete on the Quality of Those Processes**

New Acquisition Paradigm

- Performance Based
- Government Control thru system/segment specification(s) (Depth is Risk Driven)
  - Adapt approach for end item level modification programs and spares acquisition
- Contractor Controls Detailed Design and Lower Level Performance Specification
- Company Processes (in Lieu of MIL-STDS)
- Apply to existing (Enterprise & Program specific change) and new acquisition

Acquistion Reform

- Performance Based Specifications
  - Development
    - Unshackle contractors from government rqmts. and allow use/development of commercial methods where applicable
      - Eliminate duplicate processes/production lines
      - Broaden production base
  - Sustainment
    - Utilize performance based specs when it makes sense
      - Business decision
      - Technology insertion

Application of Performance-Based Acquisition

- New Development Programs - Performance Based
- Reprocurement Options for Existing Items
  - Build-To-Print if no Changes
  - Modified Build-To-Print if Changing Contractor Processes
  - F^3I if product redesigned
- Program Trades Will Decide the Appropriate Approach

Performance - Based Specifications

Requirement Allocation

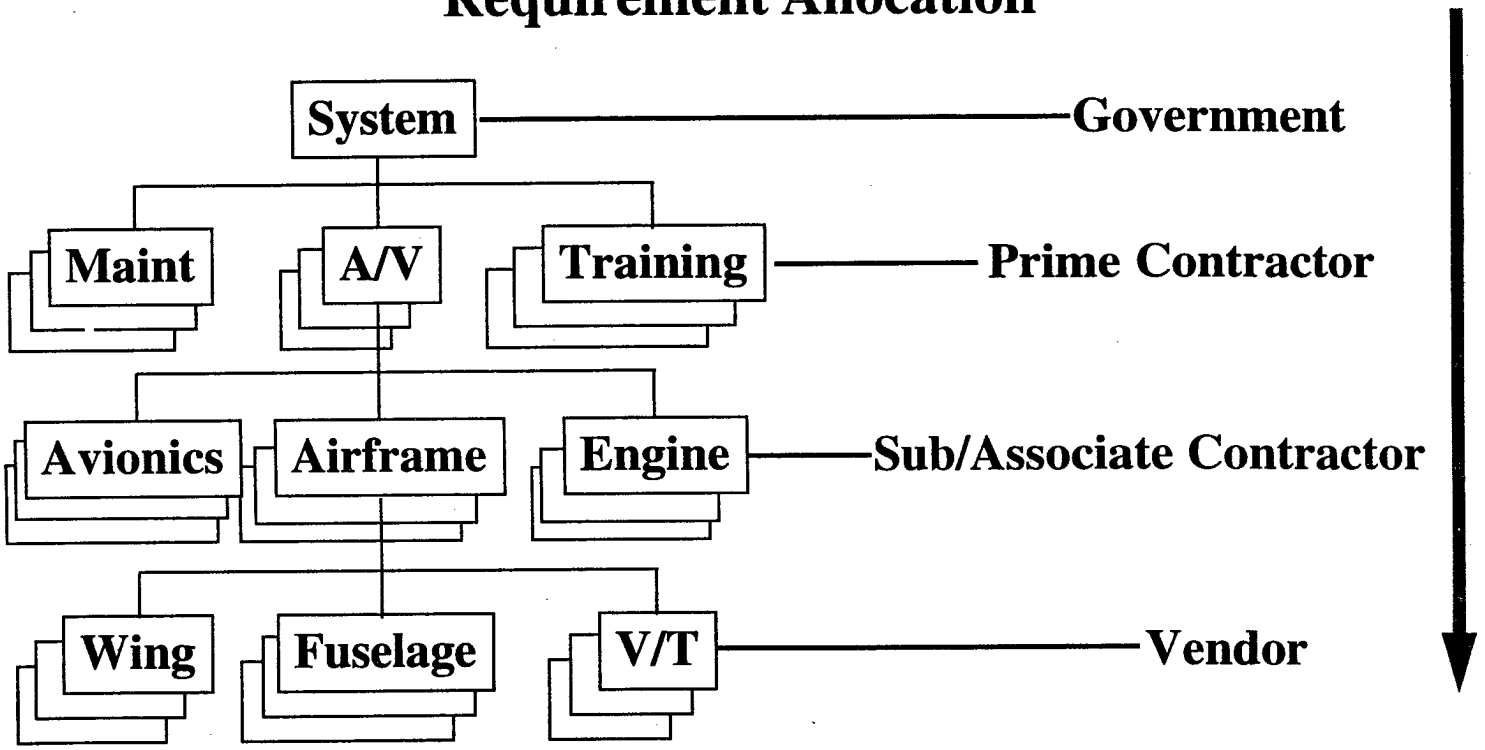

Specification Tree (Aviation)

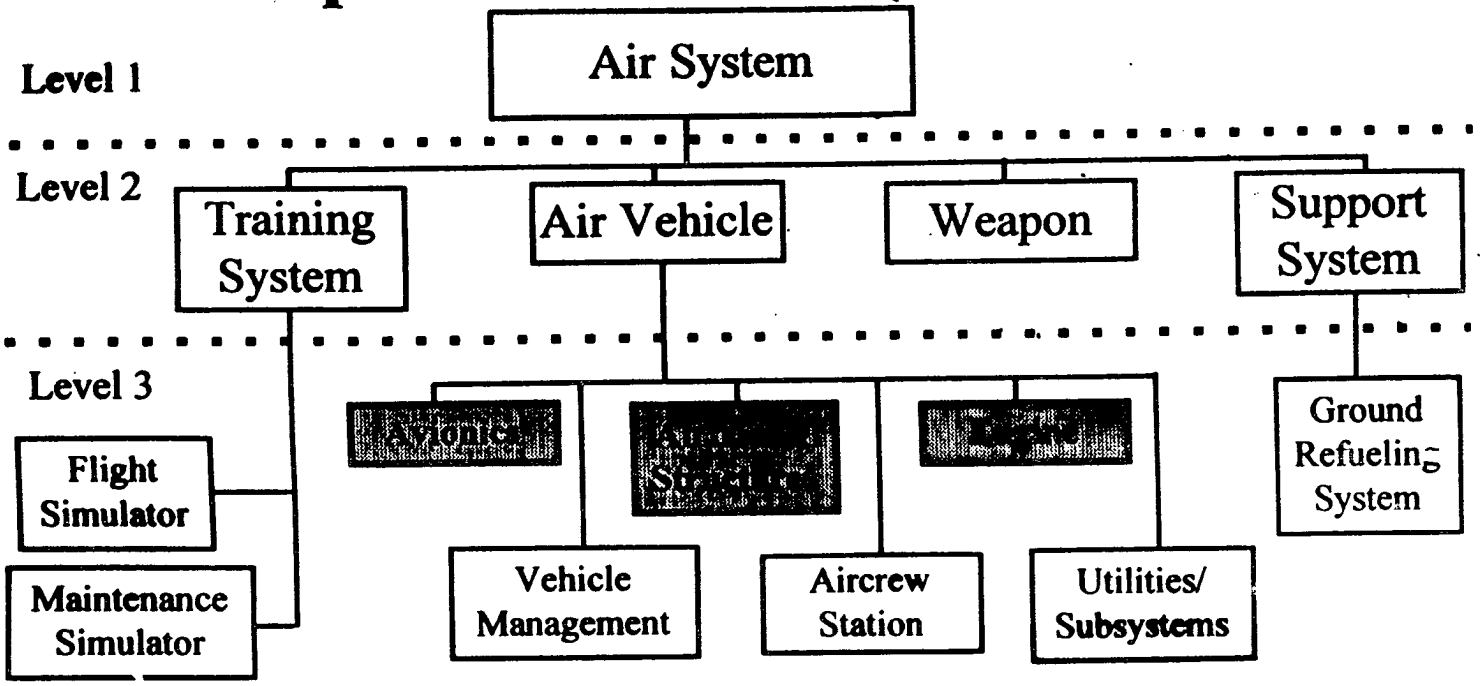

Common Use, Military Unique Specs & Stds Needed to Develop & Field Aeronautical Systems

Human Performance	Avionics Multiplex	Air Transportability	Integrated Diagnostics	Display Symbology
Electromagnetic Effects	Support System Mobility	Sound Pressure Levels	Armament Integration	Human/Computer Interface

as of 31 Oct 95

Structural Integrity Requirements

- No Reference to MIL-STD-1530 in Statement of Objectives (SOO), Instructions to Offeror (ITO) or Systems Requirements Document (SRD)
  - Utilize Structures Guide Specification for requirements language
    - Contractor to furnishes compliance methods and plans in proposal
- Contractors will be rated based on past performance, integrity program process and Manufacturing/Quality Systems
  - Draft Structures Guide Specification has requirements/guidance
    - Advanced Quality System

A Performance-Based Process -Vendor Rating

- Part of New Checks/Balances
- Earned Rating Based on Demonstrated Past Performance
- Three Levels
- Privileges Associated with Each Level

The Evaluation Process

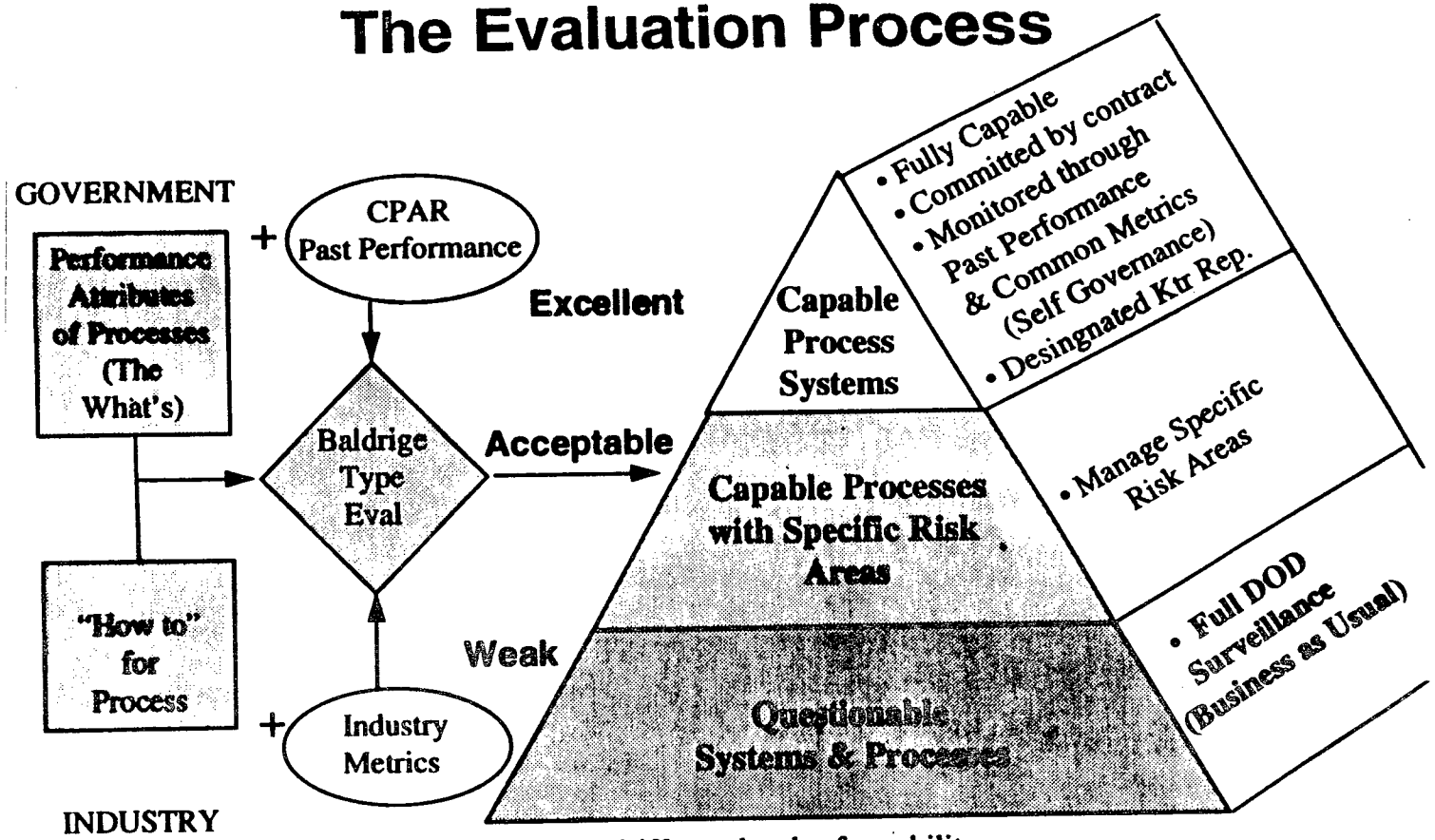

- Different levels of capability
  (CAUSE)
- Different levels of Risk Mgt and oversight
- Different Resource consumption
  (SPO size, DCMC manning, etc..)

SESSION II

STRUCTURAL JOINTS

Chairman: *D. Paul*, WL/FIB

Local Stresses and Distortions of a Three-dimensional, Riveted Lap Joint

Mr. K. Iyer[1], Dr. P.C. Bastias[2], Dr. C. A. Rubin[3] and *Dr. G. T. Hahn[3]
Department of Mechanical Engineering
Box 1592, Station B
VANDERBILT UNIVERSITY
Nashville, TN 37215

ABSTRACT

This paper presents finite element analyses for a simple lap joint for three different rivet geometries, and two levels of mesh refinement. The results describe the compliance of the connection, the rivet tilt, and the peak contact pressures, slip amplitudes and stress concentrations. The effects of plasticity are examined for the coarser model. Results are compared with similar studies. The reliability of the 3-D analyses at present refinement levels is found to be open to question, and basic features, such as the peak stress concentration at the panel hole, remain ill-defined. It is also shown that fretting may contribute to fatigue crack initiation.

INTRODUCTION

The stress concentrations, local strains, and the pressure and relative slip at the contacting interfaces, govern the fatigue life and fretting of riveted or bolted connections. These features are now becoming accessible to numerical analysis. Simple 2-dimensional analyses have been performed by Swenson, Gondhalekar and Dawicke [1], Hutchinson and coworkers [2,3], and Iyer et al. [4]. These analyses offer reliable estimates of the local stresses and strains but are unable to account for the contributions from out-of-plane bending and in-plane slip between the panels; these are especially important in a single row lap joint. More realistic, 3-

---

[1] Graduate Research Assistant, [2] Research Assistant Professor and [3]Professor, Department of Mechanical Engineering, Vanderbilt University.

D, finite element analyses have been reported by Sherbourne and Bahaari [5], Weissberg, Wander and Itzhakov [6], Fung and Smart [7], and by the present authors [8]. The 3-D analyses are demanding in terms of computer time. Even a relatively coarse mesh consumes 2 - 5 hours on an advanced machine. Fung and Smart [7] have modeled the elastic behavior of a simple lap joint, fastened with a conventional "snap" rivet and a countersunk rivet, and have examined the effects of clamping forces and low levels of interference. Iyer et al. [8] have modeled non, partial and fully countersunk configurations, and examined the effects of cyclic plasticity.

This paper presents results for a simple lap joint with 3 rivet geometries, and 2 levels of mesh refinement. The results describe the compliance of the connection, the rivet tilt, and the peak contact pressures, slip amplitudes and stress concentrations. The effects of plasticity are examined. Results are compared with similar calculations by Fung and Smart [7] and shed light on the adequacy of the present levels of mesh refinement. In both cases, the models employed relatively coarse meshes and questionable surface elements. Consequently, the reliability of the 3-D analyses is open to question, and basic features, such as the peak stress concentration at the panel hole, remain ill-defined.

ANALYTICAL PROCEDURES

The model geometry consists of two (upper and lower) sheets and a rivet. The different rivet geometries and material properties considered are shown in Table 1. Three different rivet geometries are considered: (1) Case A in which the rivet has one standard head at its lower end and one head countersunk to a depth of half the thickness of a single sheet, the included angle being 100°; (2) Case B, in which the rivet has one standard head at its lower end and one head countersunk to a depth of the thickness of a single sheet. In this case, the maximum and minimum diameter remain unchanged resulting in an included countersink angle of 60°; and (3) Case C, in which a double headed rivet with no countersinking is treated. Models A1, B1 and C1 simulate purely elastic material behavior and have a relatively coarse finite element mesh. Model B3 differs from B1 only in that it models an elastic-plastic material response (elastic linear kinematic hardening plastic, or ELKP behavior [9]). The refined elastic models are denoted as A1R, B1R and C1R. Elastic-plastic calculations have not yet been performed for the refined models.

The dimensions of the model lap joint are given in the Figure 1 caption.

A cyclic tensile load is applied at the non-overlapping end face of the upper sheet while the corresponding face belonging to the lower sheet is fixed along the x-axis. Fig. 1 shows the main features of the more refined models used in the present study. In addition, the edges A and B are fixed in the z-direction to prevent unrestrained rotation of the body in space. The geometry shown in Fig. 1 represents one unit of a multi-riveted, single row, long panel extending in the positive and negative y-directions. Lines CD and EF represent the symmetry planes and are constrained against motion in the y-direction. Material properties are defined by the following parameters: σ_E = 70 GPa, σ_K = 369.9 MPa, and M = 57.5 GPa, the elastic-plastic parameters used in Model B3.

The lap joint compliance, C = C' - C". Here, C' = δ/P, is the compliance of the model joint, P is the applied load and δ is the total displacement, and C" = L/(EA) = 93.4 m/GN, is the compliance of a continuous panel having the same length, L, as the model joint (length of the 2 panels minus the overlap) and the same cross sectional area, A, and elastic modulus, E, as the separate panels. As the load is applied and the rivet tilts, the panels displace, bend and deform around the rivet hole, distortions that are absent in the continuous panel. The joint compliance is related to these factors.

The coarse finite element meshes, features of which are shown in Fig. 2, typically consist of 1837 nodes, 390 user defined elements and 175 internally generated contact elements. Typical figures for the total number of variables and estimated RMS wavefront are 4554 and 519, respectively. A problem with ABAQUS Version 5.4-1 prevented the modeling of only half of the symmetric plates and rivet; consequently, the entire system was modeled. A later version of ABAQUS which resolves this problem is presently being implemented. Calculations with elastic material response consumed between 1400s to 6400s of CPU time on a SGI Power Challenge Array supercomputer, depending on the value of the friction coefficient. Elastic-plastic calculations consumed about 12000s (3.3 hours) of CPU time. In all cases, 8 noded, linear brick, incompatible modes elements (C3D8I) defined the bodies. For these elements, in addition to the displacement degrees of freedom, incompatible modes are added internally enabling element shearing without locking. This enhances the models' kinematic response to bending.

A more refined mesh, shown in Fig. 3, is obtained by doubling the number of elements along the circumferential edges and increasing the number of radial divisions in the overlapping portions of the sheets by 1. The refinement along the depth was left unchanged, as shown in Fig. 1. These models consist of 4569 nodes

out of which 991 are user defined, 640 user defined elements and 429 internally generated contact elements. Typical figures for the total number of variables and estimated RMS wavefront are 11332 and 739 respectively. Calculations were performed for rivet types A, B and C, elastic material response and μ=0.2, consuming about 2800s of CPU time. It is suspected that the lower coefficient of friction and the faster convergence due to improved modeling of the contact contributed to lowering the overall CPU time, while the larger size of the model contributed to an increase.

Finite element calculations performed by Fung and Smart [7] employed models consisting of 20 noded, quadratic bricks in the bulks of the sheets and the rivet, with the interfacial interactions modeled using 9 noded faces and INTER9 elements with μ=0.06; the calculations were performed using ABAQUS version 5.2. While quadratic elements are superior to linear elements in general, the mesh used in Fung and Smart's calculations consisted of one element thickness through the depth of the sheets and half as many circumferential elements compared to the refined models in the study described in this paper. It is therefore difficult to determine which mesh is superior from a refinement point of view. In addition to these differences, there are variations in the meshing, rivet head geometries, and countersink angle which could lead to different results. The interface elements used in both studies to model the contacting surfaces connect specific sets of nodes on the three interacting bodies and are most effective when slip magnitudes are much smaller than the characteristic element length. In situations involving large sliding magnitudes, they can conceivably prevent sufficient slip relaxation in the interfaces and lead to higher stresses. However, coarse elements, which satisfy the requirement that their characteristic length be much larger than slip magnitudes, can artificially stiffen the response of the joint to bending, thus lowering tensile stresses.

RESULTS

Table 2 summarizes the results of the 3-dimensional analyses described above. It refers to Fig. 3, a detail of the mesh. There are significant differences between the results obtained using the coarser and more refined meshes. For example, peak stresses are as much as 50% higher, rivet tilts are 25% higher and slip amplitudes are in most cases 30% smaller for the more refined models. Generally, it is seen that the coarse models underpredict the rivet tilt while they overpredict the slip magnitudes.

Fig. 4 shows displaced meshes for the three cases. Noticeable bending of

panels and tilting of rivets produce stress and strain gradients in the thickness direction which are absent in the 2-D representation. Countersinking makes the connection more compliant and increases rivet tilt. Rivet tilt is accompanied by local bending of the panels. Compliance values for the single row, rivet models examined here, between 27.7 m/GN and 34.7 m/GN, are effectively about 3x the values reported by Weissberg et al. [6] for a 2 row, steel bolted joint. However, as pointed out by Weissberg et al., it should be kept in mind that published compliance measurements show considerable scatter due to varying and sometimes unknown values of bolt interference and clamping force. The rivet's material properties and the method used to derive compliance can also affect the results.

As shown in Fig. 5, tensile stresses are higher near the inside panel surfaces, consistent with panel bending. For the countersunk panel this coincides with the thinned section. Peak tensile stresses in the partially countersunk case are highest. The peak stresses vary directly with tilt and bending. The stress field obtained with the 2-D model is shown in Fig. 6. The peak stress concentrations in the 3-D models are: 6.0, 5.6 and 4.0 for A1R, B1R and C1R, respectively; the stress concentration obtained from the 2D model is 6.3. The peak tensile stress for the plastically deformed case is 470.0 MPa. The peak stress concentration factor calculated by Fung and Smart is 10 for μ=0.06. Possible explanations for discrepancies can be found in the next section. Fig. 7 shows the very large relative slip at the panel-panel interface produced by plastic deformation during the first loading cycle. This is 5.7x larger than obtained for elastic deformation at the same load.

Figure 8 shows angular locations of peak stresses; the 90° direction corresponds with the direction of tensile loading. The peak tension in the countersunk panels is observed at θ =11°, and θ =169° ; in the non-countersunk case, the peaks are at θ =22° and θ =158°. The convention for labeling angles is shown on Figures 6 and 8a. for The corresponding results for the 2-D model, shown in Fig. 6, are at θ = -4° and θ =-184°.

Figs. 9 and 10 shows the distribution of the lateral stress, S11, acting at the rivet interface; this corresponds approximately to the contact pressure acting on the shank and is the dominant component of the pressure acting on the countersunk surfaces. In contrast with the 2-D representation, where pressures are uniform along the pin and panel thickness direction (direction 3), the pressures are highly localized in the 3-D case. These non-uniform distributions lead to peak pressures that are 100% larger than in the 2-D representation. For case B5, shown in Figure 10b, the high pressures acting on the rivet head produce a plastic bending buckling

of the rivet head accompanied by a relaxation of the pressure.

DISCUSSION

The traditional method of establishing the adequacy of mesh refinement of a finite element model is by ensuring that critical features, such as the stress concentration factor, do not change with further refinement. In view of the large differences between the coarse and more refined 3-D models examined here, the adequacy of the mesh refinement of models A1R, B1R and C1R is open to question. Interpenetration between the upper sheet and rivet occurred in the coarse mesh due to an excessively coarse representation of each body; this was partly responsible for increasing computation time for the coarse models, and has been eliminated in the more refined meshes. The more refined models have begun to capture gross features such as correlation between rivet tilt and compliance. Stress and slip gradients through the depth have smoothened considerably even though the number of elements along the depth axis remains unchanged. Yet there is further evidence that a convergent solution has not yet been reached; the calculated stress concentration factor continues to increase with mesh refinement.

The stress concentration factor obtained from the 2-D elastic model is about 6.3 [4], in the absence of countersinking and sheet bending. Accounting for these effects, the 3-D stress concentration should definitely be higher. Shivakumar and Newman [10] calculate stress elevation factors of 1.25 each for the two effects. Based on this accounting, the stress concentration should be about 10. However, the clamping effect of the rivet head will reduce bending at the location of the peak stresses reducing the stress concentration. Based on the calculated stress gradient under the head in the thickness direction, and the 2-D value of 6.3, a peak stress concentration of about 8 appears likely. The peak value of 10 reported by Fung and Smart [7] may reflect their larger countersink angle and/or more compliant rivet head. The present calculations show that the stress concentration increases with rivet tilt and the severity of countersinking. These observations suggest that even the relatively refined finite element mesh represents sheets which are excessively stiff in bending. Indications are quite clear that localized mesh refinement around the interfacial region alone will be insufficient. Even regions far removed from the interfacial areas are subject to significant bending and should be sufficiently refined in order to transmit the correct response to the interface. The presence of a clamping force on the rivet head will in fact push the region of the sheet, where severe local bending begins, outward from the center of the rivet, accentuating the need for a uniformly refined mesh. The asymmetry of the calculated deformations about the symmetry plane are an additional indication of

the inadequacy of the model.

The 3-D calculations also demonstrate that a 2-D model does not offer reliable descriptions of the deformation of a lap joint. The 2-D model cannot provide for contersinking and clamping, and does not account for the effects of rivet tilt and panel bending. It understates slip amplitudes and peak contact pressures and may understate the peak stress concentration as well. Panel bending shifts the peak stresses to the interior panel surfaces where fatigue cracks are observed to initiate. The fact that the peak stresses at that location are higher for the fully countersunk case than for the partially countersunk panel is consistent with experience that fully countersunk installations are inferior. The tilting of the rivet head produces contact pressure at the panel-panel interface below the hole, coupled with large slip-amplitudes at the panel-panel interface. It is thought that the lower sheet crimps plastically at the edge of the hole on its top surface and frets along the undersurface of the upper sheet, leading to the experimentally observed fretting scars. The shape of the regions in compression resembles the fretting scars observed experimentally and visible in Fig. 11.

The angular position of the peak stresses in the countersunk cases, $\theta = 11°$, does not coincide with sites of crack initiation in panels with the same configuration tested by the authors [8]; these are observed, on average, to occur between $\theta = -11°$ and $\theta = -14°$. The implication, that fatigue is not driven by the tensile stress amplitude, suggests that fretting at the rivet-panel interface, as well as fretting between the panels, and contributing to the fatigue crack initiation process. Considering the values of local slip amplitude and contact pressure at the river shank-panel interface and at the panel-panel interface, the propensity for fretting wear of the 3-D lap joint is greater than that calculated for the 2-D model [4].

CONCLUSIONS

1. A 2-D finite element model is not a valid representation of a single rivet-row lap joint.

2. Meshes more refined than the ones employed here are needed to reproduce the local bending of the panels.

3. The rivet tilt of a single rivet-row lap joint, joint compliance, slip amplitudes, local panel bending and the peak stresses are related.

4. The stress concentration in a single rivet-row, lap joint can be as high as 8 to 10 (in the absence of interference, clamping forces and adhesive).

5. Slip amplitudes of about 159 μm at the panel-panel interface coupled with high contact pressures arising from the tilted rivet head promote fretting at the edge of the rivet hole.

6. Fretting can contribute to fatigue crack initiation.

ACKNOWLEDGMENTS

The authors are grateful to Hibbitt, Karlsson and Sorensen, Inc. for permission to use their finite element Code ABAQUS. This research was supported with a grant from the Air Force Office of Scientific Research (F49620-93-1-0488).

REFERENCES

1. Swenson, D.V., Gondhalekar, S. R., Dawicke, D. S., "Analytical Developments in Support of the NASA Aging Aircraft Program with an Application to Crack Growth from Rivets", (ISSN 0148-7191), SAE General, Corporate and Regional Aviation Meeting and Exposition. Wichita, Kansas, 1993.

2. J. L. Beuth and J. W. Hutchinson, "Fracture Analysis of Multi-site Cracking in Fuselage Lap joints," Computational Mechanics, Vol. 13, 1994, pp. 315-331.

3. K. F. Nilsson, "Interaction Between a Major Crack and Small Crack Damage in Aircraft Sheet Material," Int. J. of Solids and Structures, Vol 31, 1994, pp. 2331-2346.

4. K. Iyer, G. T. Hahn, P. C. Bastias and C. A. Rubin, "Analysis of Fretting Conditions in Pinned Connections," Wear, Vol 181-183, 1995, pp. 524-530.

5. A. N. Sherbourne and M. R. Bahaari, "3D Simulation of End-Plate Bolted Connections," J. Structural Eng. Vol 120, 1994, pp. 3122-3136.

6. V. Weissberg, K. Wander and R. Itzhakov, "A New Approach to Load

Transfer in Bolted Joints," Proc. Int. Council of Aeronautical Sciences, Vol.1, 1988, pp. 96-101.

7. C. P. Fung and J. Smart, "An Experimental and Numerical Analysis of Riveted Single Lap Joints," Proc. Inst. Mech. Eng., Part g, J. Aerospace Eng., Vol 208, 1994. pp. 79-90.

8. K. Iyer, M. Xue, R. Kasinaduhni, P. C. Bastias, C. Rubin, J. J. Wert and G. T. Hahn, "Contribution of Fretting to the Fatigue and Corrosive Deterioration of a Riveted Lap Joint," Proc. Symp. Structural Integrity in Aging Aircraft, San Francisco, Nov. 15, 1995.

9. Hahn, G.T., Bhargava, V., Rubin, C.A., Chen, Q. and Kim, K., "Analysis of the Rolling Contact Residual Stresses and Cyclic Plastic Deformation of an SAE 52100 Steel Ball Bearing," *Journal of Tribology*, Vol. 109, pp. 618-626, 1987.

10. Shivakumar, K., N., Newman, J., C., Jr., "Stress Concentration Equations for Straight-Shank and Countersunk Holes in Plates," Journal of Applied Mechanics, Vol 62, 1995, pp. 248-249.

Table 1. The finite element models.

Model	Rivet heads	Coefficient of Friction, μ	Mesh	Material Behavior
2-D	Rivet modeled as pin in plane strain. Single sheet.	0.2	highly refined	elastic
A1	1 standard 1 countersunk (to ½ panel thickness)	0.2	coarse	elastic
B1	1 standard 1 countersunk (to full panel thickness)	0.2	coarse	elastic
B3	1 standard 1 countersunk (to full panel thickness)	0.2	coarse	ELKP
C1	2 standard	0.2	coarse	elastic
A1R	1 standard 1 countersunk (to ½ panel thickness)	0.2	refined	elastic
B1R	1 standard 1 countersunk (to full panel thickness)	0.2	refined	elastic
C1R	2 standard	0.2	refined	elastic

Table 2. Comparison of results from two sets of meshes

MODEL		A1	B1	B3		C1	A1R	B1R	C1R
Feature	Location*			Loading	Unloading				
Joint Compliance (m/ GN)	—	40.8	32.9	—	—	25.4	34.7	34.2	27.7
Rivet Tilt, degrees	—	3.2	3.3	7.33	3.33	2.6	4.3	4.2	3.0
Total in-plane slip at rivet-panel interface (μm)	a	62.4	61.2	692.31	638.58	27.7	28.6	29.1	25.0
	a'	89.8	45.2	471.94	442.98	37.0	17.1	31.9	18.2
	a''	-67.5	-61.1	-96.44	-35.54	-67.5	-64.9	-67.9	-67.2
	b	114.4	73.8	725.54	648.92	49.3	64.5	64.7	48.0
	b'	110.3	87.4	877.8	763.7	49.7	75.7	75.7	52.0
	b''	-31.5	-56.5	-111.09	-52.88	-36.4	-67.3	-68.1	-73.0
Total in-plane slip at panel-panel interface (μm)	g	225.4	184.4	1072.35	852.63	122.1	160.2	176.4	120.7
	h	215.3	201.1	1116.9	874.13	159.3	159.3	166.7	135.8
Total out-of-plane slip (μm)	c	-50.9	-3.4	-2.58	-12.3	4.37	-1.8	-33.3	-5.4
	c'	-30.2	23.5	246.25	235.66	5.85	-8.6	-32.1	0.0
	c''	24.1	21.9	19.3	-0.65	22.83	16.0	10.2	7.0
	d''	0.8	-1.3	-8.48	-2.52	0.3	2.4	0.3	-2.0
Peak tensile stress in elements adjacent to rivet hole (MPa)	e	443.4	407.8	43.8	-166.9	389.0	455.8	392.5	447.7
	e'	370.3	380.3	210.3	-190.6	248.2	700.0	591.1	414.4
	e''	550.9	488.8	352.3	-143.9	545.1	532.6	528.1	505.1
	f	213.9	481.9	107.8	-21.6	191.6	311.8	236.9	341.6
	f'	590.5	589.1	277.9	-206.2	339.5	747.5	697.9	434.6
	f''	330.8	300.0	133.8	-110.8	324.1	419.7	408.4	440.2
Contact Pressure (MPa)	panel-panel	—	—	—	—	—	-79.2	-111.5	-115
	panel-rivet head	—	—	—	—	—	-93.6	-117	-74.9

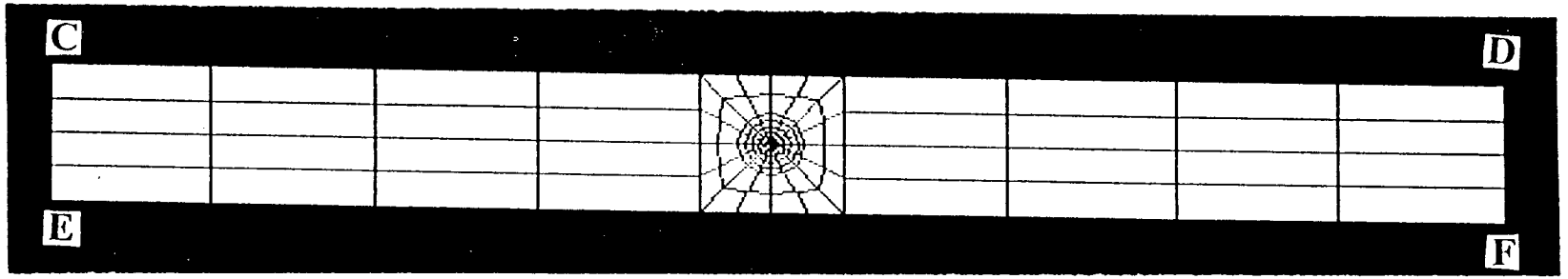

(a)

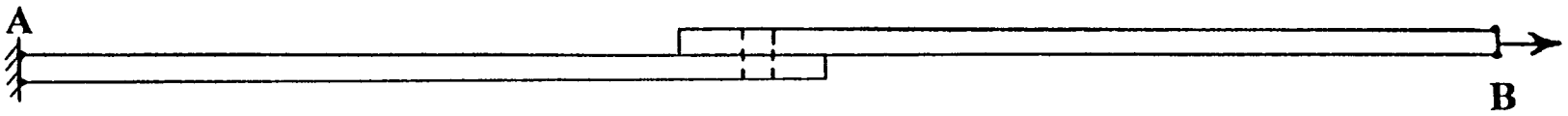

(b)

Figure 1. 3D-finite element model of a single rivet-row, lap joint: (a) plan-view of refined mesh, and (b) schematic of model profile. More detailed descriptions of the coarse and refined meshes can be found in Figures 2 and 3. The overall length of the model is 168.3 mm; the length of the overlap region is 30.6 mm; the width of the panels (repeat distance) is 30.6 mm; the thickness of the panels is 1.53 mm; the rivet shank diameter is 6.12 mm; the rivet head diameter and height are 9.792 mm and 3.83 mm respectively.

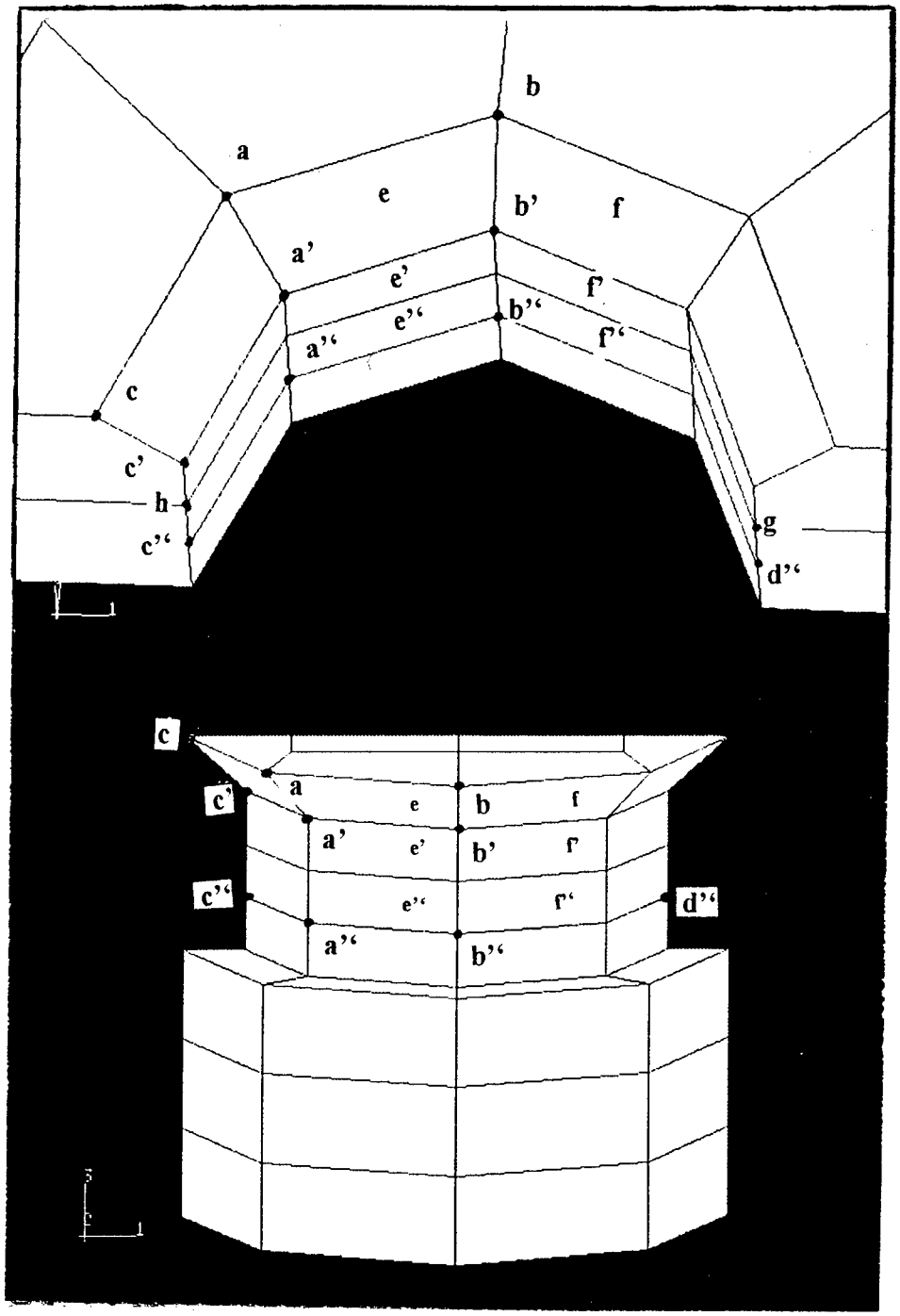

Figure 2. Details of the "coarse" mesh Model A1 (see Table 1) showing the rivet and ajacent panel. Values of the stresses and slip amplitudes at locations a-h are given in Table 2.

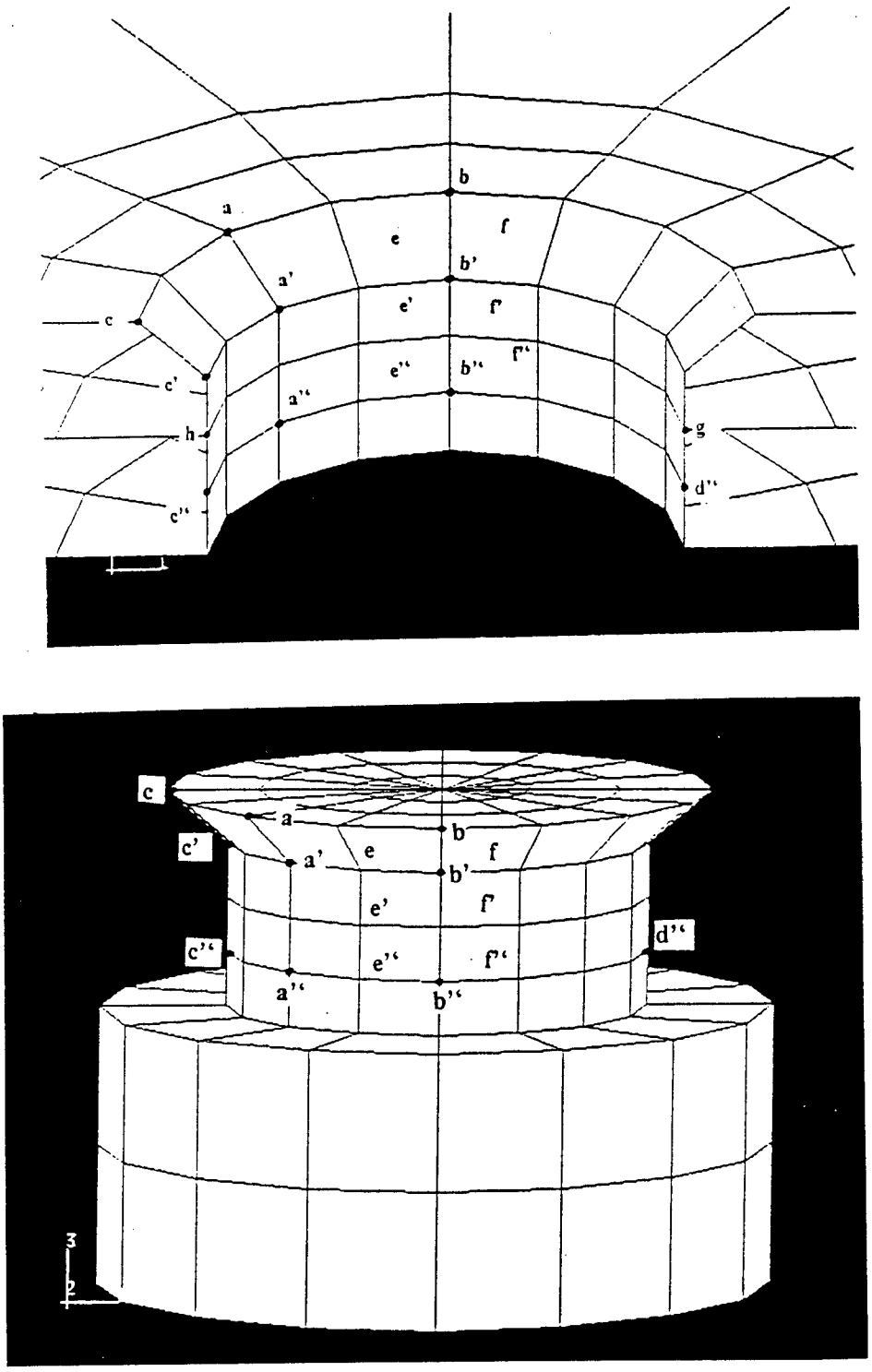

Figure 3. Details of the "refined" mesh Model A1R (see Table 1) showing the rivet and ajacent panel. Values of the stresses and slip amplitudes at locations a-h are given in Table 2.

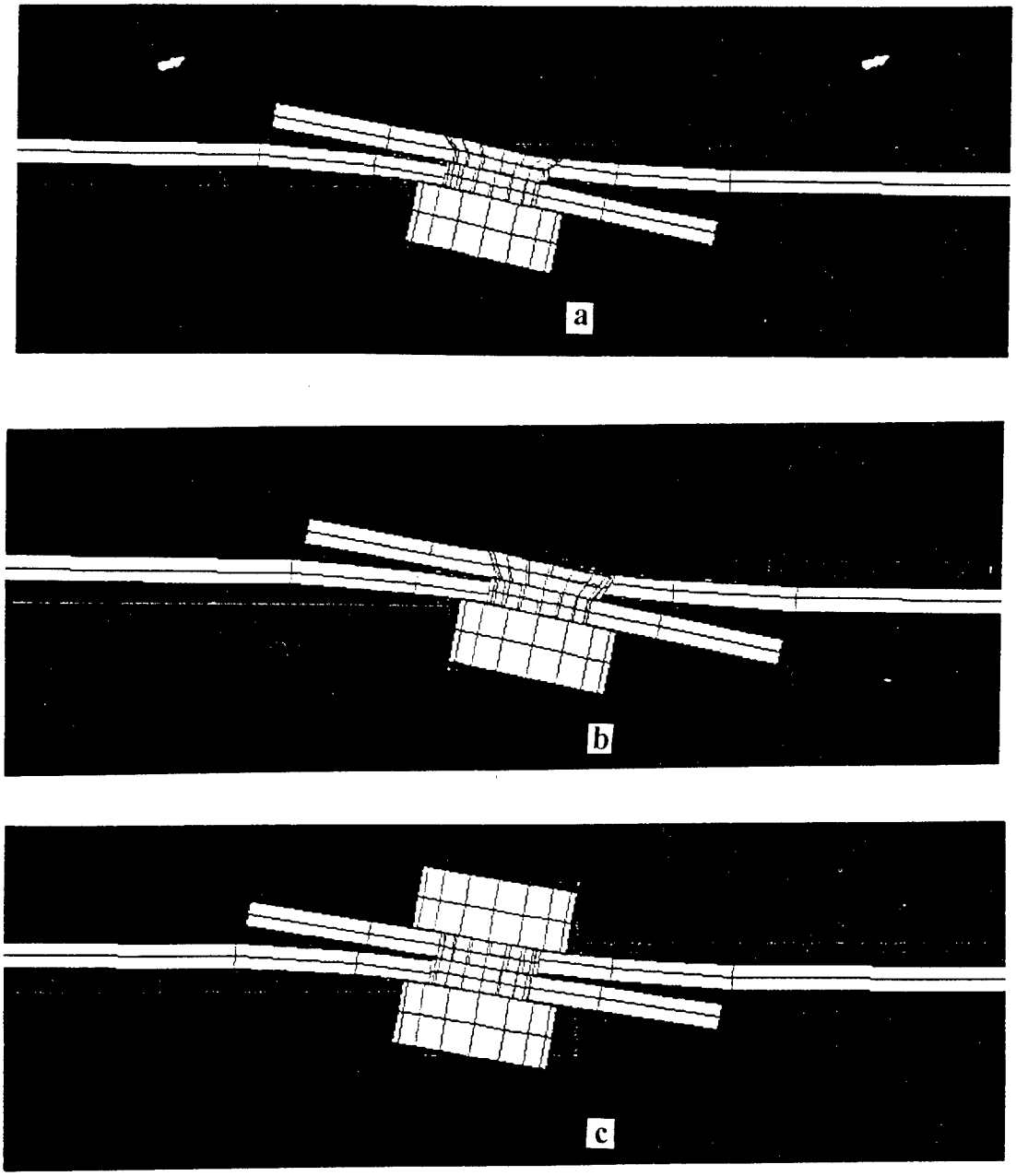

Figure 4. Profile view of the displaced meshes for a nominal applied stress of σ = 125 MPa: (a) Model A1R, partial countersink, (b) Model B1R, full countersink, and (c) Modle C1R, no countersink. Displacements are magnified by 3x.

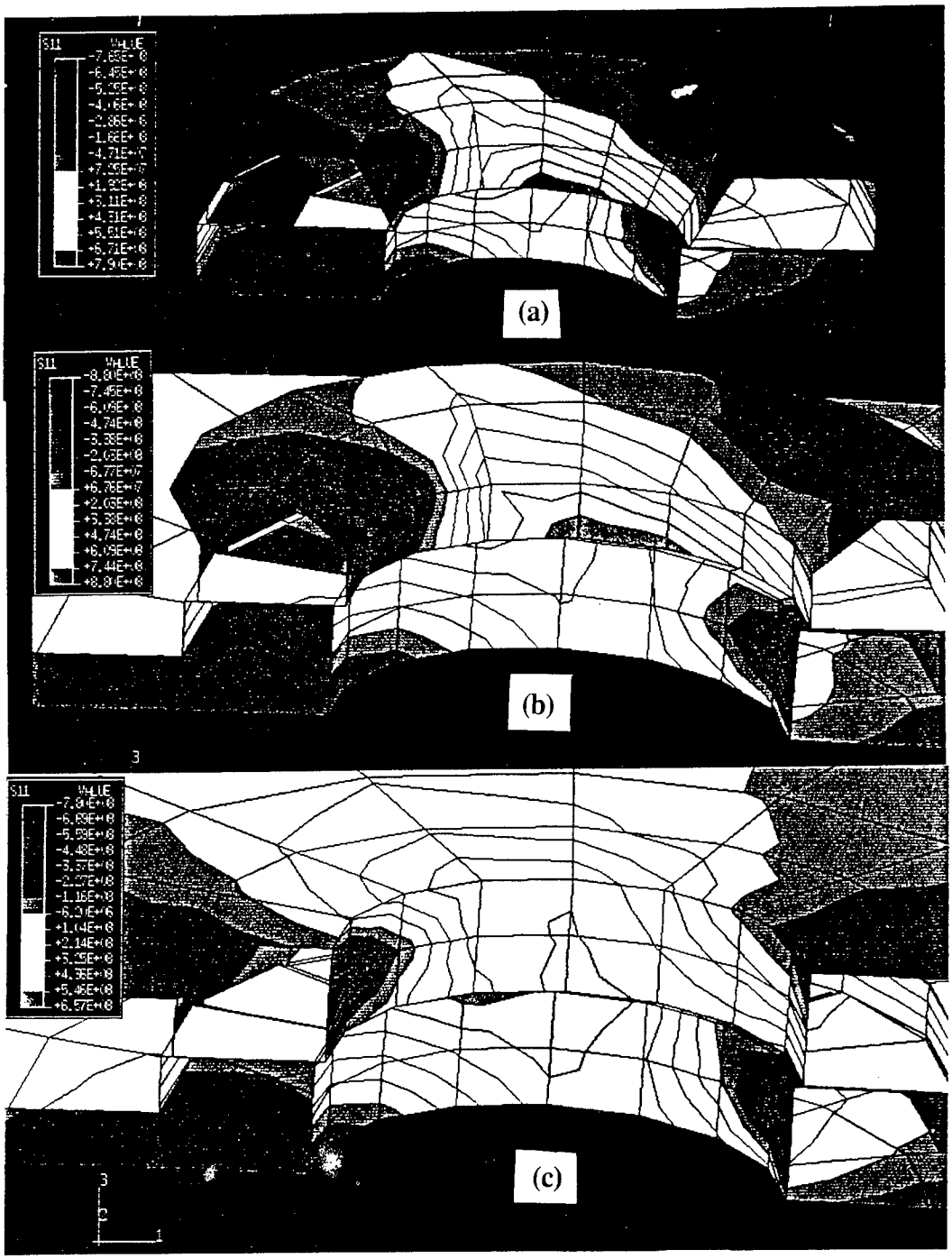

Figure 5. Normal stress fields -- σ_{11}, where direction 1 is the loading direction-- generated in the models: (a) Model A1R, (b) Model B1R and (c) Model C1R. Displacements are magnified 3x.

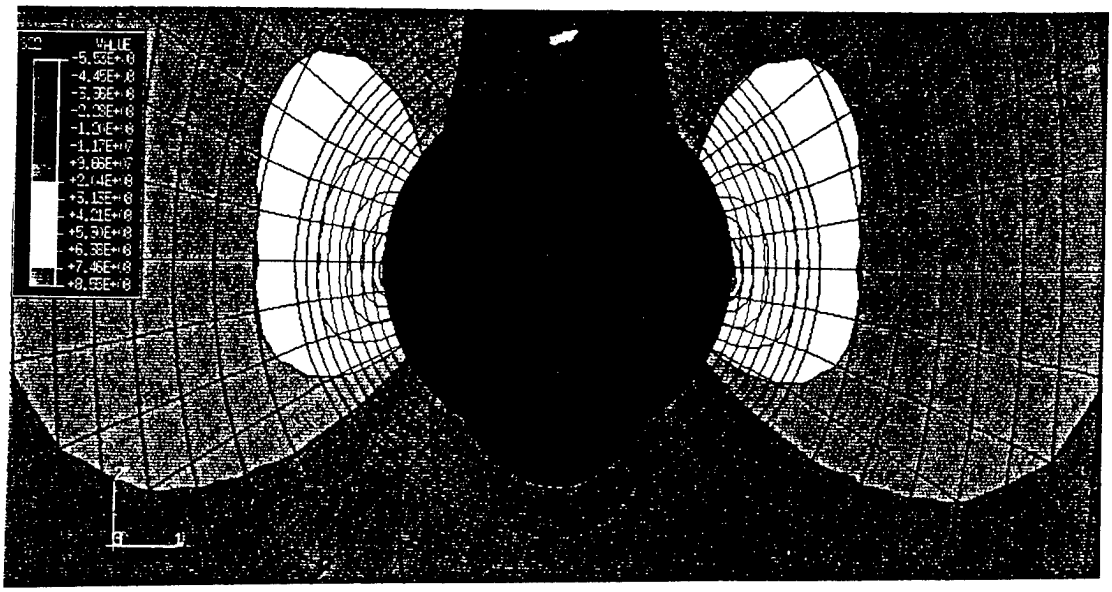

Figure 6. Normal stress field -- σ_{22}, where the direction 2 is the loading direction --generated in a 2D model of a pinned connection at a nominal stress, σ = 125 MPa.

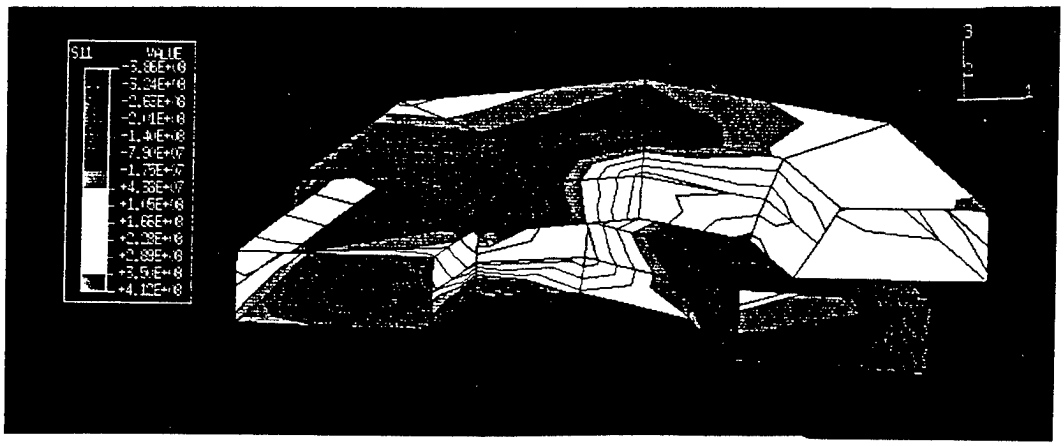

Figure 7. Normal stress field -- σ_{11}, where direction 1 is the loading direction -- generated by elastic-plastic deformation in the Model B3. Displacements are magnified 3x.

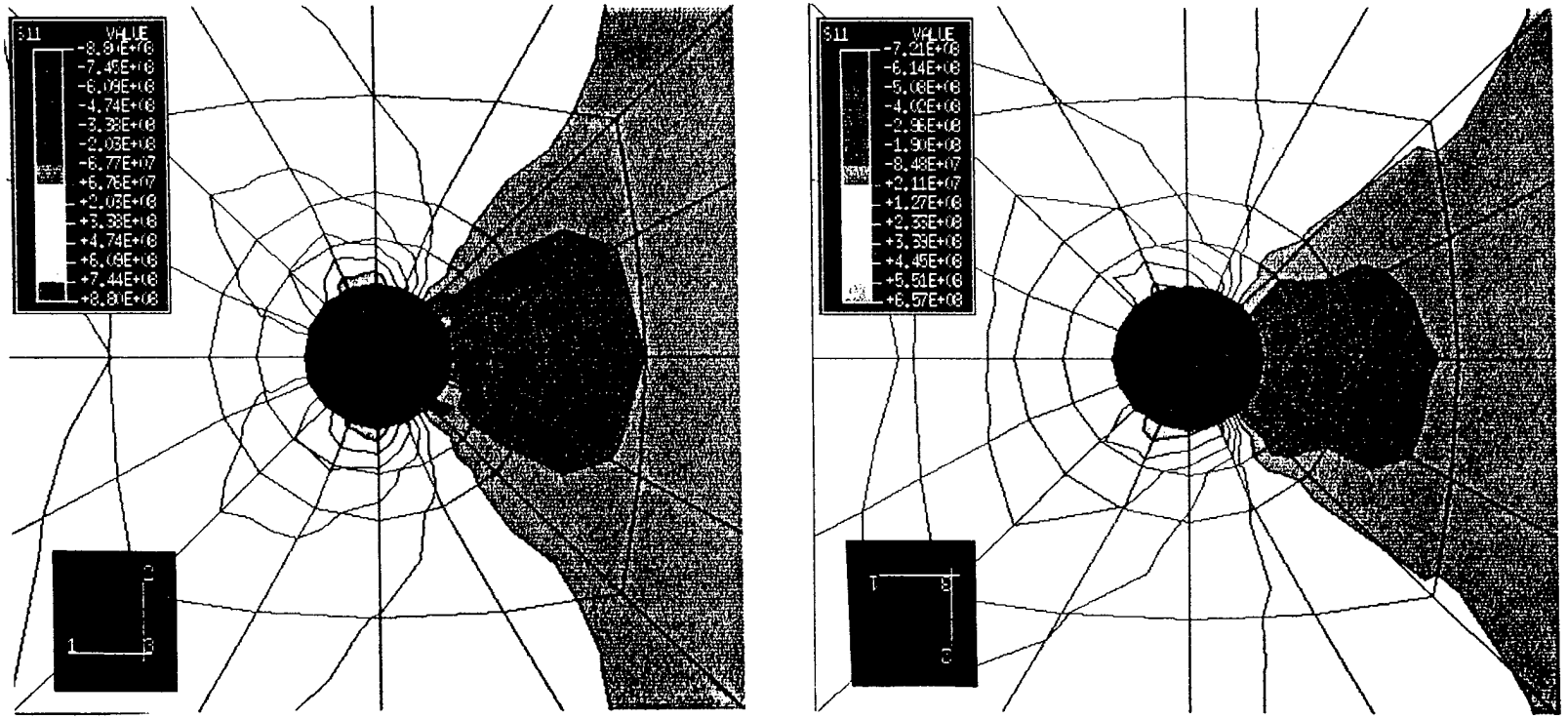

Figure 8. Normal stress fields -- σ_{11}, where the direction 1 is the loading direction-- viewed on the inner panel surface: (a) Model A1R, and (b) Model C1R.

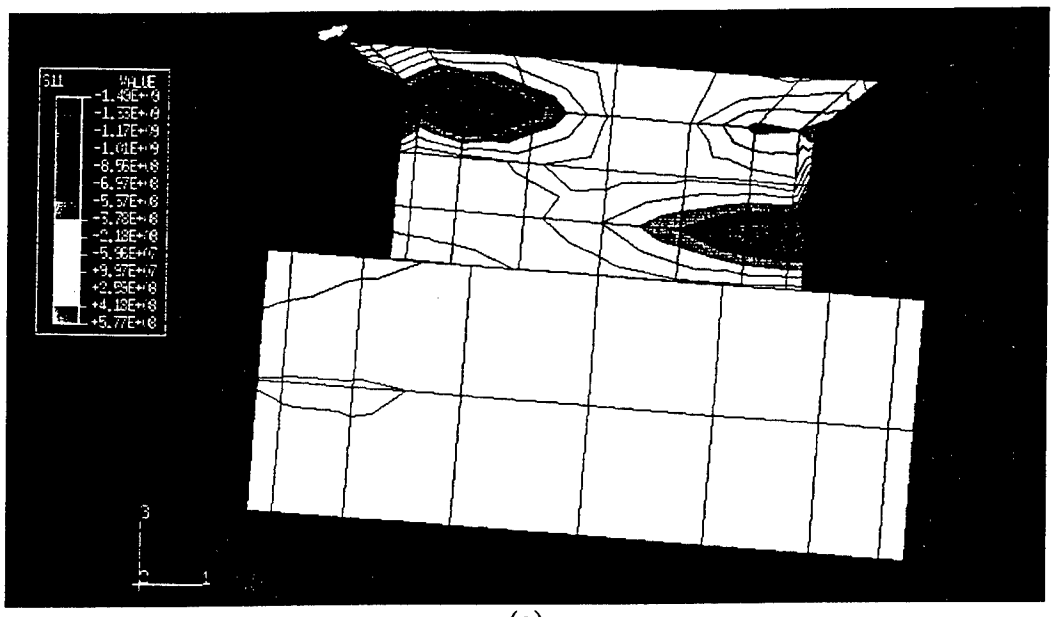

(a)

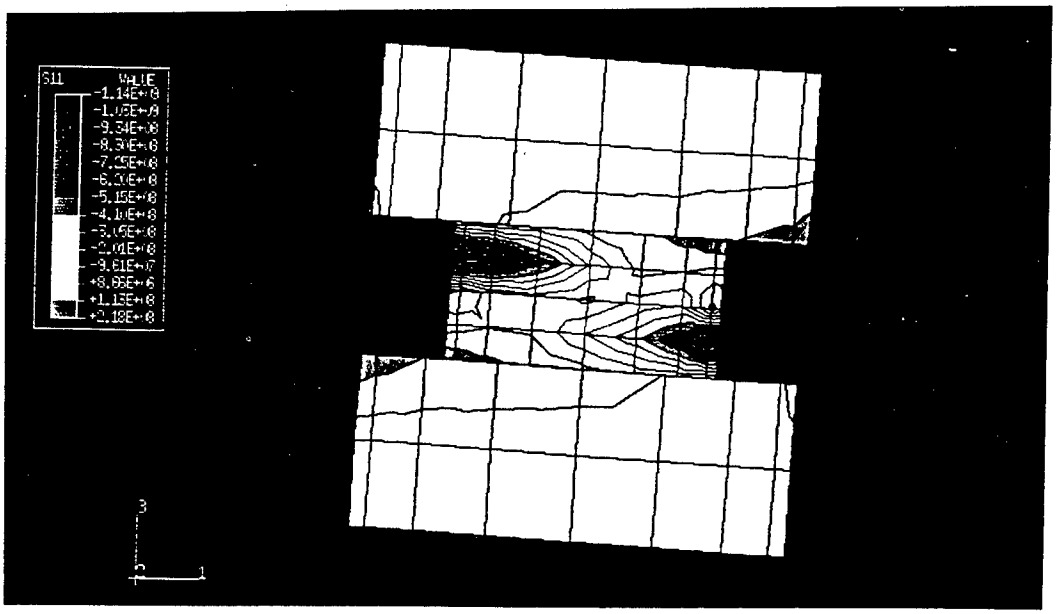

(b)

Figure 9. Contact pressure distribution on rivet shank: (a) Model A1R and (b) Model C1R.

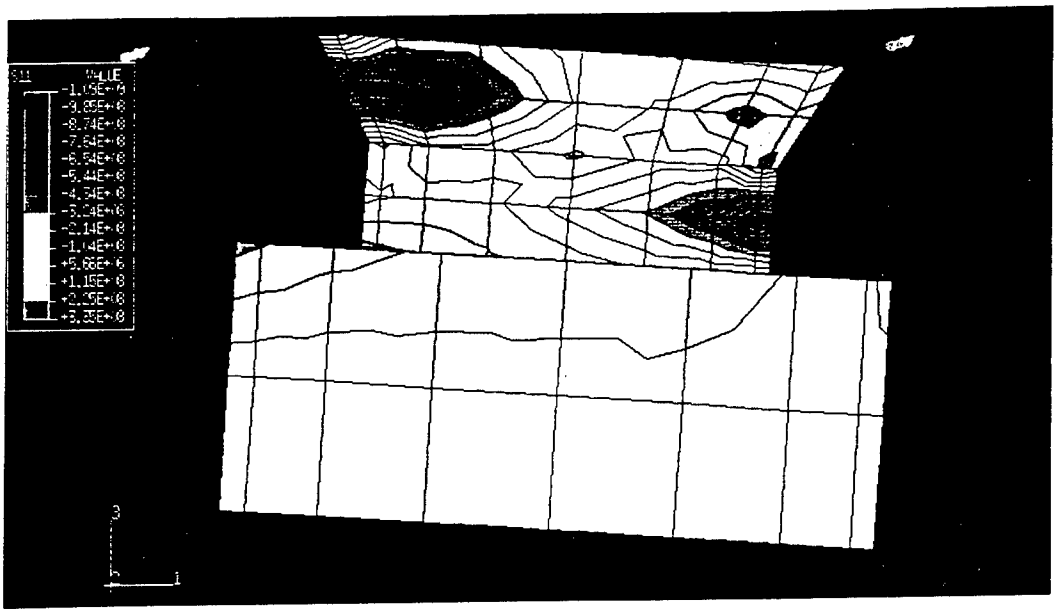

(a)

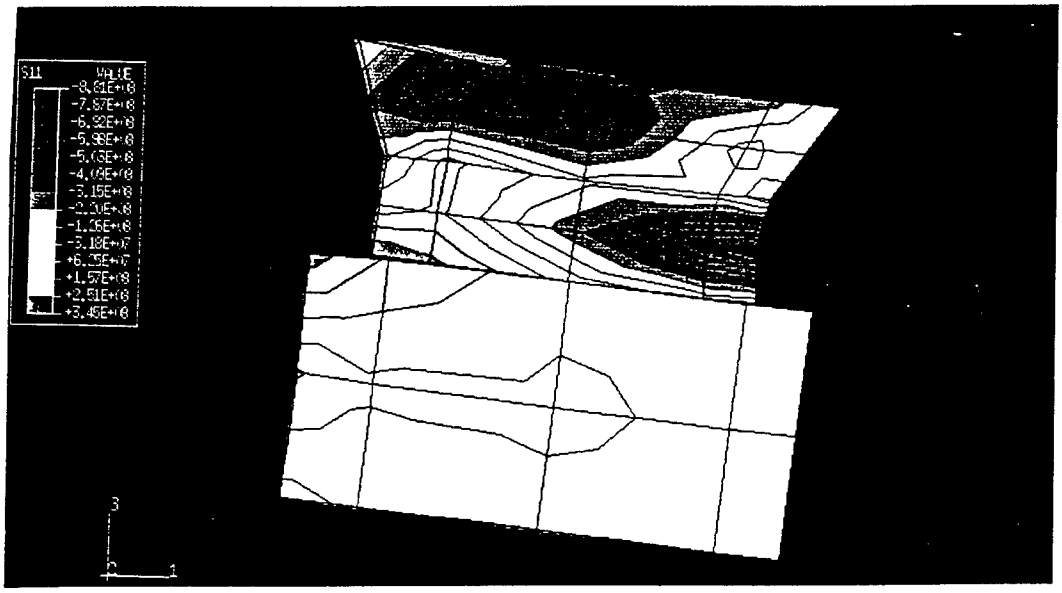

(b)

Figure 10. Contact pressure distribution on rivet shank: (a) elastic deformation of "refined" Model B1R and (b) elastic-plastic deformation of "coarse" Model B3.

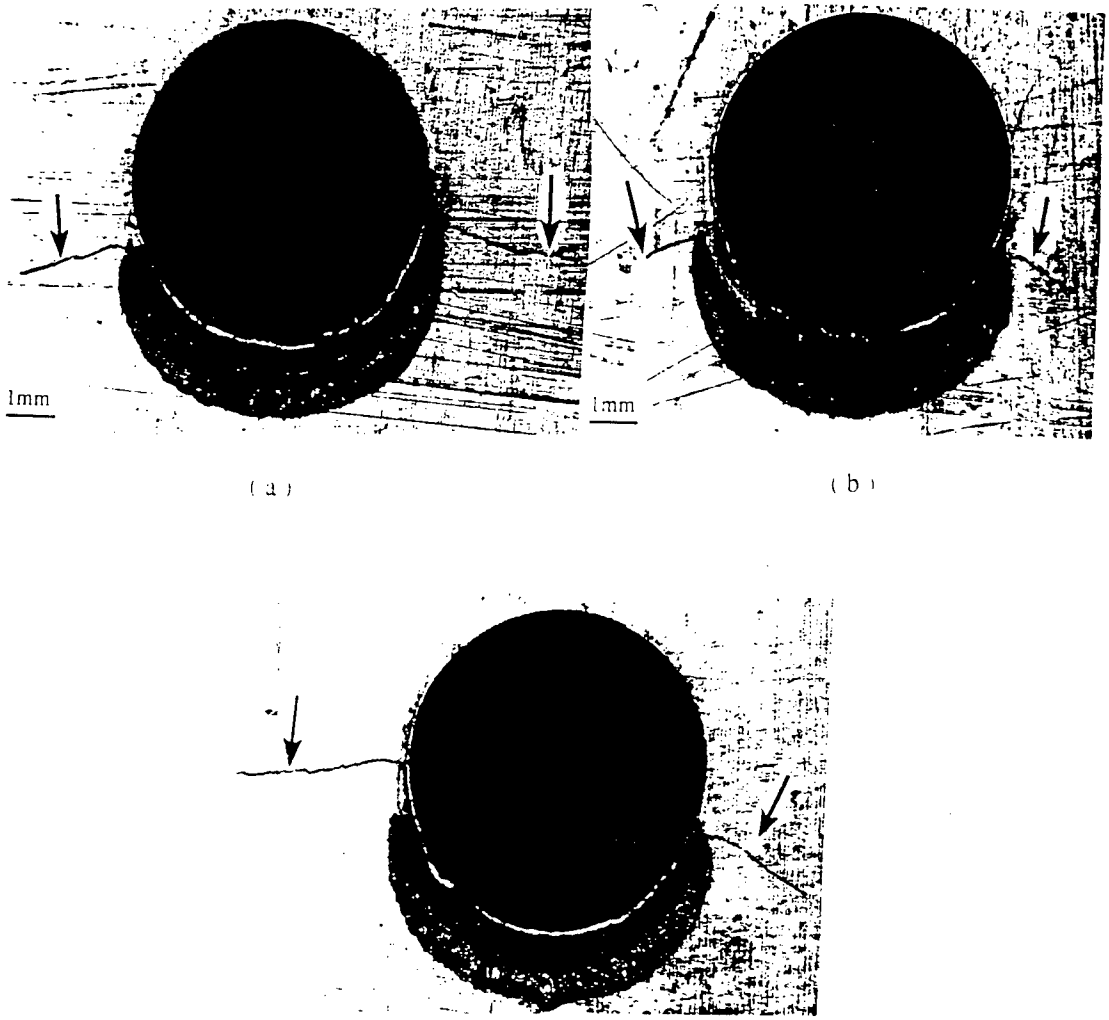

Figure 11. Examples of fatigue cracks produced in a 7075-T6 aluminum, 3-rivet, single-row lap joint subjected to N = 3261 cycles of nominal stress range, $\Delta\sigma$ = 106 MPa, R = 0.1. The dimensions of the lap joint are nearly identical to Models B1 and B1R and the cracks are viewed on the inner surface of the countersunk panel. The cracks intiate on average at the angular locations, θ = -11°, 169°. The dark, "half-moon" shaped regions below the rivet holes are fretting damage. Magnification 8x.

Experimental Strain Field Characterization of Boeing 737 Lap Splices with Analytical Correlations

*Dr. David Y. Jeong [1], Mr. Dennis P. Roach [2], Mr. Joseph V. Canha [1], Dr. John C. Brewer [1], and Dr. Thomas H. Flournoy [3]

[1] U.S. Department of Transportation
Volpe National Transportation Systems Center
Cambridge, MA 02142

[2] Sandia National Laboratories
Aging Aircraft NDI Validation Center
Albuquerque, NM 87185

[3] U.S. Department of Transportation
Federal Aviation Administration
Atlantic City, NJ 08405

ABSTRACT

The Federal Aviation Administration Technical Center (FAATC) is currently conducting and managing research related to aging aircraft. This paper describes the procedures and results of a series of ground pressurization tests conducted to measure strains in a retired Boeing 737 aircraft. The strain-gage tests were conducted at the Aging Aircraft NDI Validation Center (AANC) located at Sandia National Laboratories. The data collected from these tests are compared to computational models of fuselage lap-splice structures developed by the Volpe National Transportation Systems Center (Volpe Center). The data are also compared with results from other areas of the FAATC's National Aging Aircraft Research Program (NAARP). In particular, the AANC data are compared to: (1) laboratory measurements from curved stiffened panels, and (2) data obtained from strain gage tests performed by the National Aeronautics and Space Administration (NASA).

BACKGROUND

In support of the Federal Aviation Administration Technical Center's (FAATC) National Aging Aircraft Research Program (NAARP), the Aging Aircraft NDI Validation Center (AANC) at Sandia National Laboratories and the Volpe Na-

tional Transportation Systems Center (Volpe Center) are conducting research to determine if current rules for design, inspection, and maintenance are sufficient to ensure the safe operation of the aging fleet. Particular emphasis has been given to a phenomenon of multiple cracking that appears to be an attribute of airplanes that have been in service for some time. Multiple cracking along a longitudinal lap splice in the fuselage contributed to the structural failure of Aloha Airlines Flight 243 in 1988 [1]. Such multiple cracking is sometimes referred to as "Widespread Fatigue Damage" (WFD).

In 1992, the AANC acquired a retired Boeing 737 for use as a transport test bed. During January and February 1994, a series of ground pressurization tests was conducted on this airplane with gages installed at critical areas on the fuselage to measure strains [2]. The objectives of the tests were: (1) to monitor the strain field at the probable location of failure initiation in Aloha Airlines Flight 243, (2) to verify the accuracy of empirical results from laboratory aircraft panel tests, and (3) to validate results from finite element models of curved stiffened panels containing lap splices. For these purposes, five (5) lap-splice bays on the AANC aircraft were instrumented with 98 strain gages.

The airplane acquired by the AANC is a Boeing 737-200, Serial Number 19058, Line Number 49. Figure 1 shows a photograph of the FAA/AANC Boeing 737 aircraft. According to the Aircraft Utilization Database [3], this airplane was in service between August 1966 and February 1992. During these dates, the airplane accumulated 46,358 cycles in 38,342 flight hours. An important structural feature of the airplane is that the lap splices were not altered by the terminating action[1]. In other words, the lap splices in this airplane all contained shear head countersunk rivets only.

Strains and displacements on a Boeing 737 aircraft have been measured previously by NASA Langley Research Center [5]. The NASA data, however, were obtained from a small area near a lap joint at the tail end of the fuselage. Moreover, the FAA/AANC data provided an expansion of the NASA tests since 98 strain gages were used to monitor 5 different lap-splice bays compared to 36 strain gage channels and one lap-splice bay in the NASA test.

STRAIN GAGE DEPLOYMENT

Briefly, the selection of strain gage locations on the FAA/AANC B737 airplane was based on accommodating the following issues:

[1] The terminating action is a remedial repair which entails the replacement of shear head countersunk rivets with universal head rivets that have a larger shank diameter. Boeing Service Bulletin 737-53A [4] describes this remedial action repair for fuselage lap splices.

(1) instrumentation of several key lap-splice bays, both inside and outside;
(2) instrumentation of similar bays forward and aft of the wing to assess variations due to bending;
(3) selection of strain gage locations to resemble the strain-gage layouts in the NASA tests and in laboratory tests performed by Foster-Miller, Inc. [6,7] to allow for straightforward comparisons;
(4) determination of strain levels in high gradient areas on the skin as well as on substructure elements such as tear straps, stringers, and frames;
(5) configuration of gages in single-arm bridges to measure uniaxial strains with some rosettes used to provide principal strain data; and
(6) pressurization of the aircraft up to 6.5 psi with strain measured during increasing and decreasing pressure to determine any hysteresis effects.

The relative locations of the five instrumented lap-splice bays on the AANC airplane are shown schematically in Figure 2. The distribution of the strain gages in each test section of the aircraft is summarized in Table 1.

Table 1. Summary of Strain Gage Deployment on AANC Airplane.

Stringer Number	*Body Station Locations*	*Number of Gages in Bay*	*Remarks*
S-4L	BS470 - BS480	36	Compares with FMI full-scale panel
S-10L	BS470 - BS480	36	Compares with initiation site on Aloha B737.
S-14L	BS780 - BS790	10	Affected windows and floor beams.
S-4L	BS780 - BS790	8	Affected by fuselage bending. Also, compares with NASA test.
S-10L	BS780 - BS790	8	Affected by fuselage bending.

The strain-gage layout for the most heavily instrumented lap joints (36-gage array, see Table 1) is shown in Figure 3. Strains are measured primarily in the hoop direction, although some are also measured in the longitudinal direction. In the 8-gage and 10-gage configurations, the gages are located along the midline (between the tear strap and the frame). Two of the test sections between Body Stations 470 and 480 were instrumented with the most gages because one location (at stringer

S-10L) is directly related to the failure initiation site on the Aloha airplane [1], and the other (at stringer S-4L) is relatively isolated from the structural effects of windows, floor beams, and fuselage body bending.

The strain gages used in these tests were all encapsulated constantan foil gages with a nominal resistance of 350 ohms and a gage length of 0.125 inch. All biaxial and three-element 45° rosette gages were in single plane or unstacked configuration. The gages were manufactured to match the thermal coefficient of expansion of 2024-T3 aluminum so that the installation was considered as a self-temperature compensated (STC) set-up. The result was a flat thermal output (i.e., almost zero thermally induced strain) over a temperature range between 0 and 200° F. The sensitivity or gage factor for these gages, which relates the change in resistivity to actual strain level, was 2.05.

AIRCRAFT GROUND PRESSURIZATION

The FAA/AANC airplane was pressurized using an Airstart Unit borrowed from Kirtland Air Force Base. The unit was calibrated to provide the maximum allowable flow rate for the Boeing 737 duct work. The maximum differential pressure applied to the aircraft was dictated by flow restrictions and aircraft leakage. The aircraft was equipped with pressure relief valves that were calibrated to prevent inadvertent pressurization beyond 8.5 psi. Pressurization rates were chosen to closely match those associated with normal climb rates. Data were recorded during loading and unloading of the fuselage to determine hysteresis effects. Strain gage measurements were recorded for cabin pressures between 0 and 6.5 psi at 0.5 psi increments. A schematic of the test-up for ground pressurization and data acquisition on the FAA/AANC B737 airplane is shown in Figure 4.

EXPERIMENTAL STRAIN DATA

In the data obtained from the FAA/AANC ground pressurization tests, particular attention was given to the state of strain near the lap splices and to the variation of strain through the joints. For instance, gages were installed in each of the 5 instrumented lap-splice bays to monitor strain levels at locations above and below the joint as well as in the upper, middle, and lower rivet rows of the lap itself. Figure 5 shows the hoop strain at different locations along the midline at one of the instrumented lap-splice bays (S-4L, BS475) as a function of pressure. In general, the hoop strains are reasonably linear when plotted with respect to pressure. In addition, hysteresis effects are usually confined to the lower rivet row.

Table 2 summaries the measured strain variation in the upper skin across the 5 different lap joints at the peak pressure of 6.5 psi. Most of the load in the upper skin above the lap-splice joints is transferred into the lower skin around the upper rivet row. In addition, strain levels below the lap joint on the lower skin are approximately equal to the strain level above the joint. The strain levels are shown to decrease drastically across the circumference of the lap joint from the upper rivet row to the lower rivet row. Referring to the table, the middle rivet row of the S-4L lap joint experiences 17% of the strain above the lap splice, while the same area of the S-10L lap joint experiences 56% of the total strain. A possible reason for this difference could be a difference in bond quality between these two joints.

Although internal pressurization of the fuselage generally produces positive hoop strains, strains in the skin around the lower rivet row in each of the instrumented bays are negative. Reverse or compressive type bending develops in the lower rivet row as the lap joint deforms. Deformation of the lap joint, shown schematically in Figure 6, shifts the neutral axis of the structure, inducing a bending load into the lap skins. This reverse bending creates compressive or negative bending strains around the lower half of the lap joint. The total strain in the area, however, includes a membrane component that is positive but smaller in magnitude than the bending component. The magnitude of the membrane component is relatively small because nearly all of the load at this point is transferred into the lower skin of the lap. Since the negative bending strains are greater in magnitude than the positive membrane component, the gages show a net compressive strain.

Another way to view the strain variation across the lap joint is to examine the strain values on both skins of the riveted assembly. Figure 7 shows strains measured on the inner and outer skins at the lower rivet row at the S-4L, BS475. Comparing these results with those shown in Figure 5, the strains in the lower rivet row of the inner skin and the upper rivet row of the outer skin are on the same order of magnitude. Therefore, these two areas should be treated similarly in fatigue and damage tolerance analyses.

The strains measured from the hoop and longitudinal gages in the FAA/AANC tests can be used to calculate the corresponding membrane stresses from the following equations:

$$\sigma_\theta = \frac{E}{1-\nu^2}\left[\varepsilon_\theta + \nu\varepsilon_z\right] \qquad \sigma_z = \frac{E}{1-\nu^2}\left[\varepsilon_z + \nu\varepsilon_\theta\right] \tag{1}$$

where E is the modulus of elasticity and ν is Poisson's ratio. According to MIL Handbook 5, these material properties for 2024-T3 aluminum are 10.5 msi and 0.33, respectively.

Table 2. Strain Variation Through Different Lap Splice Joints at 6.5 psi.

(a) Stringer S-4L, Body Station 475

Location	*Microstrain*	*Percent of Strain from Skin Above Lap Joint*
Above Lap Splice	813	100%
Upper Rivet Row	771	95%
Middle Rivet Row	141	17%
Lower Rivet Row	-153	NA
Below Lap Splice	1071	131%

(b) Stringer S-10L, Body Station 475

Location	*Microstrain*	*Percent of Strain from Skin Above Lap Joint*
Above Lap Splice	907	100%
Upper Rivet Row	754	83%
Middle Rivet Row	506	56%
Lower Rivet Row	-104	NA
Below Lap Splice	906	100%

(c) Stringer S-14L, Body Station 475

Location	*Microstrain*	*Percent of Strain from Skin Above Lap Joint*
Above Lap Splice	911	100%
Upper Rivet Row	729	80%
Below Lap Splice	-263	NA

(d) Stringer S-14L, Body Station 790

Location	*Microstrain*	*Percent of Strain from Skin Above Lap Joint*
Above Lap Splice	956	100%
Upper Rivet Row	925	97%
Below Lap Splice	933	98%

(e) Stringer S-10L, Body Station 790

Location	*Microstrain*	*Percent of Strain from Skin Above Lap Joint*
Above Lap Splice	953	100%
Upper Rivet Row	1039	109%
Below Lap Splice	819	86%

Stresses in an actual aircraft are sometimes compared to the values calculated from the thin-walled cylinder approximation. From engineering mechanics considerations, the hoop and longitudinal stresses in a thin-walled cylinder are

$$\sigma_\theta = \frac{pR}{t} \qquad \sigma_z = \frac{pR}{2t} \tag{2}$$

where p is the differential pressure, R is the radius of curvature (74 inches)[2] and t is the skin thickness (0.036 inch). The stresses computed from the measured strains are compared to the stresses calculated from the theoretical thin-walled cylinder estimate in Table 3. It should be noted that this comparison is valid only at the midbay location[3]. As shown in Table 3, the actual stresses are between 10% and 30% less than the theoretical thin-walled cylinder estimates because load is transferred to the stiffening elements (i.e.; frames and stringers) in the actual fuselage structure.

Table 3. Comparison of Stresses at Midbay in Each Test Section at 6.5 psi.

Test Section	*Hoop Stress σ_θ (ksi)*	*Longitudinal Stress σ_z (ksi)*	*Ratio σ_z/σ_θ*
S-4L, BS475	9.7	4.8	0.495
S-10L, BS475	11.0	5.5	0.503
S-14L, BS475	10.8	5.2	0.475
S-4L, BS785	11.3	6.0	0.536
S-10L, BS785	11.3	5.6	0.499
Theoretical	*13.4*	*6.7*	*0.500*

Figure 8 shows strain data at the same location over different pressure cycles. The maximum variation in strain from one pressure cycle to another was less than 10% at any pressure level. Moreover, this plot shows the repeatability of the measured hoop strains in the FAA/AANC B737 tests.

The structural effects of windows, floor beams, and fuselage bending on the strain fields were examined by comparing the data among the various lap-splice

[2] The numbers within parentheses refer to nominal dimensions for the B737 airplane.

[3] The thin-walled cylinder approximations are not applicable for strains near the lap splice. Finite element models were developed to examine the strain distribution near the lap splice, and are discussed in the next section of this paper.

test sections. These correlations revealed that the structural influence of windows and floor beams can increase strains from 4% up to 46%. Furthermore, fuselage body bending can increase strains by approximately 30%.

CORRELATIONS OF STRAIN DATA

Having established a database of strain data from a retired Boeing 737 airplane, the data were compared with results from other research activities in the aging aircraft program. Three comparisons are discussed in this paper: (1) correlations with computational models, (2) correlations with laboratory panel data, and (3) correlations with data collected from the NASA B737 test.

Comparisons with Finite Element Models

Finite element models of fuselage lap-splice structures are being developed at the Volpe Center using a commercially available finite element code, ANSYS. These finite element models include structural details such as tear straps, stringers, frames, stringer ties, and rivets. Two models were developed for direct comparisons with the data collected from the AANC airplane. The first model assumed that the skins, tear straps, and structural fillers were attached by an adhesive bond, and all other components are attached by rivets. In this paper, this model is referred to as the adhesive lap-splice model. The second model, referred to as the riveted lap-splice model, assumed no adhesive, and all structural components were attached by rivets only. Thus, the two models effectively bound the possible conditions of bonding in the lap joint between entirely bonded and completely debonded.

Both finite element models employed four-noded shell elements to represent the skins, tear straps, structural fillers, frames, and stringer ties of the aircraft fuselage. In the adhesive lap-splice model, the adhesive bond between the skins, tear straps, and structural fillers was modeled using three-dimensional, eight-noded, anisotropic material elements. In the riveted lap-splice model, three-dimensional beam elements represented the rivets at the individual rivet locations throughout the model. Rivets were assumed to behave as linear elastic springs. The flexibility of these rivets was estimated using the empirical formula derived by Swift [8]. All rivets in the model were assumed to have the same rivet flexibility. The riveted lap-splice model consisted of 13,382 nodes and 12,740 elements which resulted in a total of 76,737 active degrees of freedom. The adhesive lap-splice model used 6,684 nodes and 7,042 elements which combined for 37,739 active degrees of

freedom[4]. The adhesive model also included 144 beam elements and 1,112 adhesive elements. Figure 9 shows the finite element mesh pattern used to model a section of the aircraft fuselage containing a riveted lap joint.

Figure 10 compares the measured hoop strains at various locations across the lap splice at Body Station 475, Stringer S-4L, with results from the riveted lap splice model. The solid, dotted, and dashed lines in the figure represent results from the finite element models; the symbols indicate the measured strain gage data. Figure 11 compares the same experimental data with results from the adhesive lap-splice model. Clearly, the strain data are characterized more accurately by the riveted lap-splice model, especially in the upper rivet row, suggesting that the cold-bond adhesive has substantially degraded at that location in the FAA/AANC airplane. This result was later confirmed when nondestructive inspection detected extensive corrosion and debonding in the lap joints.

Comparisons with Full-Scale Laboratory Panel Data

The FAA/AANC strain data were also correlated with data obtained from curved, stiffened panels tested by Foster-Miller, Inc. (FMI) on a unique fixture that uses water rather than air as a pressurization medium [6,7]. Fatigue testing of one full-scale panel resulted in linkup of multiple cracks which ultimately lead to structural failure[5] after 75,263 pressurization cycles [9]. This panel was initially undamaged, except for an intentionally debonded lap joint. A limited number of strain gage measurements were collected from this laboratory panel to ensure accurate and realistic loading. Although the strain data were in reasonable agreement with other available data, the measurements were not sufficient to accurately characterize strains in areas experiencing large gradients. Thus, the FAA/AANC strain data were used to verify whether the strains produced in the laboratory panels were representative of those in actual lap-splice structures.

Twelve (12) coincident locations on the laboratory panels and a corresponding section on the B737 fuselage were identified relative to a common lap-splice stringer. In general, the overall comparison between the FMI and FAA/AANC test data is reasonable. Except for one location, the hoop strains from both tests agree within 30% at all pressure levels. Based on differences in skin thickness and radius

[4] The riveted lap-splice model contained more nodes and elements than the adhesive model because nodes were placed at every rivet location in the lap joint. Also, a more refined mesh was generated within the lap joint to examine the strain gradient between rivets.

[5] "Failure" as used here means the size and distribution of multiple cracking was such that hydraulic pressure could not be maintained to continue testing.

of curvature, a "perfect" correlation would show the FAA/AANC data to be 10% higher than the FMI data.

Correlations with NASA B737 Data

Strain gage data from a Boeing 737 airplane have also been collected by NASA Langley Research Center during a ground pressurization test [5]. In the NASA test, the peak pressure was 6.2 psi. One section, located at the longitudinal lap splice between Body Stations 857 and 867 at stringer S-4R, was monitored with 36 channels. The most comparable test section on the FAA/AANC B737 airplane was the one between Body Stations 780 and 790 at stringer S-4L.

The strains from both tests are within 20% agreement, except at one location. In the upper rivet row location, the FAA/AANC hoop strains are about 40% higher than those measured in the NASA test. Figure 12 compares data it the upper rivet row from both the FAA/AANC and the NASA tests. The figure also compares the results from the riveted and adhesive lap-splice finite element models. As shown previously, the results from the rivet lap-splice model correlate reasonably well with the FAA/AANC data in the upper rivet row. The NASA data, however, correlate better with the results from the adhesive lap-splice model. Apparently, the bond in the lap splice of the NASA B737 airplane is effective, and the adhesive in the lap splices of the FAA/AANC airplane has degraded.

CONCLUSIONS

The major conclusions from this research are given as follows.

(1) Strain gage data have been collected from a retired Boeing 737 airplane which can be used to validate analytical models of fuselage structures and laboratory data from other experiments.

(2) The data from the FAA/AANC B737 airplane correlate better with the riveted lap-splice model than with the adhesive lap-splice model. Detection of corrosion and debonds in the lap splices of the aircraft through nondestructive inspections confirmed this finding. Conversely, data from the NASA B737 airplane agreed better with results from the adhesive lap-splice model than with the rivet lap-splice model. This result suggests that the adhesive bond in the lap-splice test-section of the NASA B737 is still effective.

(3) Reasonable agreement was obtained between the strain data from the FAA/AANC B737 airplane and data collected from the curved, laboratory panels used by Foster-Miller, Inc.

(4) In each test section of the FAA/AANC B737 airplane, most of the load in the skin above the lap joint is transferred into the skin around the upper rivet row. Differences in load transfer among the different test sections appear to be related to differences in bond quality.

(5) Even though internal pressurization of the fuselage generally produces positive hoop strains, strains around the lower rivet row in all instrumented bays were negative. These negative or compressive strains were a consequence of reverse bending that develops when the lap joint deforms from internal pressure loading.

(6) The lower rivet row of the inner skin experiences the strains on the same order of magnitude as the upper rivet row of the outer skin. Therefore, these two areas should be treated similarly in fatigue and damage tolerance analyses.

(7) Hoop and longitudinal stresses at the midbay location were between 70% and 90% of the theoretical thin-walled cylinder estimates. These percentages are reasonable since the actual airplane contains stiffening elements that carry load and generally reduce strain.

ACKNOWLEDGMENT

The work presented in this paper was conducted in support of the Federal Aviation Administration Technical Center's National Aging Aircraft Research Program.

REFERENCES

[1] National Transportation Safety Board, "Aircraft Accident Report - Aloha Airlines Flight 243, Boeing 737-200, N73711, Near Maui, Hawaii, April 28, 1988," NTSB/AAR-89/03, PB89-910404, June 1989.

[2] Jeong, D.Y., Roach, D.P., Canha, J.V., Brewer, J.C., and Flournoy, T.H., "Strain Fields in Boeing 737 Lap Splices: Field and Laboratory Measure-

ments with Analytical Correlations," Final Report, DOT/FAA/CT-95/25, June 1995.

[3] Aircraft Utilization Database, Aviation Research and Support Limited, United Kingdom.

[4] Boeing Service Bulletin No. 737-53A1039, "Body Skin Lap Joint Inspection and Repair," Revision 3, August 20, 1987.

[5] Phillips, E.P., and Britt, V.O., "Measurements of Fuselage Skin Strains and Displacements Near a Longitudinal Lap Joint in a Pressurized Aircraft, NASA Technical Memorandum 104163, October 1991.

[6] Samavedam, G., and Hoadley, D., "Fracture and Fatigue Strength Evaluation of Multiple Site Damaged Aircraft Fuselages - Curved Panel Testing and Analysis," Final Report, DOT/FAA/CT-94/10, January 1994.

[7] Samavedam, G., Hoadley, D., and Thomson, D., "Full-Scale Testing and Analysis of Fuselage Panels," Final Report, DOT/FAA/CT-93/78, December 1993.

[8] Swift, T., "Development of the fail-safe design features of the DC-10," *Damage Tolerance in Aircraft Structures, ASTM STP 486,* American Society for Testing and Materials, Philadelphia, PA, 1971, pp. 164-214.

[9] Samavedam, G., Thomson, D., and Jeong, D.Y., "Evaluation of the fuselage lap joint fatigue and terminating action repair," *FAA/NASA International Symposium on Advanced Structural Integrity Methods for Airframe Durability and Damage Tolerance,* NASA Conference Publication 3274, Part 2, September 1994, pp. 653-664.

Figure 1. FAA/AANC Boeing 737 test bed.

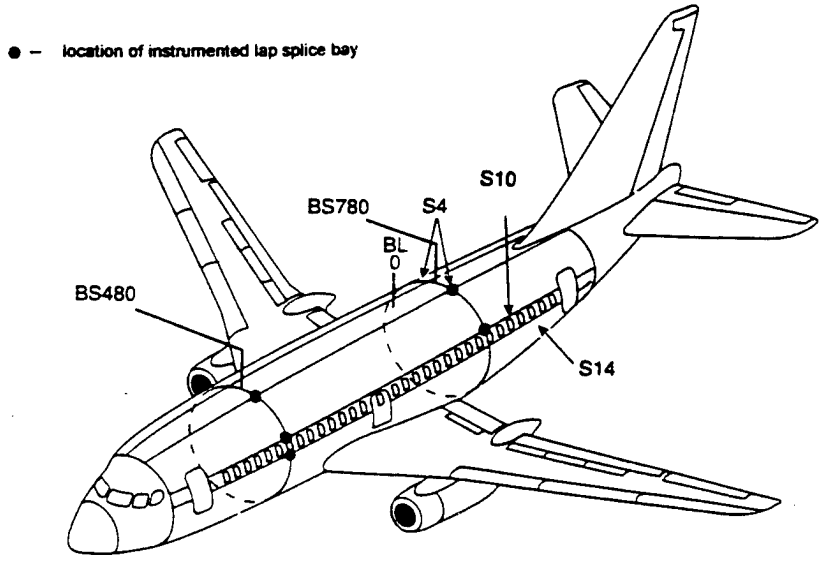

Figure 2. Locations of lap-splice test sections on FAA/AANC airplane.

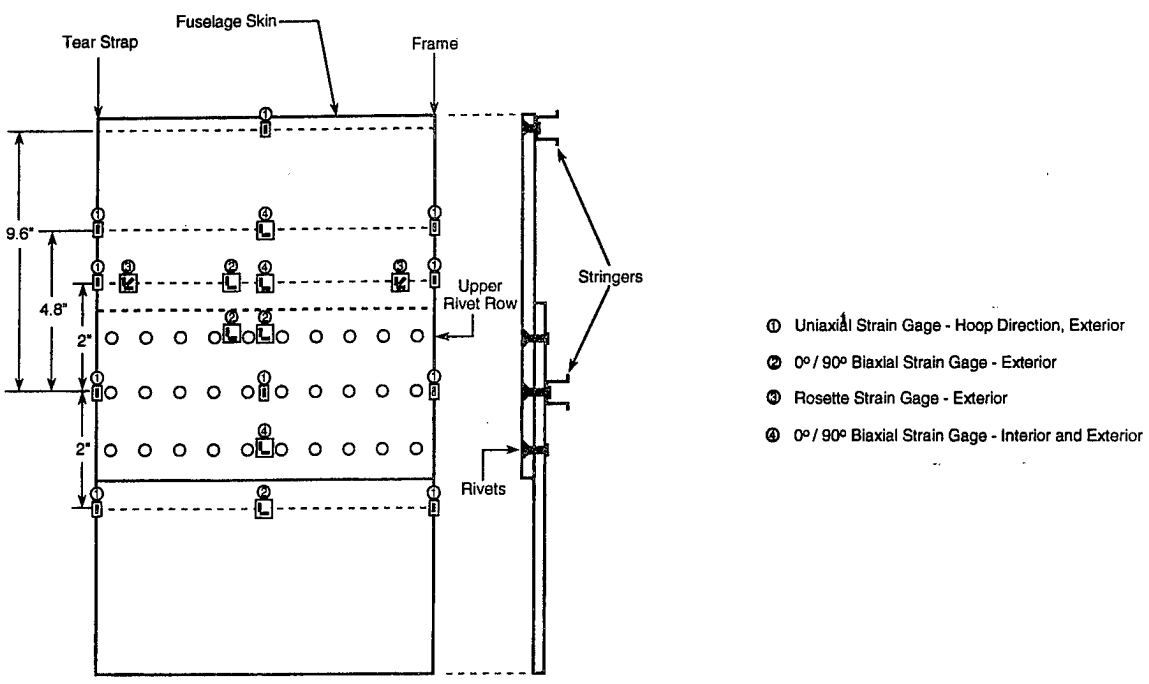

Figure 3. Strain-gage layout for 36-gage array.

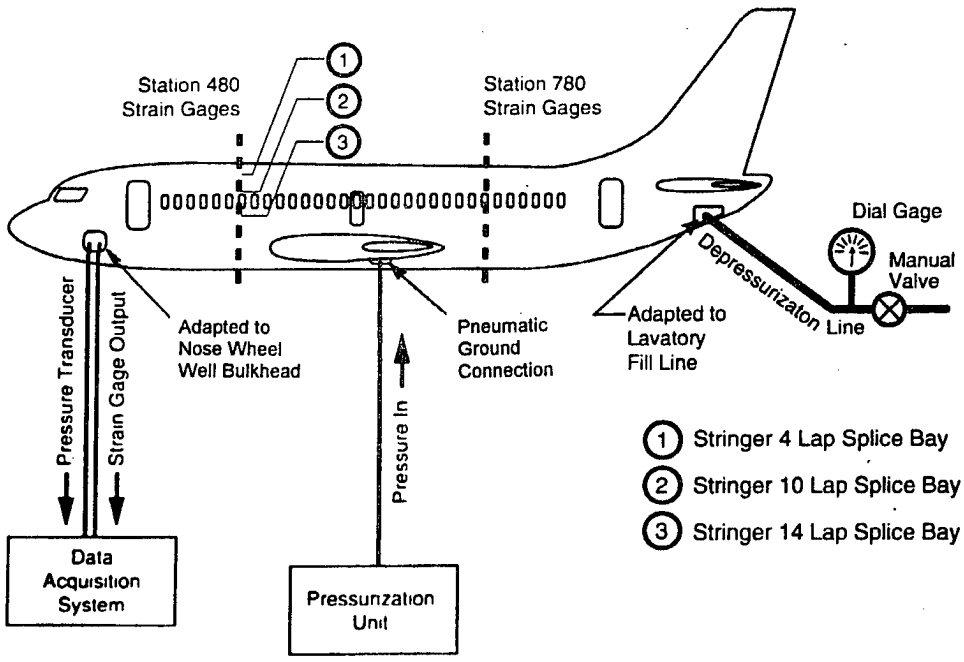

Figure 4. FAA/AANC B737 strain monitoring test set-up.

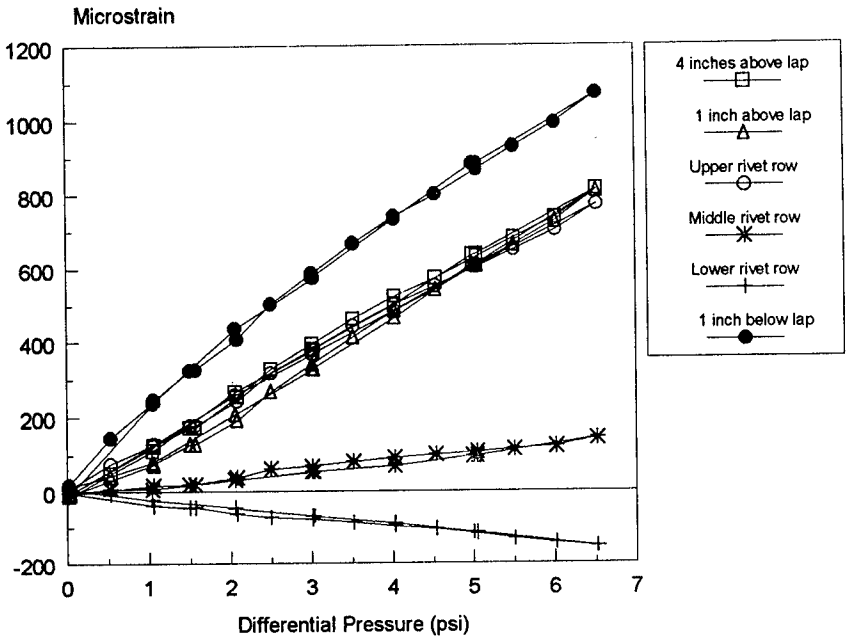

Figure 5. External skin hoop strains along midline of S-4L, BS475.

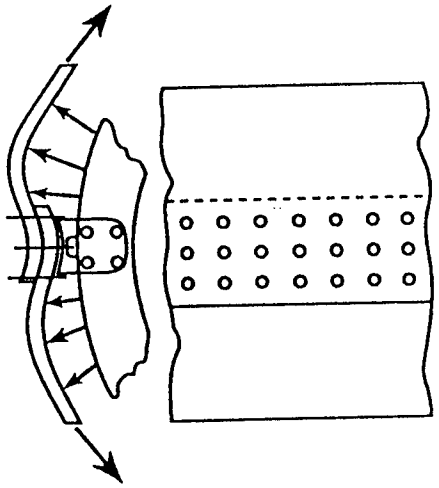

Figure 6. Schematic of lap splice deformation due to internal pressurization.

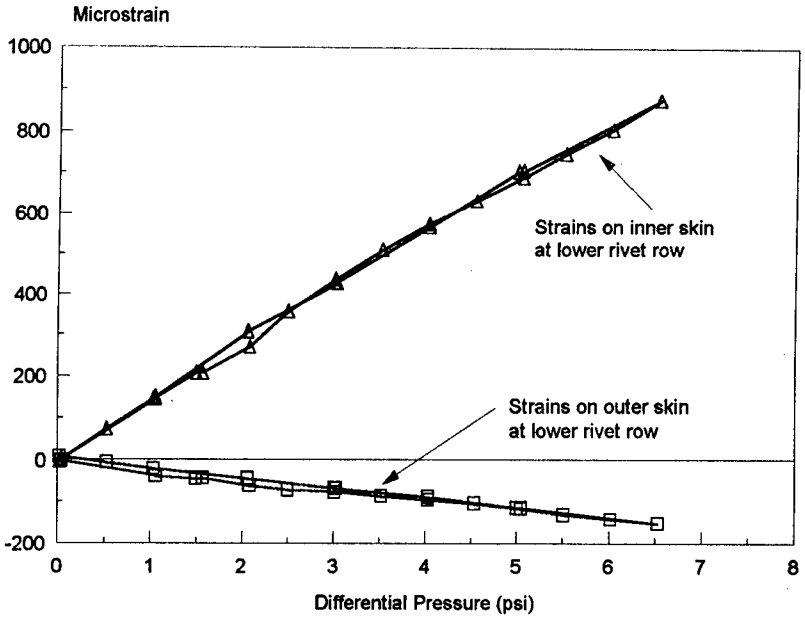

Figure 7. Hoop strains in lower rivet row on inner and outer lap skins (S-4L, BS475).

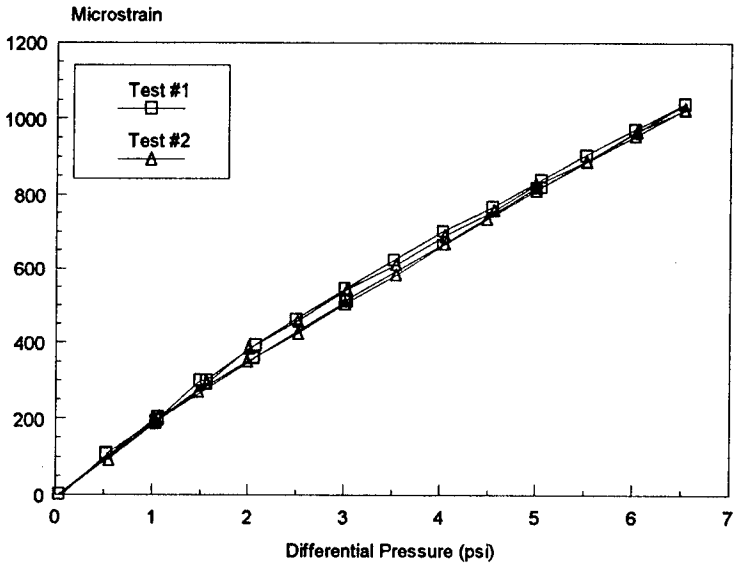

Figure 8. Repeatability of strains measured at the upper rivet row (S-10L, BS785).

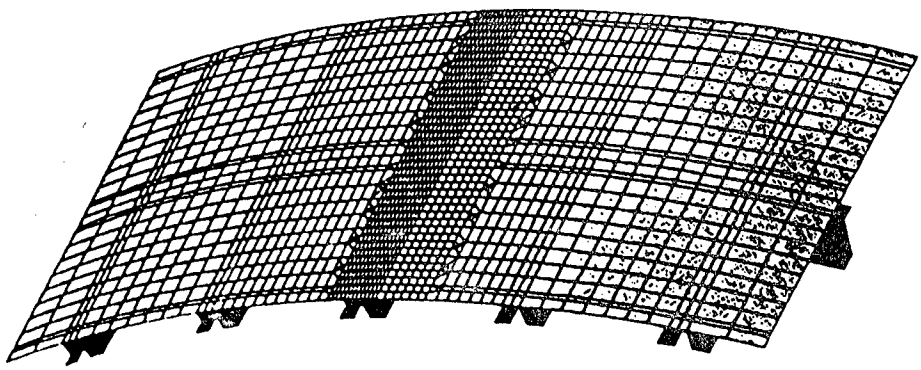

Figure 9. Finite element mesh pattern for pressurized aircraft section.

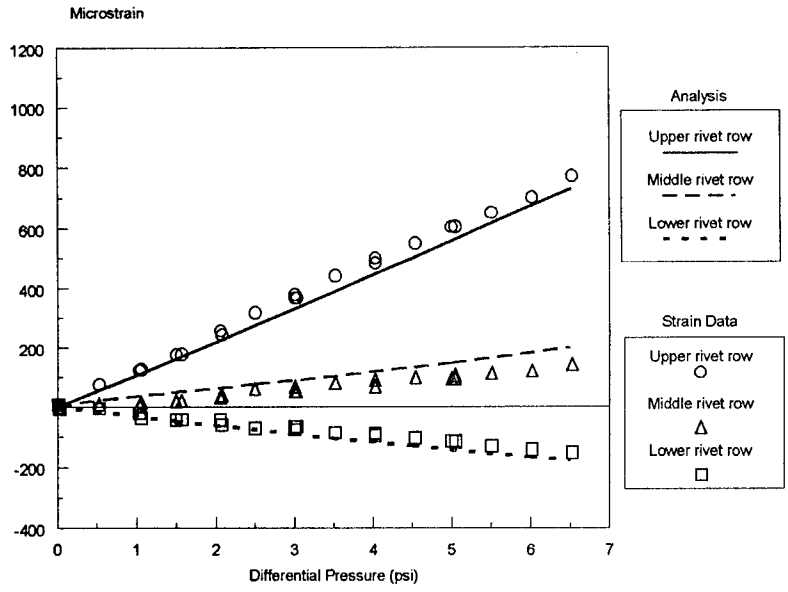

Figure 10. Comparison of strains across lap splice: riveted lap-splice model versus experimental data.

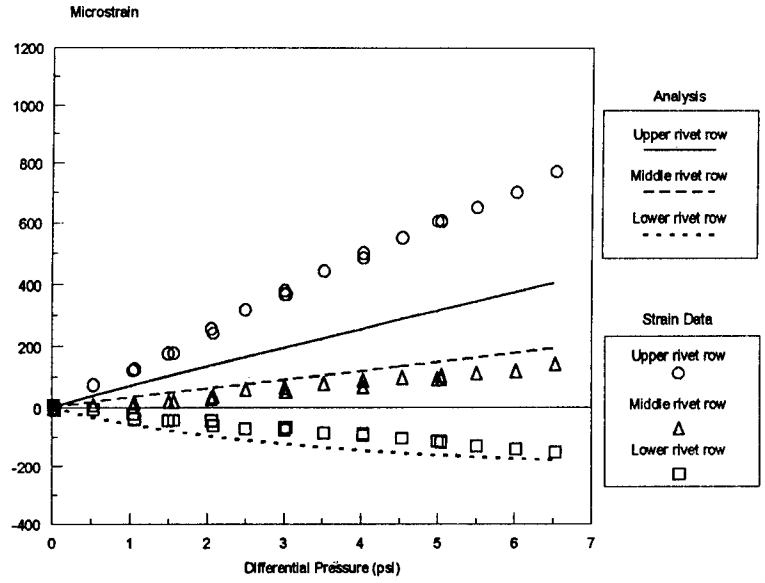

Figure 11. Comparison of strains across lap splice: adhesive lap-splice model versus experimental data.

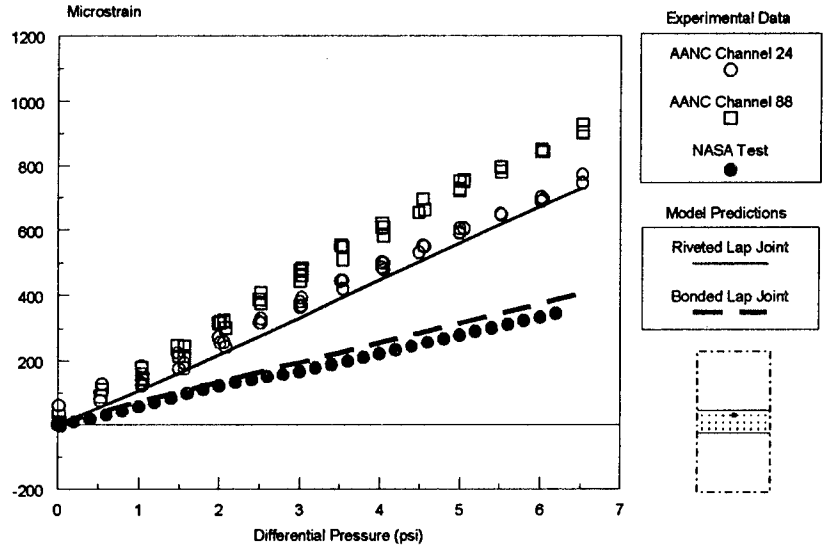

Figure 12. Comparison of strains in upper rivet row of FAA/AANC and NASA B737 lap splices with results from finite element models.

USAF Aircraft Structural Integrity Program Conference
28 November 1995

Assessing Structural Integrity of Bonded Joints Using Fracture Mechanics

Larry Butkus, Captain, USAF
George W. Woodruff School of Mechanical Engineering

Prof. Steve Johnson
School of Materials Science & Engineering

Assessing Structural Integrity of Bonded Joints Using Fracture Mechanics

Project Summary

Larry Butkus
School of Mechanical Engineering
Georgia Institute of Technology
(404)894-2853, FAX (404)853-9140

Professor Steve Johnson
School of Materials Science and Engineering
Georgia Institute of Technology
(404)894-3013

Advances in aerospace technology have been made possible, in part, through the use of lightweight materials and weight-saving structural designs. Joints, in particular, have been and remain areas in which weight can be trimmed from an airframe through the use of novel attachment techniques. In order to save weight over traditional riveted designs, to avoid the introduction of stress concentrations associated with rivet holes, and to take full advantage of advanced composite materials, engineers and designers have been specifying an ever-increasing number of adhesively bonded joints for use on airframes.

This project will investigate the mixed mode fracture (modes I and II) of adhesively bonded joints used for aircraft structural assembly and airframe repair. Joint durability will be examined through mechanical testing following environmental exposure. The goal of this project is to develop a fracture mechanics based approach to understanding: 1) the behavior of adhesive joints under mixed mode loading and 2) adhesive joint durability and changes in mechanical behavior associated with long-term exposure.

The number of adherend/adhesive combinations used or proposed for use on military and commercial aircraft is large, and the intent of this project is not to test all combinations. However, in working closely with the FAA, the USAF, and airframe manufacturers, a representative variety of adhesives, adherends, and end uses is sought. Samples will be obtained from materials used on the F-22 fighter, the C-141 transport, and the High Speed Civil Transport (HSCT) project, thereby spanning a spectrum of new, in-service, and future adhesive joints. In addition, this collection of specimens also permits the evaluation of various adhesives with either aluminum or boron- or carbon-fiber reinforced composites.

Monotonic fracture and fatigue crack growth tests will be conducted using three specimen geometries to investigate the mixed mode fracture behavior of the joints. These geometries are the double cantilever beam (DCB), the end-notched flexure (ENF), and the cracked lap-shear (CLS). Specimens will be tested in the as-received condition and following aging or cycling in temperature and humidity levels indicative of aircraft operation. Crack growth will be monitored using compliance measurements, crack growth gages, and visual inspection. SEM and finite element analyses will be used to characterize fracture surfaces and analyze joint mechanics. Some "neat" resins may also be tested under a parallel program to determine the durability of the adhesive alone.

Results from this program will aid in the specification of adhesives for future airframe usage, assist in the design of bonded joints through increasing the understanding of likely fracture modes, and permit life extension of current aging aircraft by adding to the knowledge base of bonded repair techniques.

Principal Advisor:	Prof. Steve Johnson, School of Materials Science and Engineering
Thesis Committee:	Prof. David McDowell, School of Mechanical Engineering
	Prof. Jianmin Qu, School of Mechanical Engineering
	Prof. Richard Neu, School of Mechanical Engineering
	Prof. Erian Armanios, School of Aeronautical Engineering
	Mr. James Rudd, Leader, Aging Systems Integrated Product Team, Wright-Patterson AFB, OH
Material Suppliers:	Lockheed Aeronautical Systems Company, Marietta, GA
	Boeing Commercial Airplane Company, Seattle, WA

Acknowledgements

Assessing Structural Integrity of Bonded Joints Using Fracture Mechanics

Sponsor: **Federal Aviation Administration Technical Center**

Technical Monitor: **Dr. Don Oplinger**

Grant Number: **95G023**

Material Suppliers:

- **Lockheed** Marietta, GA
- **Boeing** Renton, WA
- **Cytec** Havre de Grace, MD
- **3M Corp.** St. Paul, MN

Overview

Assessing Structural Integrity of Bonded Joints Using Fracture Mechanics

GOAL

To refine the use of fracture mechanics for the durability assessment, analysis, and design, of bonded aircraft joints

OBJECTIVES

- **Characterize the mode I, mode II and mixed mode behavior of several adhesive joint systems**
- **Quantify degradation due to environmental exposure**
- **Develop a methodology to assess joint structural integrity**

Introduction

Assessing Structural Integrity of Bonded Joints Using Fracture Mechanics

Overview
Goal & Objectives

Background

Technical Review
Stress-Based & Fracture Mechanics Analyses

Proposed Research

Some Preliminary Results

Summary

Background

Assessing Structural Integrity of Bonded Joints Using Fracture Mechanics

KEY HISTORICAL MILESTONES

- **1920s - Bonding used for wood assemblies**
- **1940s - Metal-to-metal bonding developed**
  - Schliekelmann (Fokker), de Bruy (Aero Research)
- **1955 - First flight of Fokker F27 "Friendship"**
  - 500 bonded assemblies with 4000 parts
- **1958 - USAF Aircraft Structural Integrity Program**
- **1975-80 - USAF's PABST Program**
  - **P**rimary **A**dhesive **B**onded **S**tructures **T**echnology
- **1980s-Present - Increased use of bonding**
  - repairs, composites, subassemblies

Background

Assessing Structural Integrity of Bonded Joints Using Fracture Mechanics

ADVANTAGES

- Inexpensive
- Lighter
- More Aerodynamic
- Good Sealing Capabilities
- Improved Fatigue Resistance
- High Strength-to-Weight Ratio
- Corrosion Resistant
- "Benign" Failure Modes

DISADVANTAGES

- Cure Time Required
- Weak in "peel"
- "Different" Skills Required
- Special Surface Preparation
- NDI Required
- Unforgiving

Technical Review

Assessing Structural Integrity of Bonded Joints Using Fracture Mechanics

STRESS-BASED ANALYSES

- Formulated on economical, industry tests and classical mechanics approaches
- Basis for current ASTM and industry standards
- Focus: static strength analysis

FRACTURE MECHANICS ANALYSES

- Recognizes the existence of flaws in bondline
- Focus: strain energy release rate, G, rather than stress intensity, K
- Addresses fatigue

Technical Review

Assessing Structural Integrity of Bonded Joints Using Fracture Mechanics

STRESS-BASED ANALYSES - *Previous Research*

- **Goland & Reissner** (1944)
  - Pioneering analysis identified bending moment, stress concentrations, and non-uniform shear stress
- **Adams, *et al.*** (1980s-Present)
  - Principal stresses cause adhesives to fail in tension
- **Hart-Smith** (1970s-Present)
  - Basic premises:
    - avoid peel stresses
    - make bond stronger than adherends
    - use only for thin or moderate thicknesses
    - avoid short overlaps
  - Designs based on static strength

Technical Review

Assessing Structural Integrity of Bonded Joints Using Fracture Mechanics

Adhesive Peel Stresses in Short- and Long-Overlap Single-Lap Joints

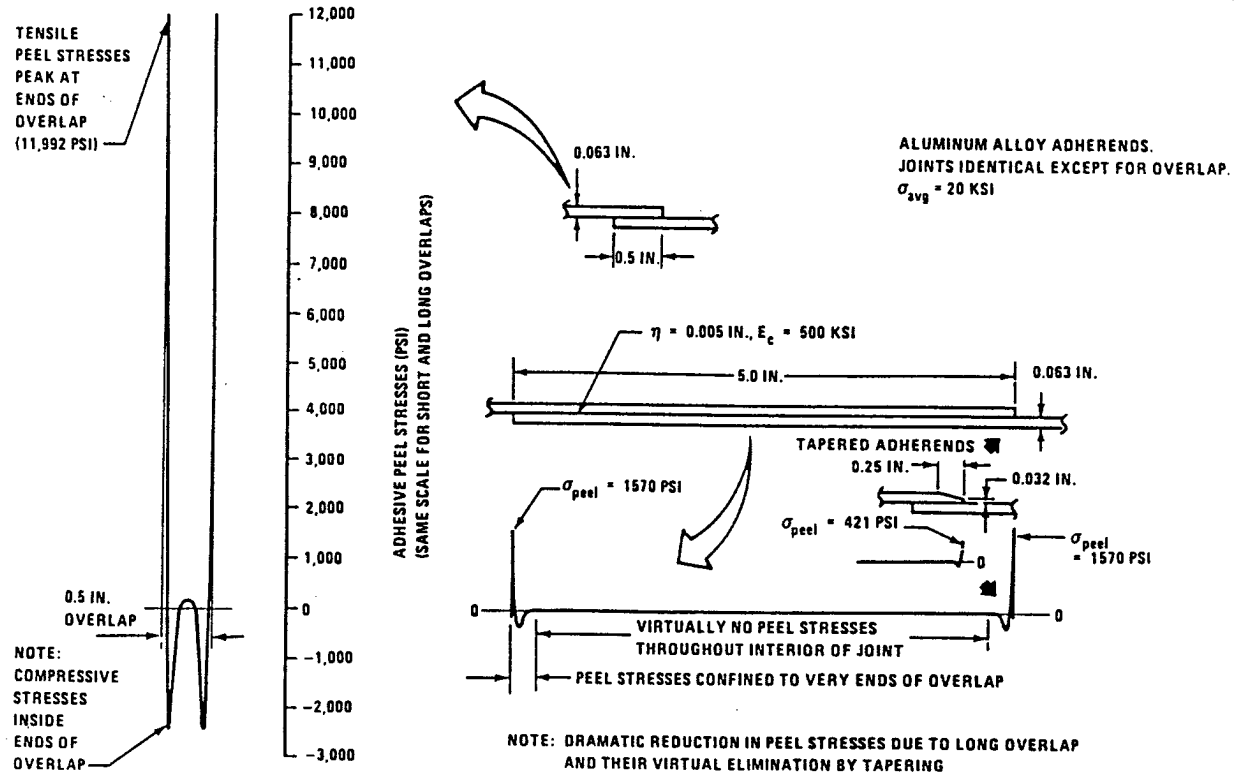

Source: Hart-Smith, L.J., "Designing to Minimize Peel Stresses in Adhesive Joints," in Delamination and Debonding of Materials, ASTM STP 876, W.S. Johnson, ed., American Society for Testing and Materials, Philadelphia, 1985, pg. 248.

Technical Review

Assessing Structural Integrity of Bonded Joints Using Fracture Mechanics

FRACTURE MECHANICS - *Previous Research*

- **Ripling, Mostovoy, and Patrick** (1964)
  - Applied theories of Griffith and Irwin
  - Developed specimens to test for G_{IC} and G_{IIC}
  - Used a strain energy release rate (G) analysis
- **Shaw** (1983)
  - Investigated plastic-zone constraint
  - Used fracture mechanics to analyze exposure effects
- **Martin & Murri** (1990)
  - Investigated single & mixed mode adhesive behavior
  - Employed and analyzed end-notched flexure tests
- **Fernlund & Spelt, *et al.*** (1994)
  - Used J-Integral, mode partitioning, and special test fixture to obtain closed-form mixed-mode solution

FRACTURE MECHANICS - *Previous Research*

- **Johnson, *et al.*** (1982-87)
  - Found cyclic debonding in absence of peel stress
  - Correlated G_T and da/dN for fatigue crack growth
  - Showed debonding at G_T values an order of magnitude lower that static toughness (G_{TC}) values
  - Determined static strength exceeded fatigue strength by a minimum of 2.3:1
  - Investigated effects of tapered adherends

Technical Review

Assessing Structural Integrity of Bonded Joints Using Fracture Mechanics

Double Cantilever Beam (DCB)

$$G_I = \frac{3P^2C}{2ba} = \frac{12P^2C}{b^2h^3E} \quad \text{where,} \quad C = \frac{8a^3}{bh^3E}$$

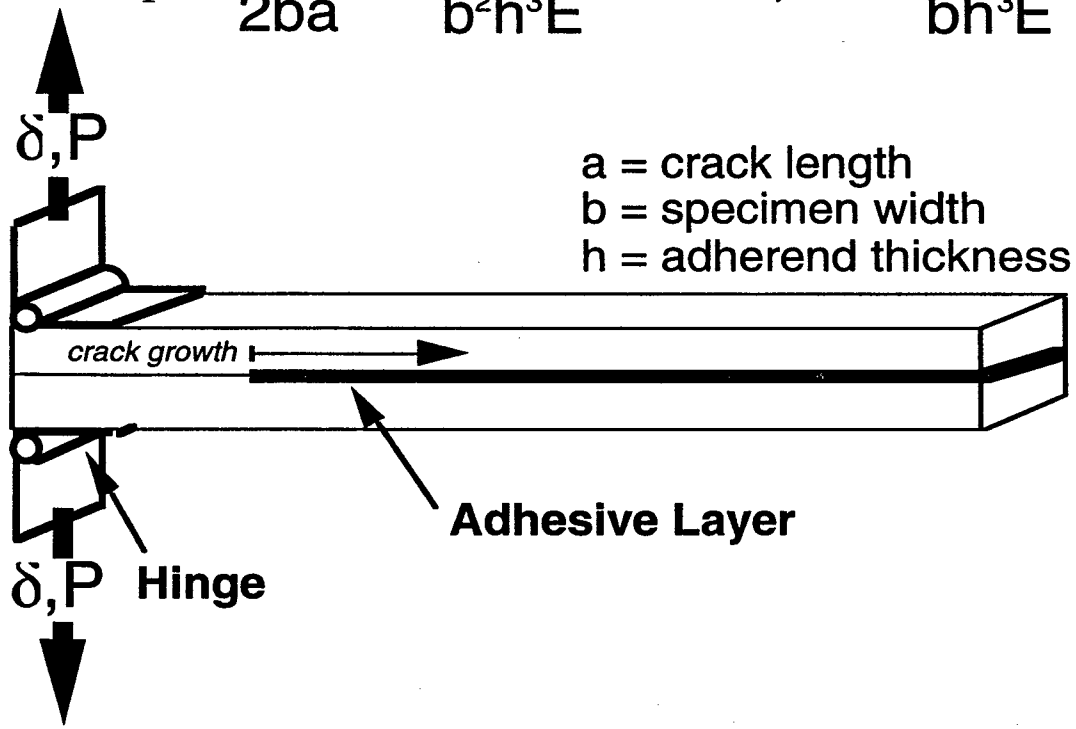

Technical Review

Assessing Structural Integrity of Bonded Joints Using Fracture Mechanics

End-Notched Flexure (ENF)

$$G_{II} = \frac{9P^2a^2C}{2b(2L^3 + 3a^3)}$$

where, $C = \frac{2L^3 + 3a^3}{8bh^3E}$

a = crack length
b = specimen width
h = adherend thickness

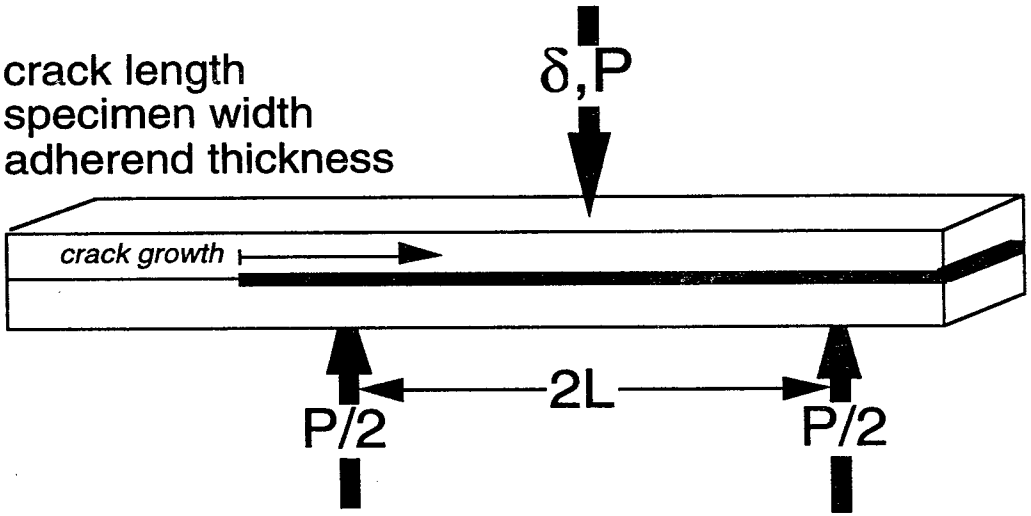

Technical Review

Assessing Structural Integrity of Bonded Joints Using Fracture Mechanics

Cracked Lap Shear (CLS)

$$G_T = \frac{P^2}{2b^2}\left[\frac{1}{(Eh)_s} - \frac{1}{(Eh)_s + (Eh)_L}\right]$$

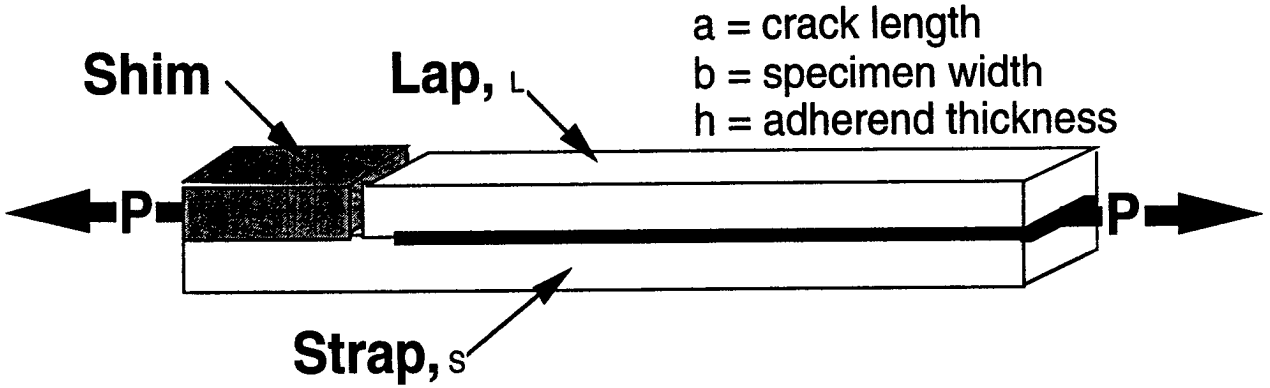

Technical Review

Assessing Structural Integrity of Bonded Joints Using Fracture Mechanics

Mixed-Mode Fracture Toughness For Several Adhesive Systems

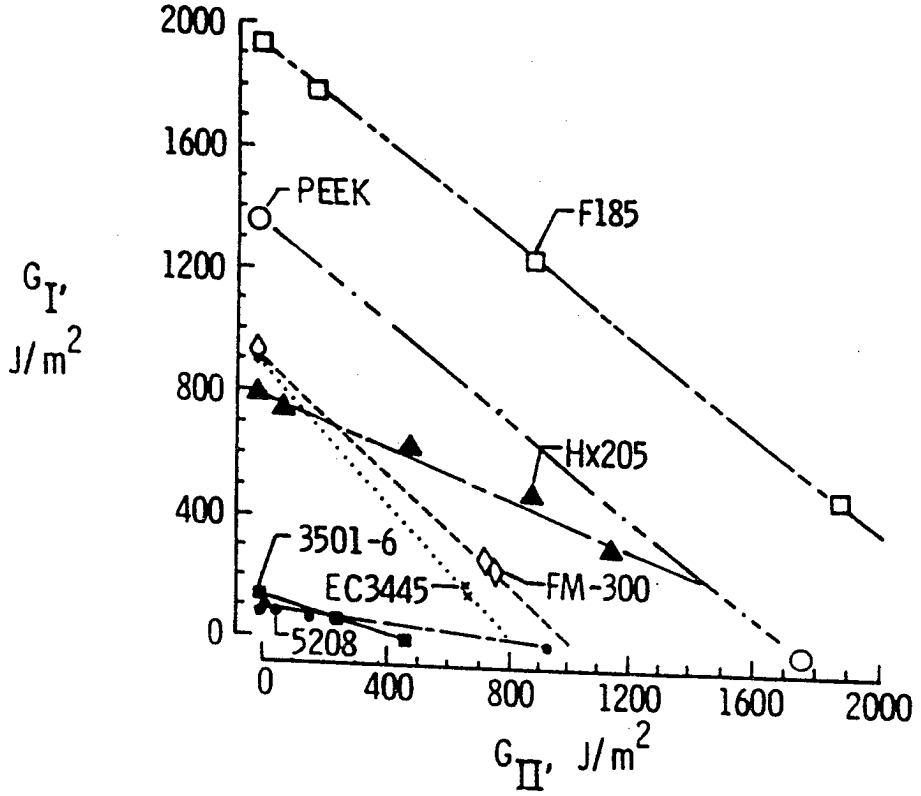

Source: Johnson, W.S. and Mangalgiri, P.D., "Influence of the Resin on Interlaminar Mixed-Mode Fracture" in Toughened Composites, ASTM STP 937, N.J. Johnston, ed., American Society for Testing and Materials, Philadelphia, 1987, pg. 309.

Technical Review

Assessing Structural Integrity of Bonded Joints Using Fracture Mechanics

Relation Between Total Strain Energy Release Rate and Debond Growth Rate

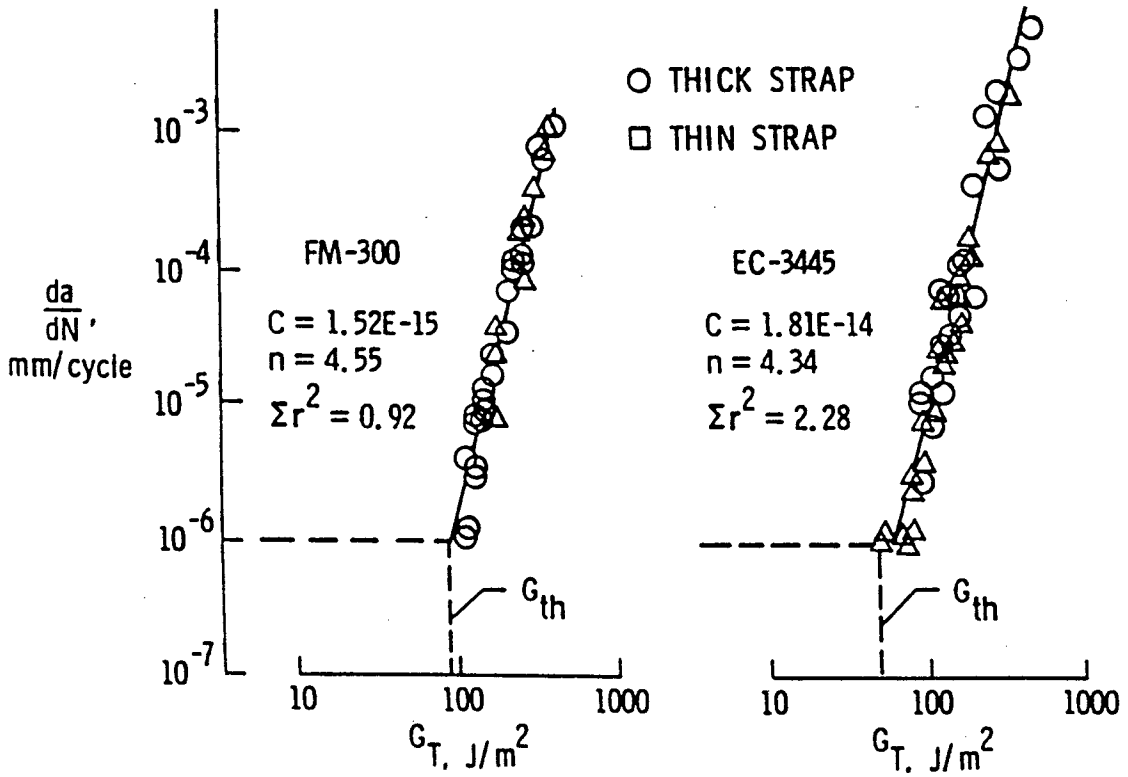

Source: Johnson, W.S. and Mall, S., "A Fracture Mechanics Approach for Designing Adhesively Bonded Joints" in Delamination and Debonding of Materials, ASTM STP 876, W.S. Johnson, ed., American Society for Testing and Materials, Philadelphia, 1985, pg. 191.

Technical Review

Assessing Structural Integrity of Bonded Joints Using Fracture Mechanics

Comparison of the Predicted and Experimental Maximum Stresses for No Debonding

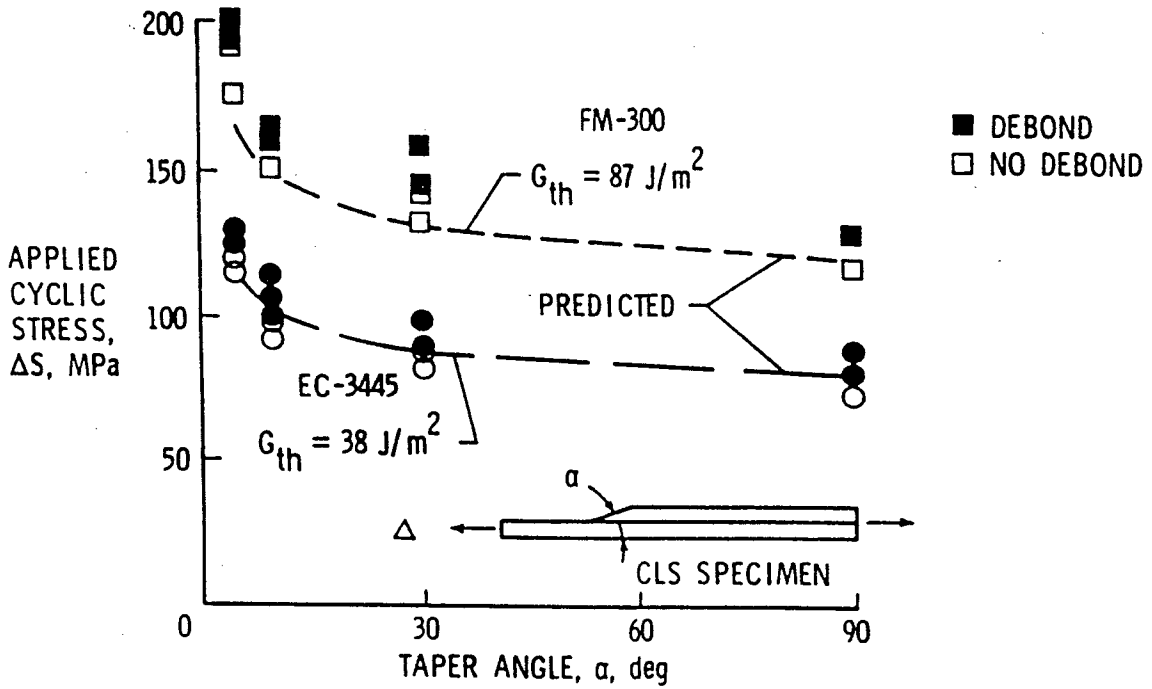

Source: Johnson, W.S. and Mall, S., "A Fracture Mechanics Approach for Designing Adhesively Bonded Joints" in Delamination and Debonding of Materials, ASTM STP 876, W.S. Johnson, ed., American Society for Testing and Materials, Philadelphia, 1985, pg. 196.

NUMERICAL ANALYSIS - *Previous Research*

- **Rybicki & Kanninen** (1977)
  - Employed constant strain elements in "Indirect Method"
  - Used nodal forces and displacements to find G, then K

- **Dattaguru, *et al.*** (1984)
  - Used GAMNAS (**G**eometric **A**nd **M**aterial **N**onlinear **A**nalysis for **S**tructures)
  - Pronounced nonlinear effcts in CLS specimen
  - G_{IC} is main governs the location of cyclic debonding

Proposed Research

Assessing Structural Integrity of Bonded Joints Using Fracture Mechanics

RESEARCH "DRIVERS"

- Supplement current stress-based approach to bonded joint design
- Link knowledge of environmental effects with fracture characteristics
- Address FAA and industry concerns about specific bonded material systems
- Respond to increased emphasis for life extension of commercial and military "aging aircraft"

Proposed Research

Assessing Structural Integrity of Bonded Joints Using Fracture Mechanics

SPECIMENS

- Three geometries for single and mixed mode fracture
- Representative of existing and future materials

ENVIRONMENTAL ISSUES

- "Building Block" approach, determine G_c & da/dN of:
  - as-received specimens
  - exposed specimens (5K and 10K hrs)
  - thermally cycled specimens (50 and 100 cycles)

ANALYSIS

- Compare results with numerical analysis (ABAQUS, GAMNAS) and suggest uses in design methodolgies

Proposed Research

Assessing Structural Integrity of Bonded Joints Using Fracture Mechanics

MATERIALS & ENVIRONMENTS

- ***Lockheed*, C-141 Program**
  - Application: Bonded Repairs
  - Adherends: Aluminum-Aluminum (7075-T651)
    Boron/Epoxy-Aluminum
  - Adhesive:
    - FM-73 modified epoxy
    - 121°C (250°F) cure/82°C (180°F) use
  - Environments:
    - 71°C (160°F)/95%rh exposure
    - -54°C (-65°F) to 71°C (160°F) cycling

Proposed Research

Assessing Structural Integrity of Bonded Joints Using Fracture Mechanics

MATERIALS & ENVIRONMENTS

- ***Lockheed*** **, F-22 Program**
  - Application: Aileron Trailing Edge/Torque Box
  - Adherends: Carbon/Bismaleimide composite
  - Adhesive:
    - AF-191 modified epoxy
    - 177°C (350°F) cure/ 121°C (250°F) use
  - Environments:
    - 104°C (220°F) exposure
    - -54°C (-65°F) to 104°C (220°F) cycling

Proposed Research

Assessing Structural Integrity of Bonded Joints Using Fracture Mechanics

MATERIALS & ENVIRONMENTS

- ***Boeing*** **, High Speed Civil Transport Program**
  - Application: Fuselage and Wing Structure
  - Adherends: Titanium (Ti-6Al-4V)
  - Adhesive:
    - FM-X5 new polyimide resin
    - 343°C (650°F) cure/ 177°C (350°F) use
  - Environments:
    - 177°C (350°F) exposure
    - -54°C (-65°F) to 177°C (350°F) cycling

Proposed Research

Assessing Structural Integrity of Bonded Joints Using Fracture Mechanics

ANTICIPATED RESULTS

- Influence of fracture mode and mode ratio on da/dN
- Relationship between G_c and da/dN
- Influence of environment on joint performance
- Application to structural/repair design and analysis
- Correlation between numerical, analytical, and experimental results

Preliminary Results

Assessing Structural Integrity of Bonded Joints Using Fracture Mechanics

- ***Lockheed*, C-141 Program**
  - Double Cantilever Beam (Mode I)
    Al/FM-73/Al
    Al/FM-73/Boron-Epoxy
  - Monotonic Loading - G_{TC} and G_{IC}
    displacement control, 1mm/min
  - Fatigue Testing - da/dN vs. G_{max}
    displacement control, R = 0.1, 10 Hz
  - Fractography

Preliminary Results

Assessing Structural Integrity of Bonded Joints Using Fracture Mechanics

Typical Bondline Regions

Al/FM-73/Al

Al/FM-73/Boron-Epoxy

Preliminary Results

Assessing Structural Integrity of Bonded Joints Using Fracture Mechanics

Monotonic Test of Al/FM-73/Al

Load vs. Displacement

Aluminum/FM-73/Aluminum

Mode I, Double Cantilever Beam

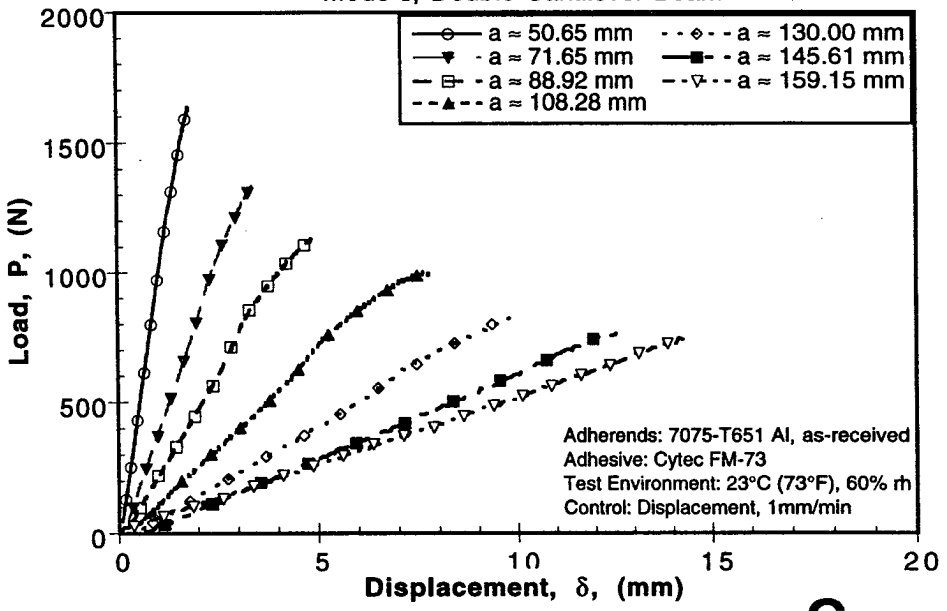

$G_{IC} \approx 2392\ J/m^2$

Preliminary Results

Assessing Structural Integrity of Bonded Joints Using Fracture Mechanics

Monotonic Test of Al/FM-73/Boron-Epoxy

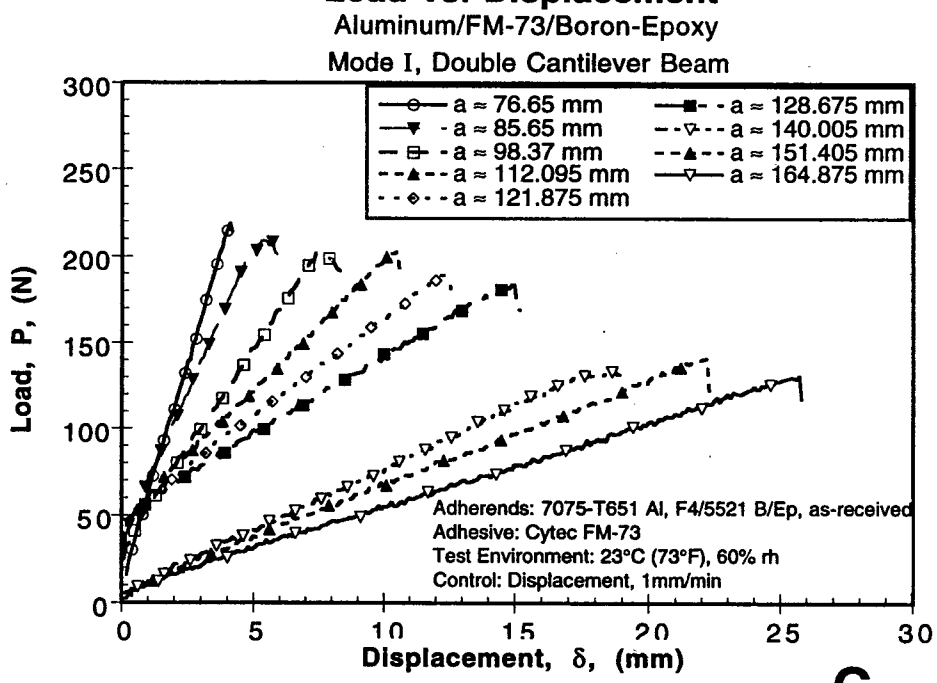

$G_{TC} \approx 915$ J/m^2

Preliminary Results

Assessing Structural Integrity of Bonded Joints Using Fracture Mechanics

Fatigue Test Results

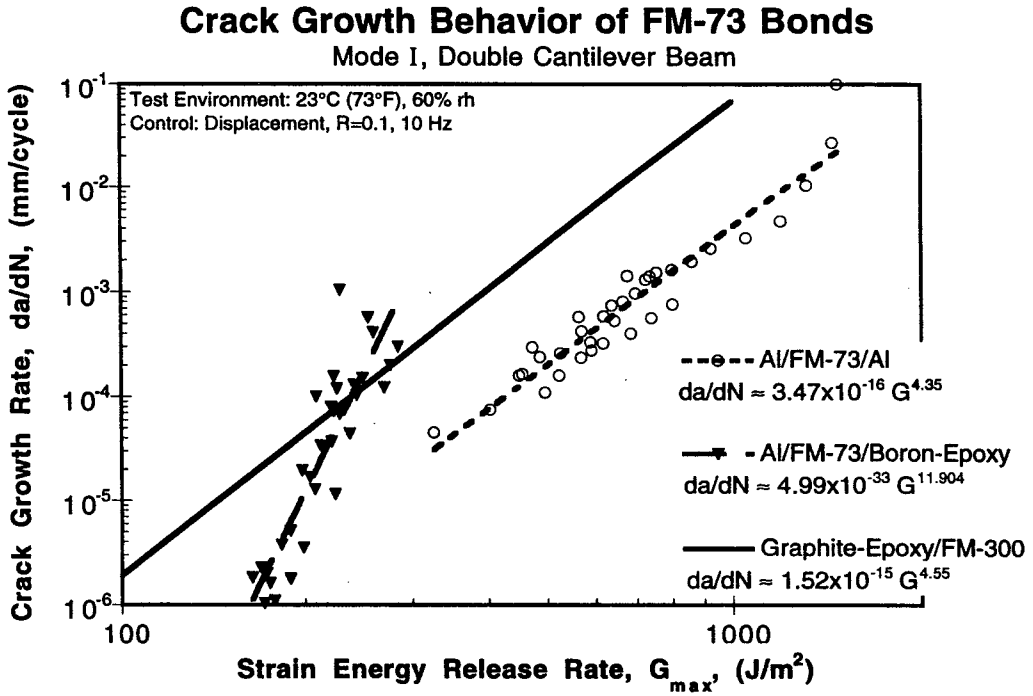

Summary

Assessing Structural Integrity of Bonded Joints Using Fracture Mechanics

- New aircraft designs and repairs are increasing use of bonded assemblies
- Opportunity exists to apply fracture mechanics to analyze effects of simulated service conditions on joint integrity
- Proposed work will seek to refine the use of fracture mechanics for the analysis and design of bonded (aircraft) joints
- Preliminary results:
  - bondline flaws are inherent
  - adherends and surface prep contribute to distinct differences in bondline mechanics

Experimental Observation of the Effect of Contact Parameters on Fretting Fatigue Crack Nucleation

*Mr. Matthew P. Szolwinski
Mr. G. Harish
Prof. Thomas N. Farris
School of Aeronautics and Astronautics—Purdue University
West Lafayette, Indiana 47907-1282

Abstract

The onset of multiple-site damage and corrosion is often found to occur at fastener/hole interfaces in lap joints or other airframe structural members. The nature of the load transfer at the contact interface results in a damage process known as fretting. The combination of micro-slip at the contact surfaces and the cyclic contact stresses associated with fretting reduce the number of cycles required to nucleate a crack from the fastener hole, compared to predictions that neglect these effects. The current experimental program focuses on the study of fretting fatigue crack formation in common aircraft aluminum alloys, including 2024-T3 and 7075-T6 alloys, with the goal of verifying lives as predicted by a numerical method based on multiaxial fatigue life models. The experiments will assess (a) the effect of the contact parameters, including the magnitude of the normal and tangential loads transferred, (b) friction coefficient at the interface, and (c) material properties, on crack nucleation through the use of a fretting fatigue test rig. The following details the relationship between the test program and aging aircraft concerns; the design and verification of a fretting fatigue test rig; and a system developed for automated data acquisition.

Background

Fretting is the damage process associated with the small-scale oscillatory relative motion of two contacting clamped surfaces; the damage process involves wear, fatigue and corrosion phenomena, each driven by the localized shear traction and microslip at the contact surface. Occurrences of fretting in structural

members such as bolted flange joints, riveted lap joints or even rocket propulsion fuel tanks have been well-documented (Hattori (1994), Rollins et al. (1989)) and often attributed to unpredicted early failures of a myriad of mechanical components and structural members.

The nucleation of cracks under the influence of the oscillatory contact stresses and strains arising from the fretting action is of particular interest to the community of officials, researchers and technicians charged with insuring the safe operation of both civil and military aging aircraft well beyond their intended design lifetimes. Critical to this effort is the proper inspection, identification and evaluation of widespread fatigue damage (WFD) on the airframe. With hundreds of joints and hundreds of thousands of individual rivet holes, the nucleation of cracks under the influence of fretting is inevitable and the task of complete inspection nearly impossible. The presence and interaction of large numbers of these small cracks in structural components, a state often referred to as multi-site damage (MSD), can lead to sudden and catastrophic failure of the airframe during service.

In light of the consequences of the nucleation of cracks, the motivation for a clear understanding of the role fretting plays is clearly evident. While several researchers (Waterhouse & Taylor (1971), Nishioka et al. (1968) and Endo & Goto (1976)) have addressed the problem of fretting fatigue with experimental studies, these early programs were primarily concerned with fretting of steel. Recent interest in aging aircraft has renewed research into the fretting of aluminum, with attention given to the phenomenon because of its role in the nucleation of cracks at the fastener/skin interface and at the interface between panels in lap joints. The current experimental effort is designed to study the role of fretting contact on the formation of fatigue cracks in aircraft aluminum.

Figure 1 illustrates the relationship between the fretting conditions experienced in aircraft operation and the localized contact stresses at the rivet/skin interface modeled in the experimental setup. During the life of an airframe, its various structural members carry a variety of cyclic loads. For example, turbulence or aeroelastic effects lead to oscillatory loading of the wing and repeated pressurization and depressurization of the cabin causes cyclic stresses in the fuselage. This global effect is represented schematically in Figure 1 with a lap splice subjected to a cyclic remote stress. The load transfer to the structure takes place on a local scale, though, at the rivet/skin interface. The remote global load causes both normal and shear loading of the rivet, an effect that induces both a normal pressure and shear traction over the area of contact between the rivet and rivet hole.

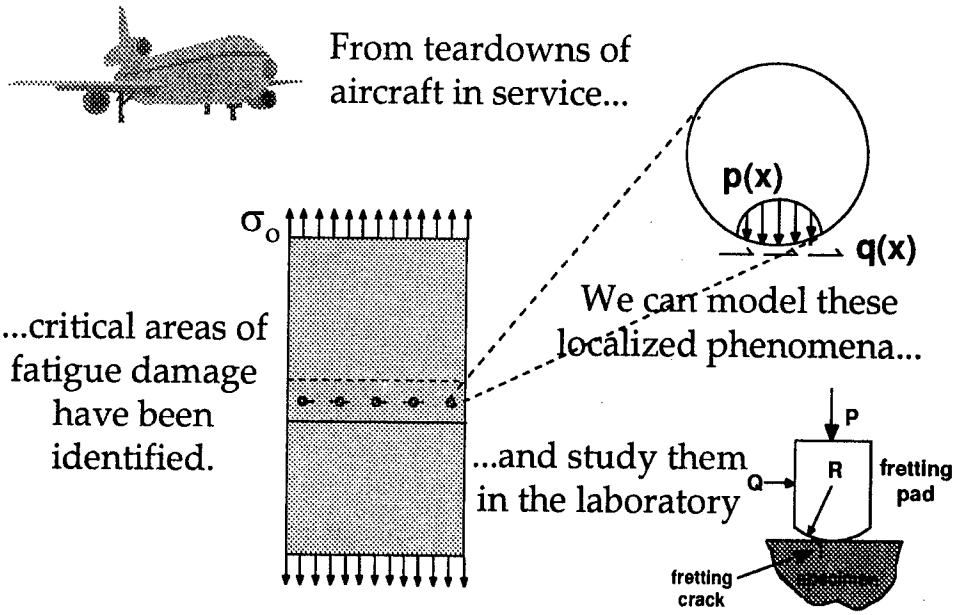

Figure 1: An illustration of the relationship between an aircraft lap splice structural joint and the fretting contact problem.

The normal pressure distribution can be approximated using Hertzian or non-conformal contact theory that holds for contact sizes much smaller than the characteristic sizes of the contacting bodies. The applied tangential force (Q) must be less than the global frictional force (μP) to prohibit sliding at the rivet/skin interface. This condition leads to a region of stick spanning the middle of contact flanked by a region of microslip. It is this stick/slip configuration that must be achieved by the fretting fatigue rig via controlled and measurable application of normal and tangential forces to the fatigue specimen. In addition, the magnitudes of the loads must be chosen so as to generate contact stresses similar to those at the rivet/skin interface.

Fretting Fatigue Test Rig

Simulation of basic fretting contact typically involves clamping either a spherical or cylindrical indenter into contact with a flat specimen and then applying an oscillatory tangential load to the indenter. An alternative configuration applies the oscillatory load to the specimen. Such a configuration can be achieved using a rig and a standard uniaxial servo-hydraulic testing machine as shown in Figure 2. The rig (similar to one suggested by Hills et al. (1988)), designed for plane-strain fretting contact, allows for the controlled

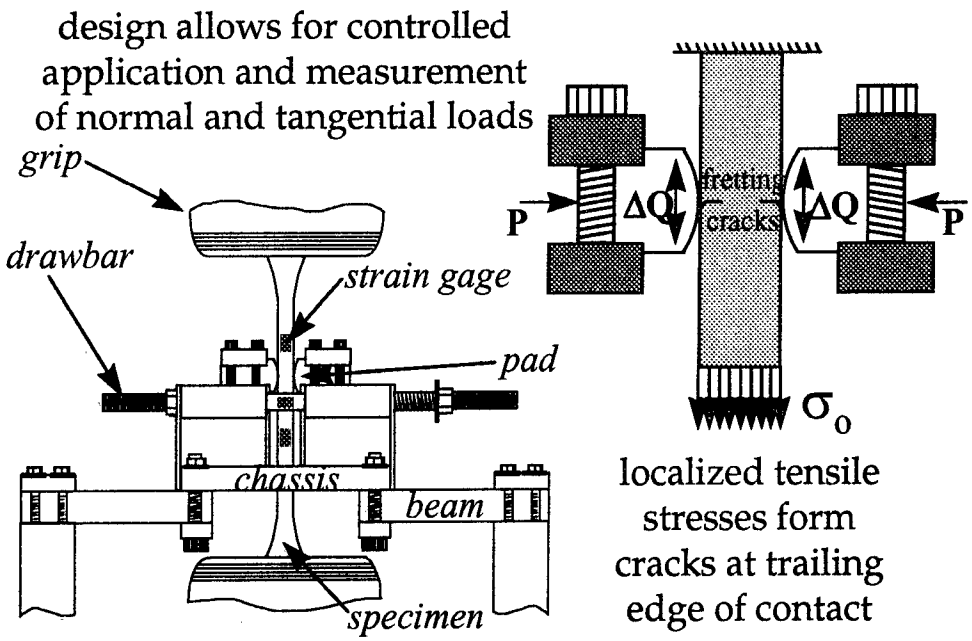

Figure 2: A schematic of a fretting fatigue test rig highlighting the relationship between its structural features and the fretting loads.

application and measurement of both the normal and tangential loads. With a specimen mounted in the grips of the load frame, the curved fretting pads are clamped into contact with the flat surface of the specimen by two drawbars. Compliant springs mounted over the drawbars ensure a constant normal load as the contact surfaces wear and wear particles are ejected. Upon application of a load by the lower grip/actuator assembly, the specimen transmits loads to the beams through friction between the specimen and pads. The beam stiffness and applied load must be chosen in tandem to assure stick/slip contact characteristic of fretting. Note that a bulk tension is superposed on the fretting contact stresses in the specimen.

Control of the contact parameters involved in fretting contact is done by varying the geometric characteristics and applied load conditions in the experimental setup. Changing the radii of curvature of the fretting pads or the clamping force P alters the size of the contact area and the maximum Hertzian contact pressure, a value that is directly proportional to the amplitudes of the elastic contact stresses and strains. The magnitude of the shear force can be increased by increasing the applied remote stress or the stiffness of the beams mounted to the rig chassis.

Measurement of critical contact parameters, P, Q and the average coefficient of friction, μ, is done with an array of strain gages, placed at various locations on

the rig and specimen. The total normal force, P, is obtained from load washers mounted over each of the drawbars. The shear force, Q, can be measured in two ways: (1) with strain gages placed above and below the contact point on the specimen, and (2) with strain gages bonded onto the beams. With the first approach, global static equilibrium of the rig/specimen combination is considered: the load transmitted by the rig is calculated as the difference between the load applied by the actuator to the portion of the specimen below the contact and the reaction load detected by a pair of gages above the contact. This method is also used to determine a calibration relationship between the tangential force, Q, and deflection of the beam, as measured by strain gages mounted on the beams. This calibration eliminates the need for mounting gages on each test specimen.

An estimate of the apparent coefficient of friction can be obtained by a method suggested by Nowell and Hills (1990). Recall that global sliding occurs when the applied tangential force, Q, equals the global applied frictional force, defined as the product of the apparent coefficient of friction, μ, and the global clamping force, P. If the value of μ is desired after a given number of cycles of fretting, the constant amplitude cyclic loading is terminated and a separate cyclic tangential load with steadily increasing amplitude is applied until gross sliding is detected.

Data Acquisition

As with any fatigue test involving a large number of cycles, automated testing and data acquisition is important. The need for an efficient data acquisition system is magnified when considering the number of measurements required to characterize the conditions of fretting fatigue. This fact is emphasized by Attia (1992) in a summary of a series of papers aimed at developing a fretting fatigue test standard. Attia (1992) notes that measurement of contact parameters and automation of the testing procedure and data acquisition are still areas to be addressed by the fretting fatigue test community.

Braun (1994) assesses the past, current and future directions of automated fatigue and fracture testing, identifying the characteristics of a next-generation test setup. These characteristics include: (1) a digital control system that implements the control loop and function generation for the waveform applied by the servo-hydraulic loadframe via software, (2) a flexible data acquisition scheme allowing for a wide variety of experimental configurations and (3) an intuitive software-based user interface that relies on a graphical-user interface (GUI). Several diversified approaches have been taken to realize such a system, including use of a UNIX-based workstation and analog controller (McKeighan, et al. (1990)) and general purpose fatigue testing software (Dharmavasan and Peers (1990)) with a

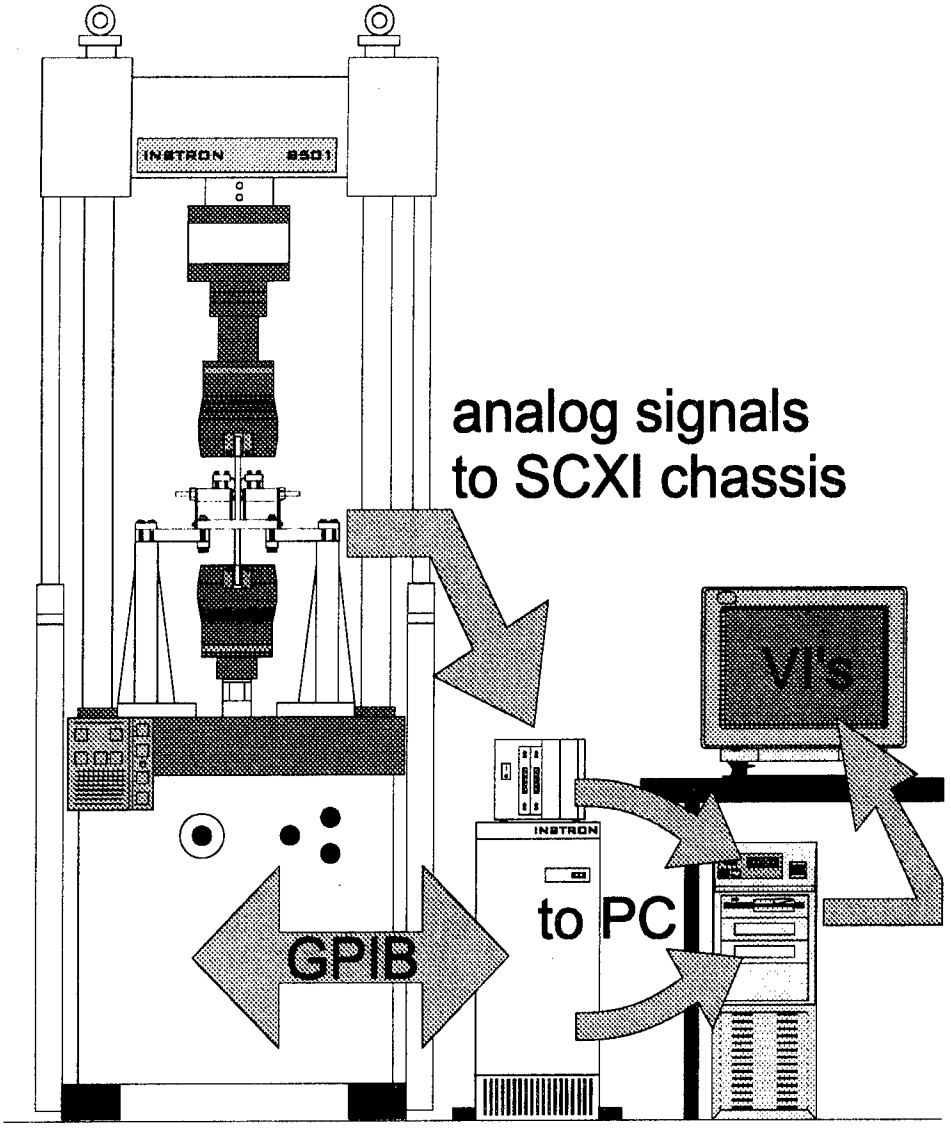

Figure 3: A schematic showing the experimental setup and associated computer control, monitoring and data acquisition system

digital controller. Each of these approaches required a significant investment of time and effort for constructing the base code for efficient communication between the myriad of components in the test system.

The current experimental setup relies exclusively on commercially-available hardware components and software package to achieve a single, flexible

graphically-oriented, Pentium™ personal computer (PC) based system for control, data acquisition (DAQ) and on-line data processing. A schematic of the system is presented in Figure 3. The fatigue loading of the specimen is accomplished with an Instron 22 kip servo-hydraulic load frame fitted with hydraulic wedge grips. The requisite control signals corresponding to a given set of frequency, waveform and amplitude parameters are sent to the servo-valves by an Instron 8500 digital controller. The controller can operate either stand-alone through an attached panel-style user interface or remotely through a digital input/output (I/O) line that relies on a standardized general purpose interface bus (GPIB). It is this GPIB connection that allows for integration of the controller with the standard PC bus architecture.

The pairs of strain gages mounted on the beams and above and below the contact are wired into half-bridge Wheatstone bridge circuits constructed on a printed circuit board. The load cells require a similar full-bridge circuit. The excitation of each of these bridges and subsequent conditioning of the analog signals from the sensors is achieved with a general-purpose Signal Conditioning eXtensions for Instrumentation chassis (SCXI) manufactured by National Instruments. The module allows for user-definable excitation voltages (3.333 or 10 V), two-stage signal gains (from 1 to 1000) and two-stage filters (4Hz or 10 kHz). The current configuration offers up to eight channels, with the potential for expansion to twelve.

The preconditioned analog signals from the array of sensors are then read from the SCXI chassis in either a multiplexed or parallel mode by a 16-bit analog-to-digital (A/D) data acquisition card in the PC. This card, an AT-MIO-16FE card also manufactured by National Instruments, can read up to 16 single-ended or 8 differential channels at a maximum of 20 kilosamples/second 10 kHz and a maximum resolution of 3 μV. It is completely software-configurable, complying with the latest "Plug and Play" hardware standards. This software configuration thus eliminates the need for cumbersome hardware jumper adjustments for varied experimental configurations.

The real strength of this experimental setup lies not necessarily in the performance and flexibility of its hardware, but in the ability for the hardware to be integrated into a single suite of user-friendly GUI panels that allow for the on-line control, monitoring and analysis of each fatigue experiment. This software platform was developed using National Instrument's LabVIEW™ (the **L**aboratory **V**irtual **I**nstrument **E**ngineering **W**orkbench package for Microsoft Windows). In short, LabVIEW is a general purpose graphical "language" that allows the user to develop complex virtual instruments (VI) for interfacing with a myriad of DAQ entities by "wiring" basic subroutines together in a diagram. Since many of the base level operations such as direct communication with the DAQ hardware,

generation of complex GUI's and data file creation and management are inherent parts of the LabVIEW subroutines, the time required to develop flexible, powerful software platforms for large-scale experimental setups is slashed.

The current experimental effort relies on an integrated suite of custom-designed virtual instruments to control, monitor and analyze the fretting fatigue tests, as presented in Figure 4. An initial panel serves as an interface to the 8500 digital controller for the load frame. The user selects parameters from dialog boxes such as the control channel (load or position); waveform type, amplitude and frequency; and any limit values. Complete remote operation of the loadframe is possible from this GUI. Two other GUI panels serve to configure, control and monitor graphically the data acquisition of both the load and position digital signals from the 8500 and the multiple channels of analog signals from the array of sensors on the fretting rig. The user can configure the number of channels collected, the frequency of data collection and the number of points collected per cycle. Once this data is collected from the various sources, it can be manipulated in several ways: presented in real-time on screen in graphical format, processed on-line with a wide variety of mathematical functions provided in LabVIEW, or written automatically in binary or ASCII format to a storage device at user-defined cycle numbers for subsequent post-processing.

Verification of the Fretting Fatigue Rig

A finite element model of the rig (Figure 5) was developed using ANSYS to assist in the design refinement and verification process for the fretting fatigue rig. (ANSYS™ is a commercial finite element package provided on an academic license to Purdue University by Swanson Analysis Systems.) The purpose of this model is threefold: (1) to characterize the relationship between the loads applied by the actuator and drawbars and the associated shear load on the pads, (2) to help predict the magnitude of any dynamic load effects associated with the forced vibration of the fretting fatigue rig, and (3) to compare measured and predicted shear force magnitudes, Q.

The rig was modeled using two-dimensional beam elements with shear deformation and the subsequent analysis was linear elastic. The specimen-pad contact was assumed to be adhesive, imposing the condition of no relative motion at the contact surfaces. No stress stiffening was considered. Finally, the drawbars were assumed to deform predominantly along their axis and hence were modeled as spring elements.

From an analysis of the results, it was concluded that the thickness of the cantilever beams had the largest effect on the compliance of the fretting rig. Subsequent analyses were performed for varied structural configurations and compared with the corresponding stiffness values measured experimentally. The

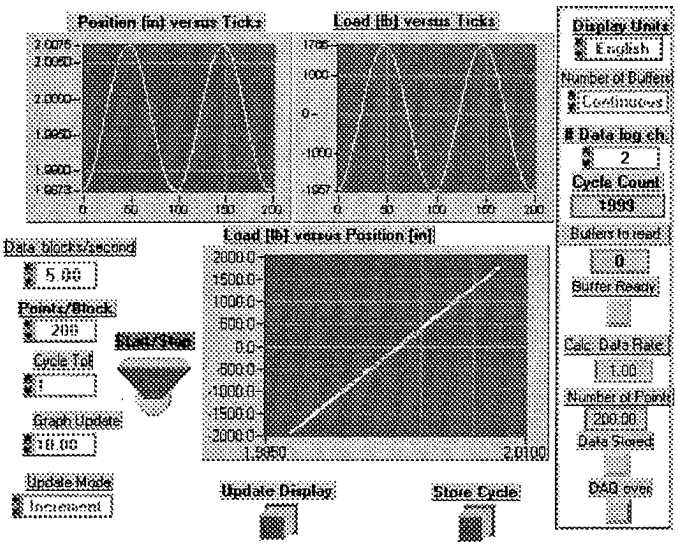

Figure 4(a)

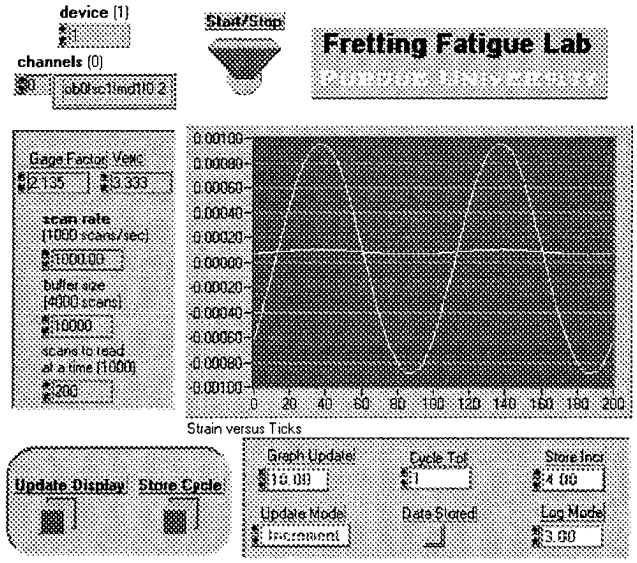

Figure 4(b)

Figure 4: Snapshots of two virtual instrument (VI) panels used in the fretting fatigue experiments. Figure 4(a) shows the panel configuring and monitoring the DAQ over the GPIB connection with the Instron 8500 controller, while Figure 4(b) displays the GUI used with the converted analog signals from the SCXI chassis and A/D board.

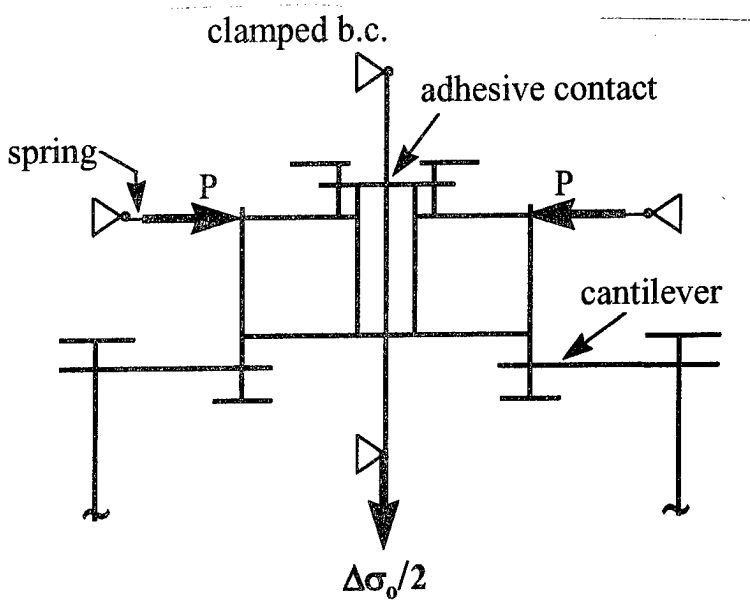

Figure 5 : A two-dimensional finite element model of the fretting fatigue test rig. The model was used as a design and verification tool during the current experimental program.

parameter used to benchmark the stiffness of the rig was Q/F , with Q being the transverse force in each cantilever and F the bulk load applied by the servo-hydraulic load frame.

Two experimental configurations that employ different cantilever stiffnesses are being used in the current study. The experimental value of F was taken from the load cell of the servo-hydraulic load frame, while the value of Q was taken from the difference in the specimen strain gage readings above and below the contact. For the first configuration, the FEM solution predicted a Q/F ratio of 8.8%, agreeing well with the experimental ratio of 9.2% . For the second configuration, the FEM solution predicted a ratio of 12.9%, compared to the experimentally-obtained ratio of 12.7%. Thus the FEM model is established as a useful design tool to predict effects of modifications of the individual rig components on the ability of a given configuration to generate the requisite forces for fretting fatigue contact. It was also observed that the compliant springs mounted on the drawbars reduce the effects of the coupling between the cyclic remote loading and the pressure transmitted through the drawbars onto the fretting pads.

In the spirit of ASTM standard E 467-90, a modal analysis of the rig was performed to investigate potential structural dynamic effects. Results of this effort

revealed the principal natural frequency of the rig to be approximately 174 Hz. As this first resonant frequency is over an order of magnitude higher than the operating frequency range of 5-15 Hz for the fretting fatigue tests, the effect of structural resonances on the applied fretting loads can be neglected comfortably. The modal analysis also showed the response of the system to be linear in the operating frequency range.

Further refinement of the model is currently underway to correlate the strain readings from the cantilever beams with the induced tangential force on the fretting pads. As alluded to earlier, such a calibration will enable direct measurement of the tangential force, Q, from the strains experienced by the cantilevers.

Current Experimental Effort

The thrust of the current experimental effort is to correlate the nucleation behavior of fretting fatigue cracks with predictions made by the multiaxial fatigue life model detailed elsewhere (Szolwinski & Farris (1995)). Past studies of fretting fatigue have focused primarily on the role of fretting fatigue in reducing total fatigue life. The studies that have concentrated on fretting crack nucleation have presented only either empirical observations or data on cycles to failure.

By choosing an appropriate range of contact parameters (contact halfwidths greater than approximately 1 mm and a ratio of applied tangential force to clamping force (Q/P) between 0.25 and 0.50) the fretting fatigue crack formation

Experimental Parameter	Level 1	Level 2	Level 3
p_o (ksi)	24	28	32
σ_o (ksi)	12	14	16
R (in)	5	9.5	12
Q/P	0.25	0.35	0.5

Table 1: Summary of typical experimental parameters chosen for the fretting fatigue crack nucleation study

damage mechanism dominates over any wear or corrosion processes. This study thus focuses on determining the number of cycles required to form a crack of length 1 mm, to allow for correlation with multiaxial fatigue life predictions. Values of maximum contact pressure and bulk applied stress amplitude were chosen to reflect conditions similar to those experienced by the rivet/skin contact. Typical experimental parameters are summarized in Table 1.

These parameters, when combined with the apparent coefficient of friction at the contact interface, characterize fully the cyclic stresses and strains associated

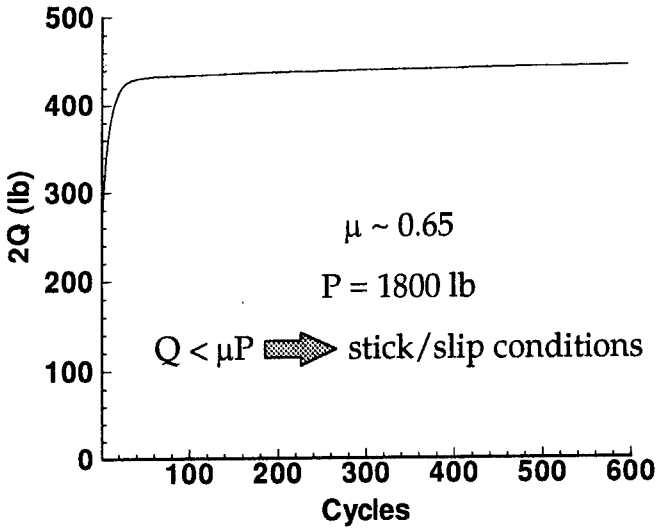

Figure 6: A plot of two times the tangential load, 2Q, over the first 600 cycles of a fretting fatigue experiment. Note how the tangential force increases rapidly in the first few cycles and then levels out corresponding to a rapid increase and eventual stabilization of the friction coefficient at the contact interface.

with the 2-D, plane strain fretting fatigue contact problem present in the experimental setup (Szolwinski (1995)). While each of the parameters in Table 1 can be monitored during the course of the experiment, the apparent coefficient of friction cannot be determined directly during the course of the fatigue experiment. Reviewing Figure 6, a plot of the applied tangential force, Q, during the initial 600 cycles of an experiment, reveals that within the first few cycles, the tangential force rises rapidly and then begins to approach an asymptotic level. This behavior is attributed to the rapid increase and stabilization of the apparent coefficient of friction under the partial slip conditions present in the fretting contact zone, a behavior reported by others (Nishioka & Hirakawa (1969), Hills et al. (1988)) in studies of the fretting of steel and aluminum, respectively.

The apparent coefficient of friction is determined by halting the constant-amplitude cyclic loading of the pads and specimen and then applying a low frequency (~ 1 Hz) cyclic waveform with an increasing amplitude envelope. Global sliding is detected by monitoring the tangential force response. As the applied load cycles, the tangential force varies in phase until global sliding commences. Once this occurs, the peaks of the tangential force response are "clipped," as the surface shear traction at the contact interface can no longer resist the applied tangential load. At this point of incipient sliding, the apparent

coefficient of friction is defined as $\mu = Q/P$. Preliminary test results for contact between 2024-T351 aluminum indicate that the steady-state apparent coefficient of friction ranges between 0.65 and 0.70, confirming observations reported by others (Hills et al. (1988)) for aluminum-on-aluminum contact.

Since this estimate of friction coefficient at the contact interface completes the characterization of the fretting fatigue contact conditions, predictions about the nucleation behavior of fretting fatigue cracks based on multiaxial fatigue theory can be made. Figure 7 presents comparisons between the life predictions and data both published in the literature (Nowell & Hills (1990)) and generated as part of this study. The necessary fatigue constants for the material used in the published study (assumed to be 2024-T4) and the current material (2024-T351) were obtained in the literature (Fuchs & Stephens (1980)). Comparison between the predictions and observed lifetimes shows strong agreement between the theory and experiment. The stress calculation in this prediction is a modified version of the Mindlin stresses field that does not account for the effect of the bulk tension on the tangential shear traction. Finite element analysis of the fretting contact in the experiment by McVeigh (1995) justifies this assumption.

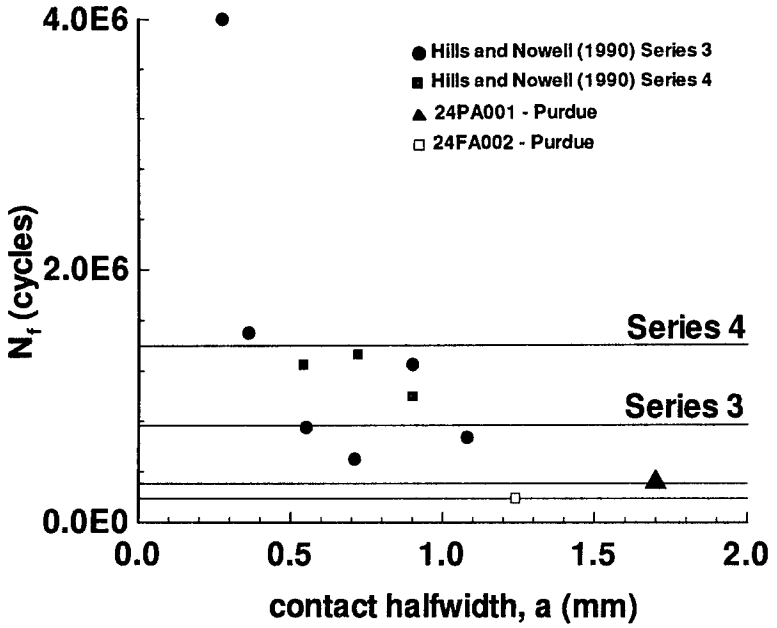

Figure 7: Comparisons between multiaxial life predictions and experimental observations.

Implications to Aging Aircraft

Application of the multiaxial fatigue life criterion to the three structural configurations presented in Figure 8 delivers a striking commentary about the critical role contact plays in the nucleation of cracks at the rivet/skin interface. Each member (a simple strip, a strip with a hole and a hole/rivet assembly experiencing load transfer) is subjected to a bulk oscillatory stress of 12 ksi, typical of those seen by a common aircraft member during service. For the first member, the stress amplitude of 12 ksi is well below the 22 ksi endurance limit for 2024-T3 aluminum and runout occurs. However, for the second member, the plate with a hole, the stress concentration of approximately three at the edge of the hole results in the nucleation of a crack in about 500,000 reversals (2 reversals = 1 cycle). Finally, for a typical case of 36% load transfer through a single rivet/skin contact, the life to nucleate a crack of 1 mm in length is predicted to be only 50,000 reversals (Farris et al. (1996)). The importance of this prediction is amplified by recalling that these rivet hole cracks are not isolated damage sites; they have the potential to interact and lead to sudden, catastrophic failure.

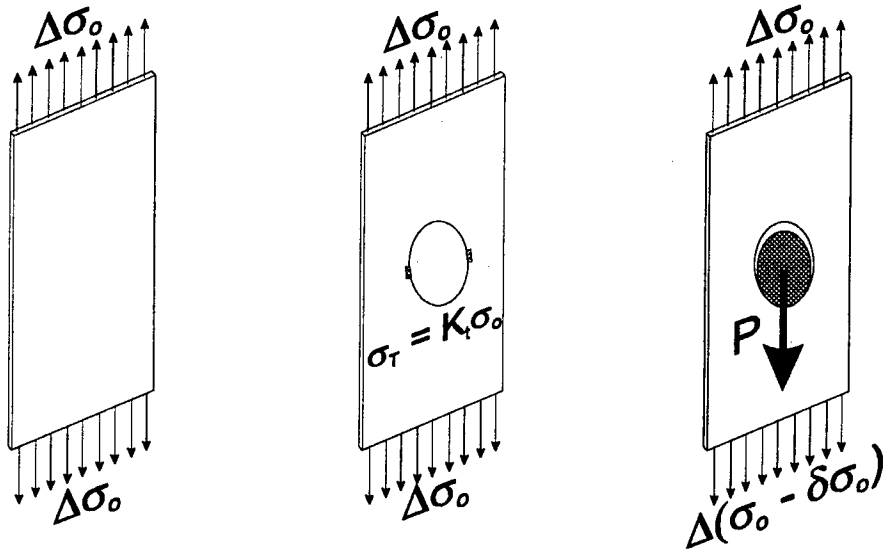

$2N_f > 10^7$ reversals $2N_f \sim 5 \times 10^5$ reversals $2N_f < 5 \times 10^4$ reversals

Figure 8: A sketch of three simple structural components with identical remote loadings and the associated number of reversals to nucleate a crack. Note the sharp reduction in life due to the contact between the rivet and hole.

Conclusions

Fretting is important to the nucleation of MSD in aging aircraft. A fully-automated test procedure for examining fretting crack formation lives is underway. Preliminary results indicate that multiaxial fatigue theory can be combined with the fully-characterized stress state to predict crack formation life.

Acknowledgment

This research is supported in part by AFOSR through contract #F49620-93-1-0377 and a National Defense Science and Graduate Engineering (NDSGE) fellowship for M. P. Szolwinski.

References

Attia, M.H. (1992), Fretting fatigue testing: current practice and future prospects for standardization, *in* 'Standardization of Fretting Fatigue Test Methods and Equipment', ASTM, Philadelphia, 263-275.

Braun, A. A. (1994) A historical overview and discussion of computer-aided materials testing, *in* 'Automation in Fatigue and Fracture—ASTM STP 1231', ASTM, Philadelphia, 5-17.

Endo, K. & Goto, H. (1976), 'Initiation and propagation of fretting fatigue cracks', *Wear* **38**, 311-324.

Farris, T. N., Grandt, A. F., Harish, G. & Wang, H. L. (1996), Analysis of widespread fatigue damage in structural joints, *in* '41st International SAMPE Symposium & Exhibition', SAMPE, Anaheim, in press.

Fuchs, H. O. & Stephens, R. I. (1980), *Metal Fatigue in Engineering*, Wiley & Sons, New York.

Hattori, T. (1994), Fretting fatigue problems in structural design, *in* 'Fretting Fatigue', European Structural Integrity Society, Sheffield, England, 437-451.

Hills, D. A., Nowell, D. & O'Connor, J. J. (1988), 'On the mechanics of fretting fatigue', *Wear* **125**, 129-146.

McKeighan, P. C. and Evans, R. D. and Hillberry, B. M. (1990), Fatigue and fracture testing using a multitasking minicomputer workstation, *in*

'Applications of Automation Technology to Fatigue and Fracture Testing—ASTM STP 1092', ASTM, Philadelphia, 52-67.

McVeigh, P. A. (1995), 'Finite Element Analysis of Fretting Fatigue Stresses', M. S. Thesis, Purdue University, West Lafayette.

Nishioka, K. & Hirakawa, K. (1968) 'Fundamental investigations of fretting fatigue, part 1', *Bulletin of JSME* **11** (45), 437-445.

Nishioka, K., Nishimura, S. & Hirakawa, K. (1969) 'Fundamental investigations of fretting fatigue, part 3', *Bulletin of JSME* **12** (51), 397-407.

Hills, D. A., Nowell, D. & O'Connor, J. J. (1988), 'On the mechanics of fretting fatigue', *Wear* **125**, 129-146.

Nowell, D. & Hills, D. A. (1990), 'Crack initiation criteria in fretting fatigue', *Wear* **136**, 329-343.

Szolwinski, M. P. (1995), 'Mechanics of fretting fatigue crack initiation', M. S. Thesis, Purdue University, West Lafayette.

Szolwinski, M. P. & Farris, T. N. (1995), Mechanics of fretting fatigue crack nucleation, *in* 'ASME Symposium on Structural Integrity of Aging Aircraft', ASME, San Francisco, 141-157.

Waterhouse, R. & Taylor, D. (1971), 'The initiation of fatigue cracks in a 0.7% carbon steel by fretting', *Wear* **17**, 139-137.

Experimental Observation of the Effect of Contact Parameters on Fretting Fatigue Crack Nucleation

M. P. Szolwinski, G. Harish & T. N. Farris

School of Aeronautics & Astronautics
Purdue University
West Lafayette, IN 47907-1282

This research is supported in part by AFOSR through contract #F49620-93-1-0377 and a National Defense Science and Graduate Engineering (NDSGE) fellowship

PURDUE

Overview

- Introduction
- Overview of fretting and aging aircraft
- Description of fretting fatigue test program
- Automated testing and data acquisition
- Verification of the test rig: FEM model
- Preliminary results of test program
- Implication of contact to aging aircraft
- Conclusion and questions

PURDUE

Defining fretting contact

- description of phenomenon
  - small-scale oscillation
  - clamped structural members
  - microslipping at contact interface
- damage process
  - wear
  - fatigue
  - corrosion

Fretting and Aging Aircraft

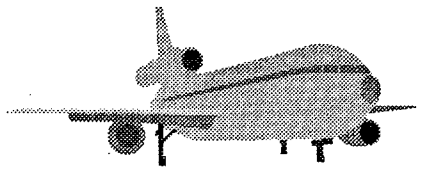

From teardowns of aircraft in service...

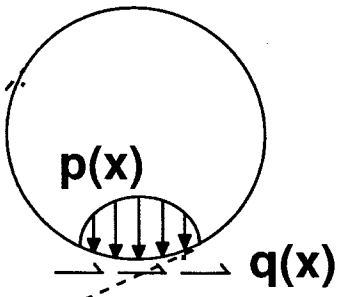

We can model these localized phenomena...

...critical areas of fatigue damage have been identified.

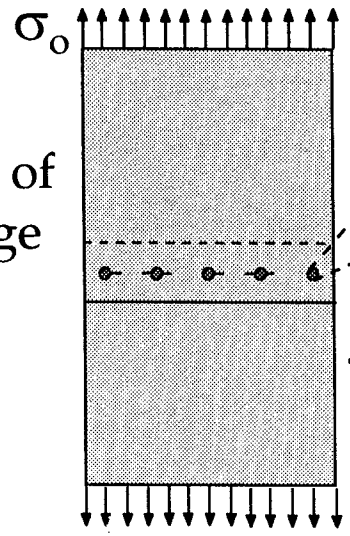

...and study them in the laboratory

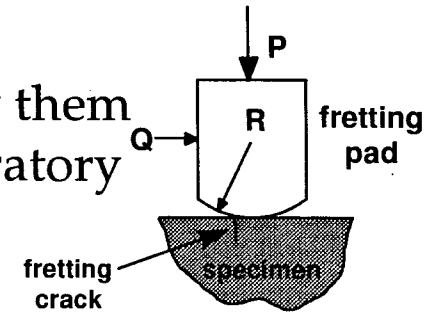

Experimental Setup

design allows for controlled application and measurement of normal and tangential loads

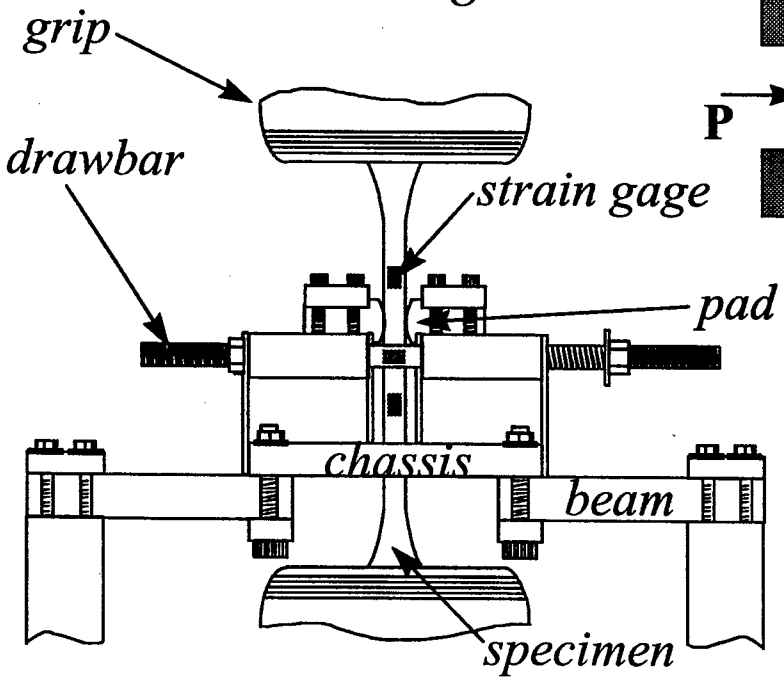

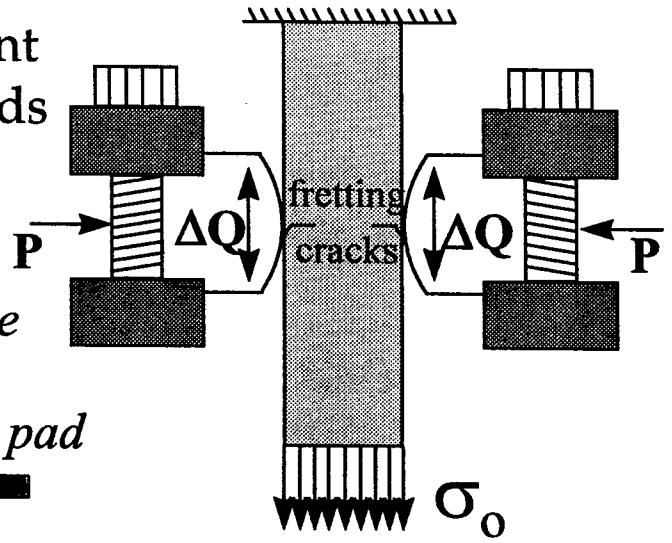

localized tensile stresses form cracks at trailing edge of contact

PURDUE

Automated Testing and DAQ

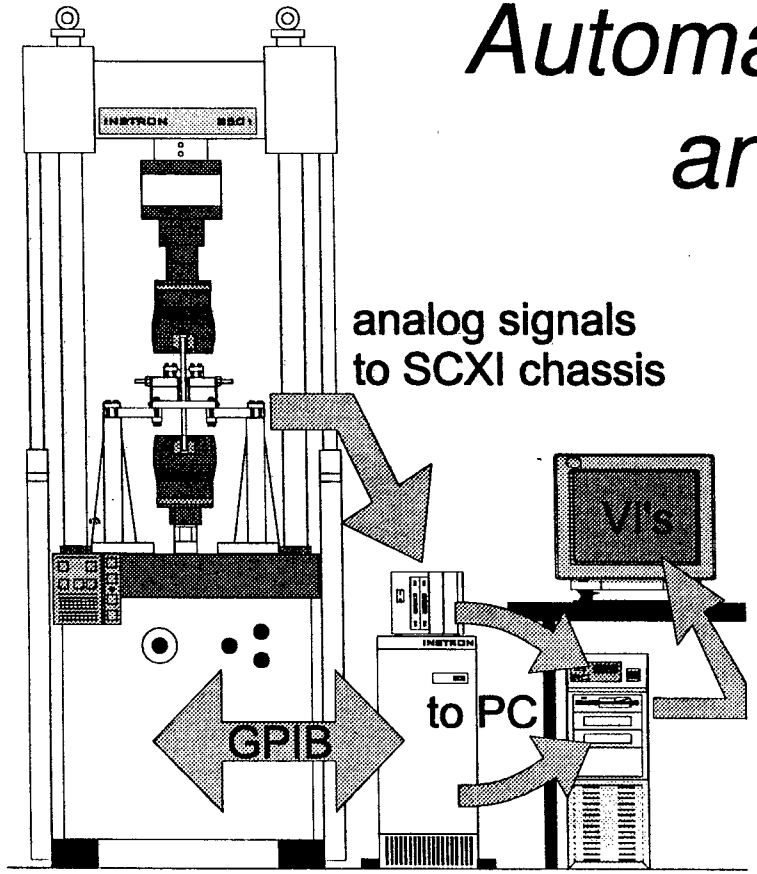

The system offers:

- complete computer control
- integrated signal monitoring
- on-line data processing

Virtual Instrument Panels

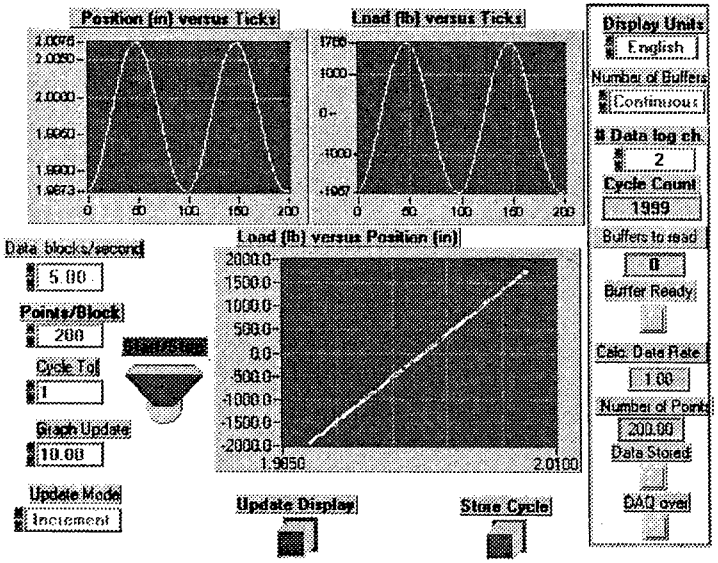

loadframe panel

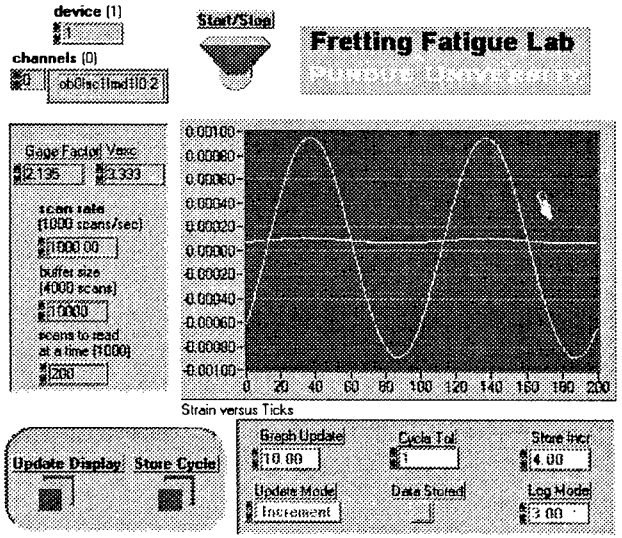

analog signals

PURDUE

FEM Model

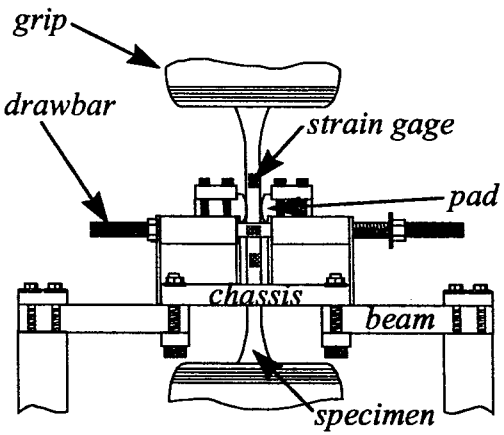

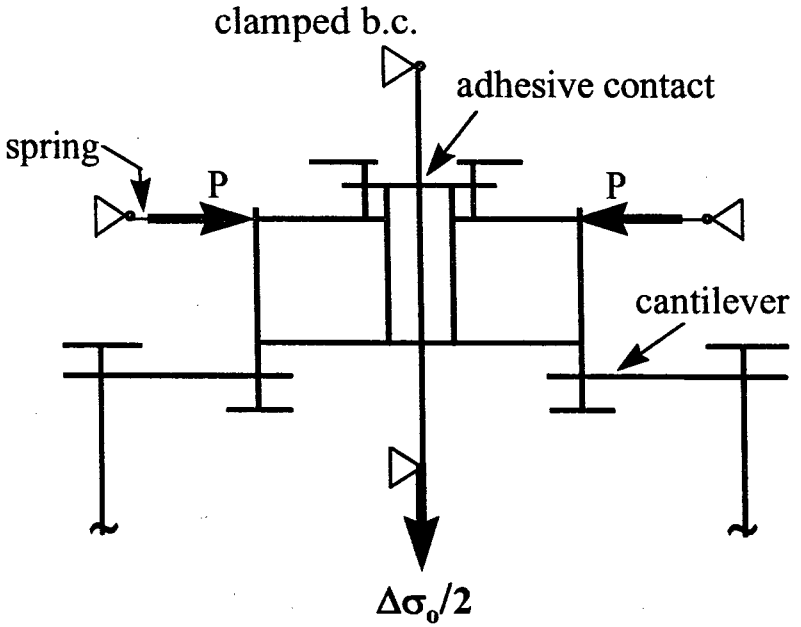

PURDUE

Verification of Test Rig

- rig modeled with 2-D beam elements with shear deformation
- model used as a tool to predict the ability of a given design to generate fretting loads
- modal analysis performed: $\omega_n \sim 175$ Hz
- further refinement underway to correlate strain in beams and tangential force

PURDUE

Evolution of tangential force amplitude

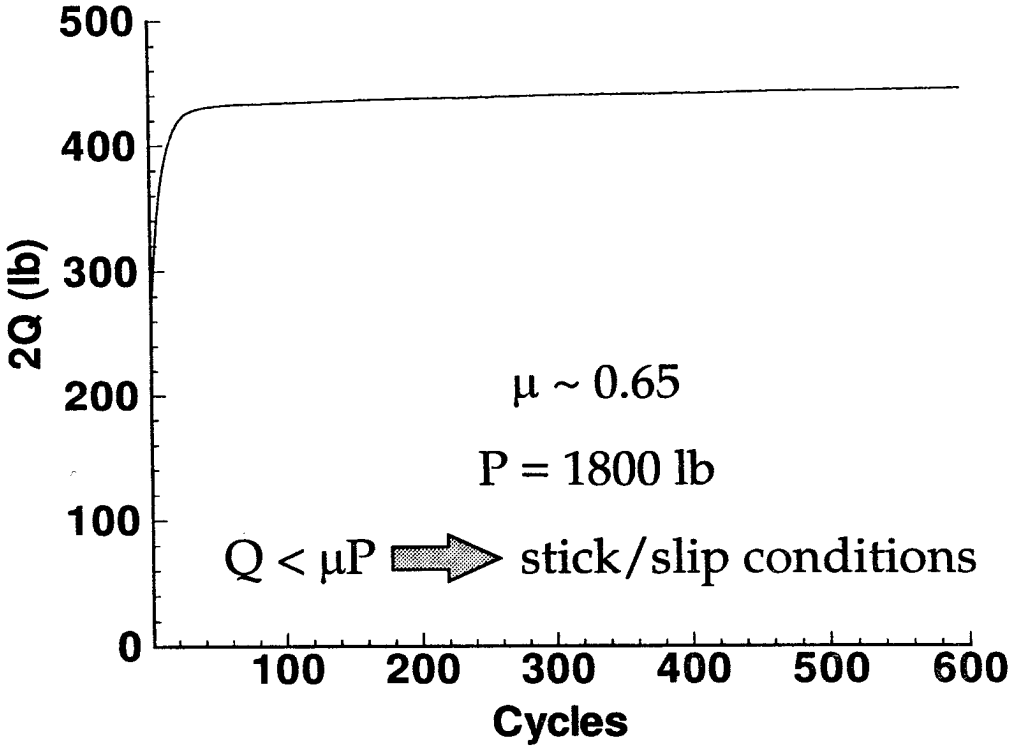

PURDUE

Fatigue Life Comparisons

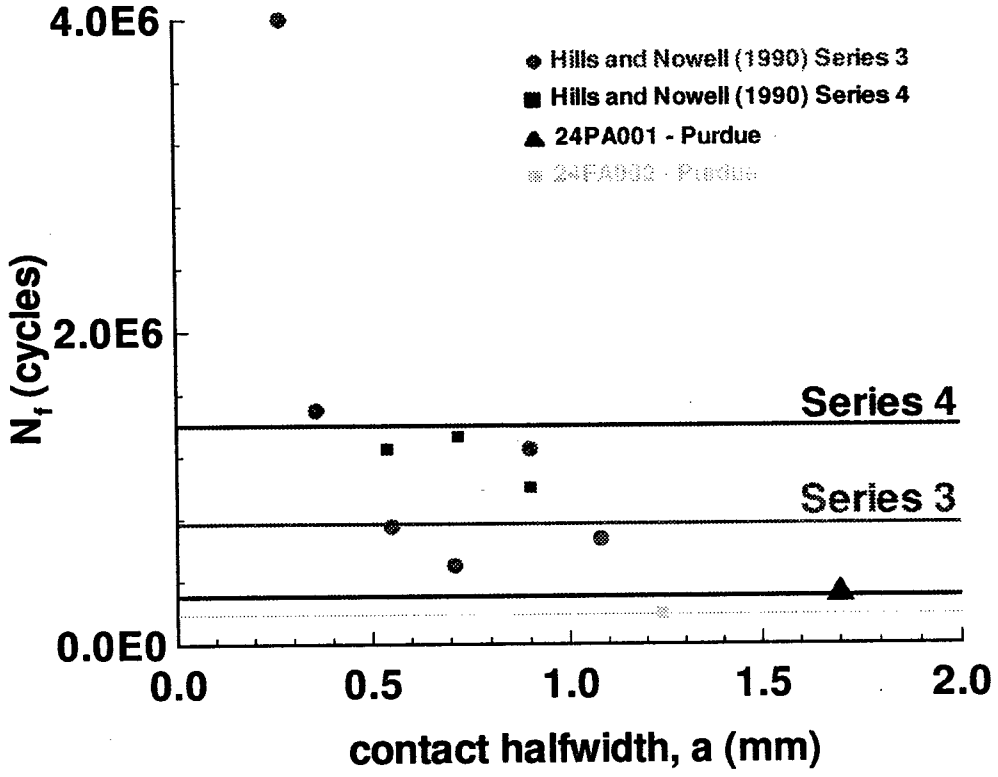

Contact and Crack Nucleation

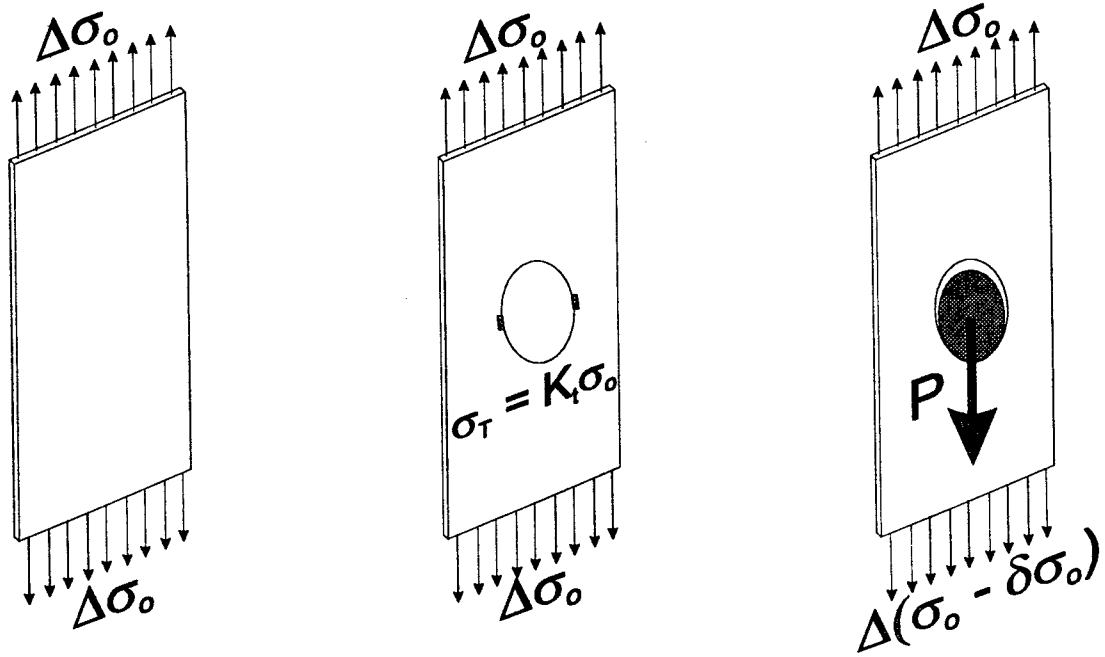

$2N_f > 10^7$ reversals $2N_f \sim 5 \times 10^5$ reversals $2N_f < 5 \times 10^4$ reversals

PURDUE

Conclusions

- Contact stresses play a critical role in nucleating cracks at the rivet/skin interface
- A well-defined fretting fatigue experiment has been designed and verified at Purdue
- A graphically-oriented automated testing and data acquisition system has been developed for application to fretting fatigue experiments
- A full test program is underway to validate further the multiaxial fatigue life predictions for fretting fatigue crack nucleation

Fatigue Crack Growth in Riveted Lap Joints

*Capt. S. Fawaz
Prof. J. Schijve
Faculty of Aerospace Engineering
Delft University of Technology
Kluyverweg 1, 2629 HS Delft, The Netherlands

Abstract

Fatigue life predictions of longitudinal riveted lap joints in a transport aircraft pressurized fuselage has been a growing concern due to recent catastophic failures and the large number of geriatric aircraft in both the military and civil fleets. An adequate prediction methodology has yet to be developed which models representative structure under combined loading. Predictions in coupon specimens under combined tension and bending have proved successful for the part through crack growth; however, the through crack portion remains inadequate. For the asymmetric riveted lap joints tested, obtaining a crack growth history in is difficult since the cracks nucleate on the faying surface of the joint. However, employing a simple marker load spectrum, understanding of the crack growth rate and stress intensity is obtained.

Introduction

The inherent complexity of mechanically fastened joints has restricted development of prediction techniques which accurately model the physical structure in the operational environment. The discussion here will focus on those parameters germane to riveted, single shear, lap joints common to transport aircraft fuselages. Specifically, the sheet material is quite thin, 1.0 - 2.2 mm, rivet diameter 4.8 mm, rivet pitch 20 - 25 mm. Although only joints with two rivet rows have been investigated thus far, the number of rivet rows used in practice ranges from two to five with stiffening elements running the length of the joint inside the fuselage. The primary load condition is pressurization of the fuselage

giving hoop stresses ranging from 70 - 100 MPa[1]. How the hoop stress is distributed through the lap joint is of fundamental importance. The local behavior in the lap joint significantly contributes to the stress state at the fatigue critical locations.

Background

Little experimental evidence is available regarding fatigue crack growth in riveted lap joints. In order to understand the fatigue behavior in the actual built up structure, the behavior in the component parts must first be understood. This research is evolutionary in development beginning with simple sheet specimens containing an open hole and ultimately concluding with component sized stiffened curved panels. The goal of each phase in the program is to understand the effect of geometry and load conditions on the crack growth rate, crack front shape, and stress intensity factor.

In light of the complexity of the riveted lap joint, special consideration is given to employing various experimental techniques to facilitate measurement of the aforementioned parameters of interest. Specifically, crack growth in the lap joint is extremely difficult to monitor in situ since the crack is not visible until penetration of the back surface. Recall, in a single shear lap joint the maximum bending occurs on the mating surface not on the free surface; therefore, the part through crack must grow through the thickness before becoming visible. Also, due to the significant amount of bending, the back surface (free) crack front does not catch up to front surface (faying) as quickly as in fatigue under pure tension. Continuous crack growth monitoring provides information regarding crack growth rate and stress intensity, but crack front shape can only be accurately determined by destructive inspection of the fracture surface. As a result, tests are conducted to obtain all three parameters of interest.

The loading in lap joints is a combination of remote tension (biaxial), remote bending, local bending, rivet load, rivet interference, clamp up, and friction. The magnitude of the bending stress due to the hoop stress ranges from one half to two times the remote tensile stress.[2] The first series of tests, open hole specimens, were designed to investigate the effect of the bending stress on the crack growth behavior. The second series, asymmetric lap joint, targeted the effect of pin loading.

Experimental

A method of reliably introducing cyclical tension and bending in a thin sheet fatigue specimen was developed. Nam et al. had developed such a specimen which was asymmetrically milled from thick plate material.[3] The stress intensity factor depends on thickness and manufacturing process (for example, cold rolling, extruding, forging); therefore, using a milled to thickness specimen introduces another unwanted degree of variability. In addition, to maintain the representation of typical aircraft structure, the thin sheet specimen was chosen.

Several open hole tension and bending specimens were tested. Typical specimen design is shown Figure 1.

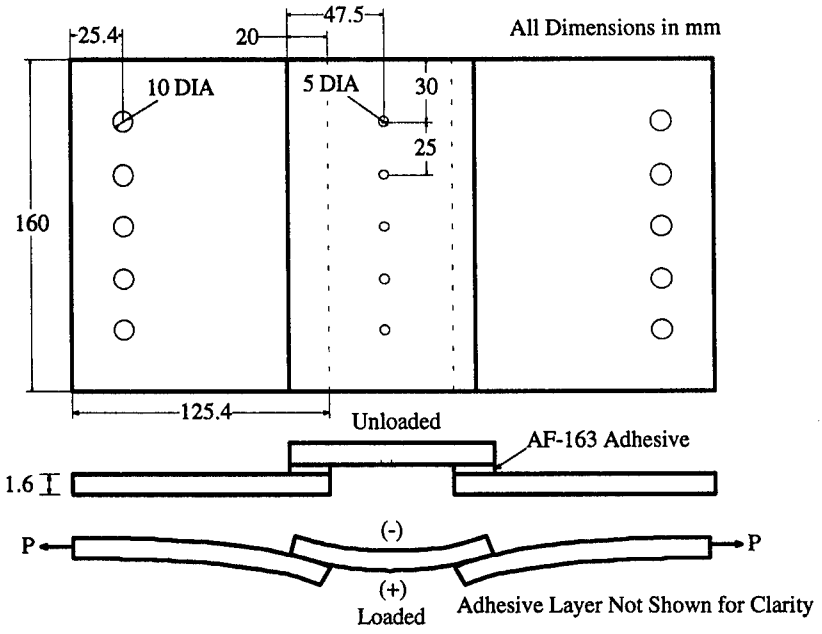

Figure 1. Typical Open Hole Specimen

Due to the eccentricity in the bonded joint, a controllable bending moment is introduced in the specimen as a non linear function of the applied load. The bonded joint allows for smooth load transfer into the specimen unlike that of a mechanically fastened joint. The specimen was designed to obtain a bending factor of 1.0 where the bending factor is defined as

$$k = \frac{\sigma_{bending}}{\sigma_{tension}}$$

Müller has shown the secondary bending in a riveted lap joint can yield bending factors ranging from 0.5 - 2.0. All three test series performed with 2024-T3 clad aluminum designed to have k = 1.0, thickness of 1.6 mm, and hole diameter of 4.8 mm. The width varied to accommodate the number of holes, one, five, or seven, while maintaining a hole pitch of 25 mm. The length was chosen by convenience keeping in mind the effect on the bending moment is negligible if greater than the width. The holes were drilled undersized then reamed to 4.8 mm. Fatigue and static tests were performed on 60 and 250 kN electro servo hydraulic load frames For each specimen type, a strain survey was completed to determine the stress field in the area of interest in addition to verifying the applicability of the analytical solution for predicting the bending moment. Each of the three specimens had a unique purpose even though they were fundamentally common. The five hole specimen was tested first in order to determine the utility of the specimen design in creating the desire bending moment. In addition, crack initiation, crack growth rate, and fatigue life were obtained. Next, the single hole specimen was intended to negate any crack interaction which may be present in the multi-hole specimens. Lastly, the seven hole specimen was used to determine the effect of secondary bending on part through and through crack development from crack detection to failure.

An asymmetric single shear riveted lap joint was also investigated and is shown in Figure 2. The asymmetry negates the difficulty in calculating the load

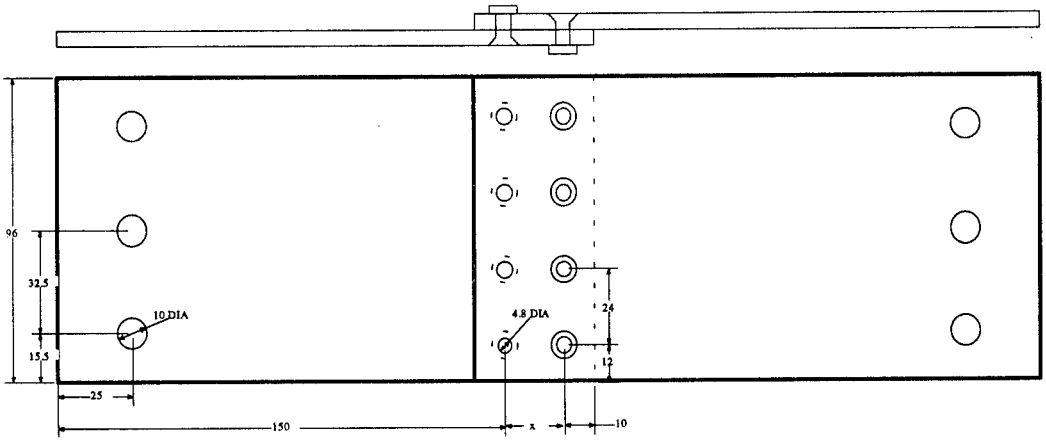

Figure 2. Asymmetric Riveted Lap Joint

transfer, but still allows for observation of the effect of the rivet load on fatigue.

The lap joint test is the first step towards built up structure offering the benefits of realism and complexity of variability. Much of this specimen design was effected by Müller's work with respect to specimen size and rivet squeeze force. To avoid the edge effect seen in coupon size lap joints, a relatively narrow width was chosen. In the overlap region, the thickness and therefore stiffness of the specimen is greater offering a higher resistance to poisson contraction with respect to the single sheet areas. The edge effect is premature cracking at the outer rivets due to the higher rivet loads caused by the poisson constraint. Müller the force with which the rivet is driven can have a significant effect on load transmission, crack nucleation, and fatigue life[2]. A low rivet squeeze force was chosen in an attempt to isolate load transmission by the rivet only and not by friction and clamp up forces which are present at higher squeeze forces. In addition, less hole expansion thus less residual stresses around the hole are present which effect small crack growth behavior.

In situ crack detection and growth was monitored using traveling optical microscopes ranging in magnification from 20 - 80X. Since cracks nucleating and growing in lap joints do so on the faying, hidden, surface; the cracks are not visible until they have penetrated the back free surface. The gel electrode method was also attempted but due to the high stress levels was not successful. A viable in situ crack monitoring techniques for small crack has yet to be developed.

Discussion and Results

By isolating each contributing factor to crack growth in riveted lap joints, a better understanding of the the individual factors can be obtained. Tension and bending being the predominant loading were investigated first. As seen in Figure 3, the analytical model predicts both the tensile and bending behavior of the open hole specimens. This model was used to design all subsequent specimens; however, each new design was validated with a strain survey in the area of interest.

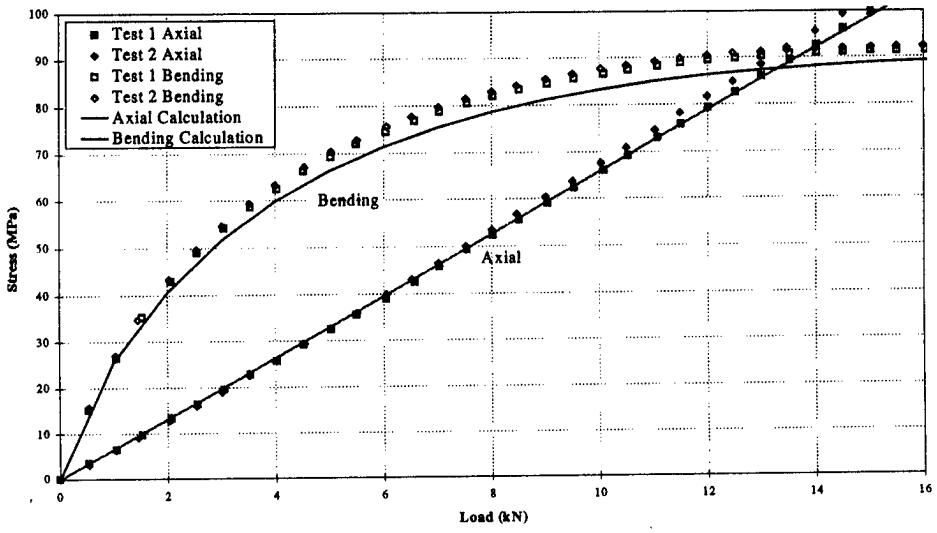

Figure 3. 1-Hole, Open Hole Specimen Stress Behavior and Prediction

The effect of secondary bending has a large effect on the fatigue performance as seen in Figure 4.

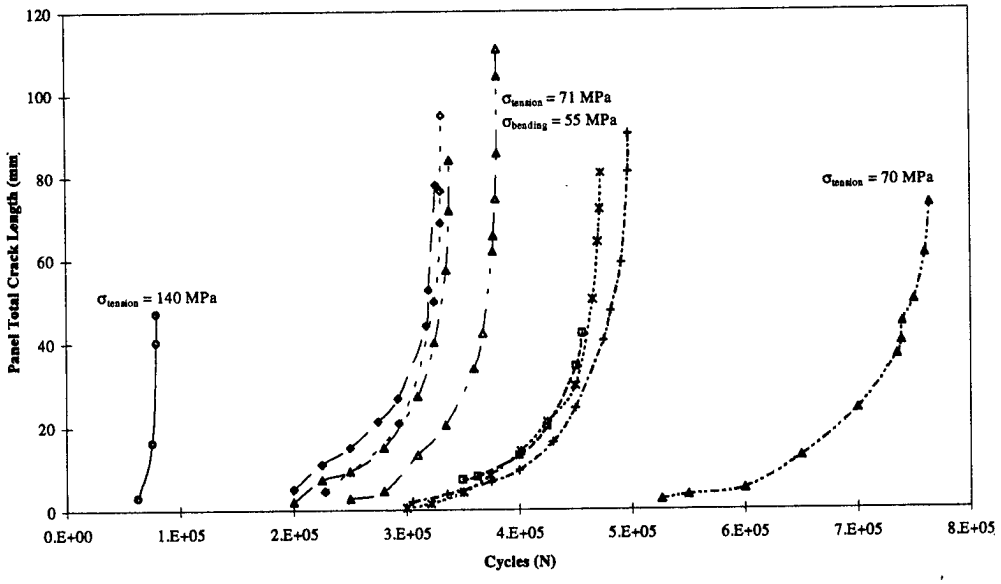

Figure 4. Effect of Secondary Bending on Fatigue Life of 5-Hole Open Hole Specimen

Predictions of the fatigue crack growth for the single and seven hole specimens have been made for the part through crack using the Newman/Raju finite element stress intensity solution.[4] Figure 5 depicts five separate cracks from one 7-hole specimen that was statically overloaded prior to fatigue failure. The crack growth behavior is strongly influenced by the flaw shape; therefore, the small errors in the predictions can be attributed to a poor initial flaw shape assumption. In a pure tensile fatigue test, the crack depth grows faster than the crack length on the free

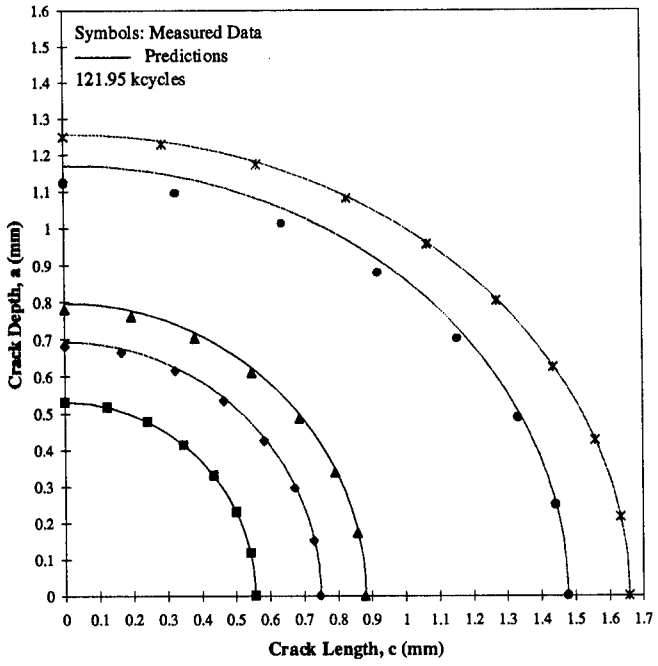

Figure 5. Part Through Crack Predictions for 7-Hole Open Hole Specimen

surface due to the higher stress intensity in the depth direction. However, with bending present, the stress at the free surface is higher than at the crack depth which appears to result a similar crack driving force at both locations. As might be expected, as the bending factor changes so does the aspect ratio; increasing k leads to shallow cracks, decreasing k deep cracks. The aspect ratio for all cracks measured ranged from 0.75 - 1.1 with a mean value of approximately 0.95.

Predicting the through the thickness cracks has not resulted in similar success as that of the part through crack. The NASGRO TC09 solution was used for all through cracks and yielded poor results. For instance, the single open hole specimen results are shown in Figure 6[5,6,7,8].

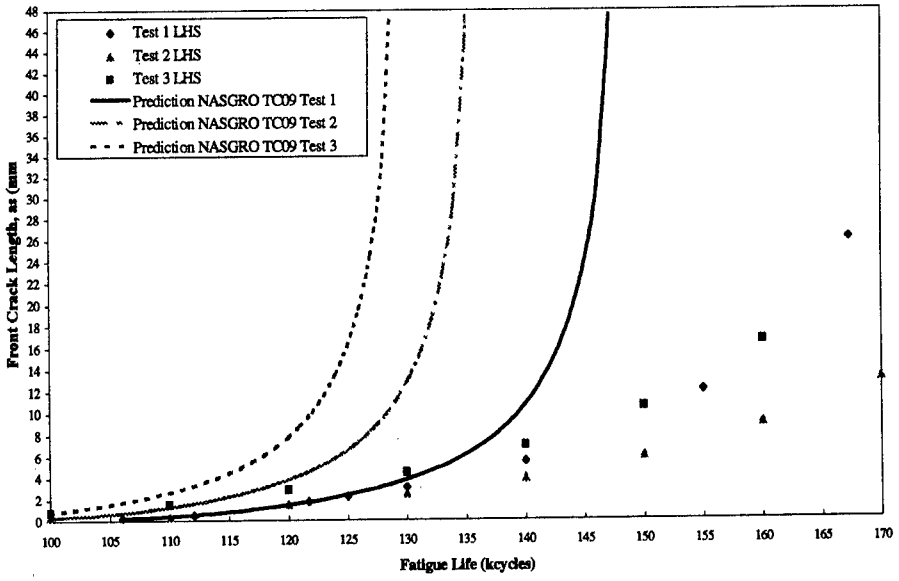

Figure 6. NASGRO TC09 Predictions for 1-Hole Open Hole Specimen

The poor performance of this solution for the given test data, in addition to the asymmetric lap joint data, has three possible sources. With respect to the bending component, either the bending stress in the area of interest in incorrectly characterized, or the boundary correction factor equation is inadequate. This solution has been shown to satisfactorily predict fatigue life for tension only fatigue tests. The crack front shapes of the through crack, as shown in Figure 7, are oblique.

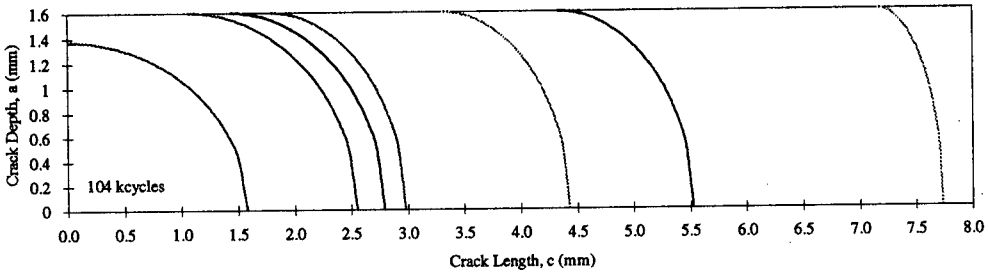

Figure 7. Oblique Crack Front in 7-Hole Open Hole Specimen

Once the part through crack penetrates the back surface, the back surface crack tip does not "catch up" to the front surface crack tip as it does under pure tension. The crack front remains oblique until the onset of instability. This solution does

not account for a non straight crack front. The cause of the error in predicting the bending behavior has yet to be determined, but all predictions under estimate the fatigue life meaning the stress intensity is being over estimated. Three dimensional finite element analysis is being used to develop the stress intensity factor solutions for an oblique through crack.

The fatigue tests of the asymmetric lap joint have shown the dependence of the crack nucleation site on the rivet squeeze force. For the NAS 1097AD6-6 rivet, a squeeze force of 10 kN, resulting in a ratio of the driven head diameter to nominal diameter of 1.1, yields cracking at the net section. Increasing the rivet squeeze force shifts the nucleation site above the hole. Müller found that with a diameter ratio of 1.75, the cracks do not nucleate at the hole, but above the hole where the local bending is highest[2]. Due to the difficulties in measuring the penetrated crack length, a crack length versus cycles curve could not be reliably constructed. Crack measurement is hindered by the plasticity around the crack and the distortion of the area surrounding the crack due to the compressive stress on the free surface during a majority of the load cycle.

An alternative to visually measuring the cracks during the test is to add a marker load cycle to the otherwise constant amplitude spectrum to mark the fracture surface. By examining the fracture surface with a scanning electron microscope, the crack length versus cycles can be deduced. The clearest marker bands were visible with a fatigue cycle stress ratio, R, of 0.5 and a marker cycle with R = 0.0. The fatigue cycle stress ratio was systematically decreased to determine the minimum value which would produce reliably countable marker bands. Ideally, the test stress level should mirror the operational environment stress level which yields an R = 0 for the ground-air-ground cycle; however, for marker bands the minimum R is 0.2. The spectrum used 50 fatigue cycles followed by only one marker cycle. Marker bands were visible for cracks as small as 0.03 mm. As can be seen from Figure 8 the crack growth rate determined from fractography is consistent with that from visual observation.

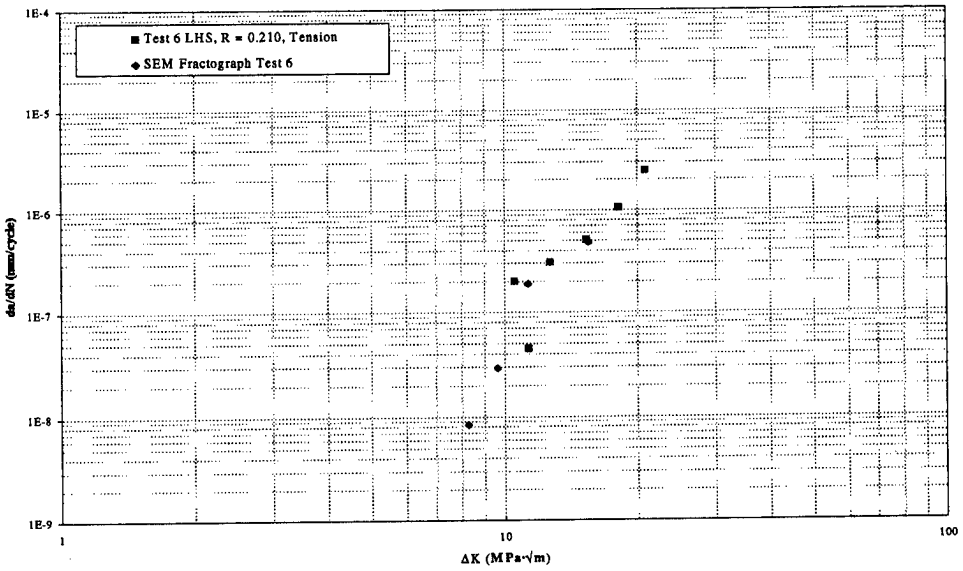

Figure 8. CCT Specimen with Marker Load

The introduction of the marker load in the fatigue tests of the asymmetric lap joints may give insight to the magnitude of the stress intensity for small cracks around the rivet hole. The marker bands tend to disappear at higher crack growth rates, therefore, constructing a crack length versus cycles history for the complete fatigue life doesn't not appear possible.

Conclusions and Future Work

Predictions for the open hole specimens loaded under remote tension and bending are excellent. Once the crack penetrates the back surface the current methodology is lacking. Work is currently underway to develop stress intensity factor equations for a through crack with the an oblique front under general combined loading. The marker load spectrum offers potential insight to the fatigue crack growth in rivet lap joints and will be explored further. As prediction methods for the simple structure are validated, the realism of the structure will be increased in an attempt to predict fatigue crack growth in a longitudinal riveted lap joint of a pressurized fuselage in a transport aircraft.

References

[1] Swift, T., "Damage Tolerance in Pressurized Fuselages," 11th Plantema Memorial Lecture, Proceedings 14th International Committee on Aeronautical Fatigue Symposium, Ottawa, Canada, 1987.

[2] Müller, Richard Paul Gerhard, "An Experimental and Analytical Investigation on the Fatigue Behaviour of Fuselage Riveted Lap Joints, The Significance of the Rivet Squeeze Force, and a Comparison of 2024-T3 and Glare 3," Ph.D. Dissertation, Delft University of Technology, Faculty of Aerospace Engineering, Delft, The Netherlands, November 1995.

[3] Nam, K. W., K. Ando, N. Ogura, and K. Matui, "Fatigue Life and Penetration Behaviour of a Surface-Cracked Plate Under Combined Tension and Bending," *Fatigue and Fracture of Engineering Materials and Structures*, Vol. 17. No. 8, 1994, pp. 873-882.

[4] Newman Jr., J. C. and I. S. Raju, "Stress Intensity Factor Equations for Cracks in Three-Dimensional Finite Bodies," Fracture Mechanics Fourteenth Symposium, Vol. I: Theory and Analysis, ASTM STP 791, J. C. Lewis and G. Sines, Eds. pp. I238-I265, 1983.

[5] Roberts, R. and T. Rich, "Stress Intensity Factors for Plate Bending," Transactions of ASME, *Journal of Applied Mechanics*, Vol. 34, No. 3, September 1967, pp. 777-779.

[6] Roberts, Richard, and John J. Kibler, "Some Aspects of Fatigue Crack Propagation," *Engineering Fracture Mechanics*, Vol. 2., 1971, pp. 243-260.

[7] Hsu, T.M. and J.W. Markham, "Interaction Effects of Multiple Cracks," *AIAA Journal*, Vol. 15, No. 3, March 1977.

[8] Shivakumar, V. and R. G. Forman, "Green's Function for a Crack Emanating from a Circular Hole in an Infinite Sheet," *International Journal of Fracture*, Vol. 16, No. 4, August 1980, pp. 305-316.

Analytical Methodology to Predict the Onset of Widespread Fatigue Damage in Airframe Structure

Dr. Charles E. Harris

Dr. James C. Newman, Jr.

Dr. James H. Starnes, Jr.

and

Dr. Robert S. Piascik

presented at the

1995 USAF Structural Integrity Program Conference

San Antonio, TX

November 28-30, 1995

Langley Research Center

Research and Technology Group

FAA-NASA-USAF COOPERATIVE PROGRAM IN AGING AIRCRAFT RESEARCH

NAARP

Technical Center
Atlantic City, NJ

NASIP

Langley Research Center
Hampton, VA

AFAASP

Wright Laboratory
Wright-Patterson AFB, OH

NASA AIRFRAME STRUCTURAL INTEGRITY PROGRAM

Goal: Economic life extension through continued airworthiness assurance

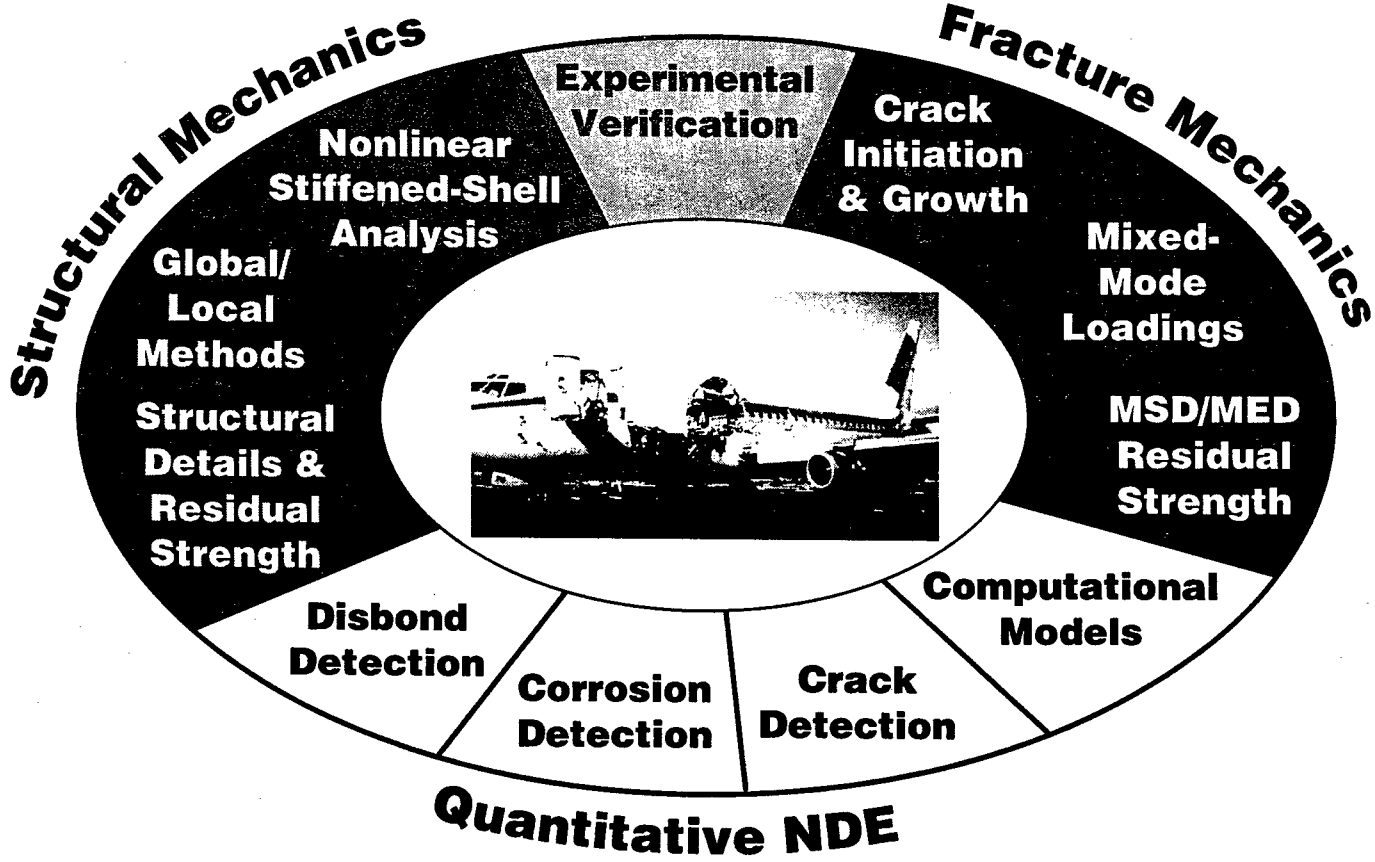

NASIP COMPUTER CODES

Capability \ Codes	FADD*	FRANC2D	ZIP2D	FASTRAN II	STAGS	FRANC3D/STAGS	FRANC3D*	ZIP3D	NASGRO*
Plane Stress/Strain	X	X	X	X				X	
Axisymmetry		X			X			X	
Plate Bending	UD	UD			X	X			X
Thin Shell					X	X			
3D Solid	UD				UD		X	X	
Straight Cracks	X	X	X	X	X	X	X	X	X
Curving (nonplaner) Cracks	X	X				X	X		UD
Layered Structure		UD			X	X		X	
Contact		X			X	X		X	
Interface		X			UD				
Elasto-Plastic		UD	X		X	X		X	
Crack Closure/Variable Amplitude			X	X				X	UD
Anisotropy	UD	X			X	X			
Residual Strength Analysis		UD	X		UD	UD		X	
Graphical Interface	X	X				X	X		
Life Prediction				X					X
Mesh Generation	X	X				X	X		
K vs. A History	X	X			X	X	X		

*FADD is also implemented into NASGRO and FRANC3D
UD -- under development

NASIP COMPUTER CODE/CHANGES

Analytical Methodology to Predict the Onset of Widespread Fatigue Damage (WFD)

I. Crack Initiation

NASA Deliverables: small crack methodology and FASTRAN II

II. Fatigue Crack Growth

NASA Deliverables: NASGRO w/ FADD, and FRANC2D

III. Residual Strength

NASA Deliverables: FRANC3D / STAGS, CTOA fracture criterion

Analytical Methodology to Predict the Onset of Widespread Fatigue Damage (WFD)

I. Crack Initiation

- Equivalent initial flaw sizes (material defects, fretting, manufacturing)
- Approximations for interference fit and clamp-up stresses
- Stress analysis with local details of the uncracked geometry

- Verified by coupon data and structural tear-down fractography data

NASA Deliverables: small crack methodology and FASTRAN II

FRACTOGRAPHY OF WSFD IN STRUCTURAL FATIGUE TEST ARTICLE

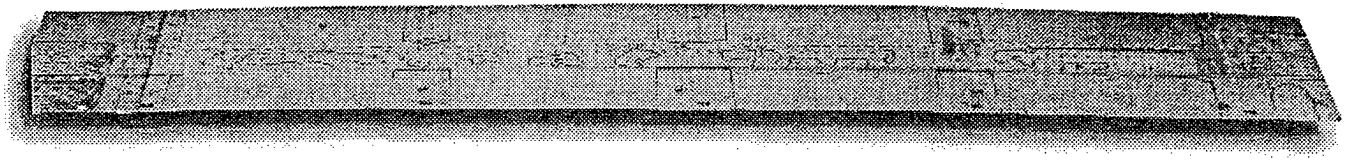

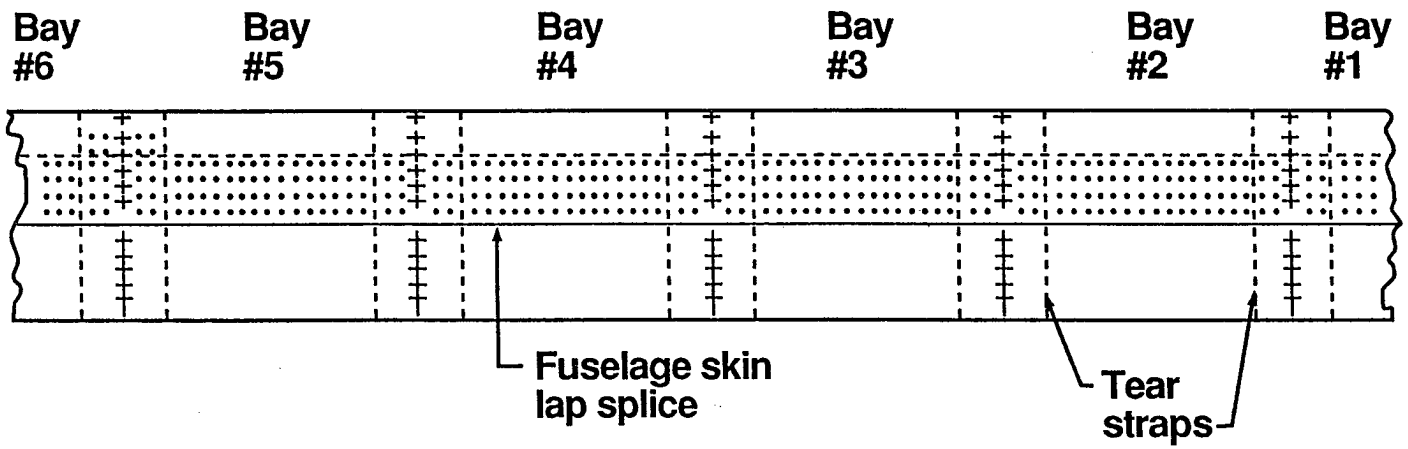

WSFD Panel Bay #1

1 J 4

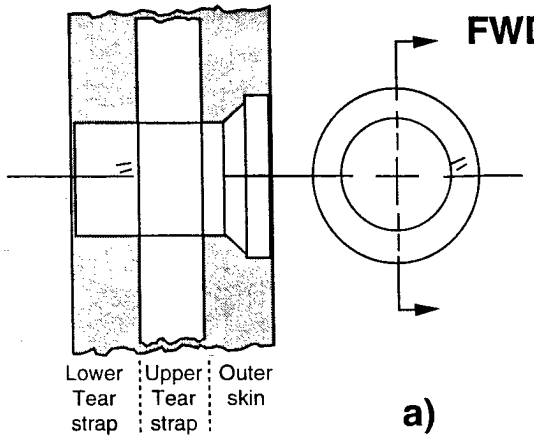

a)

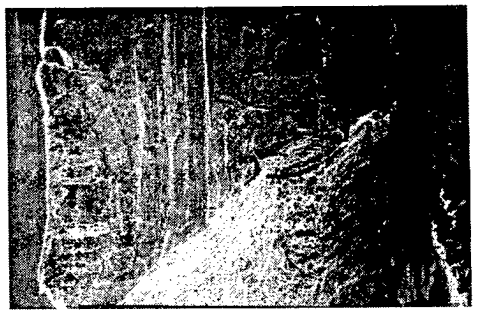

250 µm

b)

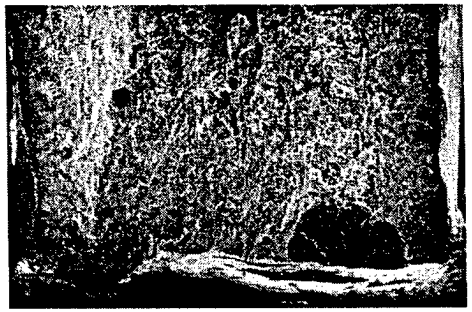

250 µm

c)

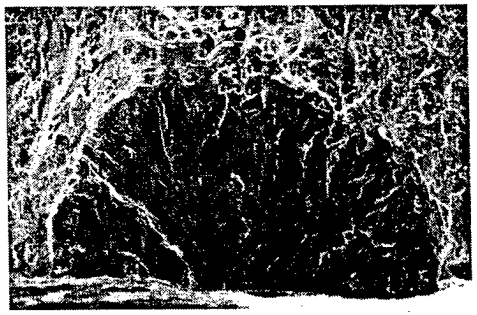

100 µm

d)

FASTRAN II

Closure Model for Fatigue Crack Growth

(Available through COSMIC and currently being used by industry)

- Plasticity-induced crack closure
- Modified Dugdale plasticity model
- Closed-form SIF's and COD equations
  (16 common crack configurations)
- Developed for spectrum fatigue analysis
  (TWIST, Mini-TWIST, FALSTAFF, FELIX, and Space Shuttle)
- Runs on Mainframe, workstations, and PC's

COMPARISON OF TEST AND PREDICTED S–N BEHAVIOR

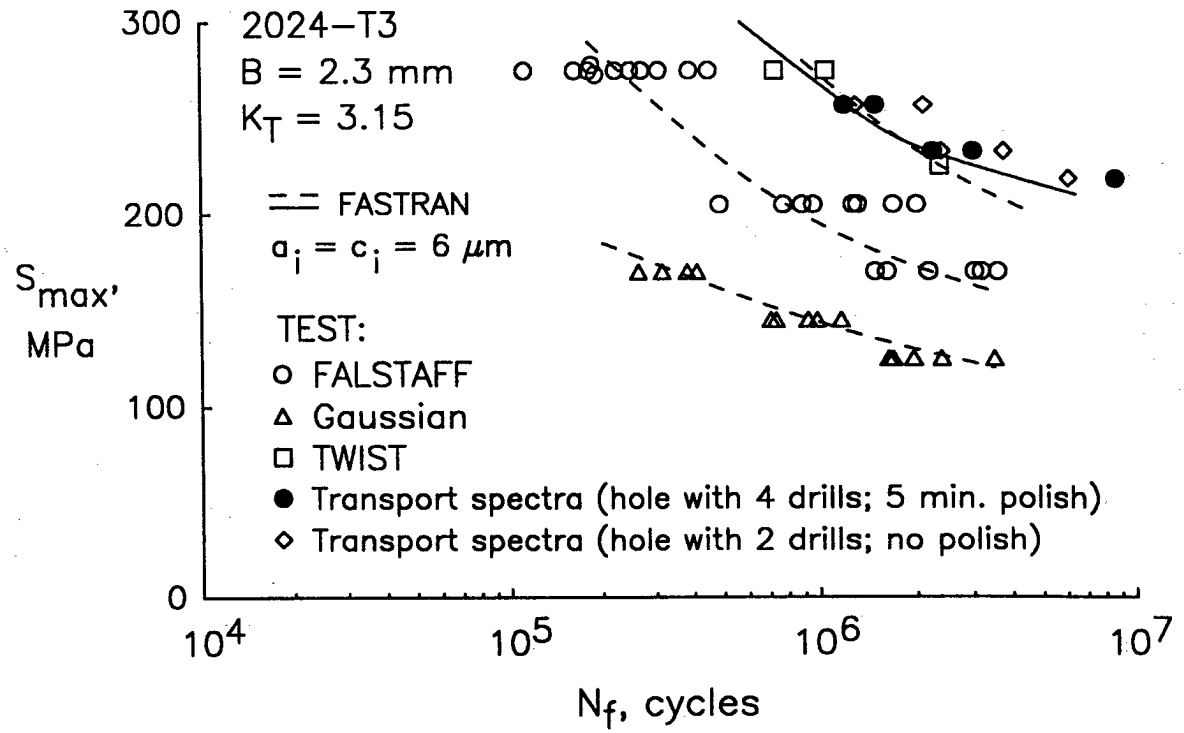

Analytical Methodology to Predict the Onset of Widespread Fatigue Damage (WFD)

I. Crack Initiation

- Equivalent initial flaw sizes (material defects, fretting, manufacturing)
- Approximations for interference fit and clamp-up stresses
- Stress analysis with local details of the uncracked geometry

II. Fatigue Crack Growth

- SIF's for part-through and through-cracks under combined loads
- Stress analysis of built-up structure with fatigue cracks modelled
- Crack closure mechanics for cycle-by-cycle crack growth
- Global-local analysis to update SIF solutions for the growing crack

- Verified by coupon, flat panel, and stiffened panel test data

NASA Deliverables: NASGRO w/ FADD, and FRANC2D

FADD

Fracture Analysis by Distributed Dislocations

(Developed at the University of Texas and NASA Langley)

Current Capabilities:

- o Elastic stress analysis of finite or infinite domains (2D)
- o Single or multiple, straight or non-straight cracks
- o Traction, displacement, or mixed boundary conditions
- o Multiple body configurations
- o Determines stress-intensity factor(s)
- o General stress analysis code for non-crack configurations

Capabilities under development:

- o Graphical interface to input configuration and boundary conditions (Workstation and PC versions)

Hardware requirements:

- o Computer mainframes
- o Unix workstations with X-windows graphics
- o PC's with microsoft windows graphics

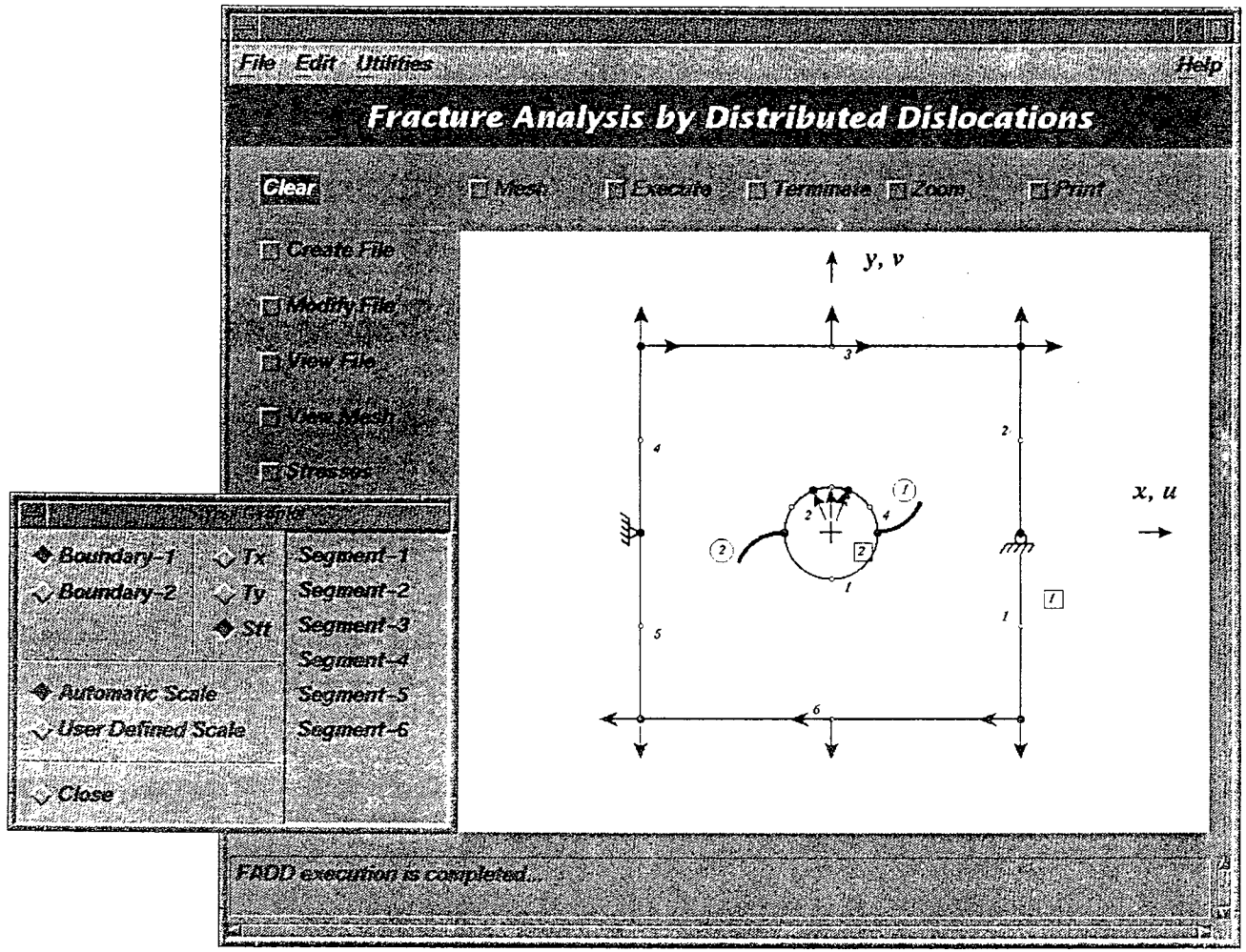
File Edit Utilities
Help
Fracture Analysis by Distributed Dislocations
Clear
Mesh
Execute
Terminate
Zoom
Print
Create File
Modify File
View File
View Mesh
Stresses
Boundary-1
Boundary-2
Tx
Ty
Stt
Segment-1
Segment-2
Segment-3
Segment-4
Segment-5
Segment-6
Automatic Scale
User Defined Scale
Close
y, v
x, u
FADD execution is completed...

FRANC2D (FRacture ANalysis Code, 2 Dimensions)

(Developed at Cornell University and Kansas State University and funded by the NASA ASIP)

Current Capabilities:

- Menu driven and interactive
- Linear-elastic finite element-based fracture mechanics of 2-D plane problems
- Automatic adaptive remeshing and mesh refinement for simulating crack growth
- Layered capability for modelling thin-sheet built-up structures
- Gap elements for modelling interference fit, friction, and bearing contact
- Integral postprocessing and visualization capabilities

Capability Under Development:

- Elasto-plastic material behavior and fracture criteria

Hardware Requirements: UNIX workstations with X windows graphics

- DEC DecStation 3000 & 5000 series
- IBM RS/6000 series
- Hewlitt-Packard 9000/700 series
- SUN Sparc stations
- Silicon Graphics, most models

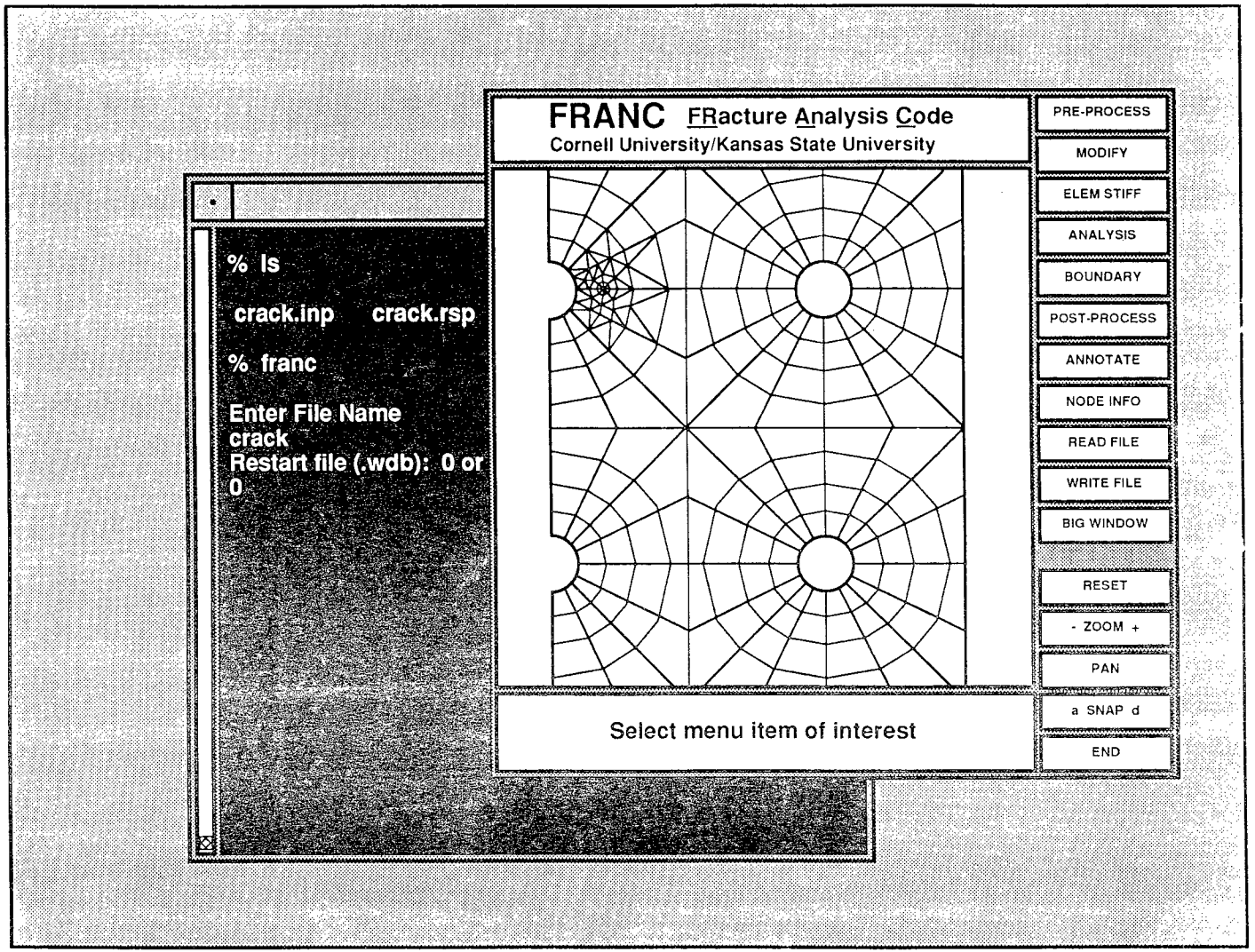
FRANC FRacture Analysis Code
Cornell University/Kansas State University
% ls
crack.inp crack.rsp
% franc
Enter File Name
crack
Restart file (.wdb): 0 or
0
PRE-PROCESS
MODIFY
ELEM STIFF
ANALYSIS
BOUNDARY
POST-PROCESS
ANNOTATE
NODE INFO
READ FILE
WRITE FILE
BIG WINDOW
RESET
- ZOOM +
PAN
a SNAP d
END
Select menu item of interest

FRANC2D STRESS ANALYSIS

EFFECT OF INTERFERENCE ON DELTA-K

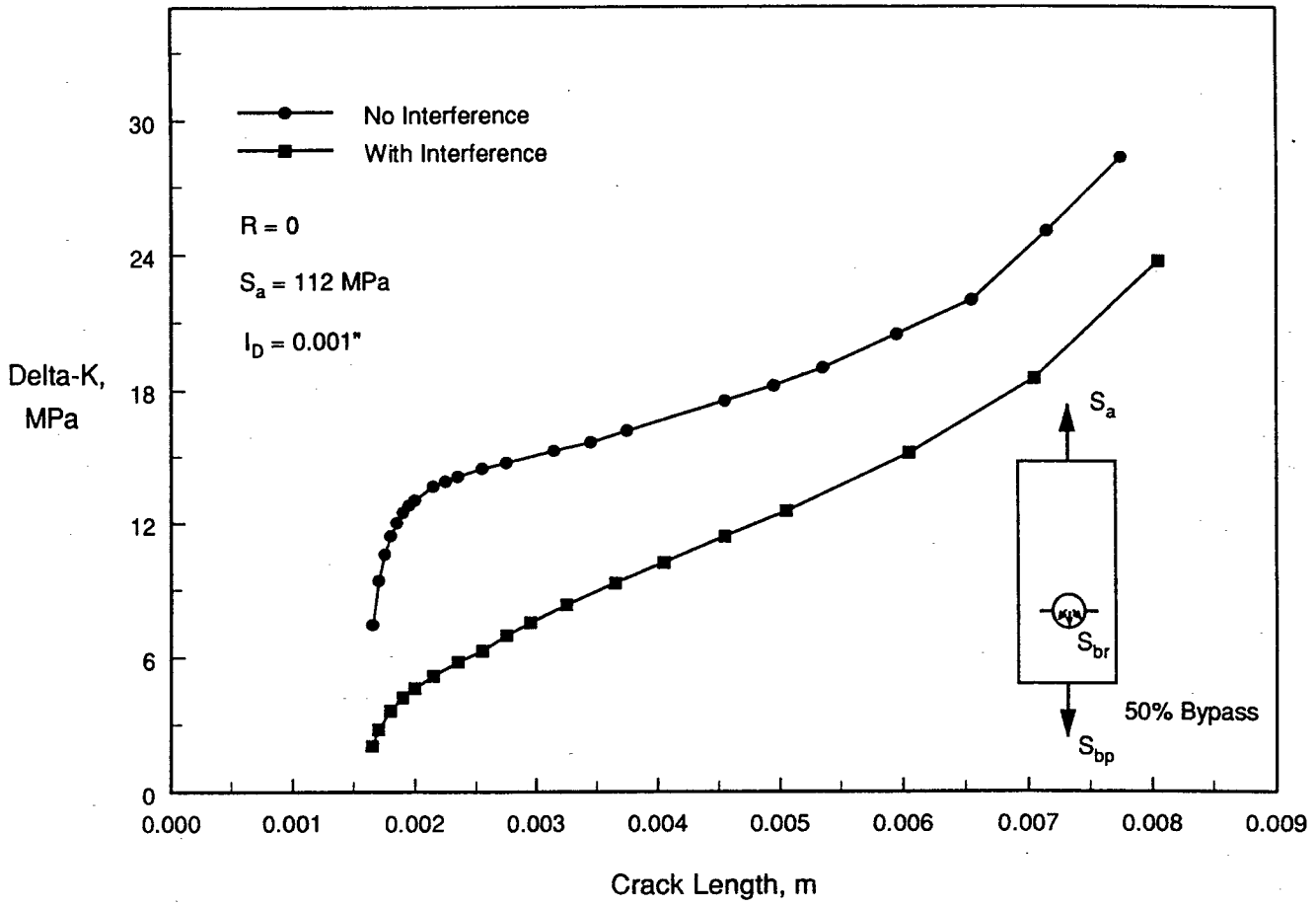

Analytical Methodology to Predict the Onset of Widespread Fatigue Damage (WFD)

I. Crack Initiation

- Equivalent initial flaw sizes (material defects, fretting, manufacturing)
- Approximations for interference fit and clamp-up stresses
- Stress analysis with local details of the uncracked geometry

II. Fatigue Crack Growth

- SIF's for part-through and through-cracks under combined loads
- Stress analysis of built-up structure with fatigue cracks modelled
- Crack closure mechanics for cycle-by-cycle crack growth
- Global-local analysis to update SIF solutions for the growing crack

III. Residual Strength

- Criteria for stable tearing and unstable crack growth (CTOA, T*, and R-curve)
- Widespread plasticity in nonlinear FEA code for analysis of built-up structure
- Global and local structural details, fastener flexibility, and combined load effects
- Uncracked element yielding (von Mises) and failure criterion (cr. effective strain)

- Verified by structural tests in LARC Pressure Box and Combined Loads D-box

NASA Deliverables: FRANC3D / STAGS, CTOA fracture criterion

FRANC3D / STAGS Residual Strength Analysis Methodology

- FRANC3D (FRacture ANalysis Code, 3 Dimensions) Code
  Software developed by Cornell University
- STAGS (STructural Analysis of General Shells) Code
  Software developed by Lockheed
- FRANC3D / STAGS Interface Code
  Software developed by Cornell University and Lockheed
- Residual Strength Analysis Methodology
  Methodology developed by NASA Langley Research Center
- Unique capabilities for fatigue and fracture mechanics analysis of structures
  - Material and geometric nonlinear structural analysis
  - Automatic mesh generation and mesh refinement
  - Automatic adaptive remeshing for non-self-similar crack growth
  - Crack growth with load relaxation to maintain nonlinear equilibrium
  - Global/local hierarchical modeling strategies
  - Stable tearing and fracture criteria

FRANC3D / STAGS (turning crack, mesh mapping)

Mesh 1: 2.0 in. initial crack

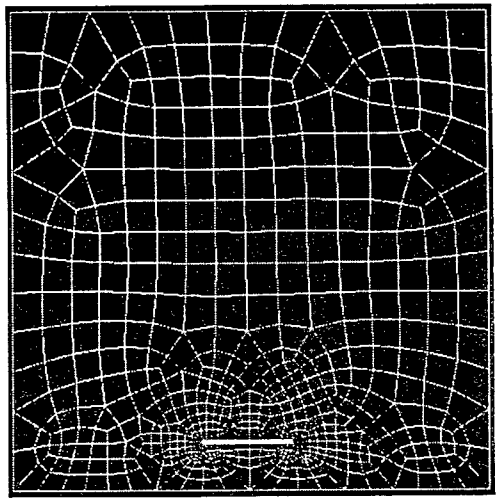

Mesh 4: Extend crack to 5.0 in., 20 deg. change in direction

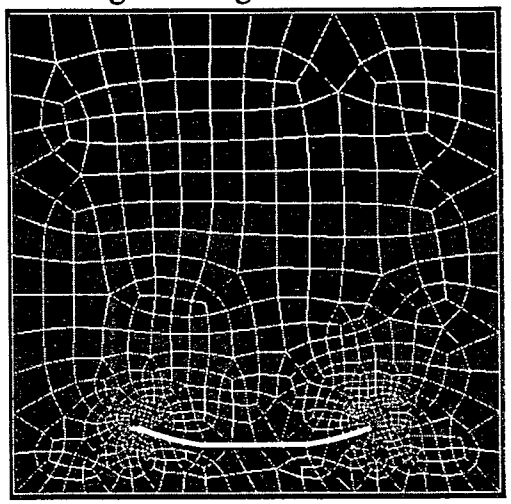

Curvilinear Crack Analysis Using FRANC3D / STAGS

- Hierarchical models: internal pressure, bending, vertical shear
- local 2-bay by 2-bay model, edge displacements from 6-bay by 6-bay model

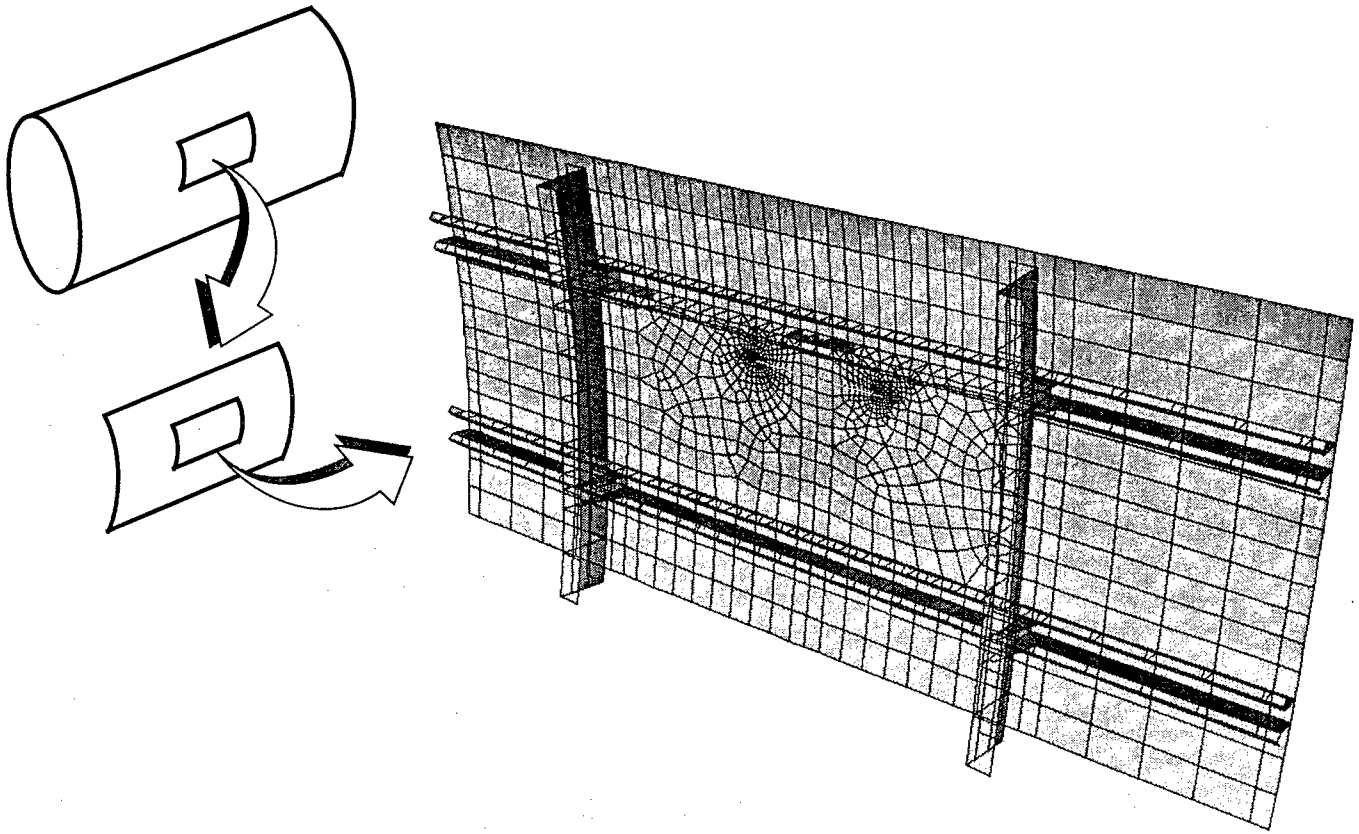

Curvilinear Crack Extension: Internal Pressure + Shear

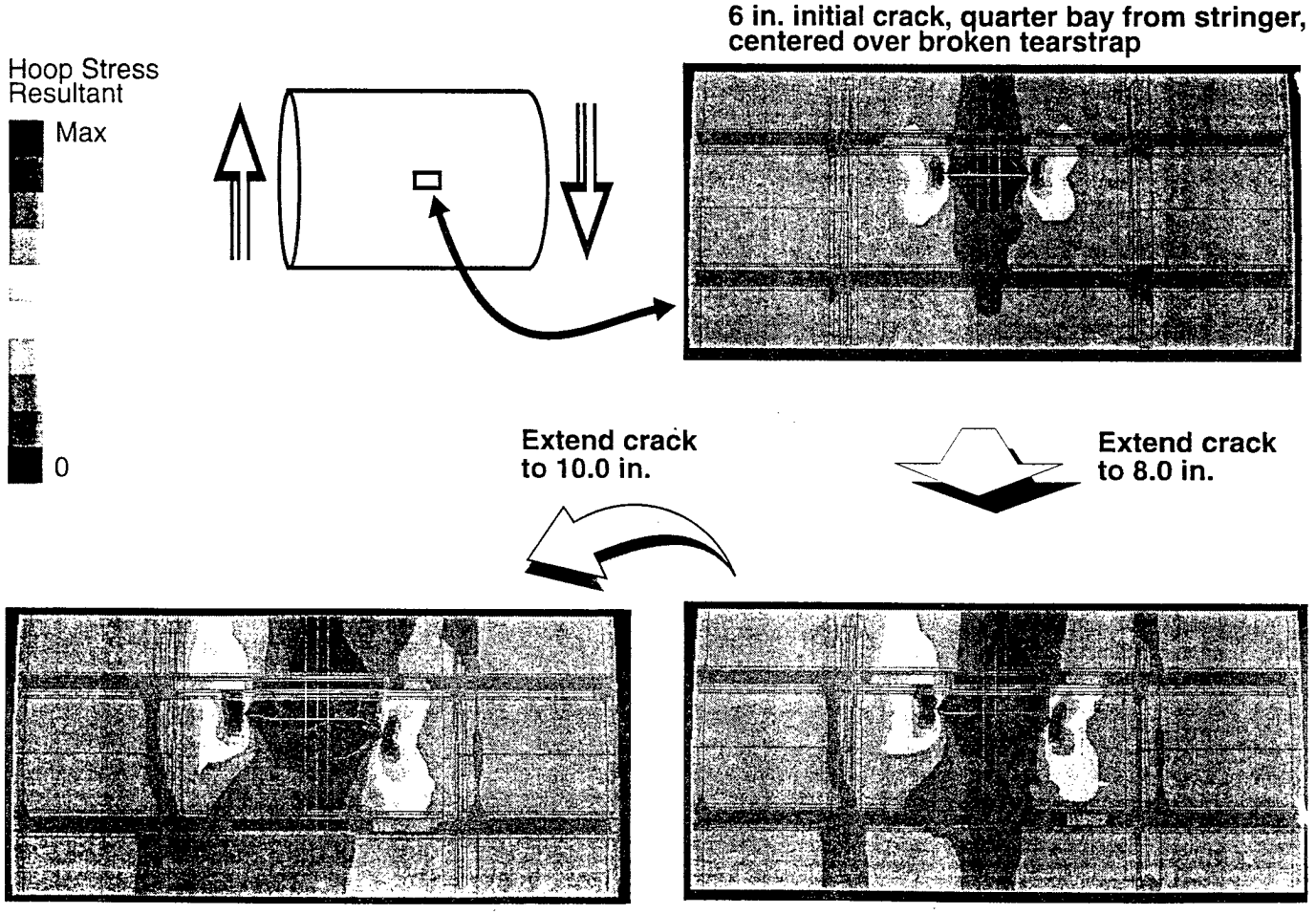

CRITICAL CRACK-TIP-OPENING ANGLE (CTOA) FRACTURE CRITERION

Experimental Verification Program

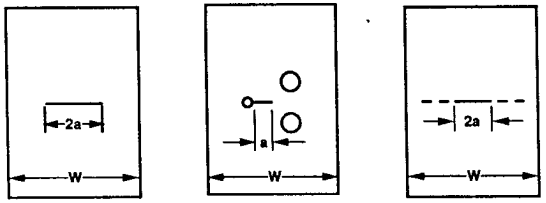

Center Crack 3-Hole MSD

Video Image of CTOA Measurement

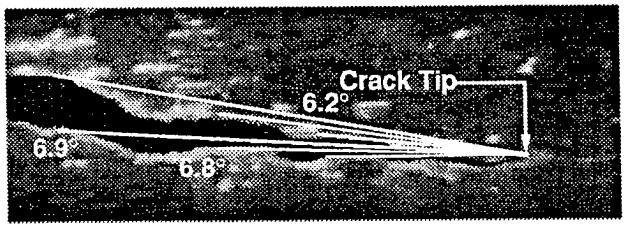

Measured CTOA as a Function of Crack Growth

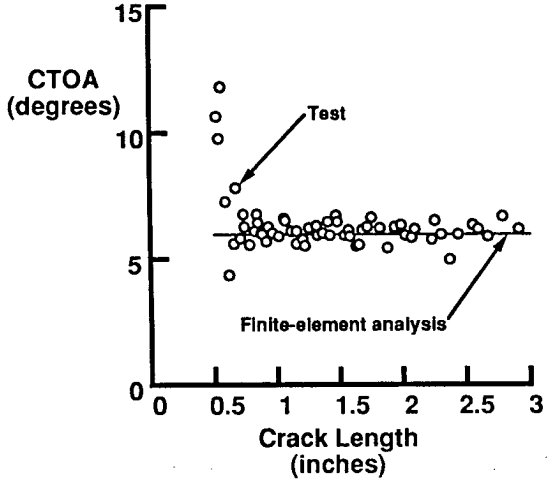

Predicted Stable Crack Growth

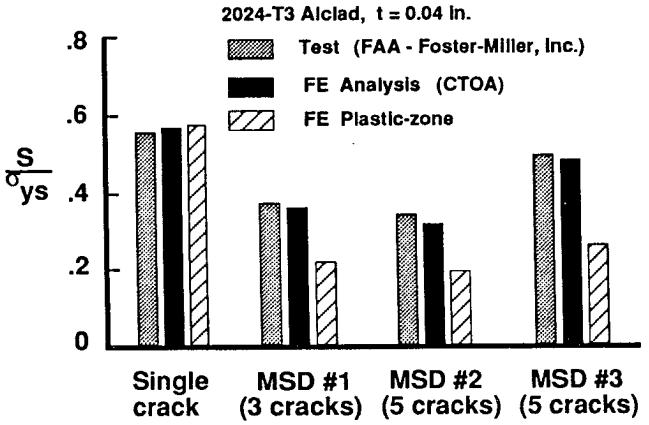

COMPARISON OF MEASURED AND PREDICTED FAILURE LOADS ON NIST MSD FRACTURE TESTS

Panel	Number of Sawcuts	Test Load kips	Predicted Load kips	Percent Error
MSD #1	1	77.0	76.8 (a)	-0.3
MSD #2	1	96.3	96.0	-0.3
MSD #3	1	64.9	65.6	+1
MSD #4	7	69.1	67.0	-3
MSD #5	7	91.2	80.9	-11
MSD #7	11	48.2	49.8	+3
MSD #8	21	47.5	50.6	+6
MSD #9	21	79.2	74.8	-6
MSD #10 (b)	11	52.2	49.8	-5

(a) Fitted to test (CTOA = 3.4 deg.; δ_i = 0.0086 in.).

(b) MSD #10 was repeat of MSD #7.

PREDICTION METHODOLOGY VERIFICATION PROGRAM

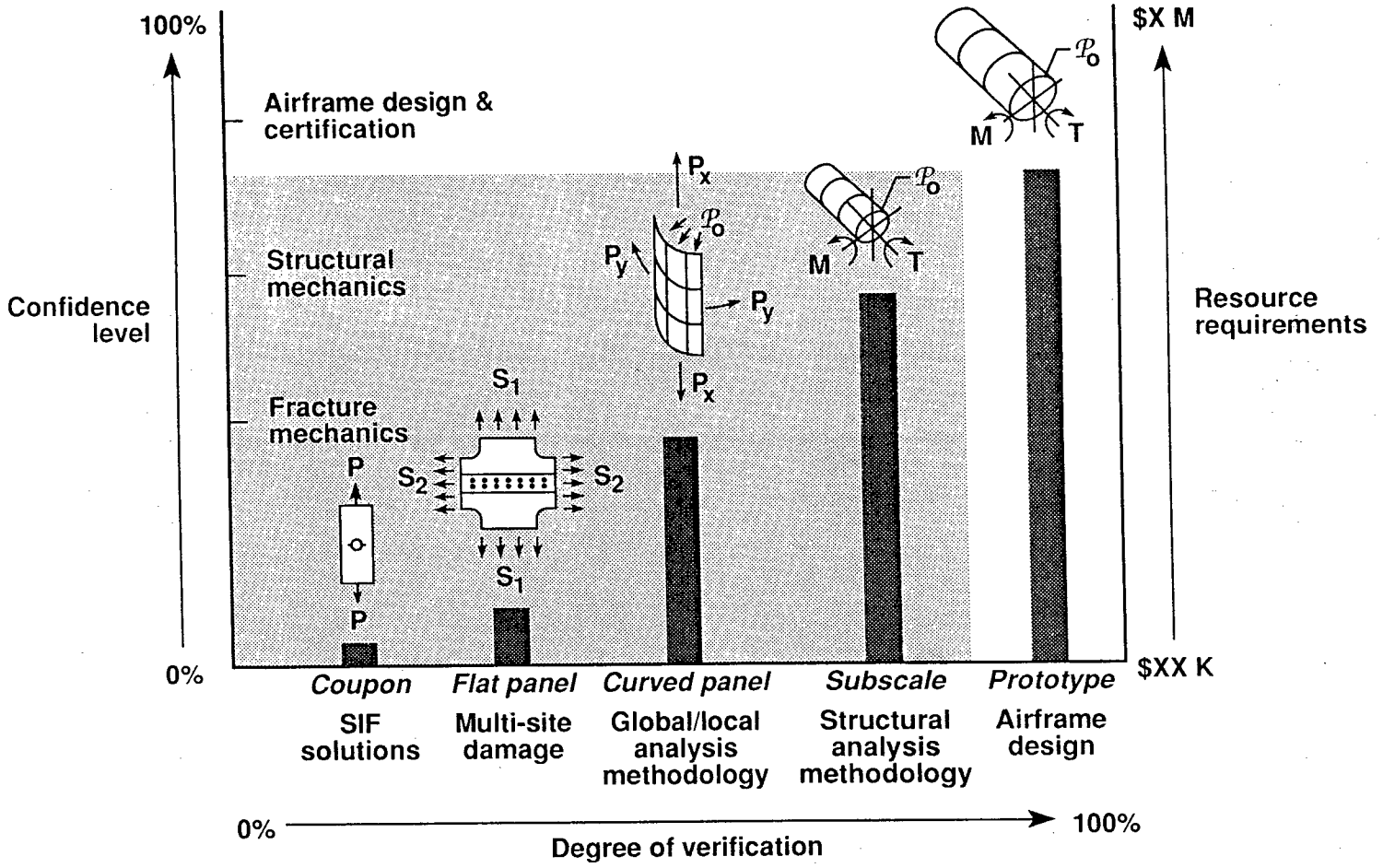

Concluding Remarks

- The methodology to predict the onset of widespread fatigue damage in aircraft structure is complex and involves the determination of:
  - crack initiation,
  - fatigue crack growth, and
  - residual strength.

- The computational tools being developed in the NASA research program are currently being evaluated by the aerospace industry.

- The keys to transferring the technology to industry include experimental verification, independent evaluation, adaptability, and user friendliness.

SESSION III

LOADS

Chairman: *M. McMahon*, NAVAIR

Landing Parameter Surveys of Transport Aircraft

Mr. Richard P. Micklos
Naval Air Warfare Center, Aircraft Division, Warminster
P.O. Box 5152, Warminster, Pa. 18974-0591

Background:

The Naval Air Warfare Center, Aircraft Division, Warminster PA., developed the Naval Aircraft Approach and Landing Data Acquisition System (NAALDAS) to collected landing parameter data for carrier landings. As part of an interagency agreement with the Federal Aviation Administration Technical Center, we have successfully modified NAALDAS to measure landing parameters of commercial jet transport aircraft. This report will describe some of the results and preliminary findings from these surveys.

Three surveys of jet transport aircraft have been performed. The first FAA sponsored survey was performed at John F. Kennedy International Airport in June of 1994. A second FAA survey was completed at Washington National Airport in June 1995. An additional FAA survey is scheduled for this fiscal year and others have been proposed. Over one thousand landings were recorded at both John F. Kennedy and National Airports. The Navy funded a survey at Tinker Air Force Base in July 1994. A much smaller sample (135 landings) of Boeing 707 type aircraft were analyzed from Tinker Air Force Base

Purpose:

These landing parameter surveys are being conducted to acquire large amounts of typical transport operational data to: (1) validate/update current design requirements, references (a), which for commercial aircraft are derived from usage data measured during the 1950s, (2) provide detailed characterization of typical transport airplane landing velocities and angular displacements, and (3) determine if there are any significant operational trends which would warrant further analysis.

Reference (b) states that landing gear was the most common commercial jet transport system involved in an accident. In addition, for all the landing/taxi accidents, hard landings events were the most common. Figure (1) presents the chronological listing of hard landing accidents by

calendar time. Figure (2) presents the hard landing accident rate data which indicates that the rate of hard landing accidents has not changes over the previous twenty years.

The first video landing survey was conducted at JFK International to collect large quantities of wide body jet aircraft data. The prior NASA surveys collected only data from narrow body B-707 and DC-8 airplanes. In fact, the preliminary results from the JFK video survey suggests that aircraft sink rates increase with airplane weight. Data from these and future surveys could be significant in the design and certification of a very large transport.

Although commercial jet transport landing loads are evaluated as part of the test and certification program, no known program exists to analyze the actual loads imposed during commercial operations. There is very little operational landing data available for commercial aircraft design, and none for wide bodied jet transports. Implementation of this new video technology permits the FAA to determine structural loads information for commercial aircraft operations. Operational and safety constraints limited the use of the Navy's film based landing parameter system in this application.

For both military and civil applications, these survey methods have the following advantages over using on-board instrumentation:

-The analysis requires no installation of equipment on the observed aircraft

- Records are obtained without interference with normal airport operations

- Records yield a large number of aircraft approach and initial contact parameters

- The system enables the study of a large number of landings at minimal costs

- Permanent records are available for reference purposes

Brief Description of NAALDAS:

The data acquisition system consists of a high resolution frame grab video camera, laser disk recorder, and computer control unit. Figure (3) shows a typical video camera installation used during the National Airport Survey.

NAALDAS has been modified for commercial transport applications by the addition of a series of four (4) video cameras located along the edge of

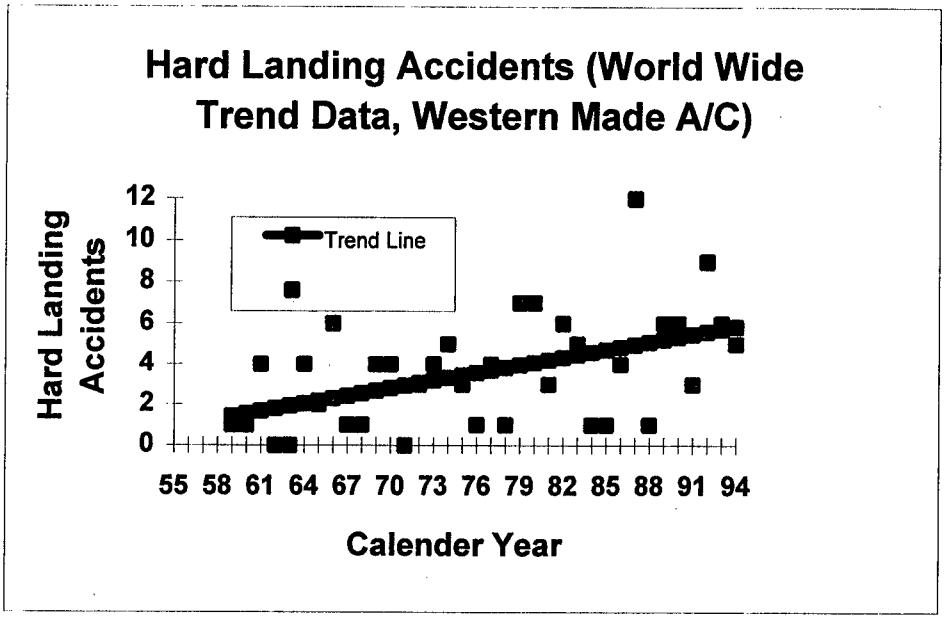

FIGURE 1: HARD LANDING ACCIDENTS BY CALENDER YEAR

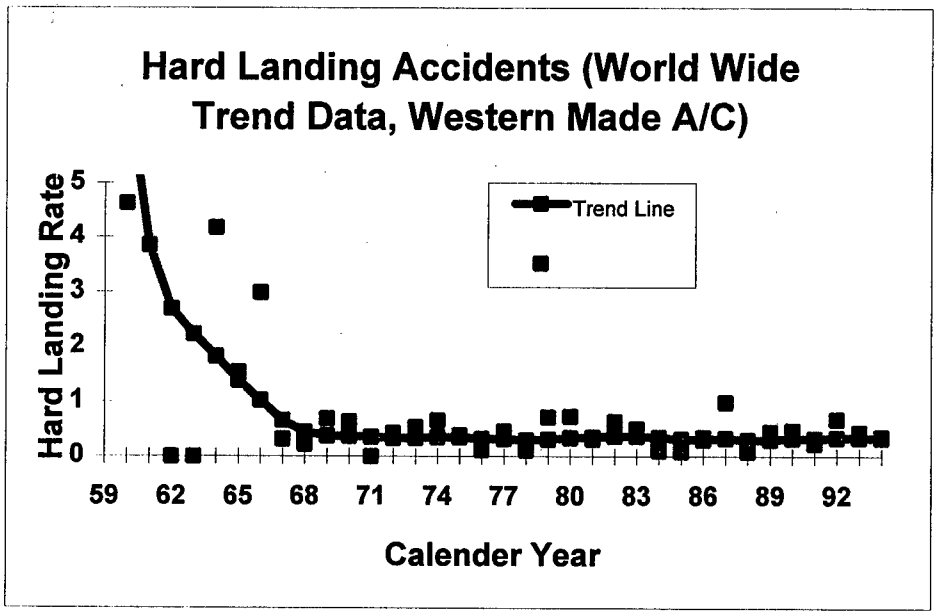

FIGURE 2: HARD LANDING ACCIDENT RATE PER 100,000 LANDINGS

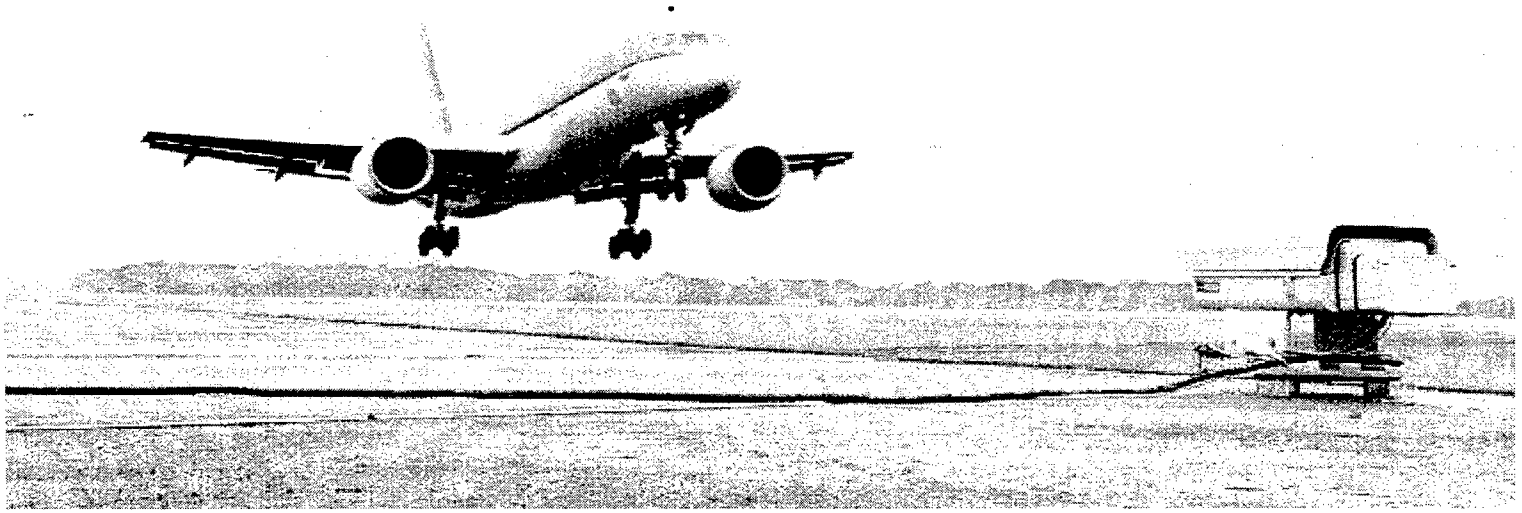

Figure 3 : Camera Installation, Showing Camera, Cabling and Boeing 757 on Final Approach at Washington National Airport, June 1995

the runway. Figure (4) is a sketch of the camera location and coverage of the multiple camera system. The images from these cameras are recorded sequentially as the aircraft passes through their field of view. This modification expands the system coverage area to approximately 2000 ft of the touchdown region of the runway. To eliminate interference and line losses between the cameras and recording station, fiber optic signal cables are used.

Image features are measured on each video frame. Figure (5) is a typical video image showing the track windows which are used to track image features. These measurements are then corrected for angular distortion caused by camera location and for aircraft roll and yaw attitude. The image measurements are compared with known dimensions on the aircraft. The differences in measured positions in successive frames are used to calculate displacement time curves of the image features. These curves are differentiated and the values of aircraft velocities are determined.

This system provides data on the following landing parameters:

Engaging Speed (Closure speed with the camera)
Approach Speed (Engaging Speed plus prevailing wind component)
Sinking Speeds of the port, starboard and nose landing gear wheels
Sinking Speed of the average position of the main wheels.
Roll attitude and rate
Pitch attitude and rate
Runway off center distance
Runway threshold to touchdown distance
Yaw angle at touchdown
Flight Path Angle at touchdown
Glide slope Angle (Instantaneous and Geometric)

A more complete description of the NAALDAS System was provided in previous Air Force Structural Integrity Program presentations, references (c) and (d).

System Operational Advantages:

The NAALDAS landing parameter survey system collects data in the actual operational environment. During these surveys, data has been collected during low visibility Instrument Landing System (ILS) landings. Landings with significant cross wind and tail wind components have been observed both at JFK International and Washington National Airport. During system testing, landings were even recorded during a snow storm at the Atlantic City International Airport.

AIRPORT CAMERA SETUP
PRELIMINARY

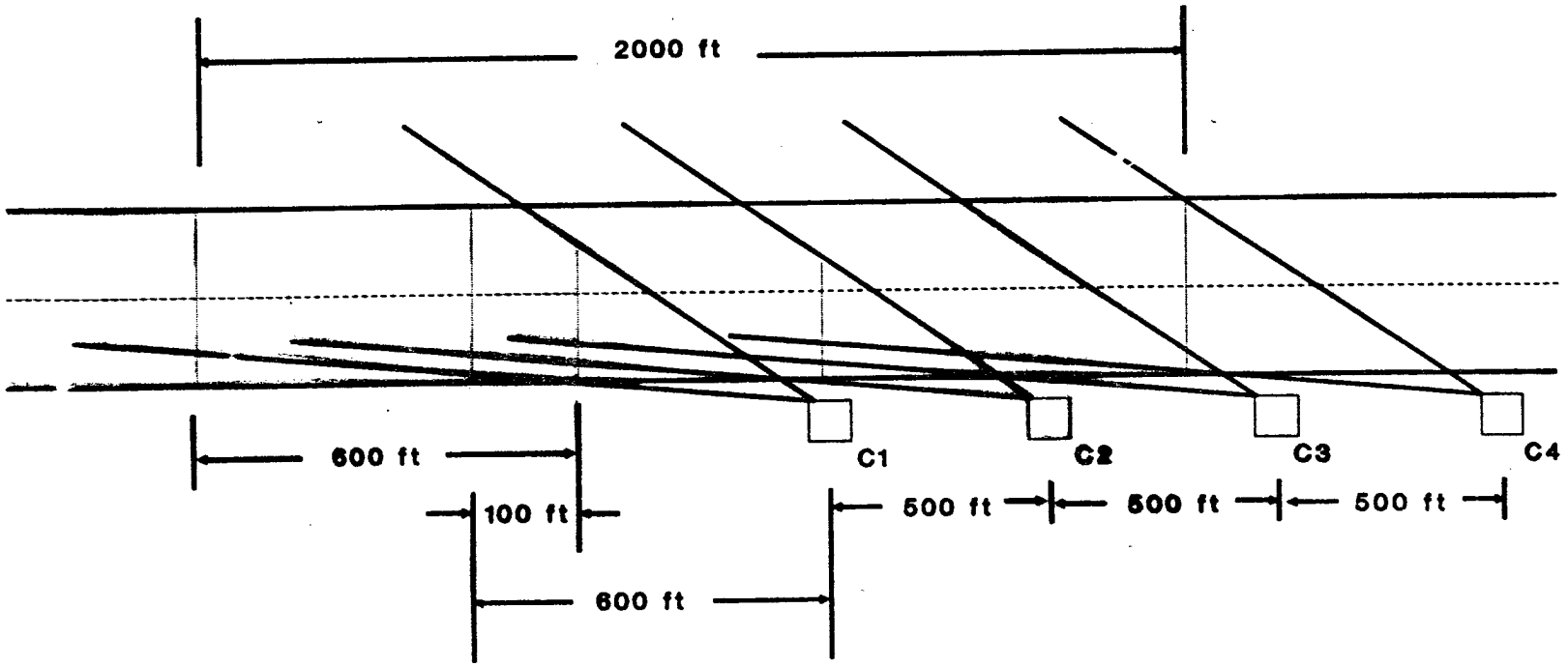

FIGURE 4: SKETCH OF VIDEO CAMERA COVERAGE DURING COMMERCIAL AIRCRAFT LANDING SURVEY

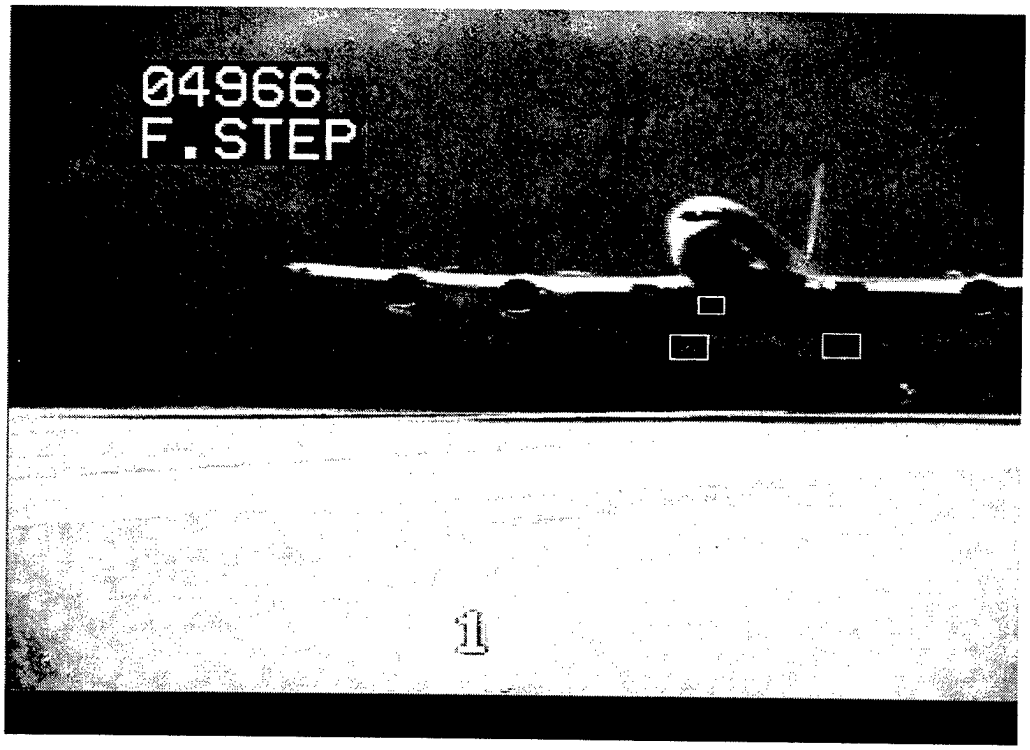

Figure 5: Video Image of NAVY E-6 Aircraft Landing Showing Track Windows Used to Track the Aircraft Landing Gear to Determine Image Feature Positions

The analysis of the video image data provides the aircraft's closure speed with respect to the camera. Approach speed is the sum of closure speed and the component of wind parallel to the centerline of the runway. The use of hourly weather summaries to provide wind data resulted in an approximate value of approach speed reported for the JFK survey. A survey anemometer was installed to collect more reliable wind information during the Washington National and Tinker Air Force Base surveys.

Current equipment constraints permitted us to instrument only one end of one runway at each survey site. We are currently expanding our capability to instrument a second location for future surveys.

JFK Airport Survey Results:

With two thirds of the 1030 JFK landings processed, some trends have been observed. However, this is only an initial data sample and the trends may not be typical of operations at other airports.

The approach to runway 13L requires a right turn on to final and the cross winds at times appeared to contribute to line up difficulties for some pilots. Discussions with airport operations personnel indicated that this was a normal operating condition in the summer months.

Landing parameters for over 230 wide body jet transports, 250 narrow bodied transports and 160 commuter aircraft landings have been processed. Statistical summaries of the principle landing parameters for the landings processed to date are presented in table 1. These summaries are grouped by aircraft categories, either wide body, narrow body or commuter. In addition six landings of the Concorde were also processed. Scatter plots of aircraft sink speed versus landing weight and approach speed versus landing weight are presented as figures (6) and (7).

The first observation made was the number of high sink speed landings in this survey. While the NAVY routinely observes aircraft sink speeds of 10 ft/sec during carrier operations, it was anticipated that an event greater than four ft/sec would be rather rare in commercial operations. The results to date indicate that over ninety landings (over 15%) had sink speeds in excess of four ft/sec and six landings were in the eight to nine ft/sec range. The design limit descent velocity is ten ft/sec. The military specification, MIL-A-8866, for transport aircraft assumes a ten ft/sec landing occurs once in two thousand landings and a nine ft/sec landing once in one thousand landings. Figure (8) compares the observed sink speed frequency distribution from JFK with the criterion of Mil A-8866.

Although the primary objective of this survey was to determine typical landing parameters for heavy wide body and wide body jet transports, significant numbers of narrow body jet transports and commuter types were recorded. During the analysis of the wide bodied jets, it became apparent

JOHN F. KENNEDY INTERNATIONAL AIRPORT SURVEY PRELIMINARY DATA

WIDE BODY AIRCRAFT DATA SUMMARY

PARAMETER	*ENGAGING SPEED* (KNOTS)	*APPROACH SPEED* (KNOTS)	*AVERAGE SINKING SPEED* (FT/SEC)	*PITCH ANGLE AT TD* (DEGREES)	*YAW ANGLE AT TD* (DEGREES)	*RUNWAY OFFCENTER DISTANCE*	*HEADWIND (KNOTS)*	*LANDING WEIGHT*
MEAN VALUE	135	140	2.7	5.87	-1.45	1.44	4.95	307477
STANDARD DEVIATION	13.40	12.39	1.83	1.58	3.32	6.65	4.31	90119
NUMBER OF EVENTS	237							

NARROW BODY AIRCRAFT DATA SUMMARY

PARAMETER	*ENGAGING SPEED* (KNOTS)	*APPROACH SPEED* (KNOTS)	*AVERAGE SINKING SPEED* (FT/SEC)	*PITCH ANGLE AT TD* (DEGREES)	*YAW ANGLE AT TD* (DEGREES)	*RUNWAY OFFCENTER DISTANCE*	*HEADWIND (KNOTS)*	*LANDING WEIGHT*
MEAN VALUE	131	136	2.1	5.32	-2.30	1.52	4.58	142555
STANDARD DEVIATION	11.72	11.48	1.57	1.48	2.94	6.24	4.20	32035
NUMBER OF EVENTS	253							

COMMUTER AIRCRAFT DATA SUMMARY

PARAMETER	*ENGAGING SPEED* (KNOTS)	*APPROACH SPEED* (KNOTS)	*AVERAGE SINKING SPEED* (FT/SEC)	*PITCH ANGLE AT TD* (DEGREES)	*YAW ANGLE AT TD* (DEGREES)	*RUNWAY OFFCENTER DISTANCE* (FEET)	*HEADWIND (KNOTS)*	*LANDING WEIGHT*
MEAN VALUE	101	106	1.5	3.47	-0.61	1.49	4.46	30095
STANDARD DEVIATION	15.45	14.16	1.07	1.59	3.33	8.01	4.50	7809
NUMBER OF EVENTS	145							

TABLE I: JFK LANDING DATA COMPARISON BY AIRCRAFT CATEGORY

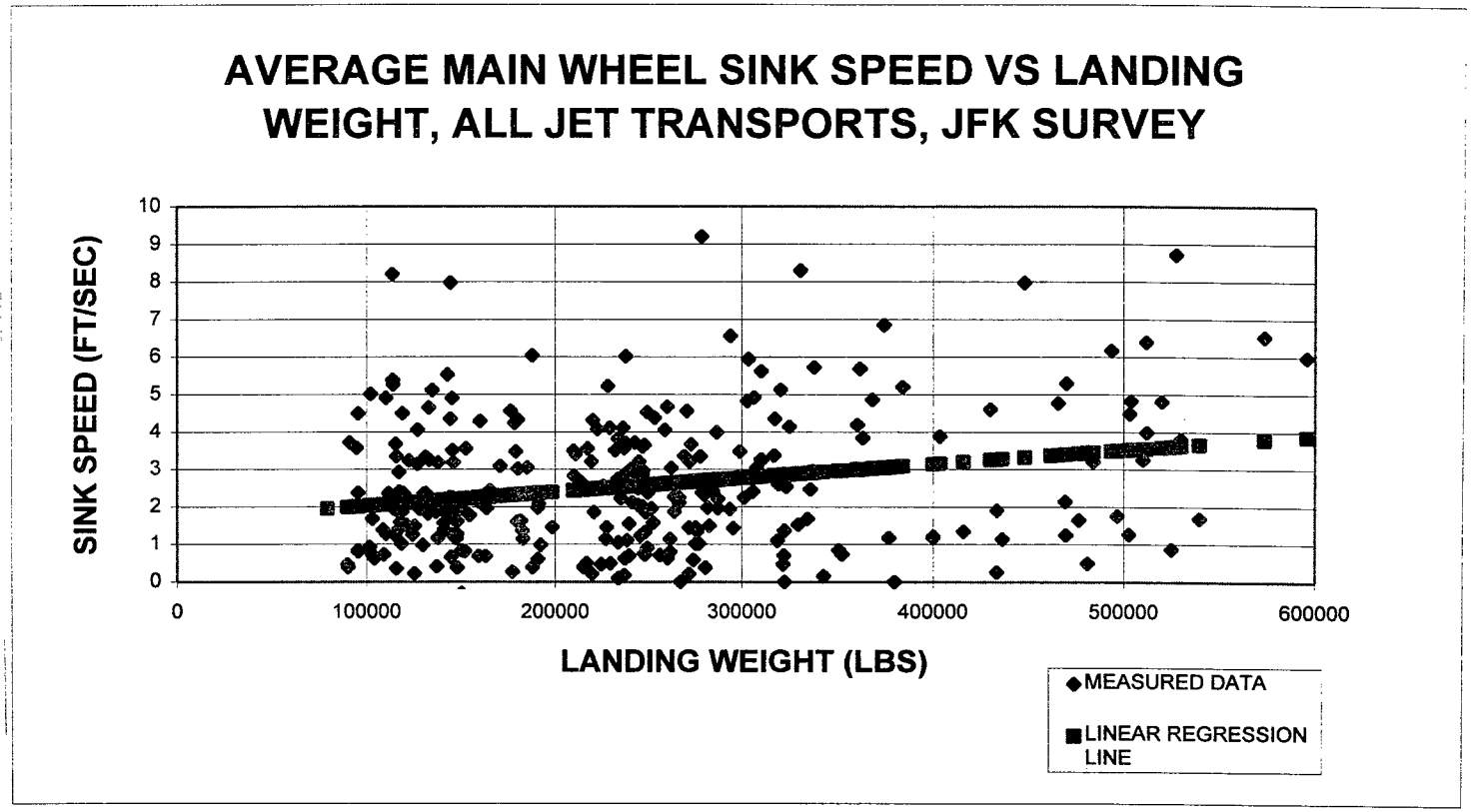

FIGURE 6: AVERAGE MAIN LANDING GEAR SINKING SPEED vs LANDING WEIGHT, ALL JET TRANSPORTS FAA JFK SURVEY

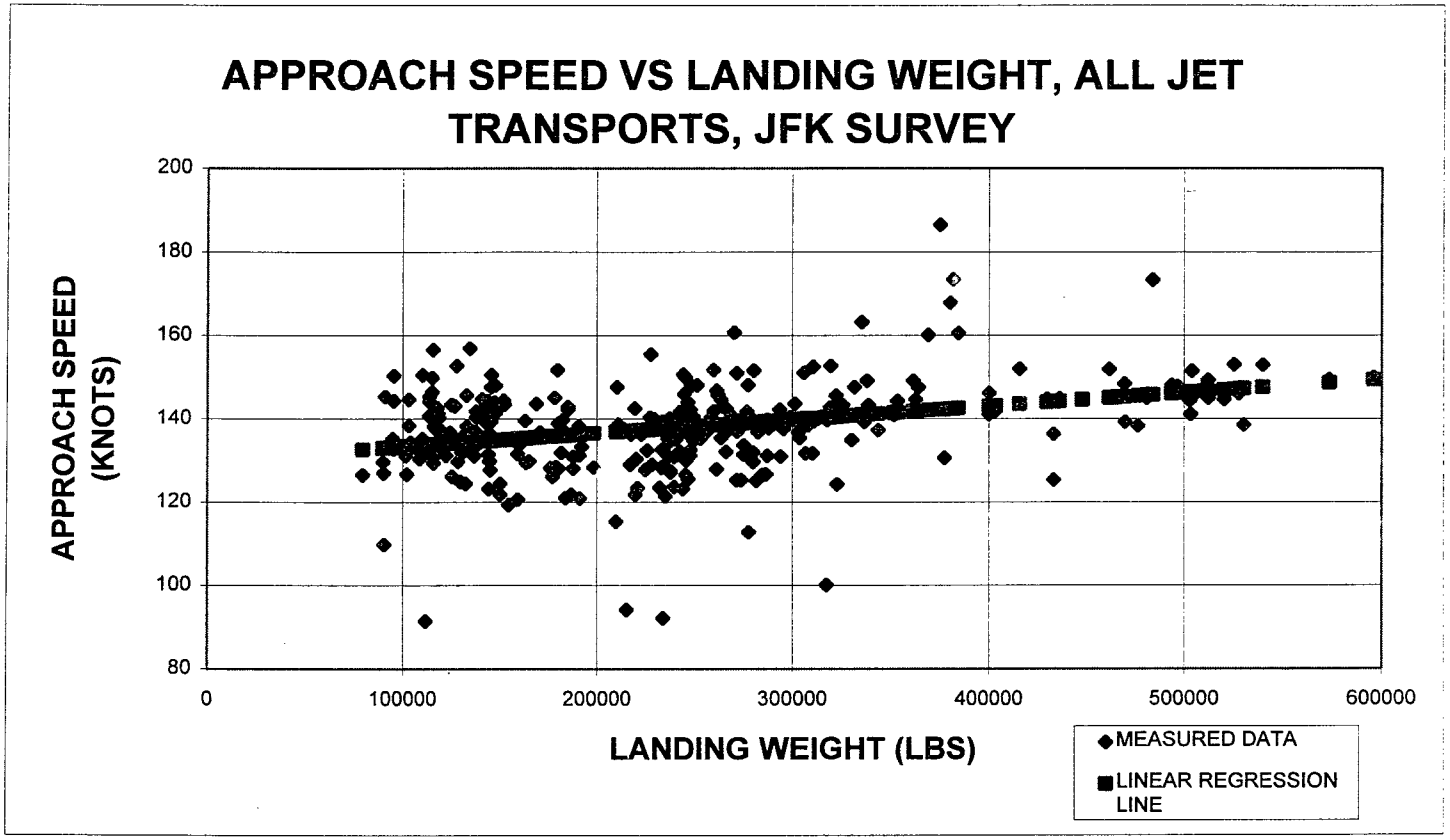

FIGURE 7: APPROACH SPEED vs LANDING WEIGHT
ALL JET TRANSPORTS
FAA JFK SURVEY

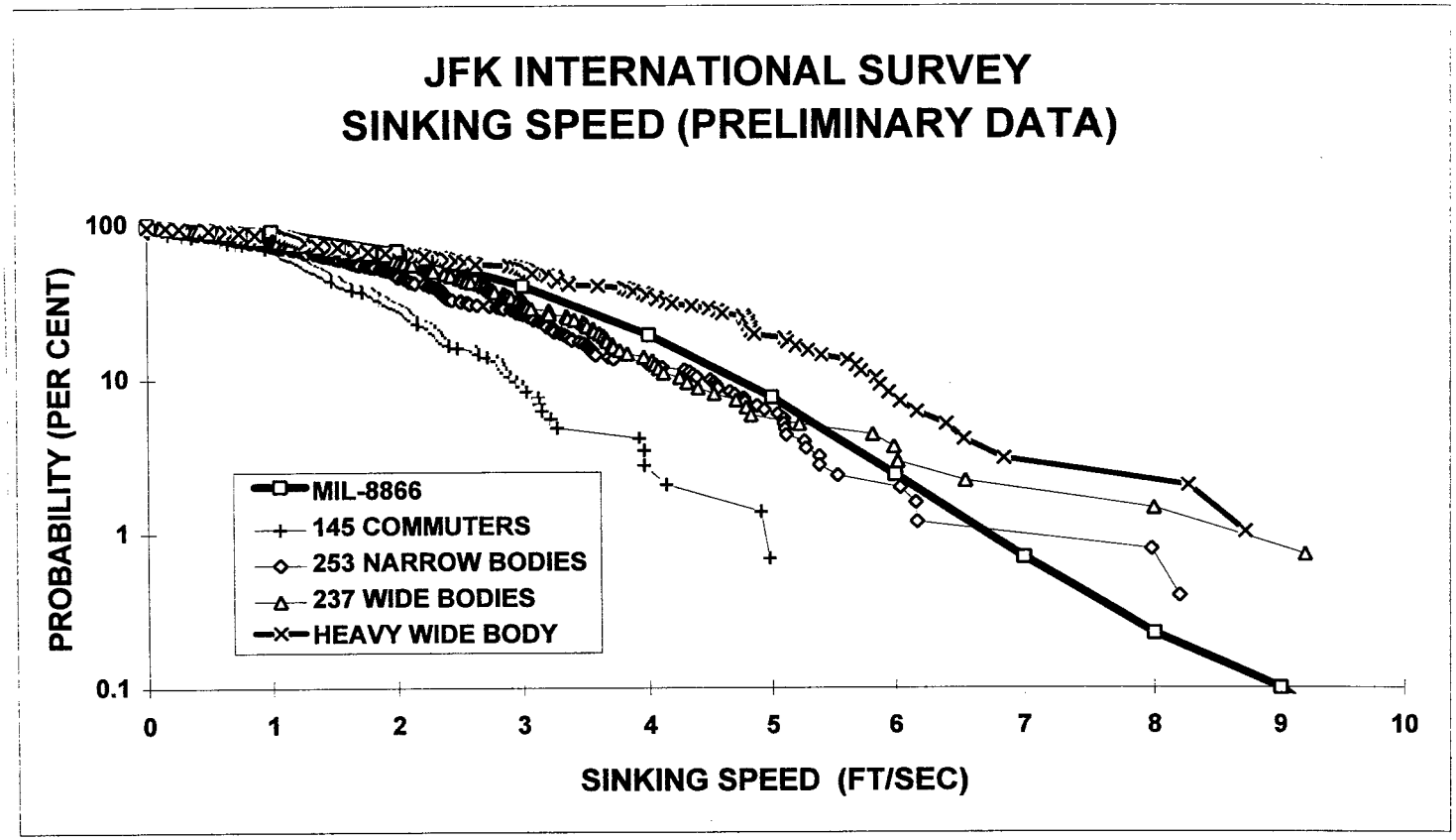

FIGURE 8: COMPARISON OF SINK SPEED PROBABILITY BY AIRCRAFT CATEGORIES

that the larger wide body aircraft were landing at an even higher sink rate than the twin jet aircraft in the same classification. The mean sink speed for the "heavy wide body jets" was found to be over 3.0 ft/sec. The "heavy wide body" category for this study was defined as consisting of the Boeing 747, McDonnell Douglas DC-10 and MD-11 as well as the Lockheed L-1011. The twin jet aircraft, Boeing 767, Airbus A300 and A310 were grouped in the "wide body jet" category. These twin jets had an average sink speed of 2.4 (ft/sec) which is much closer to the value of 2.1 ft/sec reported for the narrow body jet aircraft.

Histograms presenting the sink speed distribution for these category of aircraft are presented in figures (9), (10), (11) and (12).

Heavy Wide Body Aircraft:

Two of the six highest sink speed landings of figure (6) are heavy wide bodied aircraft; one Boeing 747, and one Lockheed L1011

The Boeing 747 landing at almost nine (9) ft/sec. and the L-1011 at over eight (8) ft/sec. The Boeing 747 landed when the prevailing cross wind component was 14 knots and the L1011 had a ten knot cross wind component. Cross wind gusts during these landings may have had a significant effect but this information was not available. Both of these landings were recorded by the first camera (closest to the runway threshold) in the four camera configuration, indicating the aircraft did not flare during these landings. Thus they landed in the first 500 ft of the camera coverage zone.

Separate plots of the heavy wide body aircraft landing parameter sets were generated. Figure (13) is a sink speed vs landing weight plot and figure (14) is an approach speed vs landing weight plot. The sink speed plot shows an increase in sinking speed in addition to an increase in scatter with increasing landing weight.

An attempt to characterize the effect of cross winds on sinking speed and approach speed is presented in figures (15) and (16) respectively. The cross wind components were derived from the prevailing winds tabulated from weather information and does not include any gust information. A plot relating aircraft touchdown position to sink speed is included as figure (17). This figure shows that the bulk of the high sink rate landings occurred in the first 1200 feet from the runway threshold.

Wide Body Aircraft:

Two of the six highest sink speed landings of figure (6) are wide bodied aircraft; both Boeing 767s. One of these jets landed with an average sink speed over nine (9) ft/sec.

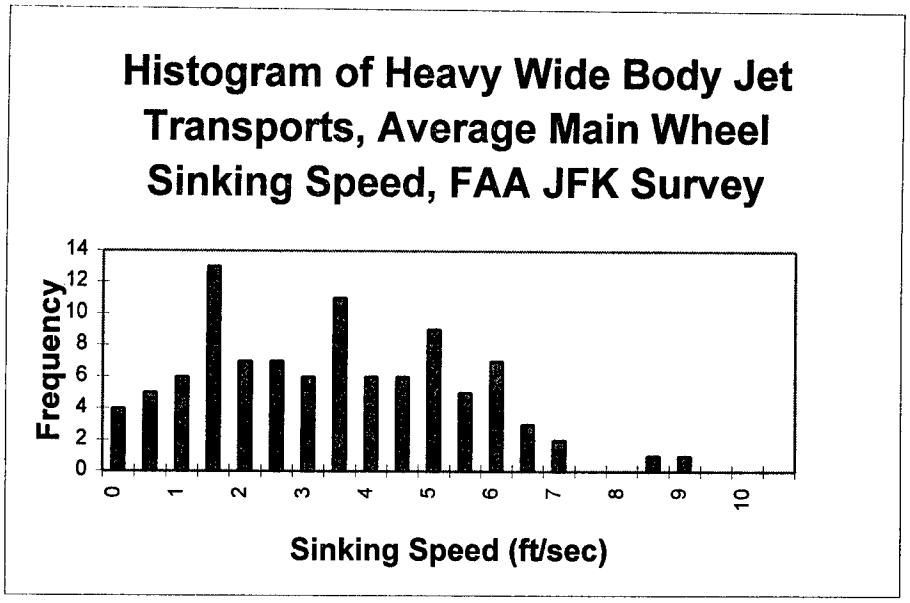

FIGURE 9: HISTOGRAM OF HEAVY WIDE BODY AIRCRAFT SINK SPEED

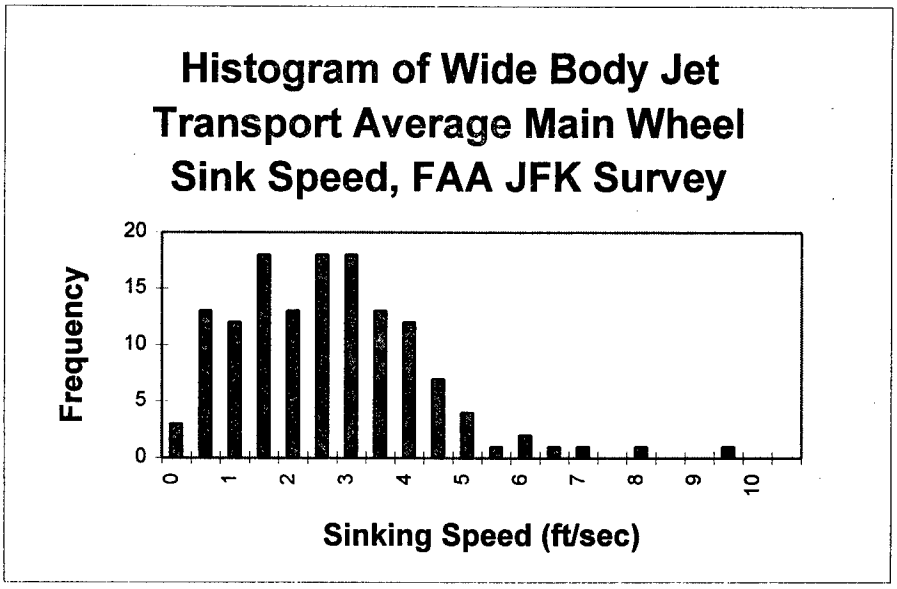

FIGURE 10: HISTOGRAM OF WIDE BODY AIRCRAFT SINK SPEED

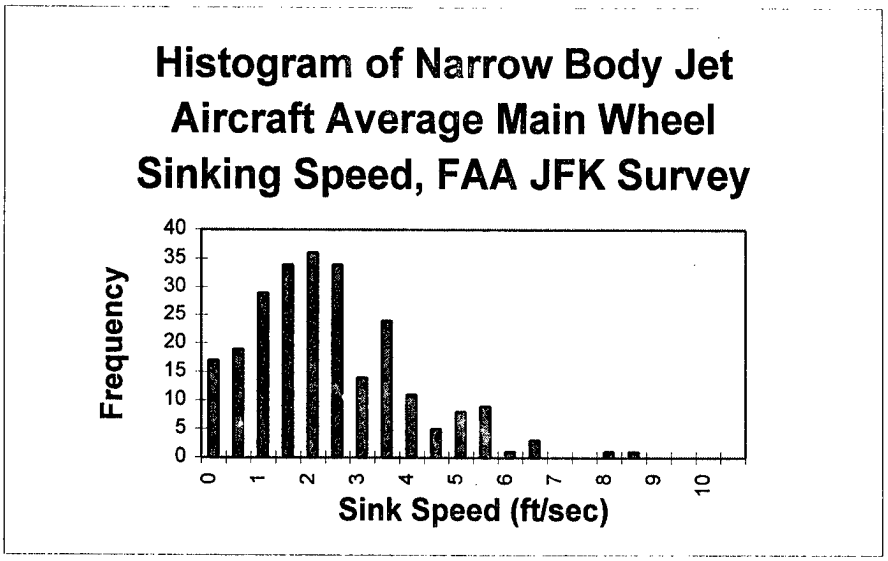

FIGURE 11: HISTOGRAM OF NARROW BODY AIRCRAFT SINK SPEED

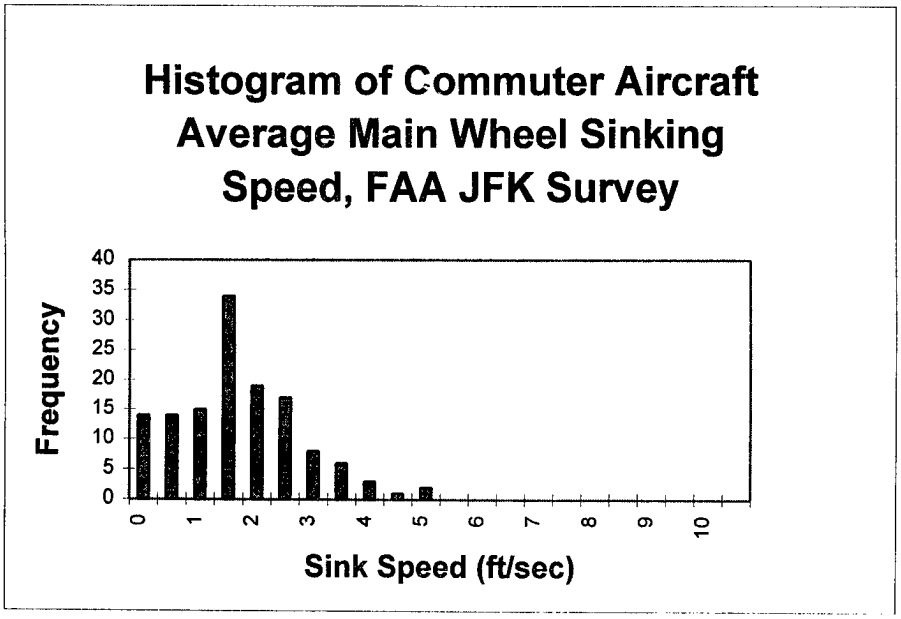

FIGURE 12: HISTOGRAM OF COMMUTER AIRCRAFT SINK SPEED

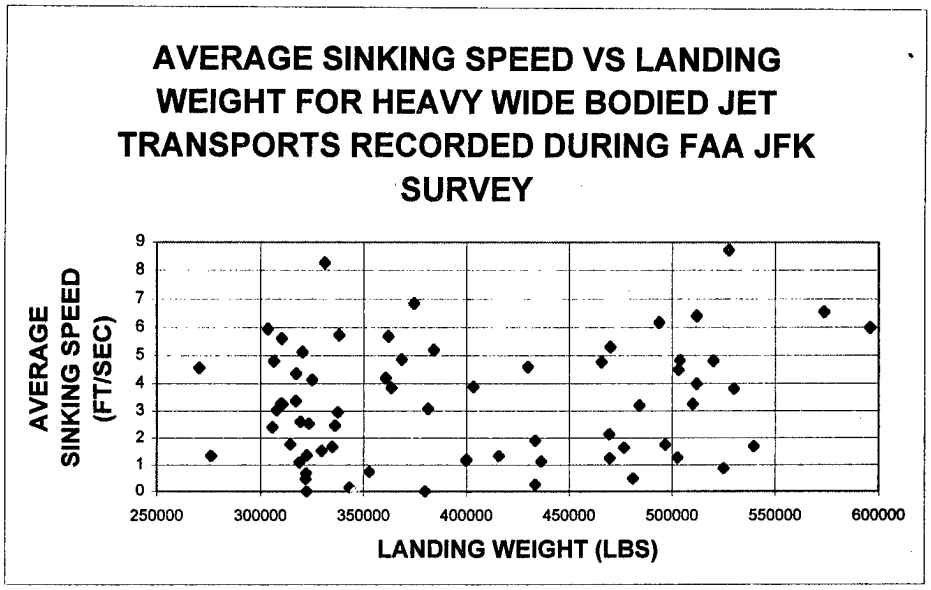

FIGURE 13: SINK SPEED DATA FOR ALL HEAVY WIDE BODY JET TRANSPORTS, FAA JFK SURVEY

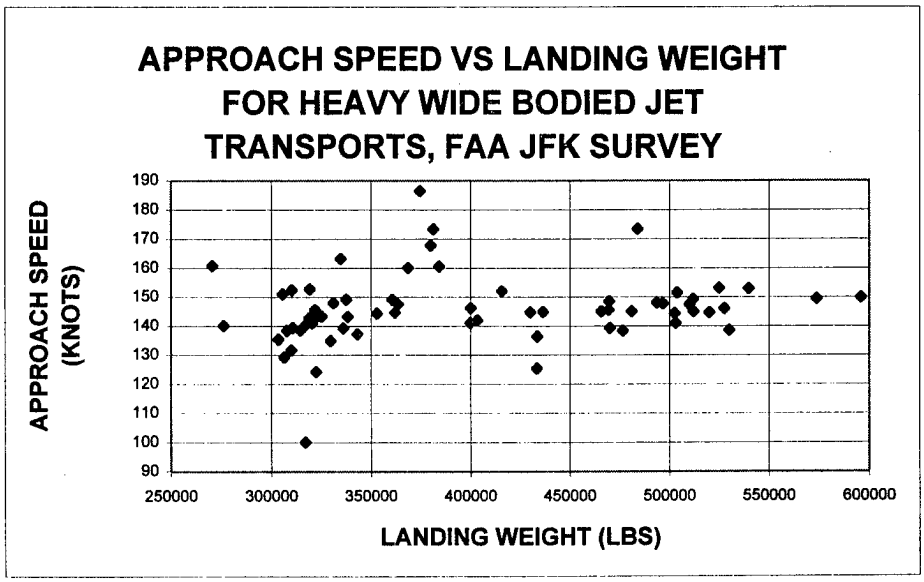

FIGURE 14: APPROACH SPEED DATA FOR ALL HEAVY WIDE BODY JET TRANSPORTS, FAA JFK SURVEY

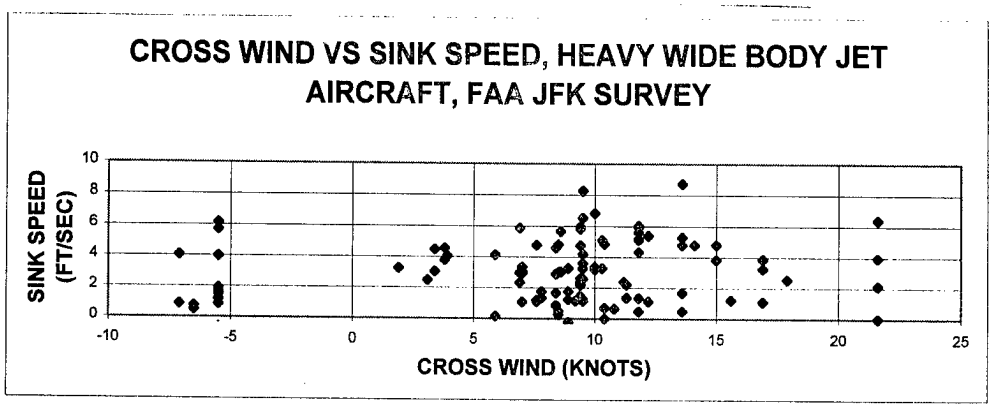

FIGURE 15: CROSS WIND VERSUS SINK SPEED, HEAVY WIDE BODY TRANSPORTS

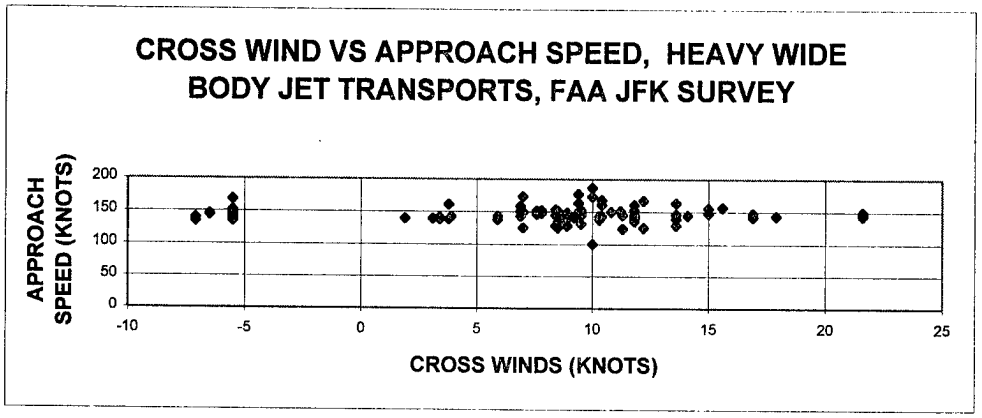

FIGURE 16: CROSS WIND VERSUS APPROACH SPEED, HEAVY WIDE BODY TRANSPORTS

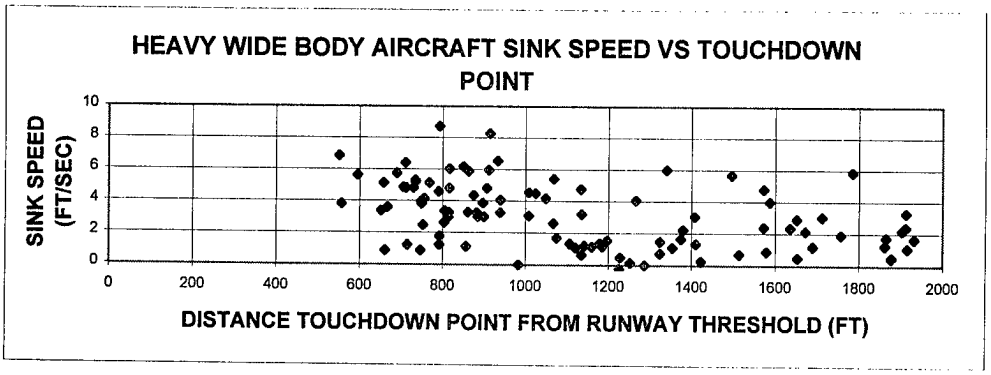

FIGURE 17: HEAVY WIDE BODY TRANSPORTS, SINK SPEED VS RUNWAY TOUCHDOWN POINT

One of the 767 aircraft had ten knot cross wind components and the other 767 landed with eight knot cross wind. One of these landings were recorded by the first camera (closest to the runway threshold) in the four camera configuration, indicating the aircraft did not flare during these landings. Thus it landed in the first 500 ft of the camera coverage zone. The other landed in the second camera's field of view, within the first 1000 feet of coverage.

Figure (18) is a sink speed vs landing weight plot of the wide body aircraft landings. This plot shows an increase in sinking speed and an increase in scatter with increasing landing weight.

A plot relating aircraft touchdown position to sinking speed is included as figure (19). This figure shows that all but one of the wide body jet landings with a sink rate of five foot per second or higher occurred within the first 1000 feet of the runway threshold.

Narrow Body Aircraft:

In this group, only two out of 173 landings were in the eight to nine ft/sec range. This aircraft classification includes Airbus A-320's, Boeing 707, 727, 737 and 757 aircraft along with McDonnell Douglas DC-8, DC-9, and MD-80 aircraft.

Both of the high sink speed landings for this classification occurred with high cross winds, an 18 knot cross wind landing of a DC-9-82 and 12 knot cross wind for a Boeing 727. Both aircraft touched down in the first 500 ft of the camera coverage area.

Approach speed and sink speed plots for these aircraft tend to confirm that these models were flying in general agreement with the original design assumptions. Sink speeds do not appear to vary with landing weight for these aircraft nor do approach speeds. See figures(20) and (21).

A plot relating aircraft touchdown position to sinking speed is included as figure (22). This figure shows that the higher sink rate landings occurred within 750 ft of the runway threshold.

National Airport Survey Results:

NOTE: The processing and analysis of landing parameters from the National Airport Survey is currently underway, these results are preliminary in nature since all the parameter data has not been tabulated and reviewed. The results presented are preliminary in nature but do reflect the broad results expected in the final analysis.

Flight operations at National airport are limited to narrow body jets and commuter aircraft. It was selected as a survey site because of the large

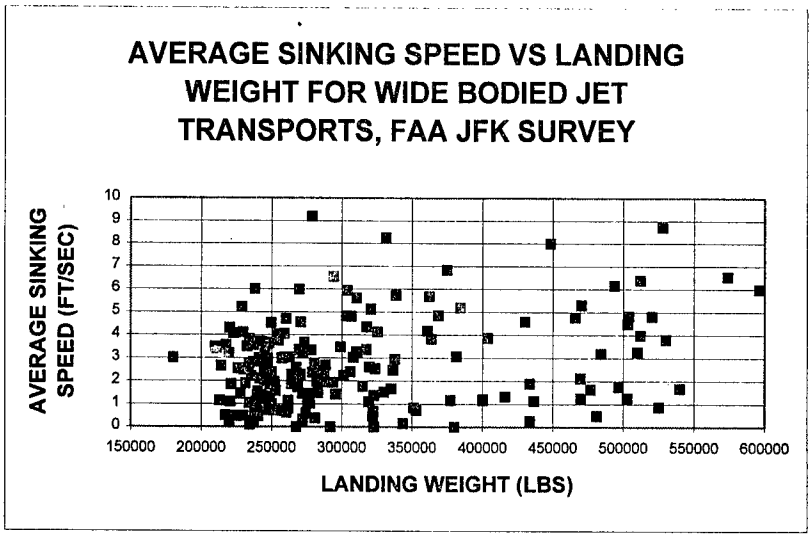

FIGURE 18: WIDE BODY TRANSPORT SINK SPEED VS LANDING WEIGHT

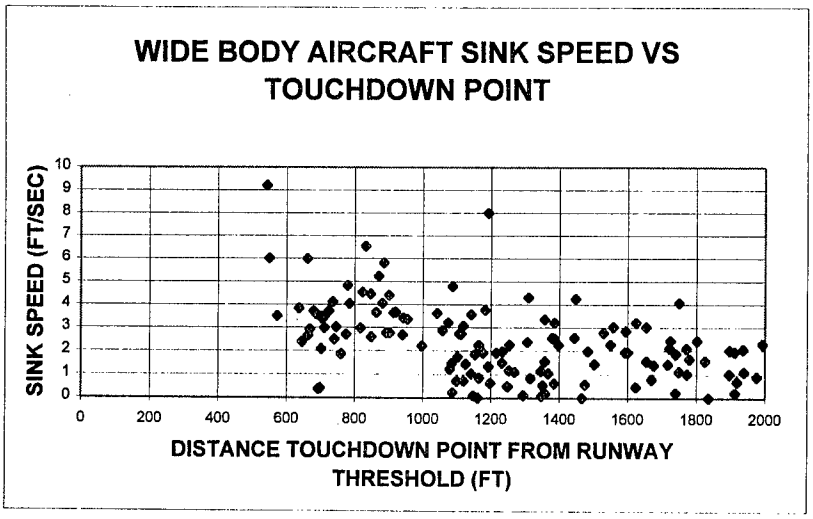

FIGURE 19: WIDE BODY TRANSPORT SINK SPEED VS RUNWAY TOUCHDOWN DISTANCE

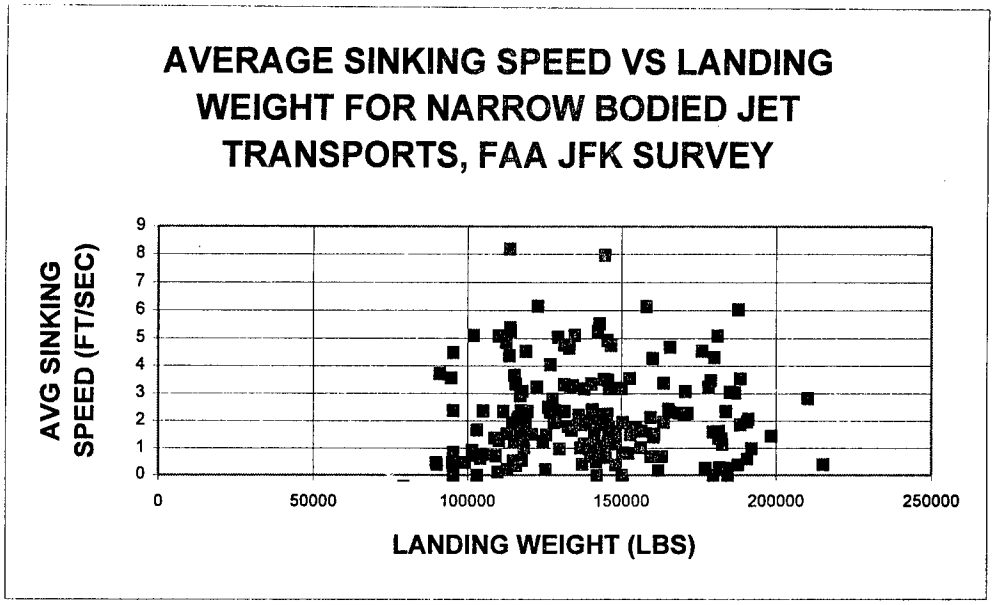

FIGURE 20: SINK SPEED DATA FOR ALL NARROW BODY JET TRANSPORTS, FAA JFK SURVEY

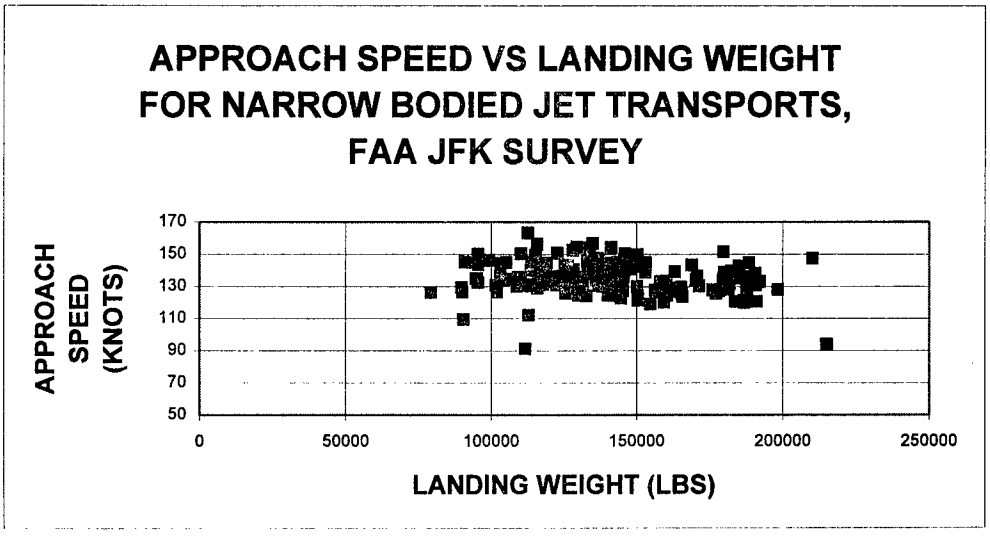

FIGURE 21: APPROACH SPEED DATA FOR ALL NARROW BODY JET TRANSPORTS, FAA JFK SURVEY

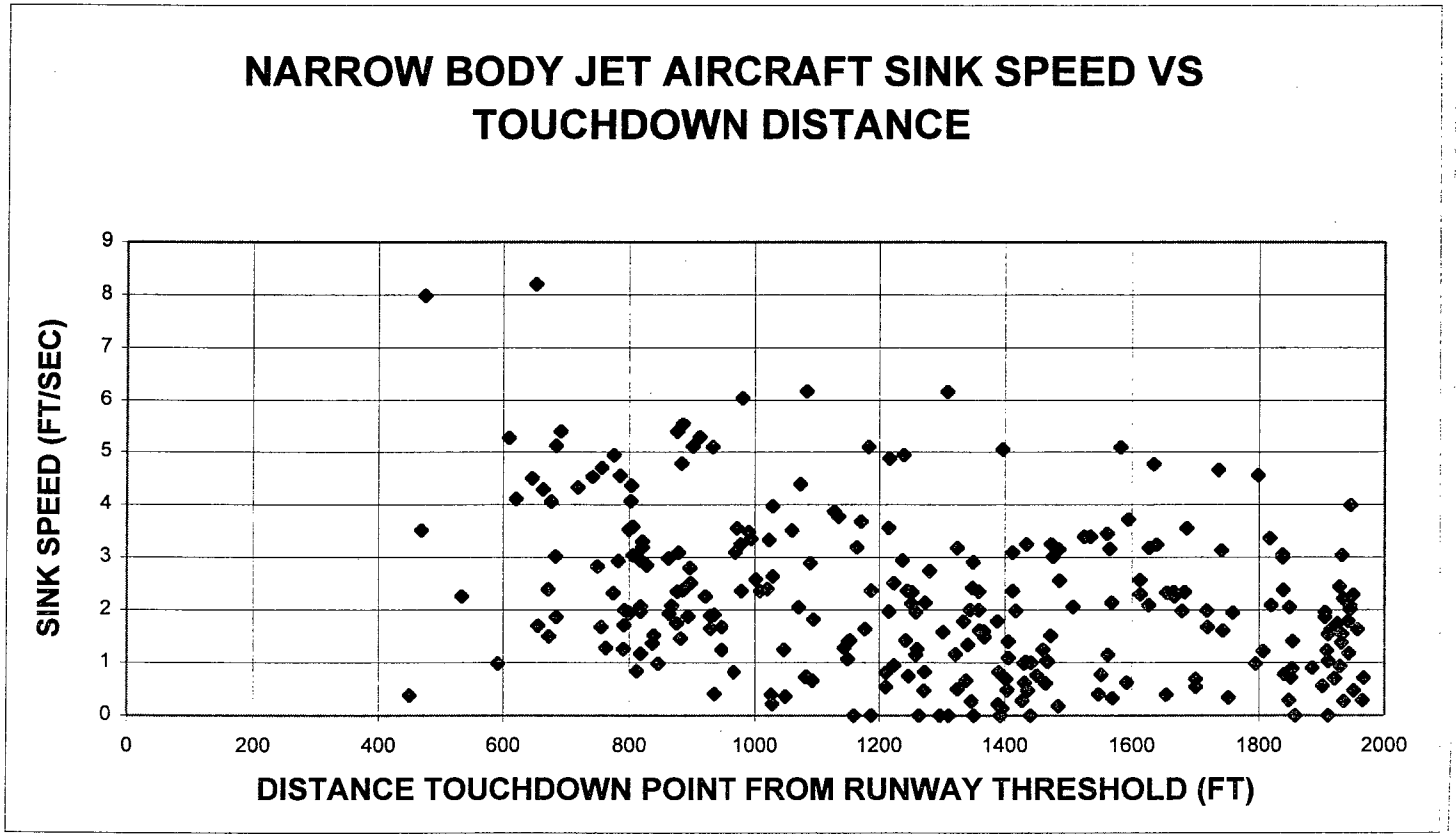

FIGURE 22: NARROW BODY JET AIRCRAFT, SINK SPEED VS RUNWAY TOUCHDOWN POINT

volume of operations on a relatively short runway. The largest aircraft routinely operating from this airport were Boeing 757 and Airbus A-320 transports. The bulk of the landings were performed by Boeing 727s, 737s along with McDonnell Douglas DC-9 & MD-80 aircraft. Thus, the survey results for all the jet transports correspond to the narrow body jet category from the JFK survey.

Figure (23) is a histogram of aircraft sink speeds for these aircraft observed at National Airport. The plot, which covers over 600 landings, is very similar to the narrow body jet category from JFK. It also indicates a number of landings with sink speeds in the range of eight to ten ft/sec. The mean sink speed for these aircraft was measured as 2.4 ft/sec with a standard deviation of 1.8 ft/sec. The comparable group of JFK landings resulted in a sink speed mean of 2.1 ft/sec with a standard deviation of 1.6 ft/sec.

The runway configurations at both JFK International and Washington National required that the camera covering the last survey area, furthest from the runway threshold, view the aircraft from the rear. This caused revisions in our software and analysis procedures. Because of this, analysis of these landings have not been completed for the National survey. As indicated from JFK, these landings tend to be at lower sink rates and the overall average at National may drop slightly once the analysis is completed.

Table (2) compares the approach speed and sink speeds for the aircraft models recorded at both NATIONAL and JFK. The results at National show higher sink rates and generally lower approach speeds than JFK. The effect of the shorter runway and larger number of landings in poor visibility conditions could cause this variation. Still the National results tend to confirm the data distribution for these aircraft from JFK.

Tinker Air Force Base Survey:

The Navy operates E-6 aircraft (a modified Boeing 707) from Tinker Air Force Base. A landing loads survey was performed during training operations to establish a data base for the landing performance of that aircraft. In addition, a limited sample of E-3, KC-135 and Boeing 707 aircraft were observed. The operations were relatively benign when compared to operations at JFK or National, with a mean sink speed approximately 2.0 ft/sec and standard deviation of less than 0.5 ft/sec. The maximum observed sink speed from this survey was 6.1 ft/sec.

Conclusions:

NAALDAS has been converted from a highly specialized tool to one suitable for use in all segments of the aviation community. The multiple camera system can survey normal field (flared) landings. It can also be used

FAA LANDING SURVEY COMPARISON
PRELIMINARY RESULTS

		NATIONAL AIRPORT SURVEY			JOHN F KENNEDY AIRPORT SURVEY		
AIRCRAFT MODEL			*APPROACH SPEED*	*AVERAGE SINK SPEED*		*APPROACH SPEED*	*AVERAGE SINK SPEED*
727	MEAN STD DEV NUMBER OF LANDINGS	110	137.0 7.96	2.30 1.81	84	139.7 7.75	2.25 1.53
737	MEAN STD DEV NUMBER OF LANDINGS	154	139.2 10.73	2.30 1.59	9	134.9 11.14	0.83 1.33
757	MEAN STD DEV NUMBER OF LANDINGS	67	129.5 5.90	2.78 2.08	79	130.5 10.27	2.01 1.46
DC-9	MEAN STD DEV NUMBER OF LANDINGS	91	133.2 9.96	2.68 1.50	42	138.2 9.37	2.22 1.85
MD-80	MEAN STD DEV NUMBER OF LANDINGS	91	134.2 9.69	3.00 1.79	36	137.2 11.09	2.11 1.56

TABLE II: COMPARISON OF APPROACH SPEED AND SINK SPEED MEASUREMENTS FOR NARROW BODY JETS FROM FAA NATIONAL AIRPORT & JFK AIRPORT SURVEYS

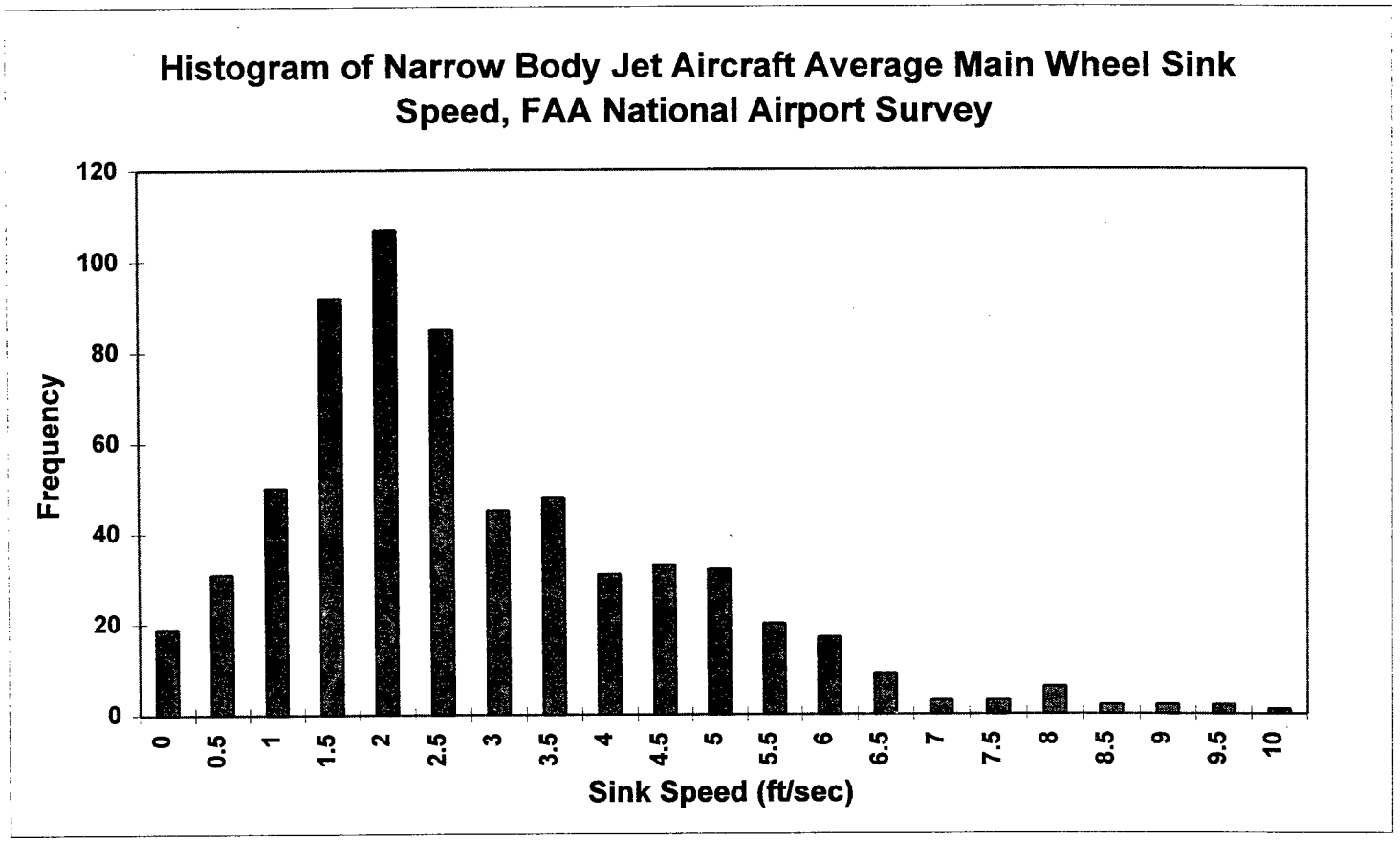

FIGURE 23: HISTOGRAM OF NARROW BODY AIRCRAFT SINK SPEED

to monitor the effect of special approach procedures, noise abatement procedures, or particular terrain problems.

The ability to temporarily install and operate NAALDAS at any location, and collect data without interfering with normal operations, makes this system unique. The technology transfer between FAA and Navy is particularly beneficial in today's environment of reduced government spending.

It is apparent that the sink rates observed for wide body aircraft in this study are higher than those of narrow body aircraft and this observation warrants further investigation. Initial results from the JFK landings indicate that the heavy wide body jet aircraft are experiencing approximately a one foot per second greater ground impact vertical velocity at initial gear/runway contact than the narrow body jets.

Figure (24) is a plot of aircraft sinking speed vs landing weight for the JFK survey. The segmented straight line on the top of the plot is a result of statistical analysis of the results of the survey. This line predicts the once-in-a-life-time maximum sink speed that could be expected for a commercial aircraft as a function of landing weight. The current aircraft design specification, reference (b) calls for a constant value of 10 ft/sec as the maximum design sink speed for transport category jet aircraft. This figure suggests that future large transport aircraft design requirements should be reviewed for higher design sinking speeds. Data for future surveys is required to verify this analysis.

A comparison of heavy wide jet body, wide body jet data, narrow body jet data and MIL-A-8866 criteria for the JFK landings is presented as Fig. (8). The measured sink speed distribution for both wide body aircraft categories exceeds that of MIL-A-8866. Further surveys are scheduled to validate this observation.

These limited data samples indicate that operations in cross wind conditions tend to increase both aircraft sink rates and approach speeds. This is a significant area for future research.

The landing data collected at JFK airport shows a strong correlation between aircraft sinking speed at the aircraft's touchdown location on the runway. The highest sink speed landings occurred in the first 1200 feet from the runway threshold. While this may be a result of local operating conditions, such as wind, weather or the pace of airport operations, this observation also warrants additional study.

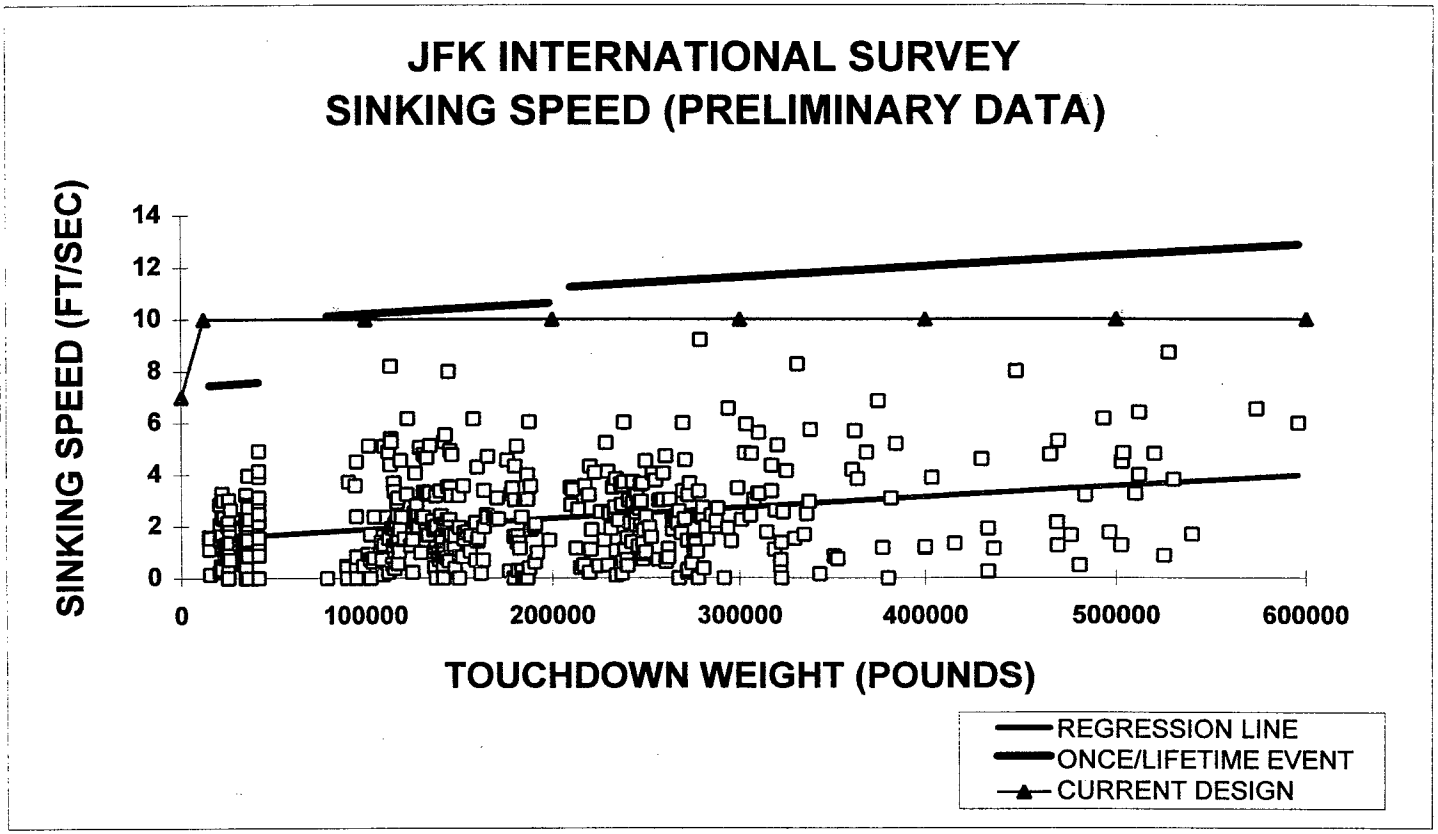

FIGURE 24: ESTIMATE OF ONCE IN A LIFE TIME SINK SPEED AS A FUNCTION OF LANDING WEIGHT FROM FAA LANDING SURVEY AT JFK AIRPORT

to monitor the effect of special approach procedures, noise abatement procedures, or particular terrain problems.

The ability to temporarily install and operate NAALDAS at any location, and collect data without interfering with normal operations, makes this system unique. The technology transfer between FAA and Navy is particularly beneficial in today's environment of reduced government spending.

It is apparent that the sink rates observed for wide body aircraft in this study are higher than those of narrow body aircraft and this observation warrants further investigation. Initial results from the JFK landings indicate that the heavy wide body jet aircraft are experiencing approximately a one foot per second greater ground impact vertical velocity at initial gear/runway contact than the narrow body jets.

Figure (24) is a plot of aircraft sinking speed vs landing weight for the JFK survey. The segmented straight line on the top of the plot is a result of statistical analysis of the results of the survey. This line predicts the once-in-a-life-time maximum sink speed that could be expected for a commercial aircraft as a function of landing weight. Once in a life time was calculated based on 50,000 landings. The current aircraft design specification, reference (b), calls for a constant value of 10 ft/sec as the maximum design sink speed for transport category jet aircraft. This figure suggests that anticipated landing weight should be considered a factor for future large transport aircraft design requirements. Additional data from future surveys is required to verify this analysis.

A comparison of heavy wide jet body, wide body jet data, narrow body jet data and MIL-A-8866 criteria for the JFK landings is presented as Fig. (8). The measured sink speed distribution for both wide body aircraft categories exceeds that of MIL-A-8866. Further surveys are scheduled to validate this observation.

These limited data samples indicate that operations in cross wind conditions tend to increase both aircraft sink rates and approach speeds, especially for light weight transport aircraft. This is a significant area for future research.

The landing data collected at JFK airport shows a strong correlation between aircraft sinking speed at the aircraft's touchdown location on the runway. All six sink speeds in excess of eight foot per second, occurred in the first 1200 feet from the runway threshold. While this may be a result of local operating conditions, such as wind, weather or the pace of airport operations, this observation also warrants additional study.

References:

(a) Code of Federal Regulations, Aeronautics and Space, Part 25.473

(b) Douglas Aircraft Company, Commercial Jet Transport Safety Statistics, 1993

(c) Technical Paper on "The Naval Aircraft Approach and Landing Data Acquisition System" presented by R. Micklos at the USAF Structural Integrity Program Conference, San Antonio, Texas, December 1992

(d) Technical Paper on "The Naval Aircraft Approach and Landing Data Acquisition System Acceptance Test Results" presented by R. Micklos at the USAF Structural Integrity Program Conference, San Antonio, Texas, December 1993.

Prediction and Control of Dynamic Loads to Improve Structural Integrity

Mr. Leonard Shaw
Mr. Larry Huttsell
Wright Laboratory
Wright Patterson Air Force Base, Ohio 45433-7542

1. SUMMARY

Many aircraft in the current Air Force fleet are facing structural life extensions rather than retirement. Several of these aircraft have had or are experiencing failures due to unsteady/separated flow. The repair and redesign to correct tail buffet problems on the twin tail fighters has been excessively expensive. Other buffet problems involve outer wing panels, fuselage missile carriage, and ventral fins. A common problem for fighters carrying external stores is Limit Cycle Oscillations (LCO) which limits performance for many store loadings. Acoustics and sonic fatigue has been a problem for many years and aircraft which carry weapons internally can have acoustic levels high enough to cause structural damage to the aircraft and the internally carried weapon.

Accurate prediction and control of dynamic loads is necessary to assure the structural integrity of the aircraft and weapons. This paper will present in-house and contractual research in the areas of aeroelasticity and acoustics, with special emphasis on buffet, LCO, and weapon bay acoustics.

2. ACOUSTICS - WEAPON BAYS

2.1 BACKGROUND

The study of flow induced cavity acoustic environments which relate to aircraft weapon bays date back to the mid 1950s when Roshko (1) and Krishnamurty (2) conducted research in this area. Roshko varied the cavity dimensions systematically while obtaining the time averaged effects in the cavity. He measured the pressure on the walls and floor. A single vortex was seen to exist for the shallow case. For very shallow configurations he noted that the shear layer reattached to the cavity floor. This observation has been repeated many times in more recent studies of very shallow cavities. As missiles became longer and smaller diameter, the need for shallower weapon bays

arose. Roshko noted that the impingement of the shear layer on the downstream wall of the cavity was the cause of increased drag which occur with open cavities. Karamcheti, conducting his research at about the same time as Roshko, studied rectangular cavities exposed to free stream Mach number flows of 0.25 to 1.5. He actually obtained sound pressure levels from his tests with levels as high as 160 dB being observed. An important observation made by Karamcheti was that there is a minimum cavity length at which the shear layer will span the opening and not impinge on the downstream wall of the cavity, thus not resulting in acoustic resonance. This is the physical basis of control of the high acoustic environment in cavities. If the shear layer can be made to span the cavity, or reattach at a stable stagnation point, no feedback process is established and hence no resonance.

One of the most referenced historical works in the flow induced cavity acoustic area is that of Rossiter (3). He made measurements of the time average and unsteady pressures on the "roof" (or floor) and behind a series of rectangular cavies set in the roof of a 2 foot by 1.5 foot transonic wind tunnel. Data for cavities with length-to-depth ratios from 1 to 10 were presented for Mach numbers from 0.4 to 1.2. His major conclusions were shallow cavities (L/D>4) produce mainly broadband acoustic spectra and deeper cavities (L/D<4) produce a periodic tone. The periodic tone was attributed to acoustic resonance in the cavity and excited by a phenomenon similar to that causing edge tones. The amplitude of the periodic tone can be as large as 0.35 times the free stream dynamic pressure. He also investigated methods to suppress the periodic fluctuations and concluded that they may be suppressed by placing a small spoiler ahead of the cavity. The only explanation given as to why a spoiler is effective is that it thickens the boundary layer. He is most referenced because of his equation to predict the possible resonant frequencies in an open cavity. Even today it is referenced often as the "Rossiter Equation" and gives a very good prediction of the resonant frequencies in a cavity, if the correct phase and convection terms are used. The equation will be presented later in the paper.

Plumbee et al (4) conducted theoretical and experimental investigations of the flow induced cavity acoustic problem. A detailed analytical prediction method was developed based on the radiation impedance of the cavity opening. A table of radiation resistance and reactance was provided to utilize the method. It is an iterative approach and does not readily converge. The method has not been referenced in subsequent publications mainly due to the difficulty in use of it. They also conducted extensive experimental tests on cavities obtaining wind tunnel data for Mach numbers from 0.2 to 5.0. The major conclusions were that the acoustic levels were higher in the rear of the cavity, width has little effect on acoustic levels, and there exist an onset Mach number below which the cavity tones are not excited. Smith and Shaw (5) formulated an empirical acoustic predictions method which was based on an extensive flight test data base. The method predicts the frequency and amplitudes of the first three acoustic modes in the cavity as well as the broadband spectrum level. The prediction method also gives the spatial

distribution of the modal energy. It is easy to use and gives a good first order prediction of the flow induced levels.

Shaw and Smith (6) presented results of a full scale flight test of an instrumented store in a weapons bay. The aircraft was an F-111 and the store was a BDU-8/B instrumented with 21 microphones. Data were recorded for altitudes of 3,000, 10,000, and 30,000 feet and Mach numbers from 0.75 to 1.3. The results showed that the acoustic levels on the store scale with free stream dynamic pressure. The levels on the store increased toward the rear. There are significant circumferential variations in the acoustic levels at different longitudinal locations.

Shaw (7) presented results from a flight test for suppression of the cavity internal acoustic levels. Numerous leading edge and trailing edge suppression devices were flight tested. Excellent suppression results were obtained for simple leading edge spoilers and rear bulkhead ramps. Nearly 30 dB suppression was obtained for the best configuration. The list of references of work related to open cavities is very long. Only a small percent of even the major efforts are referenced in this paper. As an example of the large number of reports presenting results related to aircraft cavity flow, in 1982 Betry and Rohrer (8) compiled a survey containing 144 references on this subject. Since then at least another 50-100 have been published. Thus only high relevancy efforts are referenced herein.

An example of the acoustic environment in the B-1A weapons bay is shown in Figure 1. The amplitudes of the resonant modes are well above the broadband level for the first four modes. The spectrum level of the first mode is seen to be 155 dB which is high enough to cause structural damage in a very short time. The first mode frequency is 18 Hertz and the second mode is approximately 45 Hertz. These low frequencies can easily coincide with structural resonant frequencies and thus cause structural resonant response and possibly failure. Spectra from the F-111 are shown Figure 2. The acoustic modes do not appear as broad as in Figure 4 because these spectra are 1/3 octave band and each tone includes a wider band of energy. Caution must be used to compare the two data. If the tone is at least ten dB above the broadband level in 1/3 octave band data, one can safely assume that the peak level is close to the spectrum peak of the same data. The second mode peak in Figure 2 is 161 dB but the equivalent spectrum level would be approximately 159 dB. This is an extremely high level and will cause damage. The other spectrum in the figure will be discussed later. Based on the spectra from these two aircraft the need for understanding the phenomenon and controlling the amplitudes is readily evident.

2.2 PREDICTION

In the design stage of an aircraft it is necessary to be able to predict the environment and loads that the structure and equipment must be designed and qualified for. The environment in the weapons bay includes the frequency of the acoustic modes, amplitudes of the modes, and the broadband level. There have been many methods developed to predict the cavity flow induced acoustic environment but only a few of the more useable and typical examples will be discussed.

Prediction of the resonant acoustic frequencies has been addressed at least an order of magnitude more than the amplitude. The most referenced and utilized method for predicting the frequencies is the so called Rossiter (3) equation. The equation is:

$$f\frac{L}{U} = \frac{(m-\alpha)}{M\ /\left(1+\frac{\gamma-1}{2}M^2\right)^{1/2}+\frac{1}{K_v}} \qquad (1)$$

where α is a phase lag term, γ is the ratio of the specific heats, and K_v is the convection speed of the shear layer. The equation is derived by assuming the complete cycle time is the sum of the downstream convection time and the upstream acoustic propagation time along with a phase lag of α between the two.

Prediction of the amplitudes of the weapons bay or cavity acoustic environment is much more difficult than predicting the resonant frequencies. One of the earliest theoretical amplitude prediction methods was presented by Plumblee et al (4). The method relies on the calculation of the radiation impedance of the cavity opening and then solving the wave equation with the other five sides of the cavity having infinite impendace. It is an iterative solution which must converge. It is not convenient to utilize and is not that accurate.

Smith and Shaw (5) developed an empirical prediction method for the amplitudes of the resonant frequencies as well as the longitudinal distribution of the energy in the cavity. The method is presented here because of its ease of use and very good first order prediction of the flow induced acoustic environment.

$$f_m = \frac{V}{L}\ \frac{m-0.25}{\frac{M}{(1+\frac{K-1}{2}M^2)^{1/2}}+1.75} \qquad m=1,2,3$$

$$20 \log (P_2\ max/q) = 25\ sech\ [2(M-1)]\ -3.3\ L/D - 27$$

$$20 \log (P_1\ max/q) = 20 \log (P_2\ max/q) + 1.5\ L/D - 13$$

$$20 \log (P_3\ max/q) = 20 \log (P_2\ max/q) - 13\ M + 9$$

$$20 \log (P_m/q)_{X/L} = 20 \log (P_m \text{ max}/q) - 10 \left[1 - \left|\cos \alpha_m X/L\right| + (0.33L/D - 0.6)(1-X/L)\right]$$

$$\alpha_1 = 3.5 \text{ rad}$$

$$\alpha_2 = 6.3 \text{ rad}$$

$$\alpha_3 = 10.0 \text{ rad}$$

$$20 \log (P_b \text{ max}/q) = 20 \log (P_2 \text{ max}/q) + \left[3.3\ L/D - 28 + 3(1-L/D)(1-X/L)\right]\left[1.2-0.4M\right]$$

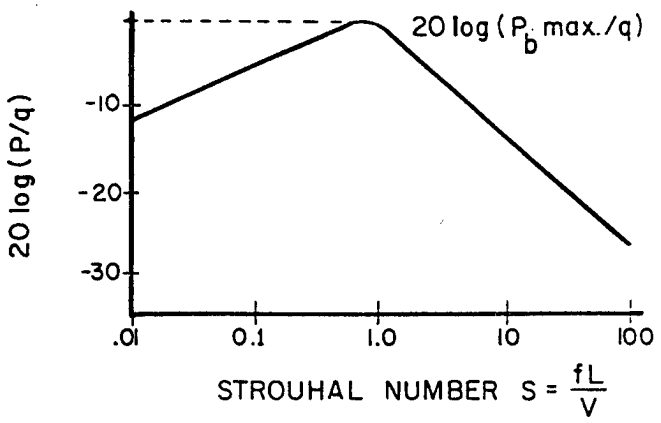

Another semiempirical prediction method was recently developed by Bauer and Dix (9). They utilized the Rossiter frequency equation but proposed a modified convection term. The amplitudes were based on a response coefficient for each mode which was a function of viscous and wave damping. The results of their effort are somewhat lacking because the predictions do not agree well with data and their predicted overall acoustic level is below the level of the resonant modes. This is totally incorrect. Figure 3 is an

example of a comparison of their prediction method (CAP code) with data. The disagreement is clearly evident. Until this method is further refined, it is not recommend.

2.3 SUPPRESSION

Literally hundreds of passive suppression concepts have been tested for their effectiveness in controlling the acoustic environment in open cavities. Tests with small scale wind tunnels up to full size aircraft have been conducted. Water table tests have been effective in evaluating a large number of devices. Rossiter (3) in 1966 concluded that the acoustic environment could be suppressed by placing a small spoiler ahead of the cavity. Heller and Bliss (10) tested a large number of suppression concepts which included both leading edge and trailing edge devices. Figure 4 shows their four most successful concepts and Figure 5 illustrates the typical level of suppression they achieved. Shaw (11) presented full scale F-111 weapon bay acoustic suppression results. The concepts tested were a leading edge sawtooth spoiler, leading edge 45 degree spoilers, and a 45 degree rear bulkhead ramp. An effective suppression for the 45 degree leading edge spoilers is shown in Figure 5 and is noted to be 24 dB for the peak one-third octave bond. The other devices were not as effective as the 45 degree leading edge spoiler. Tipton (12) documented data from the B-1A weapons bay with and without suppressers. The effectiveness of a porous leading edge spoiler is demonstrated in Figure 6. The modal tones are greatly reduced or eliminated and the broadband level is also reduced by 15 dB. However, suppression data were obtained at a wide range of Mach numbers and the effectiveness of the leading edge spoilers was observed to decrease at higher Mach numbers. This trend is shown in Figure 7. It points out the need for a better suppression technique which is effective at all speeds. Shaw et al (13) also documented the small Mach number range which a suppresser is effective in as shown in Figure 8. If a suppresser is actively controlled it then can be made to be effective at a much wider range of Mach numbers. Current research is addressing the possibility of utilizing an active suppression concept for application to the aircraft weapons bay problem. Concepts such as leading edge oscillating flaps, leading edge pulsed air jet, tunable Helmholtz resonators, oscillating walls, upstream surface excitation, and acoustic excitation are being considered. Figure 9 shows a sketch of an active flap concept recently tested. The results for the active flap are shown in Figure 10. It is evident that significant suppression is realized at all Mach numbers but different flap positions and frequencies are required for each Mach number. In the same test a high frequency tone generator, as shown in Figure 11, was tested. It excited the shear layer at a frequency above the resonant frequency. The effectiveness of it is shown in Figure 12. The resonant tones are suppressed and the broadband levels are suppressed as well. Similar success was had for other Mach numbers and configurations. Active Helmholtz resonators were evaluated and shown to be effective. The model and a

typical spectrum is given in Figure 13. The resonant tone is reduced but the broadband levels are not effected.

3. AEROELASTICITY - BUFFET AND LCO

3.1 BACKGROUND

The buffet or aerodynamic excitation associated with separated flow is normally broad-band random fluctuations with predominant frequencies associated with the air flow properties of the aircraft (e.g. vortex flow from inlets and sharp corners, wakes behind pods or other components of the aircraft). The buffeting, or structural response to buffet, can result in large oscillatory responses at resonant frequencies of the aircraft. A good review of the general principles of the buffet problem including the basic features of the fluctuating pressures and the response of the flexible aircraft structure is given by Jones (14). The effects of buffeting and other transonic phenomena on maneuvering aircraft were the subject of a study of an AGARD Working Group (15). Lamar (16) summarized this study and documented the comprehensive state-of-the-art review of buffet techniques and prediction methods by the Working Group. Another assessment of dynamic loads due to flow separation is reported by Mabey (17).

Current fighters are required to maneuver at elevated loading conditions and are experiencing structural problems due to buffet on aft components of the empenage, in particular vertical tails. The ability to accurately predict the buffet on a vertical is difficult due to the complexity of the interaction between the aircraft geometry, flow field, vortex trajectory and empenage structure. In the past, the dynamic buffet loads have been estimated from model tests by means of scaling procedures. References 18,19, and 20 report buffet testing on the F-15, F/A-18, and F-111 TACT aircraft.

Limit Cycle Oscillation (LCO) is an aeroelastic problem involving the interaction of the structural response with the highly nonlinear aerodynamic forces. An example of the nonlinear aerodynamic phenomena is incipient leading edge separation where small oscillations of the surface can drive the flow from attached to separated to attached, etc. A similar example exists for shock induced trailing edge separation. LCO is a common problem on fighters carrying external stores and limits performance for many store configurations (21).

3.2 BUFFET TESTS

In 1981, buffeting pressure measurements were made on the vertical tail surfaces of a 13 percent F-15 model (18). The test variables included dynamic pressure, angle of attack, vertical tail incidence and rudder deflection. The pressures and associated vibration response levels reached a maximum at approximately 22 degrees angle of attack.

The flow field characteristics in the vicinity of the vertical tail were investigated and are shown in Figure 14. In an in-house program, a 4.7 percent F-15 model with one flexible and one rigid vertical tail is being tested to obtain buffet data and to evaluate suppression concepts. The first entry (Oct. - Nov. 1995) will evaluate blowing concepts to control the buffet and reduce the response of the flexible tail. Three tangential blowing ports (nose, gun bump, and inboard leading edge of the wing) are being used. A second entry is scheduled in 1996 to evaluate the use of piezoelectric actuators for buffet suppression.

The vortical flow pattern on the F/A-18 aircraft at high angle of attack is shown in Figure 15. The burst vortex travels aft and upward, impinging on the vertical tail and causes very high dynamic loads. A full-scale F/A-18 aircraft, shown in Figure 16, was tested in the National Full Scale Aerodynamic Complex 80 by 120 Foot wind tunnel at NASA Ames. Buffeting pressures and the resulting structural response of the vertical tails were obtained over a range of angle of attack and sideslip conditions (22). The tests were conducted with and without the Leading-Edge-Extension (LEX) fences (installed to reduce the buffet loads). Currently the Structural Dynamics Branch of Wright Laboratory is supporting a NASA Langley buffet test on a 16 percent scale F-18 model. This support involves instrumentation from the full scale test at Ames, data acquisition equipment, and technical support. Three different suppression concepts are being evaluated (existing rudder, oscillating cylinder, and piezoelectric actuators).

Under a Phase II SBIR (Small Business Innovative Research) contract, Active Control eXperts (ACX) is developing a buffet load alleviation control system for an F/A-18 Under this contract the suppression system will be demonstrated by ground tests on a full scale vertical tail.

3.3 UNSTEADY PRESSURE TESTS

A wind tunnel test program was conducted to investigate the unsteady aerodynamic aspects of transonic Limit Cycle Oscillations (LCO) on fighter type aircraft. This program was a cooperative effort between Lockheed Fort Worth and the National Aerospace Laboratory (NLR) in the Netherlands and was funded by the Air Force and the Dutch Ministry of Defense. Two tests were conducted, a wing body configuration and a simple wing-strake configuration. The first test was conducted with the wing body configuration (Figure 17) to obtain unsteady pressures and forces necessary for identifying the transonic nature of LCO encountered on fighters with external stores. The wing panel was oscillated in pitch at amplitudes and frequencies typical of LCO. Unsteady pressure data was measured at the pressure sections shown in Figure 17. In addition to providing a detailed set of pressure data for code validation, the test provided aerodynamic time lag and damping characteristics needed to perform LCO calculations.

The simple wing-strake configuration used the wing panel from the LCO test and a strake section which was attached to and moved with the wing. This wing-strake (Figure 18) was oscillated in pitch at various amplitudes and frequencies. The test Mach numbers were 0.225, 0.6, and 0.9. The objectives were to understand the physics of high incidence unsteady flow and to provide steady and unsteady pressure data for validation of CFD codes(23). In order to better understand the flow fields that produced this data, an ongoing investigation will determine the flow field characteristics for limit cycle oscillations and transonic high alpha flow over the oscillating straked wing. Figure 19 shows the location of the light sheets for the clean wing. The locations were chosen to correspond to the pressure measurement stations and one along the vortex core. The issues of turbulence structure for buffeting and transonic pitching moment anomalies at high incidence will be addressed with this configuration. A tip launcher and tip store will be added to address tip store geometry effects and store effects on wing flow fields. The light sheet locations for this configuration is shown in Figure 20. The detailed pressure data and the associated flow field data from this test can be used to improve the prediction of various nonlinear phenomena associated with aircraft flight at transonic speeds.

3.4 LCO PREDICTION METHOD

A semi-empirical method (21) was developed specifically for F-16 LCO prediction. Under a new Wright Laboratory contract, Lockheed Fort Worth will develop a generic method for predicting nonlinear aeroelastic characteristics of wing type surfaces. The generic method will be validated on subsonic LCO, transonic LCO (shock induced separation), and buffet (ventral fin).

3.5 COMPUTATIONAL AEROELASTICITY

The advances in computer technology and the emerging Computational Fluid Dynamics (CFD) methods are providing a computational aeroelasticity capability. The ENS3DAE (Euler/Navier-Stokes 3 Dimensional AEroelastic) code (24) has been extended and improved to provide a general aeroelastic capability for complex configurations. The aerodynamic analysis procedure in ENS3DAE uses an implicit finite difference algorithm to integrate the Navier-Stokes equations. The equations are solved using a fixed time step for time-accurate cases and a spatially varying time step for steady-state computations. The linear structural dynamics equations of motion are integrated using an explicit predictor-corrector scheme. This code has been validated for steady aerodynamics , unsteady aerodynamics (pitching wing), and static aeroelastic calculations. Validation of the dynamic aeroelastic capability is underway.

An aeroelastically tailored fighter wing/body configuration (Figure 21) is shown to demonstrate the static aeroelastic capability of the code. Figure 22 shows the calculated

(rigid and flexible) and the measured pressure distribution at approximately midspan of the wing for a Mach number of 0.9 and an angle of attack of 9 degrees. As shown by the figure, the flexibility of the wing must be included for accurate pressure calculations. The computed and measured twist distribution is shown in Figure 23. The F-15 wind tunnel model (18) is being used to evaluate the new version of the ENS3DAE code. The calculations will be performed at a Mach number of 0.3 and alpha of 12 degrees. The pressure distribution and the dynamic response of the vertical tail will be calculated and compared with test data. Additional applications of this code is needed to further validate it and to determine its range of applicability for computing dynamic loads on twin tail configurations.

4. CONCLUDING REMARKS

Experimental programs are underway by several organizations to evaluate concepts to control or suppress weapons bay acoustics, buffet, and limit cycle oscillations. Computational efforts are also being conducted but lag the experimental work because of the complex nature of the nonlinear aerodynamics involved. Additional research is needed for computational aeroacoustics and computational aeroelasticity. Further testing of promising active concepts are needed to develop an active suppression system for weapons bay acoustics

5. REFERENCES

1. Roshko, A. "Some Measurements of Flow in a Rectangular Cutout," N.A.C.A. Tech. Note 3488, 1955.

2. Krishnamurty, K., "Acoustic radiation From Two-Dimensional Rectangular Cutouts in Aerodynamic Surfaces," N.A.C.A. Tech. Note 3487, 1955.

3. Rossiter, J.E., "Wind Tunnel Experiments on the Flow Over Rectangular Cavities at Subsonic and Supersonic Speeds," Royal Aircraft Establishment, ARC R.&M. No. 3438,1966.

4. Plumblee, H.E., Gibson, J.S., and Lassiter, L.W., "A Theoretical And Experimental Investigation of The Acoustic Response of Cavities In An Aerodynamic Flow," WADD -TR- 61- 75, March 1962.

5. Smith, D.L., and Shaw, L.L., "Prediction of The Pressure Oscillation In Cavities exposed to Aerodynamic Flow," AFFDL-TR-75-34, Oct 1975.

6. Shaw, L.L., and Smith D.L., "Aeroacoustic Environment of A Store in an Aircraft Weapons Bay," AFFDL-TR-&&-18, Mar 1977.

7. Shaw, L.L., "Suppression of Aerodynamically Induced Cavity Oscillations," AFFDL-TR-79-3119, Nov 1979.

8. Betry, M.R., and Rohrer , L.A., "Literature Survey of Aircraft Cavity Flow," AFWAL-TR-83-160-FIMM, May 1982.

9. Bauer, R.C., and Dix, R.E., "Engineering Model of Unsteady Flow In A Cavity," AEDC-TR-91-17, Dec 1991.

10. Heller, H. H., and Bliss, D.B., " Aerodynamically Induced Pressure Oscillations in Cavities-Physical Mechanisms and Suppression Concepts," AFFDL-TR-74-133, Feb 1975.

11. Shaw, L. L., "Full Scale Flight Evaluation of Suppressions Concept For Flow-Induced Fluctuating Pressure In Cavities," AIAA-82-0329, January, 1982.

12. Tipton, A.G., "Weapon Bay Cavity Noise Environment Data Correlation and Prediction For The B-1 Aircraft," AFWAL-TR-80-3050, June, 1980.

13. Shaw, L.L., Bartel, H., and McAvoy, J., "Prediction and Suppression of the Acoustic Environment in Large Enclosures With a Small Opening Exposed to Aerodynamic Flow" AIAA-82-0121, January, 1982.

14. Jones, J. G., "Dynamic Response of Aircraft with Fluctuating Flow Fields", Von Karmon Institute For Fluid Dynamics Lecture Series 1981-4 on Unsteady Airloads and Aeroelastic Problems in Separated and Transonic Flow, March 1981.

15. "Effects of Buffeting and Other Transonic Phenomena on Maneuvering Combat Aircraft", AGARD Advisory Report No. 82, July 1975.

16. Lamar, W. E., "Effects of Buffeting and Other Transonic Phenomena", AGARD Conference Proceedings No. 187 on Flight/Ground Testing Facilities Correlation, April 1976.

17. Mabey, D. G., "Some Aspects of Aircraft Dynamic Loads Due to Flow Separation", Royal Aircraft Establishment Tech Memo Aero 2110, July 1987.

18. Triplett, W. E., "Pressure Measurements on Twin Vertical Tails in Buffeting Flows", AFWAL-TR-82-3015, April 1982.

19. Zimmerman, N. H., Ferman, M. A., and Yurkovich, R. N., "Prediction of Tail Buffet Loads for Design Application", AIAA-89-1378 presented at AIAA Structures Structural Dynamic and Material Conference, Mobile, Alabama, April 1989.

20. Coe, C. F. and Cunningham, A. M., Jr., "Predictions of F-111 TACT Aircraft Buffet Response and Correlation of Fluctuating Pressures Measured on Aluminum and Steel Models and the Aircraft", NASA CP 4069, May 1987.

21. Meijer, J. J. and Cunningham, A. M., Jr., "A Semi-Empirical Unsteady Nonlinear Aerodynamic Model to Predict Transonic LCO Characteristics of Fighter Aircraft", AIAA-95-1340 presented at the 36th Structures, Structural Dynamics, and Materials Conference, New Orleans, LA, April 1995.

22. Pettit, C., Banford, M., Brown, D., and Pendleton, E., "Pressure Measurements on an F/A-18 Twin Vertical Tail in Buffeting Flow", WL-TM-94-3039, August 1994.

23. Cunningham, A. M., Jr. and den Boer, R. G., "Overview of Unsteady Transonic Wind Tunnel Test on a Semispan Straked Delta Wing Oscillating in Pitch", WL-TR-94-3017, August 1994.

24. Schuster, D. M., Vadyak, J., and Atta, E. H., "Flight Loads Prediction Methods for Fighter Aircraft", WRDC-TR-89-3104, November 1989.

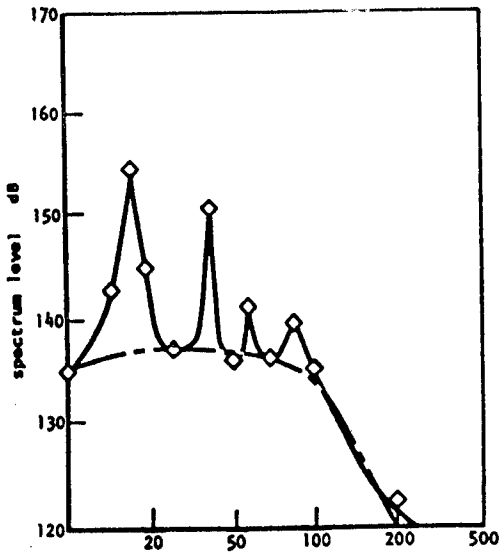

Fig 1 Full scale B-1A weapons bay acoustic levels for Mach number 0.7 at 20,000 feet

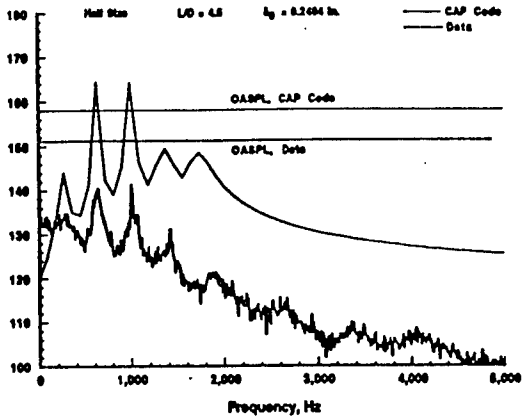

Fig 3 Comparison of Cavity Acoustic Pressure (CAP) code with Mach 0.6 Data (Ref 9)

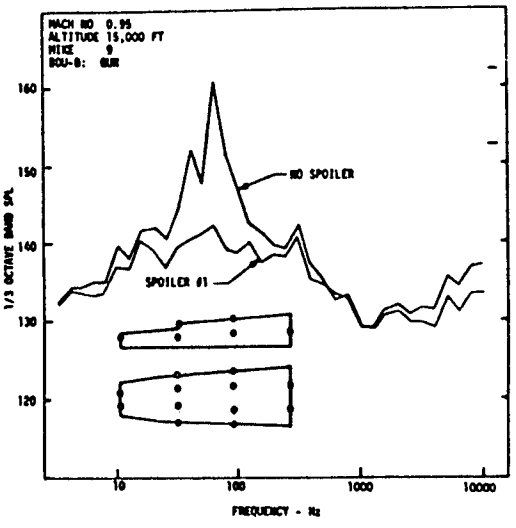

Fig 2 Full scale F-111 weapons bay spectra

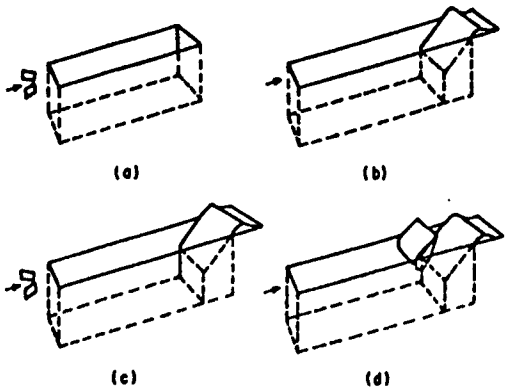

Fig 4 Four most promising suppression concepts (Ref 6)

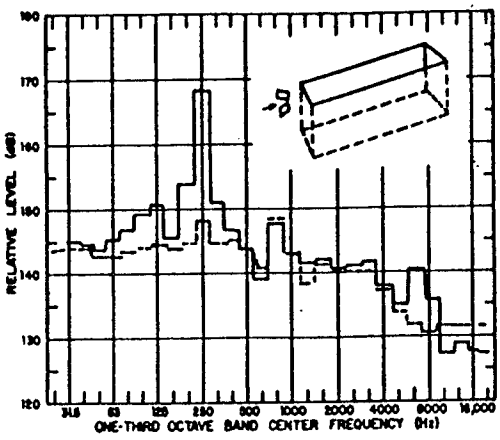

Fig 5 Example suppression of leading edge spoilers (Ref 6)

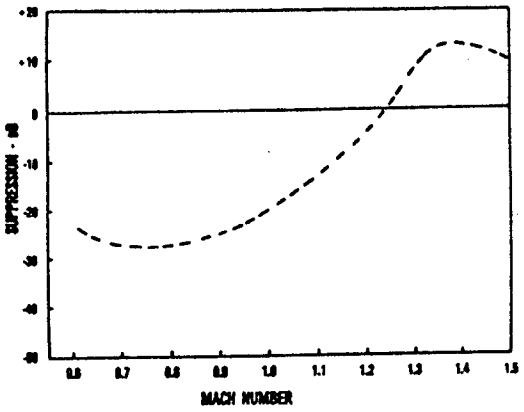

Fig 7 Variation of suppressor effectiveness with Mach number (Ref 12)

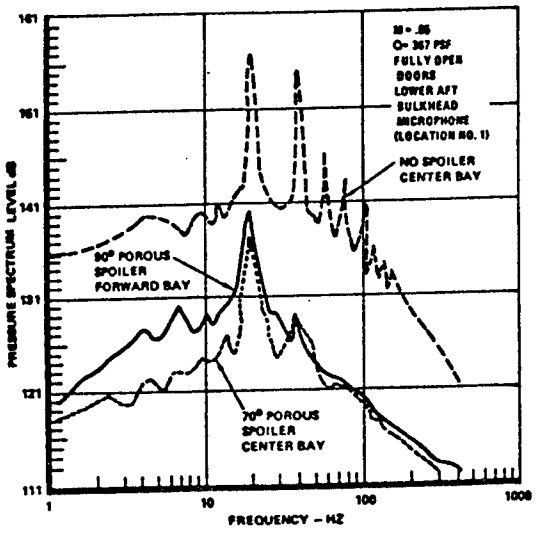

Fig 6 Forward and center bay acoustic levels (Ref 12)

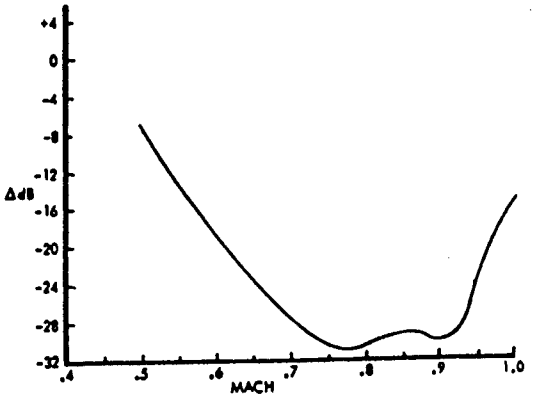

Fig 8 Optimized Suppression of Maximum Oscillation (Ref 13)

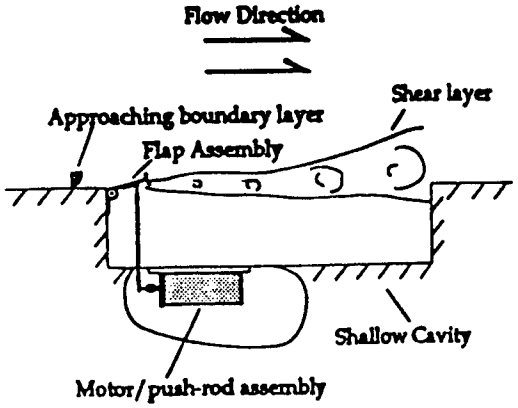

Fig 9 Sketch of recently tested active flap acoustic suppressor

Mach Number	Deflection Mag.	Neutral Height	Cavity Depth	Flap Freq.
0.6	.08°	-.03°	1.1°	29.68
0.8	.03°	0.00°	0.6°	20.01
1.5	.09°	0.00°	1.6°	4.38
1.9	.06°	0.00°	1.1°	4.57

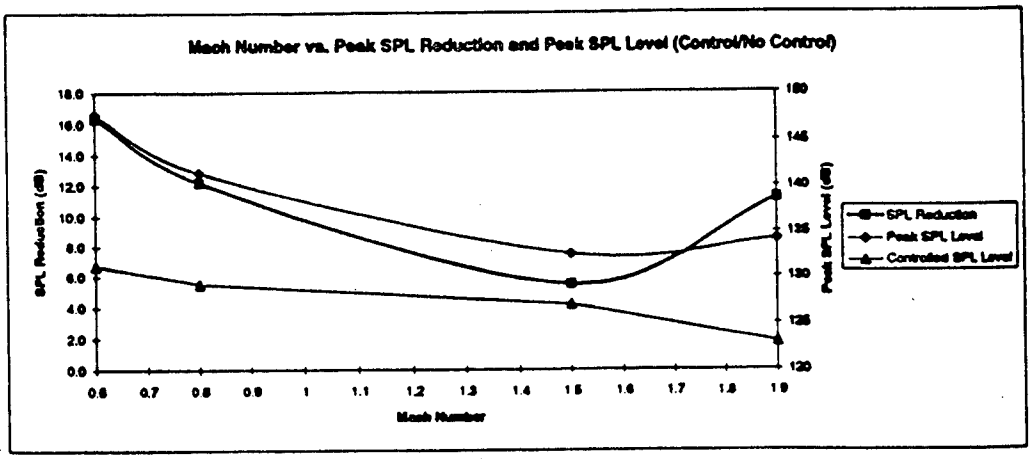

Fig 10 Summary of Results for the Active Flap

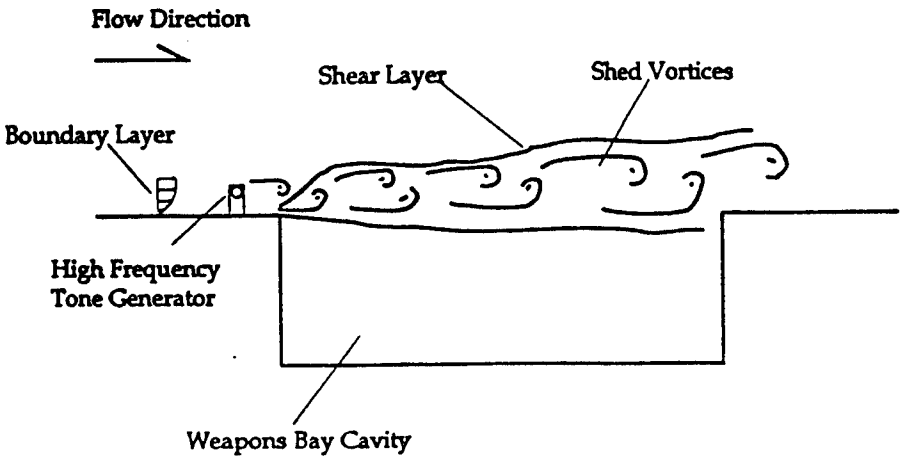

Fig 11 High Frequency Tone Generator

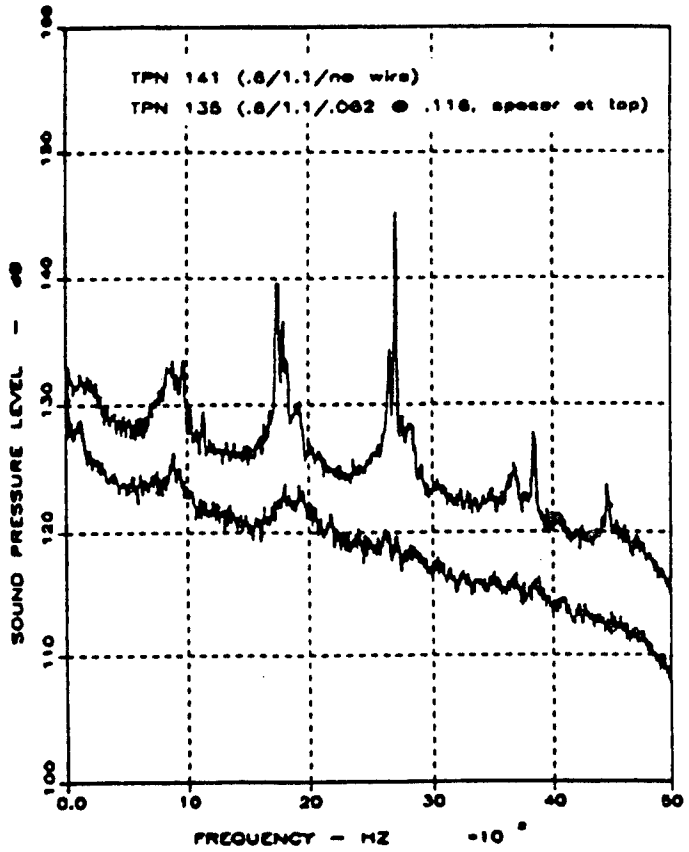

Fig 12 Results of The High Frequency Tone Generator

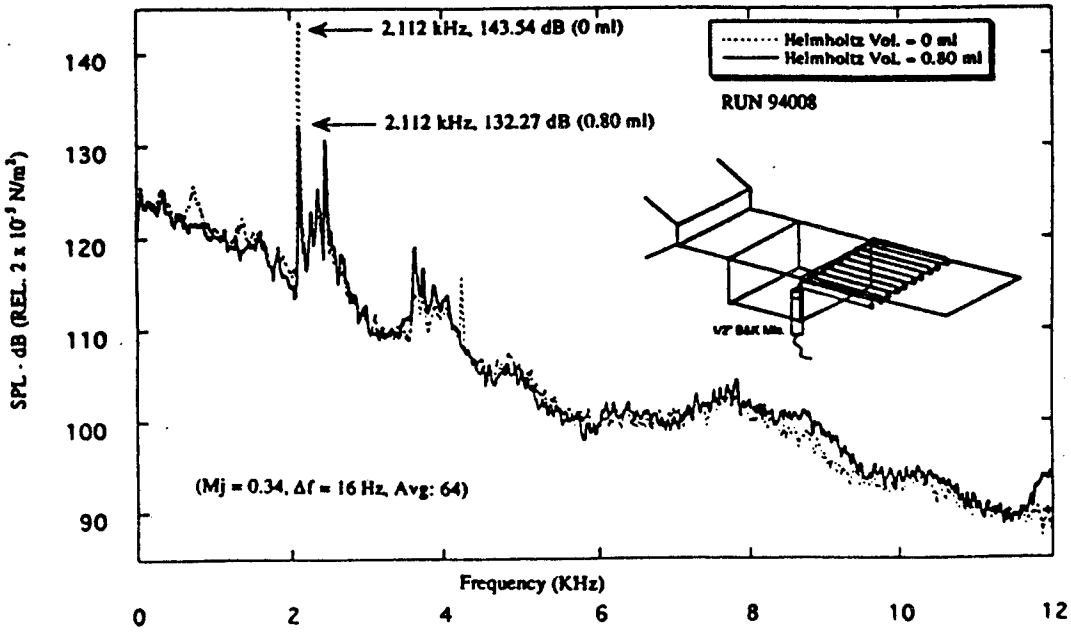

Fig 13 Helmholtz Resonator Model and Spectrum

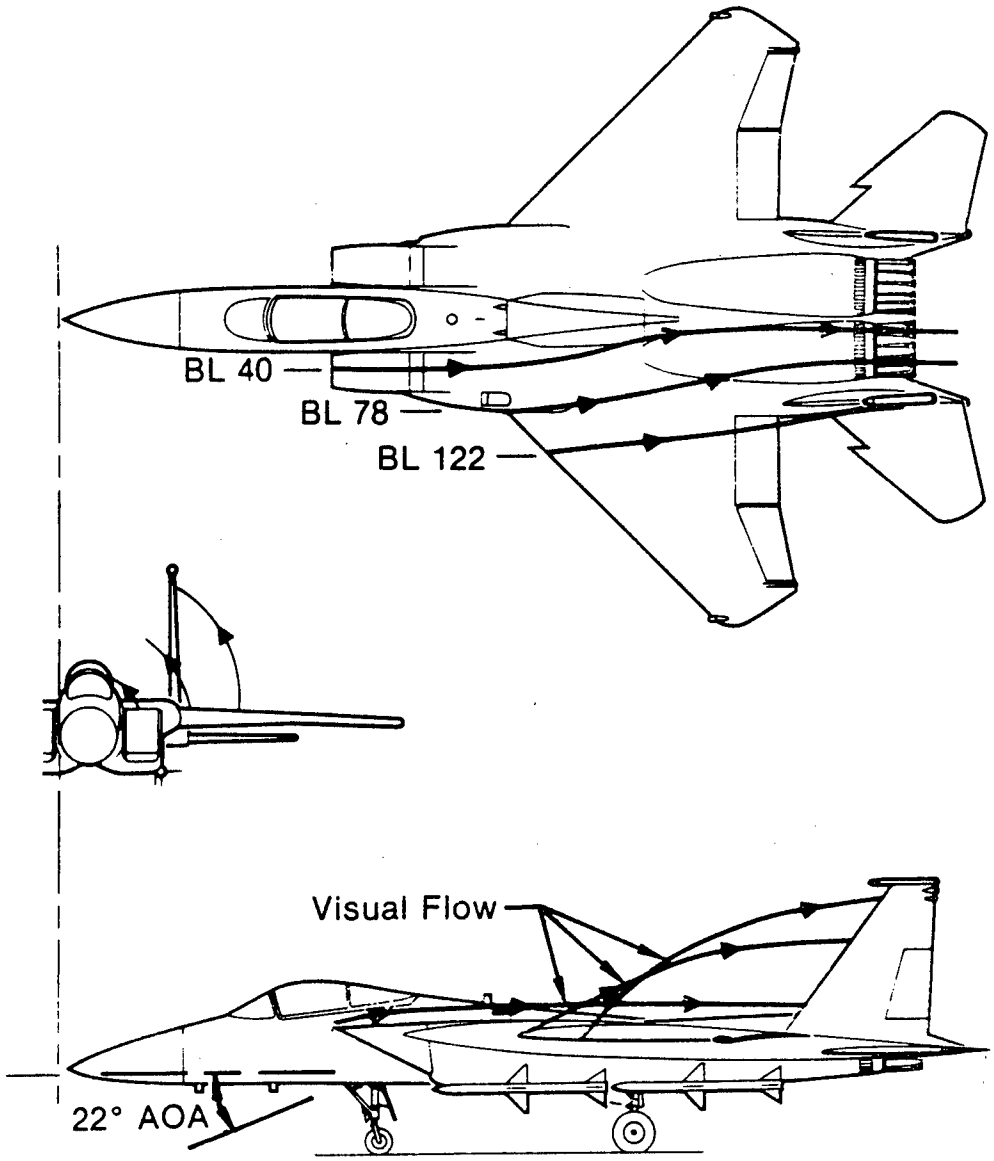

Fig 14 Vertical Tail Flowfield Characteristics at $\alpha = 22°$

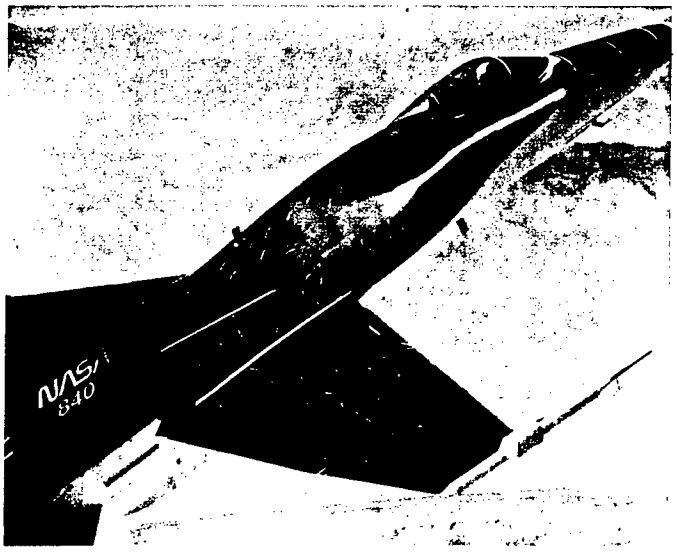

Fig 15 Vortex Flow Pattern of F/A-18

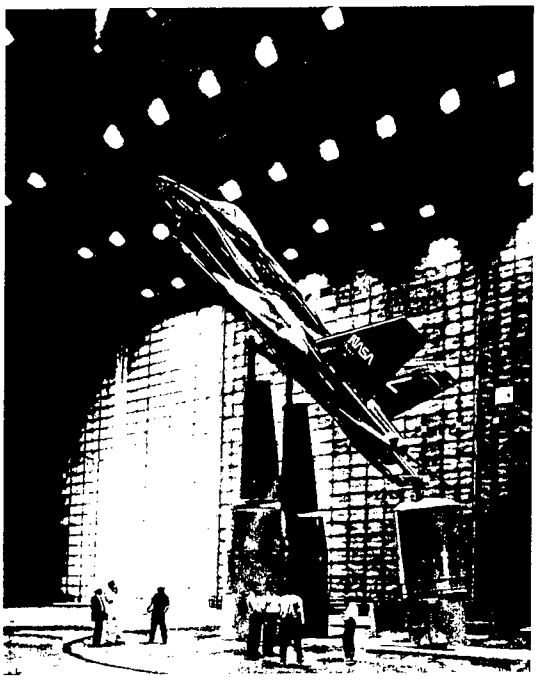

Fig 16 F/A-18 Aircraft in 80 x 120 Foot Wind Tunnel

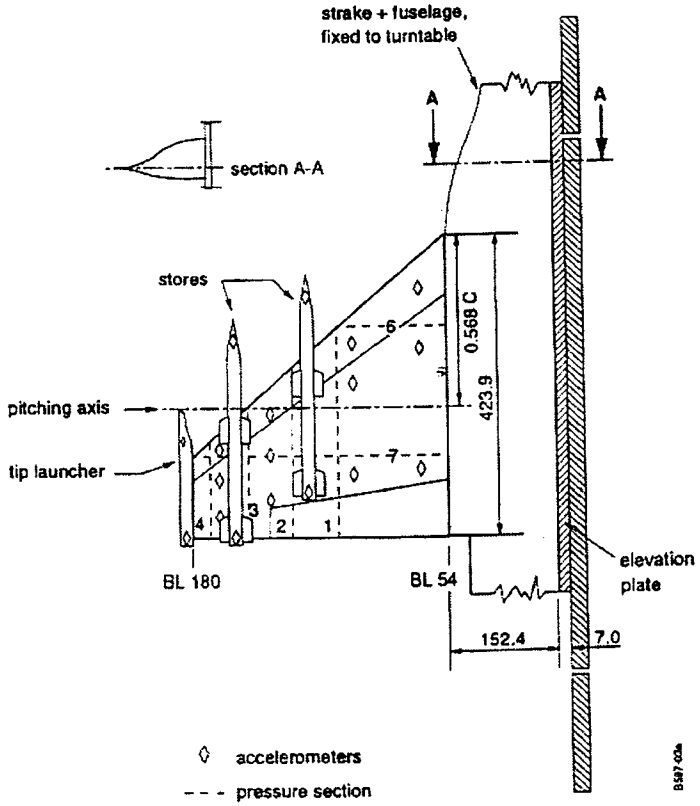

Fig 17 F-16 Wing/Store Model

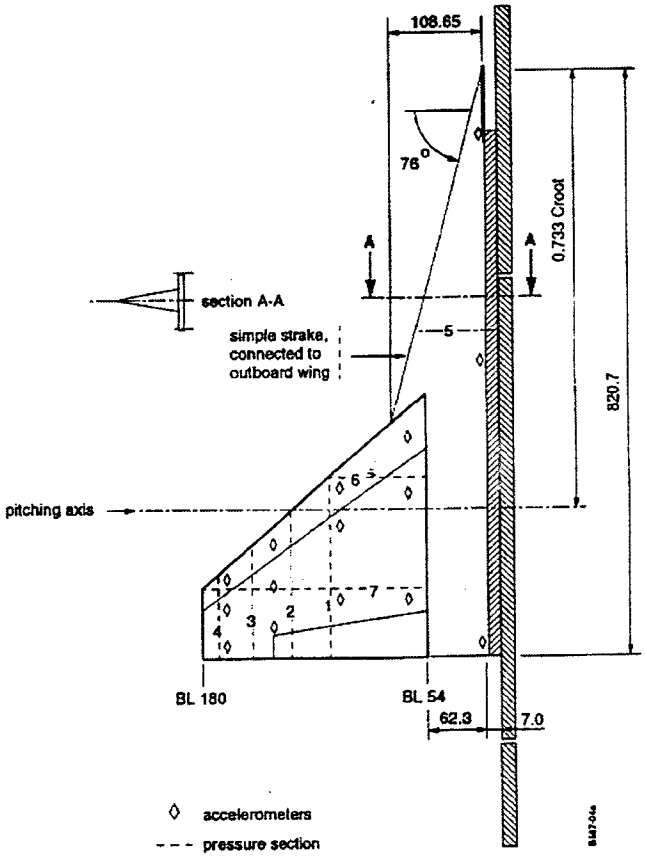

Fig 18 Simple Straked Wing Model

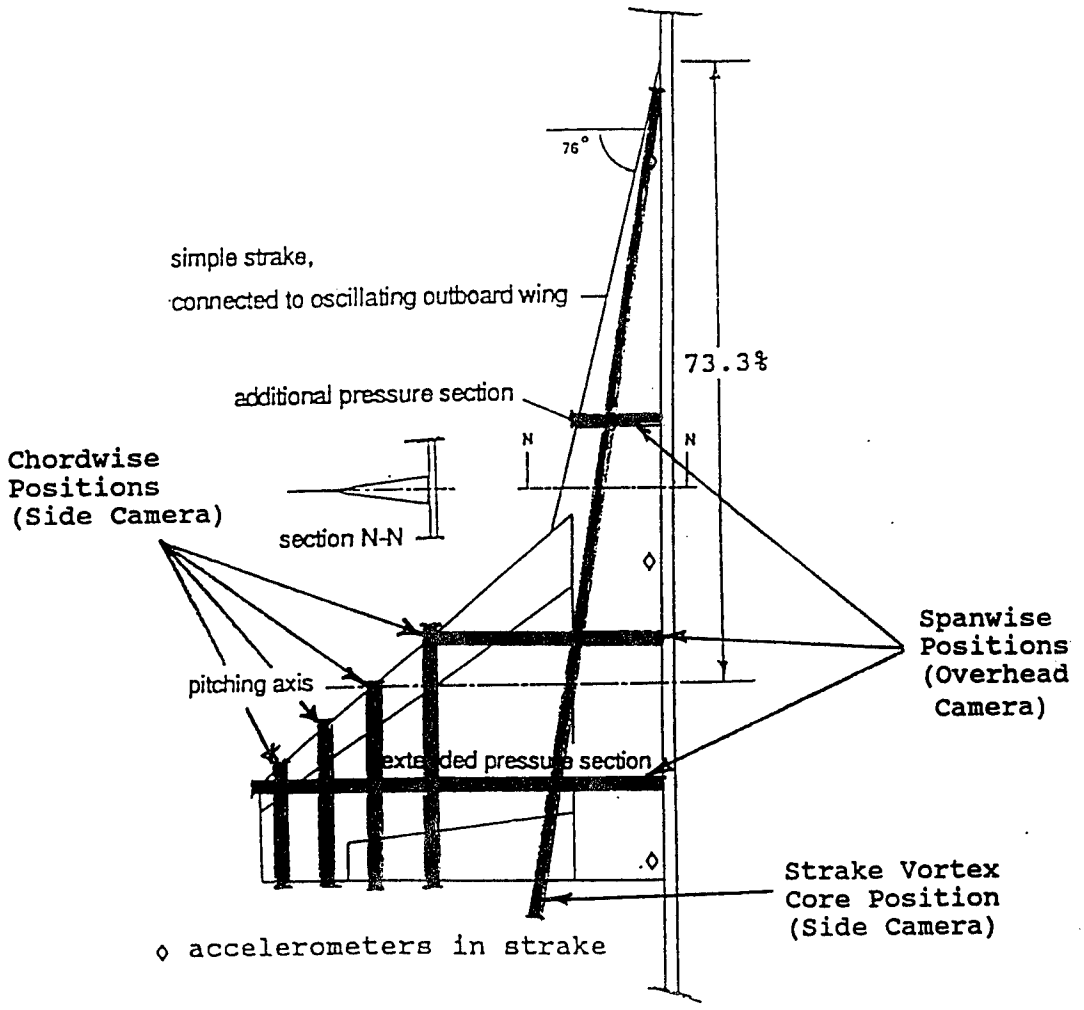

Fig 19 Clean Wing Light Sheet Locations

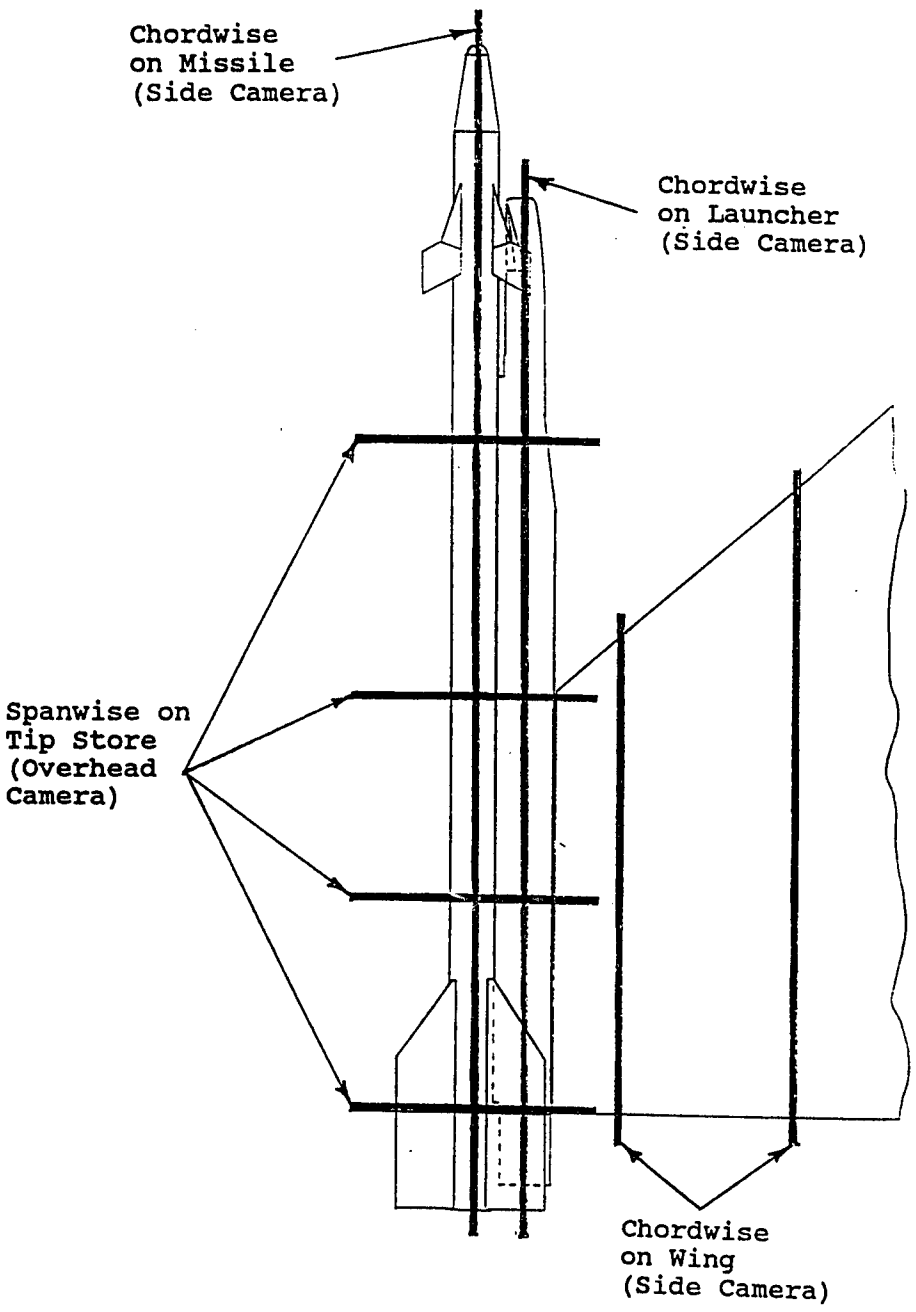

Fig 20 Tip Store Configuration Light Sheet Locations

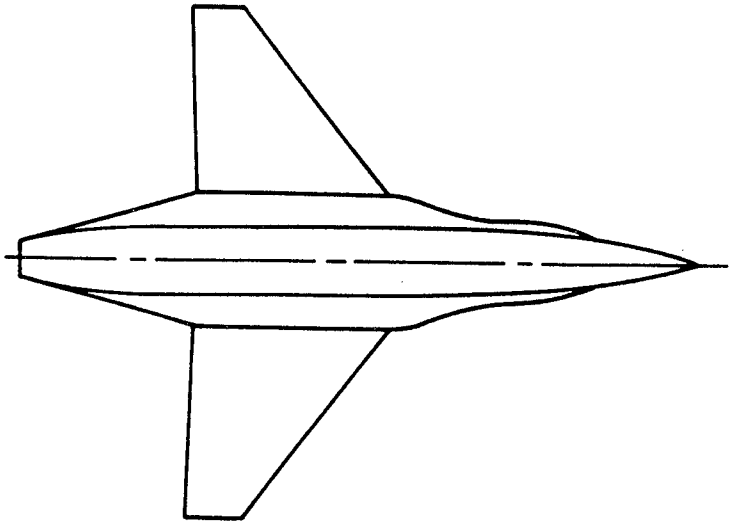

Fig 21 Aeroelastically Tailored Wing/Body Configuration

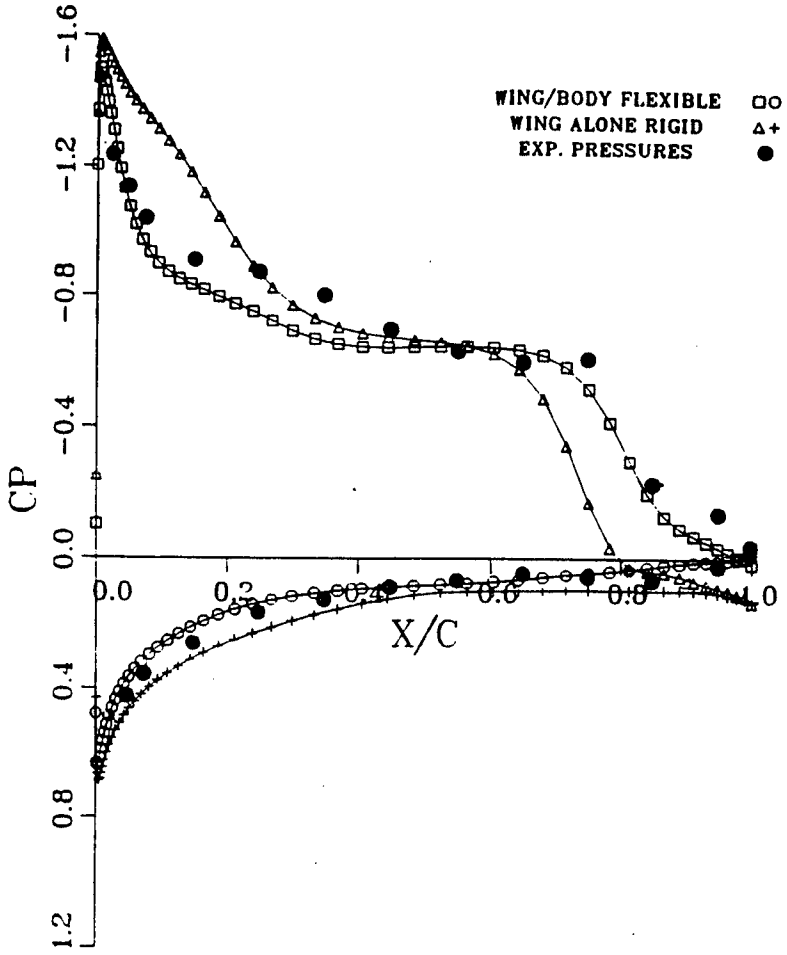

Fig 22 Computed and Experimental Pressures for an Aeroelastically Tailored Configuration (M = 0.9 and α = 9°)

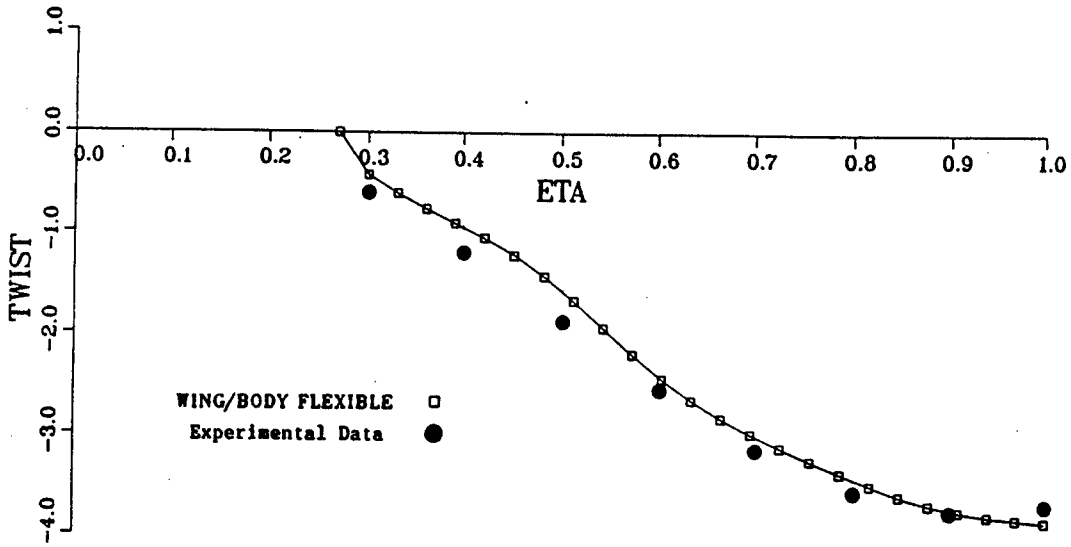

Fig 23 Aeroelastic Twist Correlation

P-3C Fatigue Tracking Methodology Update

Dr. Margery E. Hoffman
Naval Air Warfare Center, Warminster, PA 18974-0591
Mr. Nam D. Phan
Naval Air Systems Command, Arlington, VA 22243-5120
Mr. Arnold E. Anderjaska
AeroStructures, Inc., Arlington, VA 22202-4108

ABSTRACT

A service life assessment program, (SLAP) was recently completed to appraise the service life of the US Navy's P-3C aircraft. As part of this effort an interim fatigue tracking algorithm was developed to improve the accuracy of the current tracking system, and provide better service life projection. The program will culminate with the installation of a new multi-channel recorder, the AN/ASH-37, also known as the Structural Data Recording Set (SDRS), on every P-3C. The original tracking methodology used the individual aircraft's mission mix but load spectra were based on average usage at the time the system was developed. The interim methodology incorporates current individual aircraft usage data such as vertical acceleration (Nz) from the accelerometer reports. The missions and new flight segments, or points-in-the sky (PITS), were redefined based on an instrumented flight loads survey and an extensive fleet paper survey. The aircraft loads were updated to better correlate with the original flight and ground test data. A sequence accountable local strain approach was also used to calculate the accumulated fatigue damage. A future tracking system will incorporate the SDRS data to provide better individual usage tracking information. With more accurate fatigue life expended (FLE) estimates, preemptive corrective actions can be instituted in a timely manner to ensure safety and maintain fleet operational readiness.

INTRODUCTION

The current economic climate of diminishing resources highlights the need for better fleet management. Improvements in fleet management are necessary to maintain the existing airframe longer than originally planned. With better tracking of usage, more accurate fatigue life estimates and pro-active corrective actions can be made in a timely manner. The individual aircraft fatigue tracking program is performed by the US Navy as an input to optimize fleet management.

In 1990, the US Navy initiated a service life assessment program (SLAP) to estimate the structural fatigue life for the P-3C aircraft. As part of this effort, an interim tracking program was developed using improved fatigue methodology and current mission usage data. The accuracy of the fatigue estimates were improved by making use of available flight and usage information for individual P-3C aircraft.

This paper describes the interim P-3C fatigue tracking methodology that was used to re-baseline the current FLEs and produce incremental fatigue damage rates for the Navy's Structural Appraisal of Fatigue Effects (SAFE) quarterly reports until the SDRS installations are complete.

APPROACH

Major technical aspects of the P-3C fatigue life algorithm were evaluated and improved, where possible, for the interim fatigue tracking program. The primary improvements are:

a. correlated maneuver and taxi loads based on the original structural demonstration flight and taxi tests.

b. updated missions, mission mixes, and PITS definitions based on the instrumented flight loads and fleet paper surveys.

c. created capability to incorporate accelerometer data where applicable.

d. correlated effective stress concentration factors (Kn's) at critical tracking locations to P-3A full-scaled fatigue test results and/or actual service experience.

e. replaced the stress-based linear damage algorithm with a local strain-based, sequence-dependent fatigue analysis algorithm.

Compatibility with the future Structural Data Recording Set (SDRS) system was considered at every step.

The development of the interim tracking program included reviewing the current tracking locations, re-defining the nominal stress concentration factors and the reference stresses, updating the service spectra, developing the interim fatigue tracking algorithm, and calculating the fatigue life expended (FLE). These topics are described in the Vu-graphs that follow.

SUMMARY

An interim fatigue tracking program was developed for the P-3C aircraft. It uses individual aircraft information for correct sequencing of the missions and the Nz counts, if any, from the individual CAG from monthly reports. The tracking program has been written in a modular code that will allow for later incorporation of data from the SDRS system to further improve the accuracy of the fatigue life estimates. In particular with the SDRS, fuel weight, Mach number, altitude, and time will be recorded when Nz is triggered. The stress coefficients can be used for the PITS associated with the event, making the load calculation more accurate.

ACKNOWLEDGMENTS

This work could not have been performed without significant contributions from Vasile Manea, Suresh Dore, Miguel Morales, Ernie Wang and Nanu Krishnan, all of Aerostructures, Inc. We also wish to thank Mark Thomas of NAWC-Warminster for his review and helpful suggestions on this project.

REFERENCES

Additional information on the SLAP program is written in:

Aerostructures, Inc, Technical Report 91001A, P-3C Fatigue Tracking Methodology Update--1994, Volume II, Fatigue Tracking Update, April 1995.

A summary of the flight loads survey is written in:

Systems & Electronics, Inc., Report SEI-102-89-03, P-3C Aircraft Structural Flight Loads Survey, December 1989.

The flight crew paper survey was conducted fleet-wide by the Naval Air Warfare Center, Aircraft Division, Warminster PA, September 1990 to March 1991.

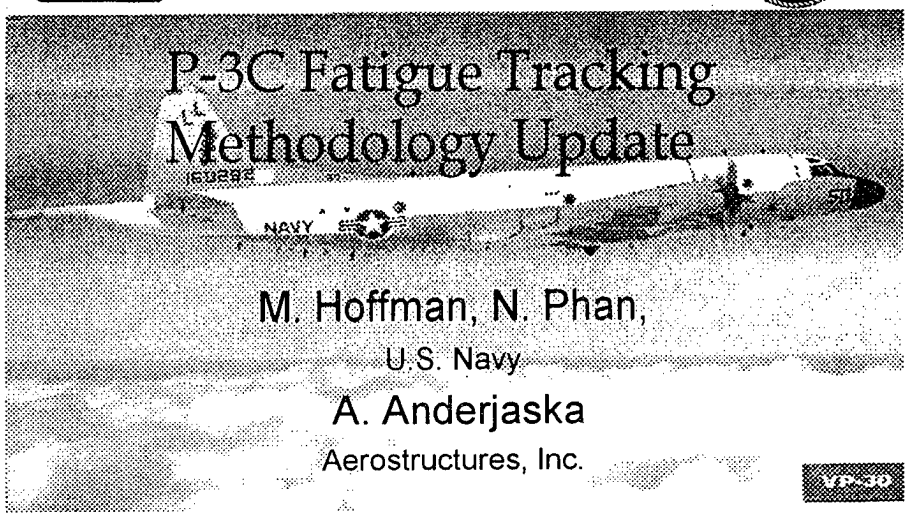

Introduction

- Motivation
  - Service Life Extension
  - Usage Changes
- Highlights of Improvements
  - Calibrated stresses
  - Incorporated CAG, log report data
- Direction
  - Parameter-based SDRS

Lockheed's Algorithm

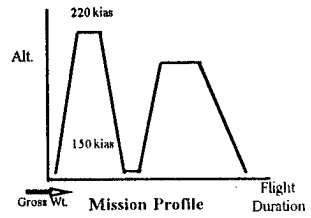

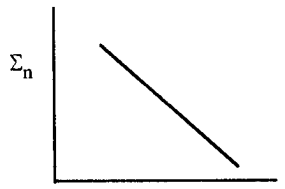

Tracking Spectra

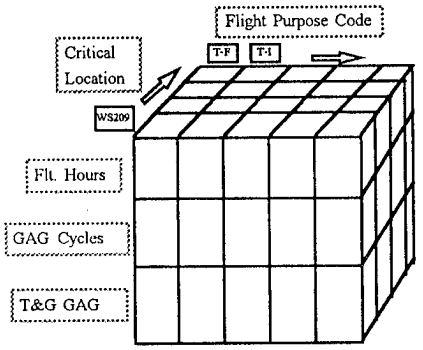

Unit Damage Matrix

APPROACH

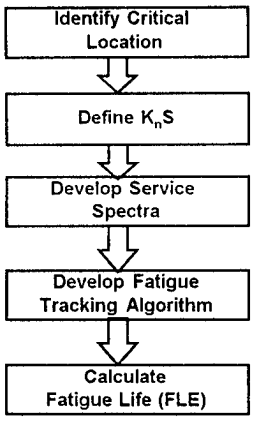

- Full Scale Fatigue Test
- Service Experience
- Analysis

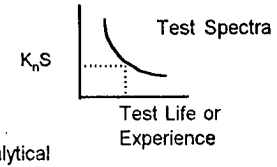

- Loads
  - > FEM/Analytical
- Usage
  - > Flt Survey/CAG data/3M
- Sequenced Stress History
- Local Strain Algorithm

Development of P-3 Tracking Program

Critical Locations

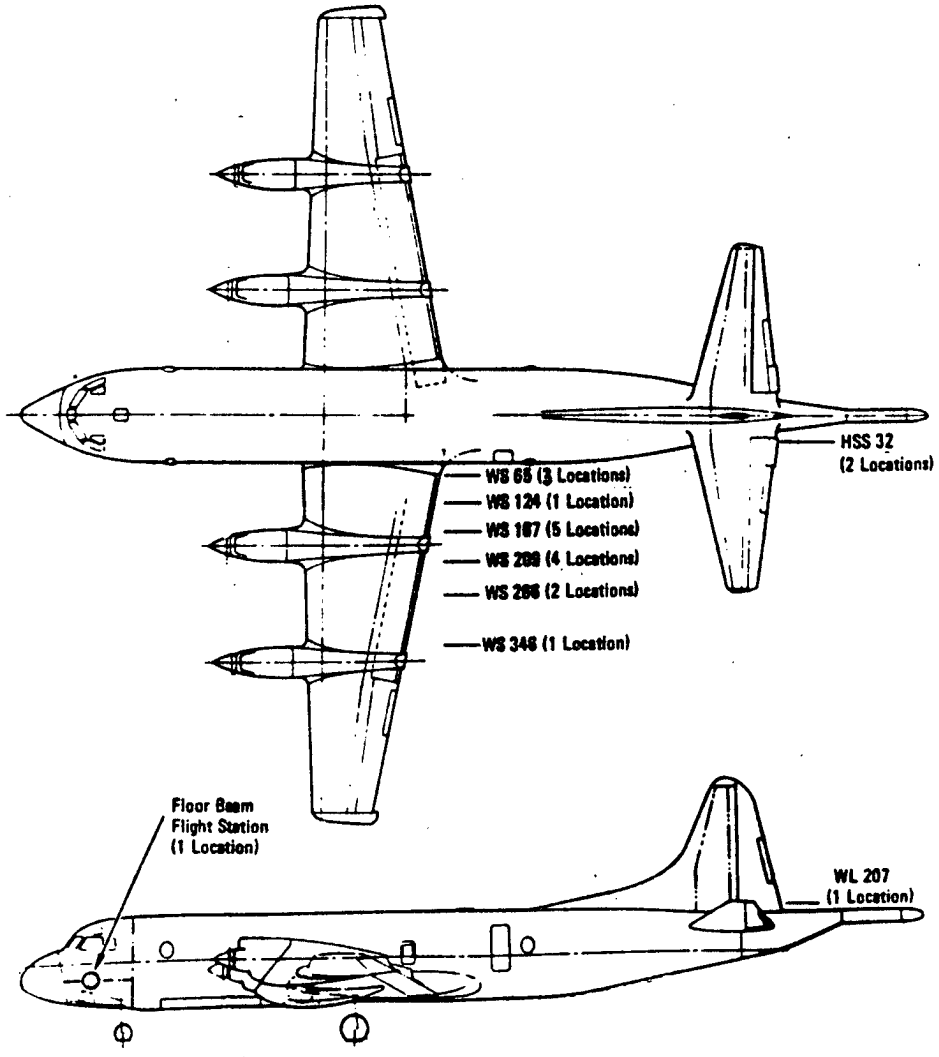

Life Assessment Surveys Mission Definition

- Flight Loads Survey- 1989
  - » Six aircraft- 1900 flight hours
  - » Nz, PITS, mission code
- Air Crew Paper Survey- 1991
  - » The Fleet- 20,000 flight hours
  - » Take-off weights, c.g., mission profiles

Nz Comparisons

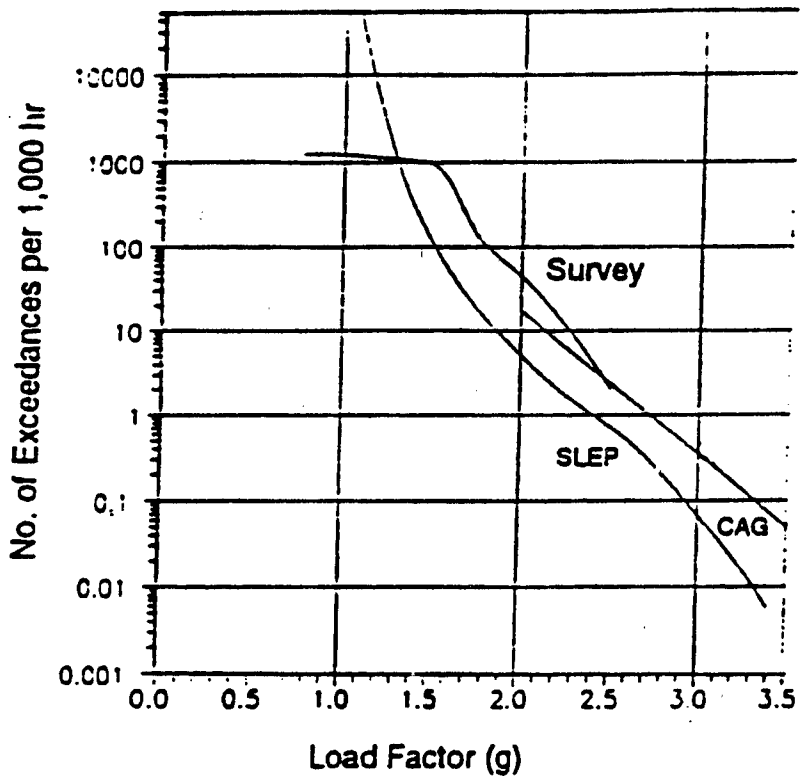

Survey PITS Comparisons

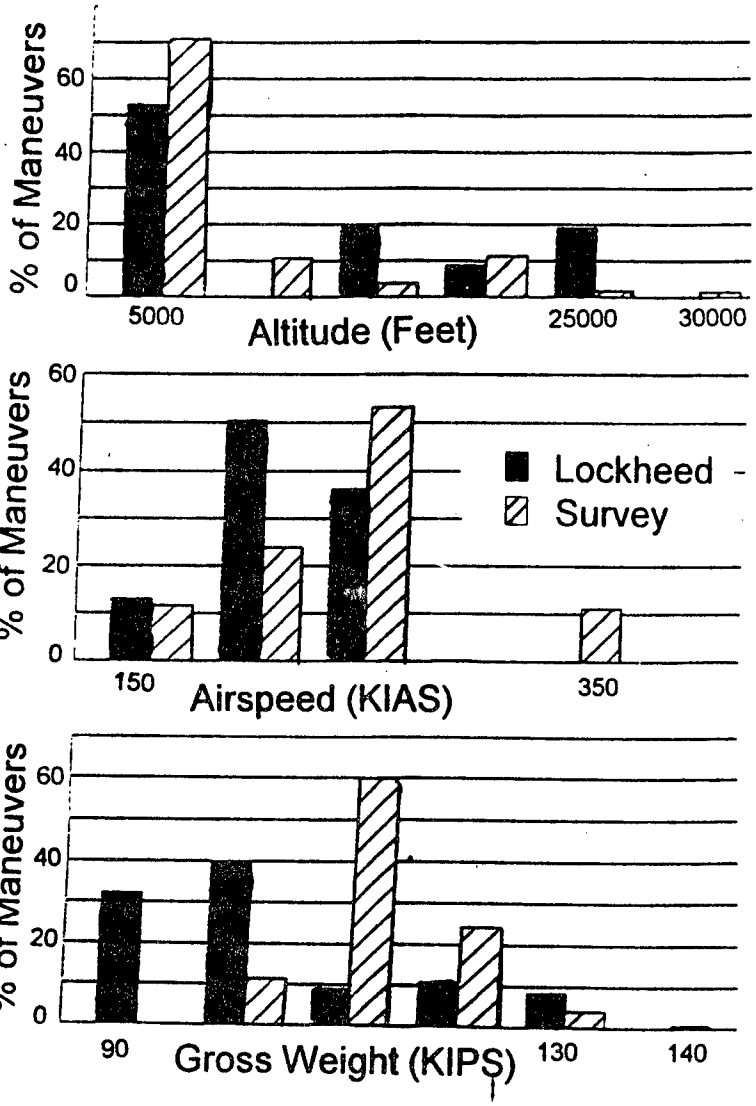

Mission Categories

Description	Training & Proficiency Fundamentals	Training & Proficiency Instrument	ASW Training Offensive ASW	Search & Rescue, Patrol Recon	Ferry Function-al Check Flight
P3-C Category	Training-Fundamentals (T-F)	Training Instrument (T-I)	ASW without Stores (ASW)	Patrol, Search, and Rescue (PSR)	Miscel-laneous (MSC)

Stress Calculation

$$PITS_i = \{GW_i, ALT_i, VEL_i\}$$

$$\sigma_i = g(PITS_i, Nz_i)$$

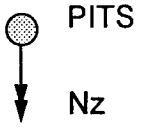

$2g < Nz < 3.5g$ is measured

$Nz < 2g$ and PITS are from survey results

Exceedance Rates

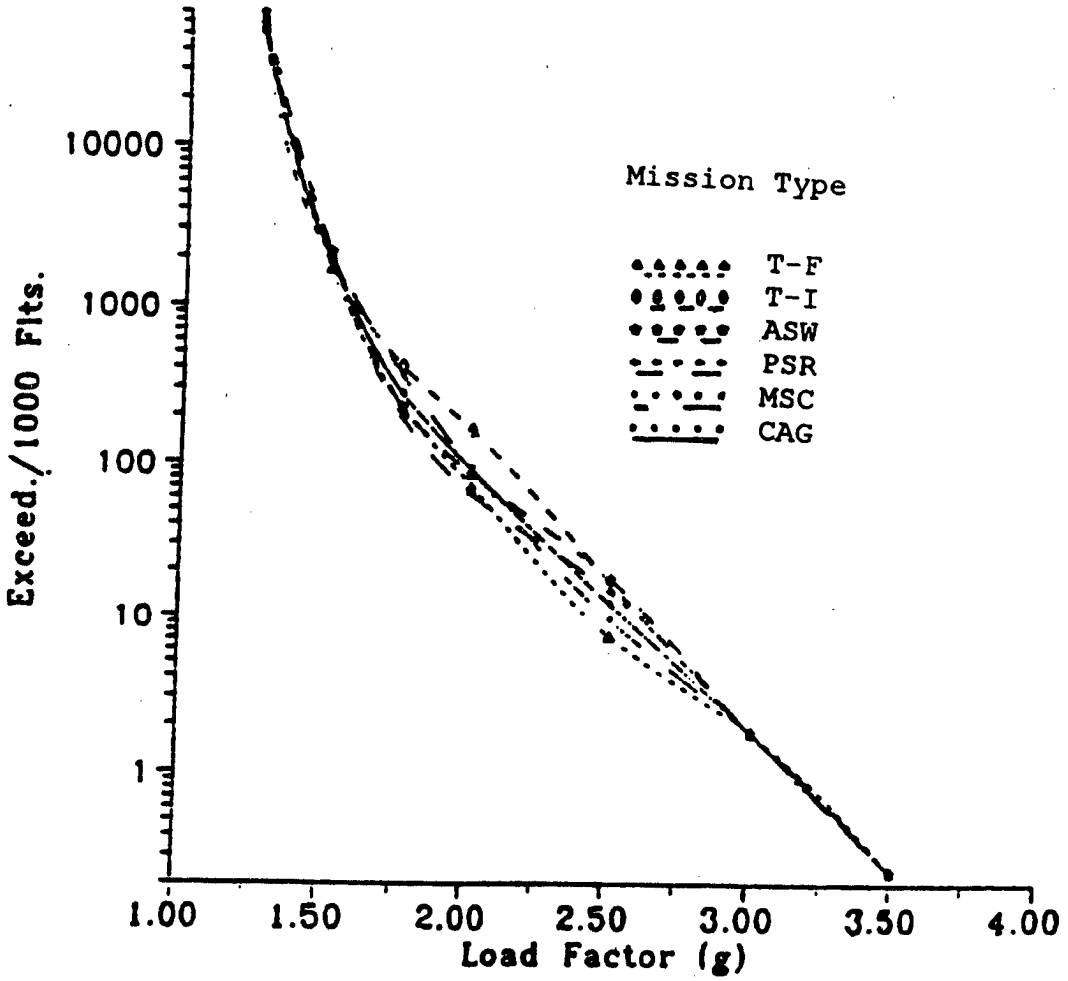

Overview of Fatigue Tracking

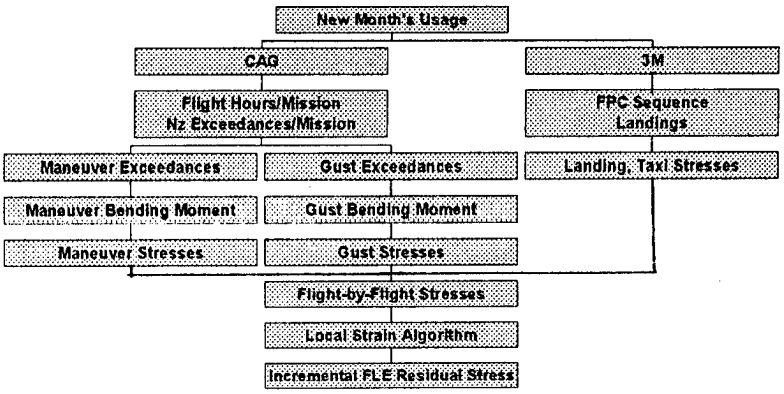

Missing CAG Data

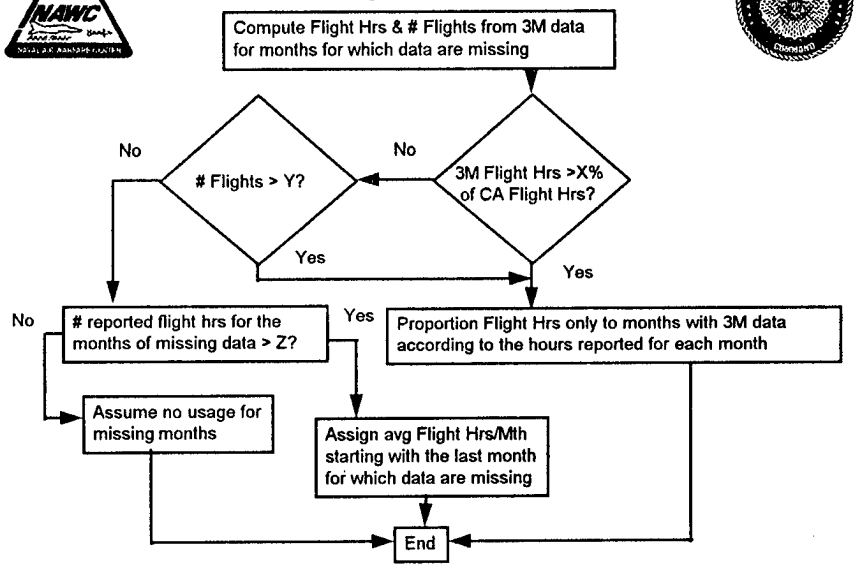

Missing 3M Data

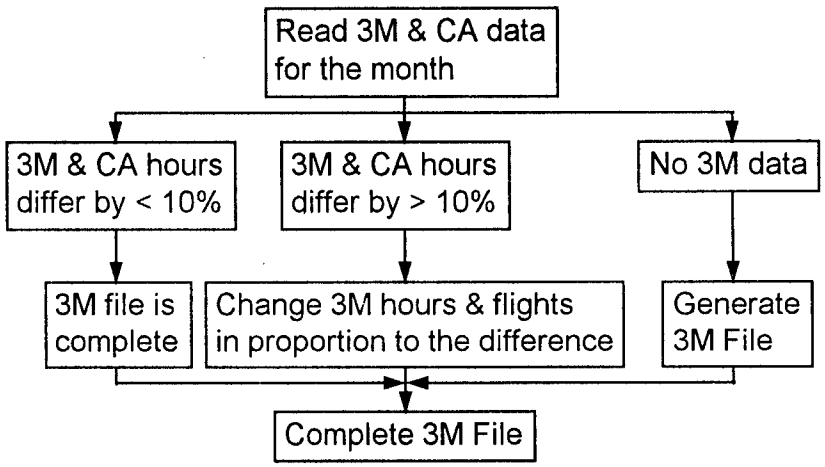

Generation of 3M File

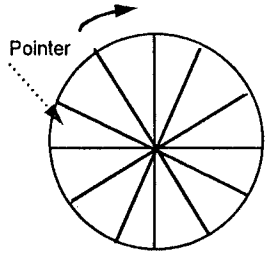

Random Mission Code Sequence (200 Total)

Mission	Avg. No. of Landings		Avg. Flight Time
	Type 1	Type 2	
1	$NL1_1$	$NL2_1$	T_1
2	$NL1_2$	$NL2_2$	T_2
.	.	.	.
.	.	.	.
.	.	.	.
N	$NL1_N$	$NL2_N$	T_N

Comparison of 12 P-3Cs

- Compared to previous tracking system
  - **Damage Index- (FLE)**
  - **Indications of Critical Areas**
- Selected representative aircraft with:
  - **Low Percentage of Quality C/A Data**
  - **High Percentage of Quality C/A Data**
  - **Average Nz Exceedances**
  - **High Nz Exceedances**
  - **Variety of Landings per Hour**

Results

- Most critical areas:
  - Front spar lower web, w.s. 167, 209
  - Fuselage floor beam
- FLEs lower when CA data is available
- FLEs higher when CA data is missing
- Exception: Test aircraft with high Nz

The Interim Tracking System Offers

- Better use of available information
  - Individual CA Data
- Updated mission/PITS interaction
- Baseline for SDRS tracking
- Template for SDRS PITS information

SAFE

SDRS TRACKING DATA FLOW

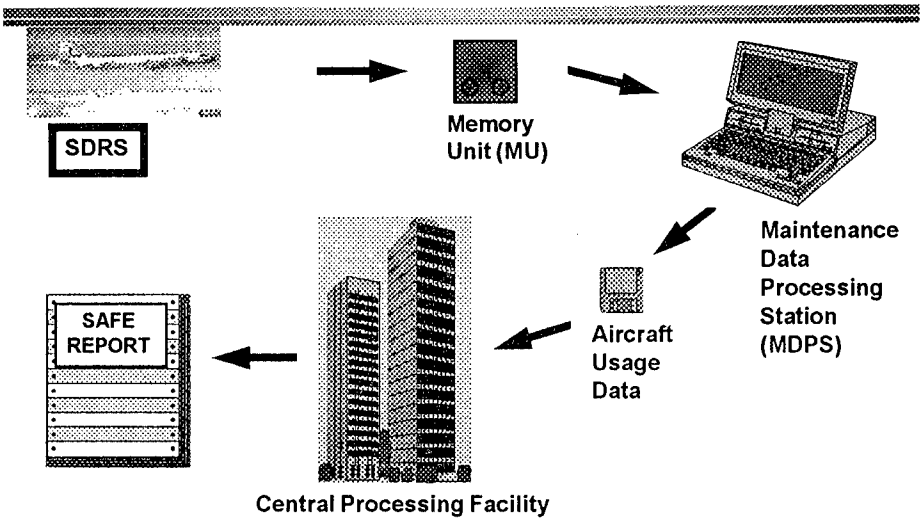

SESSION IV

ROTORCRAFT/DYNAMICS

Chairman: *T. Christian*, WR-ALC/MMSR

BRISTOL
AEROSPACE
LIMITED

LESSONS LEARNED FROM CANADIAN FORCES HELICOPTER ASIP

Implementation to Retirement

Tim Padfield -Bristol Aerospace Limited

Ken Langille - Canadian Forces,
Directorate of Technical Airworthiness

USAF ASIP CONFERENCE - 28-30 NOV 1995

BRISTOL
AEROSPACE
LIMITED

Overview

- Applying ASIP Standards
- Helicopter ASIP Background
- The ASIP Master Plan
- Usage Assessment Tools
- Maintenance Rationalization
- Fleet Management Integration
- Final Stages of ASIP
- Summary

BRISTOL
AEROSPACE
LIMITED

Canadian Forces (CF) Bell Helicopter Designations

CH118/ UH-1H / Commercial 205

CH135/ UH-1N/ Commercial 212

CH136/ OH-58A/ Commercial 206A

CH139/ Commercial 206B JetRanger III

BRISTOL
AEROSPACE
LIMITED

Original Design Philosophy

- Structure
  - Static analysis
  - No economic life determined
  - Replace as required
  - Conservative inspection schedules
- Dynamic Components
  - Fatigue tests & analysis
  - Retirement lives
  - Overhaul Intervals

BRISTOL
AEROSPACE
LIMITED

ASIP Standards & Policies

- USAF - MIL-STD-1530A & CF - D-12-010-013/SG-000 standards used
- ASIP integral part of CF Airworthiness Policy
- ASIP standards structured for life cycle support from cradle to grave. In-service application requires tailored approach.
- ASIP standard geared to damage tolerance where CF helicopter fleet were designed to safe life.

BRISTOL
AEROSPACE
LIMITED

Limitations Of Standards

- Para 1.2.1 defines application of ASIP to helicopters:

"...standard is directly applicable to manned power driven aircraft having fixed or adjustable wings and to those portions of manned helicopter and V/STOL aircraft which have Para 1.2.1 defines application of ASIP to similar structural characteristics. Helicopter-type power transmission systems including lifting and control rotors, and other dynamic machinery .... are not covered by this standard."

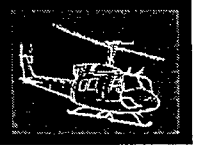

BRISTOL AEROSPACE LIMITED

Tailored Helicopter ASIP Tasks

TASK I	TASK II	TASK III	TASK IV	TASK IV
Design Information	Design Analyses and Development Tests	Full Scale Testing	Force Management Data Package	Force Management
ASIP Master Plan	Materials & Joint Allowables	Static Tests	Final Analyses	Loads/ Environment Spectra Survey
Structural Design Criteria	Load Analysis	Durability Tests	Strength Summary	Individual Airplane Tracking Data
Damage Tolerance and Durability Control Plans	Design Service Loads Spectra	Damage Tolerance Tests	Force Structural Maintenance Plan	Individual Airplane Maintenance Times
Selection of Materials, Processes & Joining Methods	Design Chemical/ Thermal Environment Spectra	Flight & Ground Operations Tests	Loads/Environment Spectra Survey	Structural Maintenance Records
Design Service Life & Design Usage	Stress Analysis	Sonic Tests	Individual Airplane Tracking Program	
	Damage Tolerance Analysis	Flight Vibration Tests		
	Durability Analysis	Flutter Tests		
	Sonic Analysis	Interpretation & Evaluation of **Test Results**		
	Vibration & Flutter Analyses			
	Nuclear & Non-Nuclear Weapons Effects Analysis			
	Design Development Tests			

BRISTOL
AEROSPACE
LIMITED

Helicopter ASIP Background

- 1983 - CH118 ASIP Master Plan
  - First application of ASIP to CF helicopters
- 1986 - CH118/CH135 ASIP Contract
  - 3 yr tailored ASIP for CH118/CH135 fleets
- 1989/90 - CH136/CH139 ASIP Contract
- Contracts extended/renewed through 1997

BRISTOL
AEROSPACE
LIMITED

ASIP Master Plans

- Crucial to the application of ASIP for in-service aircraft
- Maintains continuity in military environments where personnel changeover is frequent
- Summarizes chronological history of fleet, configurations, modifications, service difficulties and other operators experiences
- Details design substantiation & limits
- Outlines taskings, schedules & funding requirement.

BRISTOL
AEROSPACE
LIMITED

Helicopter ASIP Goals

- Safety - prevent catastrophic failures
- Economy - prescribe minimum support requirements while ensuring flight safety
- **Bristol observations:**
  - **high emphasis on safety has resulted in acceptable failure rate**
  - **not enough emphasis on economy**

BRISTOL
AEROSPACE
LIMITED

Helicopter ASIP Goals (Cont'd)

- Look for technology advances which will provide improvements in:
  - data management
  - usage measurement & management
  - maintenance management
  - overall fleet management

BRISTOL
AEROSPACE
LIMITED

Helicopter ASIP Approach

- Focus on:
  - Dynamic components
  - Critical structural problems
  - Fleet management integration

- Analysis to Substantiate:
  - Extended periodic inspection intervals
  - Extended overhaul intervals
  - Changes to retirement lives

BRISTOL
AEROSPACE
LIMITED

Helicopter ASIP Approach (Cont'd)

- Define:
  - New inspection requirements & frequency
  - Damaging operations to be eliminated or avoided
  - Cost savings from improved maintenance practices
- Fund ASIP through improved maintenance plans & resulting cost savings

BRISTOL AEROSPACE LIMITED

Identifying Maintenance Interval Drivers

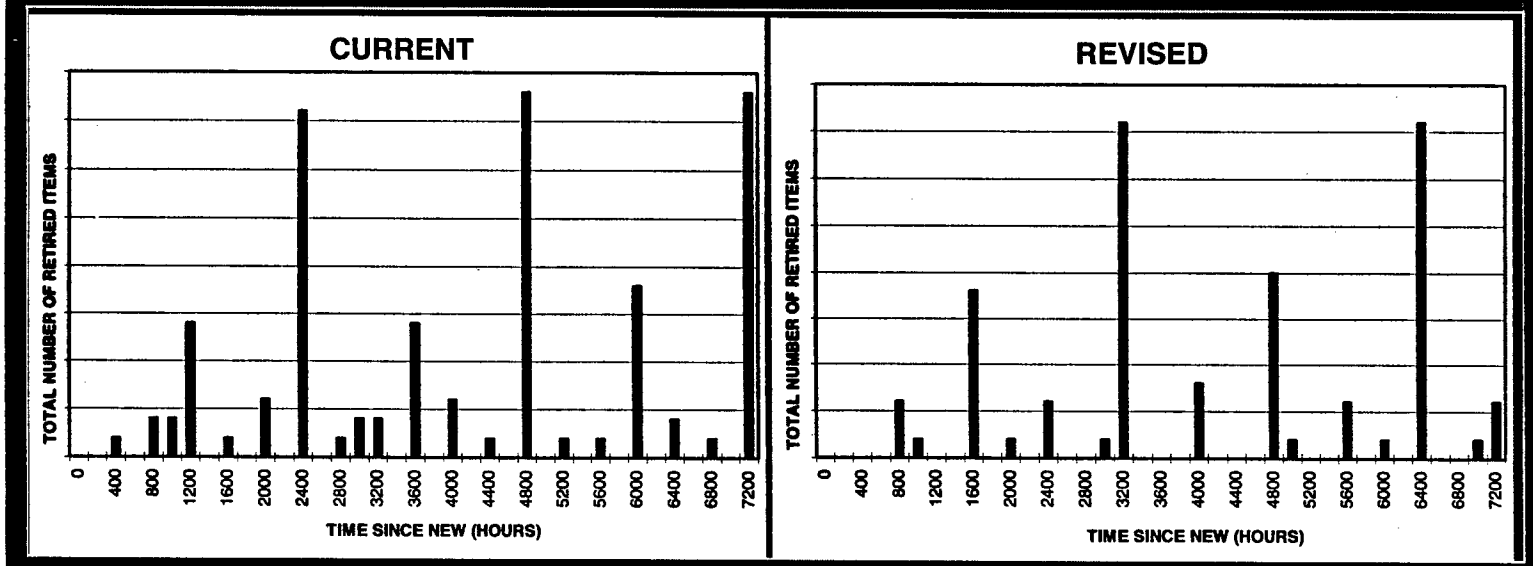

- Top assembly overhaul intervals often driven by subcomponent lives. If lowest component lives can be extended by 400 hours, in example, a 30% reduction in component replacement is achieved.

BRISTOL
AEROSPACE
LIMITED

Relationship Of Safety & Economics

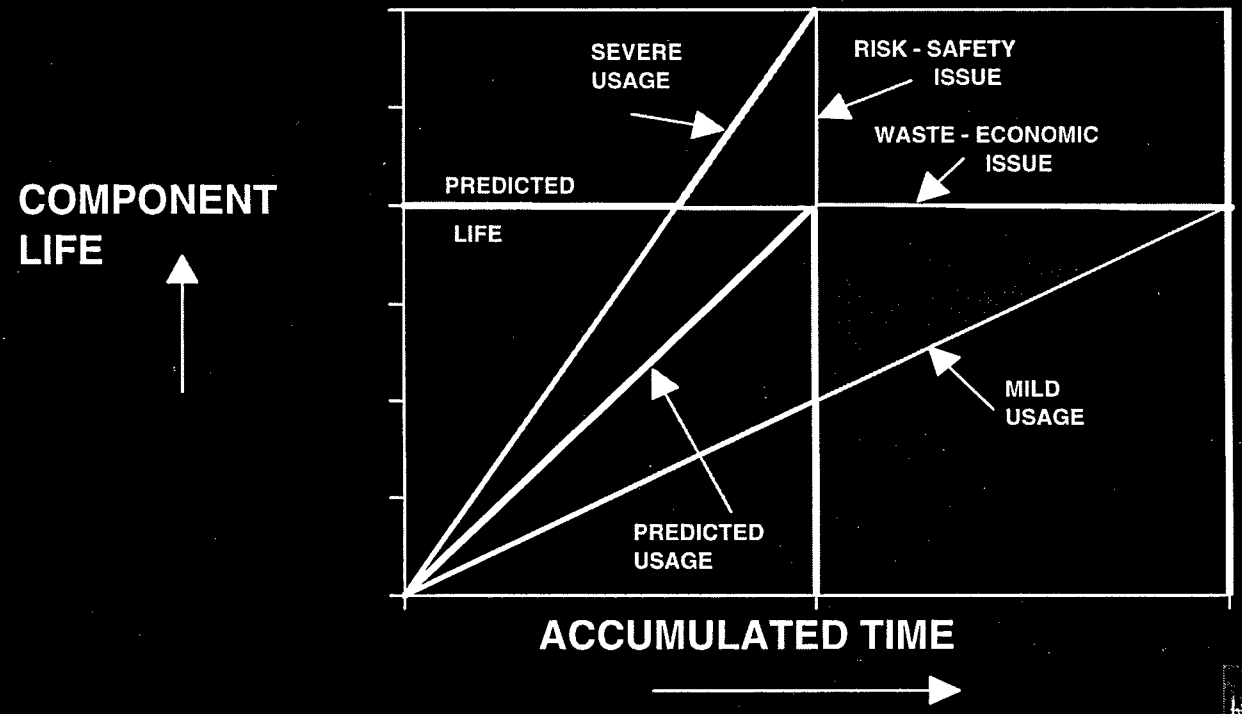

USAF ASIP CONFERENCE - 28-30 NOV 1995

BRISTOL
AEROSPACE
LIMITED

Design Usage Evaluations Logic For Change

- Level of confidence based on original criteria.
- Changes in operations, configurations, maintenance practices, and environments will affect level of confidence
- Improvements in usage definition possible and necessary
- Re-evaluation of maintenance program criteria:
  - Must not increase unknown level of risk
  - Should improve safety
  - Could provide economic benefits

BRISTOL AEROSPACE LIMITED

Usage Assessment Tools

- Pilot surveys:
  - Treat as rough-cut usage assessment
  - Pilot responses provide mixed results with questionable confidence levels
  - Pilot workload in todays aircraft takes away attention to manoeurvre detail and decreases the reliability of survey information, particularly in helicopters

BRISTOL
AEROSPACE
LIMITED

Usage Assessment Tools (Cont'd)

- Pilot survey data reduction:
  - Difficult to define mission profiles and mission mix information
  - Cannot account for pilot manoeuvre variations
  - Validation difficult
  - Good tool to define concentration areas for usage assessment systems

BRISTOL
AEROSPACE
LIMITED

Pilot Survey - Mission Breakdown

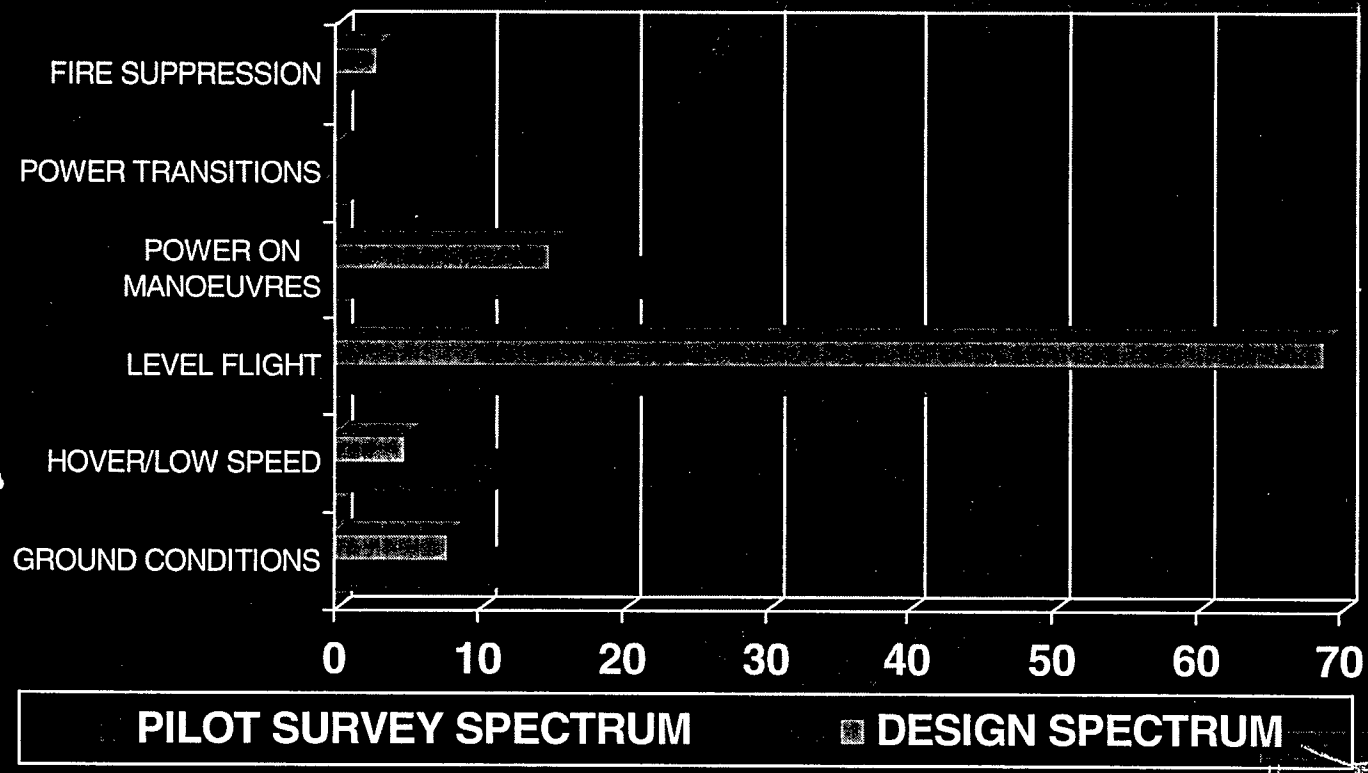

BRISTOL
AEROSPACE
LIMITED

Flight Condition Recognition Systems

- Provides measured usage data
- Many approaches exists each with various levels of accuracy, cost and pay-back scenarios
- Key is to identify number and time spent in damaging maneuvers as opposed to identifying all manoeuvres, result is lower memory requirement and less processing time
- Regime recognition is key to maximizing benefits and economic returns for initiatives in Health and Usage Monitoring Systems (HUMS)

BRISTOL
AEROSPACE
LIMITED

Manoeuvre Fatigue Damage Levels

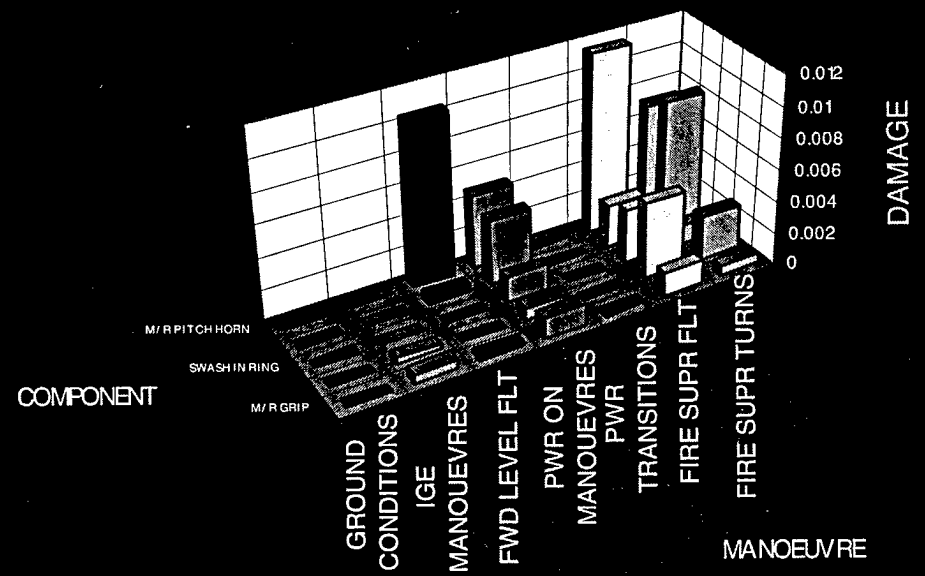

BRISTOL
AEROSPACE
LIMITED

Maintenance Rationalization Process

- Imperative to include the pilot and maintenance staff in rationalization process, many structural problems can be avoided by increased attention and awareness
- Rotor system components included in rationalization process are both life and maintenance critical; consideration must be given to both
  - RCM/MSG 3 process fails in this respect as periodic maintenance is driven by systems/powerplant logic and component safe lives are driven by structures logic

BRISTOL
AEROSPACE
LIMITED

ASIP/Life Cycle Support Integration

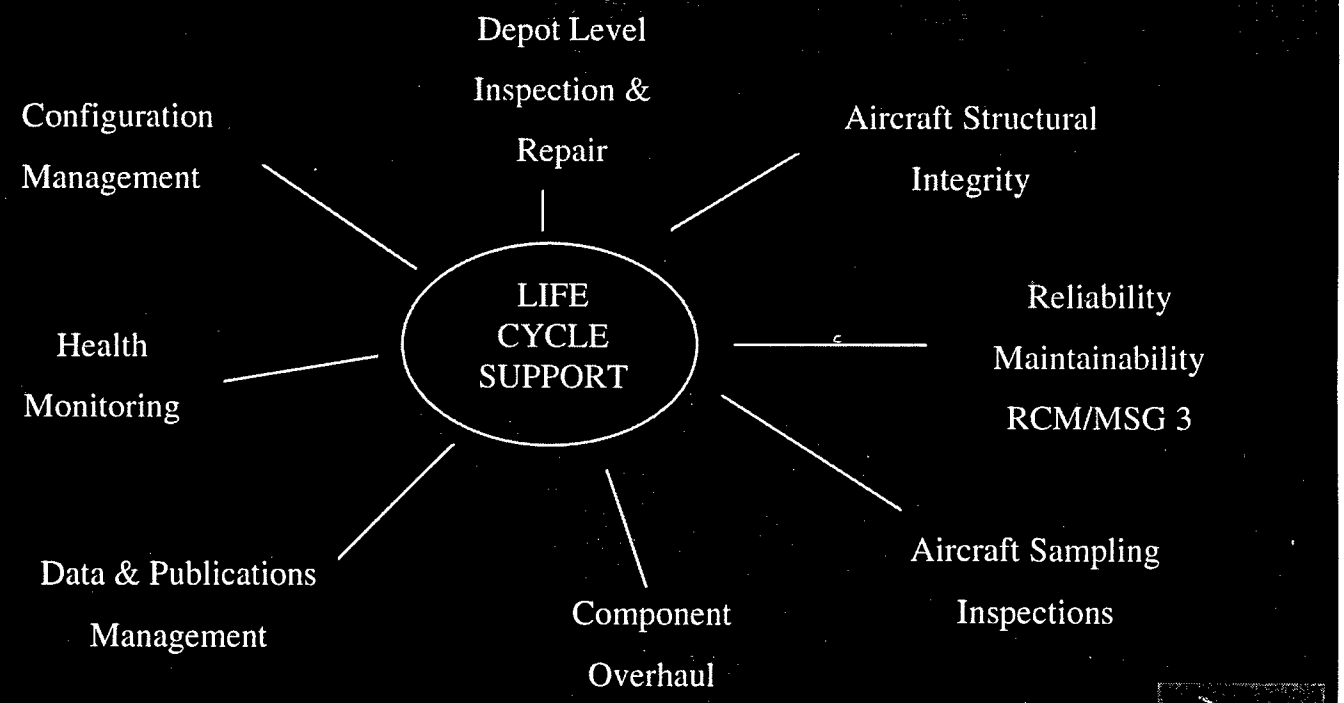

BRISTOL
AEROSPACE
LIMITED

Fleet Management Integration

- Strong interaction/understanding essential among user community, aircraft engineering officers, maintenance analysis groups and airworthiness/flight safety agencies
- Consultation with field personnel can lead to both increased understanding of problems and rapidity of engineered solutions.
- Face-to-face introduction of ASIP results to field personnel goes a long way towards the success of study

BRISTOL
AEROSPACE
LIMITED

Communication Benefits Of Today

- Engineers today have vastly superior tools available compared with those of yester-year. These enhance the effectiveness of the engineer and the success of ASIP
- Wide range of access to databases internationally:
  - FAA - Service Difficulty Reporting
  - Helicopter Association International (HAI)
  - Maintenance Malfunction Information Reporting
- Shared operator databases

BRISTOL
AEROSPACE
LIMITED

Helicopter Health & Usage Monitoring Systems (HUMS)

- HUMS integrates the latest technologies in condition monitoring and maintenance management into a unified system. Examples of features include:
  - Vibration Monitoring
  - Exceedance Monitoring
  - Usage Monitoring
  - Component Tracking
  - Cockpit Voice/Flight Data Recorders
  - Rotor Track & Balance

BRISTOL
AEROSPACE
LIMITED

HUMS (Cont'd)

- HUMS integrates existing fleet management tools and, when used effectively, may provide the user with opportunities for maintenance and retirement life credits

- **HUMS is not a replacement for ASIP but can be a highly effective tool to the ASIP engineer**

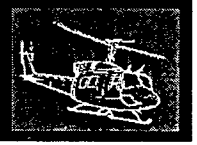

BRISTOL
AEROSPACE
LIMITED

The Final Stages Of ASIP - How Do We Wrap It Up?

- Many major benefits of ASIP can happen in the final stages of the program
- As the aircraft approaches retirement, extended maintenance and overhaul intervals become more attractive to the operator. ASIP must ensure safety is not compromised
- The ability to assess structural hot spots and define solutions rapidly is essential. Requirement exists for simple hot spot instrumentation capable of installation and operation autonomous of aircraft flight operations

BRISTOL
AEROSPACE
LIMITED

The Final Stages Of ASIP (Cont'd)

- Use ASIP expertise to assess the structural condition of aircraft and develop a matrix for selection of aircraft retirement priority
  - Ensures maximum capability in time of need
  - Reduces costs of unscheduled maintenance actions
  - Ensures safety of flight
- Target studies that have long term ramifications on future and existing fleets for cost effectiveness
- Most importantly, create a document of lessons learned to benefit future programs and industry

BRISTOL
AEROSPACE
LIMITED

Lessons Learned Summary

- Create and maintain a thorough and comprehensive ASIP Master Plan
- Only use ASIP standards as a guide; tailor standards to meet customers requirements and budget
- Treat pilot surveys as rough-cut usage assessments only
- Identify and focus efforts on aircraft maintenance drivers to maximize cost effectiveness of ASIP
- We know it is unsafe to rely on original design and usage analyses when role changes are evident

BRISTOL
AEROSPACE
LIMITED

Lessons Learned Summary (Cont'd)

- Integrate ASIP with fleet management by involving and educating all support groups on the purpose of ASIP
- Follow through with the implementation of your analyses from the drawing board to the field
- Maximize and promote the use of collective databases in industry to advance the knowledge in user communities
- Always document lessons learned to pave the path for others

Small Crack Technology for Aging Rotorcraft

*Mr. Preston R. Bates
Georgia Tech Research Institute
Atlanta, GA 30332-0844

Mr. Gary Chamberlain
Warner Robins Air Logistics Center
Robins AFB, GA 31098-1640

Abstract

Completed work is reviewed for a series of tasks required to develop a Structural Integrity Computer Program (SICP) to be used in support of Aircraft Structural Integrity Programs for USAF aging rotorcraft. A general description of the SICP is provided, followed by a discussion of helicopter fatigue failure modes and results of tasks comparing fracture mechanics techniques for large and small crack growth. Recommendations for further technology improvements are given.

Introduction

The application of damage tolerance analysis (DTA) to rotorcraft presents many technical challenges over their fixed-wing brethren. Vertical lift aircraft are more weight critical, necessitating thinner and lighter structure subjected to a high variability of applied loads. Rotorcraft components accumulate fatigue cycles much faster (typically in the 3 to 50 Hz range) than aging fixed-wing aircraft, which are often effected mainly by constant amplitude pressure-cycles. Consequently, more accuracy is required for crack growth predictions since times to failure are often on the order of a few flight hours.

Georgia Tech and Sikorsky Aircraft have supported structural integrity efforts for USAF helicopters, developing a Structural Integrity Computer Program (SICP), Figure 1, that offers a hybrid approach to aging helicopters. Until the recent RAH-66 Comanche program, DTA criteria were never specified for helicopters, and so globally applying damage tolerance based fleet management to mature weapons systems using current military standards is not practical, but is however still possible for a significant amount of selected helicopter structures [1]. The SICP provides a means to transition the application of DTA to helicopters while maintaining the traditional links to established practices.

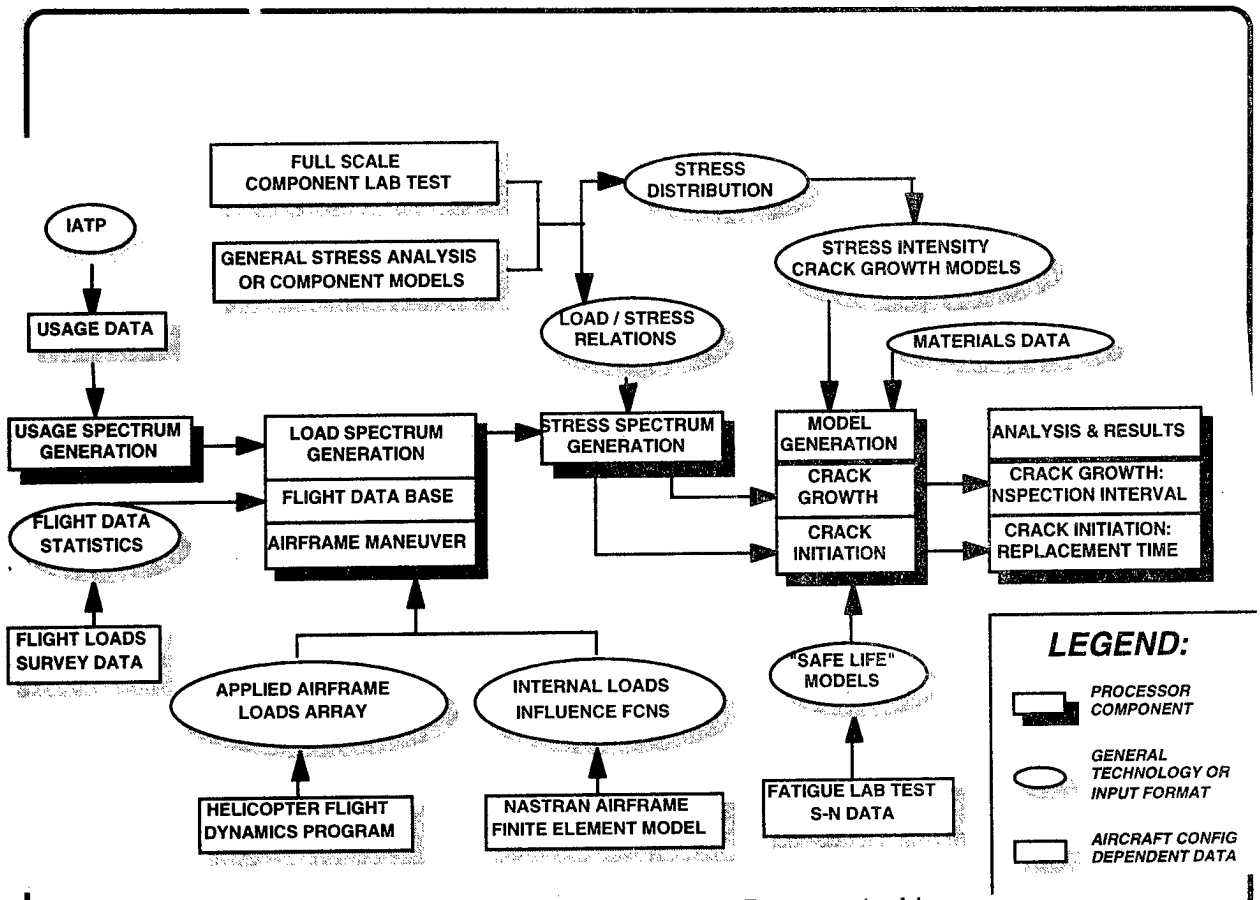

Figure 1. Structural Integrity Computer Program Architecture.

A survey of H-53 fatigue test reports and field failure data was performed to assess the variety of cracks found in rotorcraft structures [2]. The study revealed the following most frequently encountered crack geometries, which are assumed to be representative of aging helicopter structure in general:

1. corner cracks from loaded and open holes
2. multiple thru-cracks along rivet lines
3. surface cracks in plates under nonuniform and mixed mode loading
4. corner cracks in plates under nonuniform stresses
5. corner cracks in lugs
6. transverse surface cracks in hollow cylinders
7. surface cracks in thread roots

Aging rotorcraft cracks are concentrated in rotating mechanical system components occurring near structural details (e.g. fillets) and on cylindrical parts. Often, cracks propagate in mixed mode conditions and through severe nonlinear stress gradients. Rotor systems experience highly variable periodic loading and have lower safety margins because of their low weight requirements, and therefore demand more accurate analytical solutions.

The first technology task to improve SICP capabilities addressed SIF solutions and the impact of long crack material data for aging rotorcraft applications [2]. While rotorcraft fuselage structural integrity is similar to that for fixed wing aircraft, many issues are peculiar to rotorcraft applications particularly with regard to dynamic components, where the application of small crack technology is most needed. This paper researches available analytical techniques for small cracks and gives recommendations on integrating the technology into the SICP.

Small Crack Research Approaches

An appendix to ASTM Test Method E 647 (1993) defines a "small" crack as a three-dimensional crack (i.e. full or part-elliptical) whose physical dimensions compare to a microstructural feature, such as a grain, shown in Figure 1a. A "short" crack is two-dimensional (through thickness) and the dimension compares to the part width or thickness. Small cracks grow under values of ΔK which are less than the long crack threshold value and at rates higher than the long crack da/dN curve, shown in Figure 2b. The initial growth rate of short cracks is relatively high and can either go to zero (crack arrest), or drop and then increase toward long crack behavior, showing a dip in the curve. The phenomenon is effected greatly by applied stress level.

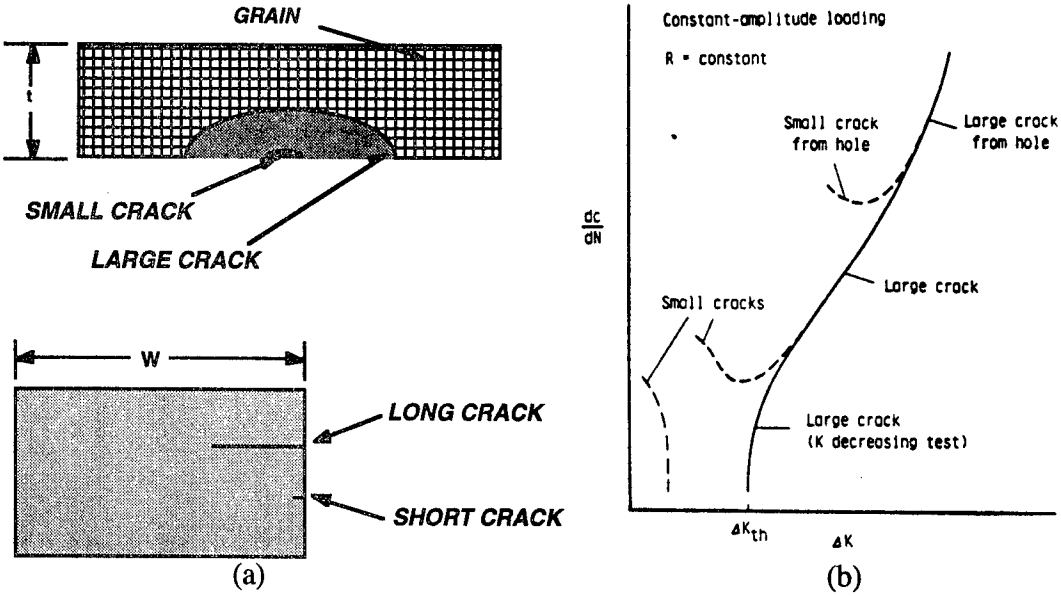

Figure 2. Small Crack Definition and Behavior.

Small crack research activity has grown steadily over the years, and since there is not yet a consensus on the most acceptable techniques to address small crack effects, research must continue to investigate this complex problem. Five general analytical approaches are found in the literature, which are not mutually exclusive:

1. linear elastic fracture mechanics (LEFM),
2. elastic-plastic fracture mechanics (EPFM),
3. crack closure,
4. probabilistic techniques, and
5. microstructural mechanics.

Long crack growth analytical procedures are based on linear elastic fracture mechanics (LEFM), which is limited by some critical assumptions, namely small scale yielding requirements. Most of the fatigue process is spent in the initiation and small crack propagation phases, with a relatively small percentage in long crack propagation. Cracks initiate in several ways, ideally from atomic slip bands or microstructural high stress concentrations in defects such as crystal imperfections, dislocations, microcracks, voids, etc. While the damage tolerant approach is sound in assuming the presence of defects, most of the defects responsible for initiating cracks and propagating small cracks are outside the analytical boundaries of LEFM.

Most LEFM small crack approaches try to correct the elastic models for plasticity effects through some artificial means to simulate the plastic zone in front of the crack. An effective elastic crack length is used for fatigue crack growth calculations. Variations on the Dugdale model are the most common. Modeling the crack growth rate in the threshold region is difficult because the rate magnitude is extremely small and hard to measure experimentally. Significant test data is often lacking to confidently define this point and observe the effect of mean stress.

EPFM is characterized by the J-integral formulation, based on deformation theory which assumes a one-to-one relationship between stress and strain. This does not account for elastic unloading and non-proportional loading, but the stress strain relationships can be improved when combined with hysteresis loops via the cyclic ΔJ parameter. J-integral solutions for various crack geometries are becoming more widely applicable to cyclic fatigue crack growth.

Crack closure observes that cracks do not immediately open upon application of tensile load. The effect is highly dependent on stress ratio, R, in terms of the actual opening stress level. Plasticity induced closure results from material deformation in the wake of the crack. Other forms of closure due to asperities from corrosion or roughness are believed to be significant. Beevers and Carlson [3] developed an asperities closure model that considers both Mode I and Mode II for roughness.

Probabilistic techniques are becoming more popular to quantify risk. Probabilistic representation of long crack threshold parameters can provide some measurement of crack growth sensitivity in this region. Stochastic models emphasize the detailed statistical nature of the problem and test data, however data of sufficient statistical quality is frequently not readily available [4]. Engineering approaches use conservative bounding techniques similar to safe-life methods, and require a large amount of test data for high statistical confidence.

Microstructural mechanics theories vary widely and consider crystallographic dislocations, persistent slip bands, and grain boundary interactions. The most complex models capture all micromechanical features while simple mechanical models try to duplicate observed behavior via correction factors and additional terms in equations. Characterizing crack growth with these considerations involves many variables and correlation with experimental observations can be difficult.

A few recent key test programs aimed at small crack effects in aerospace materials have done an excellent job of providing the fundamental information for establishing a small cracks database [5-8]:

1. AGARD Cooperative Test Program for an Aluminum Alloy (1988)
2. AGARD Supplemental Test Program for Aerospace Alloys (1990)
3. NASA/CAE Program for High-Strength Aluminum Alloys (1994)
4. Sikorsky Test Program for Helicopter Materials (1994)

These programs have focused on a approximately 10 alloys in few classes of materials, and much more testing is required for other alloy systems. Near-threshold data can be highly sensitive to the test method used, and until national standards under development become generally accepted, the problem of reliability of test data will remain. It has been observed that short and small cracks in titanium and small cracks in aluminum alloys grow faster than long cracks, but short cracks do not exhibit a characteristic dip in crack growth rate near the threshold [9]. Some steels show a distinct threshold and can be corrected, whereas aluminums lack a small crack threshold.

Comparison of Available Methods

Available long and small crack growth capabilities of several widely used computer programs were compared. Several flat plate geometries modeled in Figure 3 were selected for a benchmark helicopter component comparison:

1. Corner & Through Crack in a Lug Hole,
2. Corner & Through Crack in a 40% Loaded Hole,
3. Corner & Through Crack in an Open Hole, and
4. Corner & Through Edge Crack in a Plate

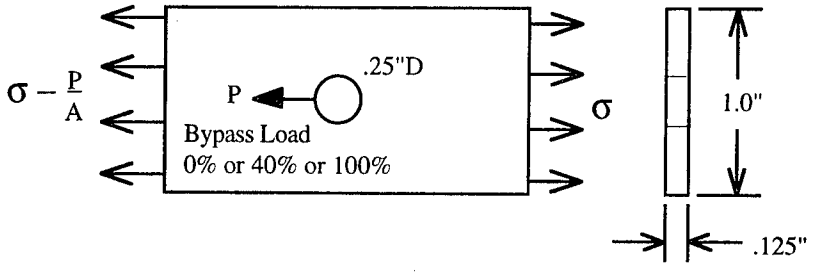

Figure 3. Benchmark Flat Plate Geometry.

Initially, the effects of stress intensity factors and long crack material data were considered for the last three geometries using 4340-180 steel data [2]. The computer codes selected for evaluation were those with which WR-ALC, Georgia Tech, and Sikorsky were most familiar: FLAGRO [10,11], MODGRO [12], and SACGAP [13]. A standard block size of 10,000 cycles was used in constant amplitude loading conditions (20, 40, 60, 80 ksi) and initial flaw sizes (.005, .010, .030 ins). Table 1 shows the maximum variations in stress intensity factor and crack growth.

TABLE 1. Results of Comparison using Long Crack Data

GEOMETRY	MAX SIF VARIATION	MAX GROWTH VARIATION
Loaded Hole	63%	43% / 65%
Open Hole	15%	17% / 97%
Edge Crack	5%	86% / 120%*

Note: Results are with/without same material da/dN data.
* For finite crack growth times only.

Stress intensity factor solutions show the most inconsistency for the loaded hole. Furthermore, the SIF for the lug geometry, the most prevalent helicopter rotor system connections, showed differences of as much as 130%. In addition, available models for general nonuniform stress fields were found to be limited. Models studied included a correction factor technique which was simple yet robust, weight function methods which were specific to geometries, and a slice synthesis technique which was robust but computationally expensive.

Predicted growth times were effected by differences in stress intensity factors, failure criteria, and default long crack da/dN material. When material data was duplicated, differences among the predictions decreased, so that scatter was usually on the order of 15%. Low stress levels (20 ksi) and flaw sizes (.005 in) produced the maximum variations. Threshold effects and material data variation accounted for the largest differences in crack growth predictions, as shown by the edge crack which had only a 5% difference in SIF, but gave the highest variation, even when the same material data was used, because of growth near the threshold. One computer code gave an infinite crack growth time, while another gave finite results.

In order to assess this highly sensitive near-threshold behavior, small crack growth analysis capabilities of available computer codes were examined. The codes selected were the latest version of FLAGRO [11], FASTRAN II [14], and PFAFAT II [15] which incorporate LEFM, closure, and probabilistic methods respectively. A dedicated cyclic EPFM code could not be found, but one is presently being developed for the NASA Marshall Space Flight Center for space shuttle main engine analysis [16].

For very small crack cases of embedded, surface, or corner flaws of .025 inches or less, early versions of FLAGRO conservatively assumed that $\Delta K_{th}=0$. The latest version uses a modified arctan rule to empirically capture the experimentally observed relationship between the LEFM threshold and stress ratio for small cracks. The following relationship is applied to all material classes.

$$\Delta K_{th} = \Delta K_0 \left[\frac{4}{\pi} \arctan (1-R) \right] \sqrt{\frac{a}{a+a_0}}$$

Here, ΔK_0 is the long crack threshold for R=0. The intrinsic crack length, a_0, has not been proven to have any physical significance but is fixed at .004 inches to provide a good fit to data points showing the onset of small crack behavior for crack lengths $\leq$ .025 inches. The threshold equation is used such that ΔK_{th} becomes constant for $R \geq .7$ due to lack of closure effects, consistent with experimental observations.

FASTRAN II is an LEFM program based on the plasticity-induced crack closure concept to account for growth near the threshold. This program has been used to model crack initiation from a microflaw in steels and has successfully captured load history effects. Crack opening stress levels are calculated from deformed material left in the wake of the growing crack which depend on load interaction effects in variable amplitude spectra. Residual stresses in the wake and crack tip plastic zone are calculated using a modified Dugdale strip yield model with rigid perfectly-plastic elements. The elastic SIF range is adjusted to an effective value based on plastic zone corrections:

$$\Delta K_{eff} = (S - S'_O)\, \beta \sqrt{\pi d}$$
$$d = c + \omega/4$$

S'_O is the crack opening stress level, β is the stress intensity , and d is the plasticity corrected crack length defined as the actual length, c, plus a fraction of the closure-corrected cyclic plastic zone size, ω. The term $\omega/4$ is based on equating estimates of ΔJ with a plasticity corrected ΔK_p and is the subject of further investigation [17]. The closure model in FASTRAN II requires da/dN data in terms of ΔK_{eff} which accounts for closure and stress ratio effects. The growth rate data for small cracks in the first three test programs discussed previously was processed in this way for constant amplitude and various spectrum load sequences.

PFAFAT II incorporates the Probabilistic Failure Assessment (PFA) approach which takes into account both test and analytical model data to quantify risk. Monte Carlo simulation is used with LEFM crack growth models to quantify the distribution of failure times based on variability in usage, dimensions, strength, load, or environment data. The following generalized Forman equation is modified

by uncertainty parameters to change the da/dN curve. The uncertainty in λK_{th} and λK_c may be characterized either by probability distributions or parametrically.

$$\frac{da}{dN} = \frac{C(1-R)^m \Delta K^n \left[\Delta K - \lambda_{K_{th}} \Delta K_{th}\right]^p}{\left[(1-R)\lambda_{K_c} K_c - \Delta K\right]^q}$$

The lug, open hole, and edge crack geometries were used in the small crack comparison. Identical SIF solutions were programmed into each computer code so that no variation due to this parameter is present in the results. The matrix of constant amplitude loading conditions and initial flaw sizes was altered to accommodate a smaller flaw size. The 4340-180 steel does not show a pronounced small crack effect but was used in this study for correlation to the previous long crack study. Because aluminum materials are more ductile and exhibit greater small crack effects near the threshold, an additional 2024-T3 alloy was selected for comparisons. The values used for the test conditions were:

1) circular initial flaw size .001, .005, .010, .030 ins
2) maximum stress levels 20, 40, 60, 80 ksi for steel
   20, 30, 40, 50 ksi for aluminum

Both constant and variable amplitude loads were applied to the problems. A rainflow cycle counted FELIX-28 spectrum was used instead of the full spectrum, which was too long for some of the programs. The spectrum was scaled so that the maximum stress corresponded to the values shown above. Identical SIF solutions were written into each computer program to eliminate variation. Table 2 shows the maximum scatter encountered for the crack geometries.

TABLE 2. Results of Comparison using Small Crack Models

GEOMETRY	MAX VARIATION 4340 Steel	MAX VARIATION 2024-T3 Aluminum
Lug Hole	89% / 254%	269% / 76%
Open Hole	98% / 465%	322% / 345%
Edge Crack	43% / 143%	246% / 715%

Note: Results are presented for constant/variable amplitude loads.
Results are for finite crack growth times only.

The highest scatter was less than a factor of 4 for constant amplitude tests and 8 for variable amplitude, generally occurring for the smallest flaw size and lowest load level. As the operative ΔK range increased, fatigue lives were closer in agreement. The edge crack showed the most discrepancies among infinite/finite life,

similar to the previous results. Steel generally does not show as much scatter since the small crack threshold is more predictable than the aluminum alloy. For the steel material, the largest scatter was found in the lowest applied stress levels. For the aluminum, the maximum variation was for the smallest crack sizes. Small crack ΔK_{eff} data used in FASTRAN II, combined with closure effects due to variable amplitude loading produced significant differences between the predictions.

To quantify the influence of several parameters on small crack growth, a parametric study was done using PFAFAT II, where λK_{th} was varied uniformly to adjust the threshold from 0.0 to 6.0, the long crack value. Other parameters were individually varied by ±10%: the calculated SIF, critical SIF, and crack growth uncertainty. Growth times are presented in Figure 4 for the simulated runs. As shown, the rapid jump in the curves indicates that the threshold acts like an on/off switch between finite and infinite life prediction, and so is the single parameter which determines growth/no growth conditions. Varying the SIF by itself is actually more detrimental on crack growth times than varying the threshold by itself, but varying only the SIF parameter had no effect on the infinite mean life as noted because mean conditions were below threshold. The threshold model is therefore very important to define exactly when growth conditions are favorable. When crack growth below threshold was activated, total scatter due to simultaneously varying all parameters was approximately 200%, while scatter due only to threshold variation was 20%. This shows that varying ΔK_{th} has only a small impact on crack growth, and so eliminating the threshold altogether would not significantly effect inspection intervals.

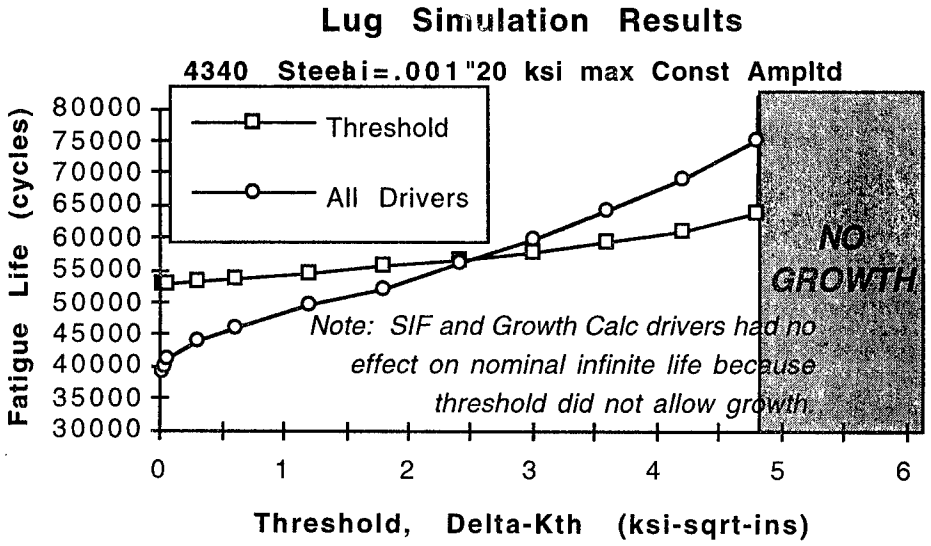

Figure 4. Driver variation results for lug geometry, 0.001 inch flaw.

Approach for Aging Rotorcraft Using Current Technology

Given the high amount of scatter in the prediction of small crack behavior, some approach for fatigue crack growth predictions in situations where short cracks are important must be defined in the SICP to establish inspection intervals. The issues that must be addressed are whether there is a need for the small crack analysis, and if so, what method can be used to conservatively predict growth.

Small crack behavior regularly dominates helicopter and engine components in defect-free conditions which are intended to be used in critical applications at large proportions of their fatigue limits. Although rotating structural components are thoroughly analyzed and tested for fatigue crack initiation, numerous circumstances associated with aging can effect the fatigue behavior which may lead to fatigue cracking that is substantially different from the laboratory conditions that established the retirement times. Heavier operating weights, widely different aircraft usage, environmental exposure, or substantial modifications due to configuration changes are real issues faced by ASIP managers.

As for most aging aircraft, without current production lines to rapidly implement engineering changes, the most attractive way to extend the inspection interval is to apply better NDI techniques to detect smaller flaws. This in turn requires better analytical capabilities to predict small crack growth. As an example, the H-53 'wet head' main rotor hub experienced a failure during TBO extension tests due to unanticipated load-stress behavior at the crack location that was not understood at the time of design. After the hubs went through modification, cracking was still not eliminated requiring a special safety inspection. However, analysis based on long crack material data and flaw size detection capabilities of the NDI procedure gave unacceptably short inspection intervals. Additionally, in contrast to dynamic components, vintage helicopter airframe structure is typically never analyzed for crack growth, with only a ground based airframe fatigue test to identify hot spots. Airframe components can benefit from small crack analysis to predict when fatigue can be expected to be a problem in critical structural members.

Figure 5 shows the extended Kitagawa diagram which is useful for defining the limitations of available LEFM technology in the context of total fatigue life. Two key crack length parameters useful for designing with small cracks are shown on the diagram [18]. Length a_1 is the largest crack whose presence does not alter the endurance limit, σ_e, of the material, i.e. the point of microcrack growth arrest. This parameter is the most difficult to measure or predict. The parameter a_2 is often referred to as the "critical crack length", since it defines the point below which small crack concepts will have to be used, signaling the end of LEFM applicability. Faced with a situation in which the initiating defect is less than a_2 in size, the early growth rates will be difficult to predict using available small crack technology. However, rotorcraft technology researchers have been able to duplicate crack initiation as the growth of small and large cracks from microstructural defects on the order of .0001 inches, indicating that a fracture mechanics approach may be the most appropriate for total fatigue life prediction.

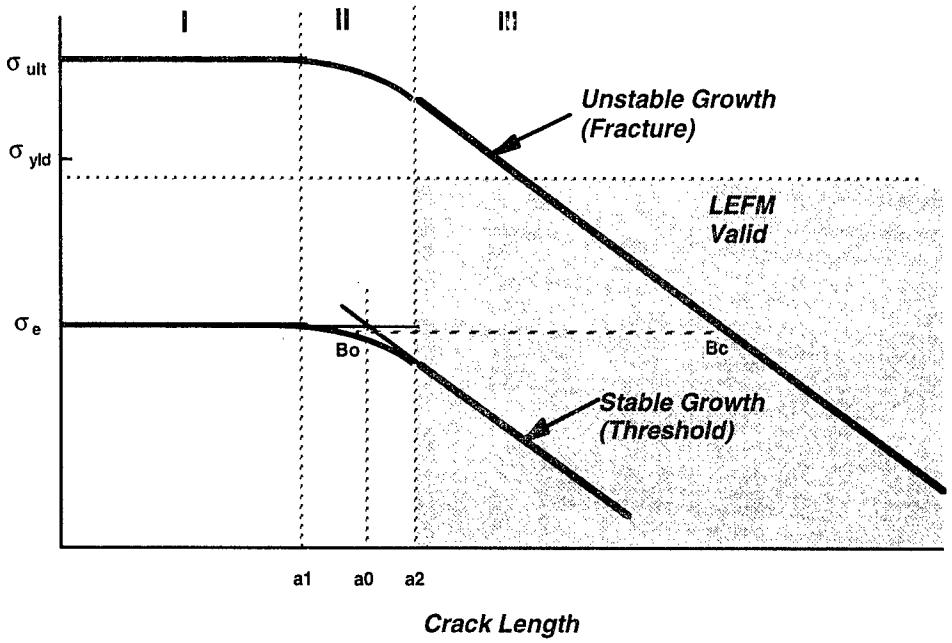

Figure 5. Small vs. long cracks on the extended Kitagawa diagram.

One conservative approach is to increase the assumed crack length to the value of a_2. This allows a safe design stress to be calculated, based on normal LEFM procedures, which must be lower than the true threshold stress which lies somewhere on the curved portion of the Kitagawa diagram. In many cases where the inherent defect sizes lie between a_1 and a_2, the difference in endurance limit stress and threshold stress at a_2 is on the order of 10–15%, sometimes as high as 30%. However, this is not a useful approach for fatigue crack growth in aging fielded systems. In that case, if stresses in the service spectrum are higher than the threshold value for a_2, and NDI procedures can detect cracks of length a_2, then small crack techniques must be used to predict, for instance, crack growth under constant amplitude shown by line B_O-B_C in Figure 5.

In the current absence of a large amount small crack test data and analytical techniques to consistently predict their growth, the following engineering approach can be taken to model the small crack effect for aging helicopter components. The threshold value (long and short) can be eliminated for all materials. This was used in the original version of FLAGRO for elliptical cracks less than .025 inches in length, and was also recommended by ALCOA to provide conservative results. Since the threshold acts like an on/off switch, safety considerations dictate the requirement that unless the exact location of the threshold can be pinpointed, there is little justification to use it if it does not severely impact inspection requirements via more frequent inspections. As the results of the probabilistic simulation in Figure 4 have shown, the impact is approximately 20%.

However, linear extrapolation of the straight line portion of the da/dN curve will not account for the small crack effect where growth rates have been shown to be higher than the long crack data (Figure 2b). The actual statistical variation of small crack growth rates at a given ΔK can be determined assuming a normal distribution or some other appropriate model using available empirical data. Based on this distribution, a weighted knockdown can be used in the small crack regime only, as shown in Figure 6. If it is assumed that no threshold exists as discussed previously, then a distribution occurs only in the crack growth rate, da/dN. Assuming a normal distribution in the rate for a given ΔK, the mean and variance can be calculated based on available small crack data for a similar alloy. Since the small crack effect is believed to be in part due to the scale of the log-log or log-normal graph, using a constant standard deviation based on the smallest measured data points mimics the scale effect. As a result, the calculated upper (99%) and lower (1%) bounds of the normal distribution appear to quickly transition into the long crack curve. The upper bound can be considered a 'weighted knockdown' factor that is applied only to the small crack region of the growth rate curve. This is similar to but not as severe as the working curve reduction technique used for safe life S/N data where the entire curve is reduced by several standard deviations.

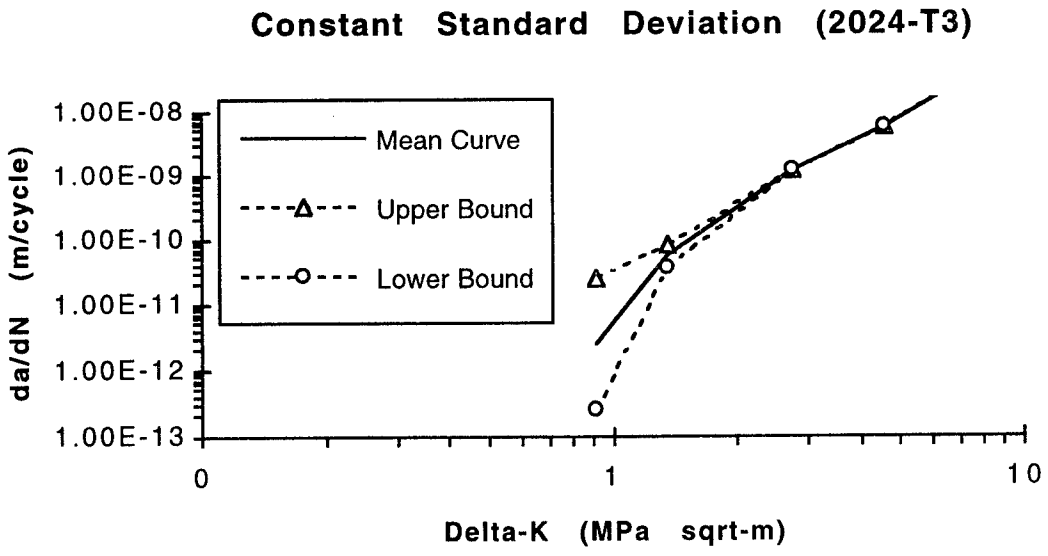

Figure 6. Statistical model for small crack scatter.

Development of New Technology

The computer codes used for the small crack growth comparison are currently available and their technologies are being considered for more widespread application. However, as there is no present consensus on which technology is most appropriate for this complex problem, further research must be performed to better correlate observed test data.

A more recent focus has been on the use of other continuum mechanics techniques for fatigue crack growth. Research is being done to apply EPFM techniques to fatigue crack growth [16]. Tasks in the current development of an EPFM computer program include deriving robust methods for determining elastic-plastic stress intensity factors, variable amplitude loading and closure correction to ΔJ, and a creep-fatigue algorithm. A great deal of other research activity focuses on multiple parameters to formulate crack growth laws [19]. Kardomateas investigated the non-hardening solution for stationary short cracks [20], proposing the use of K and the higher order T-stress term in the elastic Williams series expansion. Researchers have shown that in practice the use of the T-stress as a constraint parameter gives good estimates of crack tip triaxiality even beyond limit load for a variety of plane strain and axisymmetric crack geometries and loadings. The T-stress is readily calculable with some computational effort, has a sound physical basis, and applies to a variety of geometries and loading conditions. Multi-parameter crack growth thus far has focused only on monotonic loading conditions. Implications for fatigue crack growth laws using a two-parameter representation are being investigated.

Many agree that a few forms of closure (or lack of them) are responsible for the small crack phenomenon. Plasticity-induced closure, the technique used in FASTRAN II, results from deformed material in front of the crack tip and in the crack wake. The deformations cause interference between the crack faces and can produce significant residual stresses which effect crack growth rate. Roughness-induced closure results from crack branching and material ligaments where the roughness of the deformed crack path does not permit the crack faces to precisely fit together upon unloading. Binding of the crack flanks produces mixed mode loading conditions and discrete forces which cause the crack to remain open. Compressive loading can crush material asperities and lead to accelerated crack growth. Extremely small cracks, however, lack sufficient length to allow these mechanisms to be effective and so exhibit faster growth than available material threshold data for long cracks which does not account for these mechanisms.

To address these issues, a Mode I discrete asperity model [21] (Figure 7a) which captures the effects of both plasticity and roughness induced closure is being developed into a fatigue crack growth algorithm. A load is developed in the crack wake brought about from asperity contact. The relatively small asperities are modeled as elastic-plastic elements capable of plastic deformation under high contact stresses. Superposition is used to combine the SIF solutions of the discrete load and an applied external load.

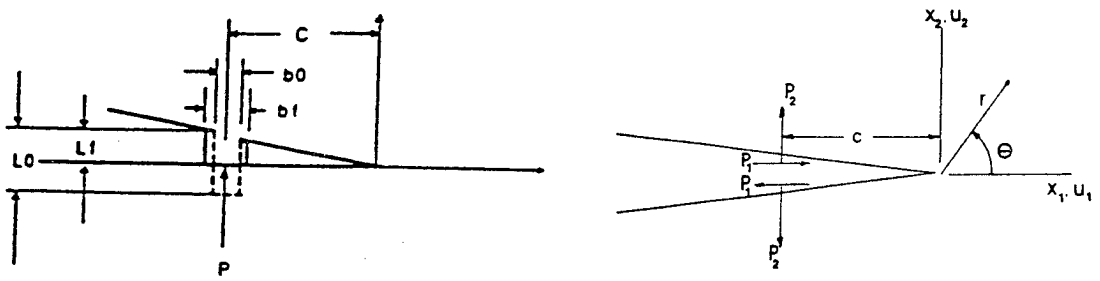

(a) (b)

Figure 7. Discrete Asperity Closure Model for Plasticity & Roughness.

Initial runs show that compressive loads will increase the rate of crack growth and result in faster crack propagation times. However, the overall impact of the asperity crushing in the test cases performed has not been dramatic, with differences on the order of only a few percent. This is partly due to the fact that the model currently is only operable for through-crack cases whereas much of the crack lifetime is spent as an elliptical crack. A SIF solution needs to be developed for elliptical flaws under a line load in the crack wake, either through finite element studies or by other numerical means. Other improvements to the code for further development of small crack analysis capability include mixed mode loading conditions [22] (Figure 7b), mixed plane strain/stress effects, and modeling microstructural features such as grain boundaries.

Conclusions

A joint Georgia Tech / Sikorsky Aircraft engineering effort is investigating fleet management for aging rotorcraft based on damage tolerant philosophy, developing a structural integrity computer program (SICP) to determine component retirement times and crack growth times of critical helicopter structures under changing mission requirements. The improved SICP technology is general enough to be applied to both rotary and fixed wing air vehicles.

A review of H-53 helicopter failure modes revealed that corner cracks from holes, multiple thru-cracks along rivet lines, and surface cracks are the most common types of cracking for vintage rotorcraft. Nonuniform stress fields and mixed modes of crack growth are also frequent. An investigation of capabilities found in several available crack growth programs revealed the following most significant conclusions for the application of damage tolerance-based force management concepts in helicopter structural integrity.

1. *Material data variation near the threshold accounts for the largest differences in crack growth predictions.* Using several available programs, results varied by less than a factor of 2, when the same long crack material crack growth rate curve was used under constant amplitude loads. When small crack data was investigated, scatter was within a factor of 4 for constant amplitude loading and a factor of 8 using a FELIX-28 spectrum. In the two alloys investigated (steel and aluminum), this high scatter resulted from small crack lengths and low load levels near the threshold. Consequently, material crack propagation data in this region must be treated carefully using test and analysis procedures that are yet to be standardized.

2. *Statistical approaches are recommended for current rotorcraft applications.* While small crack growth is important for aging rotorcraft, large differences among existing predictive capabilities necessitates a conservative engineering approach to ensure safety. Eliminating the threshold altogether does not have a severe impact on crack growth times and corresponding maintenance intervals (only 20% conservatism for the lug problem investigated). Observed variance in small crack data can be used to determine conservative crack propagation times via a knockdown factor applied only to the small crack portion of the material da/dN curve. Further studies of safety, logistics, mission readiness, and cost should be performed using a tool like the SICP to quantify the impact of the recommended approach on rotorcraft operations.

3. *Consistent small crack models are still lacking.* Plasticity, roughness, and oxide-induced closure are thought to be the most important for small crack growth, and the development of a discrete asperity closure model can potentially model all three. Other efforts should concentrate on elastic-plastic mechanics and higher order approaches to capture the effects of microplasticity and large scale yielding, the effects of variable amplitude loading, and the interaction of chemical and mechanical environments. Obtaining the required material test data and assessing the applicability of micromechanical and other mechanical models for small cracks is crucial to aging rotorcraft structural integrity.

References

1. Bates, P., Crawford, C., and Chamberlain, G., "Recent Developments in Damage Tolerance Analysis for Rotorcraft," 19th European Rotorcraft Forum, Cernobbio (Como), Italy, 1993.
2. Bates, P., and Chamberlain, G., "Progress Towards a Comprehensive Fatigue Analysis Program for Rotary and Fixed Wing Aircraft," USAF Structural Integrity Program Conference Proceedings , San Antonio, TX, Dec. 1994.
3. Beevers, C., and Carlson, R. L., "A Consideration of the Significant Factors Controlling Fatigue Thresholds," Fatigue Crack Growth 30 Years of Progress, Proceedings of a Conf. on Fatigue Crack Growth, Cambridge, UK, 1984.
4. McClung, R. C., Chan, K. S., et al., "Analysis of Small Crack Behavior for Airframe Applications," FAA/NASA International Symposium Advanced Structural Integrity Methods for Airframe Durability and Damage Tolerance, Hampton, VA, 1994.

5. Newman, J. C., Jr. and Edwards, P. R., "Short-Crack Growth Behavior in an Aluminum Alloy - An AGARD Cooperative Test Programme," AGARD Report No. 732, 1988.
6. Edwards, P. R. and Newman, J. C., Jr., "Short Crack Growth Behavior in Various Aircraft Materials," AGARD Report No. 767, 1990.
7. Newman, J. C., Jr., Wu, S. L., et. al., "Small Crack Effects in High-Strength Aluminum Alloys - A NASA/CAE Cooperative Program" NASA Reference Publication 1309, 1994.
8. Annigieri, B., Favrow, L., and Schneider, G., "Small Cracks Test Program for MH-53J Helicopter Materials," UTRC Report No. R94-470111-F, 1994.
9. Lankford, J., "Concluding Remarks - Small Cracks," Second International Conference on Low Cycle Fatigue and Elastic-Plastic Behavior of Materials, Munich, Germany, 1987.
10. NASA Johnson Space Center, Materials Branch, Structures and Mechanics Division, JSC-22267, "Fatigue Crack Growth Computer Program, NASA/FLAGRO," 1989.
11. NASA Johnson Space Center, Materials Branch, Structures and Mechanics Division, JSC-22267A, "Fatigue Crack Growth Computer Program, NASA/FLAGRO," 1994.
12. Harter, J. A., "MODGRO Version 2.3," Flight Dynamics Laboratory, Air Force Wright Aeronautical Laboratories, Wright-Patterson AFB, 1992.
13. SACGAP Computer Program, Structures Research Division, Sikorsky Aircraft, 1988.
14. Newman, J. C., Jr., "FASTRAN II - A Fatigue Crack Growth Structural Analysis Program," NASA TM 104159, 1992.
15. Moore, N. R., Ebbeler, D. H., et al., "An Improved Approach for Flight Readiness Certification - Probabilistic Models for Flaw Propagation and Turbine Blade Failure," JPL Publication 92-32, 1992.
16. McClung, R. C., Chell, G. C., et al., "Development of a Practical Methodology for Elastic-Plastic Fatigue Crack Growth," 1994 Conference on Advanced Earth-to-Orbit Propulsion Technology, NASA Marshall SFC, 1994.
17. Newman, J. C., Jr., "Fracture Mechanics Parameters for Small Fatigue Cracks," Small Crack Test Methods, ASTM STP 1149, J. Larsen and J.E. Allison, Eds., American Society for Testing and Materials, Philadelphia, 1992.
18. Taylor, D., Fatigue Thresholds, Butterworth & Co., 1989.
19. Parks, D., "Advances in Characterization of Elastic-Plastic Crack Tip Fields," Topics in Fracture and Fatigue, A.S. Argon, Ed., Springer-Verlag, 1992.
20. Kardomateas, G. A., Carlson, R. L., et al., "Near Tip Stress and Strain Fields for Short Elastic Cracks," *International Journal of Fracture*, Vol. 62, 1993.
21. Kardomateas, G. A., and Carlson, R. L., "An Analysis for the Effects of Compressive Load Excursions on Fatigue Crack Growth in Metallic Materials," Transactions of the ASME, Vol. 62, pp. 240-244, March 1995.
22. Carlson, R. L., and Beevers, C. J., "A Mixed Mode Fatigue Crack Closure Model," *Engineering Fracture Mechanics*, Vol. 22, No. 4, pp. 651-660, 1985.

Helicopter Structural Integrity with IHUMS

*Mr. Gregory P. Cleveland
Mr. Charles Trammel
Smiths Industries Aerospace - Defense Systems - Grand Rapids
4141 Eastern Avenue SE, Grand Rapids, Michigan 49518-8727

Mr. William Sullivan
Chadwick-Helmuth Company, Inc.
4601 N. Arden Drive, El Monte, California 91731

Mr. Robert Thompson
Naval Aviation Engineering Service Unit
NAS North Island, San Diego, California 92135-7066

The US Department of Defense operational readiness rate requirements of helicopters is higher today than ever before. The high utilization rates of helicopters during Operation Desert Storm provides the best evidence supporting high readiness rate requirements. These rates require more reliable equipment and a structurally sound airframe. Something, that is complicated by the fact that a helicopter is a dynamic flying platform of rotating machinery. Additionally, there is a safety concern involved with operating the traditional carry-on vibration health monitoring systems in constrained environments, such as small ship decks, and when operating under limit time constraints, such as when taking up carrier deck space. Maintenance costs, which are a significant factor in life cycle costs, have also risen dramatically. The introduction of integrated onboard maintenance system technology addresses these

issues by integrating the functions of data collection and recording, health and usage monitoring, maintenance diagnosis, and fault prediction.

Through a Cooperative Research and Development Agreement (CRADA) with the US Navy, Smiths Industries and Chadwick-Helmuth are demonstrating an Integrated Health and Usage Monitoring System (HUMS) on a SH-60B helicopter to address these requirements. The SH-60B HUMS is designed to monitor the health and usage of the engines, transmission system, rotor system, and airframe. The HUMS provides ground maintenance personnel with the necessary information to diagnose system heath, determine malfunctions, and schedule required maintenance actions. In addition to the real-time aircraft health monitoring, the HUMS provides engineering services valuable data to be used in evaluating the effects of flight states and maneuvers on airframe vibration.

The SH-60B HUMS is a highly reliable, compact multi-function system for monitoring, collecting, processing, and storing a variety of data. The SH-60B HUMS is based on Non-Developmental Item (NDI) equipment that is currently in US government inventory or procurement:

- Smiths Industries SH-60B Standard Flight Incident Recorder (SFIR) Signal Acquisition Unit and associated sensors.
- Chadwick-Helmuth MH-53J Vibration Monitoring System (VMS) and associated sensors.
- Smiths Industries Electrostatic Engine Monitoring System (EEMS™) and associated sensors.
- Smiths Industries HH-60J Combined Voice and Data Recorder (VADR™).
- Smiths Industries CH-47/OH-58D/MH-53J Data Transfer System (DTS).

The baseline SH-60B HUMS demonstration includes the following helicopter diagnostic technology capabilities:

- Onboard rotor track & balance.
- Engine exhaust debris monitoring.

- Rotor health monitoring.
- Engine health monitoring.
- Transmission and gearbox health monitoring.
- Engine life usage monitoring.

The primary elements of the SH-60B HUMS are the Onboard Monitoring Equipment and the Ground Support Equipment (GSE). A system block diagram of the baseline SH-60B HUMS Onboard Monitoring Equipment is shown in Figure 1. The baseline system has the capability for growth to include:

- Transmission and drivetrain diagnostics.
- Driveshaft and hanger bearing monitoring.
- Flight regime recognition for automatic rotor balancing.
- Structures life usage monitoring.

The SH-60B HUMS Onboard Monitoring Equipment consists of the following main Line Replaceable Units (LRUs):

- Data Acquisition Unit (DAU).
- Combined Voice and Data Recorder (VADR™).
- EEMS™ Interface Unit (EIU).
- Data Transfer System (DTS) consisting of the following items:
  - Data Receptacle Unit (DRU).
  - Removable Data Transfer Module (DTM).

The baseline SH-60B HUMS Onboard Monitoring Equipment locations are shown in Figure 2. The Data Acquisition Unit (DAU) is the main LRU component in the SH-60B HUMS. It provides monitoring and acquisition of aircraft system and HUMS specific sensors. The DAU hardware and software has been logically partitioned between the following main functions:

- Flight Data Acquisition Unit (FDAU) based on the Smiths Industries SH-60B SFIR Signal Acquisition Unit.
- Vibration Monitoring System (VMS) based on the Chadwick-Helmuth MH-53J Vibration Monitoring System.

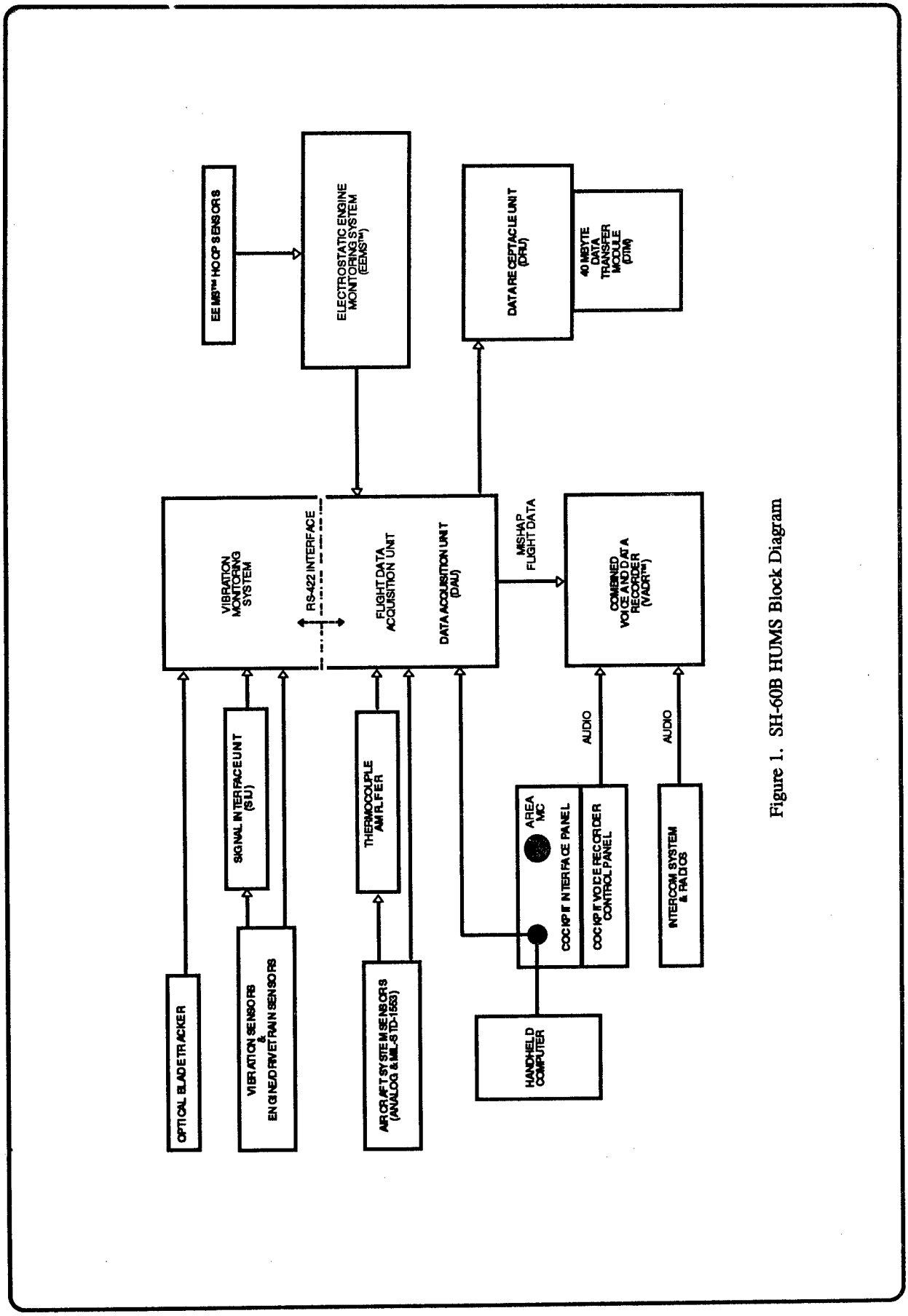

Figure 1. SH-60B HUMS Block Diagram

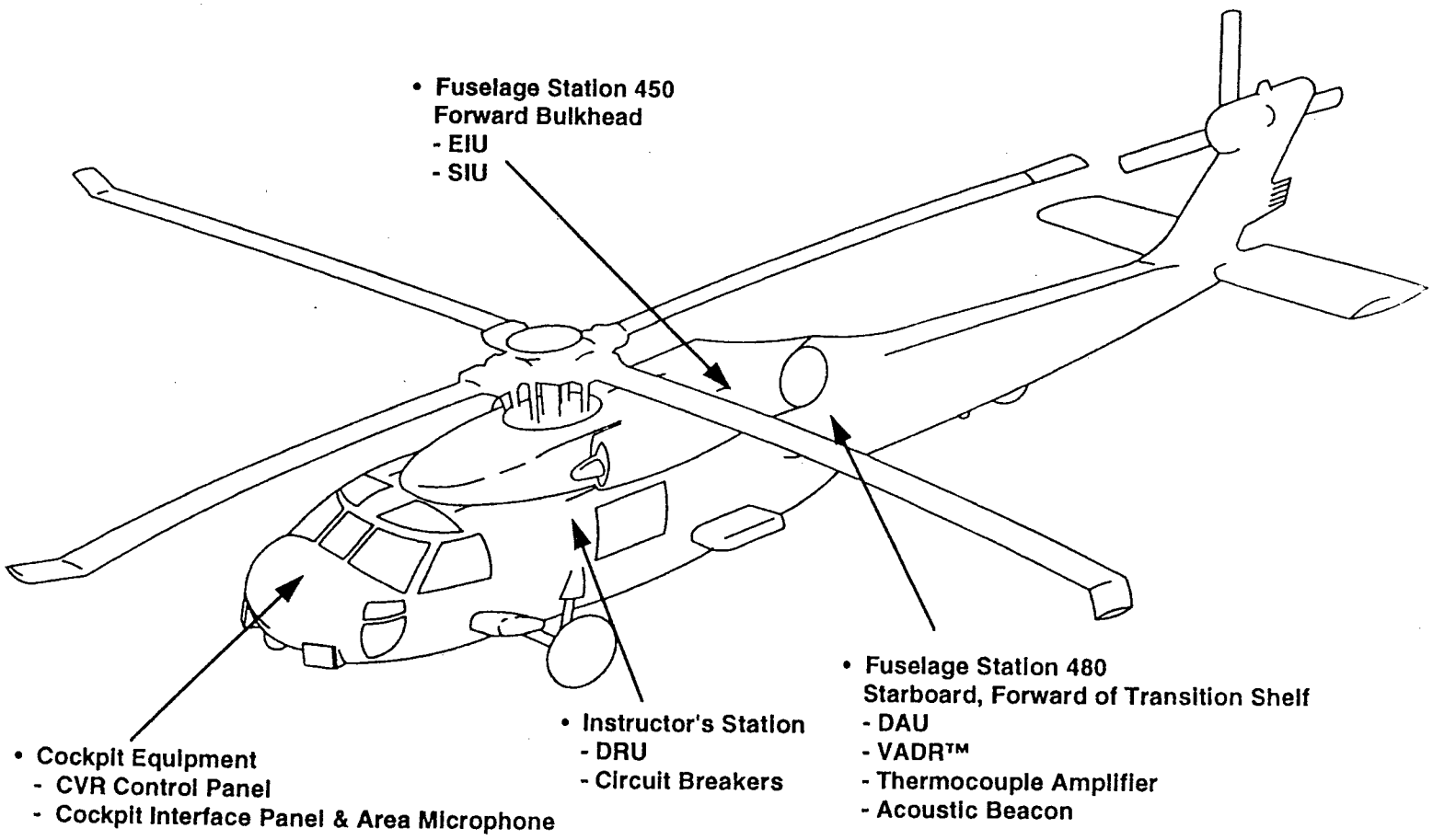

Figure 2. SH-60B HUMS Equipment Locations

The Flight Data Acquisition Unit communicates with the Vibration Monitoring System, Voice and Data Recorder, EEMS™ Interface Unit and Data Transfer System via high speed RS-422 serial interfaces with full error detection and correction protocols. The FDAU and VMS are fully isolated to prevent failure of one system from causing loss of operation of another system. The FDAU and VMS are each tasked with specific signals to condition, acquire, process and store. Computed parameters such as flight regime and alarm event status are passed at periodic intervals between the FDAU and VMS via the RS-422 serial interface. The DAU uses field proven hardware and software that was developed to meet strict system cost, size and weight goals. The system is designed to stand up to the rigors of rotary wing aircraft operations and to minimize maintenance. The system incorporates comprehensive Built-In-Test (BIT) capabilities for fault detection and isolation. The BIT is designed to allow system level and board level fault isolation. In addition, most sensor and interconnect wiring faults can be isolated by the DAU.

The SH-60B HUMS Ground Support Equipment is responsible for all data transfer functions to and from the aircraft, printing of reports, and analysis and storage of all flight data. It is modular in design with each module responsible for a specific processing function. The GSE consists of three items:

- Handheld Data Transfer Unit (DTU).
- Ground Readout Equipment (GRE).
- Ground Support Station (GSS).

The HUMS is implemented with user definable start criteria. For the SH-60B, flight data recording starts upon power application to the aircraft and the continuous vibration monitoring starts as soon as the main rotor RPM exceeds 80 percent. The FDAU subsystem interfaces with the various sensors on the aircraft as well as the MIL-STD-1553B data channels and converts the analog signals to digital form. A subset of the data required for mishap recording is processed and sent to the VADR™ for storage. Structure-related flight data as well as engine data

are processed and sent to the DTM for storage. Continuous Vibration Monitoring Data from dedicated velocimeters and accelerometers is processed by the VMS and also stored in the DTM. BIT data from both the FDAU and VMS is stored in the DTM as well. During flight operation, no specific interaction is required by the aircrew. After the flight, the HUMS stops recording, based upon user defined stop criteria, and automatically shuts down when the power is off.

After a series of flights, the DTM is removed from the aircraft and taken to the ground processing center where the GSS is resident. The GSS utilizes a Data Receptacle Unit similar to the airborne unit for data upload, download, and maintenance actions. The downloaded data is decompressed and the output is time-sequenced data in engineering units in binary form on separate files for mishap, structures, and engine. The data is now ready for analysis utilizing the Ground Support Station software analysis tools.

Although the need for crash protected VADR™ data downloading is relatively infrequent, this may be done in a similar fashion with the aircraft on the ground. This is accomplished by connecting the Ground Readout Equipment to the onboard HUMS GRE connector and applying power to the HUMS. From the menu displayed on the GRE, VADR™ downloading is selected. When the download is complete, the GRE can be used to process and playback the voice and flight data.

The SH-60B Flight Data Recorder (FDR) subsystem consists of the following major elements:

- Flight Data Acquisition Unit.
- Crash survivable combined Voice and Data Recorder.
- Data Transfer System.

The baseline SH-60B FDR subsystem provides flight data recording for mishap investigation and cockpit voice recording of the intercom system and an area microphone. The FDR subsystem also provides the capability of aircraft data recording for flight regime recognition, Individual Aircraft Tracking (IAT) for aircraft structural integrity monitoring, and engine structural integrity monitoring.

The Flight Data Acquisition Unit provides monitoring and acquisition of analog, strain gauge, MIL-STD-1553B, RS-422, discrete signals, etc. Recorded structures, engine, special event, and Built In Test data is stored the DTM and/or the crash protected VADR™. The FDAU is the primary analog/discrete/digital data acquisition, processing, and storage management component of the HUMS. The FDAU gathers data from numerous aircraft sensors which provide such information as attitude, airspeed, flight control positions, and engine performance parameters. The FDAU can accommodate the following types of signals:

- Analog signals.
- Discrete signals.
- Strain gauge (Low Level DC Analog) signals.
- MIL-STD-1553B digital signals.
- RS-422 digital signals.

The SH-60B HUMS FDAU flight data acquisition and processing functions include:

- Analog and discrete signals received and converted to necessary digital formats.
- Digital parameters acquired from MIL-STD-1553B data bus as a Bus Monitor.
- Primary interface to HUMS subsystems and Ground Support Equipment (GSE).
- Performing the flight data acquisition functions for the VADR.
- Time history recording
- Occurrence histograms, usage accumulators.
- Exceedences, overload tables.
- Snap shot and/or continuous sensor monitoring.
- Derived parameter calculations.

The FDAU interfaces with the DTS for storage of flight and maintenance data. A high performance microprocessor in the FDAU samples, scales, and processes the data before it is recorded. The aircraft mishap data and audio data is stored in the VADR™ Crash Protected

Memory (CPM) in non-volatile Electrically Erasable/Programmable Read-Only Memory (EEPROM), while the flight and maintenance data is stored in the DTM non-volatile memory. Documentary and Built In Test data is also stored in the DTM.

The VADR™ provides data collection and mishap recording of audio data, aircraft flight and system parameters to support post incident analysis. The Cockpit Voice Recorder (CVR) function of the VADR™ provides recording of cockpit voice, radio transmission and cabin area audio signals for accident investigation purposes. The Flight Data Recorder function of the VADR™ provides recording of mishap parameter data on periodic intervals. The FDR function is interfaced to the DAU via a RS-422 serial digital bus. The VADR™ complies with the crash survivability requirements of EUROCAE ED-55 (Chapter 7), EUROCAE ED-56 (Chapter 6), and EUROCAE ED-56A (Paragraph 5.3).

The VADR™ stores digital flight data and audio signals in nonvolatile memory located in a crash-protected memory housing. The VADR™ connects directly with aircraft audio systems to receive voice data. The digital flight data is received through a RS-422 serial interface to the FDAU. Discrete input and output signals are available as is an audio playback channel.

The VADR™ consists of the following three main components:

- Crash Protected Memory (CPM).
- Flight Data Recorder (FDR) and CPM Input/Output Interface.
- Cockpit Voice Recorder (CVR) Input/Output Interface.

Mishap flight data is sent to the VADR™ via a digital serial bus for storage in a specially crash protected non-volatile Electrically Erasable/ Programmable Read-Only Memory (EEPROM). A high speed RS-422 interface is also provided for data downloading and maintenance actions via the Ground Readout Equipment.

The voice recording interface accommodates four audio channels with each channel capable of storing a minimum of 1/2 hour of audio information. The audio inputs are received through analog buffers and then converted to a digital signal via an analog to digital converter. The

voice data is formatted and passed to a general purpose processor for storage in the Crash Protected Memory. In addition, the voice recorder interface provides an audio playback channel to monitor the audio input channels. Synchronization of the flight data and voice data recording functions is provided using an internally generated time tag stored in both the flight data and voice data.

The Ground Readout Equipment is used for downloading flight and voice data from the VADR™ when required. The GRE hosts the software and hardware used to download VADR™ data, display flight data and playback audio data.

The VADR™ Cockpit Voice Recorder function is supported by a CVR Control Panel designed per ARINC-557 requirements. The CVR control panel also includes the cockpit area microphone preamplifier.

Growth potential for the system includes adding vibration data from the VMS to the information stored in crash protected memory. This is considered to be extremely valuable information for helicopter incident investigation purposes.

The SH-60B HUMS incorporates a high capacity Data Transfer System which provides significant operational flexibility to the HUMS operation by the aircrew and maintenance personnel. The airborne portion of the DTS consists of a removable Data Transfer Module and a Data Receptacle Unit. The DRU is a small, rugged chassis that rack mounts in the helicopter and provides the physical mounting and electrical interface for the DTM.

The DTM is a small, rugged, solid-state portable memory cartridge used for digital information storage, loading, and retrieval. The DTM utilizes high density Flash EEPROM memory for data storage. As part of the airborne HUMS, the DTM is located within the DRU. The DTM is easily inserted in and removed from the DRU for data downloading, processing, and analysis on the Ground Support Station.

The baseline SH-60B HUMS DTM has a capacity of 40 Mbytes with as expansion capacity to 150 Mbytes if required. An additional DRU and supporting interface are incorporated in the Ground Support Station

(GSS). The DTS provides the primary data recording media for all of the HUMS subsystems during normal aircraft operation. This includes both processed (e.g. flight regimes, system health indicators, etc.) and unprocessed data (e.g. flight data compressed data files, vibration monitor log files, EEMS pulse data, etc.). Additional HUMS data transfer capability is provided via a onboard HUMS Ground Readout Equipment (GRE) connector which interfaces to the Ground Readout Equipment for HUMS installation integration, repair and troubleshooting.

The Vibration Monitoring System is an advanced vibration monitoring system that provides helicopter health monitoring and processing functions. The VMS is a compact, lightweight high performance data acquisition and processing subsystem that is a derivative of the vibration monitoring system for the US Air Force MH-53J helicopters. The VMS functions include comprehensive rotor, drive train, gearbox, engine and structures health monitoring, diagnostic data acquisition and maintenance processing. Key SH-60B HUMS VMS functions include:

- Automatic or manual collection of vibration and optical tracker data from a series of flight regimes.
- Collection of spectra from a series a flight regimes for trend monitoring.
- Capture of random spectra for analysis of intermittent aircraft events.
- Collection of spectra for health monitoring.
- In-flight check of vibration conditions for:
  - Main and tail rotor.
  - Engines and oil cooler.
  - Gearboxes (input modules, intermediate gearbox and tail rotor gearbox).
  - Shafts (high speed input shafts.)
  - Airframe (absorbers and airframe signature).
- Calculation of rotor and blade maintenance adjustments based on track and vibration data.

- Calculation of main and tail rotor and shaft balance solutions.
- Identification of vibration levels and exceedences.
- Continuous monitoring of vibration frequencies and amplitudes.

The VMS acquires main and tail rotor data and calculates and displays corrective actions, using all available adjustments to minimize aerodynamic and mass imbalance induced vibrations. Rotor smoothing experience to date demonstrates that vibration levels well below manufacturers' limits are attainable in two sets of adjustments on rotor systems with no mechanical faults. The VMS incorporates continuous engine vibration monitoring, event capture and pilot advisory for manufacturers' limit exceedence.

The VMS provides sensor interfaces for vibration sensors (velocity and acceleration), speed sensors (magnetic pickups and photocells) and a blade track sensor. The SH-60B HUMS VMS sensor locations are shown in Figure 3.

The VMS acquires main rotor track information by use of a permanently mounted Optical Blade Tracker (OBT) with shock mounted, sealed, anti-reflection optics. The OBT passively measures the blade lead, lag and track height during day and low light conditions. The OBT provides precise timing pulses of blade passage from which relative blade height and lead/lag measurements are derived. The track and lead/lag data acquisition are integrated with main rotor balance solution. The OBT is mounted on the forward fuselage, on the advancing side of the nose, oriented upward toward the underside of the rotating blades. It views each blade through a ten degree window and operates on the principle that a high-flying blade will remain in the field of view longer than a low-flying blade. This timing is then converted to distance data by use of a sensitivity constant base on the sensor-blade installation geometry. The internal circuitry is adaptive to adjust for different contrasts and changing light levels. The OBT also has its own light source that can be used for night operations.

The VMS provides a date and time stamp that is communicated to the FDAU for use in time correlation of flight parameters with continuous

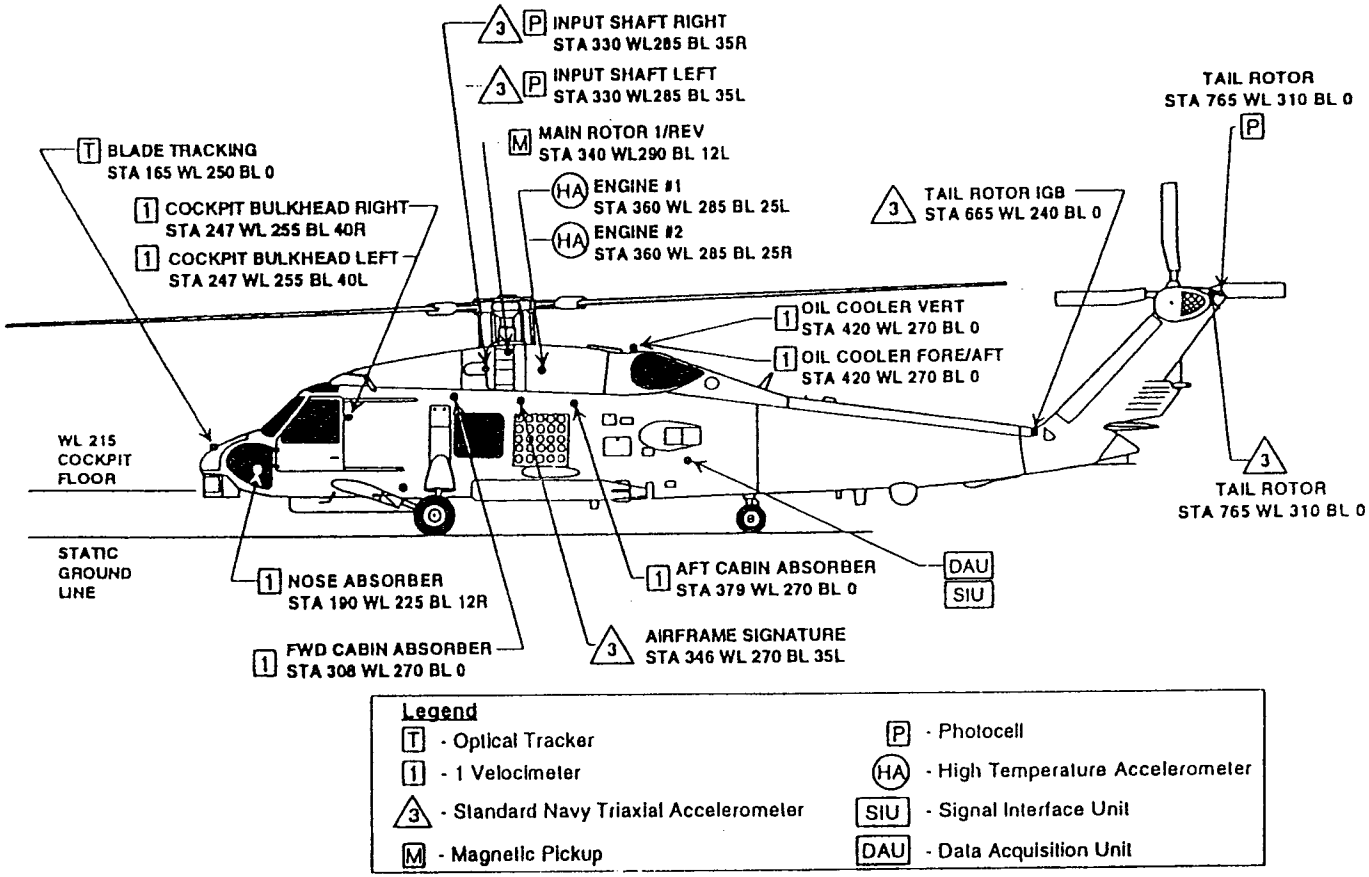

Figure 3 SH-60B HUMS Vibration Sensor Locations

vibration data. The ability exists to expand the output from the VMS to allow for triggering of flight data snapshots at the time of vibration exceedence detection.

The Ground Readout Equipment is an personal computer which interfaces to the DAU for data upload, download, and maintenance actions. The GRE allows the operator to download flight and voice data from the VADR, upload data, and perform BIT and status interrogations of the HUMS via a RS-422 interface. The GRE provides the operator with the capability to display in real time the aircraft parameters being acquired by the DAU. This procedure is used on a powered up aircraft to check suspected problems with aircraft wiring and sensors feeding data to the DAU. The GRE can provide both real-time and off-line display of flight data and playback of voice data.

The DTU provides all interfaces necessary for on-board vibration maintenance in addition to the VMS automatic data acquisition and storage functions. The automatic functions are based either upon regime recognition or by periodic acquisition and exceedence checking. The DTU is used to provide additional maintenance functions such as air crew scheduled data acquisition, input for track and balance adjustments performed by the maintenance crew, review of system faults, display of log files and maintenance actions, and upload of new operational programs or configuration files.

The GSS is an IBM compatible desktop, commercial personal computer and printer which is used to download HUMS from the DTM and host the HUMS data analysis programs. The GSS can also be used to display the mishap flight data and replay the voice data. The GSS provides the capability to archive HUMS data using a high capacity memory back-up storage unit.

The GSS software includes generalized data management and analysis packages geared toward analyzing data and managing maintenance operations. The GSS allows the user to perform manual and automatic analysis of data based on procedures established by the equipment manufacturers. The primary analysis tools for the SH-60B

HUMS are the Windows Data Review Tool (WinDRT) for flight data display and analysis and the Vibration Monitoring System (VMS) VibraLog program for vibration data analysis. The ground support analysis tools also provide correlation of flight recorder data with vibration data and engine electrostatic activity to enhance post mission analysis capability.

The Windows Data Review Tool (WinDRT) is the primary tool for analysis of flight data acquired by the HUMS. WinDRT provides the following review and analysis capabilities:

- Interactive user selection of a particular flight or other block of recorded data from those available in a downloaded data file.
- Interactive viewing and manipulation of flight data in a tabular text form including the hiding of columns of non-relevant parameters, permuting of the order in which the parameters are displayed, and rapid access to any part of the data.
- Interactive viewing and manipulation of flight data in graphical form.
- The capability to selectively print some or all of the flight data.

WinDRT is generic in its operation such that changes in the recorded parameters, method of formatting, or other recorder system specifics do not affect its operation. Once WinDRT has been directed to a particular data block within a data file, the data is presented to the user in a tabular text format. The dual plot mode of WinDRT displays a plot of user-selectable parameters. As illustrated in Figure 4, the lower graph presents the data for the duration of the recording session and is useful for spotting segments of particular interest within the data. The upper graph is a plot of the same two parameters but is a magnified view. The cursor box on the lower graph outlines the segment of the data that is plotted on the upper graph. By sliding the cursor box across the lower plot, the user can see a magnified view of any section of the data. For example, to find the value and time of the occurrence of a peak in the data, simply place the cross-hair on that peak and then read the values in the parameter field boxes. In the full plot mode shown in Figure 5,

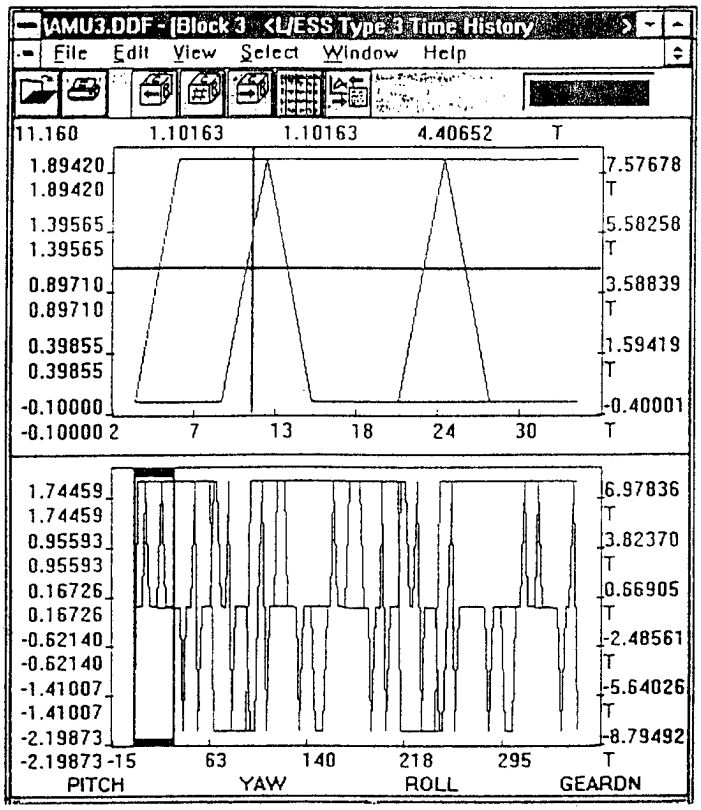

Figure 4 WinDRT Dual Plot Mode

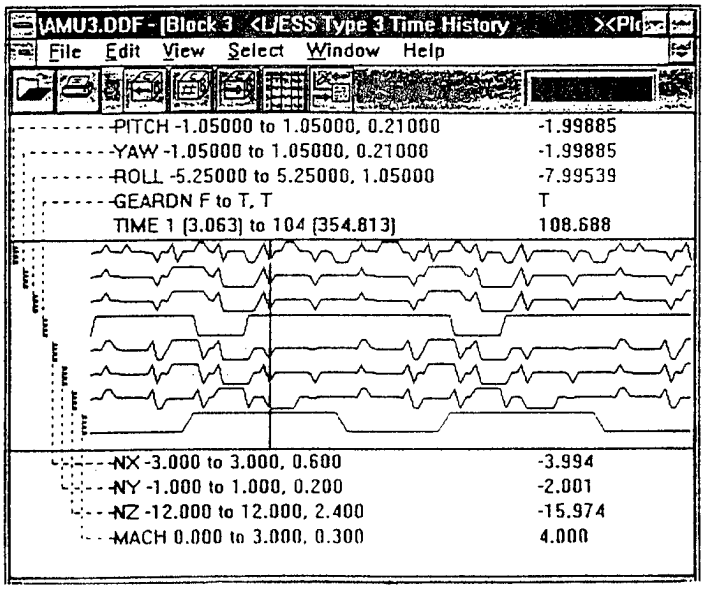

Figure 5 WinDRT Full Plot Mode

graphs of a number of flight data parameters can be displayed to allow determination of events.

VibraLog for Windows (VLFW) is the core of the SH-60B HUMS vibration analysis system. VLFW is a complete predictive maintenance productivity tool which automates routine operations for speed and simplicity while offering the widest array of analysis facilities for fault diagnostics. Unique features like aircraft templates make it possible to set up and manage very large databases easily. Other features allow for configuring airborne data acquisition functions on the ground, uploading and running the configuration files on the aircraft, and downloading and analyzing the data on the ground. VLFW functions include:

- Overall trend plotting.
- Spectrum alarm envelope.
- Frequency band alarms.
- Frequency trend plotting.
- Condition summary reports.

Figure 6 shows a simple plot of a spectrum measurement. VLFW provides more complex plot types such as the one shown in Figure 7. This plot window contains three plot panes containing a spectrum plot, a waterfall plot of that spectrum measurement over time, and the trend of one frequency of the spectrum. In any of the panes the user may step to the next measurement in time and all plots will automatically track together. In addition, the user can create his own custom plot types combining any number of plot panes.

Different types and levels of alarms can be attached to a vibration measurement. There are categories of alarms available for every supported measurement type including magnitude alarms, spectrum alarms and frequency band alarms. The levels for the alarms can be set as a constant value, a statistical value based on a given sample population, or as derived from a user defined baseline measurement.

The VLFW system also allows the creation of new vibration databases which define data acquisition and alarming parameters. The

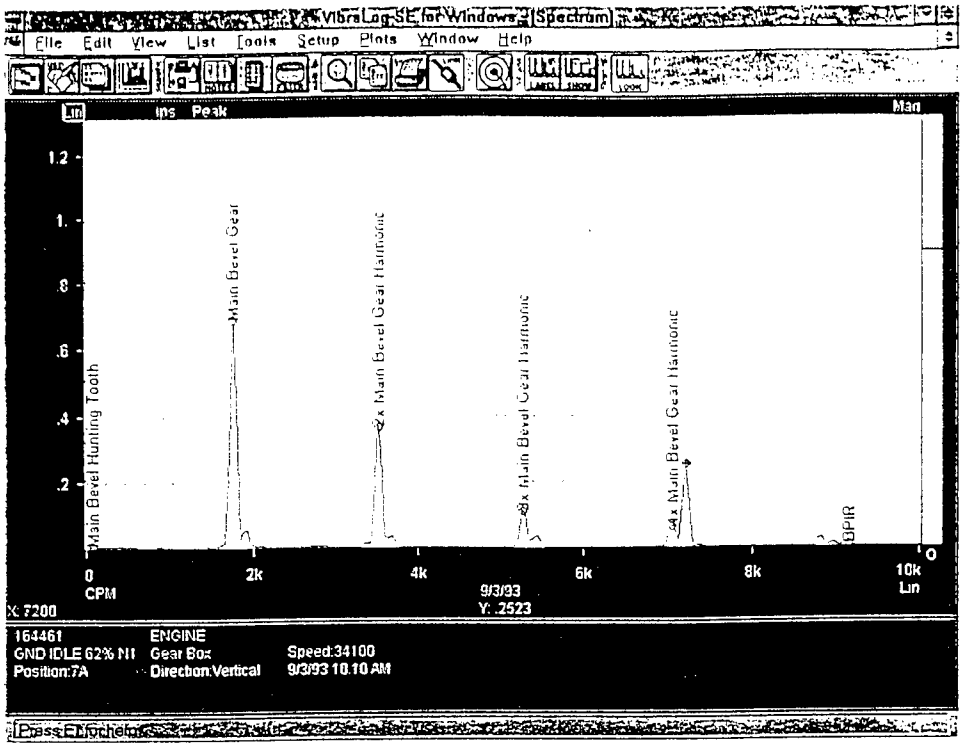

Figure 6 VLFW Single Spectrum Plot

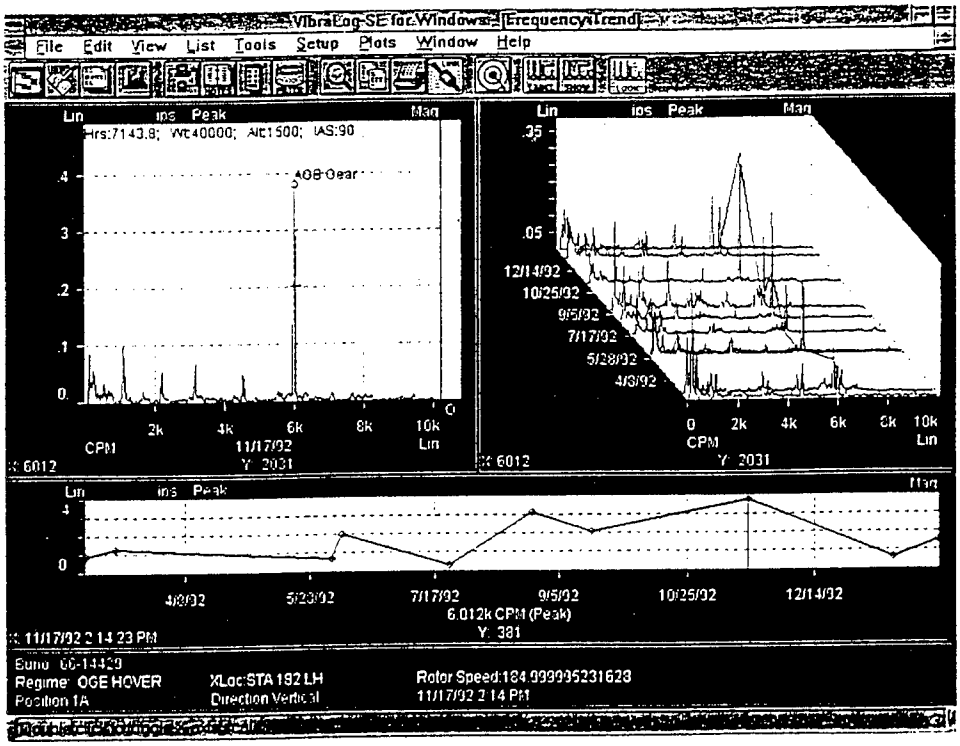

Figure 7 VLFW Combined Spectrum and Trend Plot

operator can then create a VMS configuration file which can be used to dynamically reconfigure the VMS system for testing and evaluation or for specialized vibration analysis tasks. The acquired data can then be downloaded to VLFW for storage and analysis.

The SH-60B HUMS is currently undergoing flight trials on a US Navy SH-60B helicopter at the US Navy Naval Air Station (NAS) North Island in San Diego, CA. The HUMS was installed in February 1995 and has logged over 560 flight hours to date. The following summarizes the current status of the SH-60B HUMS demonstration:

- Aircraft installation and wiring complete.
- Flight system monitoring and recording.
- Engine system monitoring and recording.
- Engine, airframe, and drivetrain continuous vibration monitoring and recording.
- All HUMS data (aircraft system data, vibration data, etc.) recorded to an onboard DTS with a removable 40 Mbyte data cartridge.
- Mishap voice and aircraft system data recorded to crash survivable memory.
- Ground support equipment and software delivered and operational.

The following baseline SH-60B HUMS capabilities are currently being implemented:

- Main rotor track and balance.
- Tail rotor balancing.
- Vibration absorber tuning.
- Onboard signature checks.
- Engine exhaust monitoring.

A significant amount of correlated flight and vibration data has been acquired by the SH-60B HUMS. This data is being reviewed on site at NAS North Island by the Naval Aviation Engineering Service Unit (NAESU) SH-60B Airframe and Vibration Specialist and at the Naval Aviation Depot (NADEP) Cherry Point by the SH-60B Engineering

Group. Evaluations are being done to determine the effects of flight on the vibration levels at the points established by the US Navy Maintenance Operating Procedures for the SH-60B and to assess if the in flight vibration levels are consistent with the predicted levels for the helicopter. Preliminary analysis of the data shows that there are certain maneuvers performed with the helicopter that significantly increase the vibration levels experienced by the airframe.

The continuous monitoring of vibration on the helicopter is also providing trending data that can be used in determining the effects on the helicopter structure that are a direct result of wear on components that cause changes in balance of the main rotor, tail rotor, and high speed shafts.

During this demonstration, trend spectrums are being collected every 150 flight hours on the helicopter for use in projecting component replacement and maintenance activity schedules.

In addition to providing data that can be used in assessing the affects of flight on the airframe, the system has been shown to have the potential to accurately track normal and exceedence usage time on the airframe, engines, and rotors of the helicopter. Data has also been used to determine the actual levels of engine torque and rotor speed experienced by the helicopter on specific flights.

The requirement for operational readiness rates of military helicopters is higher than ever before. Total health of a helicopter requires factoring in vibration data to provide component wear and mechanical integrity assessment not originally calculated in airframe lifing. The permanently installed HUMS provides the necessary correlation between vibration levels, helicopter flight regimes, and aircrew induced vibrations to give this total health assessment and improve operational readiness rates. Additionally, a permanently installed HUMS improves operational safety and provides reduced maintenance time and costs through the elimination of carry on equipment. The US Navy has also identified a requirement for on-line diagnostics for improved flight safety and maintenance of helicopter

engines and drive systems. Smiths Industries, teamed with Chadwick-Helmuth Company, has developed an Integrated Health and Usage Monitoring System (HUMS) which incorporates mechanical diagnostic technologies for airframe, propulsion and drive train monitoring to meet these requirements. The HUMS is currently undergoing flight trials on a US Navy SH-60B helicopter. This paper describes the system capabilities and summarizes the status of the SH-60B trials.

B-2 Aft Deck Redesign

B-2 SPO **ASC/YSDF**

- *2d Lt Greg Buckner (Speaker)*
- *Frank Grimsley*

NorthropGrummanB-2 Division

- *Gary Carney*

Overview

- Aft Engine Environment
- Original Aft Deck Description and History
- Redesign Process
- New Aft Deck Selection
- Current Status
- Conclusions

Aft Engine Environment -- Structural Goals

- Endure high exhaust temperatures
- Maintain structural integrity through repeated temperature variances
- Maintain aircraft low observables (stealthiness)

Solution: Aft 'Deck'

- Aft Deck Original Configuration
  - Secondary structure, exposed to engine exhaust gases
  - Titanium 6-4 material
  - Bead stiffened
  - Chem-milled pockets (between beads)

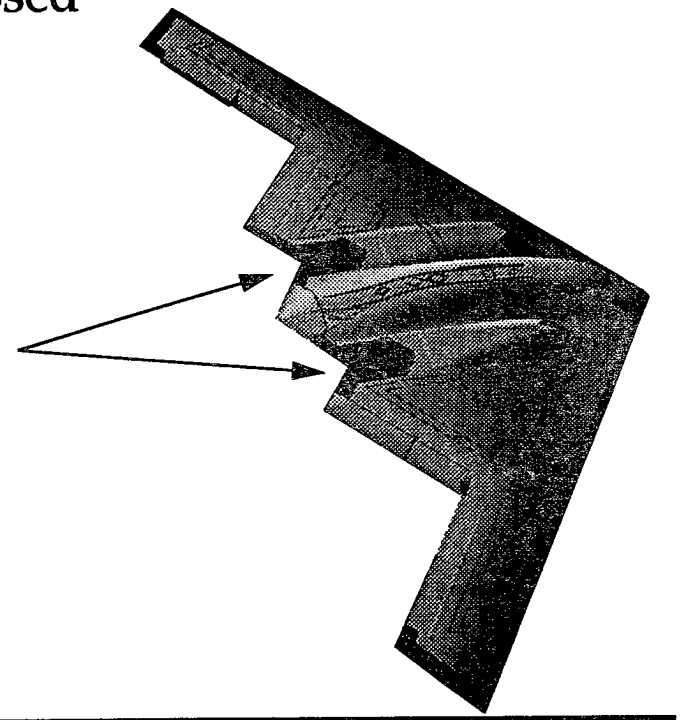

Aft Deck Failure

- March 30, 1990, the first Aft Deck cracks were discovered on AV - 1
  - 150 ground hours of engine run up
  - 30 hours of flight
- Cracks continued to occur on all six flight test aircraft
  - Occurred randomly, in rear location on either deck

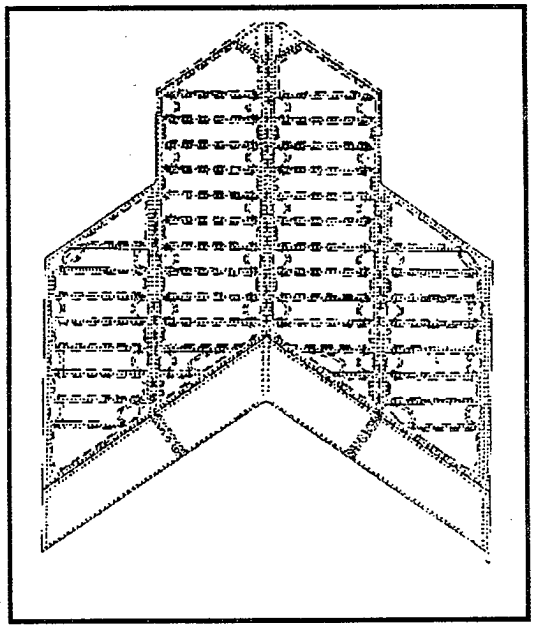

Aft Deck Cracking Locations

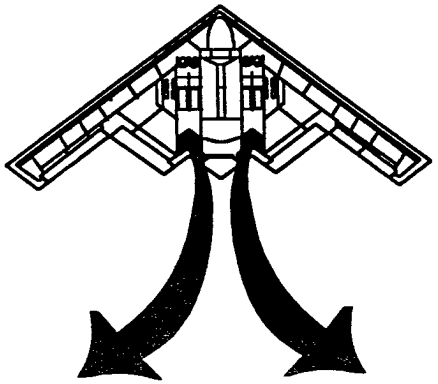

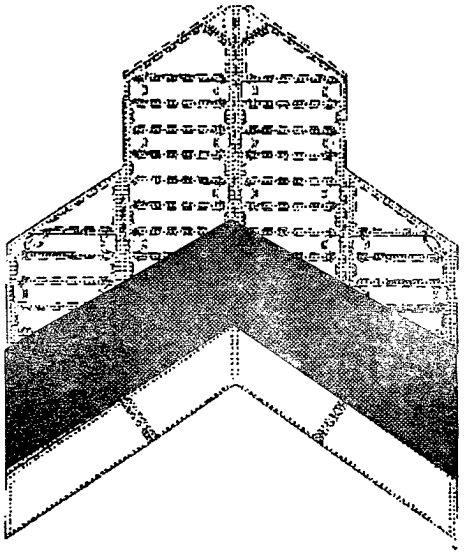

ENGINE #1 ENGINE # 2

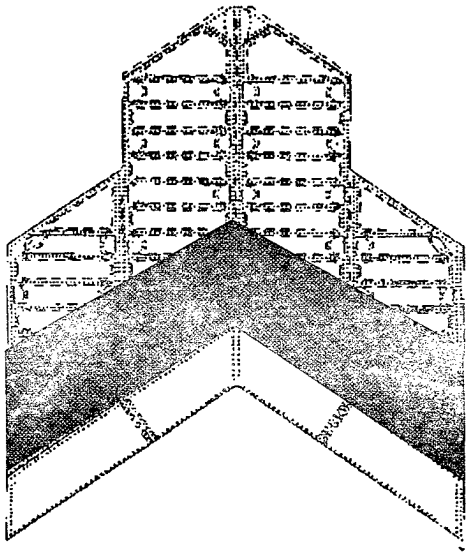

ENGINE #3 ENGINE # 4

Aft Deck Redesign

- An independent review team was established of Air Force structural experts to overview the entire redesign and failure investigation
- In June 1990, an Aft Deck Red Team was formed, membership included:

  - Vought (designer of deck)
  - Northrop
  - General Electric (tailpipe manufacturers)
  - Pratt & Whitney (engines)
  - NASA
  - Boeing
  - ASC structural and material experts
  - University Consultants

Concept Selection

- The entire spectrum of redesign options (46 in all) were evaluated
  - Cooling of the exhaust
  - Various material options and structural concepts
- As a result of the above effort, two options were selected for detailed review. They were:
  - Floating liner
    - » Cooled or uncooled
  - Modified baseline design
    - » Change material
    - » Minor structural change

Option #1: Cooled Floating Liner

- Pros
  - Liner carries no aircraft loads
  - Liner thermal loads are greatly reduced by allowing in-plane thermal expansion
  - Liner is relatively easy to repair and replace
- Cons
  - Frequent access requirement for cooling system inspection/maintenance
  - Cost/schedule

Option #2: Modified Baseline Design

- Pros
  - Material change to higher temperature Ti 6-2-4-2 (engine material)
  - Thicken the skin by removing the chem-milled pocket above the beads
  - Replace titanium fasteners with higher strength and temperature capable Inconel (steel) fasteners
- Cons
  - High Skin Temperatures
  - Difficult to analyze and predict structural life

Selection: Modified Baseline Design

- July 1991, the Modified Baseline Design option was chosen based on schedule, cost, and technical risk factors

Modified Baseline Design Analysis

- Aft Deck redesign used a second order, non-linear analysis method to insure that the complex thermal and acoustic load patterns could be accurately analyzed.
  - Typical structures analyzed with a first order analysis method.
- Calibration with AV - 2 flight test data and full scale thermal test conducted on the full-scale static test article.

Modified Baseline Design Analysis (cont.)

- Fatigue analysis was conducted that combined both thermal and acoustic loads based on ACC operational usage profiles
  - New engine ground run-up load spectrum was developed and included in the analysis
  - The usage data for this spectrum was develop by General Electric and Air Combat Command

Modified Baseline Design Component Testing

- The Titanium 6-2-4-2 material with the modified baseline structural option was qualified by testing over 500 specimens
  - Tests included both temperatures and loads
  - Tests were both static and dynamic
- The overall design was verified by 20+ component combined thermal/acoustic tests
  - These tests validated the durability and static test analyses
  - Tested at worst case temperature and acoustic levels

Modified Baseline Design Verification Testing and Schedule

- Modified Baseline Design has been flight tested for over 495 flight hours
  - The aircraft (AV - 2) is in modification prior to delivery to ACC
  - 100% NDI has revealed no defects (ring & pencil probe and ultrasonic analysis)
- AV - 14 will be the first production aircraft with the new Aft Deck design
- AV - 7 through AV - 13 were delivered with the old design and as expected, require periodic repairs

Current Status

- New Aft Deck Design
  - No crack indications during 495 hours of flight test
  - First production aircraft with deck delivered to Whiteman AFB on 14 November 1995
- Old Aft Deck Design
  - Seven operational aircraft continue missions with originally designed aft decks
  - All aircraft will return to modification line for new Aft Deck prior to 750 flight hours
    - » Predictions indicate that every deck will crack before 750 flight hours

Crack Repair Philosophy

- Stop drill up to approximate 3.0 inch crack
  - Limitation driven by crack configuration and location on deck
- Doubler repair required when crack exceeds stop drill limitation
  - Requires extensive down time because lower-side panels must be removed
  - Patch designed to meet stringent low observable requirements and prevent development of future cracks

Original Aft Deck Repairs

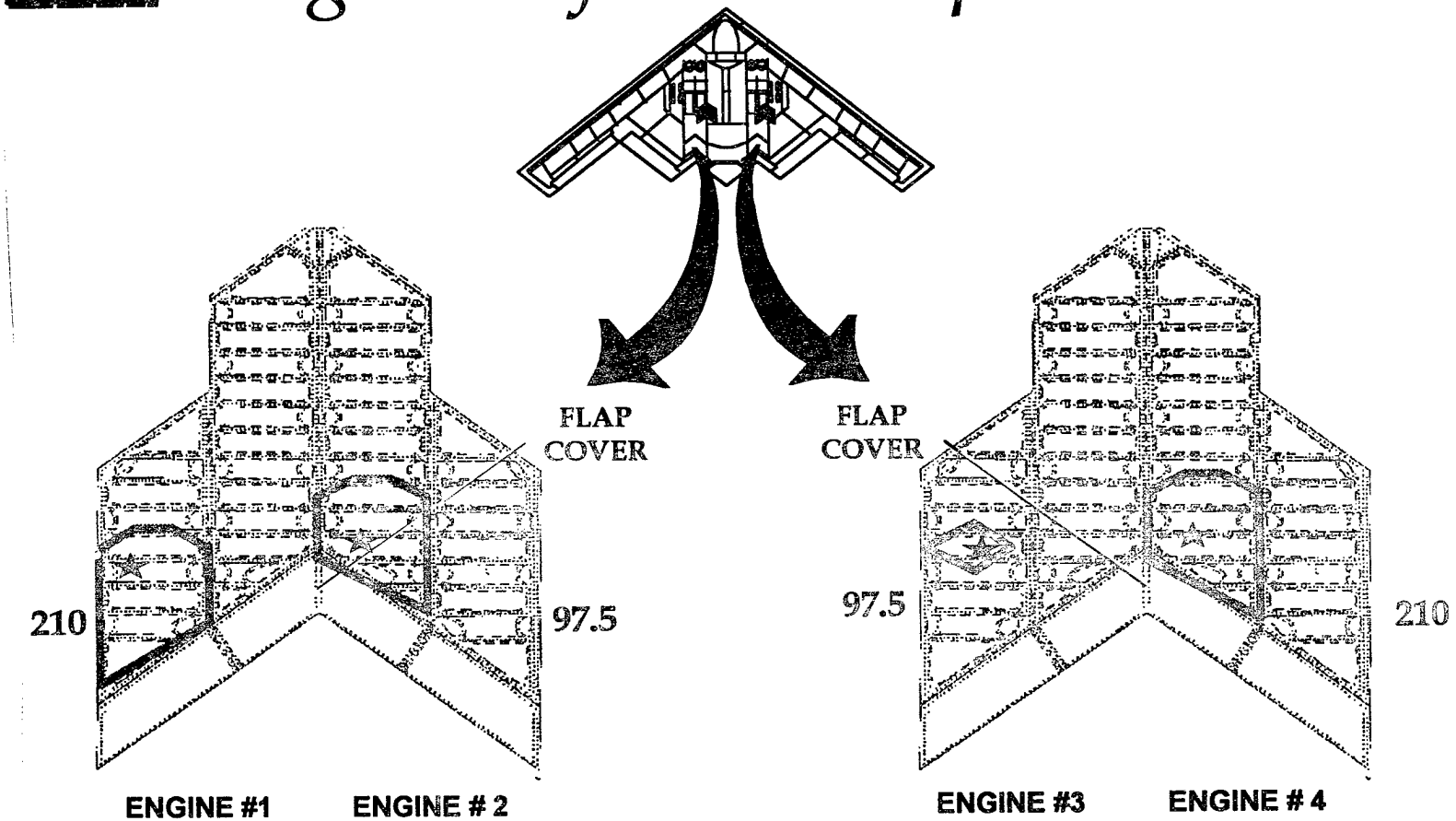

Conclusions

- Original design proved to be faulty due to incorrect temperature predictions in aft engine environment
  - Full-scale predictive tests for engine compatibility performed, temperature results were interpreted incorrectly
- Integrated team formed of technical experts across government, education, and industry to assess redesign options
  - Sped up the preliminary design time
  - Collocated at Vought in Texas

Conclusions

- Repairs for the old decks have been developed and though not ideal, will enable the operational aircraft to be useful until modification
- The new deck design was delivered to the operational wing the middle of November
  - Optimum design, verified by 495 hours of flight test

The B-2: Yesterday's Dream, Today's Reality.

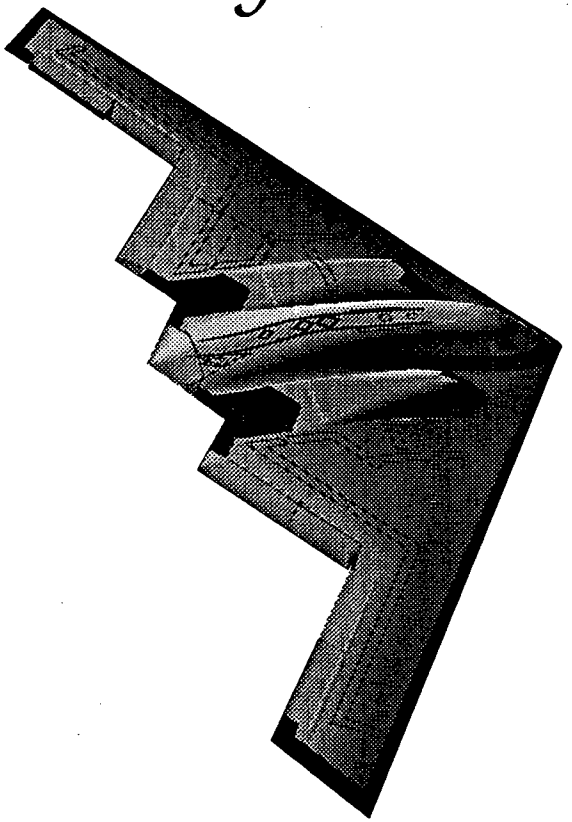

SESSION V

ENGINES

Chairman: ***Wing Cmdr C. Pomfret*****, WL/POTC**

Effect of Machining Processes on the LCF Life of Holes in High Strength Nickel Base Powder Metal Components

S. P. Kamat, Senior Engineer
W. D. Cowie, Senior Staff Engineer
Large Military Engine Life Management
GE Aircraft Engines
November 28, 1995

Outline

- Background
- Purpose/Approach
- Test Program
- Data Analysis
- Results
- Summary

Background

- Hi-strength nickel base powder metal model disk tests highlighted potential loss of LCF capability due to high speed drill and/or reaming

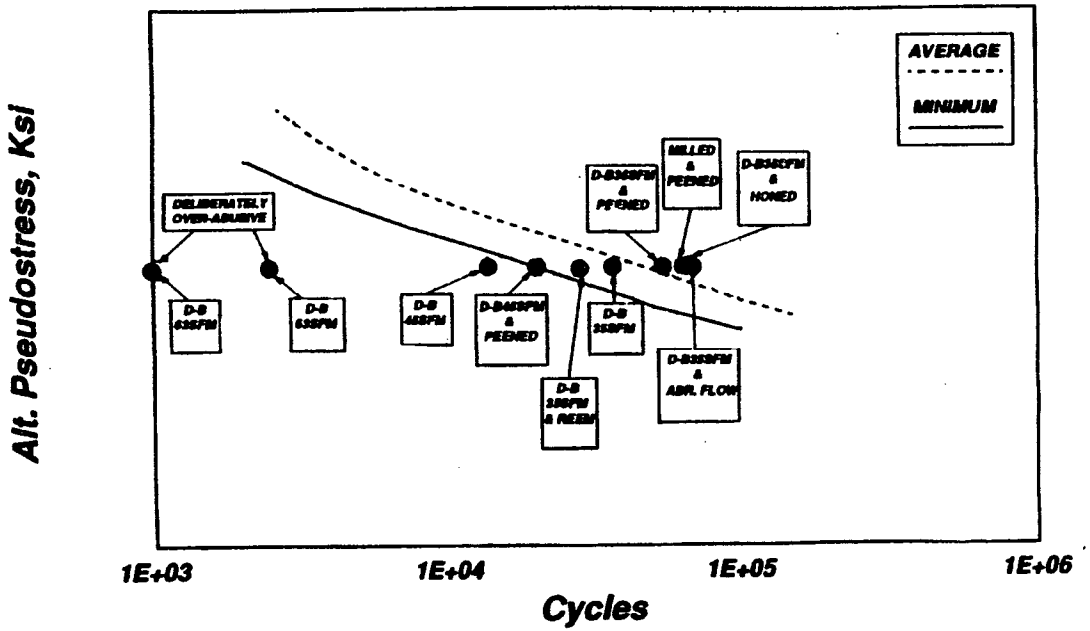

Background (Cont.)

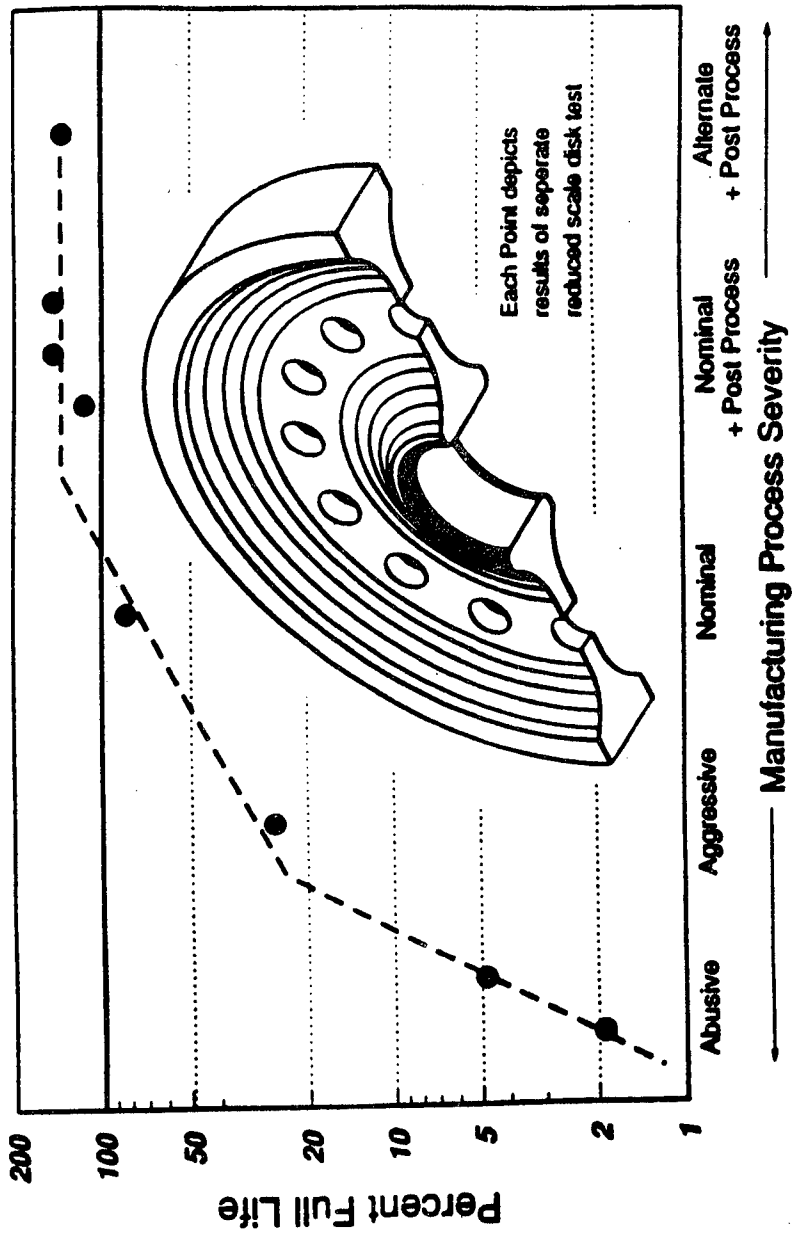

Purpose/Approach

Purpose: Define and demonstrate a practical method to evaluate the effects of manufacturing hole making processes on fatigue life of high strength Nickel Base Powder Metal Components

Approach: Evaluate various hole making processes through a cyclic test program using both feature specimens and scaled model disks for verification and compare results with standard design life predictions

Test Program
LCF Feature Specimen Tests Matrix

Component Feature	Machining Process	Tool Speed SFM	Hole Dimensions (in)		Number of Tests
			Diameter	Depth	
Rim Hole	Drill/Ream	34/21	0.263	0.923	6
Web Bolt Hole	Drill/Bore	45	0.397	0.600	6

- 750°F Test Temperature

Test Program
LCF Feature Test Specimen
To Simulate Different Hole Configurations

- Representative processes utilized to machine holes
  - Tools and speeds
- S110 Shotpeened (6-10A)
- Shims used, to simulate deeper rim thickness, when machining/peening holes

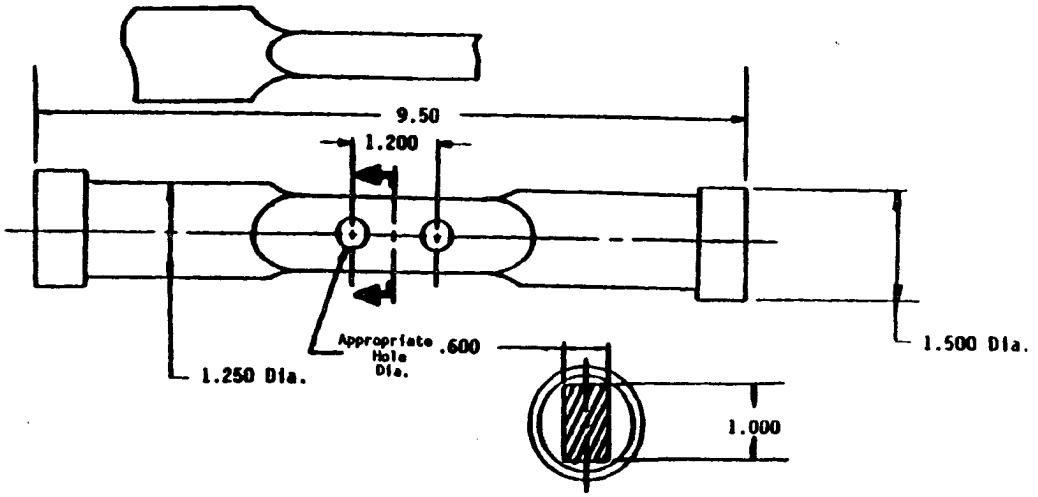

Test Program (Cont.)

Model Disk to Simulate Disk Rim Holes

- Hole machining process: 34 SFM Drill/21 SFM Ream, S110 shotpeened (6-10A)
- 750°F

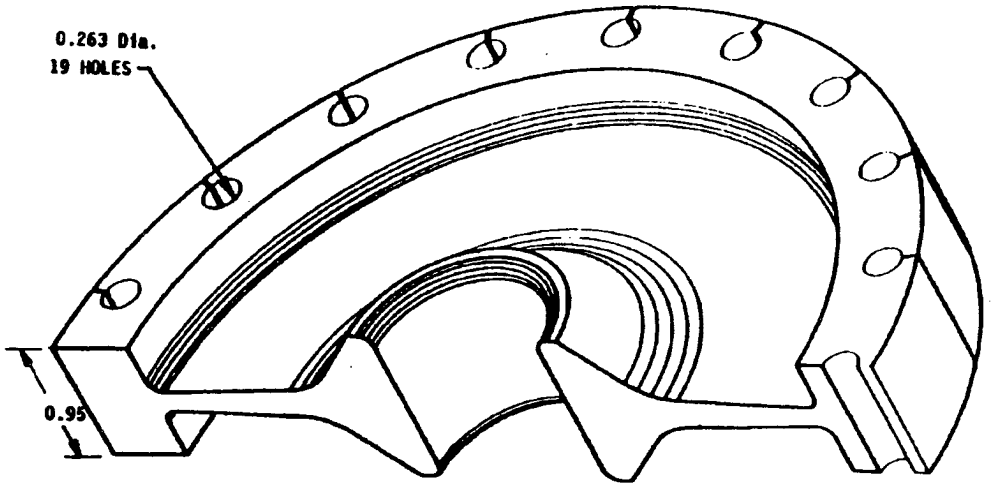

Test Program (Cont.)
Model Disk to Simulate Web Holes

- Hole machining process: 45 SFM Drill/Bore, S110 shotpeened (6-10A)
- 750°F

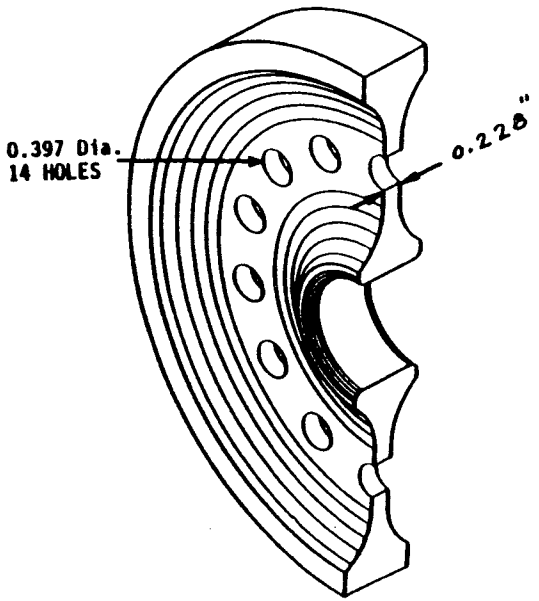

Data Analysis

- Feature test data analyzed using log normal approach (Lognorm Smith)
  - Predicts initiation life for a single hole
- Statistical methods employed to predict the first crack in the multi hole model disk from feature test data (Conditional Probability)
  - Conducted model disk tests to verify life predictions
  - Compare with life predictions from standard design curves and techniques

Data Analysis (Cont.)
Conditional Probability

- Probability of Failure for 1 Hole = $F(x)$

$\therefore$ Probability of Success = $1 - F(x)$

$\therefore$ Probability of Success for N Holes = $\{1 - F(x)\}^N$

$\therefore$ Probability of Failure = $1 - \{1 - F(x)\}^N$

Model Disk and Specimen Test Results

Test Results (Rim Holes)

- **34/21 SFM drill/ream process, S110 shotpeened (6-10A) - 750°F**

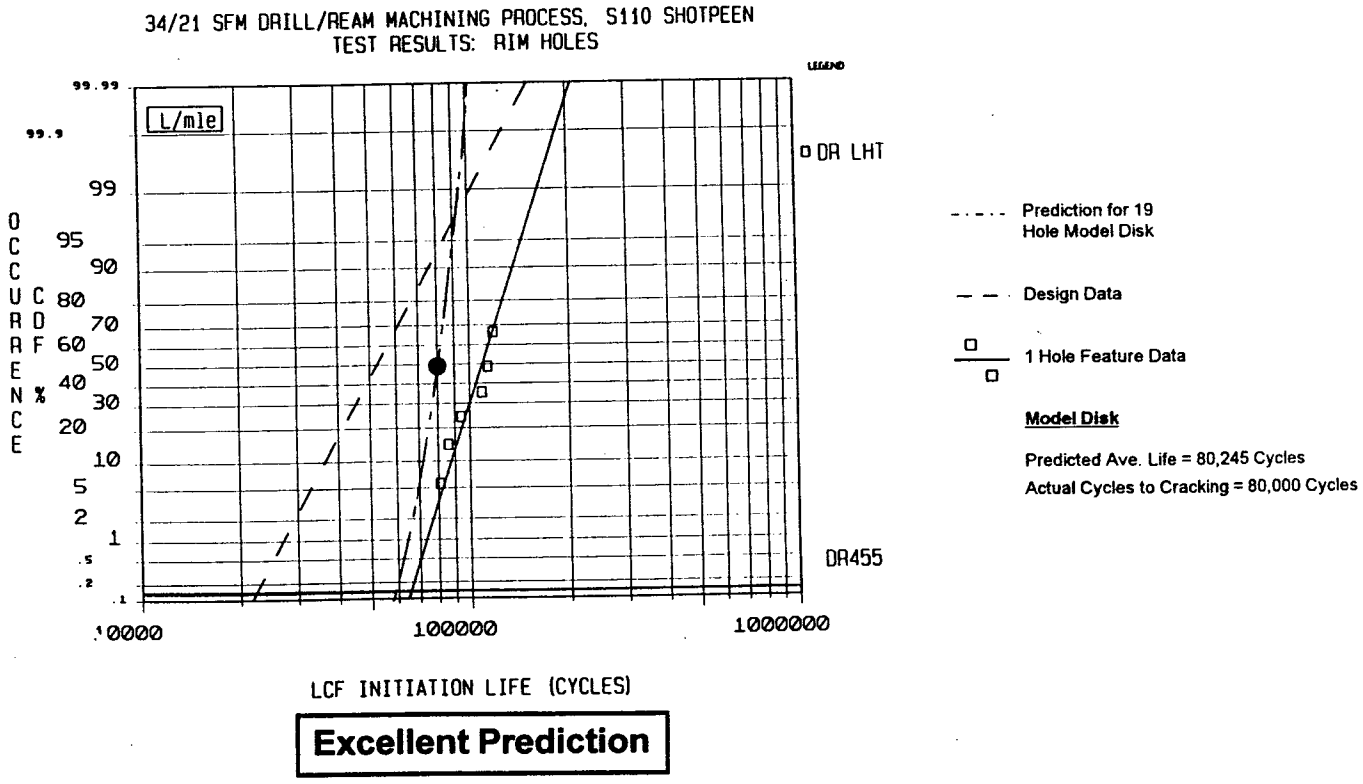

Excellent Prediction

Test Results (Web Holes)

- **45 SFM drill/bore process, S110 shotpeened (6-10A) - 750°F**

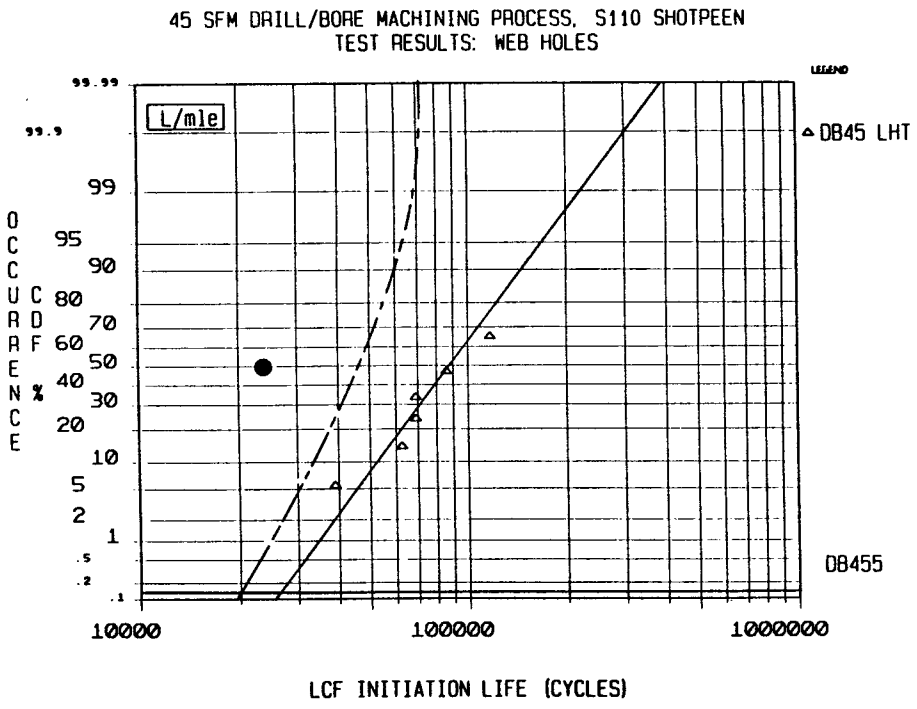

Prediction for 14 Hole Model Disk

1 Hole Feature Data

Model Disk

Predicted Ave. Life = 45,140 Cycles

Actual Cycles to Cracking = 23,500 Cycles

Prediction Not In Agreement with Test

Test Results (Web Holes)

- **45 SFM drill/ream process, S110 shotpeened (6-10A) - 750°F**

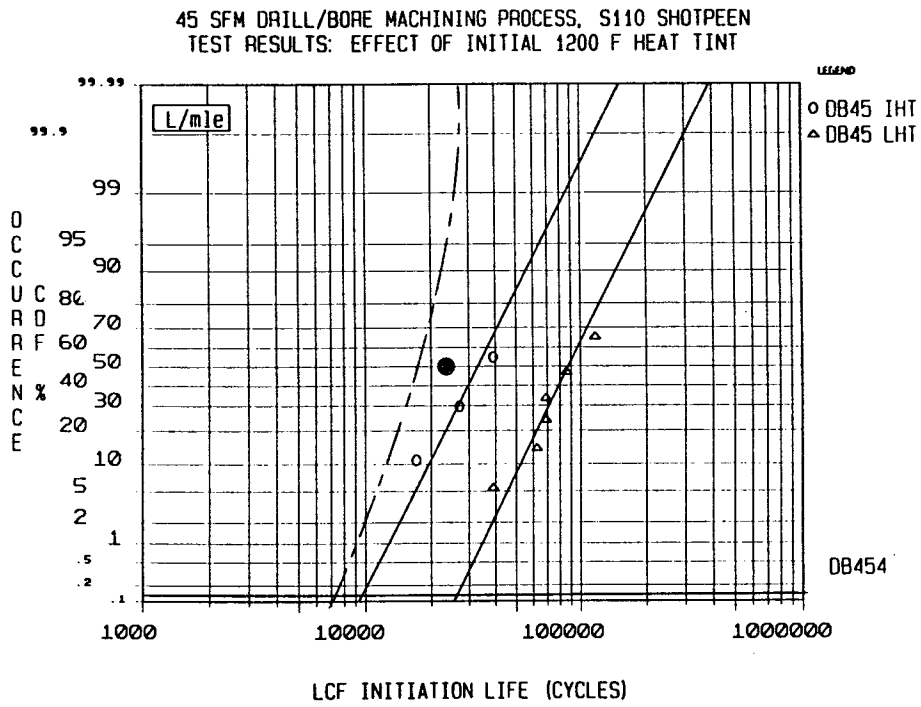

Prediction for 14 Hole Model Disk

1 Hole Feature Test Data Initial Heat Tint

1 Hole Feature Test Data Late Heat Tint

Model Disk

Predicted Ave. Life = 18,000 Cycles

Actual Cycles to Cracking = 23,500 Cycles

Recognition of Heat ~~Treat~~ TINT Influence Restores Predictability

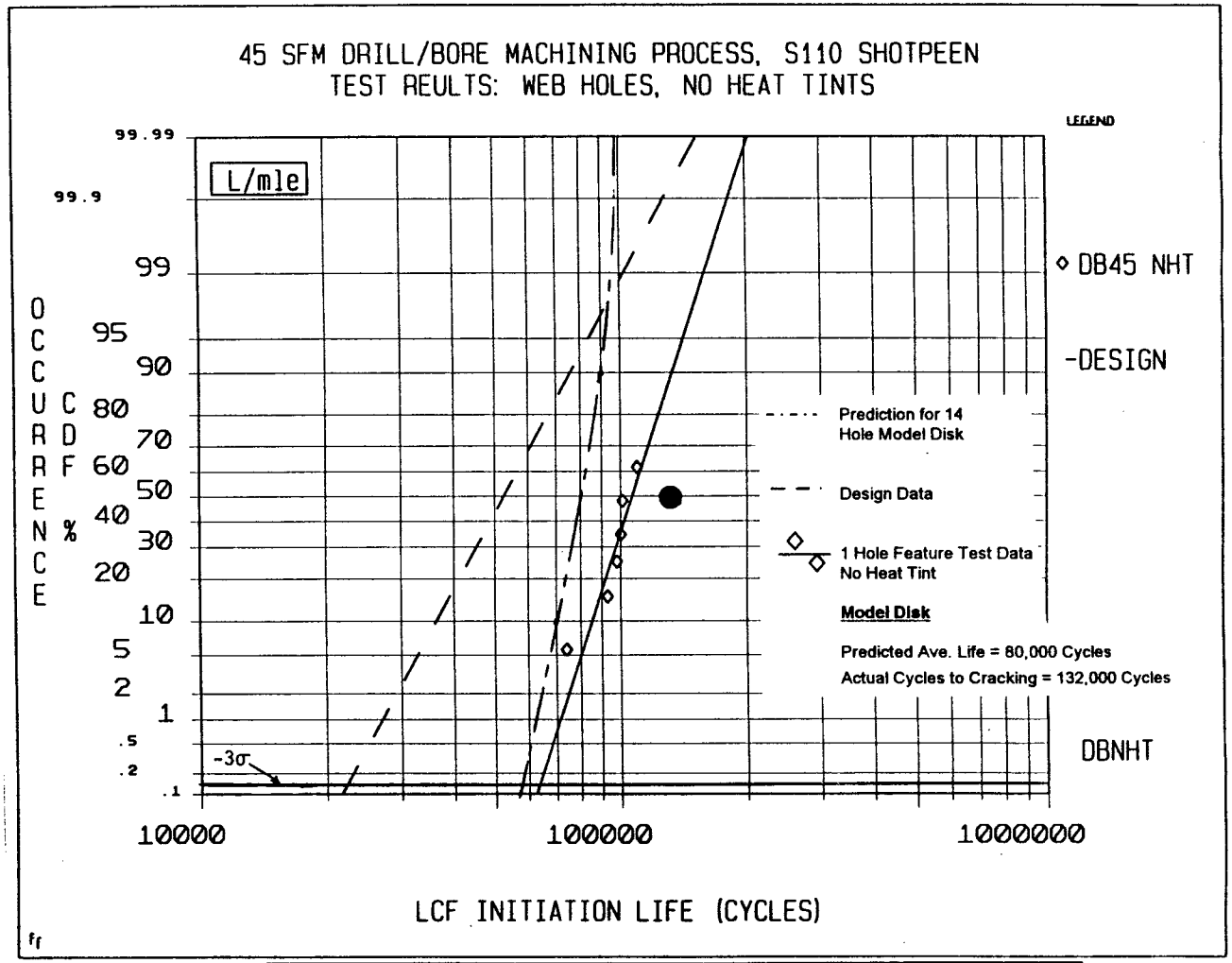

Strong Influence Relative to Design Expectations

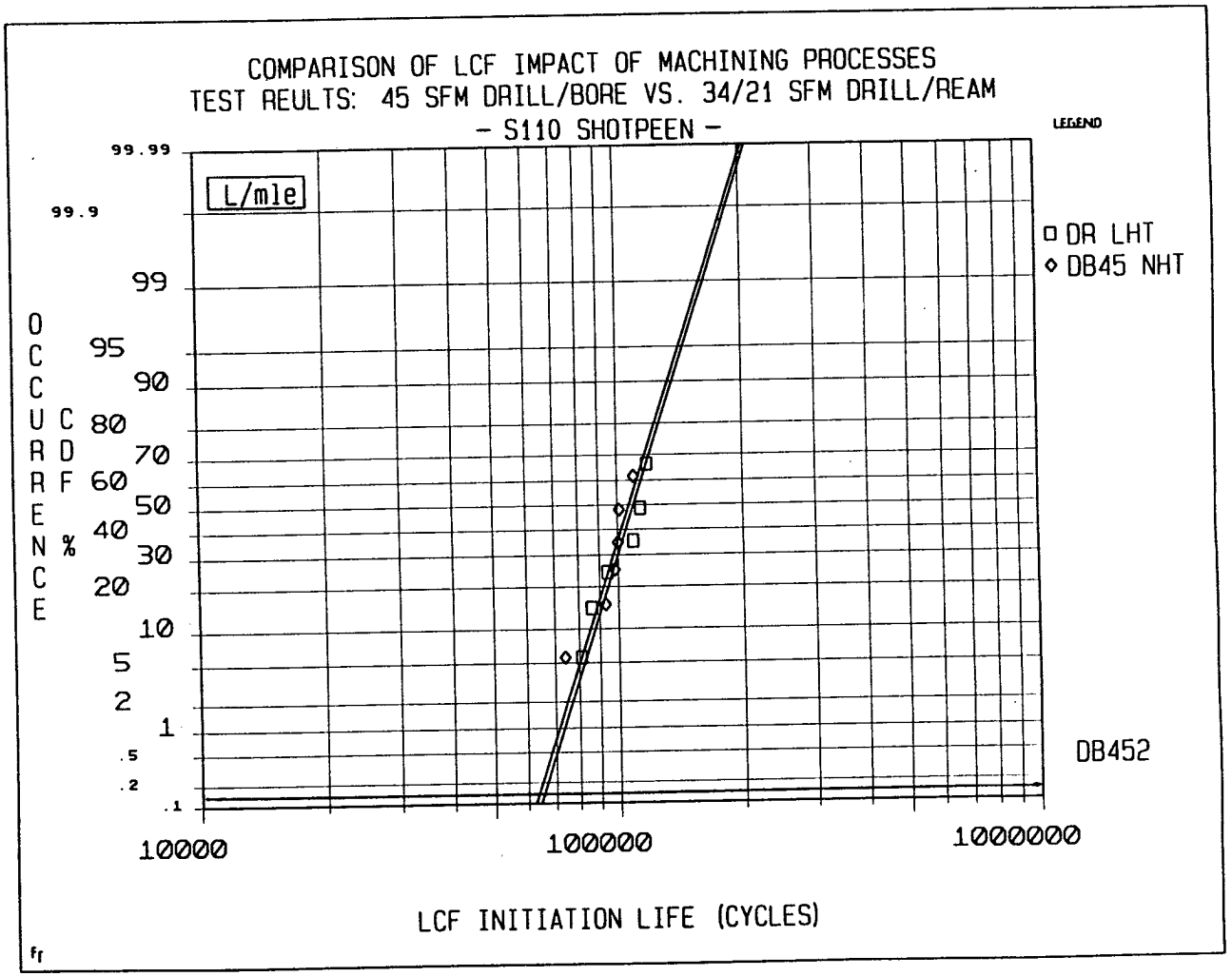
COMPARISON OF LCF IMPACT OF MACHINING PROCESSES
TEST REULTS: 45 SFM DRILL/BORE VS. 34/21 SFM DRILL/REAM
- S110 SHOTPEEN -
LEGEND
DR LHT
DB45 NHT
L/mle
99.99
99.9
99
95
90
80
70
60
50
40
30
20
10
5
2
1
.5
.2
.1
OCCURRENCE CDF %
10000
100000
1000000
DB452
LCF INITIATION LIFE (CYCLES)
fr

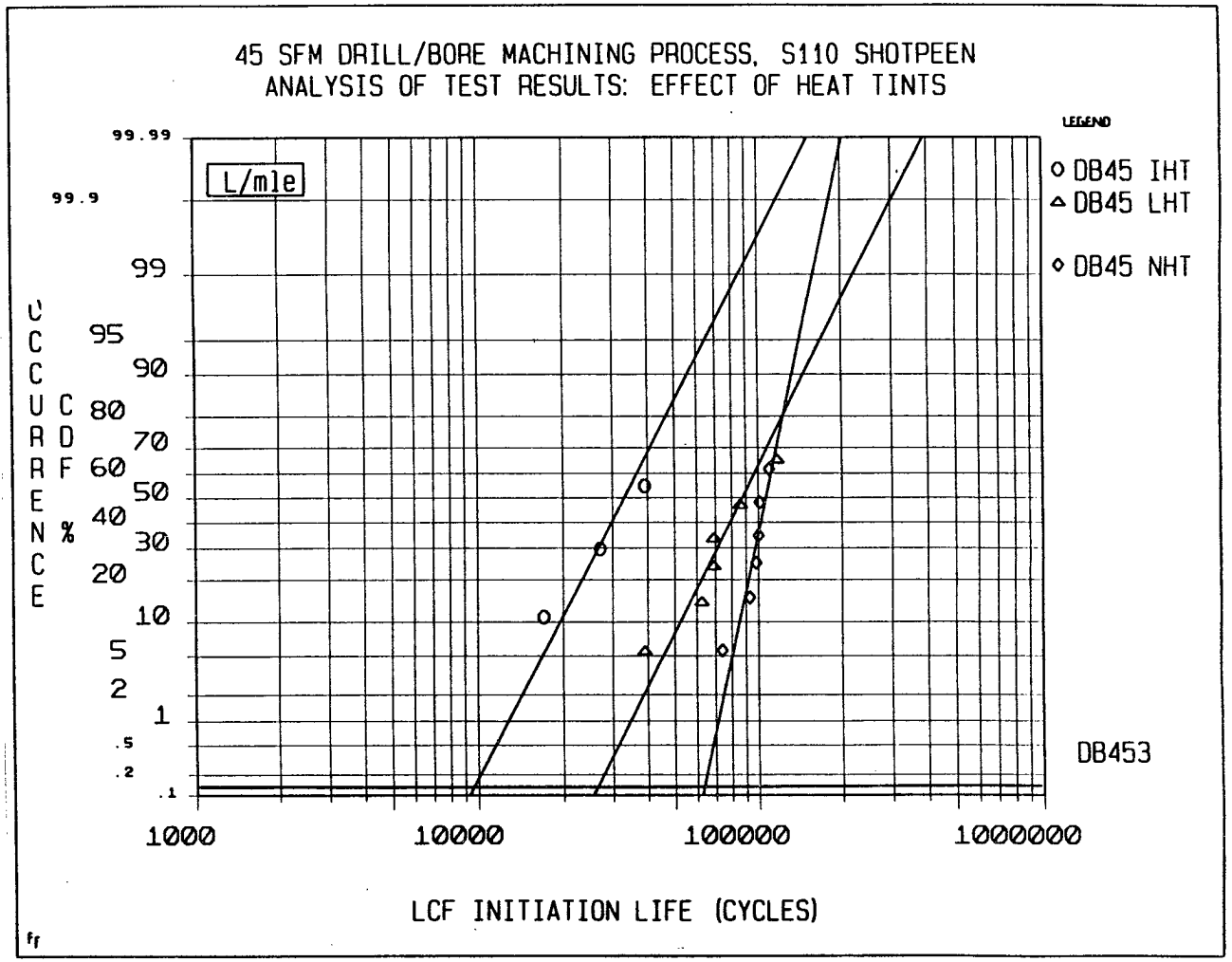

Heat Tints Play Major Role

Overall Summary

- An evaluation tool/process (multiple feature tests, Lognorm Smith analysis, conditional probability, model disk validation) which can identify the effect of various machining processes on the life of high strength nickel base powder metal materials has been identified

- This process with the addition of conditional probability can reasonably predict the life of critical areas of components
  - Recognizes influence of manufacturing processes
  - Enables identification of potential life influences (i.e. Heat tint or thermal exposure)

ACCELERATED MISSION TESTING: VALUABLE TOOL FOR ASSURING ENGINE INTEGRITY

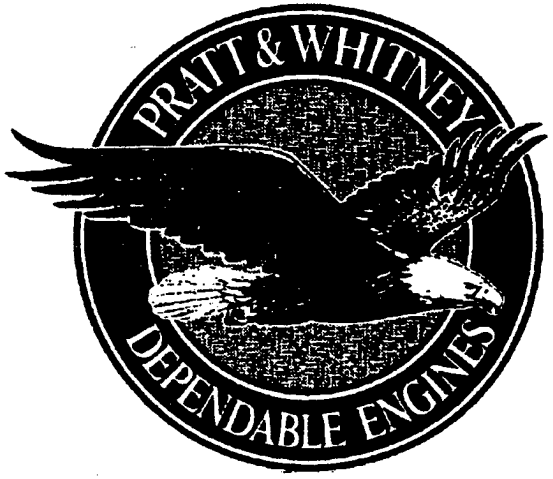

Phil Gatlin

1995 USAF Structural Integrity Program Conference

28 -30 November 1995

San Antonio, Texas

Accelerated Mission Testing (AMT)

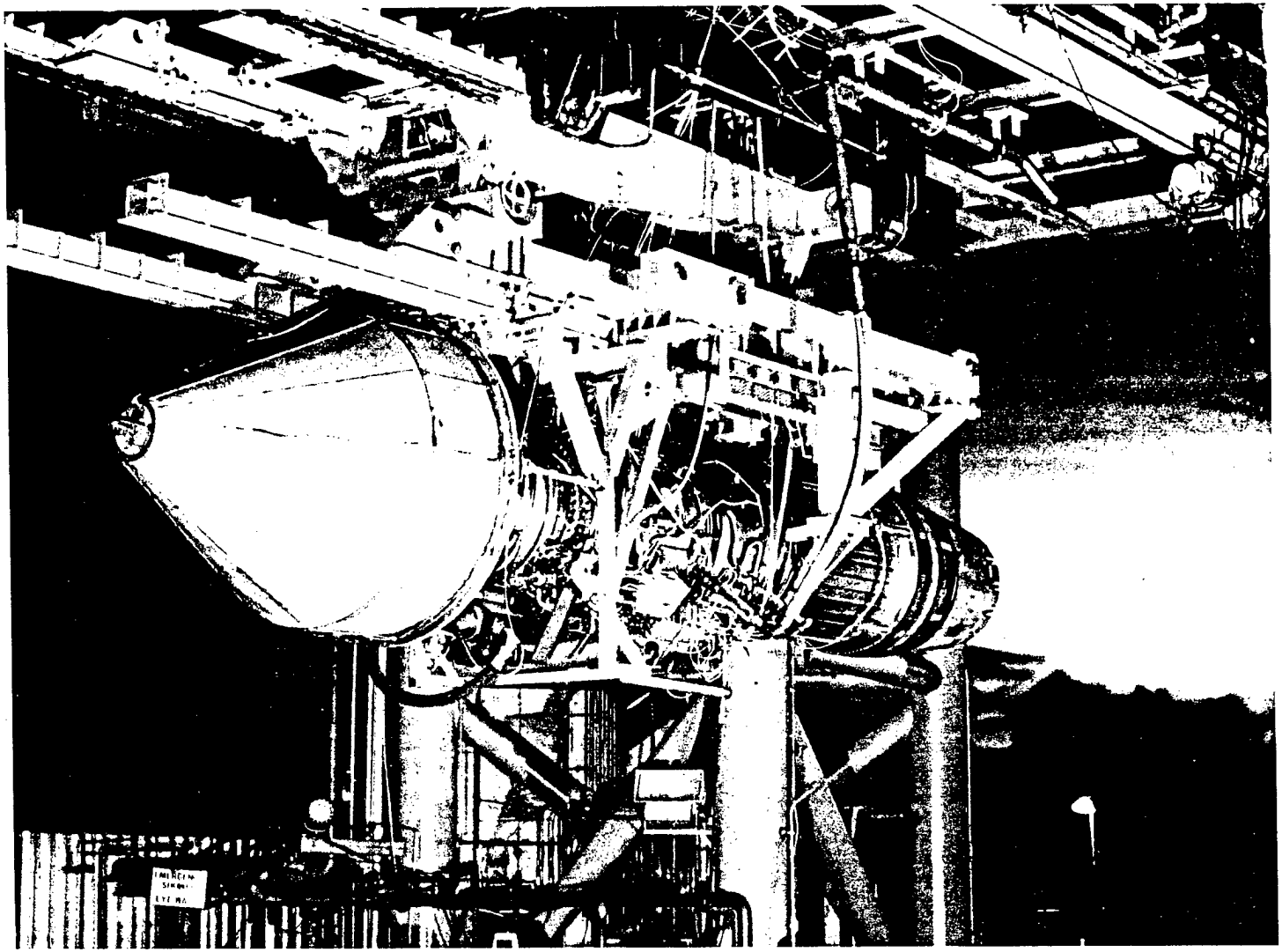

Agenda

- History of Accelerated Mission Testing (AMT)
- What is an AMT
- How are AMT cycles developed
- Have AMT test been benefical at uncovering distress modes
- What improvements are being made in AMT test

History of Accelerated Mission Testing

- AMT test have been used since 1975 as the perferred engine qualification methodology
- AMTs replaced MQT test that had been standard qualification technique since the 1950's
- Pratt Whitney has accumulated 35,000 test hours using AMTs

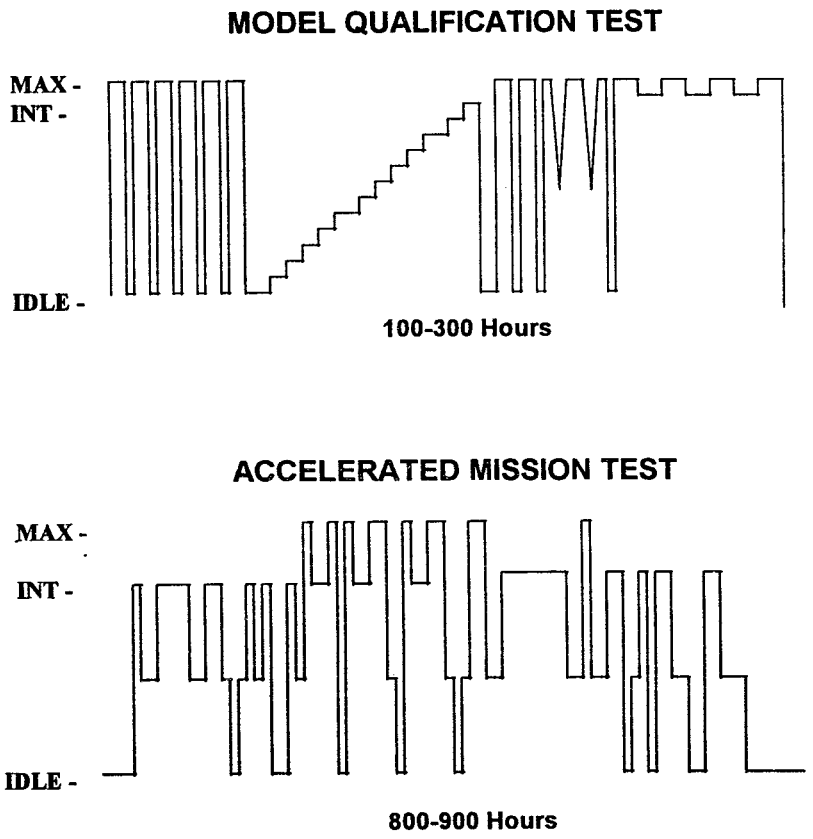

History of Accelerated Mission Testing

- MQT test results could not be related to field usage.
- AMT cycle results is directly related to field usage.
- AMT is a much better qualification or substantiation tool

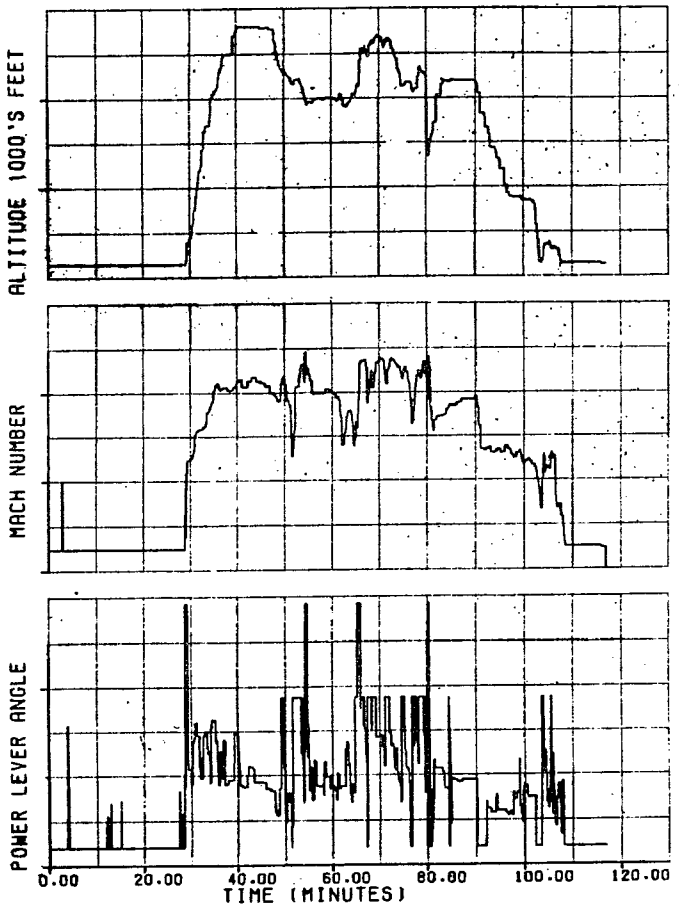

What is an Accelerated Mission Test?

- AMT is patterned after field usage..... cycles, time at power.
- Duplicates field enviromnent as closely as practical.
- Eliminates relatively non-damaging time to shorten (accelerate) test

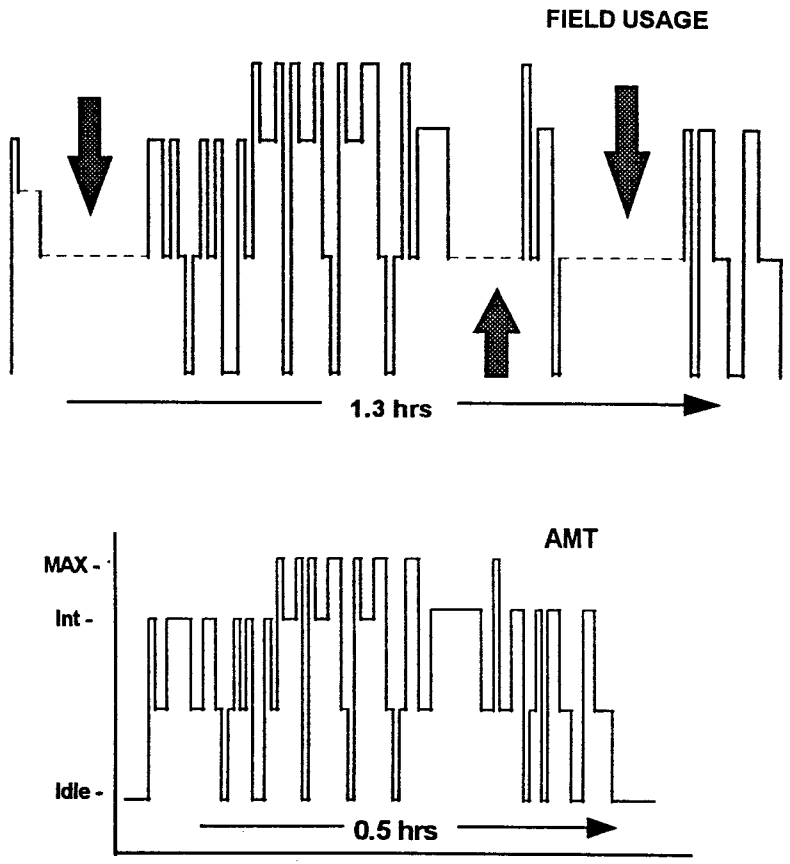

How are AMT cycles developed?

- Multiple data sources are used to define field usage profiles.
- Profiles are shortened to build AMT
- AMT profiles are run in appropriate mix to represent field usage.

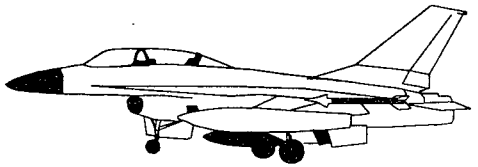

Flight Recorders
Engine Events Recorders
Pilot Interviews

Flight Profiles

How are AMT cycles developed?

- Engine environment during AMT matched closely to field usage.
  - Inlet temperature/inlet pressure
  - Power extraction
  - Customer bleed
  - Externals environment
  - Vibration

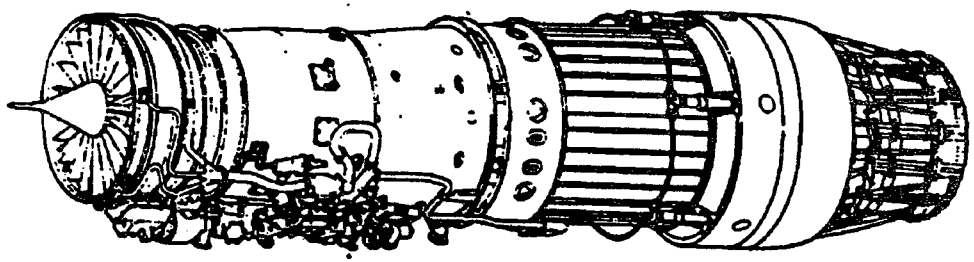

Have AMT's been beneficial?

5 Catagories of Distress Modes

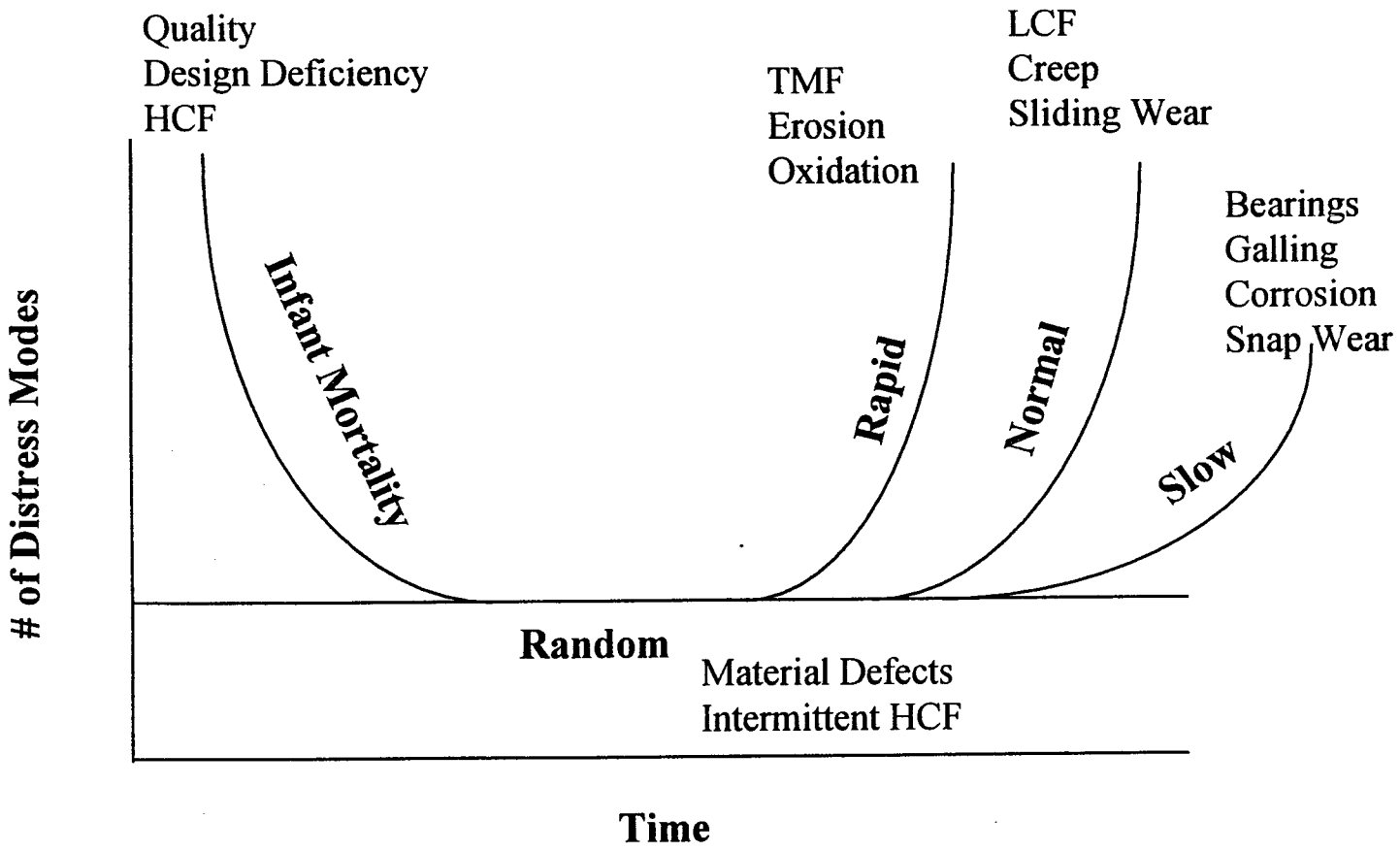

Have AMT's been beneficial?

- AMT's have been very effective at uncovering potential engine distress modes before they occur in the field.

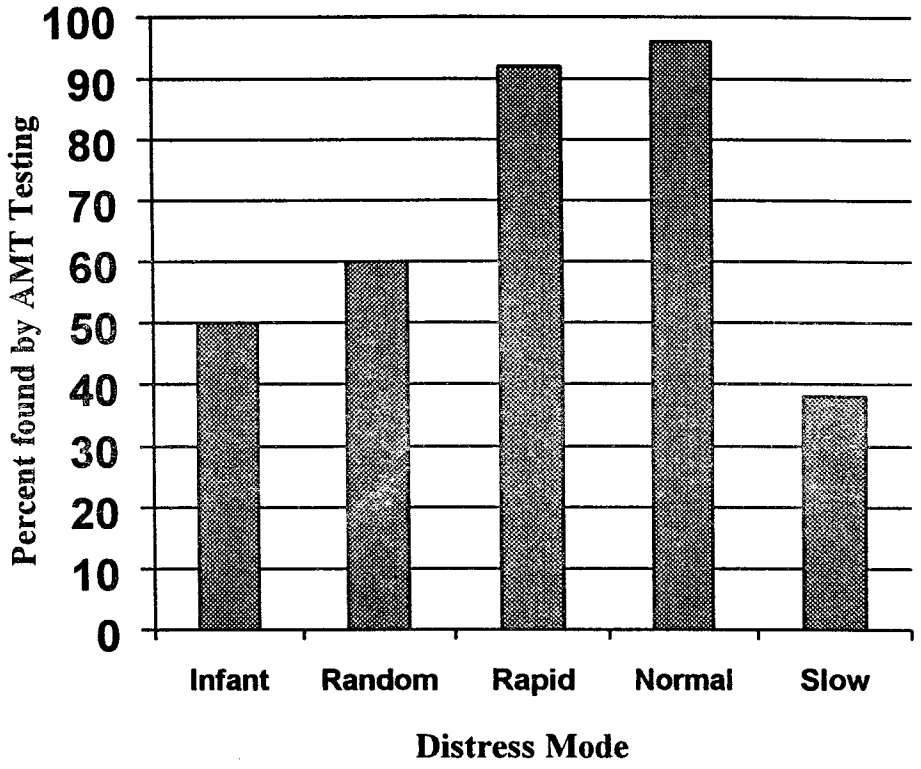

Improvements being made in AMT's

- Pre-Aged AMT engine
- Abusive Margin AMT
- Run to High side of usage distribution
- Build engine to extremes
- Continue to use components until life limit is reached

Conclusions

- Accelerated Mission Test duplicates field usage and is a better qualification/substantiation tool.
- Accelerated Mission Testing has had a very good record at finding engine distress modes before the field.
- Improvement are being made in AMT's that will make them even better at screening.
- AMT philosophy has greatly contributed to assuring engine integrity.

Plan to Control High Cycle Fatigue in Engines

Capt Neil F. Huber

WL/POTC
Wright Laboratory
Aero Propulsion and Power Directorate
1950 Fifth Street, Bldg 18
Wright-Patterson AFB, OH 45433-7251

OVERVIEW

- The Problem
- Plan Formulation
- High Cycle Fatigue (HCF) Science and Technology (S&T) Plan
  - Integrated High Performance Turbine Engine Technology (IHPTET) Connectivity
  - Example Technical Challenge
  - HCF Integrated Product Team (IPT) Structure
- Summary

THE PROBLEM

USAF PROPOSES THEORY FOR F110 SEAL FAILURES

AVIATION WEEK & SPACE TECHNOLOGY
November 7, 1994

Air Force Fighter Engine May Require Redesign

THE WALL STREET JOURNAL
May 31, 1994

F100-PW-229 FAILURES EFFECT F-15E READINESS

AVIATION WEEK & SPACE TECHNOLOGY
June 27, 1994

Engine High Cycle Fatigue is the Air Force's #1 Readiness Issue

DEPUTY DEFENSE SECRETARY
JOHN DEUTCH
May 31, 1994

THE PROBLEM

THE ENGINE DESIGN SPACE IS MURDEROUS!

31,000 PARTS

CONSTANT CHANGES OF THROTTLE
CONSTANT FLIGHT ENVELOP CHANGES
MAX. MANEUVERING TO MEET MISSION
-- EACH FLIGHT & PILOT IS DIFFERENT

1,300 PARTS ROTATE TO 16,000 rpm

"UNCLEAN" AIR

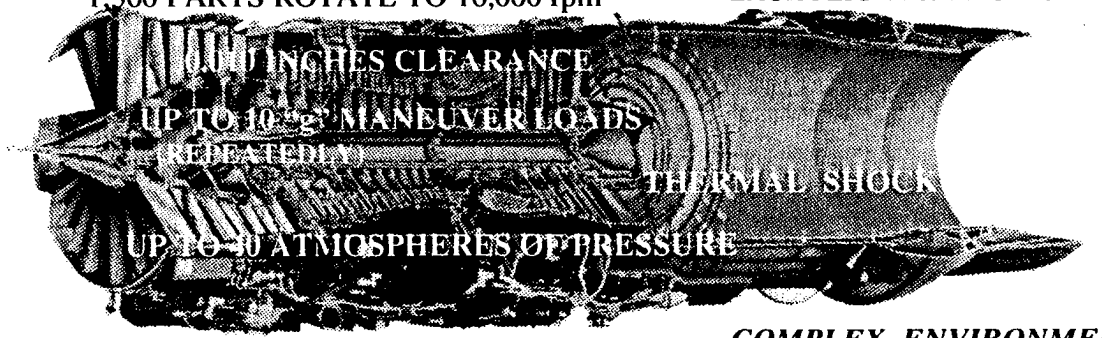

F.O.D.
RAIN
SAND
ROCKS
RIVETS
etc.

< 3 SECONDS ACCEL TIME
(IDLE TO MAX. POWER)

COMPLEX ENVIRONMENT
THERMAL STRESS
UP TO ~ 1400F ABOVE MELT TEMP
RICH IN OXYGEN & SULFUR
MECHANICAL STRESS
~ 80% ULTIMATE STRENGTH
STEADY + VIBRATORY LOADS
FLUCTUATING PRESSURE FIELDS
MECH. & THERMAL DEFLECTIONS
ACOUSTICS
IMPACT LOADS

HIGH STRENGTH MATERIALS ARE SENSITIVE
NOTCHES (<0.002 INCH)
RUBS (SMALL KISSES)
CHEMICAL ATTACK (OXIDATION/CORROSION)
SURFACE DEFECTS (NATURAL & SERVICE)
LONG TERM EXPOSURE (CREEP)
CYCLIC MECHANICAL & THERMAL LOADING ORDER
SYNERGISTIC LOADS

HCF DANGER

THE PROBLEM

CURRENT ENGINE PROBLEMS ~ 1 MILLION MANHOURS PER YEAR

PROBLEM	*ACTION*	*CAUSE*	*TYPE AFFECTED*	*# ENGINES AFFECTED*	*TIME PER ENGINE*	*START DATE STATUS COMPLIANCE*	*TOTAL MH*	*MH PER YR*
#3 FAN DISK LUG	Replace wide slot disks ASAP Redesign/Retrofit Ultrasonic Inspection	HCF driven-disk lug cracks	F100-100 -200 -220	1225 of 1225 589 of 589 1081 of 1081	140 MH/ENG	STARTED Mar 90 Long term - redesign in work Recurring Inspection F-15 every 300 cycles F-16 every 250 cycles	405,300	405,300
#4 BEARING REAR AIR SEAL	Remove/Replace Air Seal	HCF driven	F100-220+all increased life cores(upgraded cores-all types)	2988 (1081 + upgraded cores)	240 MH/ENG	STARTED Mar 92 80% complete C/W by Feb 97	717,120	232,604
#4 TURBINE BLADE	Retrofit/Re-blade	HCF caused blade failure	F100-229	270 of 270	150 MH/ENG Interim fix	STARTED Aug 93 several iterations with redesign in work// All F16 completed interim All F16 Redesign C/W NLT Dec 95	40,500	24,300
3-TOOTH SEAL	Replace seal <350 hrs	HCF caused seal failure	F101 F110-100 F110-129 F118	2 of 445 23 of 819 97 of 220 50 of 101	288 MH/ENG	STARTED Aug 94 Grounded engines should be C/W 08/95	49,536	49,536
#1 FAN BLADE	-Replace blades every 2 years -thumb nail inspect prior to 1st flight of day	HCF driven crack and failure	F110-129	220 of 220	144 MH/ENG	STARTED Nov 94 Ongoing until long term fix installed	31,680	15,840
#2 FAN BLADE/DISK	Fleet-wide Ultrasonic Inspection	HCF driven cracked blades and disk lug cracks	F100-100	670 of 819	172 MH/ENG	STARTED Mar 95 Engine will be C/W by Mar 96. This will be a -6 recurring inspection	115,240	115,240
HPT AFT BLADE RETAINER	Borescope inspection every 100 flight hours	Creep of retainer (bulge)	F110-100	819 of 819	0.5 MH/ENG	STARTED Mar 95 TCTO to be C/W by Mar 96. This will be a -6 recurring inspection	410	410
							1,359,786	843,230

THE PROBLEM

TRENDS IN ENGINE FATIGUE FAILURES

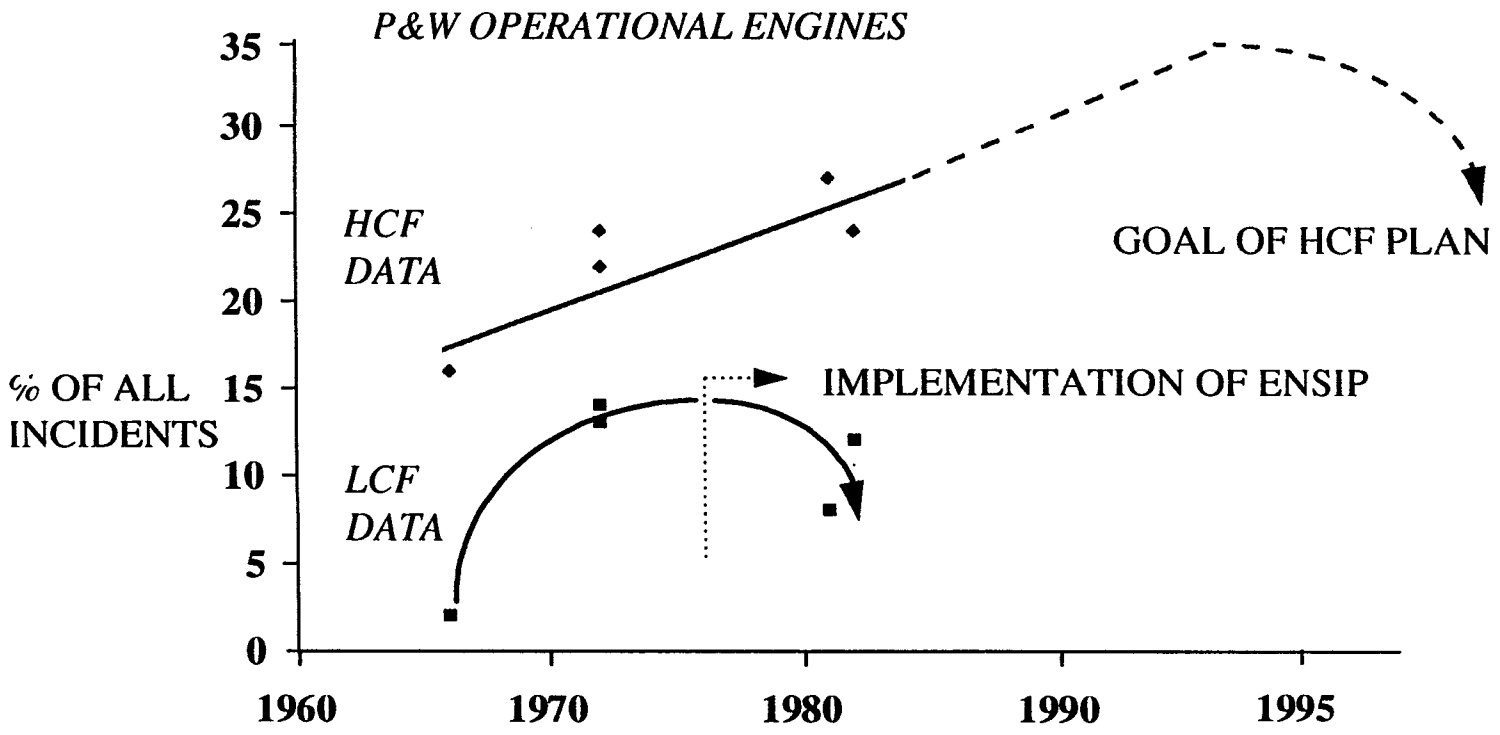

PLAN FORMULATION

ELEMENTS OF HCF
8 KEY TECHNOLOGY CHALLENGES RECOMMENDED* FOR IMPROVEMENT

Driver	*Response*	*Capability Assessment*	*Instrumentation & Test Methods*
• Industry Database	• Industry Data base	• Fracture Screening • Design Environment and Margin • Empirical Calibrations	• Standardized Stress Measurement
• User-friendly Computation Methods	• Active Airfoil Vibration Control	• Improved Conventional Goodman Diagram	• Instrumented Flight Engines
• Fan & Turbine Aero/Mech Characterization	• Passive Damping Technology	• Physics Based Approach	• Engine Test Protocol for HCF
	• Forced Response Prediction	• Material Characterization Using Fracture-Based Methods	• HCF Instrumentation Improvement
	• Engine Structural Analysis	• Component Surface Treatments	

* = WL HCF Workshop, Mar 95

HCF S&T PLAN ELEMENTS

PRODUCT:
Improved Military Specs and Contractor Design System

PLAN FORMULATION

HCF PROGRAM FLOW

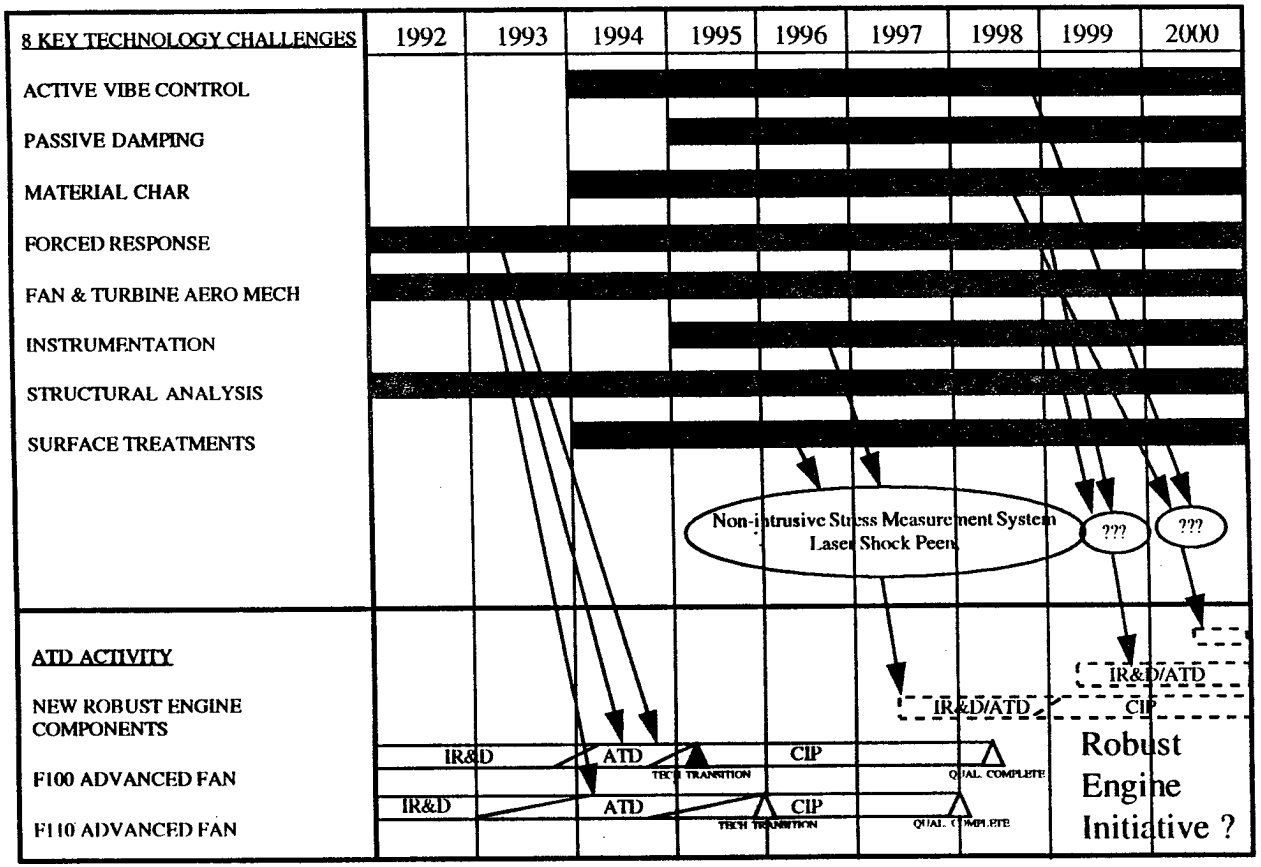

HCF S&T PLAN

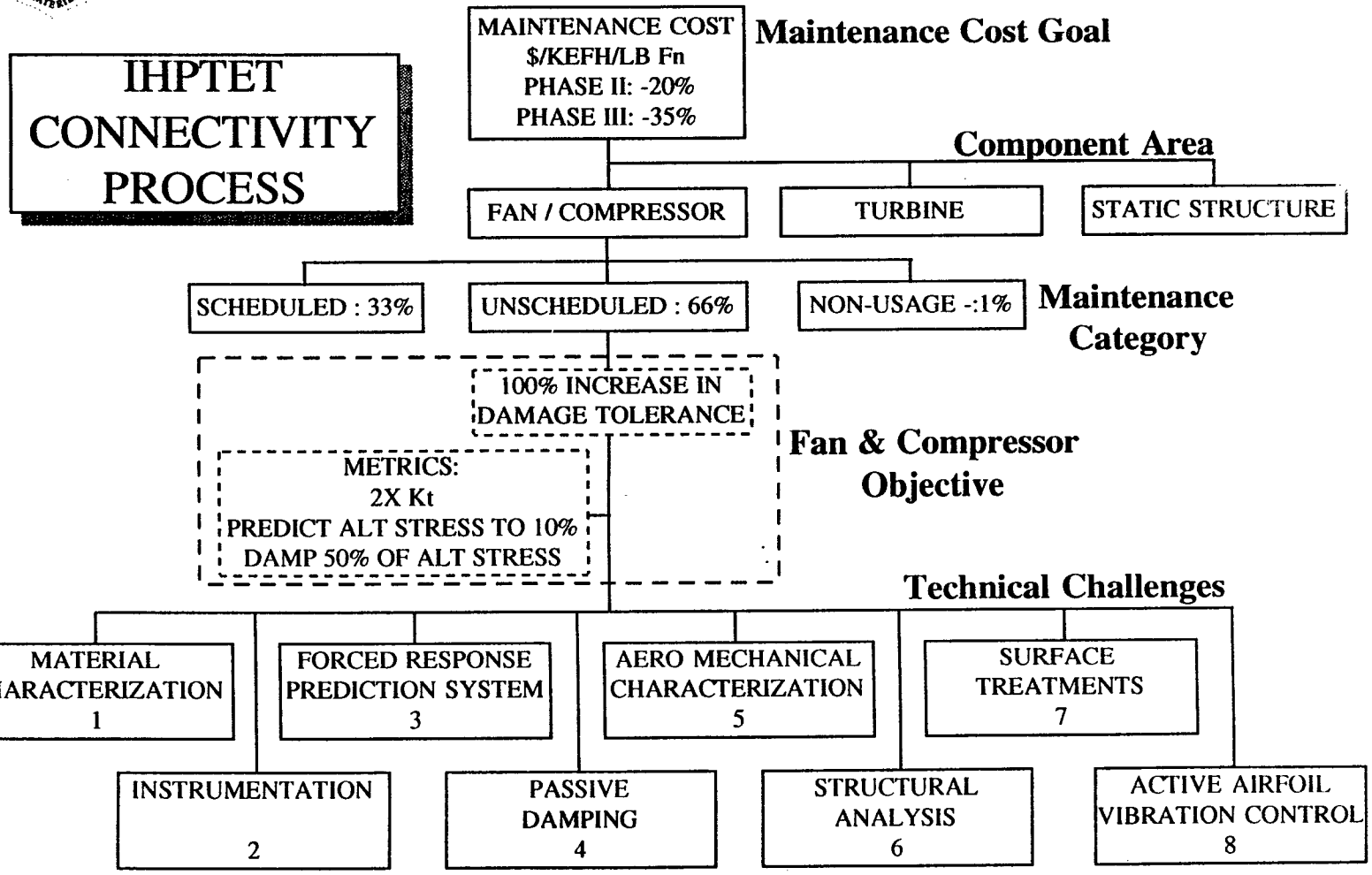
IHPTET CONNECTIVITY PROCESS
MAINTENANCE COST $/KEFH/LB Fn
PHASE II: -20%
PHASE III: -35%
Maintenance Cost Goal
Component Area
FAN / COMPRESSOR
TURBINE
STATIC STRUCTURE
SCHEDULED : 33%
UNSCHEDULED : 66%
NON-USAGE -:1%
Maintenance Category
100% INCREASE IN DAMAGE TOLERANCE
METRICS:
2X Kt
PREDICT ALT STRESS TO 10%
DAMP 50% OF ALT STRESS
Fan & Compressor Objective
Technical Challenges
MATERIAL CHARACTERIZATION 1
FORCED RESPONSE PREDICTION SYSTEM 3
AERO MECHANICAL CHARACTERIZATION 5
SURFACE TREATMENTS 7
INSTRUMENTATION 2
PASSIVE DAMPING 4
STRUCTURAL ANALYSIS 6
ACTIVE AIRFOIL VIBRATION CONTROL 8

HCF S&T PLAN

MATERIAL CHARACTERIZATION

- ***Technical Challenge:*** Material HCF damage tolerance characterization is lacking.

- ***Shortfalls / Status***
  - Materials behavior for HCF is not understood
  - Life shortening effects are not accounted for in prediction
    - —damage accumulation: galling, fretting, Foreign Object Damage (FOD), LCF/HCF interaction
  - Goodman Diagram does not account for damage / evolution of damage

- ***Approaches***
  - Develop understanding of HCF material behavior based on damage tolerance
  - Understand and quantify evolution of HCF damage
    - —(if predicted life is $1x10^7$ cycles, how much life remains at $9x10^6$?)
  - Understand crack initiation in Ti alloys and Threshold Fracture Mechanics
  - Understand effects of alloying and microstructure on HCF

- ***Exit Criteria***
  - A. Establish a modified "Goodman Diagram" that accounts for damage
  - B. Determine extent of damage as HCF cycles build up
  - C. Incorporate Threshold Fracture Mechanics into design system/ENSIP 2
  - D. Design components based on alloy contents and microstructure

HCF S&T PLAN

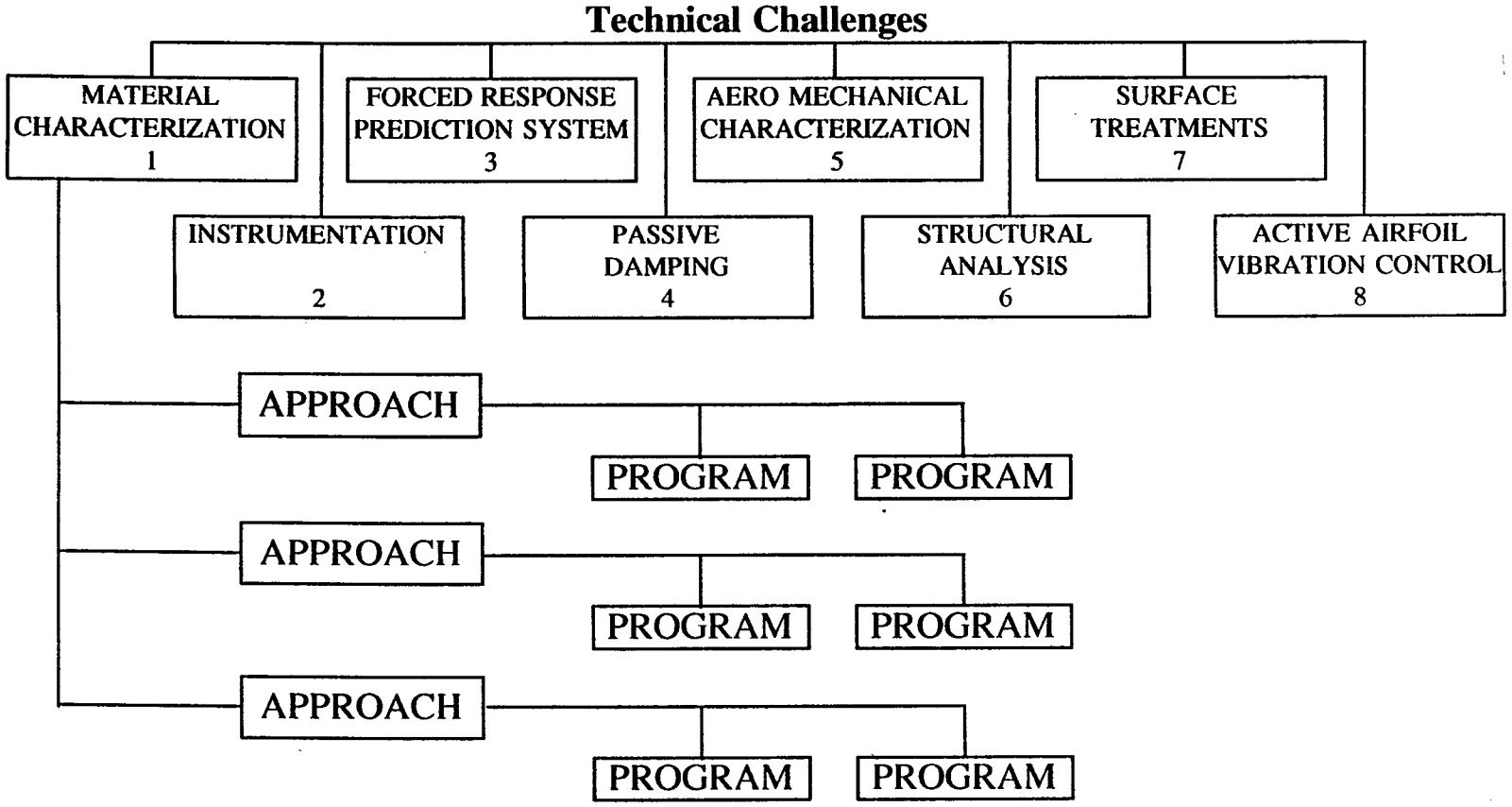
Technical Challenges
MATERIAL CHARACTERIZATION 1
FORCED RESPONSE PREDICTION SYSTEM 3
AERO MECHANICAL CHARACTERIZATION 5
SURFACE TREATMENTS 7
INSTRUMENTATION 2
PASSIVE DAMPING 4
STRUCTURAL ANALYSIS 6
ACTIVE AIRFOIL VIBRATION CONTROL 8
APPROACH
PROGRAM
PROGRAM
APPROACH
PROGRAM
PROGRAM
APPROACH
PROGRAM
PROGRAM

HCF S&T PLAN

GOAL: 35% REDUCTION IN MAINTENANCE COSTS ($/KEFH/LB Fn)

OBJECTIVES: 100% INCREASE IN DAMAGE TOLERANCE

A) INCREASE STRESS INTENSITY FACTOR CAPABILITY (K_t) BY 2X

B) PREDICT ALTERNATING STRESSES TO 10%

C) DAMP 50% OF ALTERNATING STRESSES

CHALLENGES (OBJECTIVE CATEGORY):

1. MATERIAL HCF DAMAGE TOLERANCE CHARACTERIZATION IS LACKING. (A)
2. AIRFOIL RESPONSE IS NOT ACCURATELY KNOWN DUE TO INTRUSIVE MEASUREMENT, LACK OF SENSOR PERFORMANCE, ACCURACY, DURABILITY, AND ON-LINE PROCESSING. (B,C)
3. CURRENT FORCED RESPONSE CODES ARE NOT MATURE. (B)
4. DAMPING IS NOT ACCOUNTED FOR IN THE CURRENT FAN AND COMPRESSOR DESIGN SYSTEMS; EFFECTIVE METHODS OF INCREASING DAMPING IN ROTATING COMPONENTS ARE NOT DEVELOPED. (C)
5. ENTIRE ENGINE FORCED RESPONSE ENVIRONMENT IS NOT ACCURATELY SIMULATED IN TESTING. (A,B,C)
6. HCF ENGINE STRUCTURAL ANALYSIS ACCURACY IS LACKING DUE TO INADEQUATE FINITE ELEMENT MODEL COMPLEXITY AND MODELING OF DAMAGE ACCUMULATION. (B)
7. EFFECTIVE SURFACE TREATMENTS ARE NEEDED FOR INCREASED FAN AND COMPRESSOR HCF DAMAGE TOLERANCE. (A)
8. CURRENT ENGINES DO NOT MONITOR OR CONTROL HCF. (C)

HCF S&T PLAN

GOODMAN DIAGRAM DEVELOPMENT

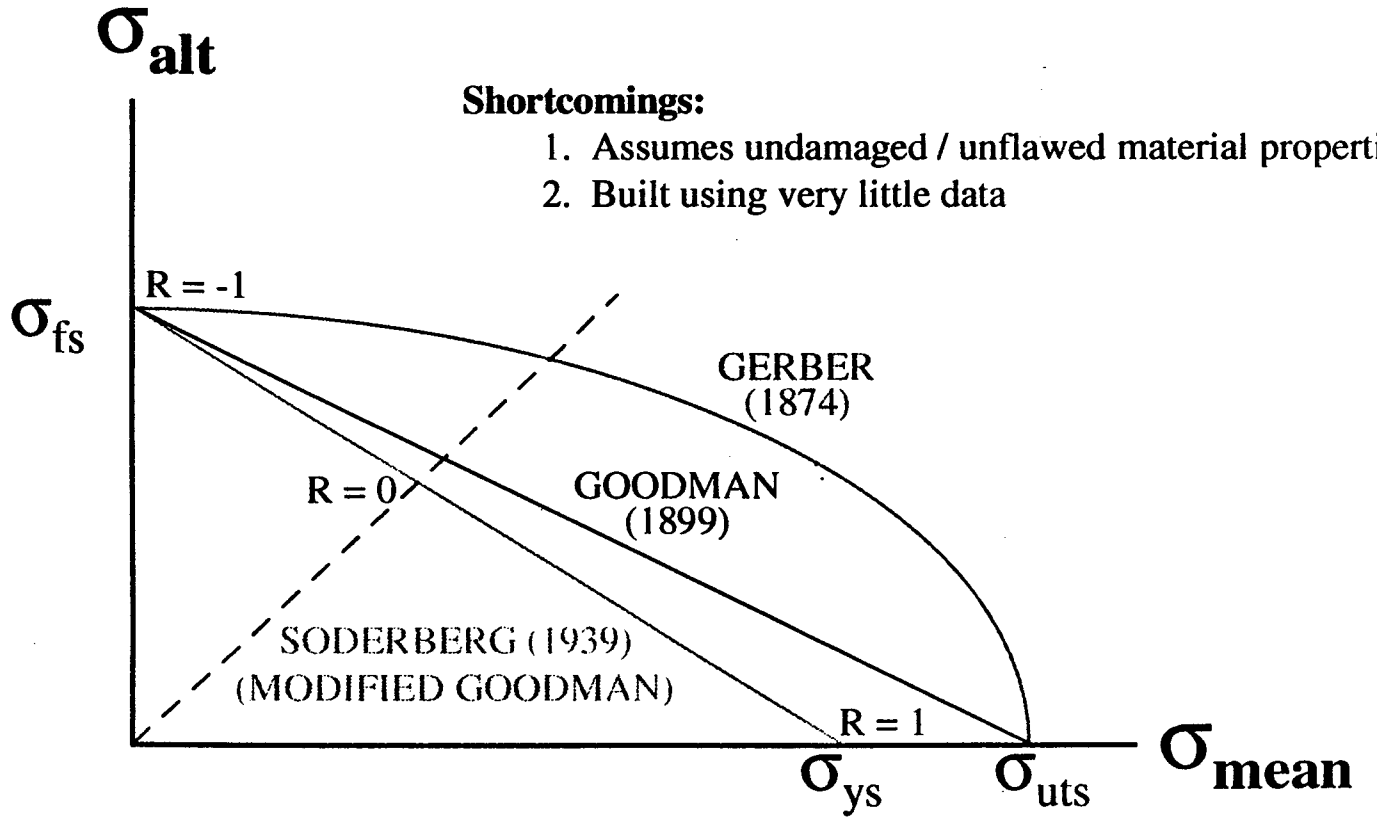

Shortcomings:

1. Assumes undamaged / unflawed material properties
2. Built using very little data

HCF S&T PLAN

THRESHOLD FRACTURE MECHANICS

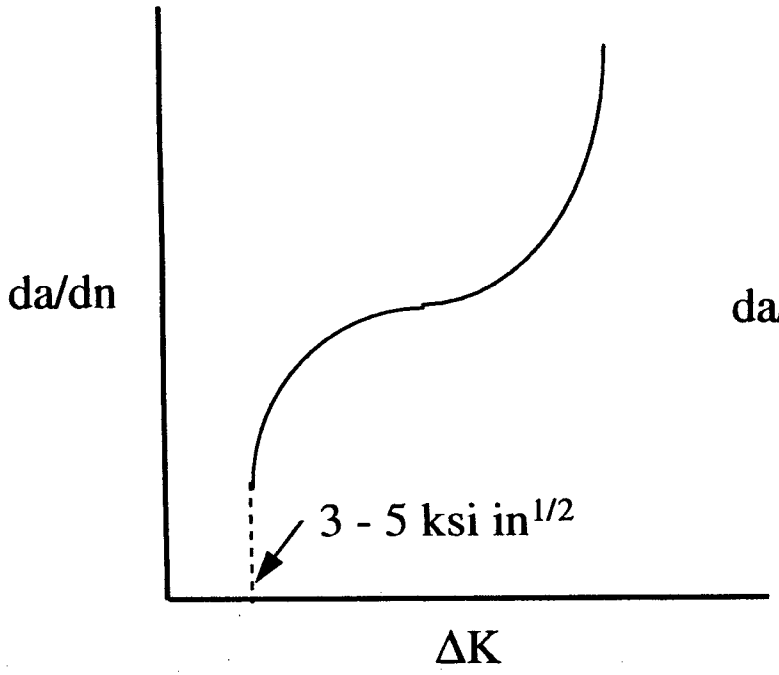

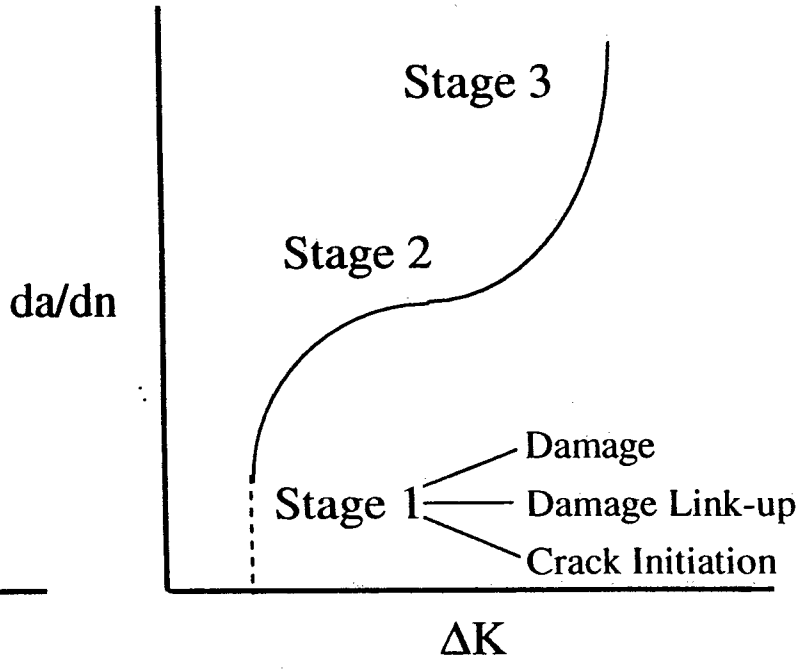

HCF S&T PLAN

MATERIAL CHARACTERIZATION

Approaches / Program Titles	FY95	FY96	FY97	FY98	FY99	FY00	FY01	$ (K)	Org
Develop Understanding of HCF Materials Behavior Based on Damage Tolerance									
- Experimental Evaluation									
-- LSP Material Characterization		150	400	300	(150)			$1,000	ML
-- Crack Initiation in Ti Alloys		25	450	700	(525)	(150)	(100)	$1,950	ML
-- HCF Crack Growth in Ti Alloys			800	1400	(1350)	(950)	(300) ◇1	$4,800	ML
Understand and Quantify Evolution of HCF Damage									
- Experimental Evaluation									
-- Crack Initiation in Ti Alloys			350	400	(600)	(500)	(100)	$1,950	ML
- Extension to Alternate Alloy					(250)	(500)	(500) ◇2	$1,250	ML
Understand Crack Initiation in Ti Alloys / TFM									
- Exp Tech for Measuring Damage (6.1)	200	200	200	200	200			$1,000	AFOSR
- Dev New Damage Tol Concepts (6.1)		300	300	300	300	300		$1,500	AFOSR
- Ti Life Prediction Methodology									
-- Crack Initiation		25	450	200	(225)	(300)		$1,200	ML
-- Short Crack Growth		(100)	100	300	300	300 ◇3		$1,100	ML
-- Long Crack Growth				100	100	100		$300	ML
-- Probabilistic Methods				(100)	(200)	(300)		$600	ML
-- Overall Life Prediction / Verification						(100)	(200) ◇4	$300	ML
- Damaged Fan Blade - Spin Pit				(250)	(250) ◇5			$500	NAVY
Understand Effects of Alloying and Microstructure on HCF									
- Rate/Control of Texture on Ti HCF (6.1)	100	100	100					$300	AFOSR
- Microstructure Effects on Ti HCF (6.1)		150	150	150				$450	AFOSR
- Mech of Short Crack Init and Prop (6.1)		400	400	400	400	400		$2,000	AFOSR
TOTAL								$20,200	
6.3 DEMONSTRATION TARGETS							2-5 △		
HCF Char. Phase III Fan Design - JTDE Test						250	250	$500	PO

1. Establish a "modified" Goodman Diagram that accounts for damage (A)
2. Determine extent of HCF damage accumulation (B)
3. Understand and quantify statistics of crack initiation and growth (C)
4. Threshold Fracture Mechanics incorporated into design system and ENSIP (C)
5. Demo damaged fan blade with Ti/LSP characterization (A,B,C)

△#,# = Milestones # & # are being demonstrated

(xxx) : Not Budgeted

HCF S&T PLAN

FUNDING BY TECH CHALLENGE

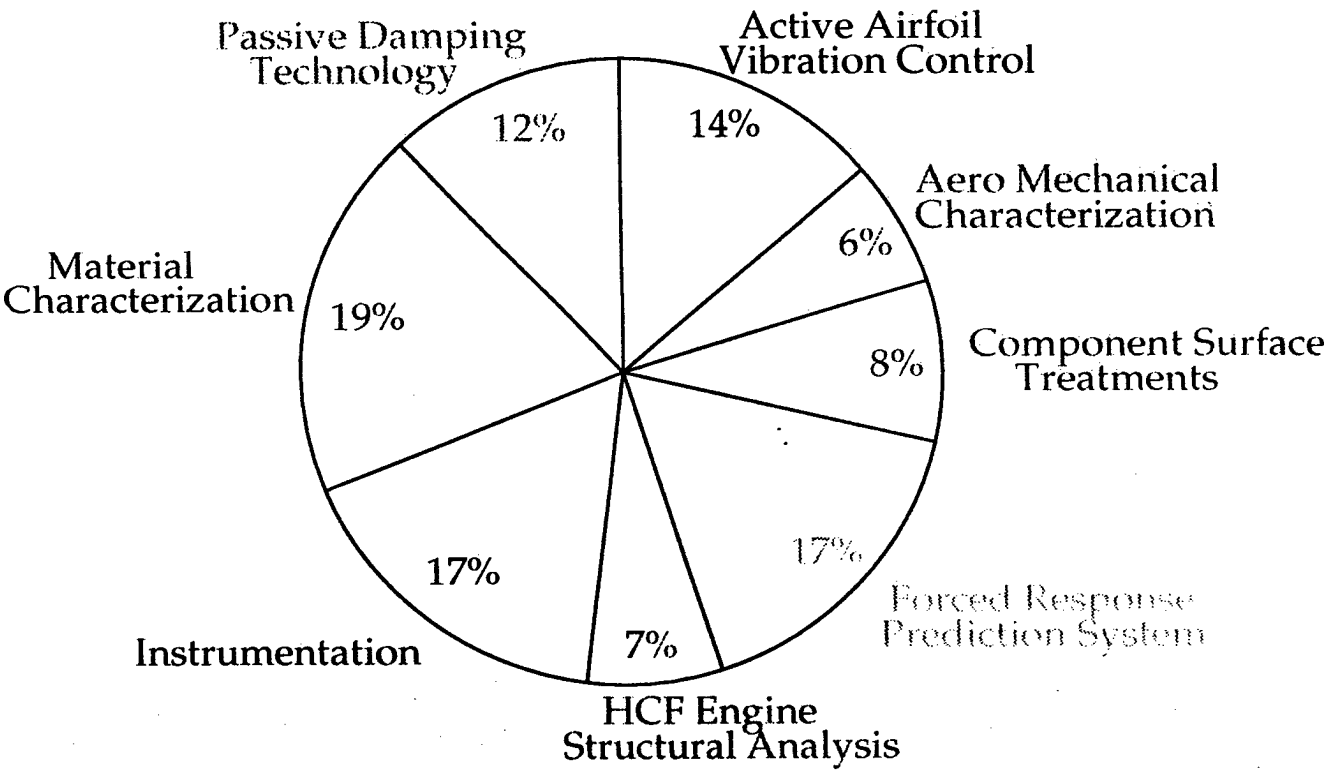

HCF S&T PLAN

Funding Sources

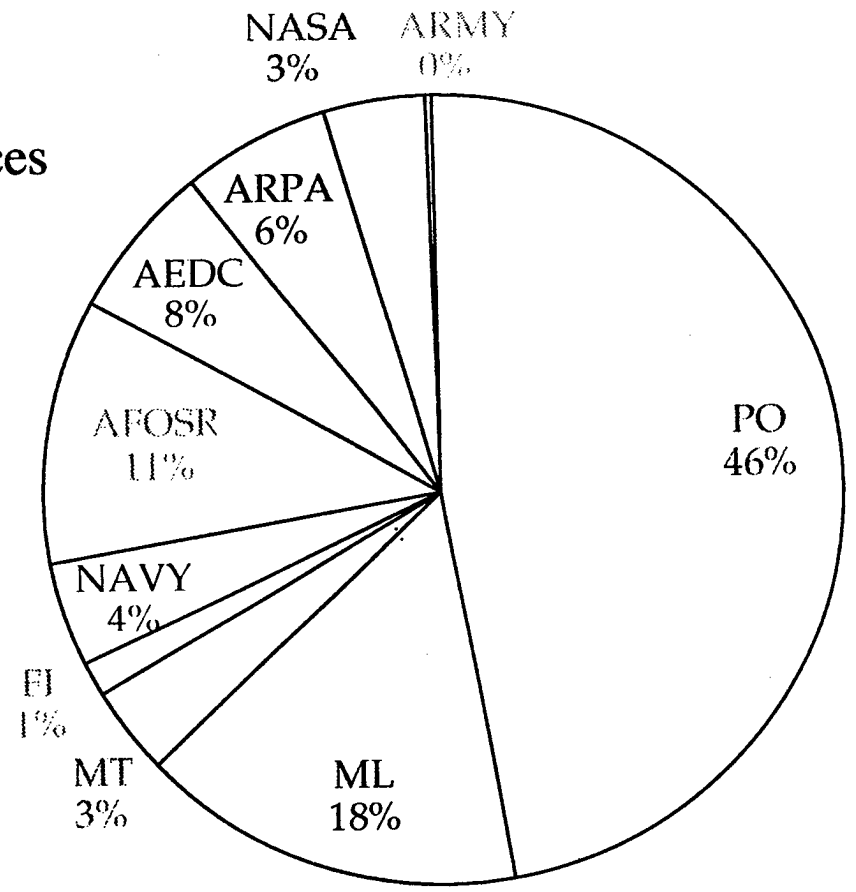

HCF S&T PLAN

HCF IPT STRUCTURE

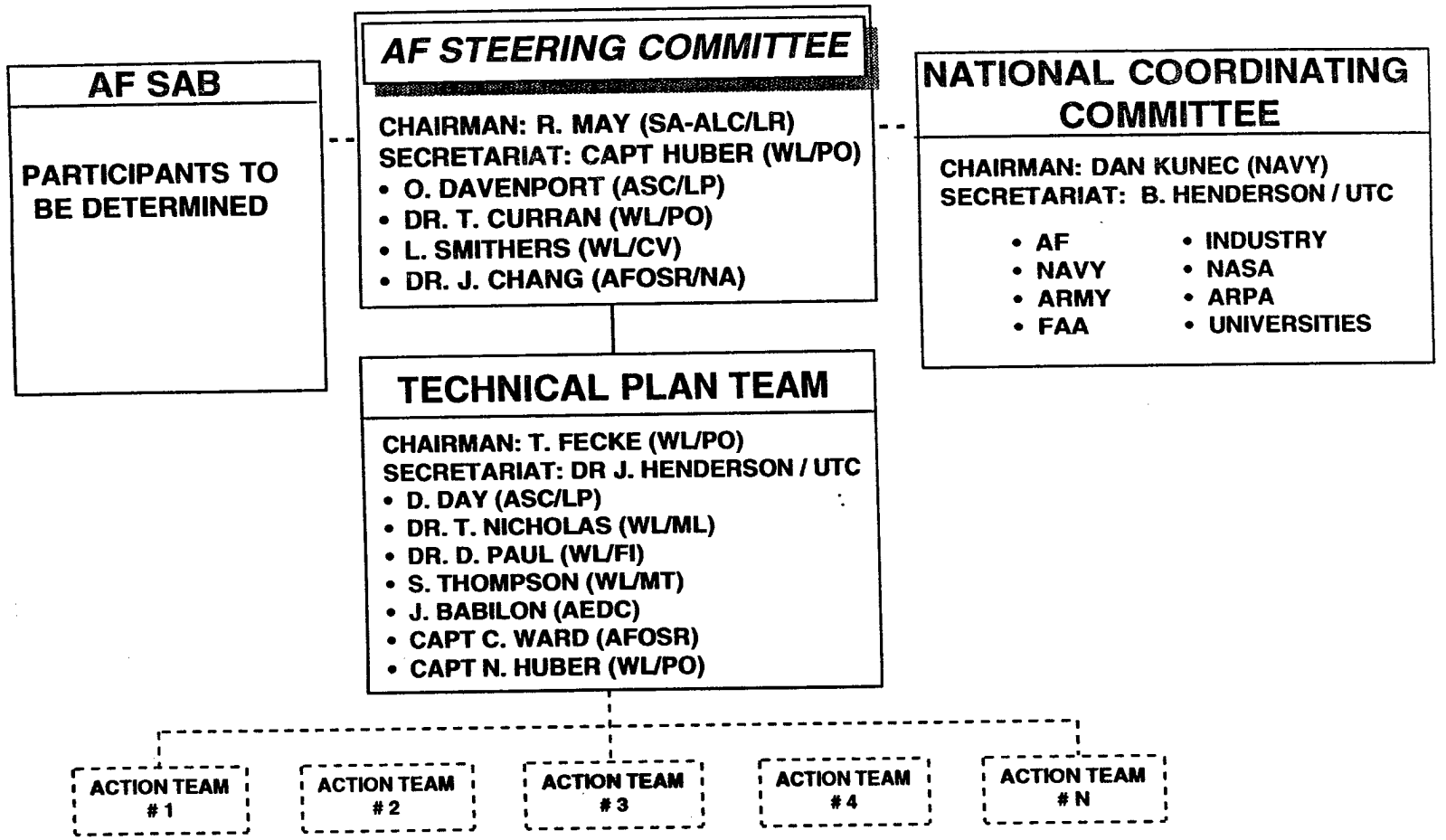

SUMMARY

- **HCF IS A MAJOR MAINTENANCE PROBLEM IN FIELDED ENGINES AND A MAJOR CONCERN FOR IHPTET FUTURE DESIGN CONCEPTS**
- **UPDATE TO HCF S&T PLAN FOCUSES ON IHPTET MAINTENANCE COST GOALS & KEY TECHNICAL CHALLENGES**
- **NEW IPT STRUCTURE IN PLACE -- PRIORITIES ESTABLISHED, KEY EFFORTS UNDERWAY, NEW PROCUREMENTS IN PROCESS**
- **FIELD ENGINE TRANSITION OPPORTUNITIES BEING INVESTIGATED**

1995 USAF Structural Integrity Program Conference
28–30 November 1995
San Antonio, TX

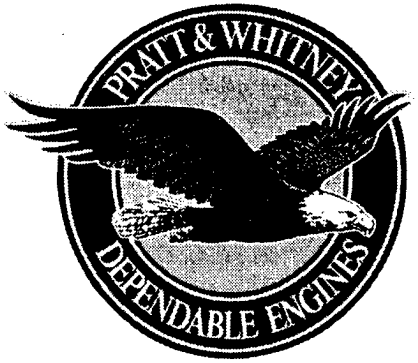

F117-PW-100 TAILORED ENSIP for FIVE PEACETIME C-17 MISSIONS

Presenter: Subhash Patel
Pratt & Whitney

Authors: Subhash Patel, Herman Johnson, Michael Mike

PRESENTATION OVERVIEW

- Background
- Tailored ENSIP Assessment
  - Program Goals and Schedules
  - P&W/USAF Teams
  - Design Criteria
  - Manufacturing and Quality Control (NDI assessment)
  - Material Characterization
  - Component Testing
  - Engine Life Management Plan
  - Life Tracking System
- Program Status
- Summary

UNITED TECHNOLOGIES CORPORATION (UTC)

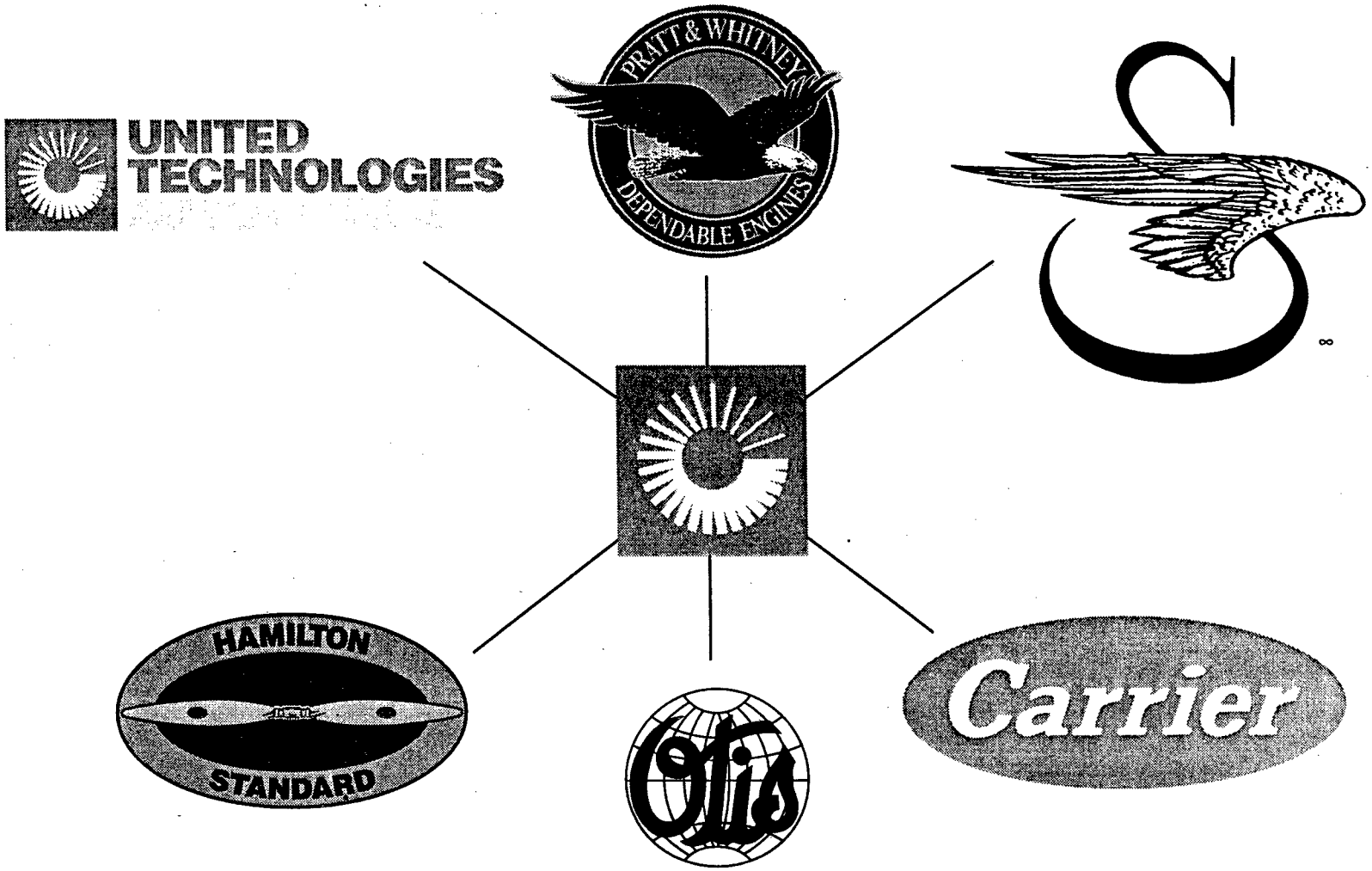

PRATT &WHITNEY PRODUCTS

POWER FOR THE WORLD'S COMMERCIAL AIRCRAFT

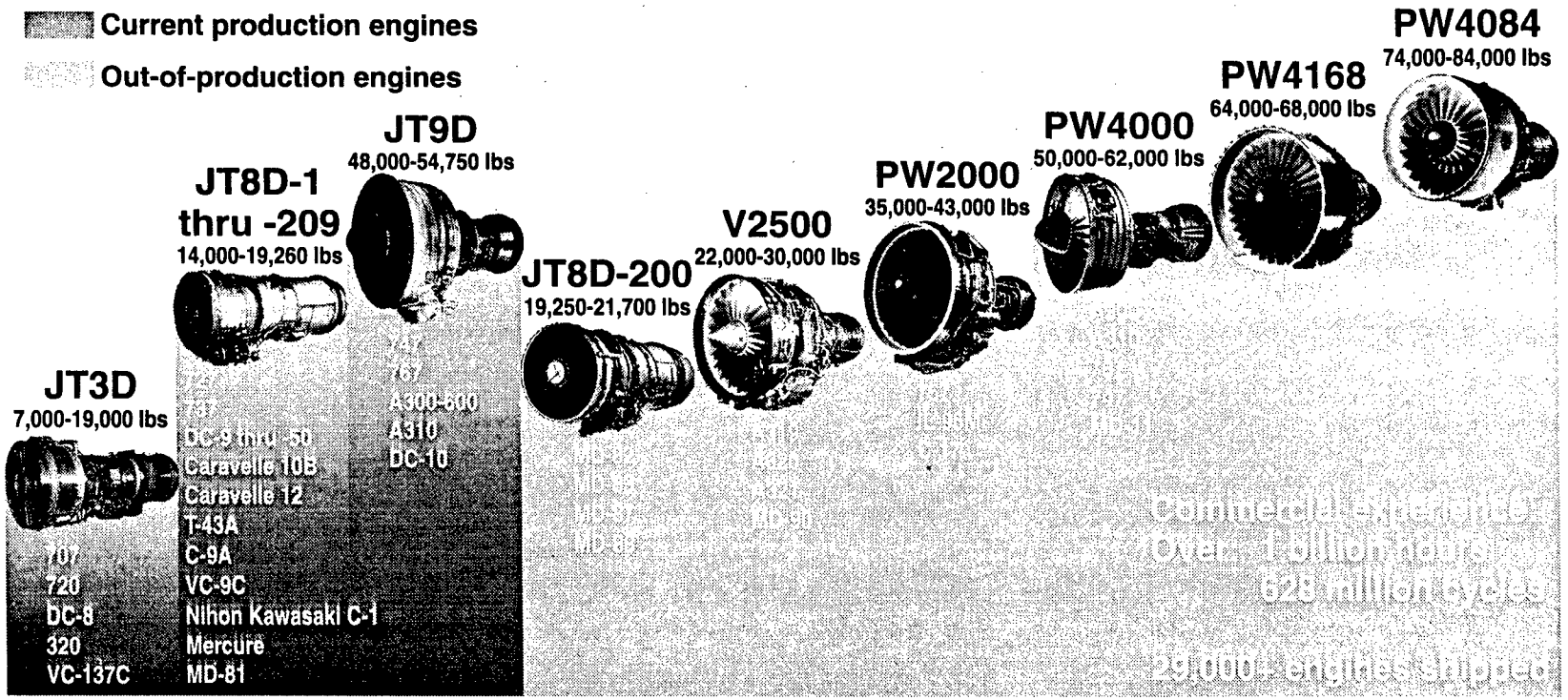

PW2000/F117 ENGINE FAMILY

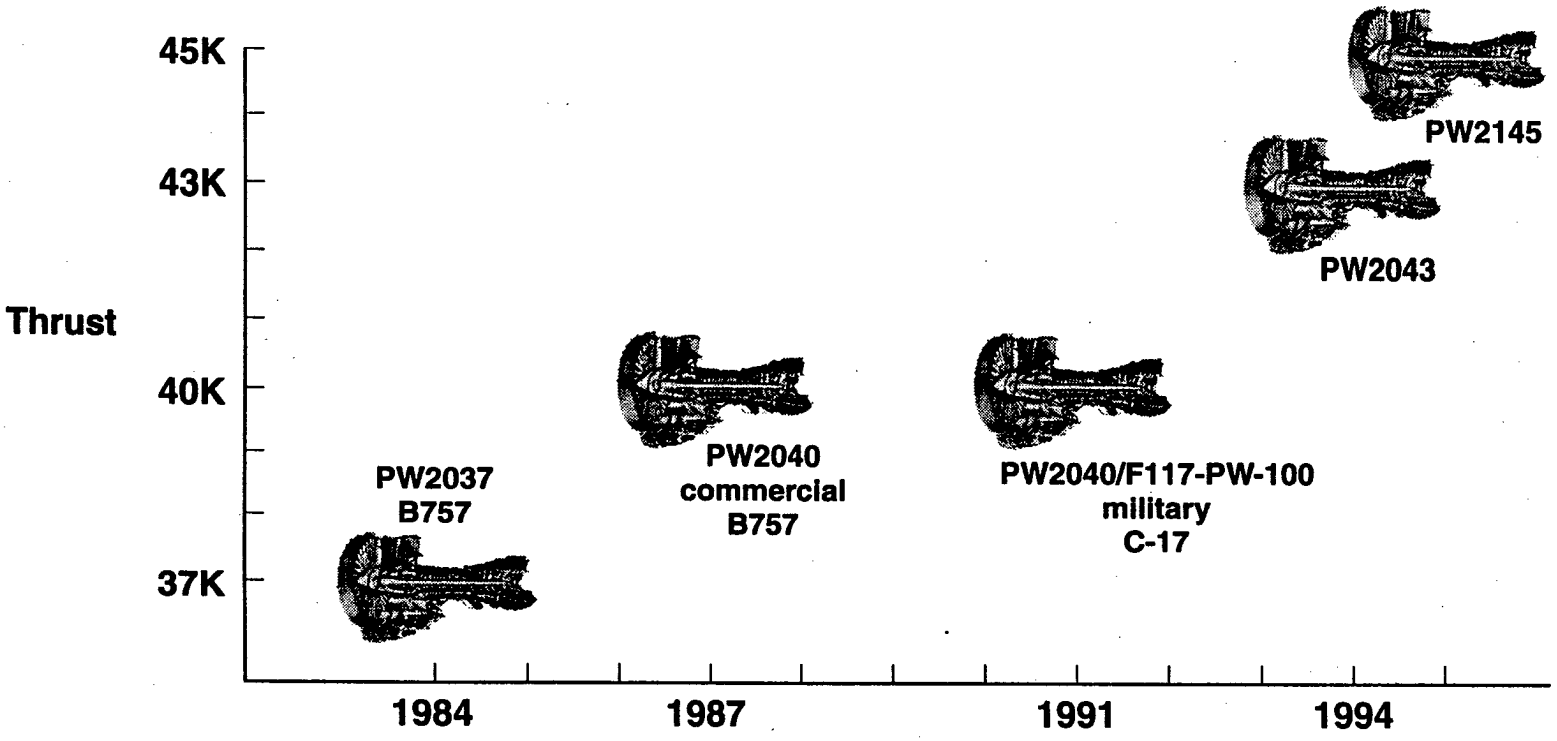

- USAF purchased off-the-shelf commercially FAA certified engine
- Advantages to the USAF
  - — No engine development funds required from USAF
  - — Preferred customer status for the USAF (cost/engine)
  - — Commercial upgrades automatically included in C-17/F117

COMMERCIALLY PROVEN ENGINE FOR GLOBEMASTER III

PW2000

Boeing 757

F117-PW-100

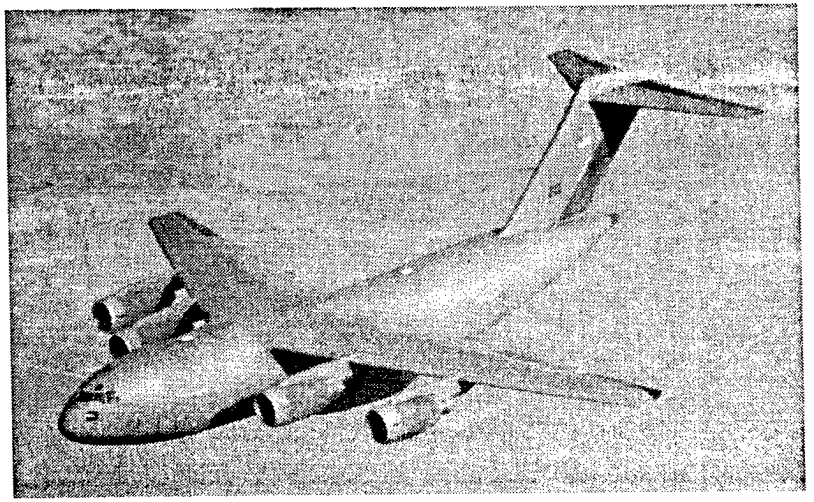

C-17 Globemaster III

F117-PW-100 (DO-3)
TAILORED ENSIP ASSESSMENT
for
'94 IMPROVEMENT PACKAGE
ENGINE

F117-PW-100 ENSIP

PROGRAM TASKS

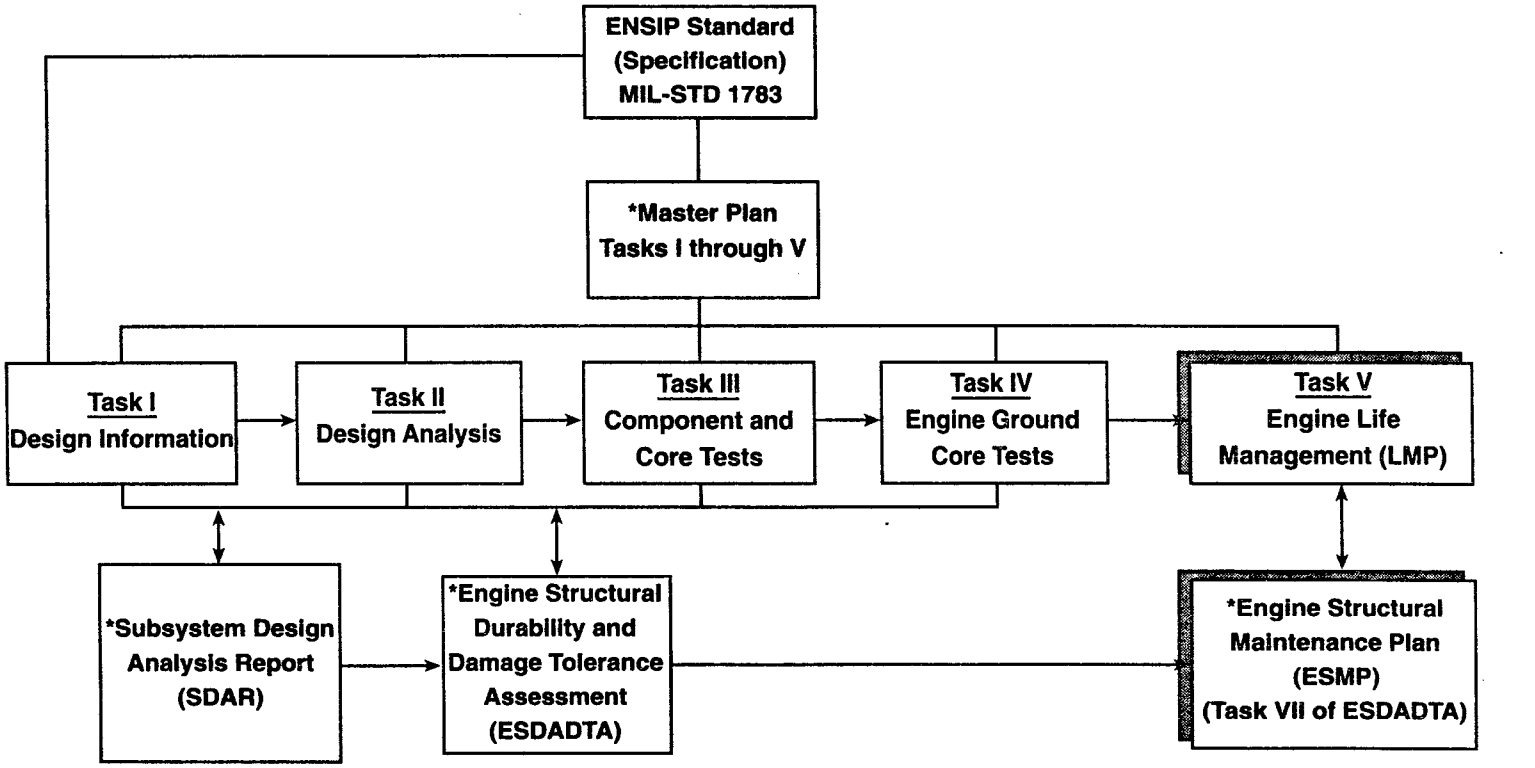

*Deliverable Documents

F117-PW-100 ENSIP

TAILORED ENSIP ASSESSMENT

- PW2000 service experience documented for initial benchmark
- PW2000 FAA tests and reports used for ENSIP as applicable
- ENSIP assessment limited to five peace time C-17 missions defined by USAF
- Damage tolerance verification tests performed on selected components
  - — HPT rotor spin test
  - — Hot diffuser case cyclic pressure test
- X-664-13 telemetry test utilized to verify latest HPT thermals
- No accelerated mission engine testing performed
  - — Commercial testing done for FAA certification
- Conceptual design improvement options for life limiting areas
  Design and implementation outside the scope of this program

Commercial Mission

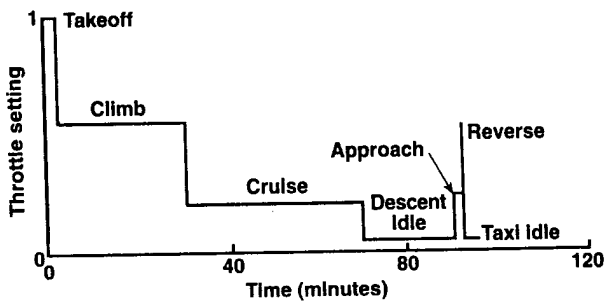

Typical commercial mission full rated takeoff

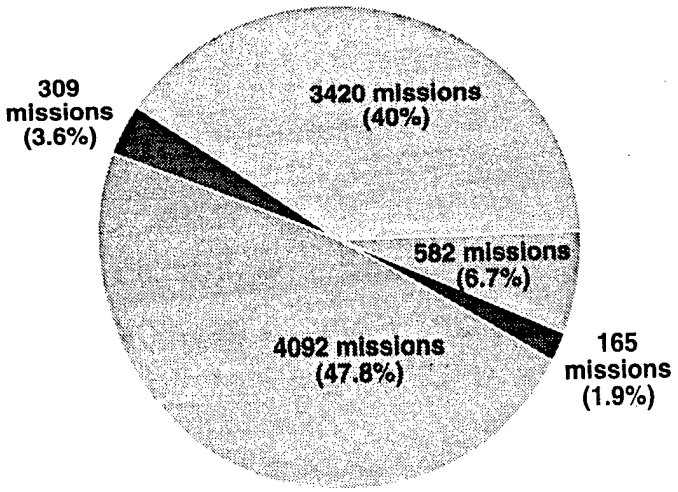

8568 missions in 30,000 EFH

Military Missions for ENSIP Assessment

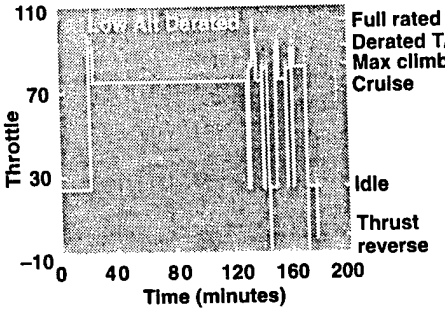

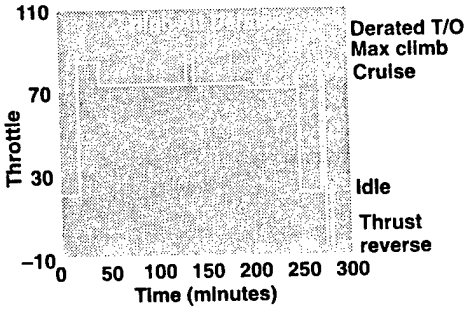

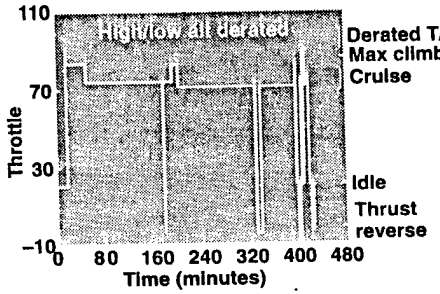

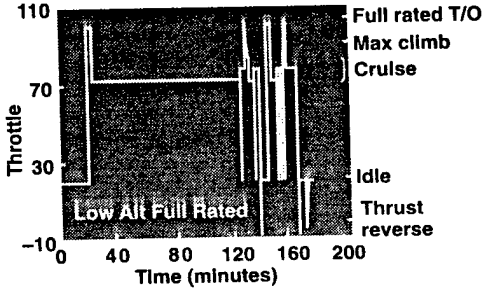

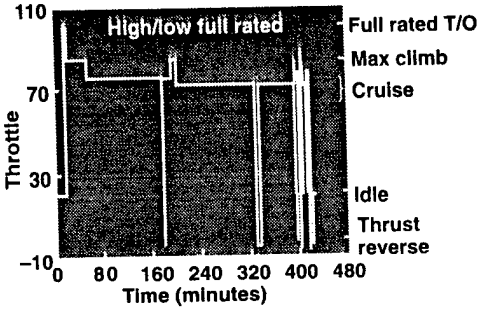

F117-PW-100 ENSIP

PROGRAM GOALS

- Durability and damage tolerance analysis for five peace time C-17 missions that meets the intent of Mil-Std-1783 for '94 package F117-PW-100 (DO-3) engine
- Integrate PW2000 service experience and ENSIP analysis to establish recommended inspection interval/ maintenance requirements
- Life Management Plan at program end provides for safe engine operation and maximizes fleet life

OVERALL PROGRAM SCHEDULE

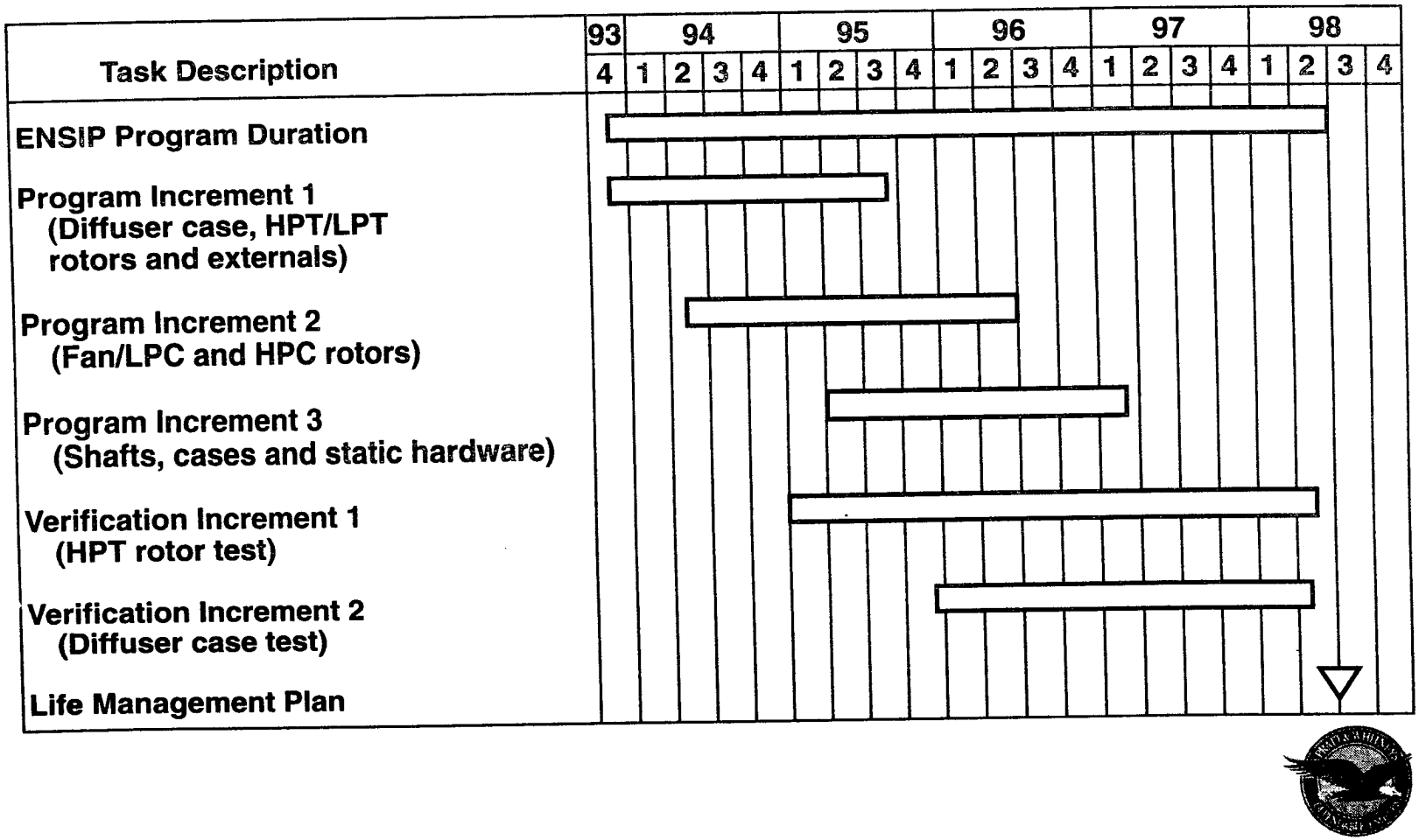

F117-PW-100 ENSIP TEAMS

PRATT & WHITNEY/USAF ENSIP EXPERIENCE INTEGRATED

- Pratt & Whitney/USAF Technical Steering Committee
  - — Detailed technical reviews held semi-annually
- Pratt & Whitney Internal Review Team
  - — Internal reviews held quarterly or as needed
- Pratt & Whitney Materials Test and Characterization Team
  - — Monthly status reviews
- Pratt & Whitney ENSIP Analysis Teams
  - — Dedicated analysis teams for Fan/LPC, HPC Diffuser/Combustor, HPT, LPT and engine Externals
  - — Bi-weekly status reviews

F117- PW-100 ENSIP

DESIGN CRITERIA

Fracture critical and durability critical components identified for analysis

F117-PW-100 design usage requirements

Parameter	Quantity
Engine Flight Hours (EFH)	30,000
Total accumulated missions	8568
Total low-altitude, full rated takeoff missions	309
Total low-altitude, derated takeoff missions	4092
Total high-/low-altitude, full rated takeoff missions	165
Total high-/low altitude, derated takeoff missions	582
Total high-altitude derated takeoff missions	3420

F117- PW-100 ENSIP

INSPECTION INTERVAL

- Assume initial flaws at critical locations (depends on inspection capabilities)
- Determine life to critical crack (safety limit)
- Inspect at 1/2 ⟶ 1X safety limit

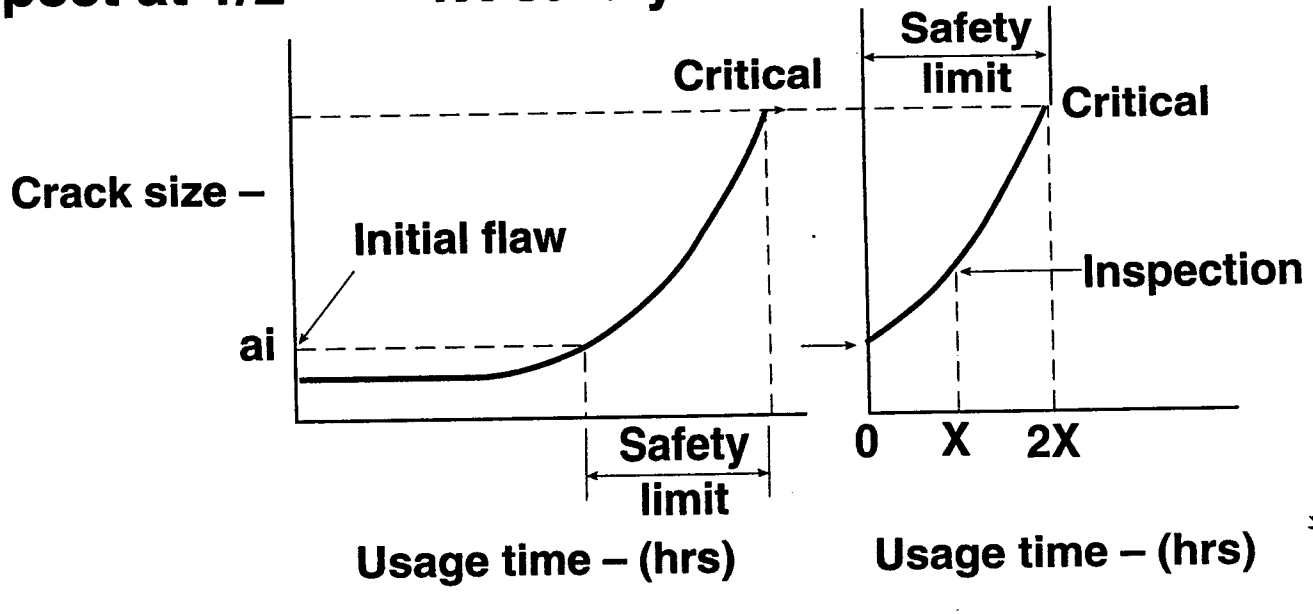

F117-PW-100 ENSIP

MANUFACTURING AND QUALITY CONTROL NDI ASSESSMENT

- F117-PW-100 recommended embedded and surface flaw sizes are based on F100-PW-229 NDI reliability experience
- Embedded flaw size based on demonstrated sonic capability
- Surface flaw size assumptions for damage tolerance calculations are consistent with F100-PW-229 demonstrated capability
- Enhanced depot inspection requirements are based on F100-PW-229 eddy current capability

F117-PW-100 ENSIP

INITIAL SURFACE FLAW SIZE RECOMMENDATIONS

- Based on F100-PW-229 reliability report, recommended F117-PW-100 initial flaw size is 0.020" x 0.040" for code 7 and 0.035" x 0.070" for code 2 FPI procedures
- Accepted alternative enhanced inspection technique for use at depot is eddy current
- 0.010" x 0.020" and 0.020" x 0.040" initial flaw size will be used for F117-PW-100 sensitivity studies

F117-PW-100 ENSIP

LCF AND FRACTURE MECHANICS TESTING PERFORMED TO SUPPORT F117 ASSESSMENT

Material	LCF	Fracture Mechanics
PWA 1100 (powder nickel)	Partial characterization	Full characterization
PWA 1085 (spheroidal Delta INCO 718)	Partial	Full
PWA 1469 (Cast + Hip INCO 718)	Partial	Full
PWA 1228 (Ti6-4)	Partial	Spot check
PWA 1224 (α-Beta Ti6-2-4-2)	Partial	Partial
PWA 1225 (Beta Ti6-2-4-2)	Partial	Full
PWA 1085 EB weld	Spot check	Partial
PWA 1224/1225 EB welded	Partial	Partial
AMS 5616 (Greek ascoloy)	Spot check	Partial
PWA 1264 (Cast + Hip Ti6-4)	Spot check	Partial

F117-PW-100 ENSIP

LCF AND F/M TEST PROGRAM

Incorporates existing data base from CEB and expands data base to cover requirements of complex military missions

- Screening tests to establish equivalency
- Additional R-ratio, temperature, frequency (dwell) tests
- Subelement verification tests to correlate life system models
  - — Constant amplitude tests
  - — Simulated duty cycle tests
- Preflawed component verification tests
  - — Verify component residual life capability
  - — Correlate models against actual component feature cyclic capabilities

F117-PW-100 ENSIP

COMPONENT TESTING

- Damage tolerance verification test performed on selected components
  - — HPT rotor spin test
  - — Hot diffuser case cyclic pressure test
- Remaining components by analysis/similarity to other Pratt & Whitney military programs
  - — HPC drum rotor per F100-PW-229
  - — Welded Fan/LPC 3 stage drum per F100-PW-220/229

F117-PW-100 ENSIP

ENGINE LIFE MANAGEMENT PLAN

LMP PROCESS UTILITILIZES SEVERAL DATA SOURCES

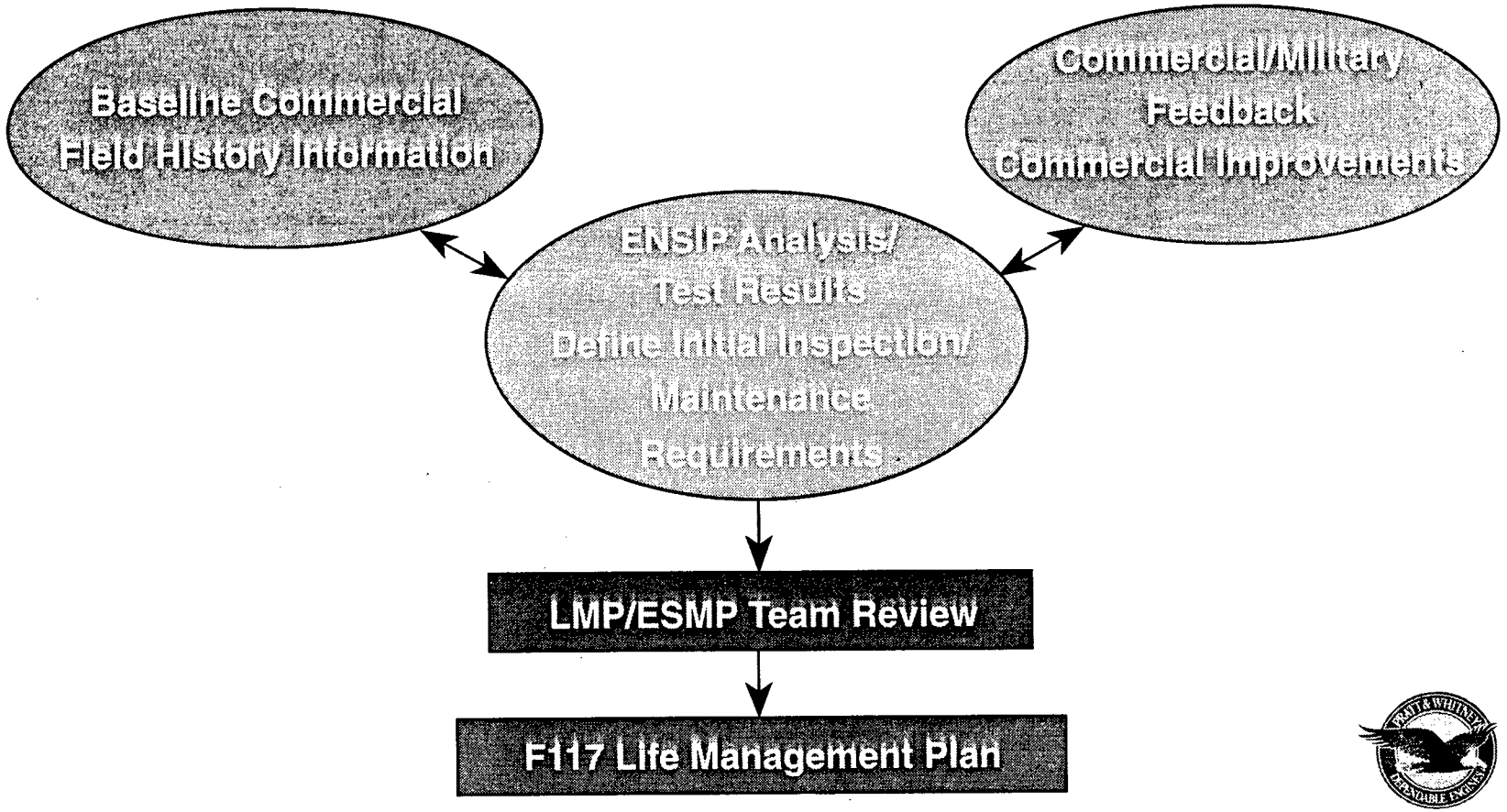

F117-PW-100 ENSIP

LIFE TRACKING SYSTEM

- Critical components tracked individually via tape downloads to ground based data system (G081)

- Multiple life tracking equations used for critical components:
  - — "K-factors" relate severity equivalency of major transients to on/off (Type I) cycle
  - — Convert to "equivalent commercial cycle"

- Track against same LCF limits used by commercial operators

F117- PW-100 ENSIP

PROGRAM STATUS

- Increment I – Diffuser case, HPT and LPT rotors, and externals
  - — Increment 1 is complete
- Increment II – Fan/LPC and HPC rotors
  - — Analysis effort is in process and on schedule
- Increment III – Cases, shafts, and static hardware
  - — Analysis effort initiated on schedule
- Verification I – HPT rotor test
  - — Hardware procurement is in process
  - — Test is planned in 1996/1997
- Verification II – Diffuser case test
  - — Hardware procurement is planned in 1996
  - — Test is planned in 1997

F117-PW-100 ENSIP

F117-PW-100 ENSIP PLANS, REPORTS, AND TASKS ARE ON SCHEDULE

Delivered:

- **Master plan** — **January 15, 1995 (annual)**
- **ESDADTA plan** — **January 15, 1995 (annual)**
- **X664 engine HPT test** — **July 25, 1994 (one time)**
- **Subsystem design analysis report** — **May 1, 1995/Oct. 31, 1995 (semi-annual)**
- **ESMP** — **August 5, 1995 (annual)**

F117-PW-100 ENSIP

ANALYSIS RESULTS STATUS

- Increment 1 and Increment 2 component analysis completed to date supports recommended inspection interval of 2000 composite missions/6000 N1 cycles

- Enhanced inspection areas and requirements identified to support inspection interval recommendations

F117-PW-100 ENSIP

SUMMARY

- PW2000 substantial commercial service and development experience made it suitable for tailored ENSIP application

- Application of ENSIP philosophy can
  - — Maximize fleet life
  - — Minimize risk thru use of "optimized" inspection/ maintenance interval requirements
  - — Reduce life cycle cost

INFORMATION SOURCE

- F117-PW-100/F100-PW-220/F100-PW-229 ENSIP documentation

- F117-PW-100 ENSIP Analysis/Team Leaders

Fan/LPC	– Dave Gatto
HPC	– Scott Billings
Diffuser/Combustor	– Jack Stetson
HPT	– Brian Chisholm
LPT	– Subhash Patel
LPT Low/Stub Shafts	– Dale Harris
Externals	– Mike Obrien
Materials Test/Design System	– Herm Johnson
Mission Analysis	– Mike Paquet
LSA/Planning and Analysis	– Paul Miller

- Viewgraph Presentation and Support – Kent Greenman

- Pratt & Whitney Canada – Archie Tannock

The Canadian Forces Experience with the Operation of Loads Monitoring Process for Efficient Structural Life Management

Capt. Serge Le Guellec
CF-18 Structural Integrity Specialist
National Defence Headquarters, Ottawa, Ontario, Canada

Mr. Mirko Zgela
Senior Structures Engineer
Martec Limited, Halifax, Nova Scotia, Canada

Summary - To improve safety and lower fleet maintenance costs, Operational Loads Monitoring (OLM) programs have been implemented by most air forces to quantify the accumulation of fatigue damage in aircraft. The Canadian Forces have recently reviewed the effectiveness of current OLM practices in providing efficient fleet management information. A key conclusion of the review is that OLM should be considered as an Information System (IS) and characterized as an information "handling process" in which information is gathered, processed and managed. OLM system development should then focus on the end user needs and on the quality and pertinence of the information provided to decision makers. Individual Aircraft Tracking (IAT) is performed by using data generated by the OLM and the Aircraft Structural Management Information Systems (ASMIS). As such, OLM can be considered as a critical element of the force management methods. High level of integration between these two information systems will allow for increased safety and optimum maintenance scheduling. OLM management and technical issues that will ensure a successful OLM are discussed. The need for timely feedback of the OLM generated data to the operational community will be emphasized in the context of a fleet Fatigue Life Management Program (FLMP). Recommendations for OLM system improvements and research areas are formulated.

1.0 Introduction

Under the auspices of the Aircraft Structural Integrity Program (ASIP), the Canadian Forces (CF) have been involved in the past ten years with the design, installation and operation of Operational Loads Monitoring (OLM) equipment for a number of its fleets of aircraft, e.g. the CT114 Tutor, CC130 Hercules, CC144 Challenger and CP140 Aurora fleets.

As a result of the above projects, the CF aeronautical engineering and maintenance communities as well as associated contractors have acquired extensive experience on aircraft loads monitoring. That practical knowledge ranges from the development of individual aircraft fatigue usage tracking strategies to database management and includes the design of dedicated OLM instrumentation suites, usage of modern fatigue and crack growth methodologies, the preparation of in-service airframe inspection packages and implementation of more effective fleet management methods.

The purpose of this paper is to summarize the CF practical experience acquired during the conduct of OLM projects, with an emphasis on managerial and technical

lessons learned. Furthermore, simple yet effective ways of monitoring the performance of a given aircraft fleet OLM capability will be proposed. Finally, new strategies for the conduct of future and/or existing OLM projects will be discussed, from technological and management standpoints.

2.0 Role of OLM within ASIP

ASIP consists of a series of engineering activities aimed at ensuring that the risk of catastrophic structural failure due to accidental damage, corrosion, fatigue, wear or other structural/material degradation is maintained at an acceptable level throughout the service life of the airplane. A detailed description of the Canadian Forces ASIP and related tasks is provided at reference [1].

The Structural Maintenance Plan (SMP) is one of the key ASIP engineering document in that it defines the airframe maintenance package which must be implemented to minimize the risk of structural failure, minimize life cycle maintenance costs and enhance aircraft operational readiness. To do so, the SMP depends, amongst other things, on the accurate tracking of aircraft in-service usage and precise measurements of in-service loads.

The relationships between the many ASIP activities with respect to the SMP are shown in figure (1). As it can be appreciated, a large number of engineering tasks must be completed to prepare the SMP and track its adequacy once implemented in-service. There, it can be seen that OLM plays a vital role in collecting the in-service usage information required to ensure that individual aircraft usage conforms to the spectra used for structural certification test purposes and that in-service maintenance packages are tailored to meet the ASIP stated objectives.

3.0 Objectives of OLM

From the above discussion, it is argued that OLM must be perceived as a complex Information System (IS) that *collects, processes, stores and communicates* structural fatigue data to a number of end users. In that context, OLM is defined as a *set of engineering and management activities that generates technical information related to the in-service usage/loading state of critical structural components in support of fleet management decisions.*

The objectives of an OLM program are therefore to:

a. improve safety of flight by identifying damaging operating techniques and/or mission profiles;

b. reduce maintenance costs by tailoring maintenance packages to actual aircraft usage;

c. identify fatigue damaging manoeuvres/missions for the purpose of defining better fatigue management measures;

d. define statistical information on fleet usage for the purpose of fatigue calculations; and

e. detect possible overstress events, for post-flight detailed inspections.

4.0 Needs of OLM end users

In general terms, three distinct groups of OLM data end users can be identified, that is the Operational community, the Weapon System Management Team and the ASIP Support Contractor.

Operational Community - Under the auspices of the Fatigue Life Management Program (FLMP), operators need to better understand the impacts of fleet operational usage on structural fatigue consumption and identify effective means of minimizing fatigue damage. Their information needs will therefore largely consist of statistical data on the effect of mission mix, external configuration mix, mission profiles, flying techniques on airframe fatigue. The information is then used to tailor specific mission profiles to satisfy both operational capability and FLMP requirements.

Moreover, typical Squadron Maintenance Organizations conduct maintenance in such a way as to minimize impact on squadron operational readiness and within the constraints of personnel, material and funds available to them. To that end, OLM information is necessary for planning purposes (e.g. aircraft rotation from different roles, storage, preventive maintenance scheduling, etc.), where airframe fatigue indicators are required on an individual aircraft basis.

Weapon System Management Team - Within the CF, fleet managers are responsible for the long term airworthiness of the fleet to which they have been assigned and, as such, must ensure that cost-effective maintenance programs are developed and implemented in a timely manner throughout the Weapon System life cycle. These include scheduled inspection packages from Squadron level to Depot Level as well as special inspections, Aircraft Sampling Inspection Program, etc. Airframe maintenance also involves the embodiment of fleet wide proactive fatigue enhancement measures and/or retrofit packages to locally rectify structural deficiencies and restore long term structural integrity.

To that end, fleet managers use OLM information coupled with aircraft specific structural configuration and maintenance packages to project future fleet usage to rationalize on an engineering basis the necessary logistical requirements to implement the maintenance programs identified above.

ASIP Support Contractor - The ASIP Contractor is responsible to provide sound engineering for the continued structural integrity of the fleet it supports. It is the ASIP Group mandate to prepare the fleet SMP, by applying sound engineering rationale to design, certification tests and in-service usage and maintenance data.

Currently, the ASIP Contractors supporting specific fleets of CF aircraft do process fleet OLM data and disseminate the information to users in the appropriate format. From an engineering standpoint, they use the processed OLM information to ensure that a given fleet usage is within the test certification envelope, that usage differences are clearly established, their impact evaluated and reflected into the detailed structural analyses which are used to rationalize the SMP and formulate recommendations to the fleet Weapon System Manager.

5.0 OLM Hardware

An OLM system can be defined as *"a set of engineering and management activities conducted to generate engineering information related to the in-service loading state of a structure aimed at supporting structural management decisions".* This definition recognizes the information generating nature of OLM programs by putting the emphasis on the end product of an OLM system: the delivery of reliable and meaningful engineering information to decision makers. To supplement this definition, an OLM system hardware can be defined as "*any equipment or electronic device which measures and acquires relevant structural parameter data for the purpose of quantifying the loading state of a structure.*"

Most OLM hardware systems can accommodate flight parameters and strain sensors and can cope with analog, digital and discrete signals. New generation systems provide digital interfaces to aircraft systems via standard databuses such as the MIL-S-1553 and/or other recognized standards. A block diagram of a typical OLM hardware system is provided in figure (2). Most systems are usually comprised of an array of aircraft sensors, a Data Acquisition and Processing Unit (DAPU) and a Mission Information Entry Device (MIED).

The sensor's array is measuring structurally significant variables such as strains at pre-determined locations and selected aircraft flight parameters that are indicative of the aircraft loading conditions. Usually flight parameters such as aircraft velocity, altitude, linear and angular accelerations and rates are captured with strain at selected locations. Also, control surface and landing gear position may be measured using Linear Velocity/Displacement Transducers or switches.

The Data Acquisition and Processing Unit (DAPU) is the heart of the system. This black box hosts the required electronic circuitry to process the measured signal originating from the sensors. Usually, the system architecture provides for signal conditioning, analog to digital conversion and filtering of the analog signals and direct capture of the aircraft digital signals via a digital input interface. The processing function consists of event counting using pre-determined thresholds and deadband levels and data compression of the acquired signal. Once processed, the data is stored into solid states memory until needed for transfer. Most of the DAPUs are software driven in that most of the key parameters for data acquisition and processing can be changed via modification to the system software. The DAPU also provides a digital interface with an external PC for further systems diagnostic.

Most DAPUs provide the capability to interface a Mission Information Entry Device (MIED) that is used by aircrew or ground crew to encode additional mission related information with the airframe signals. This information is merged with the aircraft data by the DAPU. Information needed for fleet management purposes, such as mission code, pilot identification code, airframe hours and cargo weight can also be encoded with the aircraft data.

6.0 OLM Data Processing Levels

OLM information treatment can be conceptualized as a four level process carried out at the aircraft, the squadron, the data analysis center and the fleet manager levels. Figure (3) illustrates the four levels of data processing.

The Aircraft Level - The data processing performed at this stage has been traditionally limited to filtering, data compression, sensors hysteresis and system health verifications. In some applications, real-time feedback on the loading state of the aircraft has also been provided to the aircrew. To reduce memory size requirement, the strains or flight parameter time histories must be converted into a compressed form using either peak counting, level crossing, rainflow or sequential peak and valley counting, the last two methods being the most widely used. The compressed data is downloaded by squadron maintenance personnel at regular intervals to a computer referred to as the Ground Retrieval and Display Unit (GRDU), using a data transfer medium, a largely modified laptop computer with increased memory size or non-volatile memory cassettes.

The Squadron Level - The GRDU usually takes the form of a commercially available

Personal Computer (PC) loaded with the proper downloading and system software. The data is transferred to the GRDU in binary format to speed up the transfer process. It is then converted to engineering units, verified and validated. The extent of data validation and verification at the squadron level varies substantially depending upon system design. This verification and validation task implies that errors, such as drifting sensors, unserviceable sensors and OLM system malfunctions are detected. Once downloaded, the data is structured into Aircraft Data Files (ADFs). Depending upon the data capture process adopted, some form of supplementary data is added at this stage, either entered manually or via direct link with other databases. The ADF structured information is then prepared for transfer to the Data Analysis Centre. A base level database is used to archive the ADFs that have been transferred to the Data Analysis Centre for further processing. Usually, ADFs are kept in this database for a limited amount of time and destroyed when no longer required. Transfer media are largely data cartridges and/or 3.5" data disks. To date both transfer media have been found to be adequate and cost effective.

Data Analysis Centre Level - It is at the Data Analysis Centre that nearly all of the hard processing work is performed using a fatigue tracking methodology that has been fully validated by extensive testing. Comprehensive statistical processing is performed to validate the data and to detect any long term abnormal behaviors of the sensors and/or systems hardware using pre-determined error detection algorithms. Further statistical processing is done to collate the data into fleet operational information that will be used for fleet management purposes or, if needed, in the development of new design specifications.

The validated data is then collated and sequenced into strain spectrum that are considered representative of in-service usage. Many spectra can be collated and analyzed depending upon the specific user requirements and the number of critical locations that are of interest to the user. Damage calculation is then performed for the fatigue critical locations of interest.

Data processing at this level will yield two databases and generic fatigue reports. The generic fatigue reports will contain structural fatigue consumption information that will assist the end users in making rational decisions regarding the structural integrity of the fleet or a particular airframe. An on-line database provides a summary of the fleet statistics, provides in-service structural fatigue usage trends and ideally should provide simulation capability. An off line database contains all the raw data generated for the fleet. This database will allow for quick retrieval capability.

The Fleet Manager Level - This level is key to the success of the OLM process. This level involves the interpretation of the generic fatigue reports provided by the Data Processing Centre and will result in fleet management decisions. Furthermore, with the information provided, the fleet manager will be in a position to provide feedback to operational staff on the structural integrity status of the fleet and/or individual airframe.

7.0 Management Issues

A number of issues must be dealt with early on in the OLM project. Project management methods best suited for the development and implementation of an OLM capability are first addressed. Fleet fitment strategies are then considered, where the initial and recurrent costs of the planned OLM capability must be considered. Finally, the design of an effective Fatigue Life Management Program (FLMP) is briefly discussed, with the emphasis on FLMP organizational issues and the requirement for consistent

fatigue usage management procedures for all information users.

Project Management Methods - Given the scope of the work and funds involved in the design and implementation of an OLM capability, the selection of an adequate project management method is critical. To illustrate the point, consider the following questions.

Is the project large or small? What is its impact on the overall fleet management? What is the degree of complexity envisaged? Are the project objectives clear and are they supported by all stakeholders, e.g., operators, maintainers and engineers alike? Should the project be considered as a black box integration task within the existing aircraft avionics suite, a software development project, an equipment procurement project or as an engineering database development project? What are the risks involved with the project?

In general, although the scope of OLM projects are relatively small (typically less than $ 10 M CDN), they have significant impact on the management of a given fleet. For this reason, it is essential that the project be endorsed by the appropriate Force Commander, be given a high visibility and priority and that consensus be obtained on project objectives from all stakeholders involved in the project.

Moreover, OLM projects are technically complex and require the integration of several fields of expertise, from structural engineering to the design of dedicated databases. From experience, a small project team must therefore be closely working together, as trying to compartmentalize work packages amongst a number of independent contractors, without integration, will result in significant delays, cost overruns and frustration. Clearly, integration is a key characteristic of OLM project teams.
The technical and managerial concepts which must be dealt with during OLM projects are quite well understood and are relatively well documented in published standards and/or in the open literature. A certain degree of formalization is thus inherently built-in this type of project. More to the point, given the scope of the work involved and the small size of the integrated project, needs for detailed project management procedures are not warranted.

CF experience indicates that the project management method followed for the design and implementation of Information Systems (IS) are best suited for OLM projects. A generic project management framework is provided in table (1), where the major milestones and key documents are identified. In the early stages of the project, great care must be exercised to ensure that the *Fleet Management Requirements* are well defined and that *Fleet Fatigue Management Data Specifications* are produced. These documents clearly define the fatigue information needs of all end users, a necessary step which does not always receive sufficient attention. Similarly, the preparation of performance specifications for the OLM hardware, squadron level data system, data analysis center and structural tracking database must be carefully considered before they are frozen. Thus, at every level of the OLM data processing, quality of the data should be considered as a prime concern and should be accounted for in the systems specifications.

Finally, divestment must be properly planned, where the responsibility of the routine operation of the OLM capability is transferred to the given fleet Fatigue Life Management Program (FLMP) organization.

OLM Fleet Fitment Strategies - The fleet fitment strategy which will be adopted for a particular OLM program will largely be dictated by specific fleet management requirements and funding availability, the solution being an optimum trade-off

between the two parameters. The strategy will be the object of detailed cost/benefits analyses and feasibility studies, the details of which are beyond the scope of this paper.

OLM fitment strategies can be simplified to essentially two conceptual approaches. Firstly, within a given fleet, a number of airplanes are fitted with OLM instrumentation suites of varying complexity and capability. Secondly, all fleet aircraft are fitted with an OLM instrumentation suite. A summary is provided in table (2) and relevant details are provided below.

Partial OLM fleet fitment strategy - This is accomplished by instrumenting a limited portion of the fleet. In this case, structural tracking is done at the missions, squadron or fleet level depending upon the statistical model used. The sample size is selected to be statistically representative of the aircraft in-service usage and should cover a wide range of fleet operations to minimize usage uncertainties. Based on the above, 30% of all airframe within a given fleet represents a good sample size to capture highly reliable fleet usage information. From past experience, the following should be considered when establishing a fleet fitment strategy [2];

a. each operational squadron should be assigned a minimum of three OLM instrumented aircraft, thus accounting for low flying, unserviceabilities and the need to quickly collect in-service data;

b. the total number of instrumented aircraft should not exceed 30% of all fleet aircraft and should be no less than 10 aircraft; and

c. if a large standard deviation from the mean usage is observed, e.g. above 0.15, the minimum number of instrumented aircraft should be increased to 20. This scenario is likely to happen when roles amongst squadrons differ significantly.

This type of fitment strategy will provide sufficient information to perform structural integrity management of the fleet, up to the squadron level. It will not be possible to perform fatigue management at the aircraft level. This approach should be considered if the only intent is to ensure that the assigned operational mandate of the fleet is well within its certification envelope and that roles, missions and/or manoeuvers which can jeopardize the long term structural integrity of the fleet are identified for corrective actions. Such is the case for the CT133 SilverStar fleet planned OLM program.

Full Fleet Fitment - In keeping with the intent of ASIP, true Individual Aircraft Tracking can only be achieved by instrumenting all aircraft in a given fleet. This approach is the most costly, in view of the need to instrument all fleet aircraft and the recurring costs associated with the processing of individual aircraft fatigue data. However, the incremental costs of the OLM program are justified by the need for accuracy of the OLM information obtained. Such is the case for the CF1888 fleet, whereby operational life is dictated by safe life requirements. Clearly, in view of the economic consequences attached to early retirement from service, precise fatigue consumption data is required.

Fatigue Life Management Program - In a nutshell, the objectives of a Fatigue Life Management Program (FLMP) are to monitor and tailor aircraft usage and fatigue damage accumulation so that the fleet economical life is maximized without compromising operational effectiveness. The success of the program depends on three key elements, that is fatigue awareness, usage characterization as well as guidance and control measures, as shown in figure (4). A detailed discussion of FLMP is beyond the scope of this paper and is fully addressed at reference [3].

The case of the CF188 is an excellent example of a highly effective FLMP program, where aircraft usage and corresponding fatigue data are considered during the operational and maintenance decision making processes. The program was instituted in 1987 and is the most mature of all CF OLM initiatives. The CF188 FLMP experience to date clearly indicates that the efficient use of in-service data collected via an OLM capability results in rationalized fatigue consumption, offering good return on OLM initial investment and recurring operating costs as well as added value to both fleet management and operations.

FLMP related Organizational Issues - Because of its vital role for ASIP, engineering and maintenance as well as operational communities, FLMP must be endorsed at the highest level within the Air Force chain of command. This endorsement must further be complemented by a clear definition and division of overall program management responsibilities between the respective operational Squadrons, Command Headquarters and the ASIP Contractor. The later requirement invariably translates into the need to assign personnel dedicated to support FLMP at all levels, from the early project definition stage, project divestment, capability implementation and routine operation. Clearly, senior management endorsement must be secured early on in the OLM project.

Once implemented, the Force Commander's attention must remain focused on FLMP issues in order to adequately monitor and assess fleet fatigue consumption in relation to the fleet operational mandate and provide clear guidance to operational squadrons in the form of regular feedback and the formulation of corrective control measures when required.

Definition of monitoring and control measures at Squadron level - It is the responsibility of the respective Command Headquarters to formulate and implement uniform squadron level fatigue management procedures. In particular, attention must be paid to the maintenance of squadron personnel fatigue awareness, the consistent monitoring of squadron fatigue usage and implementation of effective damage control measures and the designation of personnel assigned to support FLMP at the Squadron level. In particular, the need for clear guidelines to Squadrons with respect to individual aircraft control and its impact on fleet sustainability cannot be over-emphasized. Finally, the requirement for accurate mission and pilot identification data must be impressed on Squadron personnel to ensure that the pertinence of fleet usage statistical information is not compromised.

OLM Hardware Maintenance Issues - Given that special algorithms used for fatigue data fill-in for missing and/or faulty fatigue data are generally highly conservative, OLM instrumentation related maintenance issues must be dealt with on a priority basis at Squadron level. Clearly, maintenance turn around time must be optimized and, to that end, effective procedures must be implemented to quickly detect and correct instrumentation faults. Finally, the importance of an up to date individual aircraft OLM hardware configuration database must be stressed, as fatigue algorithms will likely require aircraft configuration specific data which will dictate the selection of appropriate correction factors for further processing purposes.

Fatigue Data Processing Turn Around Time - One of the most frequent complaints voiced by fatigue data information users is the slow processing turn-around time of fatigue usage data. To that end, the data stripping from OLM recorders, the transfer of files to the centralized data processing facility, the

actual processing and the dissemination of processed data are all activities which must be streamlined. From a user standpoint, smart use of information technology is fast becoming one of the key elements of the success of OLM programs.

8.0 Technical Issues

A technical issue is identified as any aspect of OLM that could have a detrimental effect on the quality of the structural integrity information provided to the information users.

8.1 Aircraft Level

Strain Gauging - Two major problems have been observed with strain gauges: drift and complete failure. Drift is described by the deviation of the zero setting of the strain gauge bridge under zero load conditions. Drift can be attributed to many factors ranging from strain gauge fatigue, structural hysteresis and adhesive deterioration resulting from environmental effects or bad installation and is often an indication of early failure. Drift is of prime importance since it can introduce a large error factor in fatigue calculations. ***Typically, a 15% drift from the reference strain condition can result in a factor of two in the fatigue damage evaluation.*** Complete failure of the gauge is also of concern as lost data, unlike bad or drifted strain data, cannot be recovered. To account for lost information, "fill-in" data derived from historical data trends is used and is introducing further conservatism. Finally, sensor change resulting from failed sensors also adds to the maintenance burden.

Strain gauge durability and accuracy are highly influenced by the installation procedures. Experience indicates that traditional installation methods provided by strain gauge manufacturers had to be extensively modified to provide much needed improvements in bond durability. Moreover, strain gauging is highly sensitive to surface preparation. In this regard, the surface treatment process developed for bonding of composite patching may be more appropriate procedures to use when performing strain gauge surface preparation. These procedures could provide a significant increase in strain gauge durability. Typically, the durability of strain sensors to date has been in the vicinity of 2,000 flying hours.

Data Compression - Most OLM systems hardware provide programmable parameters to adjust the level of data compression. The proper set up of these values is a compromise between the quantity of the data to be recorded and the accuracy of the fatigue damage calculations. (E.g. How relevant was the "non recorded" data to the fatigue damage?). Data compression can be altered by varying "deadband" and "threshold" values. Threshold is related to the omission of small cycles that have little influence on fatigue estimation. Increasing the threshold can reduce the volume of stored data but it can also have a significant impact on life predictions, particularly in the case of gust loads on transport aircraft. Deadband can be defined as a zone around the mean load level in which cyclic loading is considered as insignificant in the estimation of fatigue damage. Excessively small deadband and threshold values will result in an excessive amount of recorded data while too large values will result in the loss of significant data for which fatigue damage cannot be accounted for.

Threshold and deadband values must be optimized to obtain the right level of data compression appropriate to the fatigue damage evaluation methods use. This can only be performed effectively by conducting parametric studies ***and*** coupon for each critical location to be tracked. Using the fatigue calculation for validation provides

for a more practical determination of the threshold and deadband parameters.

Data compression is performed using a compression algorithm. Typically, this algorithm requires extensive validation. It has been often the case that data compression algorithms contain significant design errors that have resulted in the loss of important fatigue cycles. Usually, system hardware suppliers validate their proposed algorithms using pre-determined load sequences as test cases. A better approach would be to test the data compression algorithms using realistic sequences collected during flight or ground tests for which the knowledge base has already been established. In this regard, a real test load sequence can be properly characterized and used as a test case for verification and acceptance of the compression algorithms. This method of validation of data compression algorithms is highly desirable since it will highlight problems very rapidly.

Load/Strain Calibration - OLM calibration requirement has often been underestimated. If the strain measurement is in error, so will be the fatigue calculation. The strain gauge reading must therefore represent, as much as possible, the true value of strain state at that location and should be time invariant for a given load condition. This can only be achieved by performing calibration at regular interval. By comparing the first calibration value with existing stress models, strain sensor installation problem, such as misalignment and bad electrical connections, can be easily determined. Limited calibration using simplified calibration methods such as localized applications of weights can be used for that purpose. Also, periodic in-flight calibration using known flight reference conditions can be performed to ensure that the strain gauges have not drifted significantly over time.

Download Periodicity - How often should the stored data be downloaded? In theory, this is a function of both the OLM system hardware memory size and user's requirement for frequent information. Downloads that are too frequent will carry a maintenance overhead. Download intervals that are too sparse may result in the loss of important data due to unnoticed hardware system component failure. The best approach to determine the downloading interval is to link the download task to the aircraft maintenance schedule and to integrate the download task as an element of the scheduled maintenance package. From experience, downloads should not be more frequent that once a week (maintenance burden) or go for more than one month between downloads (lost data). It should be pointed out that these criteria, when specific aircraft operation is taken into account, will dictate the system memory size.

Mission Information Entry Device - The requirement for the installation of a Mission Information Entry Device (MIED) must be carefully weighted. This system is used to encode supplementary mission data with the loads data. This information may either be essential for the calculation of the fatigue damage or as a complement to the fleet usage statistics information. From experience, this form of data capture is unreliable because the data can be either entered incorrectly, or worst not entered at all. Thus, although this device was introduced to somewhat automate the data gathering process, extensive validation is nonetheless highly recommended, if MIED is to be used at all.

7.2 Squadron Level

Data Validation and Verification - At this stage, it is essential that as much data error as possible be identified and that a diagnosis be established on the cause of faulty data. Ideally, 90% of all the data errors should be identified at this stage. Early error detection will ensure quick rectification of problems and will avoid

utilization of conservative fill-in data to account for the data lost while awaiting for maintenance to be carried out.
Typical errors that could be identified at that stage are: complete sensor failure; sensor drift; channel chatters; channel saturation; out of range values; and sensor calibration problems. Suitable data verification and validation capability at the squadron level is an essential requirement, since it has a direct influence on the data capture rate and on the overall system efficiency.

The problem at the squadron level is that the technical expertise to perform a diagnostic assessment on data errors is not readily available. A way around this problem would be to develop automated data verification and validation algorithms that can be easily programmed to provide diagnostics as to the likely cause of data errors. These algorithms can also be designed to suggest rectification methods. The error detection and rectification algorithms could be improved over the years as experience with a particular OLM system hardware is accumulated.

Data Return Rate - Previous experience with OLM systems has indicated that a data return rate of approximately 85 to 90% could be achieved. The remaining portion is made up of missing data, due to complete system or channel failure, or bad data resulting from faulty sensors. Squadron maintenance personnel are responsible to ensure that the technical problems associated with the missing or bad data is corrected. As such, squadron personnel performance in rectifying OLM hardware problems has a direct impact on the data return rate and ultimately OLM system efficiency. A proper feedback to squadron maintenance personnel must be implemented to ensure that rapid corrective actions are prompted when problems are noted.

8.3 Data Analysis Center

Block Size Selection - The determination of the block size for processing depends on many factors. Generally speaking, keeping the block size as small as possible is desirable but not always economical, since calculation time is significantly increased. If load interaction effects (retardation) must be accounted for in the fatigue damage assessment methodology, then the most accurate solution is to perform crack initiation and/or growth calculations on a cycle-by-cycle basis. This level of precision may not be absolutely needed in all cases when retardation models are used. For transport aircraft, for example, it is considered that keeping rainflow-counted cycles in a flight-by-flight order will provide good accuracy. In the past, block size selection was a critical issue. With the increasing speed of computer hardware, sequence processing on a line-by-line basis is now possible for large quantities of data at economical cost.

Selection/Validation of Fatigue Damage Algorithms - The methods used to evaluate the fatigue damage accrual of aircraft structures using loads monitoring data has been to perform crack initiation (durability) or crack growth (damage tolerance) calculations. These predictions are compared with previous design predictions or full scale durability and damage tolerance testing data to determine the fatigue damage accrual.

The need for proper calibration of the fatigue evaluation methods cannot be over emphasizes. Regardless of the model used, every crack growth prediction or crack initiation analysis should be supported by experimental calibration, or serious over or underestimation may occur. Validation of material and geometry data, and calibration of retardation models are essential requirements and must be performed. This calibration is usually done by performing coupon fatigue testing using load spectra representative of the strain

profile. It is the accepted norm that this calibration work must be performed under spectra loading representative of the expected in-service spectrum. ***Any OLM projects must therefore include a calibration task for the fatigue damage assessment model if the model used has not been previously calibrated during design.***

Development and Validation of Transfer Functions - Transfer functions enable the development of loading sequences for fatigue critical locations based on the recorded OLM data. The OLM data used to generate transfer functions can take the form of flight parameters, strain sequence or a combination of both. Transfer functions can be developed using analytical load models coupled with Finite Element Analysis (FEA) or derived from measurements performed in full scale fatigue or flight test programs. If transfer functions have been derived using analytical models, it is strongly recommended that they be validated by flight testing. Validation will ensure that the OLM recorded strains can be predicted accurately with the analytical model used to generate the transfer functions. The validation of the transfer functions will significantly increase the confidence in the fatigue damage evaluation.

Data Validation & Verification - Not all errors will be detected at the squadron level. The DAC processing should ultimately ensure that the only data used for processing is good data. Ideally only 10% of all the potential errors would be detected at that level. Regardless of the data verification and validation strategy, all possible errors must be detected and no data should be processed that has fatigue significant data errors.

Development of Fleet Usage Database - Once the data has been processed, the fatigue damage data and fleet statistics are used to produce fatigue consumption reports that are used by the fleet manager to make their decisions. The raw rata (unprocessed) should be archived in an off-line database in the event that reprocessing of that data would be necessary. It would be highly desirable to have the historical fleet statistics and fatigue damage data accessible via an on-line database. This database, if well structured, could eliminate the requirement for printed reports. The new technology of relational database and computer network already offers cost effective solutions to information dissemination.

8.4 Fleet Management Level

Fatigue Data Interpretation - Fatigue reports have traditionally been distributed in hardcopy format. Making these fatigue damage reports easily "accessible" to the non-specialist engineer is a difficult task. This can be done however by making use of "graphical language" techniques and by condensing the relevant fatigue management information into graphs and histograms. To ensure that the information presented is in an acceptable form, it would be advisable that fleet managers be consulted on preferred fatigue damage presentation report format. The graphical fatigue management report formats could be easily be programmed into standard templates, into the fleet usage database.

9.0 Areas for Improvements

New strategies for OLM programs can offer opportunities for cost savings, improved system performance and improved system design. These are discussed below, considering new algorithms, improvements to OLM instrumentation as well as areas where research and development initiatives are required.

9.1 Methods

General - As a quick survey of the open technical literature would demonstrate, significant efforts are invested in the

development of parametric load prediction methods to derive loading. This concept is promising in that OLM instrumentation only needs to gather flight parameters, thus doing away with the need to also collect strain data. While it is recognized that this method requires a significant investment in analytical prediction capability and experimental flight testing, it could reduce the OLM life cycle costs significantly, considering the savings associated with the much simplified OLM instrumentation suite as well as reduced installation and recurring maintenance costs. A good example of parametric load formulation is provided at reference [4].

OLM Data Processing Strategy - Calculation of fatigue damage using the OLM data has been traditionally done at the Data Analysis Center. Today's technology offers the potential to use a different approach and fatigue calculation could possibly be performed in real time, on board the aircraft. This data processing strategy is called on board processing and requires a powerful computer to process flight parameters and strain data. Ideally, only the calculated values would be stored and, as such, the raw data would be lost. Thus, there would be no lag time for data processing and much smaller memory size would be required. This process has the advantage of significantly reducing OLM life cycle costs by simplifying the data management task and reducing the extent of ground base infrastructures that would otherwise be needed. The loss of raw data is perhaps the most serious drawback of the concept in that, should there be a recorder failure or fault in the fatigue algorithm, it would not be possible to retrieve the data to reconstruct the load sequences of interest.

In this case, the reduction in required memory size is traded off against the requirement for more processing power and the complexity of incorporating a software algorithm. The fatigue calculation software has to be developed for a specific aircraft and provision for software upgrades and system growth has to be provided. With the ever increasing level in computing power of microprocessors, the increasing cost of personnel to run the ground infrastructures, and in light of the lessons learned from operating first and second generation OLM systems, it is likely that this form of processing will gain in popularity.

Human Involvement in OLM Data Processing - Current processing procedures require human intervention for the downloading of the in-flight data and the merging of supplementary data to the flight-by-flight data files, data shipping and fatigue report generation and distribution. The involvement of human operators results in two problems: firstly, there is the non-negligible potential for human error in the data collation process; secondly, there is the personnel cost associated with maintaining highly skilled and trained resources to operate the ground installations. To alleviate the impact of the human operator involvement, data merging operations should be automated and manual data entry avoided as much as possible.

The need for Data Verification and Validation at an early stage of the data processing to identify most errors cannot be over-emphasized. Moreover, this important step of data processing does require well trained personnel, because a fully automated data collection system would rely on complex data verification and validation algorithms, which are still expensive to develop and maintain.

Finally, given modern computer networking and relational database technologies, OLM system designers should strive to render the process "paperless." All fatigue damage reports should be collated into an on-line fleet relational database which can be accessed by multi-users, in a user-friendly GUI type interface. Note that, for the sake of minimizing database volume,

only the critical fleet management information need be included into an on-line relational database. Raw data can simply be archived into highly compressed files using optical disk storage.

OLM System Performance Assessment - Fundamentally, the concept of OLM was introduced to improve safety and reduce maintenance costs, two parameters which can be used to assess the performance of a given OLM system. From a cost viewpoint, benefits are obtained if the total OLM life cycle costs are less than fleet management savings resulting from the interpretation OLM information. To date however, the global performance of an OLM system is not being monitored and performance indicators are required to ensure that its efficiency remains high during its service.

Three indicators are proposed, that is the data turn around time, the data capture rate and the ratio of volume of data produced over the system recurring operating cost, or cost factor. The data turn around time can be expressed in days and provides an indication of the OLM system data processing efficiency. It can be calculated from aircraft downloads to inclusion of the fatigue damage data into the fleet usage relational database. The data capture rate can be expressed as a percentage and is a direct measurement of the OLM hardware performance and of the OLM infrastructure's ability to quickly detect and correct deficiencies. Finally, the last performance indicator can be expressed in bytes of data processed per unit dollar of recurring operating cost (Kb/$). This indicator is a measure of the system efficiency variation. The Kb/$ indicator ranges from zero (i.e. no data processed) and would reach an asymptote when the system reached a maximum processing capability. The volume of data processed and operating costs only include data considered good and the recurring costs associated with the overall data processing and maintenance costs respectively.

9.2 Instrumentation

Add-On or Integrated System - It is likely that the Operational Loads Monitoring system hardware for future aircraft design will be fully integrated with existing onboard computers. Such was the case for the F/A-18 aircraft. Although this would provide a simpler approach from an engineering system design standpoint, it imposes a larger burden for software upgrades, as any software changes, for example to adjust dead band and/or threshold, of a fully integrated system would not be considered to be of major impact to justify the significant costs associated with extensive software validation and verification testing for certification purposes. Delays for OLM system upgrades could thus be substantial. The solution may lie in the design of a passive OLM system, which software can be upgraded independently, while still maintaining a degree of integration with other aircraft avionics systems, an issue which will require careful consideration for future aircraft procurement.

New Strain Sensor Technology - The utilization of flight parameters coupled to foil strain gauges have been widely used as the preferred OLM strategy. However, the inherent problems associated with strain gauges and the infrastructure overhead required to account for their deficiencies raise some fundamental questions. First, are there other means of accurately measuring strain? Secondly, can loads monitoring be done without any strain gauges?

Fibre optic strain sensing is emerging has a potential high performance replacement sensor for conventional foil strain sensors. Reference [5] provides an account of the recent developments in fibre optic technology for strain measurement. Fibre-optic strain sensor manufacturers claim that significant performance improvements

over conventional sensors can be achieved in term of accuracy, size and weight, EMI immunity and reliability. To date, no application of fibre-optic strain sensor technology has been performed in an OLM environment and in service experience is almost non existent. It is to be noted however that fibre optic strain sensors must still be bonded to the metal substrate and that surface preparation and adhesive bonding durability issues will still be present with fibre-optic technology.

Replacement of strain gauges has significant impact on aircraft maintenance and readiness as well as on the total life cycle cost of an OLM program. Consequently, the number of strain gauges used in an Operational Loads Monitoring remembering that the aim of strain gauging is only to collect gross area strains in the major load path structural members. It is therefore unlikely that strain gauging requirements should exceed eight strain sensors for most types of aircraft structures.

9.3 R & D Efforts

Whereas the last decade has witnessed significant progress in OLM technology and methods, efforts have largely been dedicated to solving fundamental hardware shortcomings, such as sensor measurements, data compression algorithms, processing power, large size solid state memory, improved reliability and maintainability. Moreover, OLM technology has rapidly become capable of collecting adequate data to accurately monitor manoeuvre and ground loads. Indeed, progresses have been remarkable. However, it is proposed that two areas now need further attention.

Firstly, the advent of highly manoeuverable fighters, such as the F/A-18, using active control system technology, has resulted in the need to better comprehend the airframe structural response to both manoeuvering and buffet induced dynamic loads. The later loads are particularly challenging in that current OLM hardware is not designed to capture the high frequency dynamic load cycles which are of interest from a fatigue standpoint. Moreover, there are currently no suitable crack initiation or crack propagation methods robust enough to predict the fatigue behavior of structural components subjected to combined manoeuvering and dynamic loads. It follows from the above that there is a need for research and development work leading to the design of third generation OLM systems, fitted with improved and robust data compression algorithm, increased memory size and improved fatigue algorithm for manoeuvering and dynamic fatigue tracking.

Secondly, new methods of processing must be devised if on board calculation is going to be the way ahead. To that end, neural networks are providing an efficient solution to the development of transfer functions in that they allow for the quick determination of mathematical relationship between measured aircraft parameters and local strain at critical locations. Also the speed at which neural network can perform the calculation, once properly trained, offer cost saving opportunity for onboard processing of the OLM data. However, the structural integrity community has been apprehensive in using neural network because of a lack of visibility on the derivation process. One possible alternative would be to use validated loads models for neural network training. The solution provided would then be a more compact and computationally efficient models that could be used on board for the fatigue damage calculation.

10.0 Conclusions

Rapid progress of the microprocessor technology over the last few years and the ever increasing memory size capacity has enable fleet wide monitoring of in-service

loads on aircraft. This large scale monitoring ability has open new perspective in aircraft structural fleet management. Fleet managers can now tailor maintenance program to suit a particular airframe requirement and provide for increased safety and lowered overall maintenance cost.

In keeping with the above, it is essential that the OLM program be sharply focused on end users information needs, a critical step in the design of the OLM information system. Furthermore, data quality and accuracy are prime concerns of the OLM system architecture. OLM system are now providing critical information to fleet managers and can be heavily relied upon for efficient fleet management.

New Information System (IS) technologies are providing opportunities to reduce OLM system life cycle costs. Automation of the data collection process by linking the OLM system with existing fleet management databases will reduce the costly personnel involvement in data entry. Also, computerized data validation and verification processes will systematically provide for high quality data. Computer networking and relational databases will provide for a near paperless OLM fatigue reporting process and for on-line availability of the OLM information to all end users.

From a system management standpoint, three performance indicators were proposed: the data capture volume, the data turn around time and the OLM cost factor. The determination of these indicators could be easily built-in the OLM information system itself.

Finally it was argued that future OLM research and development efforts should concentrate on the measurement, tracking and quantification of dynamically induced fatigue damage. To provide for a reduction in OLM system operating cost new data processing methods should be investigated. Neural networks and large scale on board processing are promising options which require further investigation.

11.0 References

[1] Canadian Forces Technical Order D12-010-013/SG-000, Aircraft Structural Integrity Program, dated July 1980.

[2] V. DeHaye, "Le coefficient de sécurité en fatigue - Calcul de niveau de sécurité associé", Centre d'essai aéronautique de Toulouse (CEAT)", AGARD CP506, December 1991.

[3] M. B. Zgela and W. B. Madley, "Durability and Damage Tolerance Testing and Fatigue Management: A CF-18 Experience", AGARD CP506, December 1991.

[4] R.J. Cazes and P Defosse, "Aircraft Tracking Optimization of Parameters Selection", DASSAULT-AVIATION, AGARD CP506, December 1991.

[5] F. A. Blaha and S. L. McBride, "Fiber-Optic Sensor Systems for Measuring Strain, and the Detection of Acoustic Emissions in Smart Structures", AGRAD CP531, April 1993.

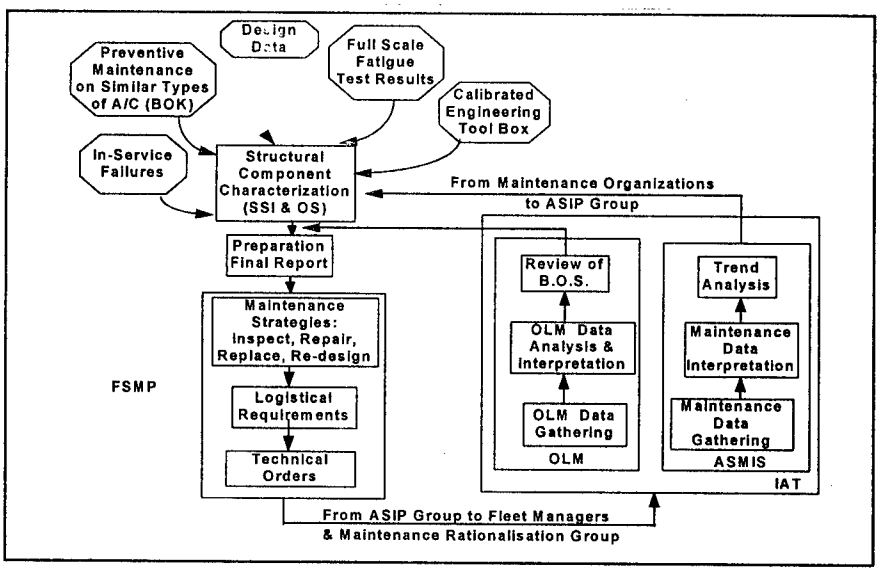

Figure 1 - ASIP & Structural Maintenance Plan

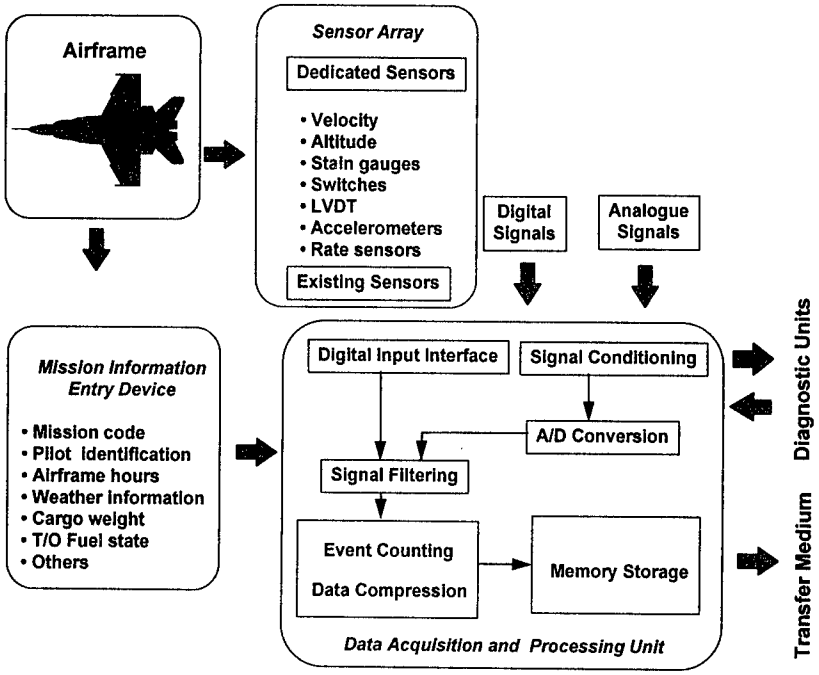

Figure 2 - Typical OLM System Block Diagram

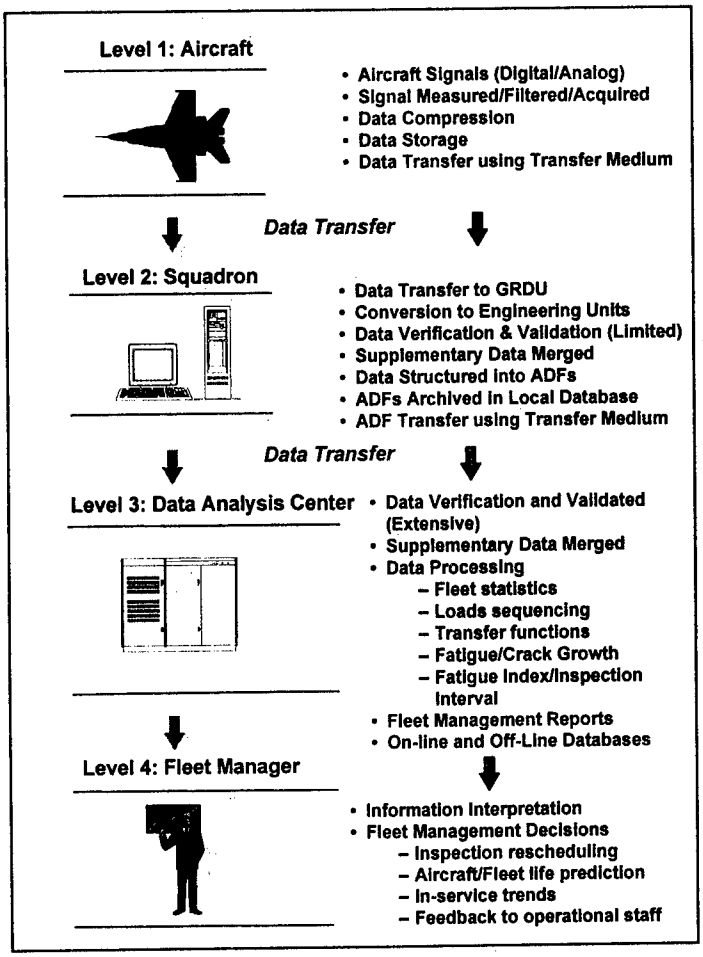

Figure 3 - OLM Data Processing Level

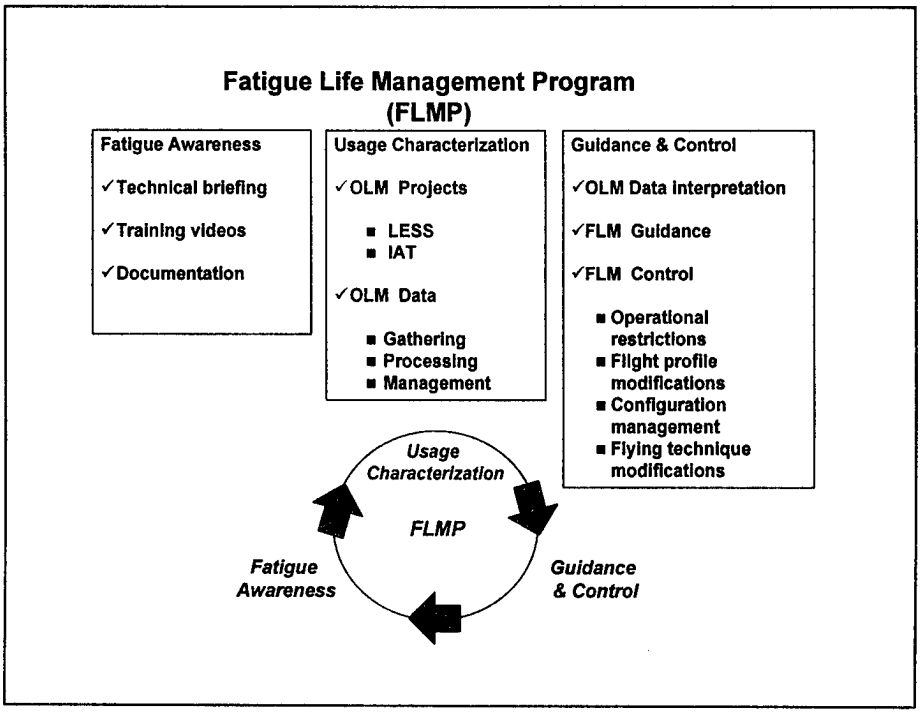

Figure 4 - Fatigue Life Management Program

Project Phases	*Decision document*	*Technical and Management Documents*
Identification	• Statement of Capability Deficiencies • Project Development Proposal • Project Charter	• Feasibility Studies • Cost/Benefits Analyses • Project Responsibility Matrix • Definition of Fleet Management Requirements
Concept Development	• Statement of Requirements	• Fleet Fatigue Management Data Specifications • CLM System Definition • CLM Project Performance Requirements • CLM Project Risk Analysis
Planning	• Project Implementation Plan	• Work Breakdown Structures (WBS) • WBS Dictionary • Master Schedule • Master Budget • CLM Equipment Prototype Functional Performance Specifications • CLM System - Base Level Data System Performance Specifications • CLM System - Data Analysis Centre Data System Performance Specifications • CLM System - Structural Tracking Database Functional Performance Specifications • CLM System - Training Requirements • Request for Proposals (RFP) that will includes Statement of Works (SOW) and the Functional Performance Specifications.
Implementation		• Project Progress Reports • Contracted DID/CDRLs
Divestment	• Project Transition Plan	• Transition Schedule & Tasks • CLM Process Maintainability & Reliability Assessment
Closure		• Project Final Report

Table 1 - Project Management Framework

Strategy	*Partial*	*Full*
Aim	Fatigue Tracking	Fatigue Tracking
Sample Size	• 10 A/C Minimum • 30 A/C Maximum	• 100 % fleet
Tracking Possibility	• Flight hours basis • Missions/role • Squadron/role	• Damage basis • Flight hours • Mission/role • Squadron /role
Risk	Medium to High	Low
Cost	Small to Medium	High

Table 2 - Fleet Fitment Strategies

SESSION VI

MECSIP

Chairman: *R. Berger*, ASC/ENFA

SIE

MECSIP ANALYSIS CASE HISTORIES
ISSUES RAISED AND BENEFICIAL DESIGN IMPACTS

presented at the

1995 USAF STRUCTURAL INTEGRITY PROGRAM CONFERENCE

San Antonio, Texas

November, 1995

Matthew Creager

Kirk Odian

STRUCTURAL INTEGRITY ENGINEERING
CHATSWORTH, CALIFORNIA

THE PURPOSE OF OUR PRESENTATION IS TO HIGHLIGHT SOME OF THE LESSONS LEARNED, ISSUES AND IMPACTS OF MECSIP

- **THE AIRCRAFT INDUSTRY HAS ALMOST FIFTY YEARS EXPERIENCE IN DURABILITY/FATIGUE ANALYSIS OF AIRFRAME STRUCTURES**
- **WE ALSO HAVE OVER TWENTY-FIVE YEARS OF EXPERIENCE IN DAMAGE TOLERANCE ANALYSIS OF AIRFRAME STRUCTURES**
- **MECSIP IS A RELATIVELY NEW REQUIREMENT**
  - MUCH OF OUR PREVIOUS EXPERIENCE IN INTEGRITY PROGRAMS IS RELEVANT
  - HOWEVER, ISSUES NOT CONFRONTED IN AIRFRAME STRUCTURAL INTEGRITY HAVE ARISEN

SIE

THE PRESENTATION WILL REFLECT THE RESULTS OF MECSIP ANALYSIS OF FIFTEEN COMPONENTS ANALYZED OVER THE PAST FIVE YEARS

- **FIVE DIFFERENT SENSORS (FOUR TEMPERATURE, ONE SPEED)**
  - PRIMARY STRUCTURAL DESIGN CONSTRAINT

    MOUNTING SYSTEM

    DRIVEN BY LOCATION AND MAINTAINABILITY
  - PRIMARY LOADS

    VIBRATION

SIE

COMPONENTS ANALYZED (CONTINUED)

- **ONE ELECTRICAL GENERATOR**
  - PRIMARY STRUCTURAL DESIGN CONSTRAINT

    STRUCTURE IS ROBUST DUE TO HEAT SINK REQUIREMENTS, HOWEVER ATTACHING COMPONENTS CAN IMPART HIGH LOADS
  - PRIMARY LOADS

    VIBRATION AND THERMAL
- **THREE ACTUATORS**
  - PRIMARY STRUCTURAL DESIGN CONSTRAINT

    WEIGHT AND ENVELOPE
  - PRIMARY LOADS

    FUNCTIONAL PRESSURE LOADS AND VIBRATION

COMPONENTS ANALYZED (CONTINUED)

- **FIVE MOUNTING BRACKETS/BEARINGS**
  - PRIMARY STRUCTURAL DESIGN CONSTRAINT

    WEIGHT
  - PRIMARY LOADS

    OPERATIONAL LOADS
- **ONE FUEL VALVE**
  - PRIMARY DESIGN CONSTANT

    MOUNTING SYSTEM/MATERIALS
  - PRIMARY LOADS

    VIBRATION

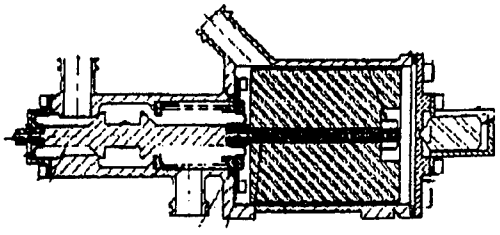

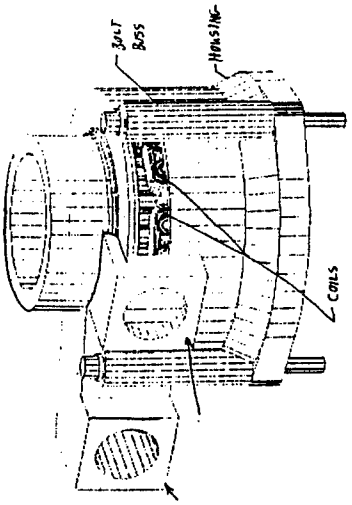
BOLT BOSS
HOUSING
COILS

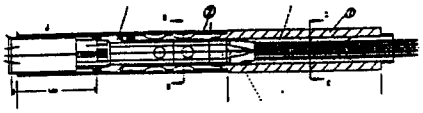

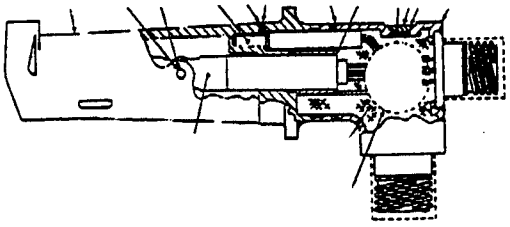

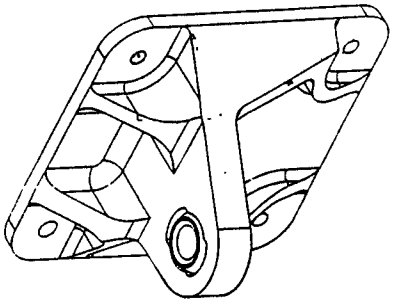

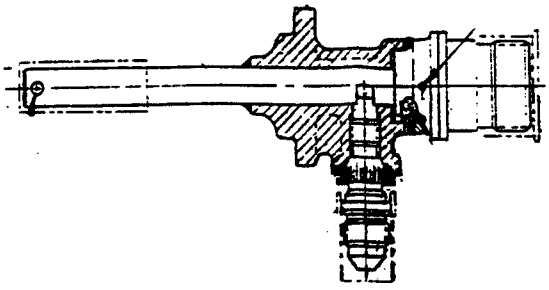

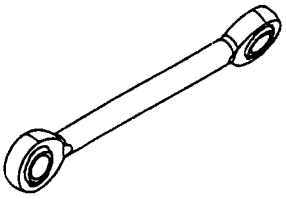

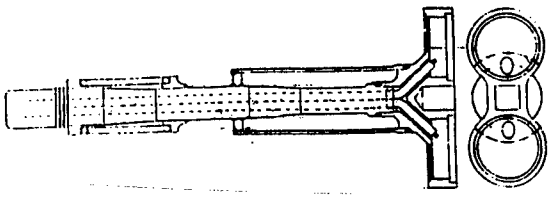

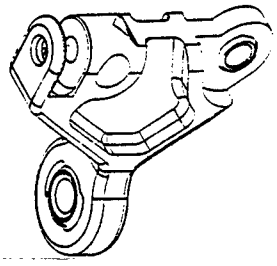

VIBRATION LOADS ARE A DISTINCTLY MORE IMPORTANT ELEMENT OF MECSIP ANALYSIS THAN AIRFRAME INTEGRITY ANALYSIS

- **THIS REQUIRES SOME NEW AND UNIQUE ISSUES TO BE ADDRESSED**
- **THESE ISSUES INVOLVE BOTH ANALYSIS AND TESTING**
- **MANY OF THESE ISSUES ARE RELATED TO THE HIGH FREQUENCIES INVOLVED**
  - 100 TO 10,000 HZ
  - AFFECTS THE DOMAIN OF RELEVANT MATERIAL PROPERTIES
  - AFFECTS TEST CONSTRAINTS AND TEST TIMES

THERE ARE TWO WAYS THAT THE ANALYTIC VIBRATION ENVIRONMENT IS BEING SPECIFIED:

- **g LEVEL VERSUS FREQUENCY**

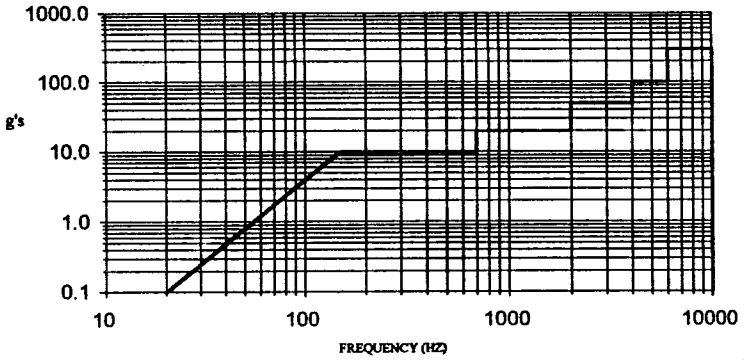

- POWER SPECTRAL DENSITY (PSD)

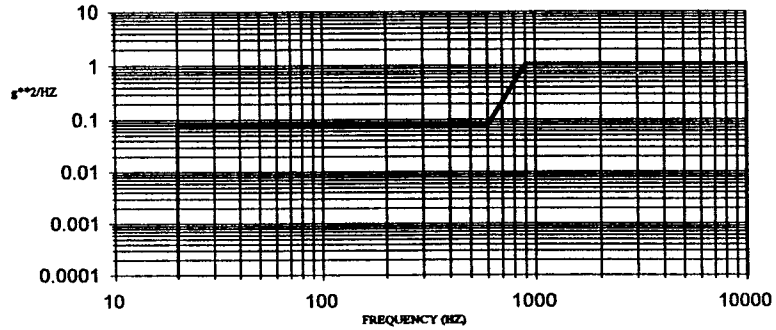

SIE

g LEVEL VERSUS FREQUENCY VIBRATION ENVIRONMENT

- **USING THIS ALONE, LOADING SPECTRA CANNOT BE DEVELOPED**
  - ADDITIONAL INFORMATION THAT GIVES TIME SPENT AT EACH FREQUENCY WOULD BE REQUIRED (e.g., PSDs) IN ORDER TO GENERATE SPECTRA
- **CONSEQUENCE - ACCEPTABILITY IS DETERMINED FOR:**
  - DURABILITY BY
    - COMPARING THE MAXIMUM VIBRATIONAL STRESS TO THE FATIGUE "ENDURANCE" LIMIT
  - DAMAGE TOLERANCE BY
    - COMPARING THE MAXIMUM CYCLIC STRESS INTENSITY FACTOR TO THE CRACK GROWTH RATE THRESHOLD

SIE

STRUCTURAL INTEGRITY ANALYSIS USING A g VERSUS FREQUENCY VIBRATION ENVIRONMENT

- **GENERATE A STRUCTURAL MODEL (usually FEM)**
- **PERFORM A MODAL ANALYSIS → $f_1, f_2, ...f_n$ AND MODE SHAPES**
- **ASSUME A DAMPING COEFFICIENT**
- **FOR EACH MODE USE A SINUSOIDAL INPUT TO GENERATE A STRESS RESPONSE AT CRITICAL LOCATIONS**
- **USE K_t AND STRESS INTENSITY EQUATIONS TO COMPARE ANALYSIS RESULTS TO " ENDURANCE LIMITS" AND CRACK GROWTH RATE THRESHOLDS**

PSD VIBRATION ENVIRONMENT

- **ALLOWS THE DETERMINATION OF A LOADING SPECTRUM**
- **USUALLY THE REASONABLE ASSUMPTION OF A "NARROW BAND" RESPONSE IS USED**
  - SPECTRUM CAN THEN BE SIMPLY DEFINED IN TERMS OF A RAYLEIGH DISTRIBUTION

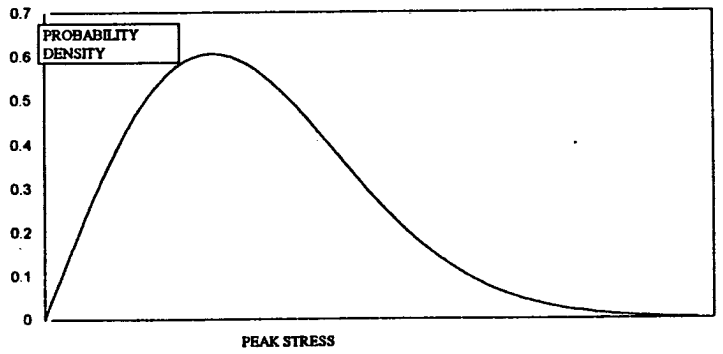

SIE

PSD VIBRATION ENVIRONMENT (continued)

- **DUE TO HIGH RESPONSE FREQUENCIES, BILLIONS OF POTENTIALLY DAMAGING CYCLES OCCUR**
  - THERE IS EVIDENCE THAT FOR RANDOM LOADING (AS OPPOSED TO CONSTANT AMPLITUDE LOADING) THERE IS NO "ENDURANCE LIMIT"
    - REQUIRES EXTRAPOLATION OF S-N DATA
      - •CURRENT APPROACH IS STRAIGHT LINE EXTRAPOLATION IN LOG-LOG SPACE
- **SHOULD ANALYTIC SPECTRUM BE TRUNCATED?**
  - WHERE? - 3 SIGMA?, 5 SIGMA?, 7 SIGMA?, etc.?
  - IN MANY CASES SIGNIFICANT AMOUNTS OF DAMAGE ARE OCCURRING BEYOND 5 SIGMA STRESSES.

SIE

STRUCTURAL INTEGRITY ANALYSIS USING A PSD VIBRATION ENVIRONMENT

- **GENERATE A STRUCTURAL MODEL**
- **PERFORM MODAL ANALYSIS → TRANSFER FUNCTION**
- **ASSUME A DAMPING COEFFICIENT**
- **USE INPUT g PSD to GENERATE AN OUTPUT STRESS PSD AT CRITICAL LOCATIONS**
- **GET STRESS RMS AND DOMINANT FREQUENCY FROM EACH STRESS PSD**
- **GENERATE RAYLEIGH DISTRIBUTION SPECTRA**
- **USE K_t, STRESS INTENSITY FACTOR EQUATIONS, S-N CURVES and da/dN vs ΔK to CALCULATE FATIGUE LIVES AND CRACK GROWTH LIVES.**

CRACK GROWTH ANALYSIS UNDER RANDOM LOADING

$$K = S \bullet Y(a)$$

$$da/dN = da/dN(K)$$

$$K_{rms} = S_{rms} \bullet Y(a)$$

Rayleigh Distribution - $f(S/S_{rms}) = f(\alpha)$

Average Crack Growth Per Cycle = $\overline{da}/dN\ (K_{rms})$

$$\overline{da}/dN\ (K_{rms}) = \int_{0}^{\infty} f(\alpha) \bullet da/dN\ (\alpha K_{rms}) \bullet d\alpha$$

$$N = freq \bullet \Delta t = \int_{a_i}^{a_f} da/\ [\overline{da}/dN(S_{rms} \bullet Y(a))]$$

BASIC CRACK GROWTH RATE
A356-T6 ALUMINUM

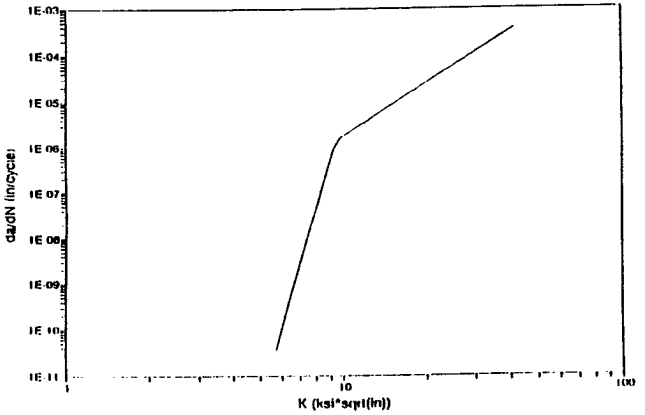

RAYLEIGH DISTRIBUTION CRACK GROWTH RATE
A356-T6 ALUMINUM CASTING

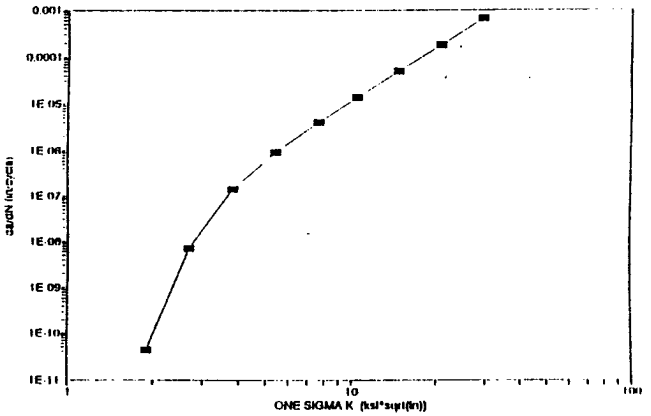

DAMAGE ACCUMULATION AT KRMS=1.4

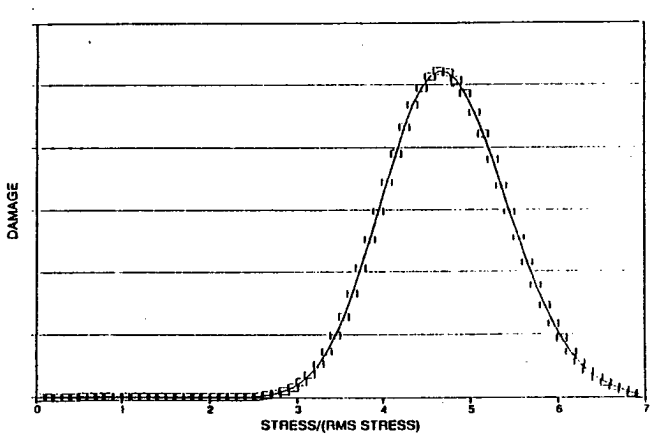

THERE ARE SIGNIFICANT DIFFERENCES IN D/DT ANALYSIS USING g VERSUS FREQUENCY AND PSD VIBRATION ENVIRONMENTS

	MATERIAL	LOAD ENVIRONMENT
g VERSUS FREQUENCY	S-N ENDURANCE LIMIT (non-conservative?) ΔK_{th}	INFINITE NUMBER OF CYCLES AT ALL FREQUENCIES (conservative)
PSD	STRAIGHT LINE EXTRAPOLATION OF LOG S-LOG N (conservative) ΔK_{th} or Bi-slope or Paris ?	INCLUDES ALL LOADS OUT TO 7 SIGMA (conservative?)

SIE

FOR SOME MATERIALS USED THERE IS EXTREMELY LITTLE OR NO FATIGUE OR CRACK GROWTH RATE DATA

- **THIS IS PARTICULARLY TRUE FOR:**
  - NON-STRUCTURAL MATERIALS (e.g., PLATINUM ALLOYS)
  - UNIQUE HARDWARE (e.g., FLEXIBLE METAL BELLOWS)
- **A RIGID REQUIREMENT ON A STATISTICALLY DESCRIBED "ENDURANCE LIMIT" OR S-N CURVE IS NOT REALISTIC.**
  - THE RESULT IS THE USE OF AN ESTIMATE OF AN EXTREMELY UNLIKELY LOWER BOUND
- **SIMILARLY, ESTIMATES ON THE LOWER BOUND OF DELTA K THRESHOLD AND UPPER BOUNDS ON CRACK GROWTH RATES MUST BE USED FOR SOME MATERIALS**

SIE

MAINTAINABILITY AND SPACE REQUIREMENTS ARE SIGNIFICANT CONSTRAINTS NOT NORMALLY ENCOUNTERED IN AIRFRAME STRUCTURAL INTEGRITY

FOR EXAMPLE IN ONE SENSOR

- **CAPTIVE BOLTS WERE CONSIDERED HIGHLY DESIRABLE FROM A MAINTAINABILITY PERSPECTIVE**
- **THREE BOLT MOUNT WOULD BE STRUCTURALLY SUPERIOR TO A TWO BOLT MOUNT**
  - PRECLUDED BY SPACE CONSTRAINTS AND THE MAINTAINABILITY REQUIREMENT OF HAVING "TWIST-IN TWIST-OUT" MOUNTING SYSTEM

IT WAS COMMON FOR THE INITIAL D/DT ANALYSIS TO SHOW NEGATIVE MARGINS

- **SOME WERE ELIMINATED BY GENERATING MORE REALISTIC MATERIAL PROPERTIES**
  - BE-COPPER
  - PLATINUM ALLOY
- **SOME WERE ELIMINATED BY RUNNING TESTS TO ESTABLISH LESS CONSERVATIVE DAMPING ESTIMATES**
- **MINOR REDESIGN ELIMINATED OTHERS**
- **ONE REQUIRED A SIGNIFICANT DESIGN CHANGE**

DESIGN CHANGES AS A RESULT OF STRUCTURAL INTEGRITY ANALYSIS

COMPONENT	DESIGN CHANGES	SUBJECTIVE ESTIMATE OF IMPACT
SPEED SENSOR	a) RECONFIGURED WELD b) CHANGED THICKNESS AND GEOMETRY OF MOUNT	MINOR
TWO TEMPERATURE SENSORS	a) INCREASED WELD DIMENSIONS b) STIFFENED THERMOCOUPLES c) INCREASED VARIOUS RADII	MODERATE
TEMPERATURE SENSOR	a) RESIZED SEAL GROOVE b) INCREASED WELD DIMENSIONS c) OPTIMIZED SECTION FOR WEIGHT SAVINGS	MODERATE
TEMPERATURE SENSOR	a) INCREASED RADII b) INCREASED WALL THICKNESS c) MOVED DRAIN HOLES d) CHANGED SUPPORT OF INTERNAL ELEMENTS e) ADDED VIBRATION ISOLATOR	IMPORTANT
GENERATOR	a) INCREASED WALL THICKNESS b) INCREASED RADII	MODERATE
MOUNTING BRACKET/BEARING	a) RESIZED LUG GEOMETRY	IMPORTANT
FUEL VALVE	a) RESIZED MOUNTS b) INCREASED WALL THICKNESS c) INCREASED RADII d) MATERIAL CHANGE (CTE)	IMPORTANT
ACTUATOR	a) MATERIAL CHANGE b) RESIZED FITTING	MODERATE

SIE

IT IS NOT SURPRISING THAT ITEMS THAT HAVE ALWAYS BEEN DESIGNED AS STRUCTURAL COMPONENTS WILL BE IMPACTED LEAST BY A MECSIP REVIEW

- **FOUR MOUNTING BRACKETS/BEARINGS AND TWO ACTUATORS WERE UNCHANGED**
- **HOWEVER, SOME CHANGES WERE REQUIRED IN A FEW "STRUCTURAL" MECSIP COMPONENTS**
  - SOME DETAILS WERE MISSED IN THE ORIGINAL DESIGN
  - MECSIP SUPPLIED AN IMPORTANT SECOND LOOK AT THESE COMPONENTS

MECSIP ANALYSIS HAD A SIGNIFICANT AND IMPORTANT IMPACT ON "NON-STRUCTURAL" COMPONENTS.

A DAMAGE TOLERANCE ANALYSIS

of a

LANDING GEAR

by

T.A. Wolff
M.P. Kaplan
T.Willis

Willis & Kaplan, Inc.

Background: ***The life of the landing gear of a CASA 212 aircraft was determined using safe-life procedures. The operator of a fleet of aircraft was approaching the life limit of the landing gear.***

Objective: ***To assess the applicability of fracture mechanics methodology on the landing gear of a CASA 212 aircraft.***

Purpose: ***To determine inspection intervals and techniques that would allow the operator to continue to use the landing gear past the safe life limits prescribed by the manufacturer.***

PROGRAM PLAN:

I DETERMINE LOADINGS

II IDENTIFY COMPONENTS

A. GEOMETRY

B. CRITICALITY

III PERFORM LOADS ANALYSIS

IV PERFORM STRESS ANALYSIS

A. CLOSED FORM SOLUTIONS

B. FINITE ELEMENT ANALYSIS

V SPECTRUM DEVELOPMENT

A. OCCURRENCES & LOADINGS

B. STRESS TIME HISTORY

VI MATERIAL PROPERTIES

VII CRACK GROWTH ANALYSIS

VIII RESULTS & CONCLUSIONS

IX MAINTENANCE PLAN

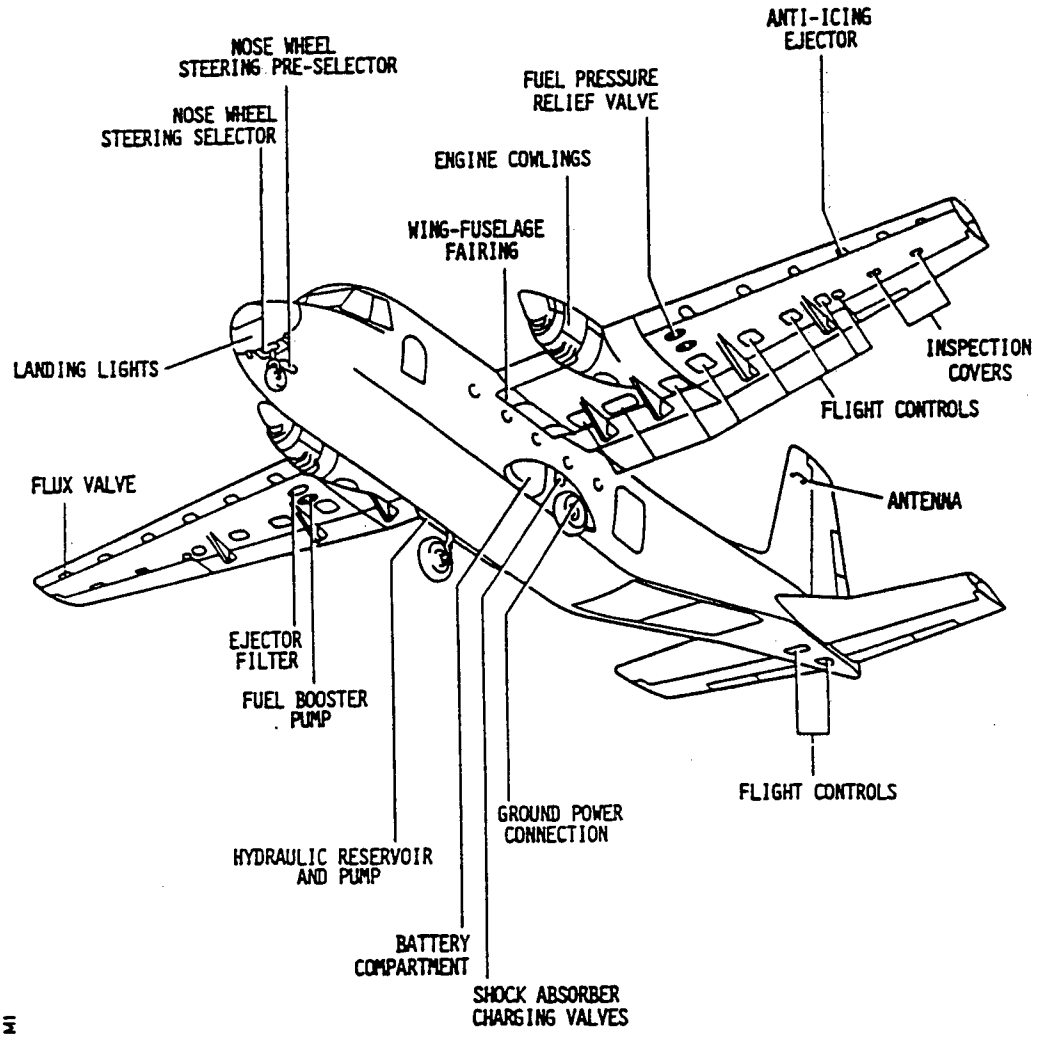

Fig. 2 Access and Inspection Panels

R

J. MAXIMUM DESIGN LANDING WEIGHT (MLW):

The maximum design landing weight is the maximum weight for landing as limited by aircraft strength and airworthiness requirements.

K. OPERATIONAL LANDING WEIGHT (OLW)

The operational landing weight of an aircraft is the maximum authorized weight for landing. It is subject to airport, operational and related restrictions. It must not exceed maximum design landing weight.

L. TARE

The tare is the weight of items such as: parking block, chocks, jacks, etc. necessary for weighing and which are not include in the weight aircraft.

1 Kg = 2.2046 lb

8.- MAXIMUM DESIGN WEIGHT

	lbs	Kgs
Maximum taxi weight	16534.5	7500 kg
Maximum take-off weight	16424.3	7450 kg
Maximum landing weight	16203.7	7350 kg
Maximum zero fuel weight	15552.4	7050 kg
Maximum fuel capacity (1991 liters)	3527.4	1600 kg
Basic empty weight	9071.9	4115 kg

Design Ramp Weight = Max. wt. for ground handling cond.s (Ramp conditions) = 16534.5 ( )

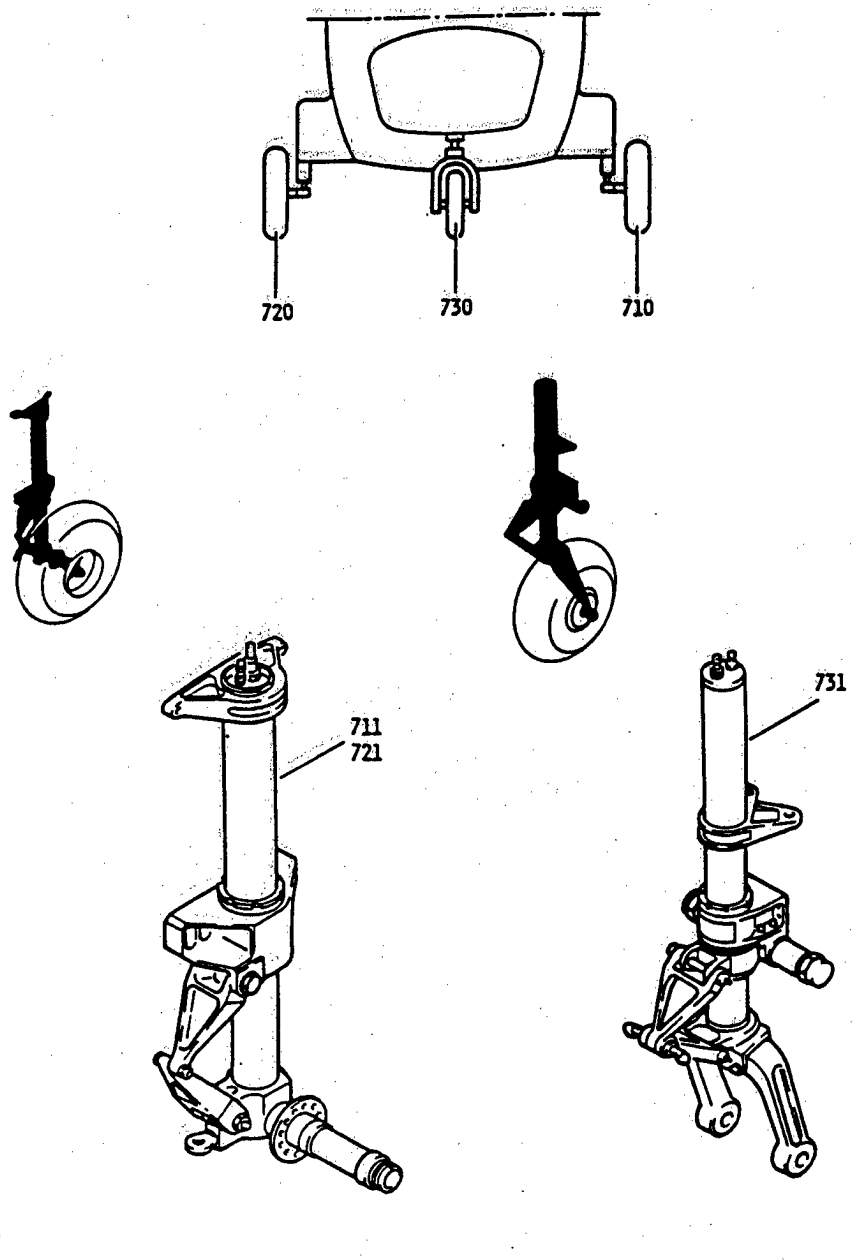

Fig. 7 Aircraft Zoning - 700 Area Breakdown

R

Effectivity: All

WKI PART NOS.

CONSTRUCCIONES AERONAUTICAS S A

C-212 AVIOCAR SERIES 200

ILLUSTRATED PARTS CATALOG

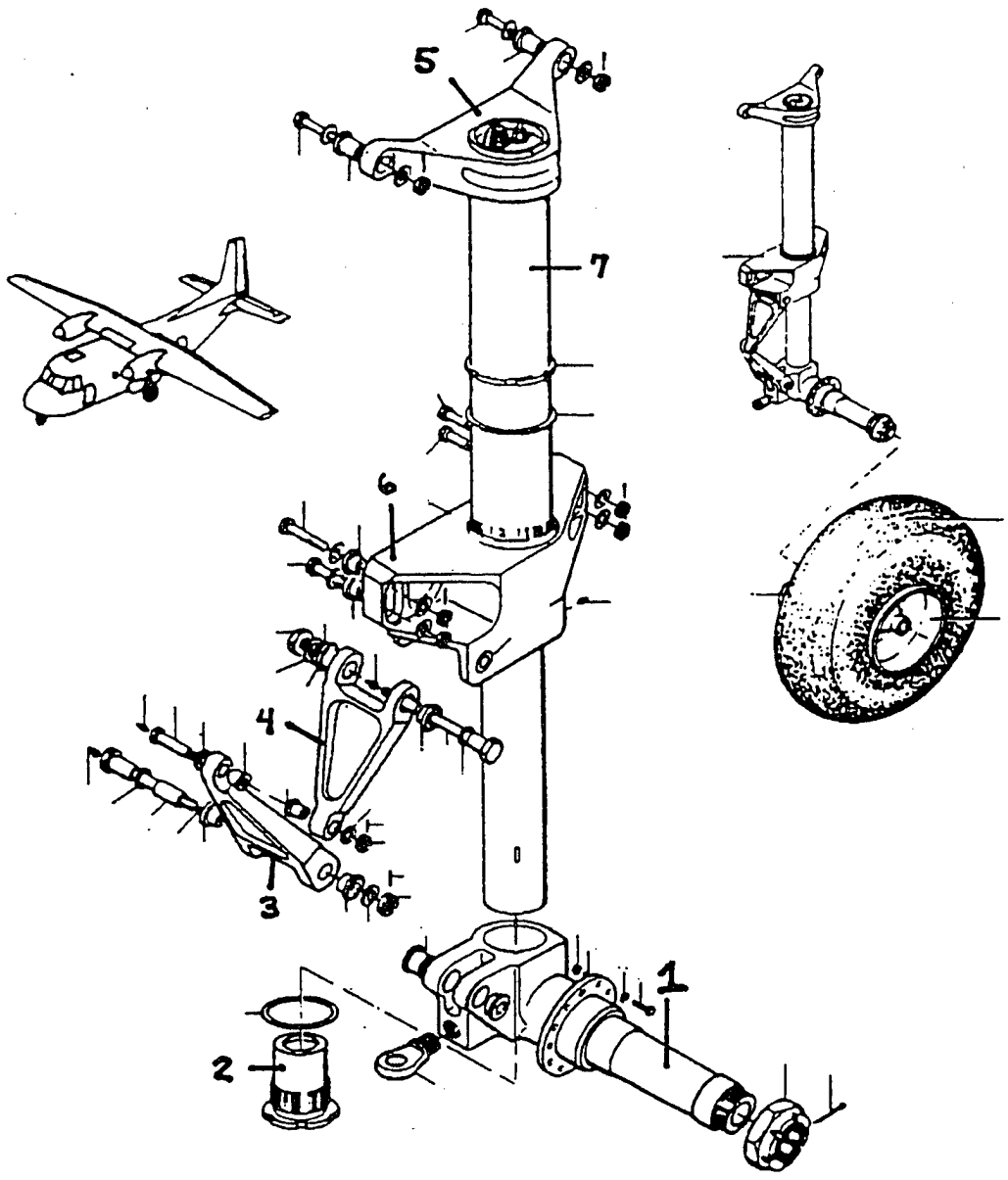

Main Landing Gear
Figure 1

32-10-00
Fig. 1

Page 0
Jan. 3/83

WKI PART NOS.

CONSTRUCCIONES AERONAUTICAS S A

C-212 :VIOCAR SERIES 200

ILLUSTRATED PARTS CATALOG

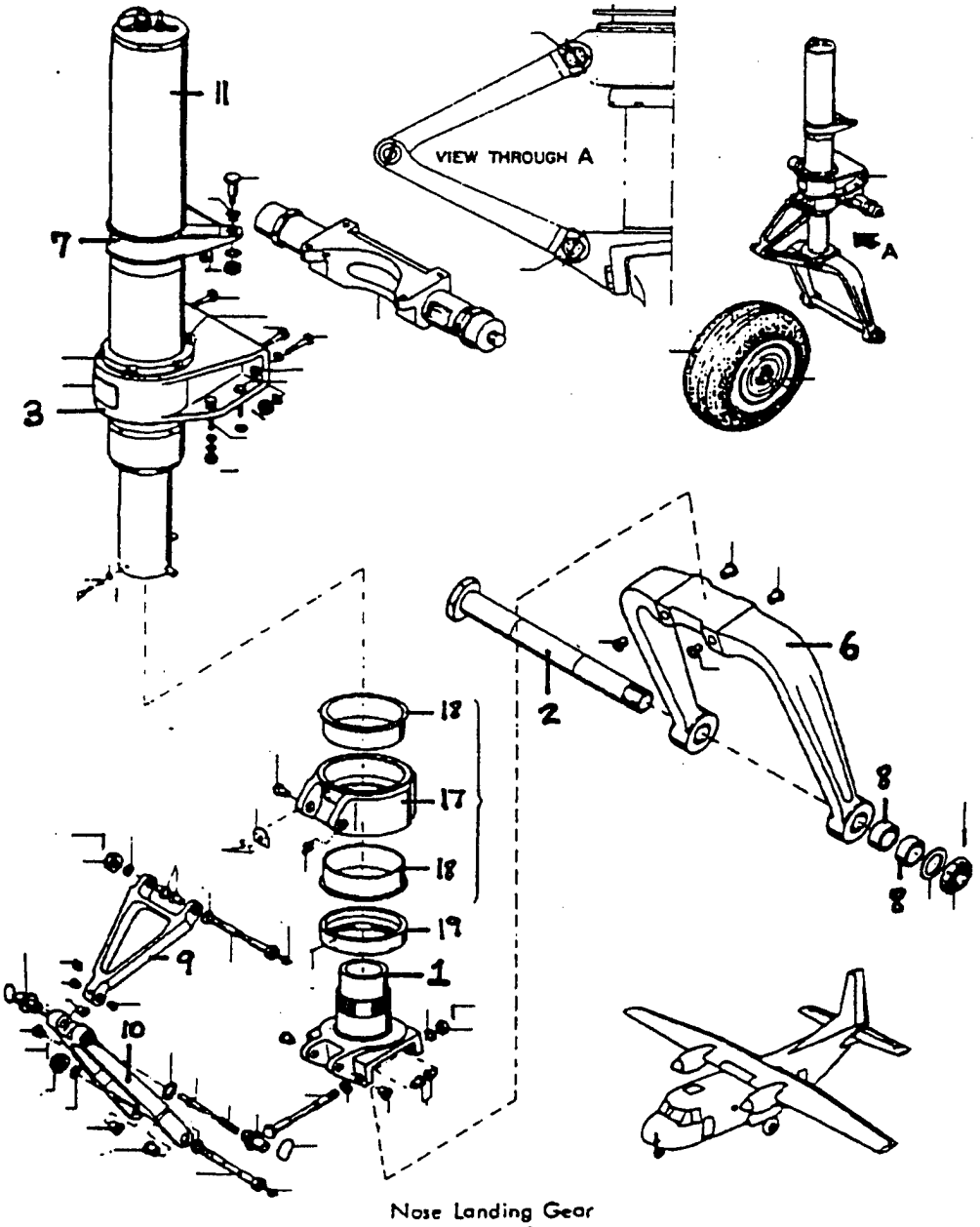

Nose Landing Gear
Figure 1

32-20-00
Fig. 1

Page 0
Sep. 12/84

the surfaces and supporting structure must be designed for the combined vertical and horizontal surface loads resulting from each prescribed flight load condition considered separately.

(Amdt. 25–23, Eff. 5/8/70)

§ 25.445 Outboard fins.

(a) If outboard fins are on the horizontal tail surface, the tail surfaces must be designed for the maximum horizontal surface load in combination with the corresponding loads induced on the vertical surfaces by endplate effects. These induced effects need not be combined with other vertical surface loads.

(b) To provide for unsymmetrical loading when outboard fins extend above and below the horizontal surface, the critical vertical surface loading (load per unit area) determined under § 25.391 must also be applied as follows:

(1) 100 percent to the area of the vertical surfaces above (or below) the horizontal surface.

(2) 80 percent to the area below (or above) the horizontal surface.

§ 25.457 Wing flaps.

Wing flaps, their operating mechanisms, and their supporting structures must be designed for critical loads occurring in the conditions prescribed in § 25.345, accounting for the loads occurring during transition from one flap position and airspeed to another.

§ 25.459 Special devices.

The loading for special devices using aerodynamic surfaces (such as slots, slats, and spoilers) must be determined from test data.

(Amdt. 25–72, Eff. 8/20/90)

GROUND LOADS

§ 25.471 General.

(a) *Loads and equilibrium.* For limit ground loads—

(1) Limit ground loads obtained under this subpart are considered to be external forces applied to the airplane structure; and

(2) In each specified ground load condition, the external loads must be placed in equilibrium with the linear and angular inertia loads in a rational or conservative manner.

(b) *Critical centers of gravity.* The critical centers of gravity within the range for which certification is requested must be selected so that the maximum design loads are obtained in each landing gear element. Fore and aft, vertical, and lateral airplane centers of gravity must be considered. Lateral displacements of the c.g. from the airplane centerline which would result in main gear loads not greater than 103 percent of the critical design load for symmetrical loading conditions may be selected without considering the effects of these lateral c.g. displacements on the loading of the main gear elements, or on the airplane structure provided—

(1) The lateral displacement of the c.g. results from random passenger or cargo disposition within the fuselage or from random unsymmetrical fuel loading or fuel usage; and

(2) Appropriate loading instructions for random disposable loads are included under the provisions of § 25.1583(c)(1) to ensure that the lateral displacement of the center of gravity is maintained within these limits.

(c) *Landing gear dimension data.* Figure 1 of the appendix A contains the basic landing gear dimension data.

(Amdt. 25–23, Eff. 5/8/70)

§ 25.473 Ground load conditions and assumptions.

(a) For the landing conditions specified in §§ 25.479 through 25.485, the following apply:

(1) The selected limit vertical inertia load factors at the center of gravity of the airplane may not be less than the values that would be obtained—

(i) In the attitude and subject to the drag loads associated with the particular landing condition;

(ii) With a limit descent velocity of 10 f.p.s. at the design landing weight (the maximum weight for landing conditions at the maximum descent velocity); and

(iii) With a limit descent velocity of 6 f.p.s. at the design takeoff weight (the maximum weight for landing conditions at a reduced descent velocity).

(2) Airplane lift, not exceeding the airplane weight, may be assumed to exist throughout the landing impact and to act through the center of gravity of the airplane.

(b) The prescribed descent velocities may be modified if it is shown that the airplane has design features that make it impossible to develop these velocities.

(2) Up and aft through the axle at 45 degrees to the ground line.

(c) For the tail-down landing condition for airplanes with nose wheels, the airplane is assumed to be at an attitude corresponding to either the stalling angle of the maximum angle allowing clearance with the ground by each part of the airplane other than the main wheels, in accordance with figure 3 of appendix A, whichever is less.

§ 25.483 One-wheel landing conditions.

For the one-wheel landing condition, the airplane is assumed to be in the level attitude and to contact the ground on one side of the main landing gear, in accordance with figure 4 of appendix A. In this attitude—

(a) The ground reactions must be the same as those obtained on that side under § 25.479(c)(2); and

(b) Each unbalanced external load must be reacted by airplane inertia in a rational or conservative manner.

§ 25.485 Side load conditions.

(a) For the side load condition, the airplane is assumed to be in the level attitude with only the main wheels contacting the ground, in accordance with figure 5 of appendix A.

(b) Side loads of 0.8 of the vertical reaction (on one side) acting inward and 0.6 of the vertical reaction (on the other side) acting outward must be combined with one-half of the maximum vertical ground reactions obtained in the level landing conditions. These loads are assumed to be applied at the ground contact point and to be resisted by the inertia of the airplane. The drag loads may be assumed to be zero.

§ 25.487 Rebound landing condition.

(a) The landing gear and its supporting structure must be investigated for the loads occurring during rebound of the airplane from the landing surface.

(b) With the landing gear fully extended and not in contact with the ground, a load factor of 20.0 must act on the unsprung weights of the landing gear. This load factor must act in the direction of motion of the unsprung weights as they reach their limiting positions in extending with relation to the sprung parts of the landing gear.

§ 25.489 Ground handling conditions.

Unless otherwise prescribed, the landing gear and the airplane structure must be investigated for the conditions in §§ 25.491 through 25.509 with the airplane at the design ramp weight (the maximum weight for ground handling conditions). No wing lift may be considered. The shock absorbers and tires may be assumed to be in their static position.

(Amdt. 25–23, Eff. 5/8/70)

§ 25.491 Takeoff run.

The landing gear and the airplane structure are assumed to be subjected to loads not less than those obtained under conditions described in § 25.235.

§ 25.493 Braked roll conditions.

(a) An airplane with a tail wheel is assumed to be in the level attitude with the load on the main wheels, in accordance with figure 6 of appendix A. The limit vertical load factor is 1.2 at the design landing weight, and 1.0 at the design ramp weight. A drag reaction equal to the vertical reaction multiplied by a coefficient of friction of 0.8, must be combined with the vertical ground reaction and applied at the ground contact point.

(b) For an airplane with a nose wheel, the limit vertical load factor is 1.2 at the design landing weight, and 1.0 at the design ramp weight. A drag reaction equal to the vertical reaction, multiplied by a coefficient of friction of 0.8, must be combined with the vertical reaction and applied at the ground contact point of each wheel with brakes. The following two attitudes, in accordance with figure 6 of appendix A, must be considered:

(1) The level attitude with the wheels contacting the ground and the loads distributed between the main and nose gear. Zero pitching acceleration is assumed.

(2) The level attitude with only the main gear contacting the ground and with the pitching moment resisted by angular acceleration.

(c) A drag reaction lower than that prescribed in paragraphs (a) and (b) of this section may be used if it is substantiated that an effective drag force of 0.8 times the vertical reaction cannot be attained under any likely loading condition.

(Amdt. 25–23, Eff. 5/8/70)

§ 25.495 Turning.

In the static position, in accordance with figure 7 of appendix A, the airplane is assumed to execute a steady turn by nose gear steering, or by application of sufficient differential power, so that the limit load factors applied at the center of gravity are 1.0 vertically and 0.5 laterally. The side ground

Insert Figs. 6 & 7

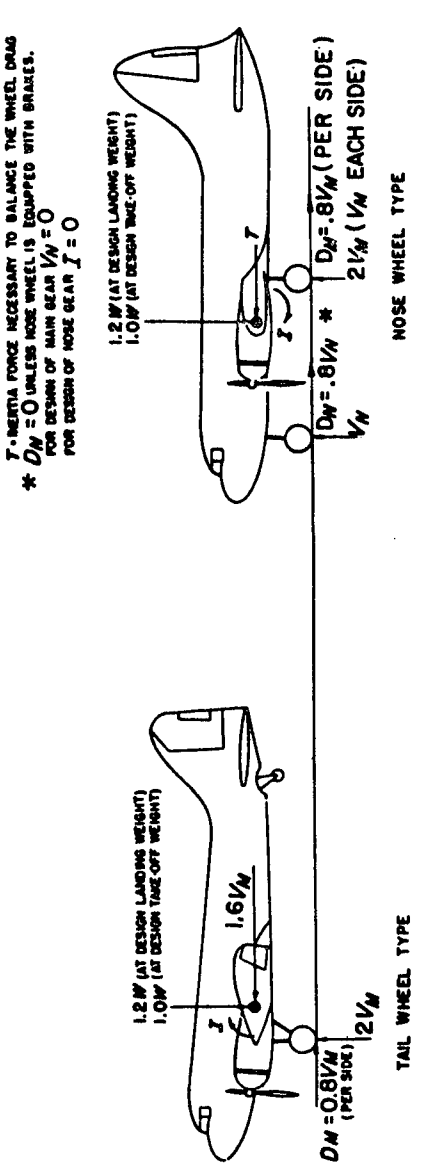

Figure 6—Braked roll.

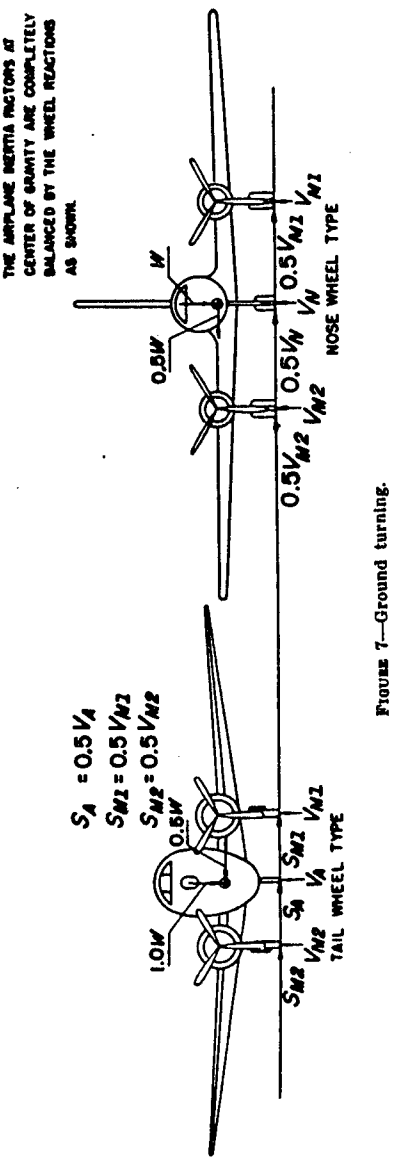

Figure 7—Ground turning.

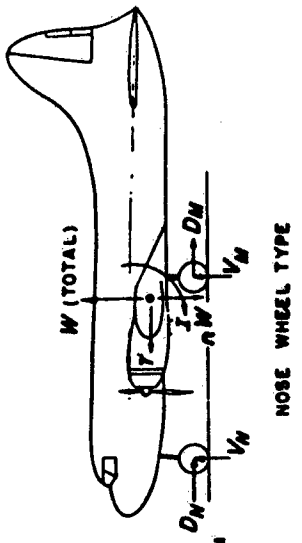

Figure 2—Level landing.

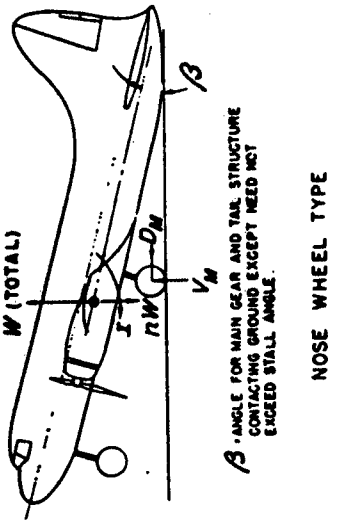

Figure 3—Tail-down landing.

$$HIC = \left\{ (t_2 - t_1) \left[\frac{1}{(t_2 - t_1)} \int_{t_1}^{t_2} a(t)dt \right]^{2.5} \right\}_{max}$$

where—

t_1 is the initial integration time,

t_2 is the final integration time, and

a(t) is the total acceleration vs. time curve for the head strike, and where

(t) is in seconds, and (a) is in units of gravity (g).

(6) Where leg injuries may result from contact with seats or other structure, protection must be provided to prevent axially compressive loads exceeding 2,250 pounds in each femur.

(7) The seat must remain attached at all points of attachment, although the structure may have yielded.

(8) Seats must not yield under the tests specified in paragraphs (b)(1) and (b)(2) of this section to the extent they would impede rapid evacuation of the airplane occupants.

(Amdt. 25–64, Eff. 6/16/88)

§25.563 Structural ditching provisions.

Structural strength considerations of ditching provisions must be in accordance with §25.801(e).

FATIGUE EVALUATION

§25.571 Damage-tolerance and fatigue evaluation of structure.

(a) *General.* An evaluation of the strength, detail design, and fabrication must show that catastrophic failure due to fatigue, corrosion, or accidental damage, will be avoided throughout the operational life of the airplane. This evaluation must be conducted in accordance with the provisions of paragraphs (b) and (e) of this section, except as specified in paragraph (c) of this section, for each part of the structure which could contribute to a catastrophic failure (such as wing, empennage, control surfaces and their systems, the fuselage, engine mounting, landing gear, and their related primary attachments). Advisory Circular AC No. 25.571–1 contains guidance information relating to the requirements of this section (copies of the Advisory Circular may be obtained from the U.S. Department of Transportation, Publications Section M–443.1, Washington, DC 20590). For turbojet powered airplanes, those parts which could contribute to a catastrophic failure must also be evaluated under paragraph (d) of this section. In addition, the following apply:

(1) Each evaluation required by this section must include—

(i) The typical loading spectra, temperatures, and humidities expected in service;

(ii) The identification of principal structural elements and detail design points, the failure of which could cause catastrophic failure of the airplane; and

(iii) An analysis, supported by test evidence, of the principal structural elements and detail design points identified in paragraph (a)(1)(ii) of this section.

(2) The service history of airplanes of similar structural design, taking due account of differences in operating conditions and procedures, may be used in the evaluations required by this section.

(3) Based on the evaluations required by this section, inspections or other procedures must be established as necessary to prevent catastrophic failure, and must be included in the Airworthiness Limitations section of the Instructions for Continued Airworthiness required by §25.1529.

(b) *Damage-tolerance evaluation.* The evaluation must include a determination of the probable locations and modes of damage due to fatigue, corrosion, or accidental damage. The determination must be the analysis supported by test evidence and (if available) service experience. Damage at multiple sites due to prior fatigue exposure must be included where the design is such that this type of damage can be expected to occur. The evaluation must incorporate repeated load and static analyses supported by test evidence. The extent of damage for residual strength evaluation at any time within the operational life must be consistent with the initial detectability and subsequent growth under repeated loads. The residual strength evaluation must show that the remaining structure is able to withstand loads (considered as static ultimate loads) corresponding to the following conditions:

(1) The limit symmetrical maneuvering conditions specified §25.337 at V_C and in §25.345.

(2) The limit gust condition specified in §§25.305(d), 25.341, and 25.351(b) at the specified speeds up to V_C, and in §25.345.

(3) The limit rolling conditions specified in §25.349 and the limit unsymmetrical conditions specified in §§25.367 and 25.427, at speeds up to V_C.

(4) The limit yaw maneuvering conditions specified in §25.351(a) at the specified speeds up to V_C.

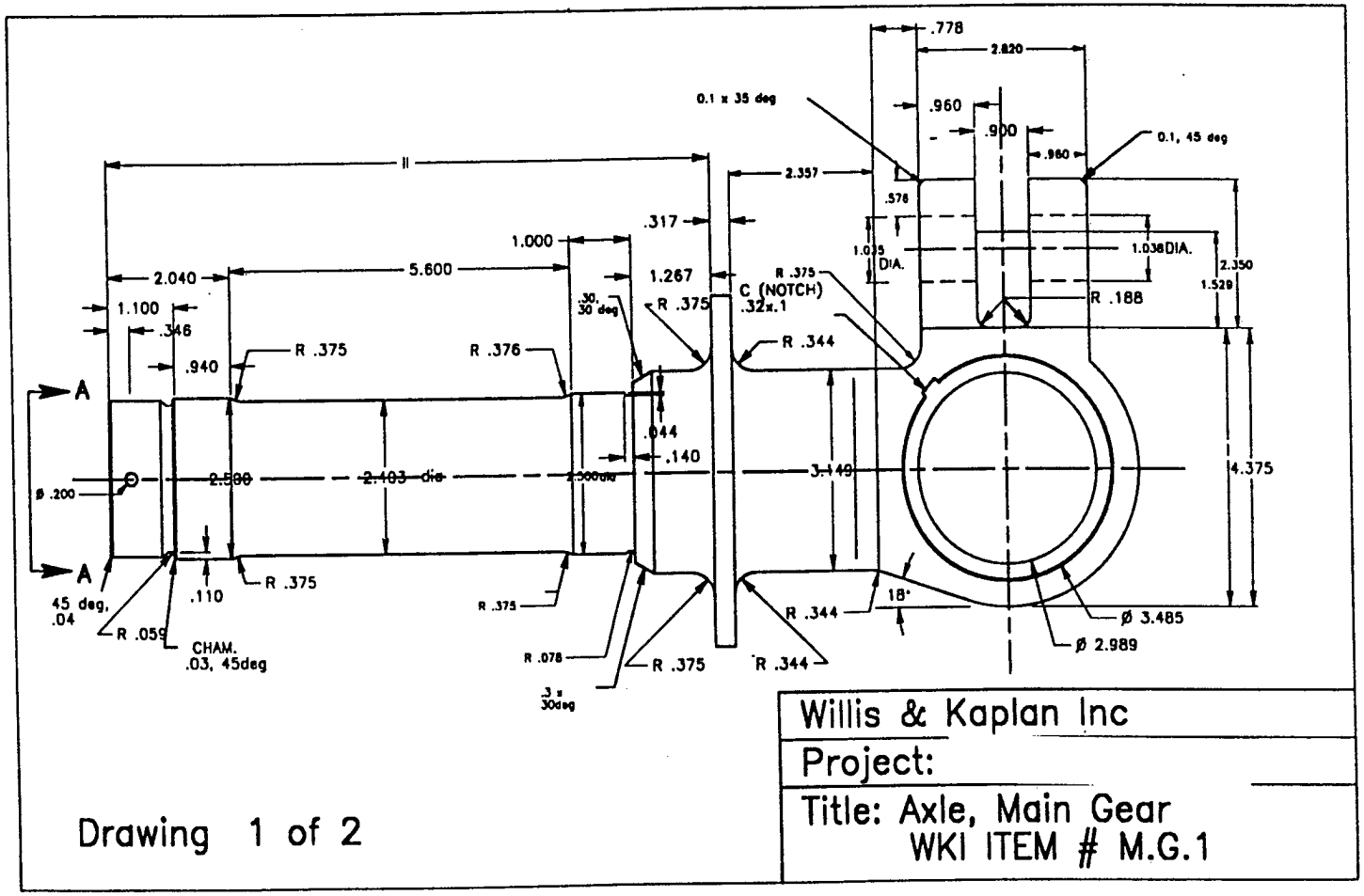
.778
2.820
0.1 x 35 deg
.960
.900
.960
0.1, 45 deg
ll
2.357
.576
.317
1.000
1.035 DIA.
1.038DIA.
2.350
1.529
2.040
5.600
1.267
R .375
C (NOTCH) .32x.1
R .188
1.100
.346
.940
R .375
R .376
R .344
A
.044
.140
ø .200
2.500
2.403 dia
3.149
4.375
A
45 deg, .04
.110
R .375
R .059
CHAM. .03, 45deg
R .375
R .078
3 x 30deg
R .375
R .344
18°
R .344
ø 3.485
ø 2.989
Willis & Kaplan Inc
Project:
Title: Axle, Main Gear
WKI ITEM # M.G.1
Drawing 1 of 2

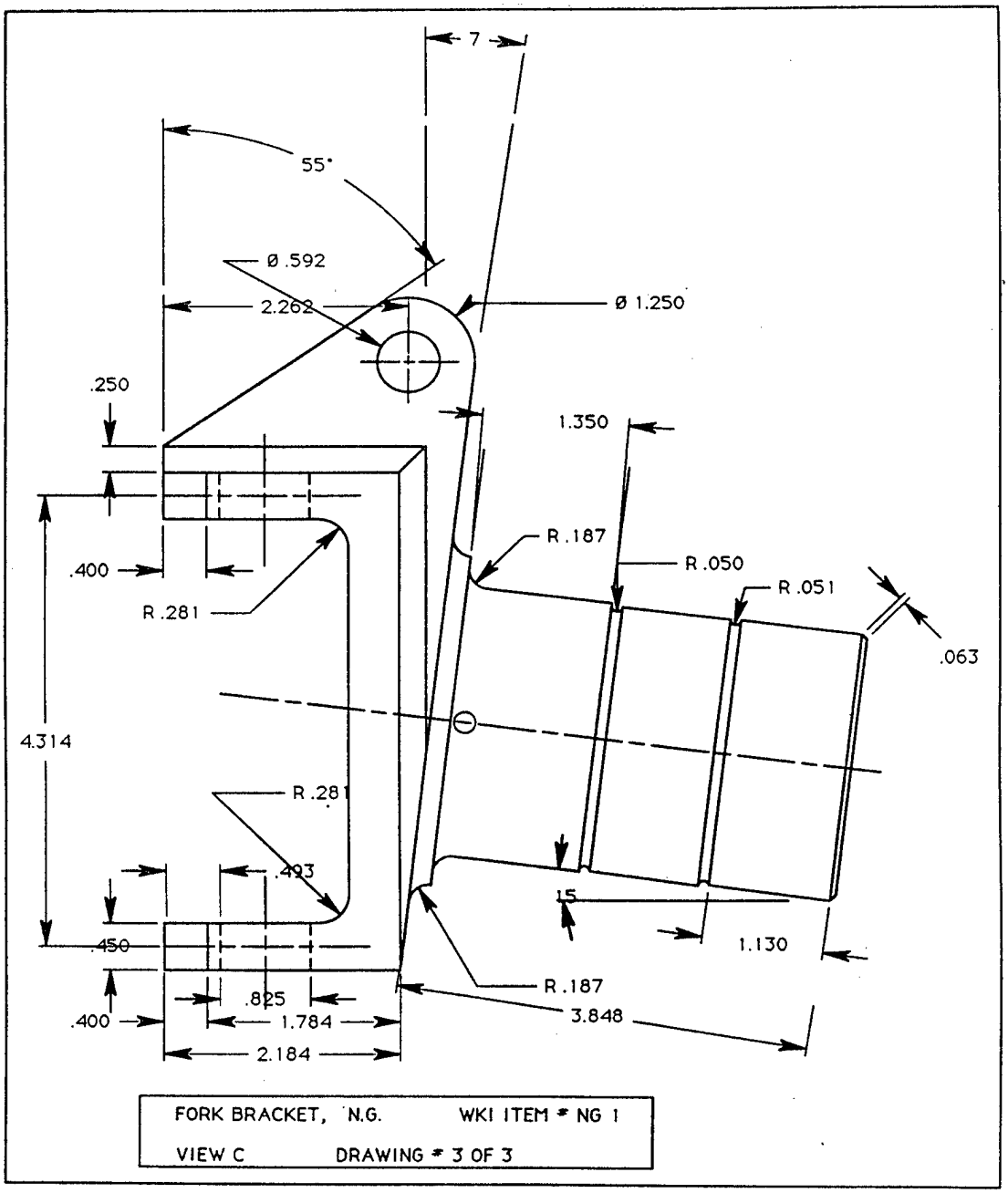
7
55°
Ø .592
2.262
Ø 1.250
.250
1.350
R .187
R .050
R .051
.063
.400
R .281
4.314
R .281
.493
.450
.825
.400
1.784
2.184
.15
1.130
R .187
3.848
FORK BRACKET, N.G. WKI ITEM # NG 1
VIEW C DRAWING # 3 OF 3

		---	LOADS ANALYSIS		4/7/95	
Parameters						
h=	C.G.Height from axle (ft) :			5.57		
h1 =	C.G. Height from Ground (ft)			6.88		
Af=	C.G. Dist. from front gear - fore (ft)			15.49		
Aa=	C.G. Dist from front gear - aft (ft)			16.57		
Bf=	C.G.Dist. from main gear - fore (ft)			2.40		
Ba=	C.G. Dist from main gear -aft (ft)			1.33		
WL=	Design Landing Weight (lbs)			16204.00		
Wr=	Design Ramp Weight (lbs)			16535.00		
Nz=	Vert load factor at C.G.			2.79		
T =	Track Width (ft)			17.90		
			Drag Forces :- +ve = aft			
Load Cases						
Case # 1	Level Landing,3 wheel,Max wheel spin-up, C.G.Fore;					
K=	0.8	W(n-1)=	29005.16			
l=	0	A-hk=	11.034			
		B+hK=	6.856			
	Vn+Vm=W(n-1)					
	(A-hk)Vn-(B+hK)Vm=0					
	Vn=	11115.6723				
	Vm=	17889.4877				
Vert load at nose=			11115.672			
Horiz load at nose (aft)			8892.5378			
Vert load at ech MLG			8944.7439			
Horiz load at each MLG (aft)			7155.7951			
Case # 2	Level Landing ,3wheel,Max wheel spin-up, C.G.Aft;					
K=	0.8	W(n-1)=	29005.16			
l=	0	A-hk=	12.114			
		B+hK=	5.786			
	Vn+Vm=W(n-1)					
	(A-hk)Vn-(B+hK)Vm=0					
	Vn=	9375.6344				
	Vm=	19629.5256				
Vert load at nose=			9375.6344			
Horiz load at nose (aft)			7500.5075			
Vert load at ech MLG			9814.7628			

Horiz load at each MLG (aft)			**7851.8102**			
Case ° 3	Level Landing ,3 wheel, max wheel vert load, c.g fore					
k=	0.25					
l=	0					
		W(n-1)=	29005.16			
		A-hk=	14.0975			
		B+hK=	2.4			
	Vn+Vm=W(n-1)					
	(A-hk)Vn-(B+hK)Vm=0					
	Vn=	4219.57169				
	Vm=	24785.5883				
Vert load at nose=			**4219.5717**			
Horiz load at nose (aft)			**1054.8929**			
Vert load at ech MLG			**12392.794**			
Horiz load at each MLG (aft)			**3098.1985**			
Case # 4	Level Landing,3wheel,Max wheel load, C.G.Aft;					
K=	0.25	W(n-1)=	29005.16			
l=	0	A-hk=	15.1775			
		B+hK=	2.7225			
	Vn+Vm=W(n-1)					
	(A-hk)Vn-(B+hK)Vm=0					
	Vn=	4411..539				
	Vm=	24593.621				
Vert load at nose=			**4411.539**			
Horiz load at nose (aft)			**1102.8848**			
Vert load at ech MLG			**12296.811**			
Horiz load at each MLG (aft)			**3074.2026**			
Case # 5	Level Landing ,3 wheels, max spring back, - c.g. fore					
K (max) =	-0.8	W(n-1)=	29005.16			
l=0	0	A-hk=	19.946			
		B+hK=	-2.056			
	Vn+Vm=W(n-1)					
	(A-hk)Vn-(B+hK)Vm=0					
	Vn=	-3333.4046	At limit, Vn=0.0			

Figure 7- Questionaire

WILLIS & KAPLAN INC

DISTRIBUTION OF LANDING GEAR LOADS ON LANDING AND DURING GROUND HANDLING

For purposes of evaluating stresses in landing gear, the FAA classifies the various landing and ground handling conditions as shown in the chart below. Please provide your best estimate of the percentage of landings and (for ground handling) the number of occasions per ground-air-ground cycle that each of the indicated conditions apply. These estimates need not be limited to CASA 212 aircraft.

NOTES: For the landing conditions:

- One wheel, two wheel, three wheel etc should be interpreted as a condition when the landing impact forces are primarily reacted by one, two or three wheels, respectively.
- The percentages you provide in the landing condition estimates should add up to 100%

LANDING CONDITIONS

	Condition	% of landings that this condition occurs
	Level Landing - with lateral drift zero or insignificant	
1	3 wheels	3%
2	2 wheels (MLG)	10%
3	1 wheel (MLG)	7%
	Level Landing - with lateral drift	
4	2 wheels (MLG)	5%
	Tail-Down Landing Lateral drift zero or insignificant	
5	2 wheels (MLG)	75%
		100%

GROUND HANDLING CONDITIONS

	Condition	No of occurences per ground-air-ground cycle
1	Braked roll (Straight ahead motion, no turns)	3
2	Turning (all 3 wheels rolling)	6
3	Pivoting (about one main landing gear)	0

Table 7 - 3

Taxi Spectrum

	Exceedances Per 1000 Operations	
	Prepared Runway	
Incremental Load Factor $\pm\Delta g$	Full Operation Pre -or Post Flight	Occurrences/1000 Operation
0.3	2094	2000
0.4	94.2	90
0.5	4.2	4
0.6	0.155	.15
0.7	0.005	.005
0.8	0	–
0.9	–	–
1.0	–	–
1.1	Exc	–

Table 7 - 4

Landing Impact Spectrum

	Exceedances Per 1000 Landings	
Incremental Load Factor Δg	Conventional Landings	Occurrences/1000 Landings
0.1	900	470
0.2	530	380
0.3	50	41
0.4	9	4.7
0.5	4.3	2.1
0.6	2.2	.9
0.7	1.3	.65
0.8	0.65	.65
0.9	0	0
1.0		

Landing Conditions

Level Landing Conditions
Tail-Down Landing Conditions
One Wheel Landing Conditions
Side Load Landing Conditions
Rebound Landing Conditions

Ground Handling Conditions

Take-off Run
Braked Roll Conditions
Turning
Nose Wheel Yaw
Pivoting
Reversed Braking
Towing Loads
Jacking Loads
Taxi Loads

Ground Load Conditions and Assumptions

Critical centers of gravity were obtained from CASA data in the Weight & Balance Manual. These data become:

C.G. Height (from axle) = 5.57 feet
C.G. Height (from ground) = 6.88 feet
C.G. Distance (from ng) = 15.49 (fwd. C.G.)
= 16.57 (aft. C.G.)
Design Landing Weight = 16204 lbs
Design Ramp Weight = 16535 lbs.

6.2.15 Sliding Tube

The sliding tube, which is manufactured from 4130 steel, is attached to the fork bracket at its lower end, and is free to slide in and out of the cylinder at its upper end. The sliding tube is subject to moments and vertical, drag, and side loads from the fork bracket. The sliding tube reacts these loads to the cylinder through the adapter and the plunger restrictor.

The stresses in the sliding tube were determined from conventional analysis. Due to its relatively simple geometry, the sliding tube was modeled as a simply supported beam subject to combined bending and compression. The maximum bending moment, and therefore, the maximum stress, were found to be significant, occurring at the point where the sliding tube contacts the adapter.

6.2.16 Inner Tube

The inner tube, which is manufactured from 2024 aluminum, is located within the cylinder and is attached to the cover. The inner tube is subject to compressive loads from the piston which is attached to its lower end. Conventional analysis indicates that the inner tube stresses are not critical.

6.3 Summary

Bases upon the stress levels determined in the main landing gear and the nose landing gear as a result of the analyses, the following components were later analyzed for fatigue crack growth:

6.3.1 Main Landing Gear Components

Axle
Cylinder
Torque Arms
Upper Trunnion
Lower Trunnion
Sliding Tube

6.3.2 Nose Landing Gear Components

Axle
Cylinder
Fork
Fork Bracket
Upper Trunnion
Lower Trunnion
Sliding Tube

Main Gear Materials Data

Component	Material	Yield Strength	Ultimate Strength
Axle	DIN 1.6747	179 ksi	225 ksi
Sliding Tube	4130 steel	145 ksi	170 ksi
Cylinder	4130 steel	145 ksi	170 ksi
Torque Arm	4130 steel	145 ksi	170 ksi
Lower Trunnion	2024-T3	42 ksi	64 ksi
Upper Trunnion	2024-T3	42 ksi	64 ksi
Inner Tube	4130 steel	145 ksi	170 ksi

Nose Gear Materials Data

Component	Material	Yield Strength	Ultimate Strength
Sliding Tube	4130 steel	220 ksi	256 ksi
Inner Tube	2024-T3	42 ksi	64 ksi
Torque Arms	4130 steel	120 ksi	140 ksi
Fork	DIN 1.6747	179 ksi	225 ksi
Fork Bracket	DIN 1.6747	179 ksi	225 ksi
Axle	DIN 1.6747	179 ksi	225 ksi
Upper Trunnion	4130 steel	120 ksi	140 ksi
Lower Cylinder	4130 steel	145 ksi	170 ksi
Lower Trunnion	2024-T3	42 ksi	64 ksi

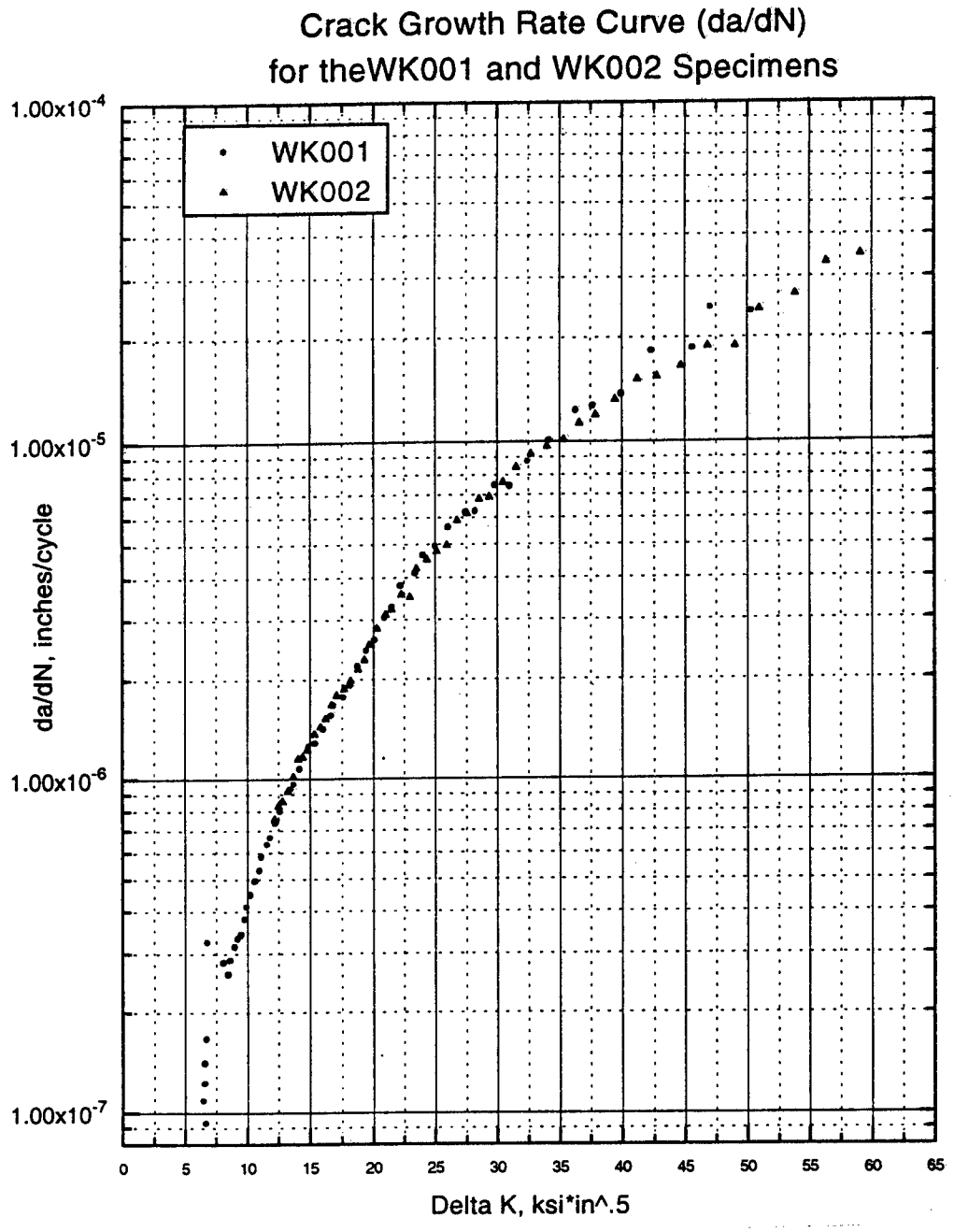
Crack Growth Rate Curve (da/dN)
for theWK001 and WK002 Specimens
WK001
WK002
1.00x10-4
1.00x10-5
1.00x10-6
1.00x10-7
da/dN, inches/cycle
0
5
10
15
20
25
30
35
40
45
50
55
60
65
Delta K, ksi*in^.5

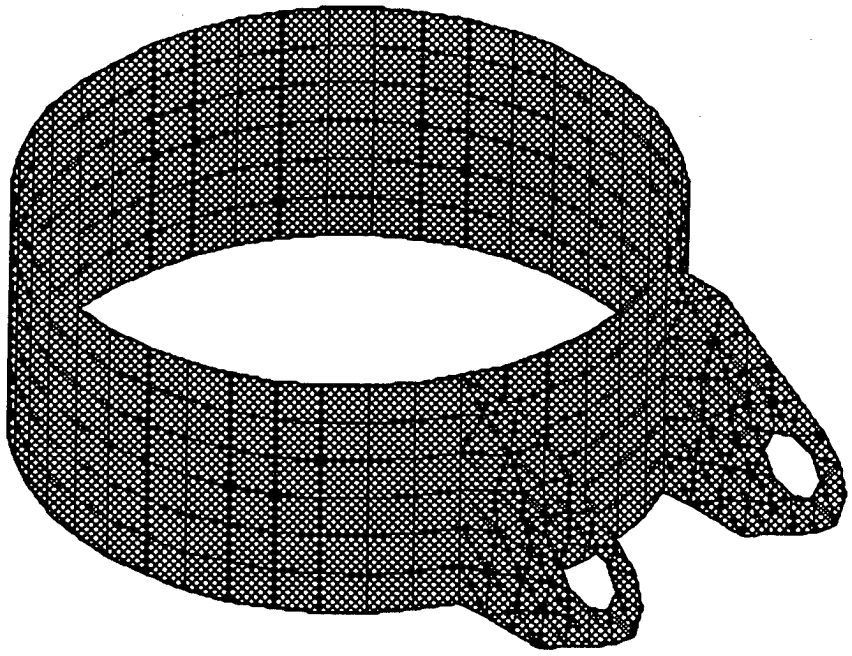

Nose Steering Collar

Figure 6-6

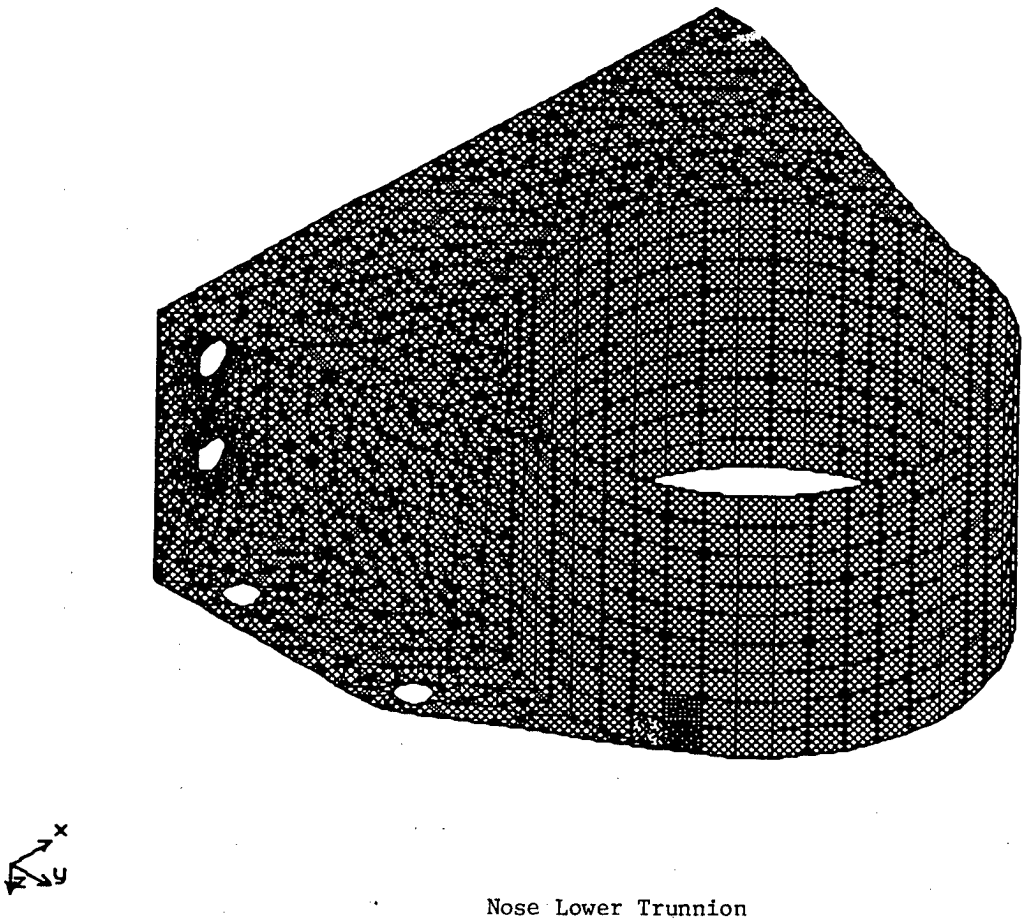

Nose Lower Trunnion

Figure 6-9

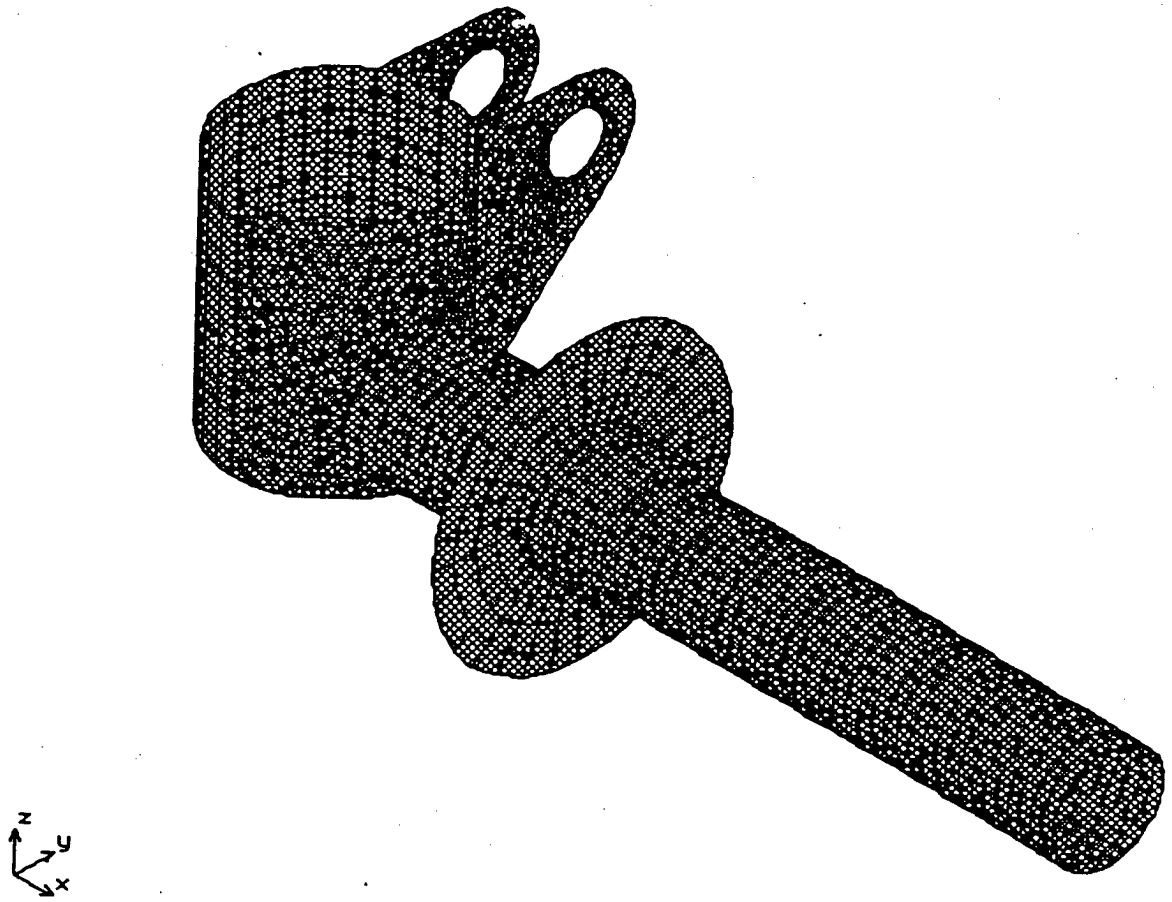

Main Axle

Figure 6-1

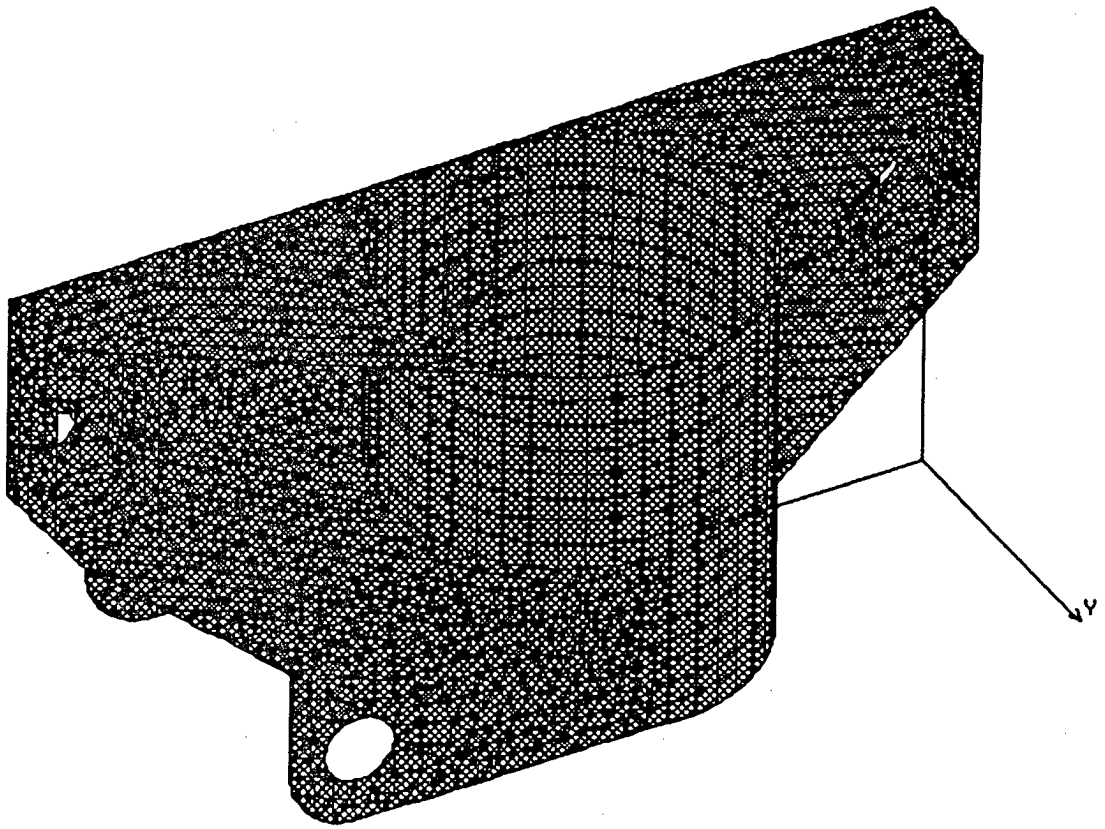

Main Lower Trunnion

Figure 6-4

Figure 8-5
Main Landing Gear - Sliding Tube

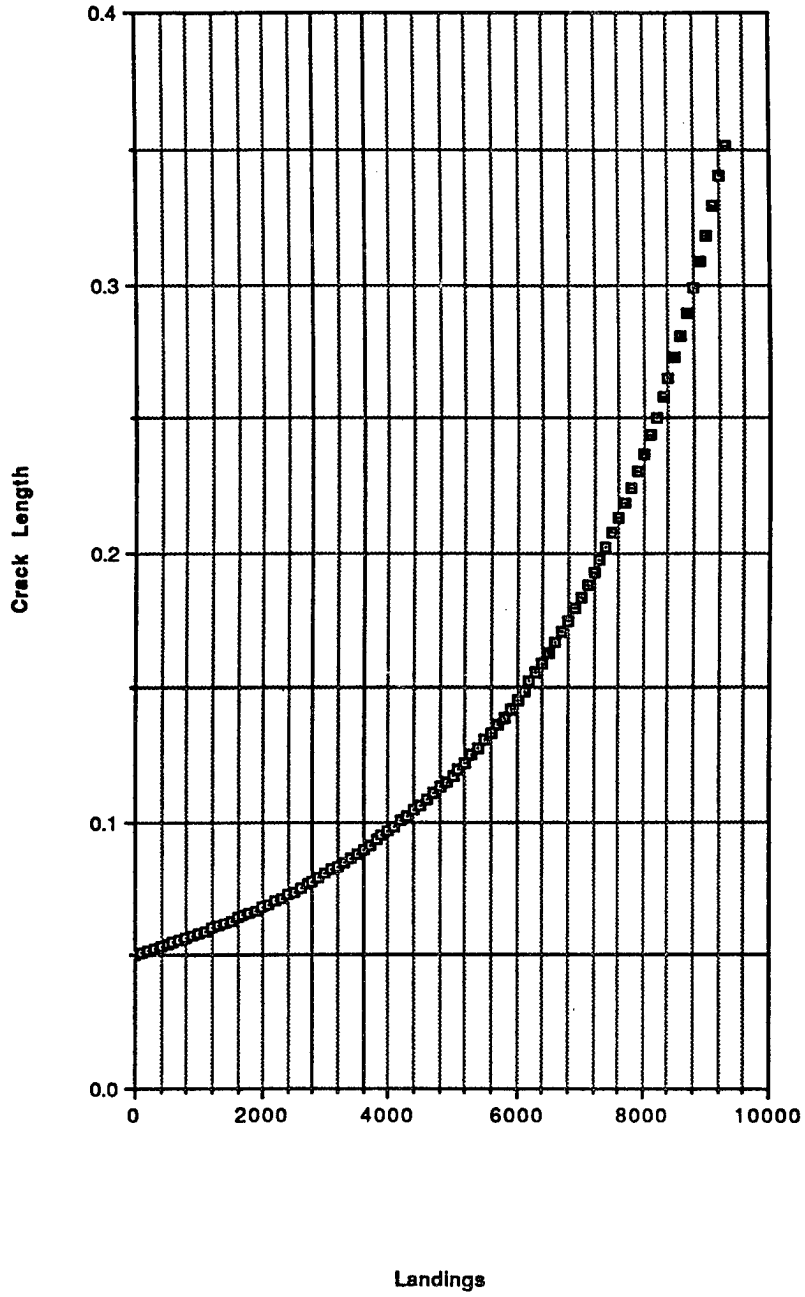

Figure 8-4
Main Landing Gear - Lower Trunnion

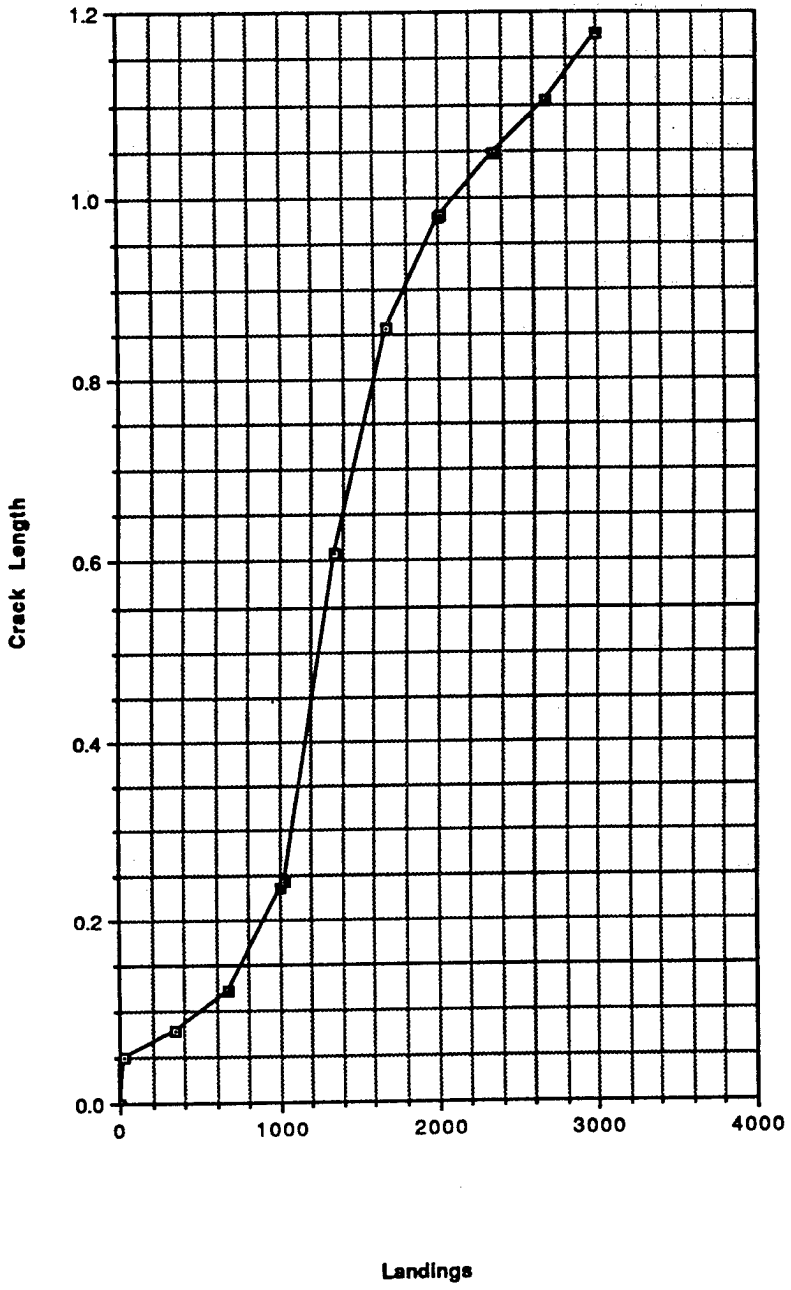

Figure 8-2
Main Landing Gear - Cylinder

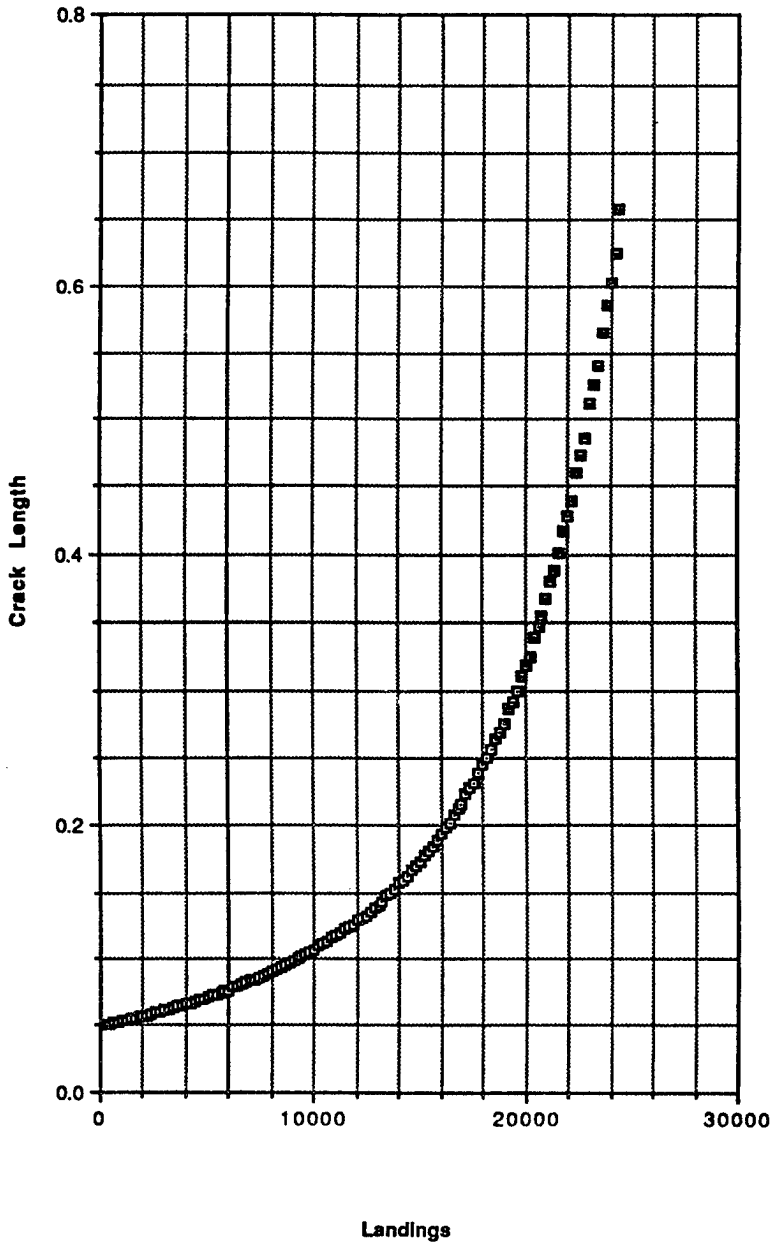

Figure 8-11
Nose Landing Gear - Lower Trunnion

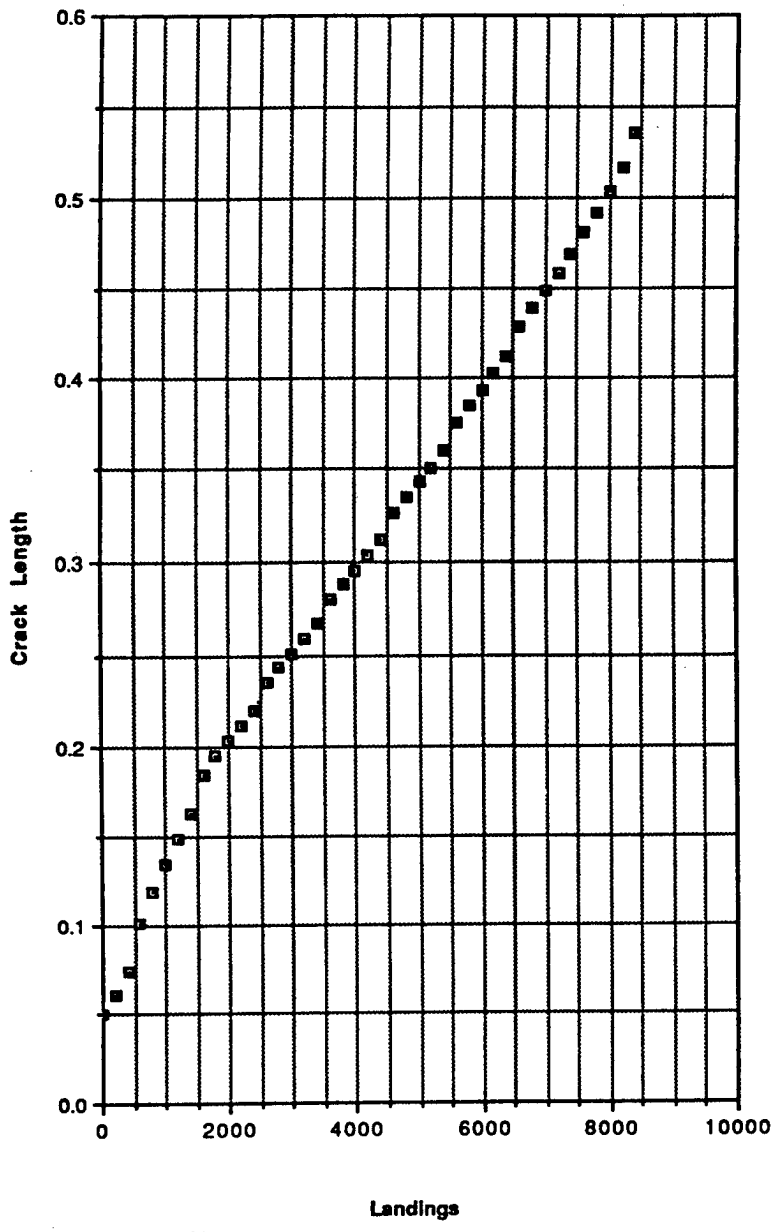

Figure 8-9
Nose Landing Gear - Fork Bracket

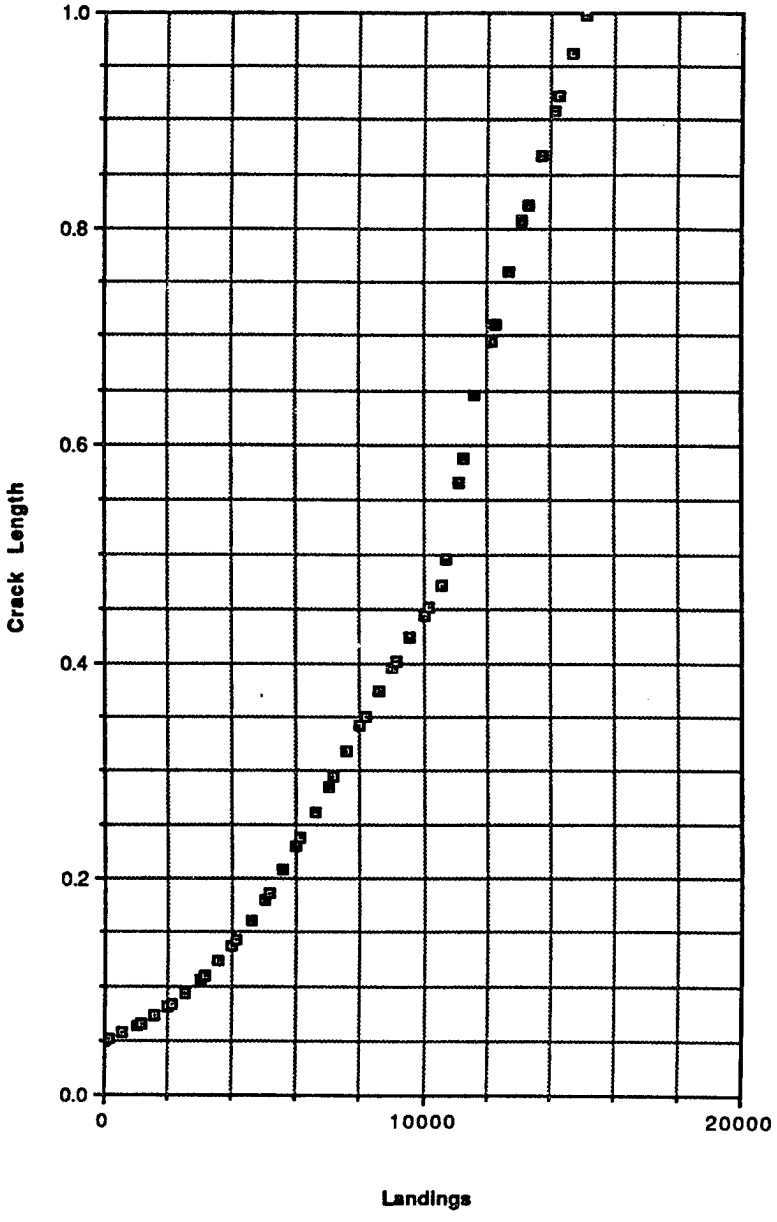

Figure 8-7
Nose Landing Gear - Cylinder

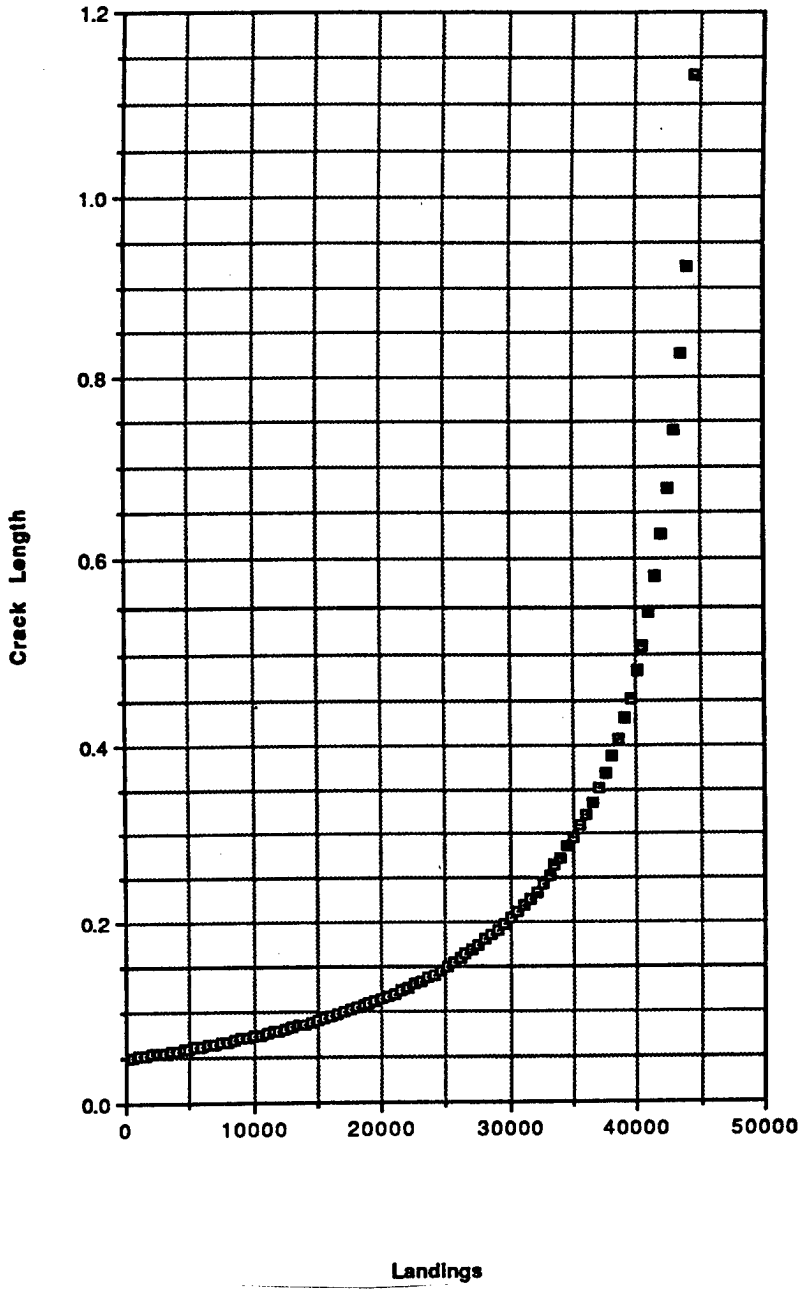

Inspection Location	
Main Gear	
Axle	Radii at Shoulders
Cylinder	Entire surface
Upper Torque Arm	Upper Flange
Lower Torque Arm	Upper Flange
Lower Trunnion	All fastener holes, cylinder hole, and radii at ears
Sliding Tube	Radii at shoulders
Nose Gear	
Axle	Radii at shoulders
Outer Cylinder	Entire Surface
Fork	All fastener holes
Fork Bracket	All fastener holes, radii at shoulders
Upper Trunnion	All fastener holes and trunnion/cylinder interface
Lower Trunnion	All fastener holes and cylinder hole

Initial Inspection Interval

All components are to be removed from the aircraft and inspected using eddy current. If any component shows a crack, then that component is to be replaced.

Repeated Inspection Intervals

Main Gear

Axle	7,100 Landings
Cylinder	10,500 Landings
Upper Torque Arm	20,000 Landings
Lower Torque Arm	20,000 Landings
Lower Trunnion	1,000 Landings
Sliding Tube	4,600 Landings

Nose Gear

Axle	19,600 Landings
Outer Cylinder	10,500 Landings
Fork	36,000 Landings
Fork Bracket	5,000 Landings
Upper Trunnion	25,000 Landings
Lower Trunnion	3,700 Landings

Critical Crack Size

Main Gear

Axle	0.400 inches
Cylinder	0.670 inches
Upper Torque Arm	0.275 inches
Lower Torque Arm	0.275 inches
Lower Trunnion	0.970 inches
Sliding Tube	0.550 inches

Nose Gear

Axle	5.000 inches
Outer Cylinder	0.700 inches
Fork	6.000 inches
Fork Bracket	0.475 inches
Upper Trunnion	0.550 inches
Lower Trunnion	1.170 inches

Case Depth and Chemistry Profile Measurements: A Novel NDI Technique

Mr. Simon Pelletier
*Dr. Normand J. Marchand
AMRA Technologies
4700 de la Savane
Montreal, Quebec H4P 1T7
Canada

ABSTRACT

In this paper a novel NDI technique which meets MECSIP requirements is presented. This technique allows the direct measurement of carbon (or nitrogen) profile and case depths in carburized components such as gears, shafts, screws, etc. The NDI technique is an advanced version of an AC-field method that was successfully employed to detect microcrack initiation in complex thermal cycle of gas turbine materials. Also, this new type of sensor makes use of a new technology named current focusing. The basic principles underneath this new system are presented and contrasted with the basic principles supporting the conventional NDI techniques.

Results which demonstrate the capabilities of this AC-field sensor to measure case depths are presented. The effectiveness and reliability of this novel technique were assessed by (1) inspecting various components taken out of production or from the field and (2) by examining these components using destructive verification procedures (cutting gears, metallographic inspections, microhardness profile, etc.). A data bank of carbon profiles (and case depths) is developed along with their corresponding AC-field electronic signatures.

1.0 Introduction

1.1 Carburizing of steels. Carburized steels are widely used for shafts, gears, bearings and other highly stressed components found in aircraft engines. Most of these components are cyclically stressed and resistance to fracture is a critical design factor. Depending on the application, resistance to rolling contact fatigue and/or to wear may be required.

During carburizing process, steel is heated above the A3 temperature and exposed to a carbon-rich environment, increasing the concentration of carbon adjacent to the exposed surfaces. At the end of the carburizing process, the steel is quenched to the ambient temperature, generally through a complex sequence of steps as to minimize distortion. In the quenching process, austenite is transformed to several decomposition phases which may include ferrite, perlite carbide, bainite, and martensite. The decomposition products have a lower density than the austenite. The austenite carbon gradients translates into hardness gradients after quenching. Case depths are usually defined as the distance from the surface where hardness drops to a given level, typically HV 510 or 50 HRC.

The increased carbon concentration at the surface lowers the martensite start temperature (M_s); thus transformation of the case austenite occurs at lower temperatures. In small cross-sections, where thermal gradients are minimal, the higher surface carbon content causes a delay in the transformation of case austenite relative to the core austenite. This time lag causes transformation dilatational strains to occur progressively, from the core to the outer case. These strains can be sufficiently high, generally exceeding yield, to give rise to progressive plastic deformation of the system and thus to distortion.

Many processing and microstructural factors affect the fatigue and wear performances, such that wide variations in endurance limits, ranging from 210 MPa to 1950 MPa have been reported [1]. However they are very sensitive to microstructural factors such as the amount and distribution of martensite and retained austenite and the development of favorable surface residual compressive stresses. **It is thus imperative that the depths of carburized layers and the associated microstructures and residual stresses be known if the field performances of the components are to be predicted and/or guaranteed.**

1.2 Carburizing and residual stresses. The chemical and transformation gradients in carburized steels produces surface residual compressive stresses. These stresses make it possible to readily manufacture high carbon martensitic structures which in quenched, through-hardened steels are difficult to produce because of surface tensile stresses and high sensitivity to quench cracking [1]. Furthermore, the surface

compressive stresses in carburized steels offset applied tensile bending stresses and thereby significantly increases fracture and fatigue resistance.

The compressive surface stresses are a result of the effect of temperature gradients established during quenching, superimposed on M_s gradients associated with the carbon gradients introduced into the austenite by carburizing. At some point during quenching, the temperature falls below the higher M_s temperature in the interior of the specimen, and the austenite begins to transform into martensite. Although the temperature is lower at the surface, the austenite there remains untransformed because of the low surface M_s. The interior formation of martensite causes an associated volume expansion which at high temperatures can be readily accommodated by the surrounding austenite. Eventually, the temperature at the surface falls below the M_s and the high carbon martensite forms. The interior martensite, now at lower temperature and significantly stiffer than the austenite, resists the expansion of the high carbon surface martensite and thereby places it in compression. Accordingly, the interior martensite is placed in tension. The following figure shows a schematic diagram of the residual stress profiles that typically form in carburized and hardened steels [2]. Also shown schematically, are the carbon profile responsible for transformation gradients on quenching and the retained austenite profile. As can be seen, the compressive residual stresses are balanced by interior tensile residual stresses. Larger amounts of austenite transformation would be expected to increase compressive stresses according to the scenarios outlined above.

Parrish and Harper [2] have also reported the results of a literature survey which included the evaluation of seventy (70) residual stress curves for carburized steels. The specimens all had case depths around 1 mm or less with the core carbon contents between 0.15 and 0.20%. Figure 2 shows the range of residual stress profiles which are typical of those associated with carburizing. As shown, the compressive residual stress zone encompasses most of the case depth.

The level of surface compressive residual stress is controlled by the surface carbon content, the carbon gradient (case depth), the quenching conditions, the hardenability of the case and of the core material, and tempering after hardening. However, although in carburizing processes, the objective is to produce a beneficial and controlled level of compressive residual stresses in the surface, subsequent manufacturing processes can create residual stresses in a way that is uncontrolled. Examples of such processes are machining by chips cutting tools, abrasive grinding, EDM, laser hole drilling, or any other surface forming or finishing process that causes local plastic deformation or intensive heating of the metal surface. The optimum microstructure and residual stress for a given carburized part depends on its intended

function. In rolling contact or gear teeth, for example, a controlled level of retained austenite is beneficial (improved toughness). However this implies that the level of residual compressive stress and hardness will be lower than if the part is refrigerated before tempering to reduce the level of retained austenite to increase the hardness (all other things being equal).

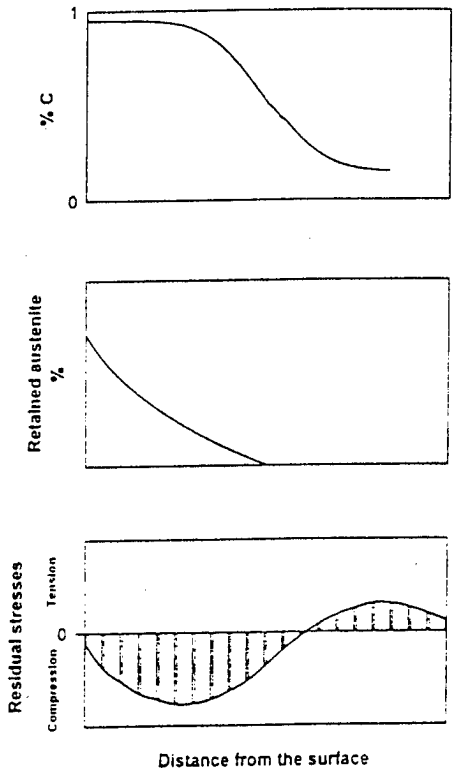

Figure 1: Schematic diagram of the residual stresses profile in carburized steels.

Being able to quantify case depths and their associated residual stresses and concurrently the changes of the residual stresses with further machining operations, is vitally important to quality and reliability of components.

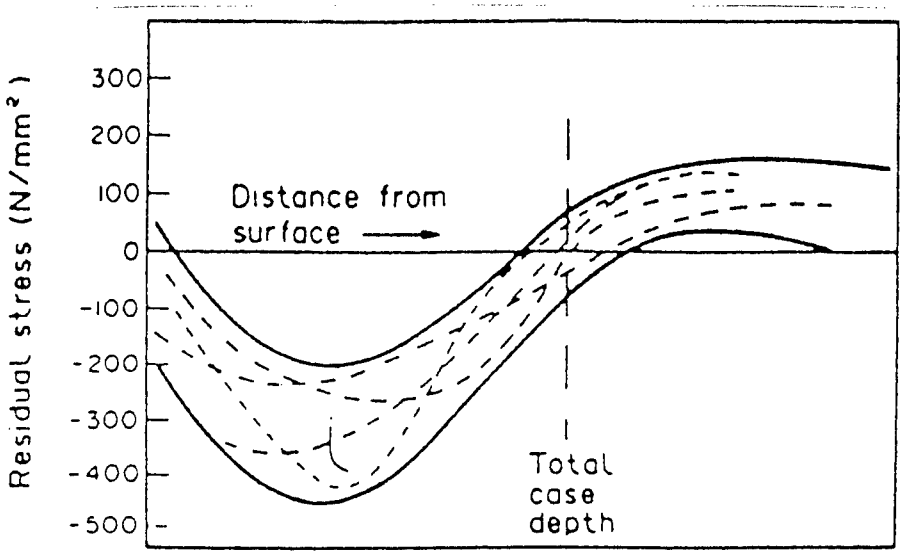

Figure 2: Range of residual stresses in carburized steels [2].

2. Measurements of Case Depths (and Residual Stresses)

2.1 Conventional Methods. A number of methods have been developed to measure case depths and residual stresses in materials. These include X-Ray diffraction, ultrasonic, electromagnetic and mechanical methods as well. These techniques are described in details elsewhere [3]. However their key features will be highlighted here as to contrast their similarities and major differences.

Mechanical methods for the measurement of case depths and residual stresses have been used longer than any of the other methods. There are many techniques used for the mechanical measurements of case depths and residual stresses, but for the most part, they all consist of cutting the component or removal of stressed material and the measurement of the resultant hardness profile and/or strain change. For residual stress measurements, the most "popular" technique presently in use is that of hole drilling. Here a specially designed set of electrical resistance strain gauges are used to measure the strain change caused by removing stressed material by hole drilling [4]. Beside the fact that these methods are destructive procedures, they also have many limitations and are not suitable where high stresses and stress gradients exist.

Case depths and surface residual stresses can be measured by X-Rays as described in great details in "X-Ray Diffraction Residual Stress Techniques" [5]. With

the X-Ray diffraction technique, the interatomic distortion or planar distance is measured and the corresponding carbon concentration or stress is calculated [4,6]. The penetration of X-Rays is of the order of only 10mm in metals. Therefore, the technique is limited to measurements of surface carbon content or stresses only (unless a surface layer is removed by chemical etching or mechanical polishing in which case it is no more a nondestructive technique). Its use has been generally limited to laboratory because of the lack of field-usable equipment and concern with radiation safety.

With ultrasonic techniques, the velocity of the ultrasonic waves in the materials is measured and related to carbon content and to stress [7]. These techniques rely on a small velocity change caused by changes in chemistry and by the presence of stress. This is known as the acoustoelastic effect [8]. In principle, ultrasonic techniques can be used to measure bulk as well as surface values of carbon and stresses. Because of the difficulty in differentiating stress effects from the effect of material texture, practical ultrasonic applications have not yet materialized. Another problem with the application of ultrasound is that carbon content and residual stresses are changing significantly over distances of tens of microns. However, the nature of the propagation of ultrasound and instrumentation for measurement of its velocity results in spatial resolution on the order of tens of milimeters to tens of centimeters, i.e. three to four orders of magnitude too coarse [4,7].

With all the electromagnetic techniques, one or more of the magnetic properties of a material (such as permeability, magnetostriction, hysteresis, coercive force or magnetic domain, wall motion during magnetization, etc) are sensed and correlated to chemical composition and to stress. The change in magnetic properties of the material caused by stress is known as the magnetoelastic effect [3,8]. Therefore, these techniques (normally) apply only to ferromagnetic materials, such as ferritic and martensitic steels. Among the many electromagnetic stress-measurement techniques the Barkhausen Noise Analysis (BNA), the Non-Linear Harmonics (NLH), the Magnetically Induced Velocity Changes (MIVC), and the Magabsorption Techniques have been shown to have limited success [3].

The inductively detected Backhausen noise (BNA) signals reflect the activity occurring very near the surface of the specimen to a maximum depth of about 0.1 mm (0.004 in.). Therefore, the BNA technique is only applicable to measuring near surface chemistry changes and stresses. As far as residual stress is concerned, the effective stress-measurement range of this technique is up to about 50% of the yield stress of the material, because the change in the Backhausen noise with stress becomes saturated at above these stress levels [3-4,8-9]. Because, the BNA signals are sensitive to slight changes in material chemical composition, phase composition, dislocation density,

microstructure, etc., as they are to residual stress, the NBA has not found broad application for the quantitative measurement of residual stress or case depth [10]. Like all other electromagnetic techniques, BNA suffers from lift-off factor, fill factor, edge effects, etc. [3]. To minimize these detrimental effects and because of the difficulty in magnetizing complex-geometry area, the application of the technique is limited to simple geometry ferromagnetic parts.

The non-linear harmonics (NLH) technique relies on the fact that mechanical stresses greatly influence the shape of the magnetic hysteresis of ferromagnetic materials. This implies that the harmonic content of the magnetic induction (B vs. time) is also affected by the stress state in the material. With the NLH, these harmonic frequencies are detected, and their amplitudes are related to the state of stress in the material [3,11]. As for the BNA, the NLH is limited to simple geometries. This stems from the fact that the amplitude of third harmonics is used to determine the state of stress in the material. The range of stress to which the technique is effective is up to about 50% of the yield stress of the material, because the response also saturates at higher stress levels [11]. Finally, as for BNA, the accuracy of the technique is about ±35 MPa (±5 ksi) which for most practical cases is inadequate.

Because of the magnetoelastic interaction, the elastic moduli of a ferromagnetic material are dependant on the magnetization of the material [8]. Moreover, the elastic moduli is also a function of the carbon content. Consequently, the velocity of the ultrasonic waves in ferromagnetic materials changes when an external magnetic field is applied to the materials [4,12]. The magnetically induced velocity changes (MIVC) for ultrasonic waves is characteristically dependant on the chemical gradient, the stress gradient, as well as the angle between the stress direction and the direction of the applied magnetic field [12]. This characteristic chemistry and stress dependence of the MIVC is used for case depth and stress determination. In theory, the MIVC technique can be used to measure bulk and surface chemical composition and stresses by applying both bulk (shear or longitudinal) and surface ultrasonic waves. The accuracy in both chemical composition and stress measurements is about ±0.2% and ±35 MPa (±5 ksi) assuming that a very high magnetic induction field is used (B $>10^6$ Amp./meter). Hence, a relatively large electromagnet is needed to magnetize the part under investigation. This is cumbersome to handle in practical applications. Furthermore, because of difficulty in magnetizing complex-geometry parts, the application of the technique is limited to simple geometry parts.

Magabsorption involves the measurement of the change in the energy absorbed from the field of an RF coil, by a ferromagnetic material placed in the field of the coil, as a function of the strength of a magnetic bias field also applied to the material. The

variation of μ_{RF} as a function of H_B (bias field) is the basis for the magabsorption phenomenon [4,8,13]. This is because the RF permeability, μ_{RF} changes as the H_B is varied sinusoidally, and that the energy absorbed by the material from the RF coil also varies as a function of H_B [13]. Due to the complexity of the electronics and data analysis procedures, only very simple geometry can be inspected and have been inspected so far (wires and flat plates). The extension of this technique to move complicated geometries has yet to be achieved.

It is obvious that all the methods discussed so far suffer from the same problem, i.e. they rely on the change of some magnetic properties to quantify case depths or residual stresses. Thus they are only applicable to ferromagnetic materials. Furthermore, since the magnetic properties vary in complicated manner with stress, chemistry, phases, etc., the calibrations require to address in-service components is extremely difficult. As a result, the actual claimed accuracy is not sufficient for on-line quality control purposes. **New technologies are required if the requirements for quality control and lifing of engine parts are to be achieved.**

2.2 The AC-Field technology

The principle by which the AC-field detects changes of electricals properties (conductivity and magnetic permeability) in surface or flaws is illustrated in figure 3. An electric current density (J_0) is introduced into the region to be inspected. Then the AC potential difference (ACPD) across a region of the specimen surface, or across some region where a crack is expected is monitored. The mapping of potential is indicative of change in chemistry, stress field or cracking. Very high sensitivity and increased accuracy is possible because the frequency of operation may be chosen to suit both the electrical properties (conductivity) and the magnetic properties of the particular metal (or alloy) under investigation. This tuning of the AC frequency induces a pronounced skin-effect enhancement of the ACPD signals.

An intrinsic property of an alternating current is that it is concentrated upon the surface of a conductor, and this is the so-called "skin effect". The skin depth (δ), which is seen in figure 3, varies with the frequency of the power source and with the properties of the material according to the following equation:

$$\delta = \frac{1}{\sqrt{\mu_0 \mu_r \sigma f}} \qquad (1)$$

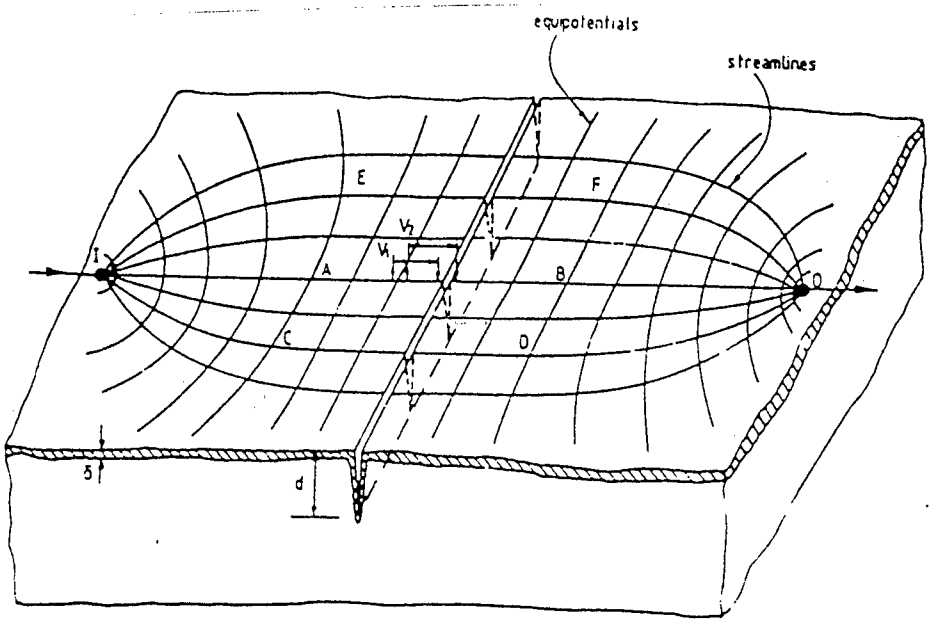

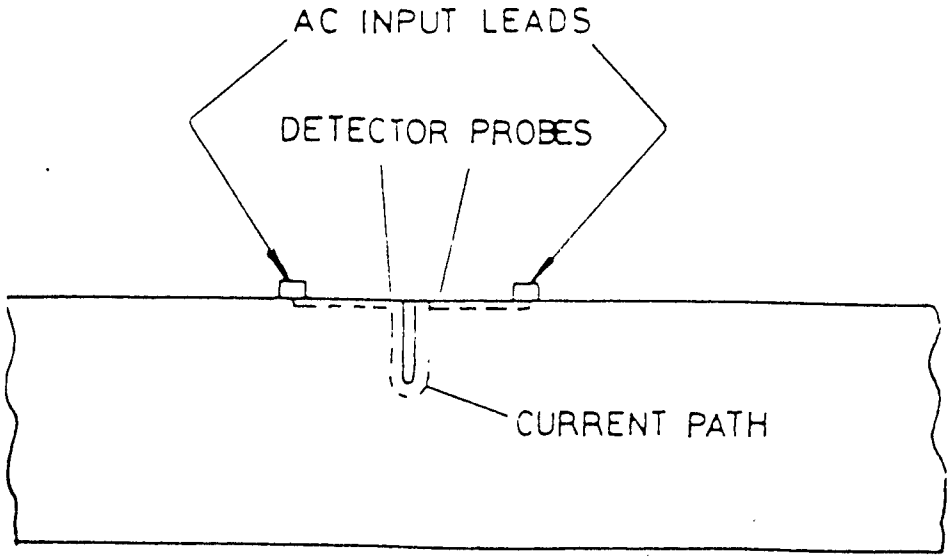

Figure 3: Illustration of the skin effect associated with a.c. conduction

where μ_0 = permeability of vacuum (H/m)
μ_R = relative permeability of conductor
σ = conductivity of conductor (Ω/m)
f = frequency of AC current (Hz)
δ = skin depth (m)

Note that both electrical (σ or ρ) and magnetic properties (μ_R) affect the skin depth. Thus any change in σ or μ_R due to the chemistry variation or residual stresses will affect δ. Changing d results in changing the current density and therefore in changing the potential difference between two points on the surface (all other parameters being equal). For a given AC current, the smaller the skin depth, the higher the sensitivity [3].

Because the skin depth decreases as the frequency of operation increases, then the AC-Field technology is useful not only for ferromagnetic materials (where the magnetic properties are responsible for small skin depths) but also for non-magnetic metals. For example, consider a mild steel and Waspalloy (aircraft engine disc material) which are respectively ferromagnetic and paramagnetic materials.

For these two materials we have:

Mild Steel: $\mu_R \gg 400$ $\rho = 2.0 \times 10^{-7}$ Ω-m

Waspalloy: $\mu_R \gg 1$ $\rho = 1.2 \times 10^{-6}$ Ω-m

Thus at a frequency of 100 Hz the skin depth for the steel is about 1.0 mm while at a frequency of 200 kHz the skin depth for waspalloy is also about 1.0 mm. Note that, ferromagnetic materials always have smaller skin depths at the same frequency than paramagnetic materials. Hence at 250 kHz the skin depth of mild steel is less than 150 μm.

The above argument imply that the electromagnetic methods (EMM) and the ACPD technology share similar features. However, as opposed to EMMs, the ACPD deals with the measurement of potentials at the surface and these potentials are integral of the electrical fields along a given between two points[1]. The lower the conductivity, the higher potential being measured [1] (all thing being equal).

[1] Here we have $J = \sigma \nabla V$. In 1-D this can be written as $J_x = \sigma(\partial V/\partial x)$ or with ΔL the spacing between two considered points $\Delta V = J_x \Delta L/\sigma$

The ACPD technique uses the fact that both magnetic and electrical properties affect the potentials at the surface. This is a significant advantage over the conventional electromagnetic methods (including the eddy-currents) because, in many commercial alloys the magnetic properties are weakly affected by large changes in composition, microstructure, state of stress, etc. This is the case of most titanium-based and nickel based alloys which are used in the aircraft industry. On the other hand, these paramagnetics (non-ferromagnetic) alloys display significant changes in their conductivities (or resistivity) as a function of impurities, composition, microstructures, residual stresses, etc. For example, the conductivity of waspalloy can be varied from 7.5×10^5 Ω/m to 1.2×10^6 Ω/m depending on the heat treatment (microstructure) [3]. These changes are therefore readily quantifiable using the ACPD.

Another important advantage of the ACPD Technique over all other conventional electromagnetic methods, is that the magnitude of the potential field varies linearly with the amplitude of the injected AC current. Since the injected currents used in ACPD are much higher (100 - 1000 times) than the induced eddy currents, much smaller changes in surface impedance due to stresses or composition, can be detected. The difference between the EMMs and the ACPD can be summarized as follow.

With the EMMs we impose a magnetic field (H_I) which creates an induction field (B_I). This induction field generates an electrical field (E) and thus eddy currents (J). In turn, the eddy-currents produces a magnetic field (H_R) which is sensed by a pick-up device. Thus measurements of changes or modifications in the materials depend mostly on changes in magnetic permeability (μ).

With the ACPD, a current field (J) is imposed which creates an electric field (E). Perturbation or modification of the electric field are measured directly at the surface. There is no intermediate. The ACPD is directly quantifying changes in surface and near surface impedance. Moreover theoretical or numerical predictions of the potentials at the surface are readily available as compared to EMMs.

2.3 Current Focusing

In the previous section we have seen that the ACPD technique implies the injection of a known current into a conductive material, and the mapping of the potentials between the injection points. However, as can be seen in figure 3, the injected current will tend to spread-out as to minimize the current density at the

surface. This new ACPD technology, which will be described in detail in the next sections, makes use of a method known as current focusing [14].

Current focusing is based on the fact that when a current flows between two conductors, some energy is transmitted by an electromagnetic field between the two. The electromagnetic field penetrates the conducting surfaces of the conductors and causes the electrons to change position. As for the skin depth, the extent of the field's penetration depends upon frequency, magnetic permeability and conductivity. This is shown in figure 4.

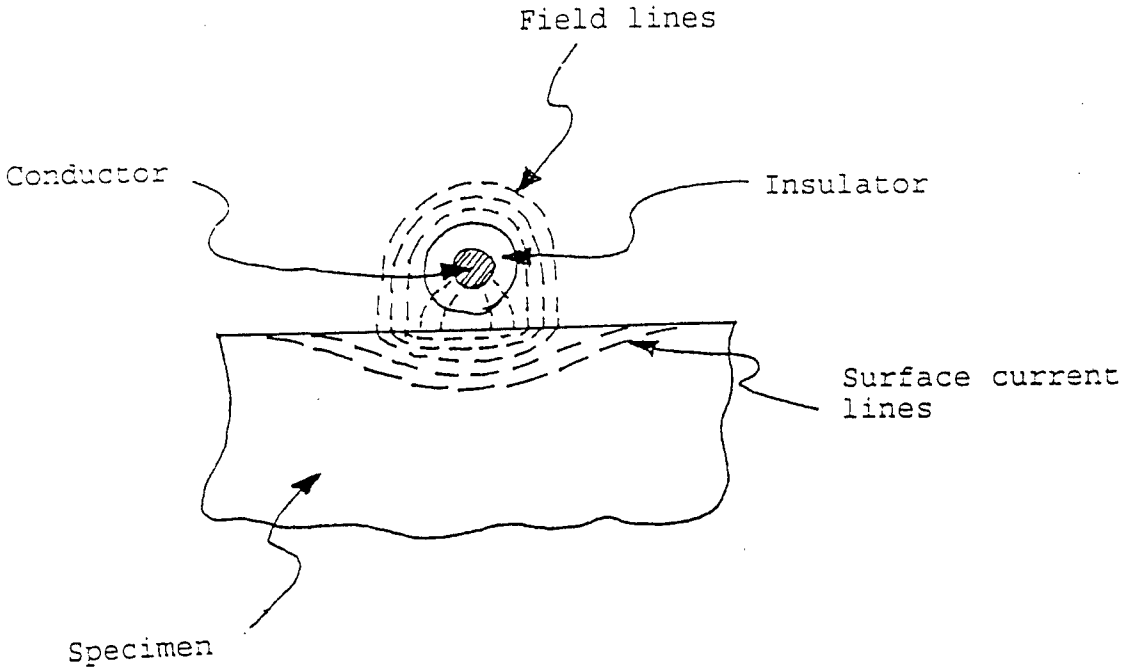

Figure 4: Schematic illustrating the current focusing method

The closer the conductor to the surface of the specimen, the more intense is the focusing of the current. **Thus the use of an AC current, in conjunction with the current focusing technique, results in having a 3-dimensional control of the current density distribution in a solid.** Hence a skin effect in the depth of the specimen and a skin-effect at the surface (moving laterally from the conductor located above the specimen) result from the use of current focusing.

The use of current focusing implies that the current densities in the area which are to be probed can be extremely high as to permit very small changes in surface impedance to be detected. Furthermore, the current focusing technique allows the monitoring of areas having extremely complex geometries. This would be problematic or impossible with the conventional EMMs.

2.4 Feasibility study for measuring case depths

To assess the true capabilities of the ACPD technology for detecting changes in surface impedance due to change in chemical composition (carburizing), two calibration procedures were carried-out. The first calibration was concerned with experimental measurements on two samples of gear teeth of different microstructures while the second calibration pertains to theoretical numerical calibration of the surface measurements assuming a given distribution of conductivity (i.e. a given profile of carbon). The details and results pertaining to numerical modelling are presented elsewhere [15].

Two geometrically identical samples of gears were used for the feasibility study. However, the samples were carburized at different level with the first sample (SMPI) beeing more carburized than the other (SMPII). The microhardness profils for the samples were been shown in figure 6. The samples were instrumented as shown in figure 5. As can be seen, the crude arrangement of current and voltage probes (used for both samples) employed the current focusing method. For both samples the probe spacing was 10 mm ± 0.5 mm. The optimal spacing to minimize noise and signal distortion has not been addressed. The measurements were carried-out using an ACPD crack growth monitor (CGM5) which was initially developed to detect crack initiation and growth in aircraft engine materials under high temperature fatigue conditions.

A current of 1 Amp. was used in all cases. The frequency of the current was varied in steps of 300 Hz, 1kHz, 3 kHz, 10 kHz and 30 kHz. The gain was set at 50 dB (X 316) for all the measurements. Each sample of gear contains three teeth, the measurements were carried-out on two teeth of each sample as to evaluate the reproducibility of the technique when using a very crude current and probe assembly.

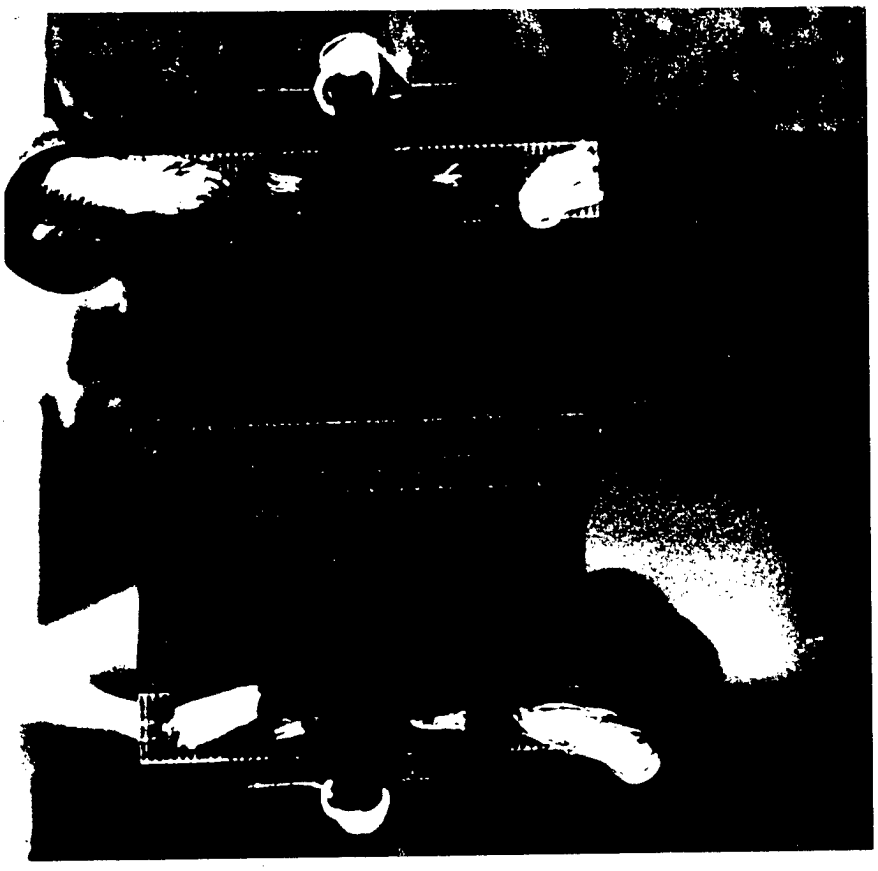

Figure 5: a) Arrangement of current and voltage probes for samples I.

The raw data for both samples are shown in figures 6 and 7. Figure 6 show the total change of the voltage (potential difference between two probes) as a function of the frequency.

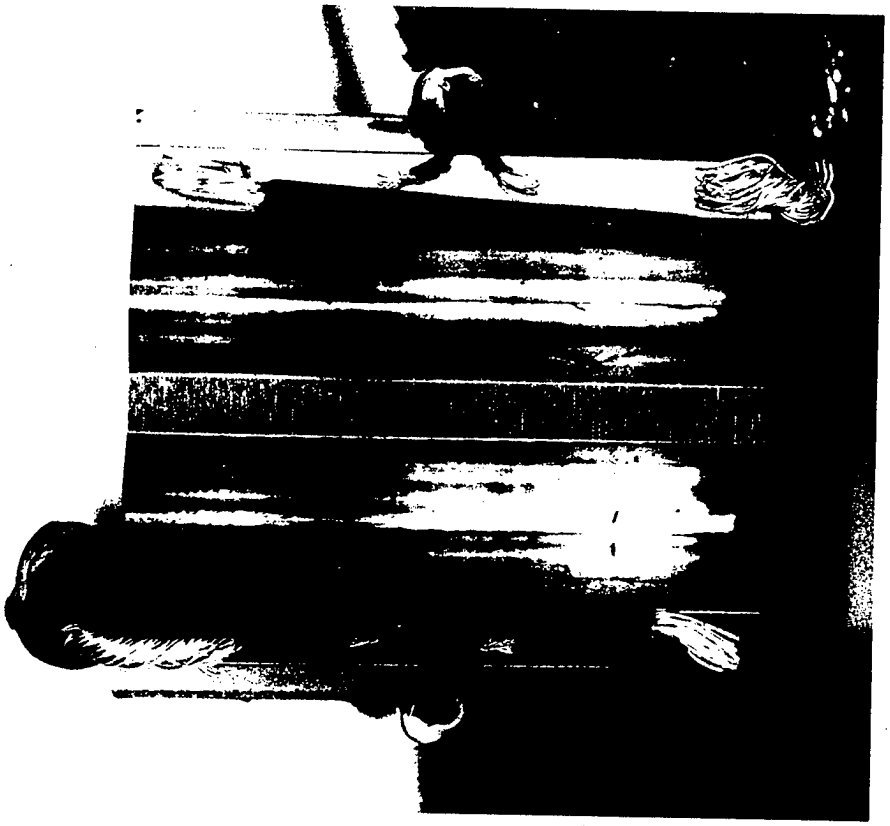

Figure 5: b) Arrangement of current and voltage probes for samples II.

The following conclusions can be drawn from these measurements:

a. The reproducibility of the ACPD technique is excellent in spite of the fact that a crude arrangement of current and potential probes was used. This conclusion stems from the fact that the ACPD signals obtained on two different teeth of the samples are (worst case) within 10%.

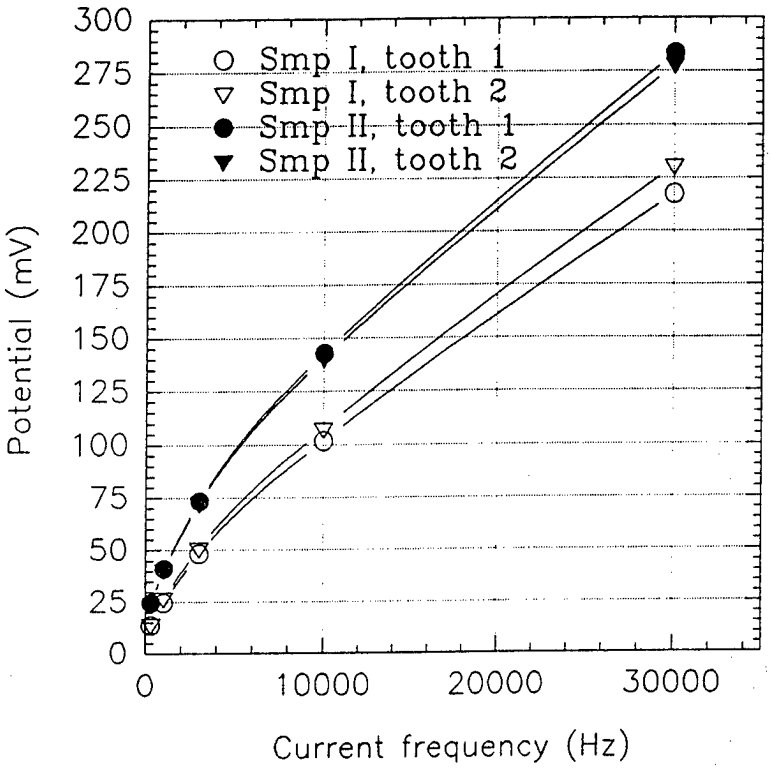

Figure 6: ACPD signal as a function of frequency (gain 50db)

b. The system that the system is very sensitive to small change in conductivity. Note that even at 300 Hz the ACPD signals of both samples are different. This difference between the two samples increases with increasing frequency. This shows that changing the skin depth clearly permits the determination of the gradient of conductivity at the surface.

c. More data points are needed at low frequencies to allow the precise determination of the case depth. Nevertheless a rough estimate of the case depth can be produced by assuming that: $\mu_R \gg 350$, and: $\sigma = 3.7 \times 10^6\ \Omega/m$. These values are those of 4340 steel which were taken from the literature [3,18]. Thus

$$\delta = \frac{1}{\sqrt{350 \times 4\pi \times 10^{7} \times 3.7 \times 10^{6} \times 3000}} = 451\mu m$$

$$\text{casedepth} \approx 2 \times \delta = 902 \mu\text{m}$$

Note that by choosing other values of μ_R, one would obtain different values for the case depths. The following table summarizes this

μ_R (assumed)	case depth (μm)
500	756
400	846
350	902
300	976

The above table shows that the knowledge of the μ_R is also required if the case depths is to be computed accurately. However, by using experimental measurements of the case depth we eliminate the need of knowing μ_R. Hence the microhardness profiles for the two samples were measured. These profiles are shown in figure 8. As can be seen the case depth of sample I is about 890 μm which is within 2% of the predicted value. Nevertheless, to better pin-point the frequency which determines the skin depth which is of the order of the case depth we have normalized the results in terms of the voltages measured at 300 Hz for which the skin depth is large. These results are shown in figure 7. As expected there is a deviation occurring near 3 kHz.

3.0 Validation and testing of actual components

Spur gears specimens, typical of those used in Pratt & Whitney Canada engines were used in this study. Figure 9 shows an example of such gears. These gears are made of AMS6265(8610), a steel which normally require carburizing.

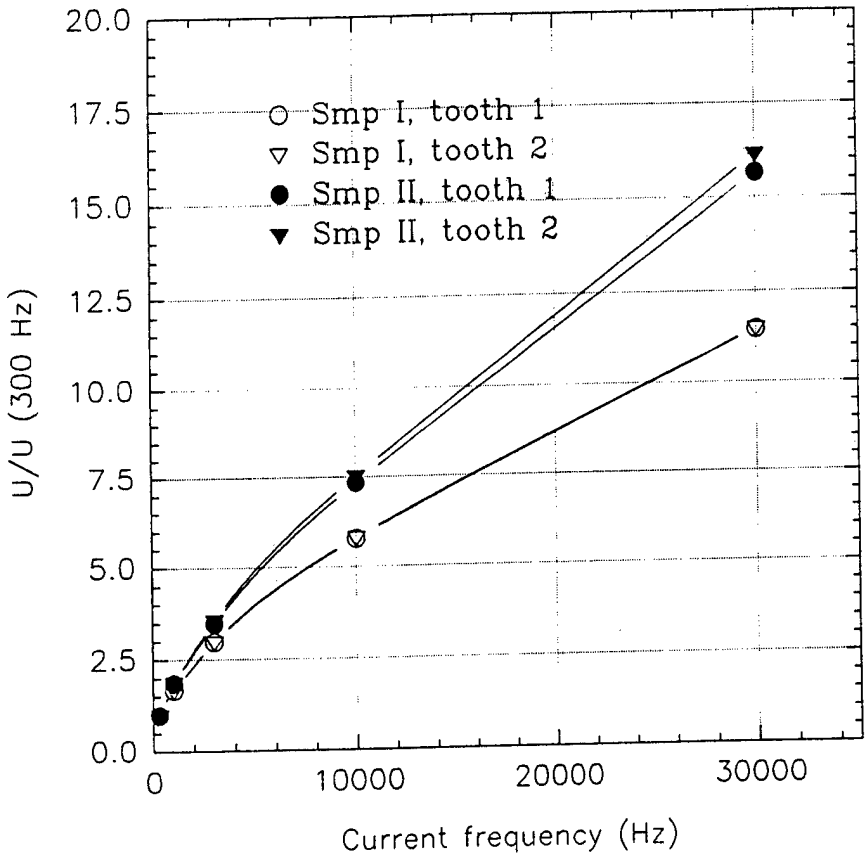

Figure 7: Normalized potential as a function of frequency

In accordance with aircraft engine manufacturers specifications, the effective case depth is usually controlled between 0.009 in and 0.030 in (230 μm to 762 μm). It is this variability of the process which requires a quality control assessment (NDT) of the actual case depths.

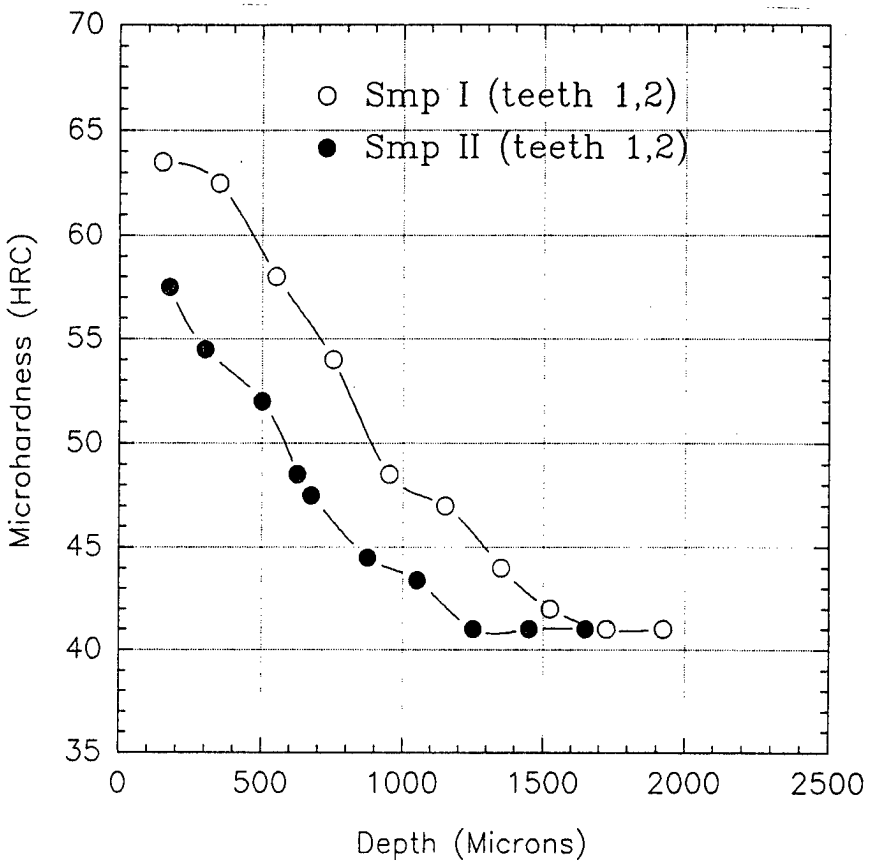

Figure 8: Microhardness profile

Hand probes that suits the spur gears geometry were fabricated (see figure 10). Several gears (about 6) of the same model were carburized under various processing conditions. Each of these gears were inspected as shown in figure 11. A Potential vs. Frequency curve was produced for each components. After the measurements, the components were sectioned and metallographically inspected to determine the total case depth and effective case depths using microhardness measurements (profiles).

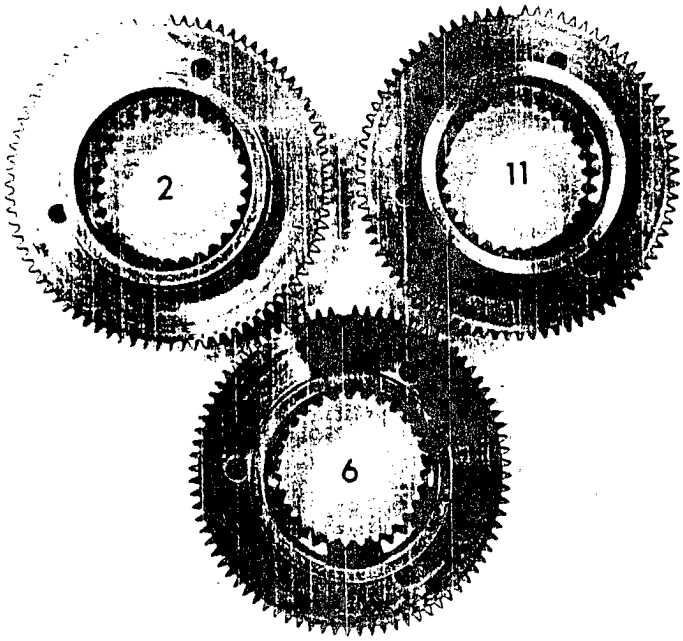

Figure 9: Typical gears samples

Figures 12 show the ACPD voltage as a linear function of the frequency for the various samples. As can be seen there is a significant difference between the carburized and uncarburized samples. Here, the effective measured case depths are reported along with their ACPD vs Frequency signature. Reporting the total case depths along with their corresponding ACPD/Frequency curves would have yielded the same results as those shown in figures 12 and 13. Note that even at 300 Hz (the lowest frequency at the which measurements were carried out) these is a difference of few millivolts between the carburized and the uncarburized samples. Obviously the present ACPD signal has very good sensitivity.

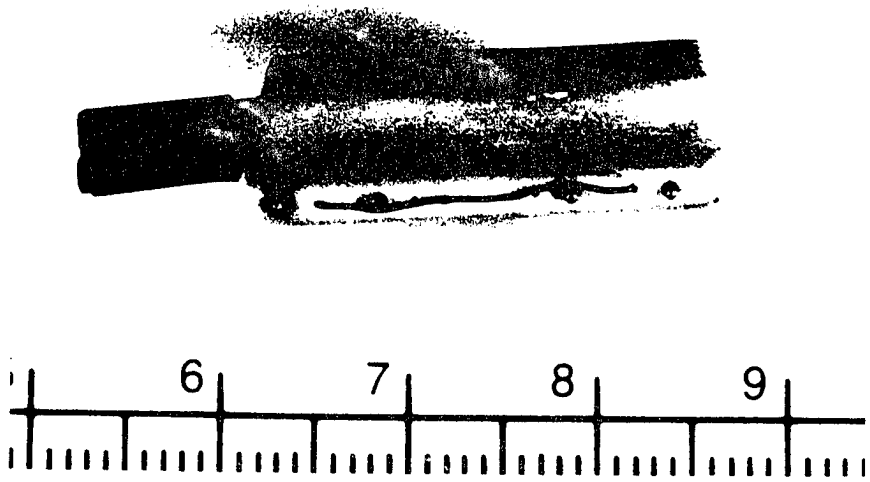

Figure 10: Hand Probe

Figure 13 shows the ACPD voltage as a function of the square root of the frequency for the various samples. Note that hypothetical sample which would have constant electricals and magnetics properties as a function of depth would present a straight line (see Eg. 1). However the two virgin samples, free of carburizing, do not show a linear behavior (ACPD vs $\sqrt{f}$). This can be explained by the fact the machining and/or previous heat treatments, on the samples, have modified the electricals and magnetics properties of the surface. In particular, the residual stress associated with machining operations have been show to modifical the ACPD vs $\sqrt{f}$ response of conductive materials [15].

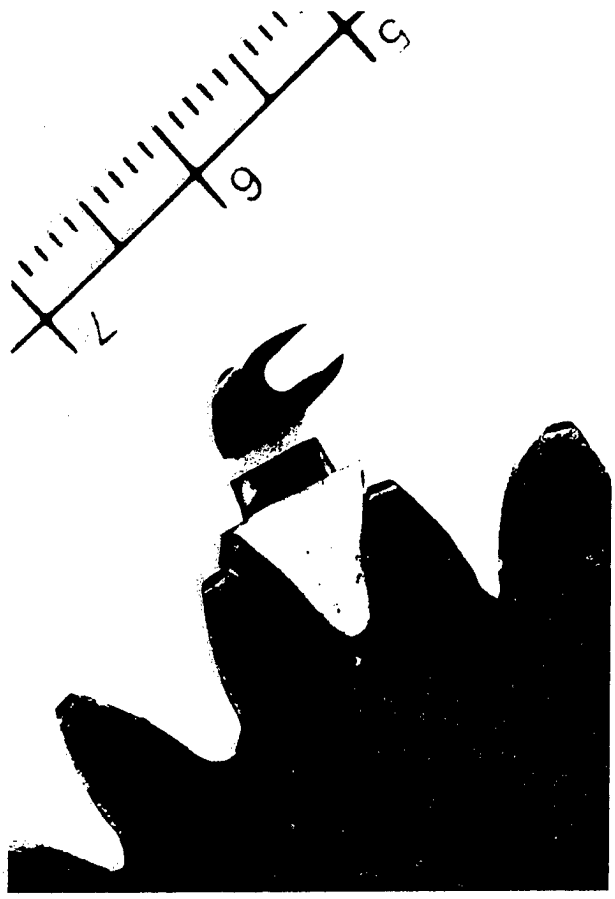

Figure 11: Probe installed on a gear sample

Figures 12 and 13 show that the case depths can be accurately determine on real components using the proposed (novel) ACPD/Current focusing technologie. With the present instrument (300 Hz to 30 kHz) the ACPD/Frequency curve can resolved case depths to within 25μm (0.001"). Furthermore, samples having identical case depth yielded the same ACPD/frequency curves. This results attests as to the reliability of the technology to quantify case depths.

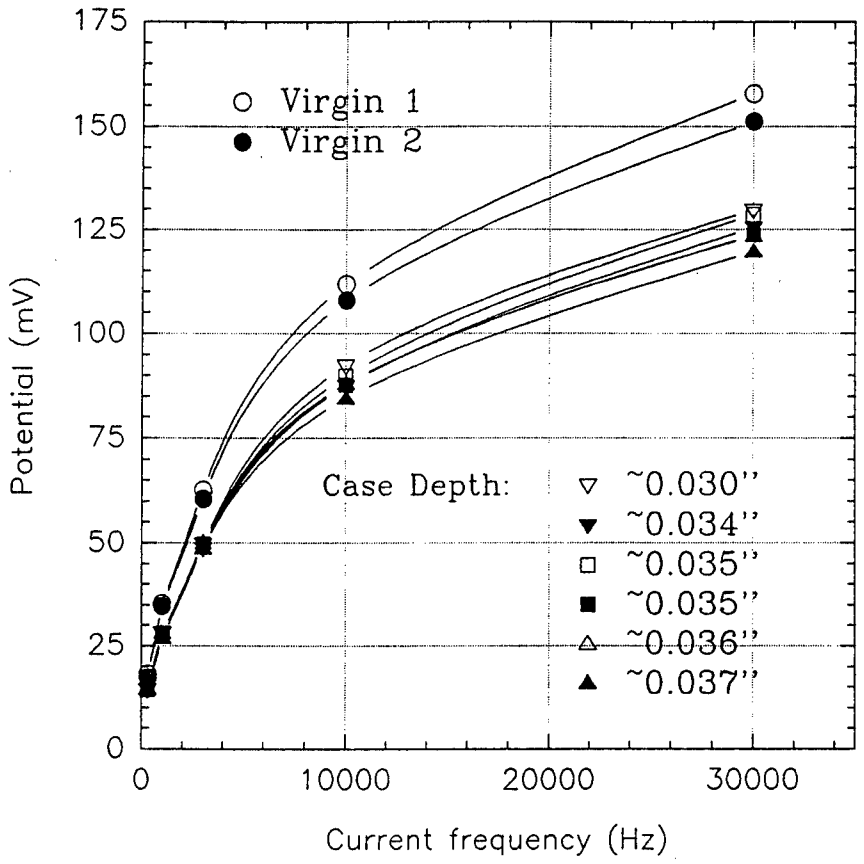

Figure12: Potential as a function of frequency

4.0 Conclusions

The main conclusions that can be drawn from this research and development program can be summarized as follows:

1) A novel NDI instrument capable of sizing case depths in carburized parts was developed. The main features of this instrument are:

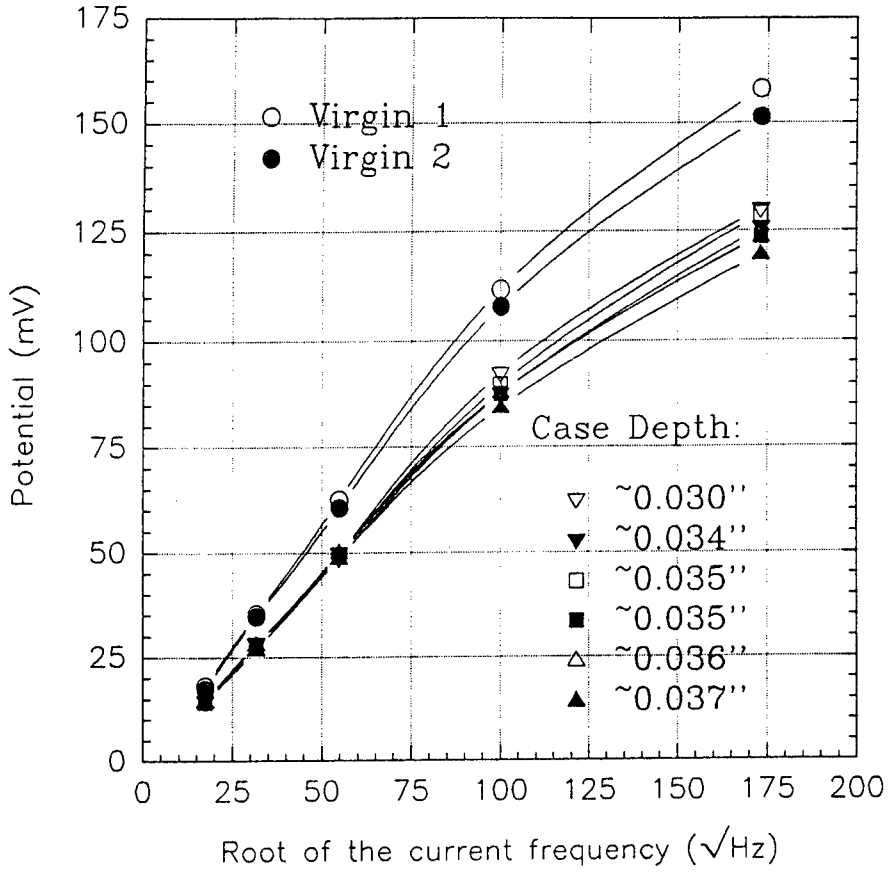

Figure 13: Potential as a function of square root of the frequency

- 100 Hz to 50 kHz frequency range;
- up to 2 Amp.;
- 2 independent channels for measurement;
- 3000 gain;
- high stability (not affected by extrinsic parameters);
- two sets of hand-probe (one for flat surfaces and one set for spur gears)
- the know-how to design and quickly fabricate hand probes to accommodate other geometries (e.g. fir tree, etc.).

2) A data bank of case depths and chemistry profiles along with their corresponding electronics signatures was produced.

3) A quality control assessment of the data including the probability of detection (POD) of case depths was obtained (the 95% POD/95% confidence level for the instrument).

This technology (ACPD and current focusing) is now being further developed to quantify depth and intensity of residual stresses induced by varying manufacturing processes including shot peening.

References

1. C.A. Stickels and C.M. Mack in Carburizing: Processing and Performance, ed by G. Krauss, pub. by ASM International, Materials Park, OH, 1989, pp 1-101

2. G. Parrish and G.S. Harper, Production Gas carburizing, Pergamon Press, New York, NY, 1985

3. Nondestructive Evaluation and Quality Control - Volume 17, Metals Handbook, Ninth Edition, pub. by ASM International, 1989.

4. C.O. Rudd, "A Review of Nondestructive Methods for Residual Stress Measurement", J. of Metals, vol. 33 no 6, 1981.

6. C.O. Ruud, in Quenching and Distortion Control ed. by G.E. Totten, pub. by ASM International, Materials Park, OH, 1992, pp. 193-198.

5. Materials Characterization - Volume 10, Metals Handbook, Ninth Edition, pub. by ASM International, 1986.

7. Y.H. Pao, W. Sachse, and H. Fukuoka, "Acousto-elasticity and Ultrasonic Measurement of Residual Stresses", in Physical Acoustics: Principles and Methods -vol XVIII, ed. by W.P. Mason and R.M. Thurston, Academic Press, 1984, pp. 61-143.

8. Handbook of Physics, ed. by E.V. Condon and H. Odishaw, McGraw Hill, 1967, pp. 4.141-4.145.

9. R.L. Pasley, "Backhausen Effect - An Indication of stress", Mater. Eval. vol 28, 1970, pp 157-163.

10. M. Mayos, S. Segalini, and M. Putignami, in Review of Progress in Quantitative NDE, vol.6, ed. by D.O. Thompson and D.E. Chimenti, Plenum Press, 1987.

11. H. Kwun and G.L. Bukhardt, "Nondestructive Measurement of stress in Ferromagnetic Steels Using Harmonic Analysis of Induced Voltage", NDT International, vol. 20, 1987, pp 167-176.

12. H. Kwun, "Measurement of stress in Steels Using Magnetically Induced Velocity changes for Ultrasonic Waves", in Nondestructive Characterization of Materials - II, ed. by J.F. Bussière et al., Plenum Press, 1987, pp. 633-670.

13. Nondestructive Evaluation and Quality Control - Volume 17, Metals Handbook, Ninth Edition, pub by ASM International, Materials Park, OH, 1989

14. "Method, Test Probe and Apparatus for Measurement of ACPD by Confining Test Current to a skin Region of a test Specimen", B.A. Unvala and N.J. Marchand, US patent #5,202,641, April 1993.

15. S. Tiku and N.J. Marchand, "On-Line Strain and Damage Measurements System (3rd Annual Report), prepared for the Department of National Defense (DND), August 1994, 152 pages.

16. J. Dai, N.J. Marchand and M. Hongoh, "Study of Fatigue Crack Initiation and Growth in Titanium Alloys Using an ACPD Technique", Can. Aero & Space J., vol. 39, 1993, pp. 35-44.

17. S. Tiku and N.J. Marchand, On-Line Strain and Damage Measurements System (2nd Annual Report), prepared for the Department of National Defence (DND), August 1993, 137 pages.

18. Properties and Selection: Irons, Steels and High Performance Alloys, Metals Handbook - Volume I, Tenth Edition, pub. by ASM International, Metals Park, Oh, 1990.